



THE FRANKLIN INSTITUTE  
RESEARCH LABORATORIES  
Philadelphia, Penna. 19103

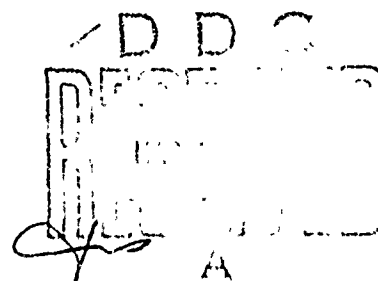
SEED-88

AD720455

**PROCEEDINGS**  
of the  
**SIXTH SYMPOSIUM ON**  
**ELECTROEXPLOSIVE DEVICES**

THE FRANKLIN INSTITUTE RESEARCH LABORATORIES

Held in  
SAN FRANCISCO, CALIF.  
JULY 8-10, 1969



Unclassified

Reproduced by  
NATIONAL TECHNICAL  
INFORMATION SERVICE  
Springfield, Va. 22151

Twenty-five Dollars

833





## PREFACE

*E.E. Hannum, Chairman*  
Manager, Applied Physics Laboratory  
The Franklin Institute Research Laboratories

The Sixth EED Symposium was attended by approximately 325 people representing 126 industrial concerns, 43 Government agencies and 4 foreign countries (England, Canada, France, and Israel). Four sessions were held on Tuesday and Wednesday July 8 and 9, 1969, at the St. Francis Hotel in San Francisco. The fifth session, classified Confidential, was held at the Treasure Island Naval Base on Thursday July 10, 1969. The proceedings therefore are in two volumes; this unclassified volume which contains 50 papers (over 850 pages) and a Confidential one with 9 papers.

The first paper describes the explosive and pyrotechnic devices used on the Apollo spacecraft which successfully landed the first men on the moon just about one week after the Symposium. About 90% of the Apollo EED's were non-destructively tested by neutron radiography; a new technique first reported at the 5th EED Symposium held at The Franklin Institute in Philadelphia, June 13-14, 1967. Papers 2-10 and 2-11 in these Proceedings are on the subject of neutron radiography.

Also in Session Two were presented and discussed a number of testing techniques and design aids which should prove very helpful to workers in the field.

In Session One a number of interesting new developments are described. In paper 1-2, Lockheed's "Super Zip" separation system evolution is traced through various design improvements to the truly remarkable culmination. One need merely scan the titles in the Table of Contents to appreciate the wide variety of new developments discussed at this meeting. It is also evident that a great deal of the industry's EED effort has been aimed at combating hostile environments which include electromagnetic energy in the forms of RF, EMP, lightning, electrostatic discharge, ionizing radiation, high heat flux, and even germs. Yes germs!

Spacecraft going to other planets must be sterilized to avoid the possibility of contamination by earth organisms. One EED has been shown to be

capable of surviving the heat cycling of the sterilization process (Paper 3-3). Since most EED's were not designed with this problem in mind, we doubt if many will be found suitable. However, Paper 5-2 describes a number of new heat resistant explosives.

Paper 4-1 on laser initiation of explosives stimulated much interest and discussion which leads us to suspect that more work is being done on lasers than was reported at this meeting.

A number of novel developments and studies were presented which include:

- Detonation by remote flash (Paper 5-4);
- Fluoric ignition device (Paper 5-5);
- Percussion-electric primer (Paper 5-7);
- Liquid desensitized initiators (Paper 3-10); and
- Solid-state initiator (Paper 4-2).

In all, 52 papers were presented in 2 1/2 days and are printed in full herein together with seven others (that were presented by title only) and the edited (condensed) discussion recorded at the meeting. Also, for convenience, the unclassified abstracts of the other volume are repeated in this volume.

Although this was our 6th EED Symposium, it was the first one held on the West Coast and the first meeting to last more than two days. We will probably plan for a three-day meeting next time, to be held in Philadelphia in 1971.

## TABLE OF CONTENTS

### Preface

*E.E. Hannum, Chairman. Manager, Applied Physics Laboratory  
The Franklin Institute Research Laboratories*

### SESSION ONE - NEW DEVELOPMENTS (Tuesday Morning, July 8, 1969)

Chairman: *Robert Wagner, Picatinny Arsenal*

#### Abstracts (Session One)

- 1-1 Apollo Spacecraft Pyrotechnics  
*William H. Simmons, NASA Manned Spacecraft Center, Houston*
- 1-2 Evolution of Linear Separation Systems for Aerospace Applications  
*I.B. Gluckman, Lockheed Missile & Space Co.*
- 1-3 A Visual Marker System for a Missile  
*P.K. Salzman, General Dynamics, Pomona Div.*
- 1-4 Development of the Saturn V Through-Bulkhead Initiator  
*L.W. Ccrwin and C.S. Greenough\*, North American Rockwell Corp.*
- 1-5 A Release Mechanism for Stored High-Pressure Gas  
*Louis G. DeGrace and L.G. Bach\*, Bendix Missile Systems Div.*
- 1-6 Vacuum Deposited Thin-Film Bridges in Electroexplosive Devices  
*J.R. Craig and O.M. Schroll, Sandia Corp.;*  
*C.E. Simpson and R. Blackshire\*, Unidynamics/Phoenix*
- 1-7 Pressure-Controlled Propellant-Actuated Devices  
*V.W. Drexelius and M.L. Schimmel\*, McDonnell Douglas Corp.*
- 1-8 Detached Electrode Electroexplosive Devices  
*D.H. Chamberlain and R.H. Stresau\*, R. Stresau Lab., Inc.*  
*R.L. Higuera and J.O. Jones, U.S. Naval Weapons Ctr., Corona Labs.*
- 1-9 Development and Characteristics of a Low-Cost Detonator for Precise Synchronization  
*Giordano Melani, Ballistic Research Labs., Aberdeen Proving Ground*  
*Presented by Boyd Taylor*
- 1-10 Electrostatic-Insensitive Detonator for Precise Synchronization  
*Boyd Taylor, Ballistic Research Labs., Aberdeen Proving Ground*
- 1-11 Further Advances in Microcircuit Bridge Technology  
*D.N. Griffin, Pelmec Div., Quantico Ind., Inc.*
- 1-12P\*\* Development of an Ordnance Circuit RF Filter  
*P.F. Mohrbach and D.J. Mullen, Franklin Institute Research Labs.*

---

\* *Speaker*

\*\*A P after the paper number indicates that this paper was presented by title only  
NOTE: Pages are numbered consecutively by paper number.

SESSION TWO - TOOLS, TECHNIQUES, AND TESTING  
(Tuesday Afternoon, July 8, 1969)

Chairman: *Douglas Durham, Lockheed Missile & Space Co.*  
Abstracts (Session Two)

A. Design Aids

- 2-1 The Second Law Applied to Pyrotechnic Systems  
*J.H. McLain, Washington College*
- 2-2 Statistical Scanning Study of Explosive End Fittings  
*R.R. Sullivan\*, S.A. Moses and G.R. Compton,  
McDonnell Douglas Astronautics, Western Div.*
- 2-3 Interior Ballistics of High-Low Propulsion Systems  
*Otto K. Heiney, Jet Propulsion Lab.*
- 2-4 Nomographical Solution of Electroexplosive Device Firing Time Equation  
*H.D. Peckham\*, Gavilan College; D.E. Davenport, Singer-General  
Precision, Inc., Link Group*
- 2-5P Withdrawn
- 2-6 Quantitative Predictions of EED Firing Characteristics  
*D.E. Davenport, Singer-General Precision, Inc., Link Group*
- 2-7P Electrical and Thermal Considerations in the Design of Electroexplosive Devices  
*R.H. Stresau, R. Stresau Lab., Inc.*

B. Testing Techniques

- 2-8 The Development of a Fixed Gap, Electrostatic Spark-Discharge Apparatus  
for Characterizing Explosives  
*L.J. Montesi, U.S. Naval Ordnance Lab.*
- 2-9 Experiments in Measurement of Output Energy of Electroexplosive Devices  
Through Metal Deformation  
*S. Barron\* and Edward G. Pierson, Conax Corp.*
- 2-10 Use of Neutron Radiography for Visual Non-Destructive Examination of Ord-  
nance Components  
*C.R. Wilson\*, GE Co., Pleasanton; W. Breakey, McCormick Selph*
- 2-11 Non-Destructive Testing of Apollo CSM Spacecraft Ordnance Devices by  
Neutron Radiography  
*W.H. Knight and A.L. Hitchens, Space Div., and N.M. Ewbank and G. Gigas\*,  
Atomics Inter., North American Rockwell Corp.*
- 2-12 Through-Bulkhead Initiator Design Margin Study  
*William B. Freeman, Martin Marietta Corp., Orlando*
- 2-13 Dynamic Output Characterization of Thrusting Type Pyrotechnic Devices  
*J.L. Lilly, Space Sys., GE Co., Philadelphia*
- 2-14 Instrumentation Control Charts  
*S. Damskey, GE Co., Philadelphia*
- 2-15P Information Sources for Explosives and Pyrotechnics  
*Gunther Cohn, Franklin Institute Research Labs.*
- 2-16P Explosive Detonator Shock Testing for Impact Sensors  
*Joseph Robin Klein, GE Co., Philadelphia*

SESSION THREE - RELIABILITY, SAFETY AND HAZARDS  
(Wednesday Morning, July 9, 1969)

Chairman: *Paul F. Mohrbach, The Franklin Institute Research Labs.*  
Abstracts (Session Three)

- 3-1 Safety of EED's in the Naval Electromagnetic Environment  
*F.J. Chesterman, Admiralty, Surface Weapons Establishment, England*
- 3-2 A Broadband RF Filter/Attenuator Plug for Wire Bridge Electroexplosive Devices  
*Theodore Marshall\*, Picatinny Arsenal; Paul F. Mohrbach, Franklin Institute Research Labs.*
- 3-3 Sterilization-Environmental Testing of Initiators  
*Laurence J. Bement, NASA, Langley Research Center*
- 3-4 The E.M.I. Hazard Measurement System  
*W.L. Watton, E.M.I. (E) Ltd. and W.B. Seamaton, RARDE, Min/Def. U.K.; Presented by W.S. Hall, British Embassy*
- 3-5 Discharge of an Electrostatically Charged Human  
*John T. Petrick, U.S. Naval Weapons Lab., Dahlgren, Va.*
- 3-6 Experiments in the Protection of EED's from Electrostatic Discharge  
*Edward G. Pierson, Conax Corp.*
- 3-7 Demythologizing Electrostatics  
*L.D. Pitts, Singer-General Precision, Inc., Link Group*
- 3-8 Initiation of Electroexplosive Devices by Lightning  
*Harvey S. North, Sandia Corp.*
- 3-9 Withdrawn
- 3-10 Liquid Desensitized Initiators  
*Robert W. Heinemann, Picatinny Arsenal*
- 3-11 Instrumentation for Making Broadband Measurements on Electroexplosive Devices  
*Jack G. Hewitt, Jr., Denver Research Institute*

SESSION FOUR - R&D STUDIES  
(Wednesday Afternoon, July 9, 1969)

Chairman: *Syl C. Piccoli, Singer-General Precision, Inc., Link Group*  
Abstracts (Session Four)

- 4-1 Some Initial Investigations of the Laser Initiation of Explosives  
*Modesto J. Barbarisi\* and Edward G. Kessler, Picatinny Arsenal*
- 4-2 The Development of a Solid-State Explosive Initiator  
*R.F. Flagg\*, E.J. Stecker and L.E. Hollander, Holes Inc.*

- 4-3 Effect of Reduced Ambient Pressure on the Hot-Wire Sensitivity of Primary Explosives, Metal-Oxidant Mixtures, and Black Powder  
*Howard S. Leopold, U.S. Naval Ordnance Lab.*
- 4-4 Functioning Time of a 1-Amp/1-Watt Detonator  
*Seranton Nesbitt, U.S. Naval Ordnance Lab*
- 4-5 The Propagation of Reaction Across a Lead Azide-PETN Interface  
*Calvin L. Scott, U.S. Naval Ordnance Lab.*
- 4-6 On the Combustion Propagation of Tungsten Delay Powders  
*Roswitha Zimmer-Galler\* and Martin Zimmer, U.S. Naval Ordnance Station, Indian Head, Md.*
- 4-7 See other volume
- 4-8 Development of RF Attenuators Utilizing Ferrite-Ceramic Component and the Effect of Nuclear Radiation of These Components  
*Nancy B. Willoughby and Stanley M. Adelman\*, Picatinny Arsenal*
- 4-9 Response of SCOUT Destruct Charges to High Heat Fluxes  
*A.E. Pierard, Missile and Space Div., LTV Aerospace Corp.*
- 4-10  $dx/dt$  vs Time Detonation Monitoring  
*Donald Baker Moore, Explosive Technology*
- 4-11 Evaluation of Detonating Cord by Framing Camera Technique  
*J.W. Blain, B.V. Carlson and A.H. Smith\*, Lockheed Missile and Space Co.*
- 4-12P Comparative Effects of CW and Radar Signals on FED Bridgewire Temperature  
*O.W. Mayes\* and Charles Carlson, McDonnell Douglas Astronautics, Western Div.*
- 4-13P EBW Firing Unit-Detonator Compatibility Tests  
*Raymond G. Amicone and Michael G. Kelly, Franklin Institute Research Labs.*
- 4-14P Determining Ratings of RF Suppression Devices  
*P.F. Mohrbach, R.F. Wood, and R.H. Thompson, Franklin Institute Research Labs.*

Abstracts (Session Five)

Attendance

Distribution

## 1-1 APOLLO SPACECRAFT PYROTECHNICS

By William H. Simmons

Manager, Apollo Pyrotechnic Subsystems  
NASA Manned Spacecraft Center

### INTRODUCTION

At the Third Electroexplosive Device (EED) Symposium in Philadelphia in 1963, the author presented a paper entitled "The Apollo Standard Initiator (ASI)." That paper described a modular-cartridge concept using a standard EED which was being adopted for the Apollo spacecraft. Concepts also were presented for the postmanufacture indexing of the initiator, for the anticipated application of pyrotechnic devices to spacecraft functions, and for a computerized data collection storage analysis system.

The pyrotechnic devices and their functions in the Apollo spacecraft on a lunar landing mission (fig. 1) are described in this paper. During the past 6 years, all pyrotechnic devices and systems have been tested extensively on the ground, in unmanned flights, and in manned flights. The last flight test objectives of the pyrotechnics were completed successfully subsequent to the Apollo 10 mission in May 1969.

The term Apollo Standard Initiator (ASI) was applied originally both to the concept of a standard EED for Apollo spacecraft and to the hardware, a specific dual-bridgewire initiator. Subsequently, a single-bridgewire initiator was developed and now is the standard device on the spacecraft; the dual-bridgewire unit is now obsolete in the Apollo program. Therefore, "Apollo Standard Initiator," or "ASI," now represent

the concept, and "Single-Bridgewire Apollo Standard Initiator," or "SBASI," describe the hardware.

Other words and abbreviations used in this paper are clarified below.

1. "Pyrotechnics" is synonymous with "explosive" and "ordnance" (pyrotechnic device).
2. "Explosive" includes both detonating and deflagrating materials. "High explosive" and "propellant" are used to differentiate between the two types of materials, when necessary.
3. "Redundant" is used in the sense of "dual" rather than "superfluous."
4. "Spacecraft" (S/C) (fig. 2) includes the following:
  - a. The command and service modules (CSM), which are abbreviated command module (CM) and service module (SM)
  - b. The lunar module (LM)
  - c. The spacecraft/lunar module adapter (SLA)
5. The Saturn IVB (S-IVB) is the third stage of the launch vehicle (LV) which inserts the spacecraft into translunar trajectory.

#### GENERAL

The Apollo spacecraft and SLA incorporate over 210 explosively loaded devices (including 143 electrically initiated cartridges of 19 different types) in the most complex pyrotechnic system ever used on any flight vehicle.



Most functions performed by spacecraft pyrotechnics are classified as "crew critical," because premature operation of the pyrotechnics or the failure of the pyrotechnics to operate properly could result in loss of the crew. The few remaining functions are, similarly, "mission critical;" that is, failure could result in an aborted mission or in an alternate mission. The high criticality assigned to spacecraft pyrotechnic functions dictated maximum redundancy in pyrotechnic systems and devices (fig. 3). Where practicable, completely redundant systems or devices are used, as in the apex-cover jettison system. Where completely redundant systems are not possible because of space or weight limitations, redundant cartridges are used, as in the canard thruster. Next in order of desirability is a single cartridge with dual initiators, as in the parachute-riser guillotines. The original dual-bridgewire initiator was developed to provide an additional back-out step, a single initiator with dual bridgewires interfacing the same explosive charge.

The electrical circuitry and associated control components, including the batteries that supply power for logic and firing, are redundant. The pyrotechnic batteries and circuits are used only for pyrotechnic system firing and control. Firing circuits A and B are completely independent and are electrically and physically isolated from each other and from all other spacecraft circuitry. Logic circuits A and B are similar, except in the earth-landing system where additional redundancy is required. In the earth-landing system, although the logic relay contacts are electrically isolated, the relay coils A and B are interconnected so that both contacts are pulled in by either logic A or logic B. This system circumvents a single-point failure in either logic system without compromising the isolation of the firing circuitry.

Early in the Apollo program, the NASA Manned Spacecraft Center (MSC) adopted the concept of modular cartridge assemblies, based on a standardized hot-wire initiator. Whenever possible, this standardization principle has been extended to cartridge assemblies at significant cost and time savings. In addition, the adoption of the modular-cartridge concept has enhanced confidence and reliability of these common components/assemblies through increased testing and use (fig. 4). Components, subassemblies and assemblies were qualified serially (that is, first the EED, then each cartridge, then each higher assembly, and so forth) to complete systems.

Because the most critical area in any EED is the electroexplosive interface, a common interface that is tested in a number of devices increases the confidence in all devices using the interface. The SBASI provides such an interface in a form that can be tested as a separate unit then tested again and again in higher devices, assemblies and systems. In addition, because of the necessity to develop and qualify only one EED, it was possible to test and understand more thoroughly the characteristics of that device than would have been possible if a number of different devices had been developed for the spacecraft.

Noninterchangeability of special-purpose cartridges is ensured by using different threads on the output ends and by using on the connector a unique postmanufacture indexing technique which provides for special keyway combinations. The indexing technique is covered by NASA-owned U.S. Patent 3,287,031 and is available on a royalty-free, nonexclusive license basis for commercial use. The technique can be used also on other nonpyrotechnic electrical connectors.

A family of special shielded connectors, which mate with the various SBASI configurations and provide radiofrequency shield continuity, were developed for

the Apollo pyrotechnic systems. On the Apollo spacecraft, these connectors are reserved for use on pyrotechnic circuits to prevent misconnection with other electrical circuitry.

In instances where the common use of hardware was not feasible, common technology was used. For example, the opposing-blade guillotine which severs the CM-SM umbilical (fig. 5) was the basis for the designs of the LM interstage guillotine, of two guillotines for umbilicals between the LM and SLA, and of the LM landing-gear uplock cutter.

To ensure consistent quality and traceability of high-explosive materials, only newly manufactured RDX and HNS high explosives are used. These bulk explosives are government-furnished material. RDX is supplied to NASA by the Army, and HNS is supplied by the Navy. The materials are shipped directly to the using supplier of explosive assemblies upon request to MSC by North American Rockwell and Grumman Aircraft Engineering Corporation.

Neutron radiography (N-ray) is a relatively new technique used to ensure high quality of assemblies. In a number of instances, such as examining the explosive core in a mild detonating fuse (MDF) for discontinuities, this technique is superior to X-ray. The relative opacity of the lead sheath and of the explosive core to thermal neutrons is the reverse of that with X-rays. However, the advantage is lost when the MDF is bonded into a charge holder with a hydrogenous material such as epoxy. Therefore, the N-ray technique is applied selectively to Apollo pyrotechnics to supplement X-rays where appropriate.

All lots of all explosively loaded components and assemblies are non-destructively tested and inspected on a 100-percent basis. The lots then are sampled at random for destructive testing at each level of assembly. In addition, one unit from each lot of each device to be installed on a spacecraft is

fired at the Kennedy Space Center before each flight to ensure that there has been no deterioration caused by shipping, handling, or storage subsequent to lot acceptance.

The Apollo Pyrotechnic Data System (APDS) was established to collect and analyze data on the spacecraft pyrotechnics. The system uses the computer complex at MSC and is now being modified to increase the capabilities. When fully operational, the APDS will be capable of storing and analyzing data pertaining to the logistics, quality, and engineering aspects of all Apollo devices by serialized parts, by lots, and by total population.

The inputs to the computer system are reports submitted on MSC Form 1275 by all Government and Contractor activities which manufacture, test, ship, install, or handle Apollo pyrotechnic devices. Each report identifies the reported devices by part, lot, and serial number. Parametric data on performance and tests are reportable, as are shipping destinations, receiving inspections, allocation to specific spacecraft, and so forth.

A typical logistics study from the stored data could be a printout of the location of every cartridge in existence; such a report could be used to locate all units of a specific lot to provide a basis for additional procurement or to "freeze" a lot pending investigation of an anomaly ~~related to~~ that lot or part. Engineering studies of specific performance parameters can be made to investigate lot-to-lot variations and trends.

## PYROTECHNIC FUNCTIONS ON A NORMAL MISSION

Pyrotechnic devices perform many and varied functions on a spacecraft. A total of 218 explosively loaded parts, including 143 cartridges, are installed on each spacecraft. The first pyrotechnic function in a normal mission, jettison of the launch escape system (LES), occurs approximately 3 minutes after launch, and the last pyrotechnic function, main parachute disconnect, occurs after splashdown. The pyrotechnic devices and locations in the spacecraft are shown in figure 6. In this paper, the devices are discussed first as used in a normal lunar landing mission (fig. 1) and then as used in aborted missions.

### Launch Escape System (LES) Jettison

In a normal mission, the LES is not used and is jettisoned immediately after second-stage booster (S-II) ignition (fig. 7). Simultaneously with ignition of the tower-jettison motor by dual igniter cartridges, a frangible nut in the base of each tower leg (used to secure the tower to the command module structure) is fractured by dual detonators (fig. 8).

### CSM-Launch Vehicle Separation

The next pyrotechnic event, CSM separation from the launch vehicle, occurs after translunar injection by the third (S-IVB) stage of the launch vehicle (fig. 9). The four SLA panels are separated by redundant explosive trains on the forward, aft, and inner and outer longitudinal splice plates (fig. 10). Pyrotechnic thrusters powered by dual cartridges rotate each panel outwardly around a center hinge. After a rotation of approximately  $45^\circ$ , the panel hinges separate and spring thrusters jettison the panel. At the time of splice-plate separation, a

high-explosive-operated guillotine severs an umbilical between the LM and one SLA panel, a spring reel then retracts the umbilical arm to the panel for jettison with the panel, and a high-explosive charge in a frangible-link disconnect separates the SM-SLA umbilical just aft of the SM. The entire system is explosively interconnected, with dual detonators initiating the separation trains and confined detonating cords connecting these trains to the SM-SLA umbilical disconnect and to the LM-SLA guillotine.

#### LM-SLA Separation

After separation from the S-IVB, the CSM returns and docks with the LM, an electrical umbilical is attached to the LM separation firing circuits through the docking interface, and the four frangible links that attach the LM to the fixed portion of the SLA are fired (figs. 11 and 12). Because the detonators in the links are located on the SLA side of the LM-SLA interface, a high-explosive guillotine severs this umbilical bundle 30 milliseconds after the frangible-link detonators are fired.

#### LM Pyrotechnics

All LM pyrotechnic functions occur during the next phases of the mission which involve lunar descent, landing, and ascent. The LM devices and locations are shown in figure 13. The relatively new explosive hexanitrostilbene (HNS) is used in all LM high-explosive devices and in the docking ring separation system of the CM. In all other CSM and SLA high-explosive applications, cyclotrimethylene trinitramine (RDX) is used because, at the time of initial system development, relatively little information on HNS was available and the supply of HNS was limited.

### LM Landing Gear Deployment

In lunar orbit and prior to separation of the LM from the CSM, the LM landing gear is deployed by firing guillotines (fig. 14) which sever tension straps that hold the gear in the retracted position. When the straps are severed, springs deploy the gear to the downlocked position.

### LM Main Propulsion and Reaction Control Systems

#### (MPS and RCS) Pressurization

A number of normally closed explosive valves (fig. 15) are used in the LM main propulsion system and in the reaction control system (RCS). The valves pressurize propellant tanks by opening the lines to ambient and supercritical helium storage vessels, provide for propellant tank venting, and perform compatibility functions. The valves are used singly or in pairs, depending on their function; redundant cartridges are used when valves are not redundant. A total of 16 valves and 22 cartridges are used for these functions.

The explosive valves in the descent propulsion system (DPS) and in the RCS are functioned and the systems are checked out prior to undocking of the LM for descent to the lunar surface. The valves in the ascent propulsion system (APS) are fired during preparation for launch from the lunar surface.

### LM Staging

On the lunar surface and prior to launch of the ascent stage, the LM stages are separated by an explosive nut and bolt (fig. 16) at each structural attachment point. The interstage electrical circuits are deadfaced by two electrical-circuit interrupters (fig. 17), and the interstage umbilical (electrical and fluid lines) is severed by a guillotine (fig. 18).

In an abort during descent to the lunar surface, actuation of the "Abort Stage" switch initiates the staging and the pressurization of the ascent section of the main propulsion system in an electrically timed sequence, the descent stage is jettisoned, and the ascent stage then returns to lunar orbit to rendezvous with the CM.

#### LM Jettison

After rendezvous, docking, and LM crew transfer to the CM in lunar orbit, the LM is jettisoned by severing the docking-tunnel structure with redundant explosive trains (fig. 19). The docking-ring-separation charges and associated long-reach detonators are the only CSM devices which use HNS high explosive.

#### CM-SM Separation and SM Jettison

Before the spacecraft enters the atmosphere of the earth at approximately 400 000 feet, the CM RCS propellant tanks are pressurized by helium, which is released by explosive valves of the same configuration as that shown in figure 15. By using the RCS, the crew then orients the CSM to separation attitude. At separation (fig. 20), the critical electrical circuits between the CM and the SM are deadfaced by electrical-circuit interrupters (fig. 21), the CM-SM umbilical is severed by a high-explosive-operated guillotine (fig. 5), and structural separation is accomplished by dual linear-shaped charges (fig. 22) on each of the three tension ties between the modules. The SM backs away from the CM using the +X thrusters of the SM RCS.



### Earth Landing System (ELS) Operation

Approximately 8 minutes after atmospheric entry (fig. 23), the spacecraft has descended to approximately 24 000 feet where the CM apex cover is jettisoned by a redundant thruster system (fig. 24). As the cover separates from the CM, a lanyard-operated switch fires a drag parachute mortar in the cover. The parachute prevents the cover from recontacting the CM or interfering with drogue parachute deployment.

Two seconds after cover jettison, the two reefed drogue parachutes are deployed by mortars (fig. 25). At "line stretch," the time-delay reefing-line cutters in each parachute (fig. 26) are actuated and disreef the drogues 10 seconds later.

Approximately 40 seconds after deployment, the drogues are disconnected by severing the risers with propellant-gas-operated guillotines (fig. 27) and the three pilot parachutes are deployed simultaneously by mortars (fig. 25). The pilot parachutes deploy the main parachutes, which inflate to a full-reefed condition. Main parachute riser deployment actuates six 8-second-delay line cutters which release spring-loaded deployment mechanisms on two VHF antennas and on a flashing beacon light to assist in recovery operations. At line stretch of the main parachutes, four 6-second and two 10-second-delay reefing-line cutters are actuated on each parachute, effecting disreef in two stages to lower the inflation shock loading on the parachutes.

Immediately after splashdown, the three main parachutes are disconnected by guillotines in the parachute disconnect assembly (the "flowerpot") (fig. 27).

## PYROTECHNIC FUNCTIONS FOR ABORTS

Missions may be aborted at any time. However, special pyrotechnic functions or sequences are involved only in the aborts occurring between crew insertion (manning of the spacecraft on the pad) and orbital insertion of the spacecraft. Aborts from the launch pad and at low altitudes require highly complex sequences of pyrotechnic events; the combination and sequence of events are functions of altitude. To minimize risk to the crew, onboard automatic control, onboard manual control, and ground control of abort initiation is provided.

From the pad to approximately 30 000 feet (fig. 28), abort begins with the following essentially simultaneous pyrotechnic functions ( $T = C$ ).

1. CM-SM electrical circuit deadfacing (four circuit interrupters)
2. CM RCS propellant pressurization (four explosive valves)
3. CM RCS helium, fuel, and oxidizer interconnects (four explosive valves)
4. CM RCS oxidizer dump (two explosive valves)
5. CM-SM structural separation (three dual linear-shaped charges)
6. CM-SM umbilical separation (one guillotine)
7. Launch escape motor ignition (two cartridges)
8. Pitch control motor ignition (two cartridges)

At  $T + 5$  seconds, the CM RCS fuel dump is initiated by firing two more explosive valves. At  $T + 11$  seconds, a thruster deploys canards in the LES to reverse the attitude of the CM for LES jettison and parachute deployment (fig. 29), and at  $T + 14$  seconds, the docking ring is explosively separated and jettisoned with the launch escape tower to which it is attached by a tension tie.

At approximately T + 14.5 seconds, the apex cover is jettisoned as in normal landing, and at T + 16 seconds, the drogues are deployed. At T + 18 seconds, the RCS fuel and oxidizer lines are purged, and the residual helium pressurant is dumped through four explosive valves.

The drogues disreef at approximately T + 27 seconds and are disconnected simultaneously with main parachute deployment at T + 28 seconds. Recovery-aid deployment, descent, and landing are the same as in a normal mission.

#### 30 000 Feet to Normal LES Jettison

In an abort from 30 000 feet to LES jettison, the pyrotechnic functions are similar to the abort described previously. However, rapid jettison of RCS propellant is inhibited, and the propellants are disposed of as in a normal mission. The time interval between events is changed slightly, and above 100 000 feet, the crewmen may elect to jettison the LES and follow normal landing procedures.

#### LES Jettison to Normal CSM Launch Vehicle Separation

After tower jettison and prior to normal CSM separation from the launch vehicle, missions are aborted by using the SM service propulsion system (SPS). The CSM is separated from the launch vehicle as in a normal mission and, at crew option, either normal entry and landing procedures are followed or the CSM aborts into orbit with the SPS.

#### EED AND CARTRIDGE ASSEMBLIES

Three general types of cartridges are used in the spacecraft: igniter cartridges in rocket motors, pressure cartridges in mechanical devices, and detonator

cartridges in high-explosive systems. The number of special-purpose cartridges has been minimized, and all but one type of cartridge electrically initiated.

To achieve high confidence in the critical electroexplosive interface, a standard EED, the SBASI, was developed and qualified as an independent module. By adding booster modules containing various types of charges, special-purpose cartridge assemblies are obtained. The resulting spacecraft cartridge family is shown in figure 30. The only nonelectric cartridge, that used to operate the SLA panel thrusters is fired by confined detonating cords to minimize the electrical circuitry and to ensure simultaneity in SLA panel separation.

#### The EED Module

The heart of the Apollo spacecraft pyrotechnic systems is the SBASI. Early in the Apollo program, a dual-bridgewire four-pin initiator was developed as the standard unit and was used in the early development and qualification of CSM and LM pyrotechnic systems. During the development of the device and system, the following limitations of the dual-bridgewire initiator became apparent.

1. Low interbridge electrical resistance (characteristic of conductive mixes) imposed limitations on electrical systems design.
2. The body material (17-4PH steel) had inadequate impact resistance in detonator applications at low temperatures (below -65° F).
3. In the detonator and in some high-pressure cartridge applications, the electrical pins in the EED could be blown out.
4. In the circuit-to-circuit mode, the initiator had high sensitivity to electrostatic discharge.

It also became apparent that the dual-bridgewire feature of the device was not required because the necessary redundancy could be better achieved at higher levels of assembly and, as a result, it was possible to eliminate one bridgewire. Thus, the SBASI came into existence. The SBASI retains the performance and desirable electrical characteristics of the original unit and incorporates the following improvements.

1. The body material was changed to Inconel 718 for improved impact resistance at cryogenic temperatures.

2. The wall thickness was increased for higher internal pressure capability.

3. The electrostatic discharge survival capability was increased from 9000 to 25 000 volts, and the spark gap providing this capability was moved to the interior of the unit for environmental and contamination protection.

4. A stepped Inconel 718 header was incorporated, with the contact pins glassed to the header and the header welded to the body. This design, together with the increased wall thickness, raised the internal pressure capability to over 35 000 psi.

5. The technique for postmanufacture indexing of the connector was incorporated.

In development of the SBASI, the body-header assembly was hydrostatically tested, after repeated thermal shocks from -320° F to 500° F, to over 100 000 psi without failure. In production, all units are tested to 35 000 psi. All production units are also tested for electrostatic survival capability and leak tested with helium to ensure proper hermetic sealing. Sectioned and exploded views of the SBASI are shown in figure 31. The technical requirements and the physical

configuration of the SBASI and the component parts are defined in NASA/MSC documents which comprise the SBASI procurement package. Space Ordnance Systems, Inc., developed the dual-bridgewire unit and the SBASI. Subsequently, Hi Shear Corporation was qualified as a second source of the SBASI. The units produced by these two manufacturers have been tested extensively to ensure complete interchangeability.

The capability of indexing the connector end of the SBASI after manufacture is a unique and important feature which permits manufacture and stocking of the unit in a general-use configuration and subsequently configuring any unit to any of nine special keyway combinations to meet special requirements. This technique eliminates the need for stocking the various indexed configurations which may be needed on short notice. With this technique, indexed SBASI can be reconfigured if required.

The indexing technique consists of broaching two (or more) additional keyways in the connector at the time of manufacture. In the SBASI, the two additional keyways are in the 1 o'clock and 11 o'clock position with the master keyway at 12 o'clock and the other four ways at the normal positions of 3, 5, 7, and 8 o'clock (fig. 32). SBASI are procured and stocked in U.S. government-bonded storage in the "all open" (xx0) configuration. However, no SBASI may be shipped in that configuration without special MSC authorization because such a unit will mate with any connector. Prior to shipment, two keyways are blocked by staking appropriate keyways inwardly to within 0.001 inch of the inner surface of the connector. Configuration xx1 is normally found on initiators, but that configuration is prohibited on the Apollo spacecraft; it is reserved for developmental, experimental, nonflight, and rejected flight units. SBASI which are rejected at any time can be restaked to this nonspacecraft xx1 configuration to prevent mating of any firing circuit on the spacecraft if a rejected

unit is installed by mistake. The special indexing system on the Apollo spacecraft may not be used in any system other than pyrotechnics, thus preventing possible mixups in the connection of circuits.

The complete part numbering system for the SBASI is shown in figure 32. The first digit of the dash number indicates the flight status, the second digit indicates whether a weld washer is installed on the part, and the third digit indicates the keyway indexing combination.

Another unique feature of the SBASI is the spanner-type torquing section that is used instead of the usual hexagonal section (fig. 33). This feature is used to prevent applying torque to the SBASI, with attendant damage to the hermetic seal, when a cartridge assembly is installed in the spacecraft. Because a special tool is required to install or remove a SBASI, only authorized personnel possessing this tool can perform this operation.

A third feature is the method of hermetically sealing the SBASI into a cartridge assembly. A thin metal washer is welded to the underside of the torquing section (fig. 33) during the preshipment configuration operations. After installation of the SBASI into the cartridge, this washer is welded around the outer edge to the top of the cartridge body.

For the Apollo spacecraft program, the SBASI is government-furnished equipment to all cartridge manufacturers upon request to MSC by North American Rockwell Corporation and Grumman Aircraft Engineering Corporation. MSC stocks the unit in the xx0 configuration with only the basic part number marked on the unit (in addition to lot, serial, and so forth). Prior to each shipment, the required quantity of units are staked, fitted with washers if required, marked with the appropriate dash number, and tested nondestructively. Units which

fail the shipping tests are reconfigured to xxl, color coded as rejected flight units, and shipped to MSC for removal from the flight stock. Any SBASI or cartridge assembly which becomes nonflightworthy at any time can be handled similarly.

The SBASI has a perfect reliability record to date; the SBASI and its predecessor unit has not been known to have failed to fire when subjected to the recommended minimum all-fire current pulse. The Inconel 718 body and header resists high-explosive shock loading at cryogenic temperatures, and the autoignition (cookoff) temperature of the explosive mix is well over 600° F.

The SBASI and its predecessor unit have undoubtedly undergone more exhaustive and extensive testing than any other initiators. More than 20 000 dual-bridgewire units were used in the Apollo spacecraft development, followed by perhaps 5000 to 6000 SBASI units. The extent of testing and use of the units in non-MSC programs is not known with any degree of exactness; however, it is known that the SBASI is being tested and used elsewhere in a variety of programs and is being considered for even wider use. MSC is vitally interested in acquiring such information, especially test results which indicate areas where improvements are desirable or which demonstrate acceptable characteristics under extended environmental conditions.

The personnel of the MSC believes strongly in the standard initiator concept and encourages the use of the SBASI, within the limits of its capabilities, on other programs. The advantages of standardization have been clearly demonstrated on the Apollo program where significant reductions in cost and development time were realized. In addition, the demonstrated reliability and confidence level in the SBASI are being significantly increased as the Apollo flight program progresses because approximately 140 SBASI are flown on each Apollo mission.



The present SBASI design represents a stage in the evolutionary process and will undoubtedly undergo modifications as necessary improvements are uncovered for future programs. The present SBASI will be used in the Apollo Applications Program. Each new MSC program will start with the then-current SBASI configuration, with improvements being incorporated as required. Thus, the SBASI and the ASI concept are dynamic rather than static end-of-the-line devices and concepts.

#### Cartridge Assemblies

Modular cartridges (incorporating the SBASI as a component) are used throughout the spacecraft and are designed for common-use where possible.

The physical configuration, performance, and spacecraft usage of the Apollo cartridge assemblies are shown in table 1. The SBASI is included because it is used as a pressure cartridge in one application. The indexing of the SBASI in the cartridges is also shown. Cartridges with different outputs have different threads where necessary to prevent improper installation, and those having the same output but which are located close to each other in the spacecraft and are fired at different times are differently indexed. Thus, the same thread and indexing may be used in various locations on the spacecraft.

Each cartridge assembly (except the SLA thruster cartridge) consists of one or two SBASI and a cartridge body hermetically sealed together by the weld washer. The Type 100 pressure cartridge contains no charge other than that in the SBASI; the cartridge module is an adapter necessary to install the SBASI in a small explosive valve. Right- and left-hand threads are used on variations of these, and other, cartridges because of installation near other cartridges with different functions or different firing times.

The parachute disconnect assembly (figs. 27 and 34), known as the flowerpot, provides an excellent example of the need for indexing initiators. Because of the limited space available, only one cutter blade, powered by one cartridge, could be used for each of the five risers. The maximum attainable redundancy was to install two SBASI in each cartridge, one connected to each of the two electrical systems. In figure 35, the connectors are shown mated to the SBASI and the figure clearly illustrates the space problem often encountered in the spacecraft. In this one case, the space was so limited that weld washers could not be used because the washers would overlap. Therefore, the SBASI are epoxied in place and lockwired together. The necessity for correct connection of firing leads is apparent because a mistake could result in disconnecting a main parachute before deployment. To ensure circuit redundancy in each cartridge, both system A and system B must be connected to each cartridge. As a result, five cartridges with ten SBASI are in proximity where proper cartridge installation and connector mating is mandatory. The solution to this problem is shown in figure 36. Proper cartridge installation is ensured by different threads on the two cartridges, and proper connector mating is ensured by four different indexing combinations.

#### CONCLUSION

The Apollo spacecraft has a pyrotechnic system which is undoubtedly the most complex ever used on any flight vehicle.

Undoubtedly the greatest innovation in the Apollo spacecraft pyrotechnic systems is the use of a standardized initiator. This technique, with modular cartridges and postmanufacture indexing of the initiator, resulted in significant cost reductions, shorter development times for higher assemblies, and higher demonstrated reliability of the most critical area, the electroexplosive interface.

TABLE 1.- APOLLO SPACECRAFT CARTRIDGES

Cartridge type	Variations, (cartridge dash number)	SBASI dash number	Cartridge thread (a)	Nominal performance			Use	Number on each spacecraft
				psi	Bomb			
					Volume	Type (b)		
Pressure cartridges								
Canard	None	216	1-1/2 x 12 RH	13 500	20 in <sup>3</sup>	C	Canard thruster	2
Type I	None	216	7/8 x 14 RH	14 500	52 cc	V	Drogue parachute mortar	4
Type II	None	216	11/16 x 12 RH	11 200	8.9 cc	V	Pilot and drag parachute mortar	8
Type IV	0034	218	15/16 x 16 RH	2 250	8.8 cc	C	CM RCS propellant valve	5
Type IV	0054	216	15/16 x 16 RH	2 250	8.8 cc	C	SM circuit interrupter	4
Type IV	1034	217	15/16 x 16 LH	2 250	8.8 cc	C	CM RCS propellant valve	1
Type VI	None	216	1-1/16 x 18 RH	14 500	4.8 in <sup>3</sup>	V	Apex cover thruster	4
Type 100	0121	216	11/16 x 24 RH	9 000	0.5 cc	C	CM and LM RCS helium valve	12
Type 100	0122	212	11/16 x 24 LH	9 000	0.5 cc	C	CM RCS helium valve	2
Type 200	None	216	3/4 x 16 LH	12 900	7.0 cc	C	CM circuit interrupter	4
Drogue disc	None	252/253 (c)	13/16 x 20 RH	5 800	0.9 in <sup>3</sup>	C	Drogue parachute disconnect	2
Main disc	None	253/259 (c)	1 x 16 RH	10 500	1.2 in <sup>3</sup>	C	Main parachute disconnect	3
LM valve	None	216	3/8 x 24 LH	1 600	10 cc	C	LM propulsion system	22
Electrical circuit interrupter	None	216	7/16 x 24 RH	1 000	10 cc	C	LM circuit interrupter	4
Explosive nut	None	216	9/16 x 24 RH	6 800	2.7 cc	C	LM interstage separation	4
Explosive bolt	None	216	1-1/16 x 18 RH	1 000	2.5 cc	C	LM interstage system	4
SBASI	Many	256	3/8 x 24 RH	650	10 cc	C	Docking probe retraction	4
SLA thruster	None	(d)	1-1/16 x 18 RH	4 200	4 in <sup>3</sup>	C	SLA panel deployment	8
Igniter cartridges								
Type I	None	216	5/8 x 18 RH	2 100	10 cc	C	Launch escape/pitch control motors	4
Type II	None	218	3/14 x 16 RH	2 100	10 cc	C	Tower jettison motor	2
Detonator cartridges								
CSM standard	0007	216	9/16 x 18 RH	0.045 dent in aluminum		Various on CSM		26
CSM standard	0008	218	9/16 x 18 LH	0.045 dent in aluminum		SLA separation		2
End type	None	216	9/16 x 18 RH	0.018 dent in steel		LM guillotine and landing gear uplocks		10
Long reach	None	216	5/8 x 18 RH	0.022 dent in steel		Docking-ring separation		2

<sup>a</sup>RH, right hand; LH, left hand.<sup>c</sup>Two SBASI per cartridge.<sup>b</sup>C, closed; V, vented.<sup>d</sup>Nonelectric cartridge initiated by confined detonating cord.

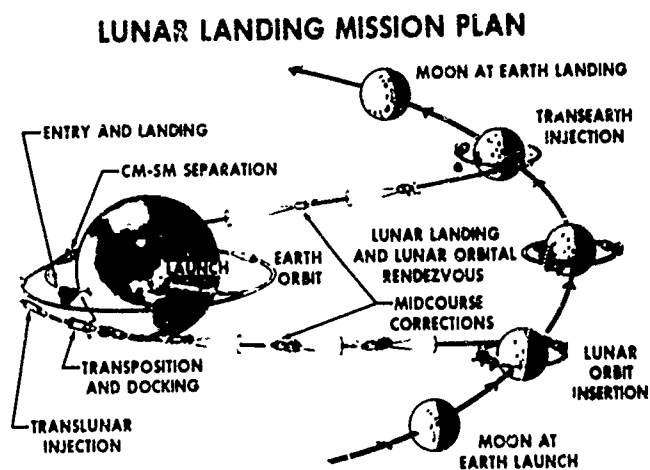


Figure 1

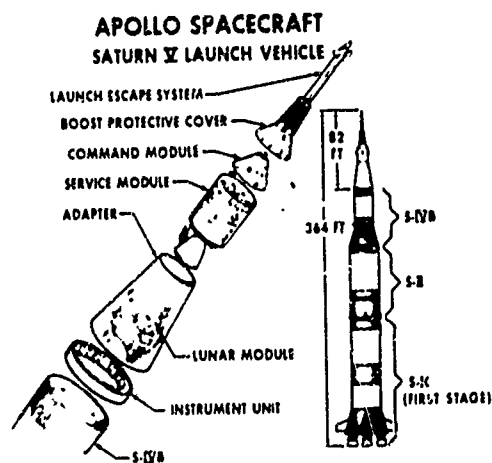


Figure 2

## SYSTEM/DEVICE REDUNDANCY

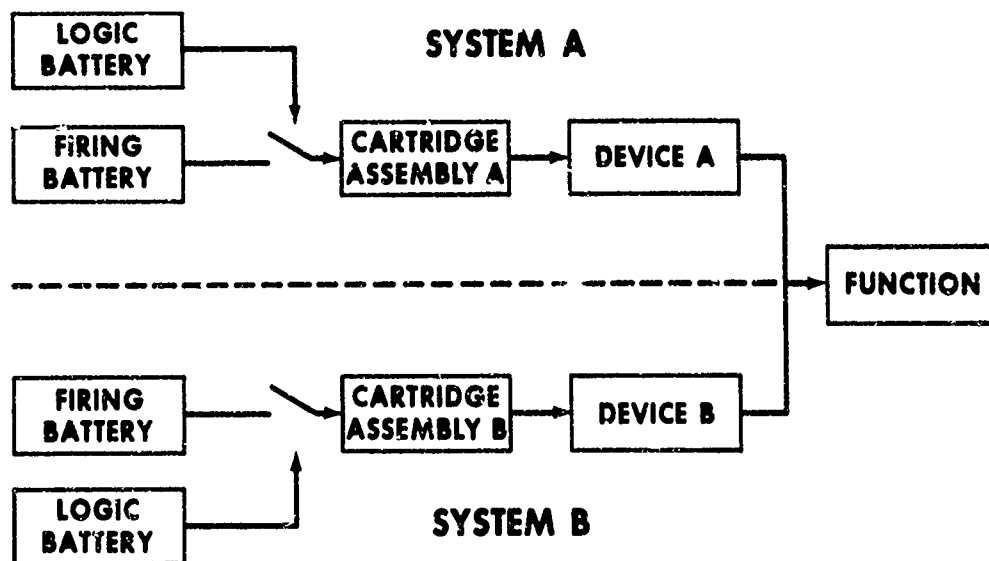


Figure 3

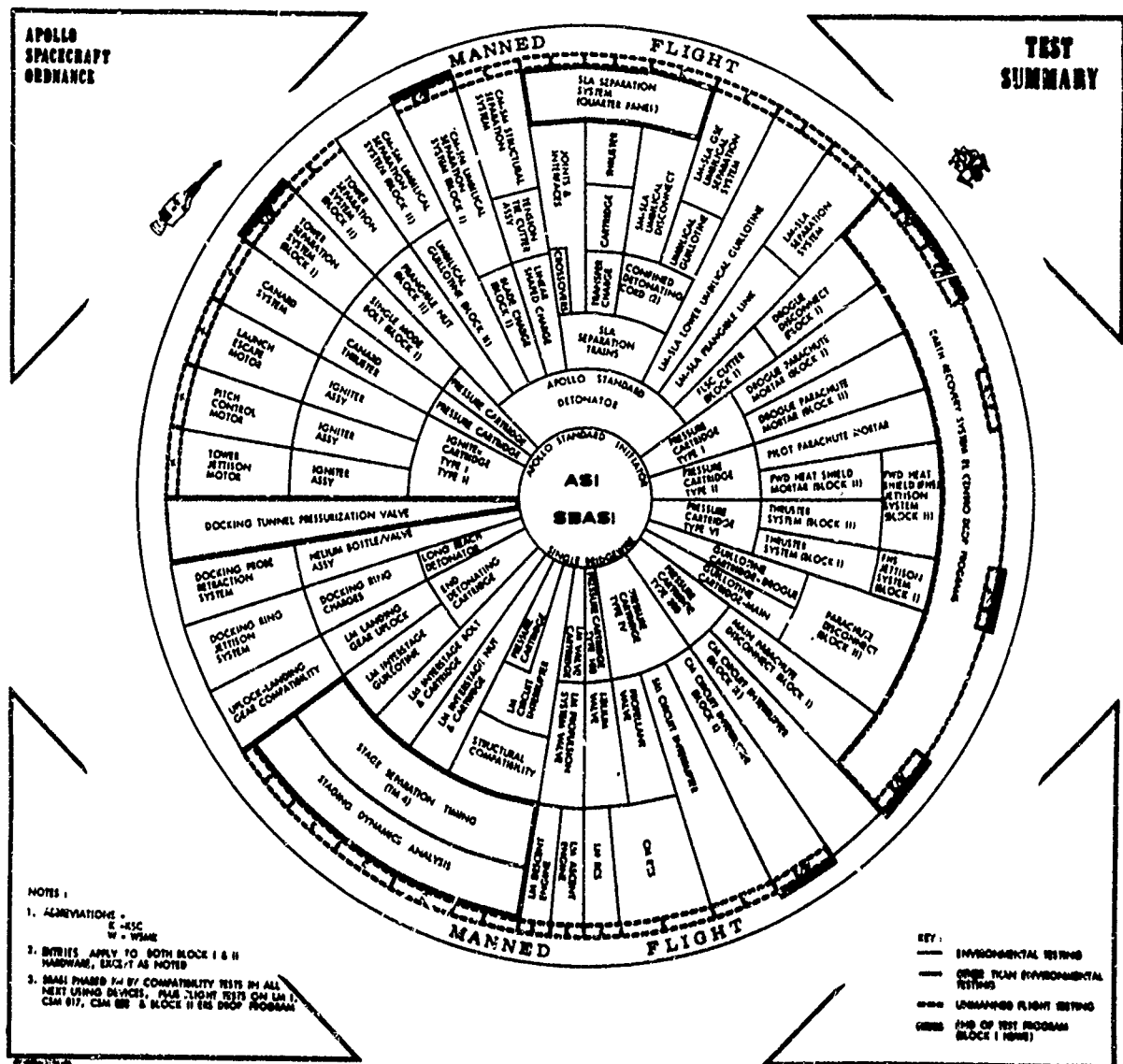
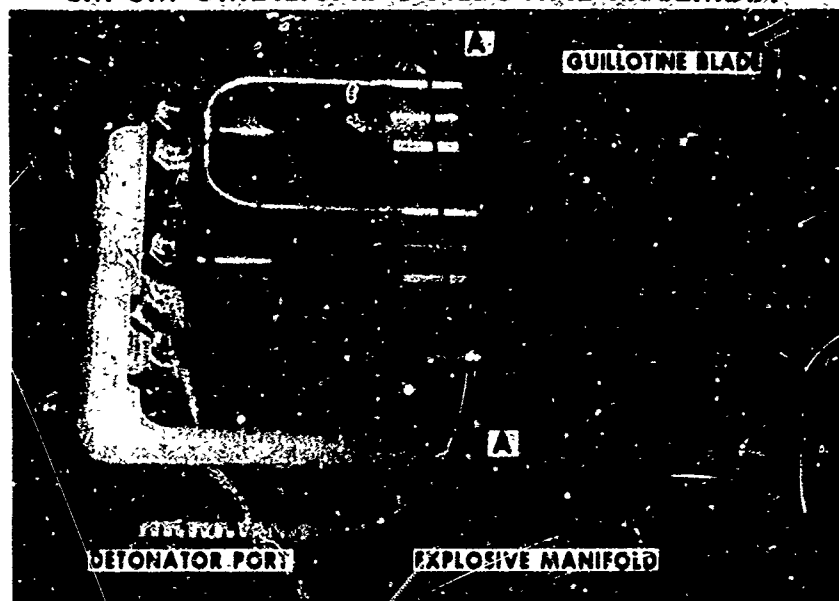


Figure 4

1-1.23

## CM-SM UMBILICAL GUILLOTINE ASSEMBLY



## CM-SM UMBILICAL GUILLOTINE, (CONT)

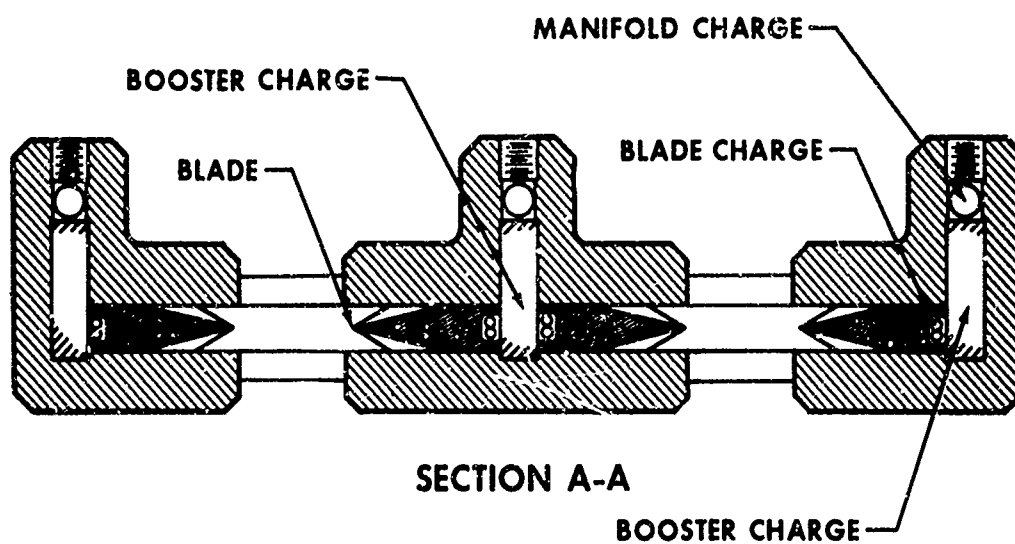


Figure 5

1-1.24

## APOLLO PYROTECHNICS AND THEIR LOCATIONS ON THE SPACECRAFT

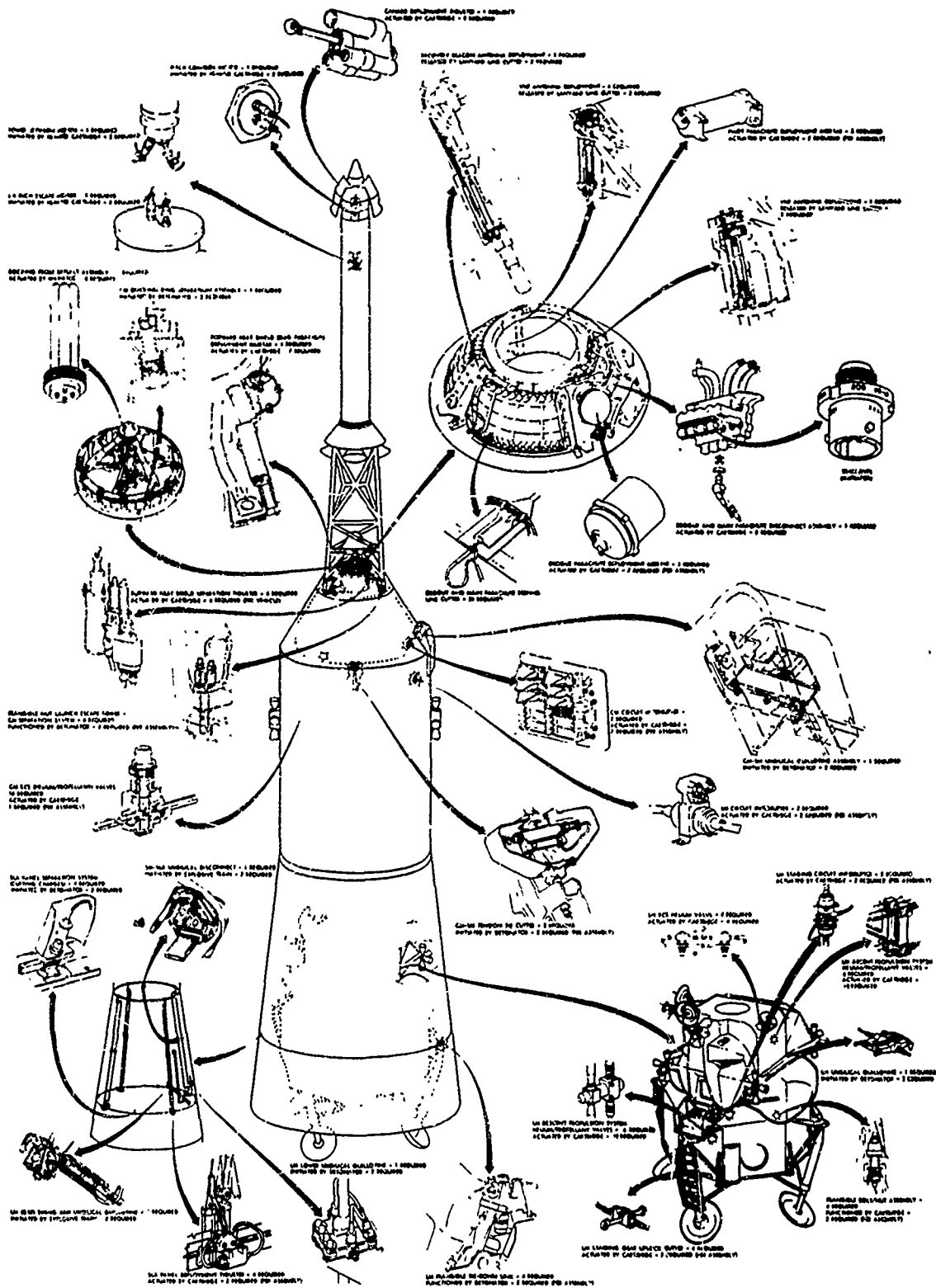


Figure 6

# NORMAL TOWER JETTISON

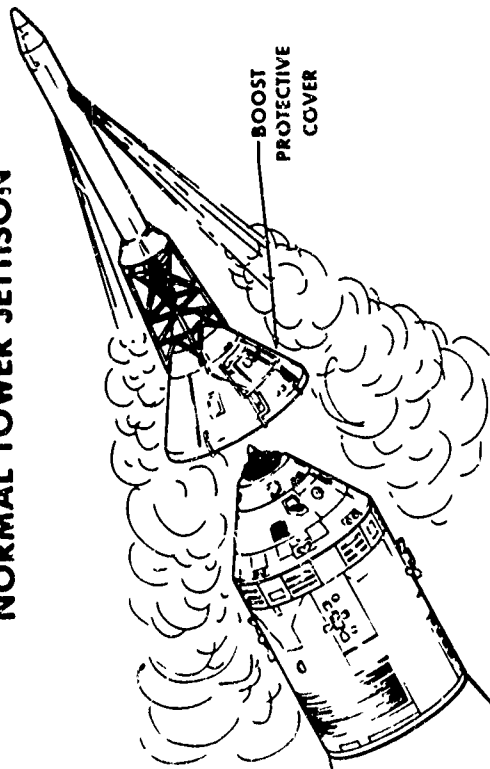


Figure 7

# NORMAL CSM/LV SEPARATION

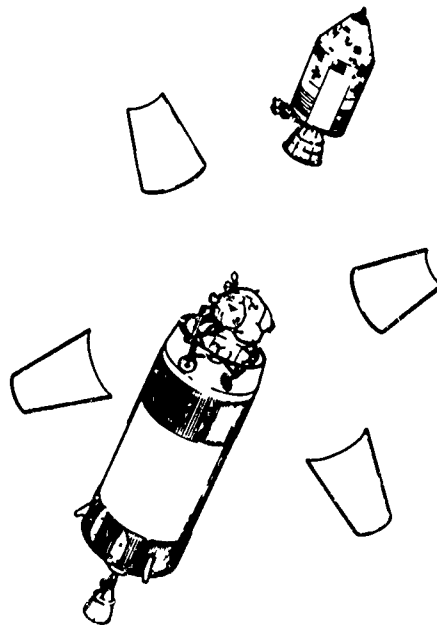


Figure 9

# TOWER SEPARATION SYSTEM

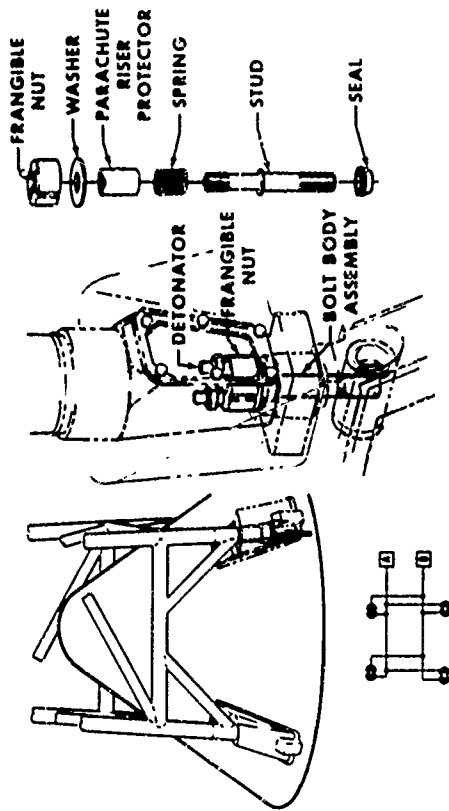


Figure 8

# SEPARATION OF THE SLA PANELS

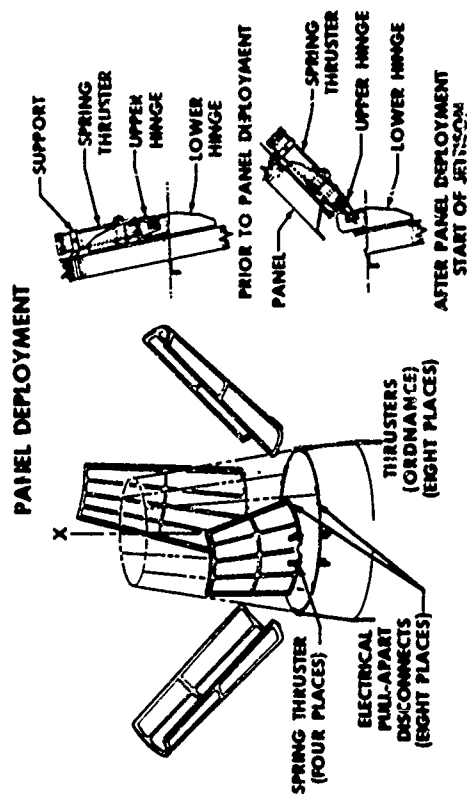


Figure 10(a)



# SEPARATION OF THE SLA PANELS, (CONT)

## PANEL SEPARATION

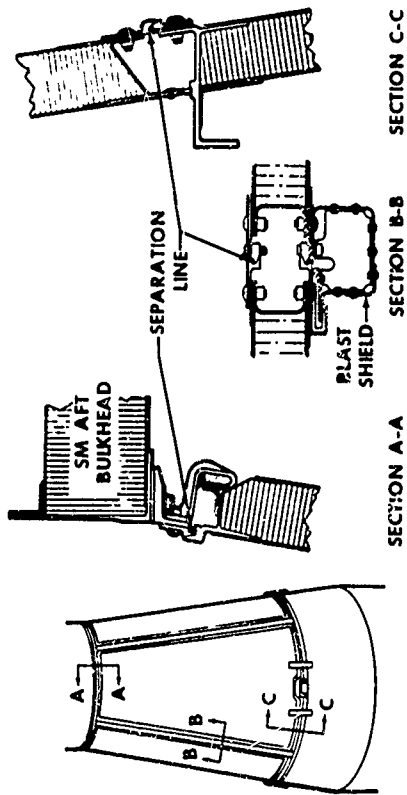


Figure 10(b)

# SEPARATION OF THE SLA PANELS, (CONT)

## EXPLOSIVE TRAINS

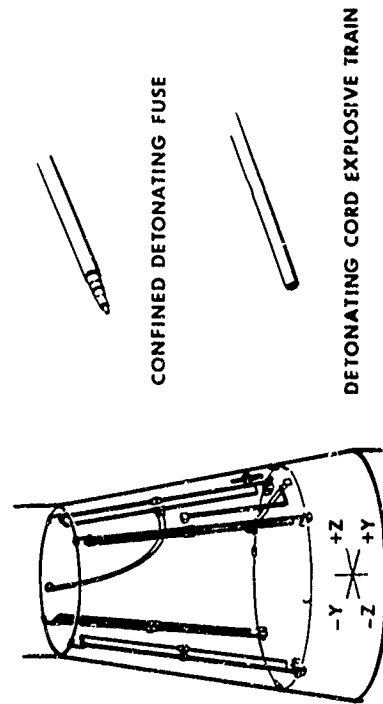


Figure 10(c)

# SEPARATION OF THE SLA PANELS, (CONT)

## ASSOCIATED DEVICES

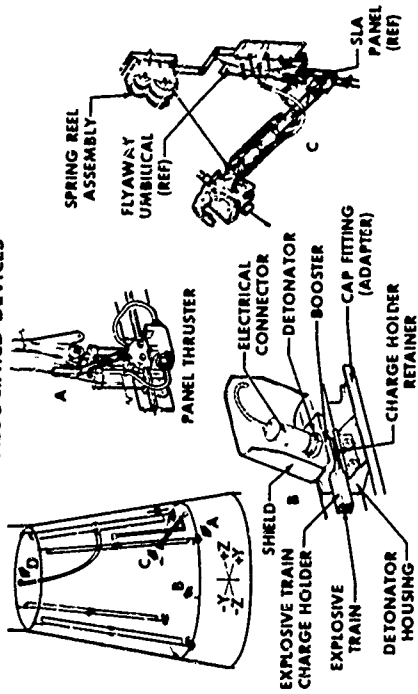


Figure 10(d)

# SEPARATION OF THE SLA PANELS, (CONCL)

## ASSOCIATED DEVICES, (CONCL)

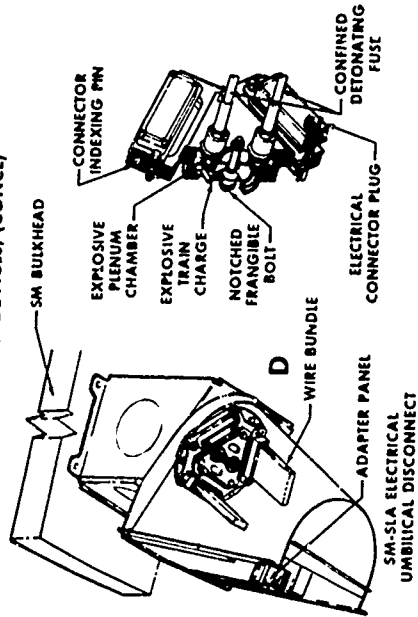


Figure 10(e)

## TRANSPOSITION, DOCKING, AND SPACECRAFT SEPARATION

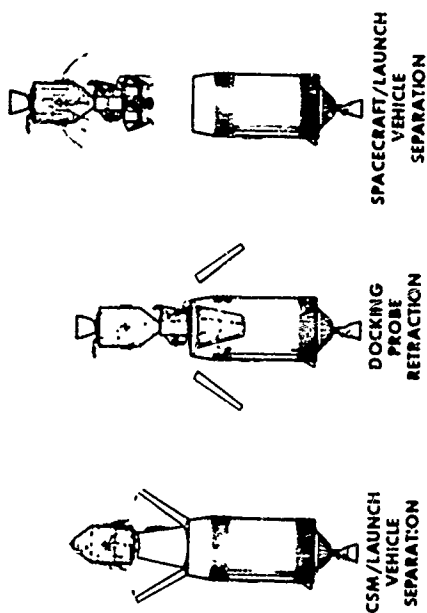
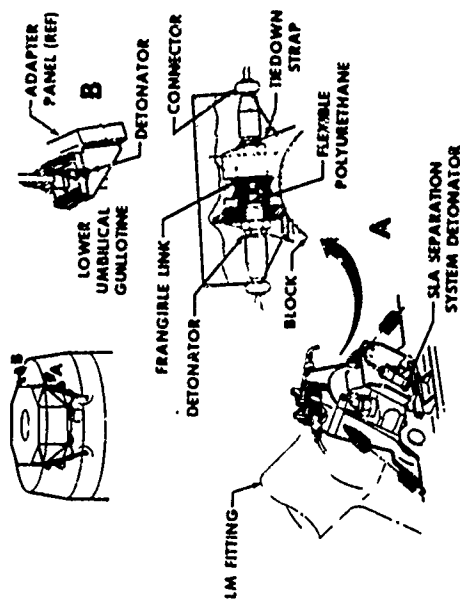


Figure 11

## LM-5LA SEPARATION SYSTEM



**Figure 12**

## LM EXPLOSIVE VALVES

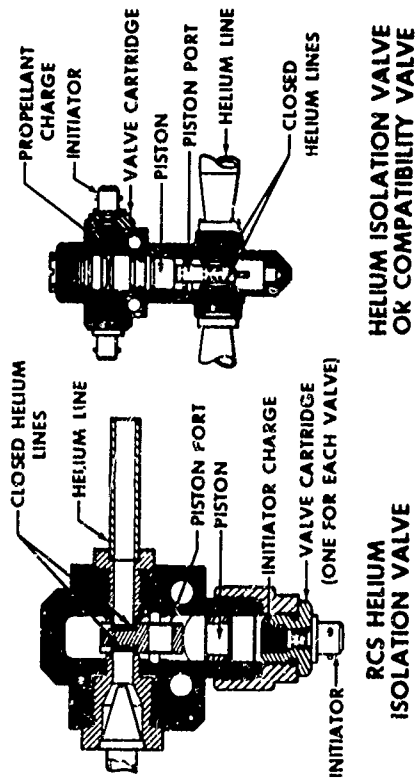


Figure 15

## INTERSTAGE STRUCTURAL CONNECTION NUT AND BOLT ASSEMBLY (LM)

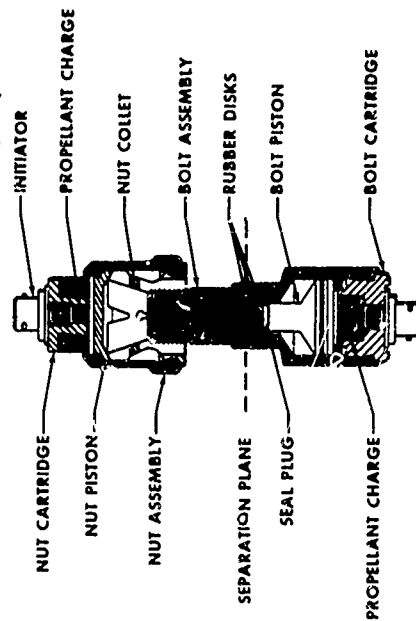


Figure 16

33

## LM ELECTRICAL CIRCUIT INTERRUPTER

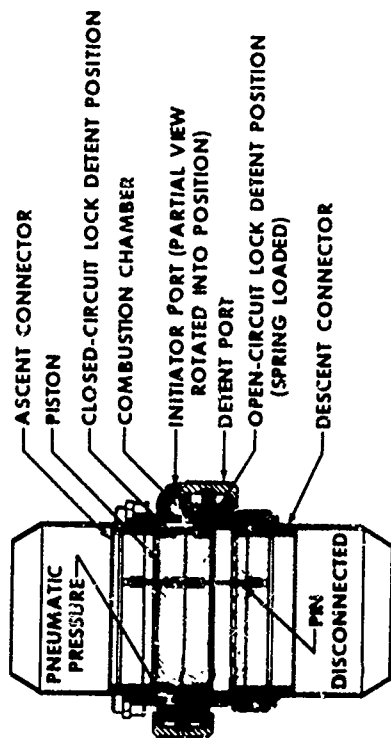


Figure 17

## LM INTERSTAGE GUILLOTINE ASSEMBLY

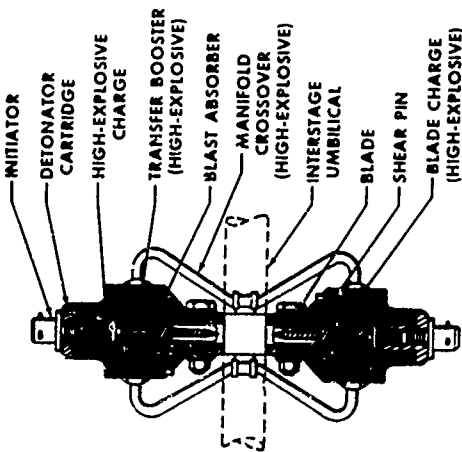


Figure 18

34

# LM JETTISON SYSTEM

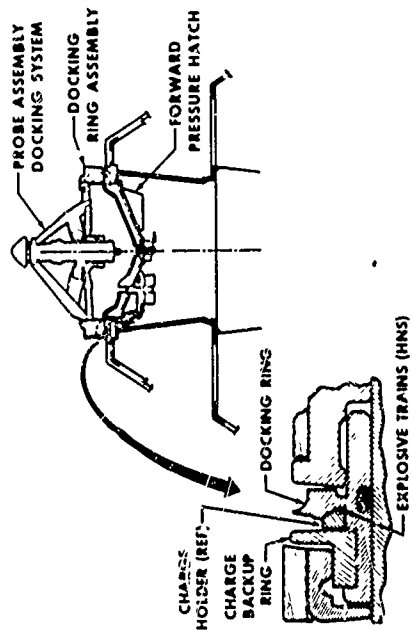


Figure 19

# CM-SM SEPARATION AND SM JETTISON

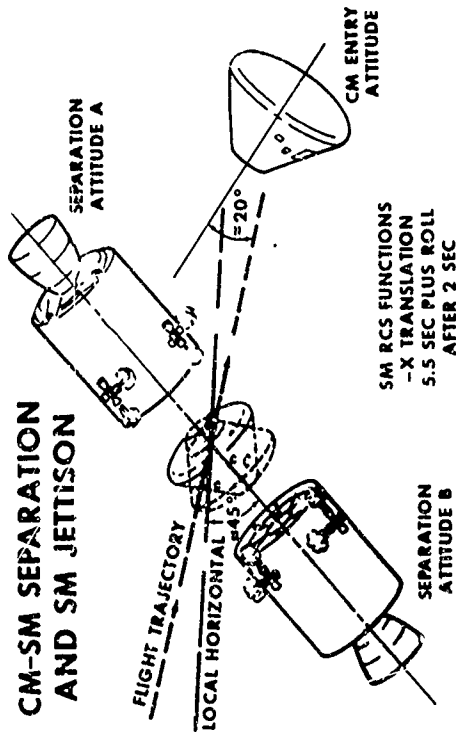


Figure 20

# CSM ELECTRICAL CIRCUIT INTERRUPTER

## COMMAND MODULE

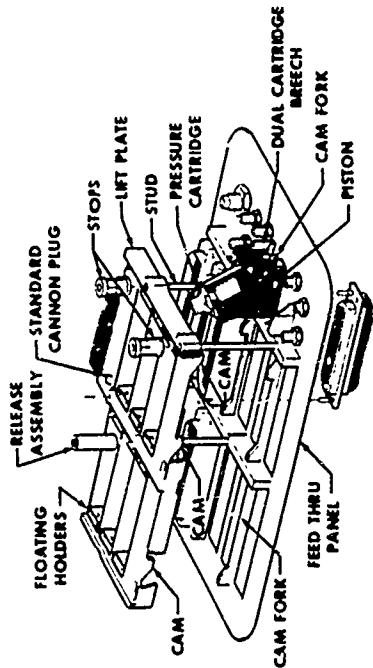


Figure 21(a)

# CSM ELECTRICAL CIRCUIT INTERRUPTER, (CONT)

## SERVICE MODULE

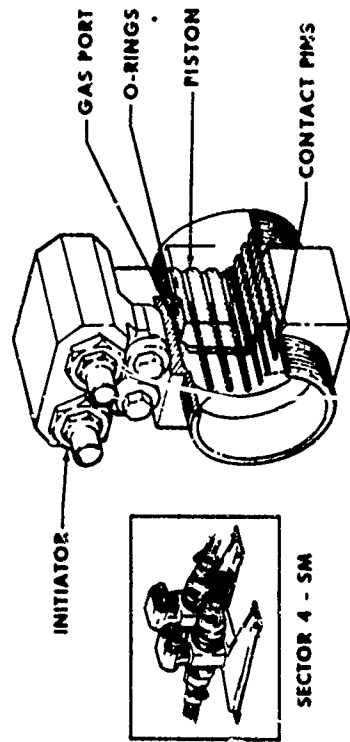


Figure 21(b)

### CM-SM STRUCTURAL SEPARATION SYSTEM

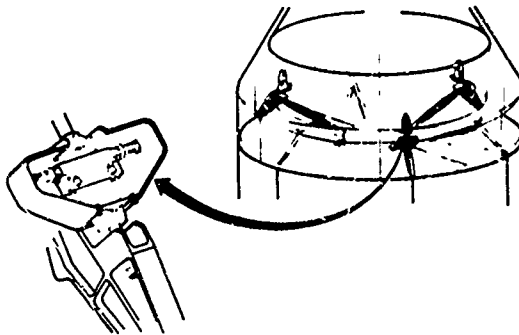


Figure 22(a)

### CM-SM STRUCTURAL SEPARATION SYSTEM, (CONT)

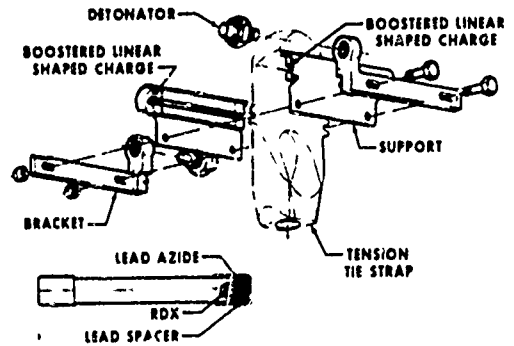


Figure 22(b)

## EARTH LANDING SYSTEM

### NORMAL SEQUENCE

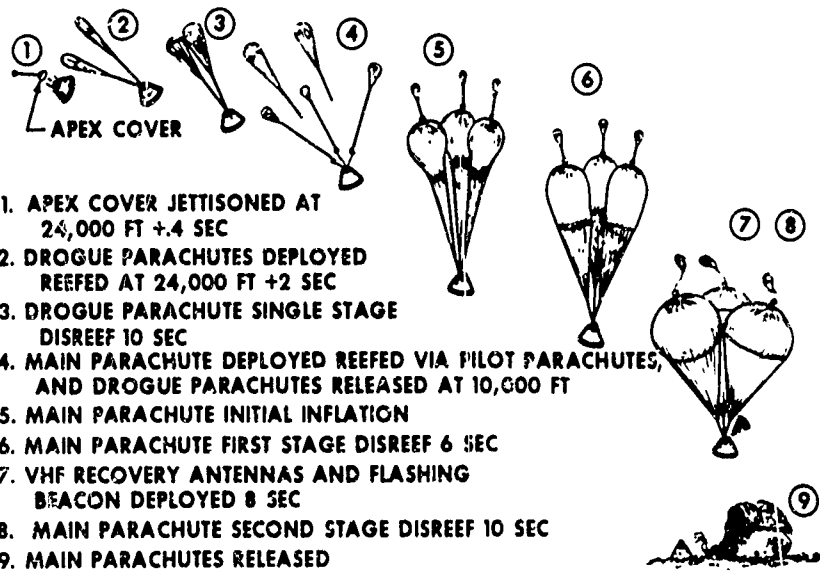


Figure 23

# APEX COVER JETTISON SYSTEM THRUSTER SYSTEM

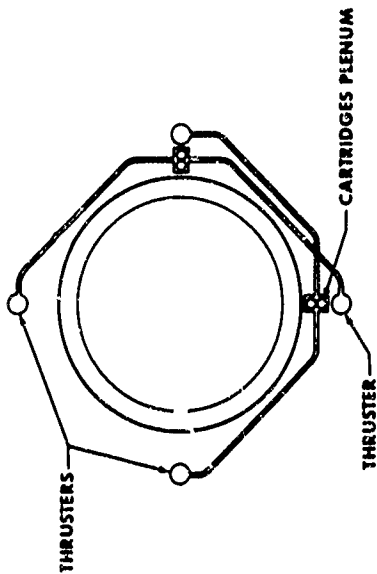


Figure 24(a)

# APEX COVER JETTISON SYSTEM, (CONT) DRAG PARACHUTE MORTAR

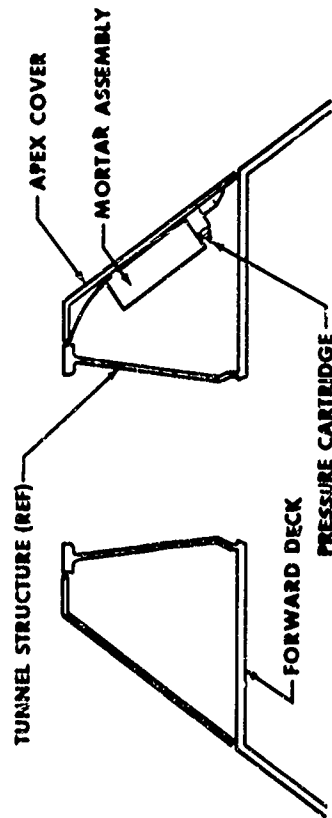


Figure 24(b)

# PARACHUTE MORTAR ASSEMBLIES

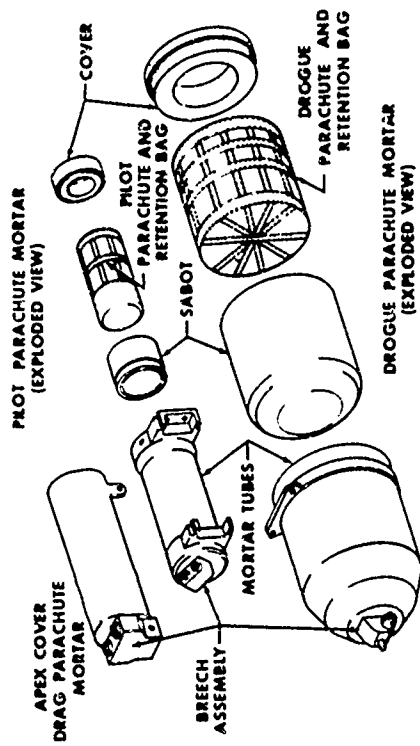


Figure 25

# REEFING LINE CUTTERS (6, 8, AND 10 SECOND)

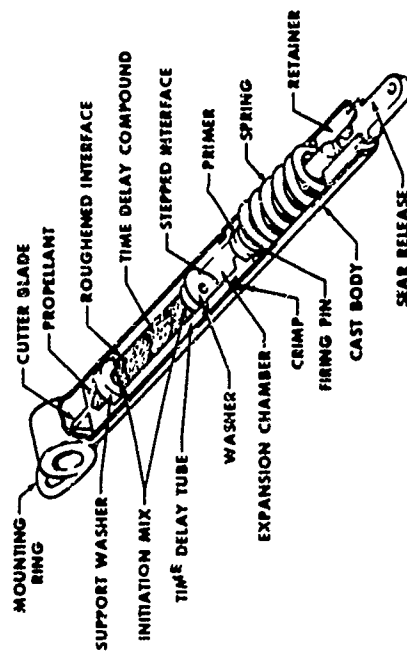


Figure 26

## PARACHUTE DISCONNECT (FLOWER POT)

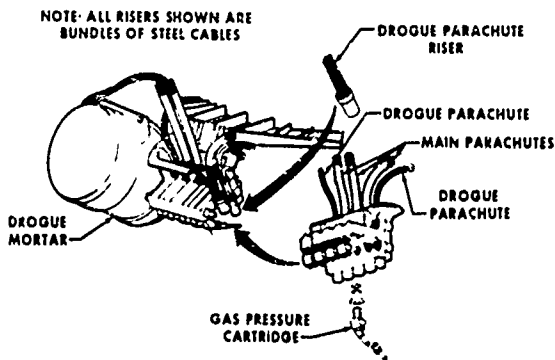


Figure 27(a)

## PARACHUTE DISCONNECT (FLOWER POT), (CONT)

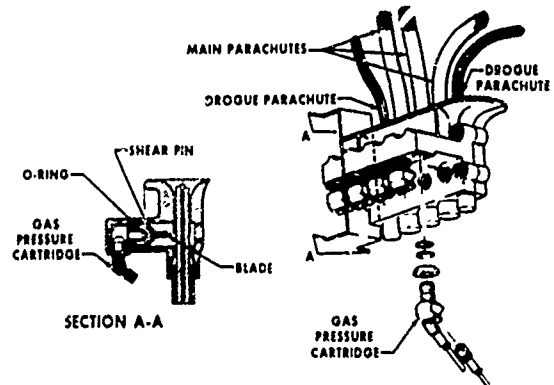


Figure 27(b)

## ABORT PROFILE - PAD TO ~ 30,000 FEET

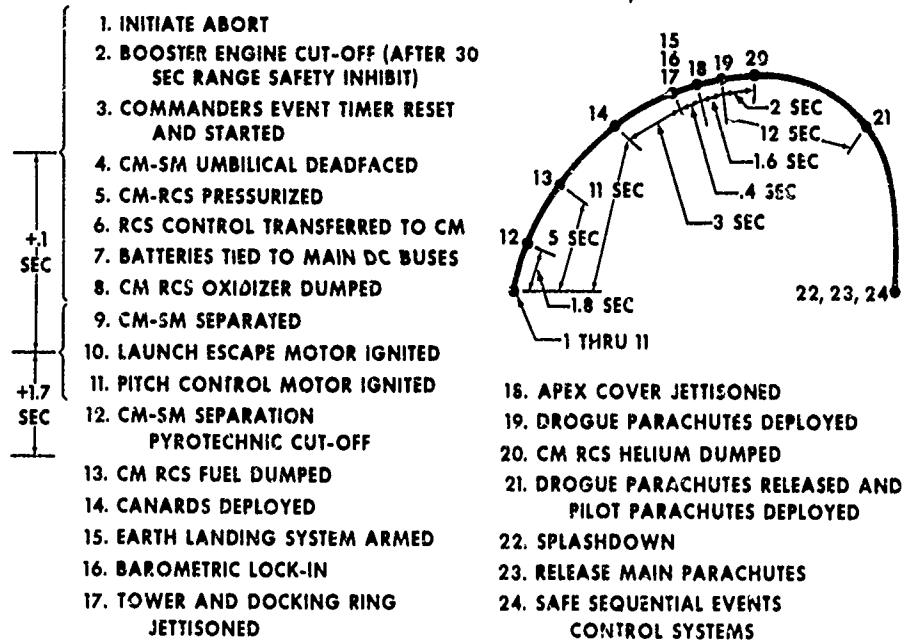


Figure 28

# CANARD DEPLOYMENT SYSTEM CANARD THRUSTER AND MOTOR IGNITER CARTRIDGES

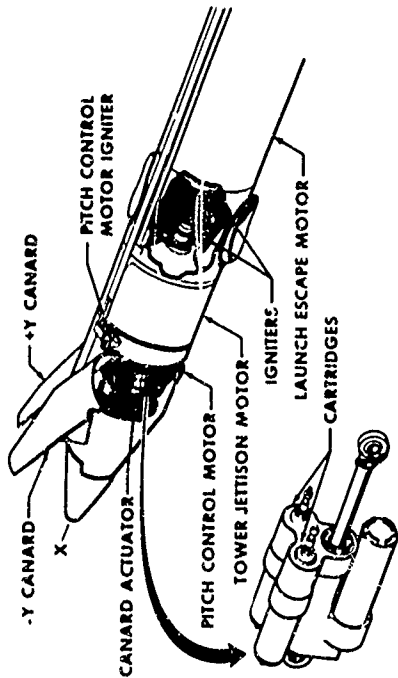


Figure 29(a)

# CANARD DEPLOYMENT SYSTEM, (CONT) CANARD THRUSTER

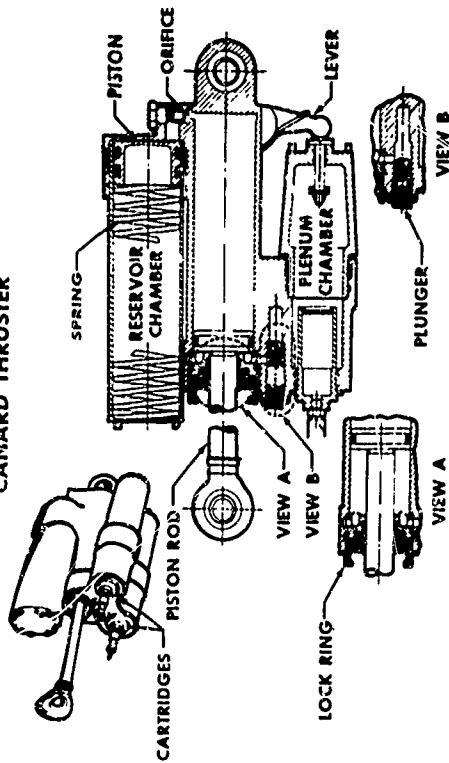


Figure 29(b)

# SPACECRAFT CARTRIDGE FAMILY

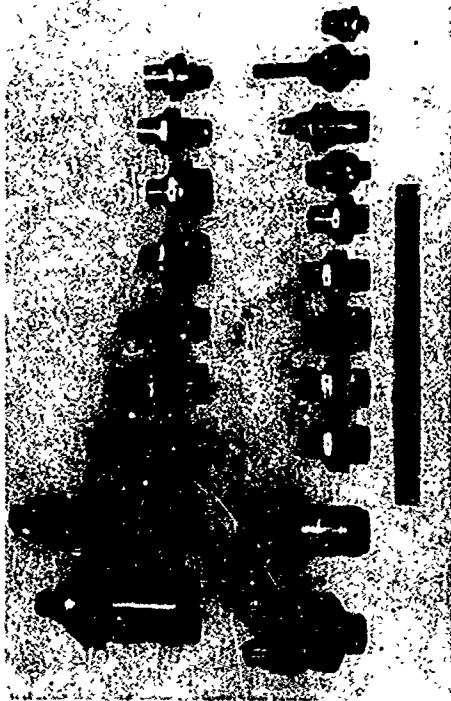


Figure 30

# SINGLE BRIDGEWIRE APOLLO STANDARD INITIATOR - EXPLODED VIEW

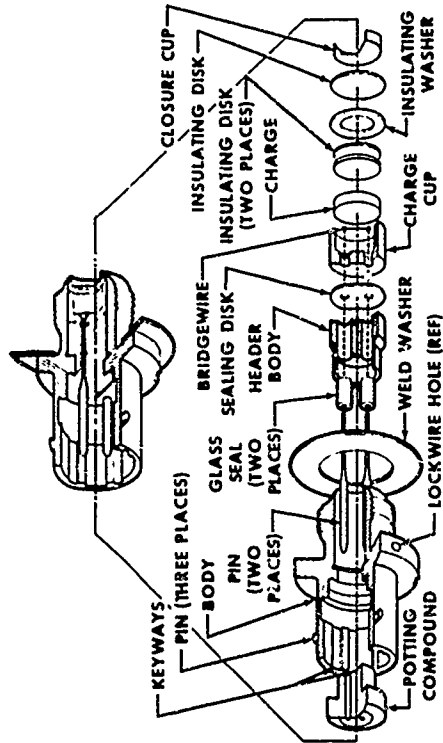
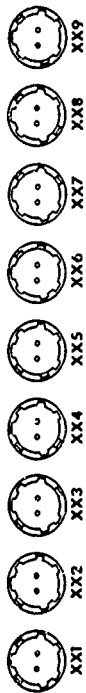


Figure 31



# SBASI INDEXING AND DASH NUMBERING



BASIC PART NUMBER	DASH	DESIGNATION
SE026100001	- 1XX	PROTOTYPE, DEVELOPMENTAL EXPERIMENTAL FLIGHT CONFIGURATION, QUALIFIED OR QUALIFIABLE
	- 2XX	INERT DEVICE
	- 8XX	WELD WASHER ATTACHED
	- XIX	NO WELD WASHER
	- XX0	KEYWAYS 1 AND 6 CLOSED (NONLIGHT FLIGHT)
	- XX1	KEYWAYS 1 AND 6 CLOSED (FLIGHT)
	- XX2	KEYWAYS 1 AND 6 CLOSED (FLIGHT)
	- XX3	KEYWAYS 1 AND 6 CLOSED (FLIGHT)
	- XX4	KEYWAYS 1 AND 6 CLOSED (FLIGHT)
	- XX5	KEYWAYS 1 AND 6 CLOSED (FLIGHT)
	- XX6	KEYWAYS 1 AND 6 CLOSED (FLIGHT)
	- XX7	KEYWAYS 1 AND 6 CLOSED (FLIGHT)
	- XX8	KEYWAYS 1 AND 6 CLOSED (FLIGHT)
	- XX9	KEYWAYS 1 AND 6 CLOSED (FLIGHT)
	- XX0	ALL KEYWAYS OPEN (REQUIRES SPECIFIC MSC AUTHORITY FOR USE)

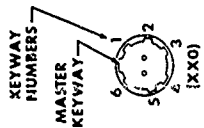


Figure 32

## SINGLE BRIDGEWIRE APOLLO STANDARD INITIATOR

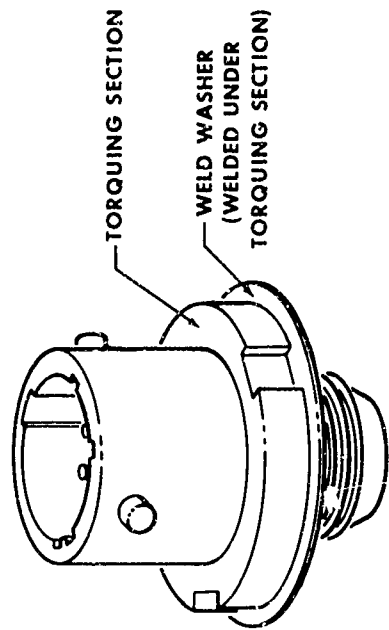


Figure 33

## PARACHUTE DISCONNECT CARTRIDGE INSTALLATION



Figure 34

## PARACHUTE DISCONNECT CARTRIDGES WITH FIRING CIRCUIT CONNECTORS MATED



Figure 35

# PARACHUTE DISCONNECT CARTRIDGE THREADS/SBASI INDEXING

PARACHUTE ELECTRICAL CIRCUIT	XX2 XX3		XX8 XX9		XX8 XX9		XX8 XX9		XX8 XX9		XX2 XX3	
	A	B	A	B	A	B	A	B	A	B	A	B
THREAD	13/16 X 20		1 X 16.		1 X 16		1 X 16		1 X 16		13/16 X 20	
SBASI DASH NUMBER	-252	-253	-258	-259	-258	-259	-258	-259	-258	-259	-252	-253

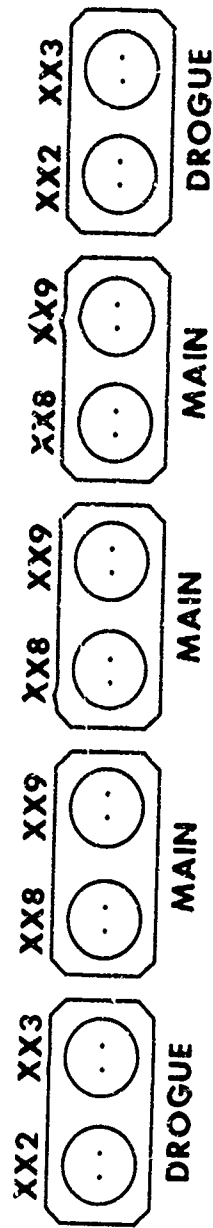


Figure 36

## 1-2 EVOLUTION OF LINEAR SEPARATION SYSTEMS FOR AEROSPACE APPLICATIONS

by

I. B. Gluckman

Lockheed Missiles & Space Company

### ABSTRACT

A presentation is made of the history and evolution of linear separation systems at LMSC, starting with the MDF concept used on the Polaris and Agena, continuing with refinements as used on fairings for the Vela and other government programs, and concluding with the SUPER\*ZIP concept. Systems using Flexible Linear Shaped Charge and ZipCord are also covered. Reasons for design changes and selection, such as shock mitigation and debris containment are discussed. Separation films conclude the presentation.

### INTRODUCTION

Separation of stages in missiles was accomplished until about 1957 almost exclusively through release or severance of mechanical or pyro-mechanical devices which served as attachment points between stages, and were located around the circumference of the separation plane. The devices used were explosive bolts, explosive or release nuts, pin-pullers, ball-lock systems, Marmon-type clamps, and other similar designs.

These multi-point attachment and separation designs have been very successful and are still being used in some applications. Towards the end of the last decade, however, this concept began sharing the spotlight with a different approach, that of the Stressed Skin or Linear Separation System which offered distinct advantages for some applications. The new approach consisted of a length of detonating cord installed around the circumference of a specially designed continuous joint on the airframe skin, which was an integral and functional part of the structure. Separation was by cutting or fracturing the skin. Various systems were developed: MDF (Mild Detonating Fuse) or MDC (Mild Detonating Cord), Flexible Linear Shaped Charge, and more recently, LMSC Zipcord and SUPER\*ZIP. This paper covers some of the highlights in the evolution of these systems over a little more than a decade.

#### ADVANTAGES AND DISADVANTAGES OF LINEAR SEPARATION SYSTEMS

Considerations leading to introduction of the Linear Separation concept were primarily reliability and simultaneity. By-products were weight reduction and lower cost.

The Reliability Model for a multi-point attachment system is a series arrangement requiring successful operation of three or more independent units, each unit most likely using redundant initiators. Failure of either unit can result in a catastrophic failure. On the other hand, the Reliability Model for a linear separation system is a single primary device, usually initiated by redundant initiators. This analysis is obviously an over-simplification; nevertheless, it illustrates the basic difference (and advantage) in concept reliability and the favorable simplicity of the linear separation system.

Instantaneous separation is an important factor in staging or fairing separation, especially in large and complex vehicles, as angular movements must be limited to prevent misalignment and possible mechanical interference during separation. Such performance requires simultaneity of separation between the various attachment points. In a multi-point attachment system using three or more independent units, the degree of simultaneity is dependent on the functioning time dispersion between the various units. The dispersion can normally be reduced by augmenting the current to the EED's, substantially above the all-fire current. There are limits, however, to current availability. Another method for dispersion reduction is selection of faster acting EED's and mechanical devices. Even under the best practical conditions of electric current supply and EED selection, a dispersion as low as that achieved with a linear separation system cannot be assured. For example, a dispersion of up to 6 msec is a practical design criterion for a multi-point system. On the other hand, a total mechanical separation time of less than 1 msec is automatically achieved in a 5 ft. diameter linear separation joint by virtue of continuity of the single charge and high velocity of detonation (approx. 6500 meters/sec or higher). The simultaneity consideration, therefore, also favors a linear separation system.

Weight reductions of the joint of approximately 50 percent and more were achieved in changing to linear systems by simplification of the structural design. Such simplification also resulted in cost savings.

On the other hand, it is recognized that the earlier linear separation systems using unconfined detonating cord generated debris and that the shock levels were sometimes higher than with a multi-attachment system. These disadvantages were later overcome or reduced by advance designs to be discussed below.

This paper does not intend to discredit the multi-point attachment systems, some of which are still being used successfully. As with any other equipment, trade-off studies in depth are always necessary in order to select the proper system for the specific application.

### MILD DETONATING FUSE (MDF)

At Lockheed, the Polaris missile was the first major project to utilize the linear concept for separating the first stage from the second. A frangible joint was designed around 1957, using magnesium-thorium alloy because of its light-weight qualities and excellent brittleness. The joint (shown conceptually in Figure 1) used round detonating cord, with lead-jacketed explosive core of 10 grains per foot. The explosive was originally PETN, then RDX, and several years later, HMX (9 grain core). The cord was covered with a 10 mil layer of polyethylene for waterproofing and lubrication to facilitate installation. In those days, use of such a small core-load was considered rather daring; it appeared that way to most designers who were used to the typical 100 grain Corps of Engineers detonating cord. Nevertheless, based on manufacturer's representations and test results which indicated high reliability with core loads of 10 grains and less, a decision was made to proceed with a system based on a cord of this size. These cords were identified then as "Low Energy Detonating Cord" (LEDC), and later as "Mild Detonating Fuse" (MDF) or "Mild Detonating Cord" (MDC). The major suppliers were Ensign Bickford, Dupont, and later, Explosive Technology.

The separation of the Polaris joint was effected by detonation of the cord which induced a shock impulse, fracturing the center notch of the skin and forcing it outward; the separated segments hinged around the two external notches which also fractured.

The internal design of the joint was such that the products of combustion and lead debris were forced outward with only a relatively small amount moving inward.

The explosive system (Figure 2) consisted of a circumferential strand of cord as discussed above, with the two ends initiated by two EED's, each with an auxiliary explosive lead and booster charge. Originally, a conventional type safe and arm device was used. This device was later eliminated although the same in-line fuze train design was retained until the advent of EBW. The initiation of the cord was end-on. The system's reliability analysis indicated that two failures were required for separation failure; e.g., any two of the following: defective EED(s), non-transfer(s) between donor and acceptor, or interruption(s) in the cord.

As a result of highly successful use on the Polaris, the Agena, which had previously used explosive bolts and pinpullers for separation from the booster, adopted the 10-grain RDX MDF system in 1961, with the exception of the initiation system. The initiation was end-on directly from two 100 milligram RDX detonators in lieu of the fuze train as initially used in the Polaris. The two detonators were "potted" in an aluminum block with a common electrical connector. This block was assembled on the vehicle to another block which secured the ends of the MDF, so as to align these ends with the detonators. This system has been used successfully in more than 250 Agena flights, including the Gemini missions involving the Agena rendezvous.

#### FLEXIBLE LINEAR SHAPED CHARGE

About 1962, the increase in size of nose fairings for space vehicles required a more effective and faster separation than the axial translation (over the nose) heretofore used which was accomplished by a single plane severance at the base only, resulting in long

periods of deployment of the separated structure. Penalties in overall system performance of larger fairings suggested a clamshell design, separating at the base and also longitudinally with sections hinging away from the vehicle. This resulted in less overall time for jettisoning and avoidance of mechanical interference problems.

The first program at Lockheed to consider the clamshell were the Vela and several NASA projects. As there was constantly a desire to reduce both shock and contamination, especially in the proximity of sensitive optical equipment, it was felt that this could be achieved by using a flexible linear-shaped charge (FLSC) of lesser cord load. Several designs were generated using 5-grain and 7-grain per foot shaped charge cord. In spite of successful beginnings, subsequent failures in propagation during full system test indicated that additional development of system and/or product was necessary. Tight schedules did not allow such development and a decision was made to abandon this approach in favor of the well-proven 10-grain round cord (MDF). Based on published reports by various companies in the fields, it appears that the problems with this low core load linear shaped charge have since been resolved. There has been no occasion to re-introduce this product (in low core loads) in LMSC separation applications. However, a strap cutter used for separation, consisting of a 40-grain per foot RDX linear shaped charge, approximately 4 inches long, was developed and flown successfully.

#### FAIRING SEPARATION SYSTEMS USING MDF

Several clamshell design fairing programs have incorporated an MDF system. A typical design is shown in Figure 3. Both the circumferential joint and the two vertical joints contain 10-grain MDF, the frangible section design being very similar to that previously shown for the Agena and Polaris staging.



The method of initiation was changed through a two-step evolution. The first step was to use a detonator block on each side of the fairing at its base. Each block (Figure 4) contained one terminal of each of the two semi-circular sections of the circumferential joint and the lower terminal of one vertical section; the terminals were capped with lead azide loaded booster relays. Two detonators (100 milligram RDX each) were used in each block for side initiation of the relays. The upper ends of the two vertical legs used shaped bottom detonators (170 milligrams each), for side initiation of the cord. This system was successfully flown several years ago.

More recently, however, with the advent of more effective detonators, another step was taken towards simplification by eliminating the booster relays and adopting direct side initiation of the cord exclusively (Figure 5). This proved a highly reliable method and is being used in several five foot and ten foot diameter fairing joints.

A program using a ten foot diameter fairing instituted a requirement for full redundancy of separation systems, and the resulting design looked as shown in Figure 6. In this case, two parallel, separate, and independent 5-grain HMX cords are routed in a continuous loop along the length and top of the fairing, all ends being initiated at the bottom. Otherwise, the joint is similar to the mag-thorium joint previously discussed.

This same fairing also incorporates another type of frangible joint circumferentially around its base. The circumferential joint (Figure 7) is made of beryllium panels, backed by an aluminum extrusion. Two detonating cords are used, these being 2-1/2 grain RDX cord. This core load was found to be more than adequate as satisfactory fracture was obtained with core loads as low as 1-grain per foot. The same circumferential separation joint is also used for booster separation and was selected for reasons of weight and anticipated shock reduction.

## DETONATOR DEVELOPMENT

As part of these programs, several EBW and conventional detonators were developed to meet desired characteristics. EBW development being a special subject in itself, peculiar to the Polaris, will not be covered in this paper.

The construction of the conventional detonators is of the two-pin connector type, in stainless steel bodies for screw-in to the next assembly. The output charges are 100 to 110 milligrams of RDX with a high L/D ratio and heavy peripheral confinement. Both .5 amp no-fire and 1 amp - 1 watt no-fire versions are available. A typical detonator is shown in Figure 8.

These detonators have proven quite reliable in side-initiating MDF (2-1/2 and 10-grain RDX, 5 and 9-grain HMX) at air gaps from zero to .3 inch and more. Bruceton testing was conducted but was found to be unrealistic as the  $\bar{X}$  in several cases that were tried, was considerably above the maximum design gap. It was felt that intensive testing within the configuration design limits but with slight exaggeration would be more meaningful than a Bruceton. Additional tests were conducted with off-loaded detonators to further strengthen the confidence in the reliability of transfer.

An interesting problem that was investigated also in connection with transfer was the question as to whether partial disintegration of a detonator during its functioning had any effect on the integrity and proper initiation of the cord. This question was raised in view of the fact that a sleeve containing the explosive was observed to be ejected from the detonator during functioning and it wasn't known definitely whether this event occurred prior or subsequent to initiation of the detonator *base* charge and MDF. Flash X-ray techniques at LMSC's Santa Cruz Base were used for this investigation.

The procedure was to mount the detonators in aluminum blocks on a steel plate. A section of 10-grain/ft. MDF was placed under the detonator and taped to the steel plate. Several initiation tests were conducted and radiographs were taken during each event to determine location of the base charge sleeve at various times following detonation. Oscilloscope photographs were used to verify the delay time of the radiographs. Two of these radiographs after 12  $\mu$ sec and 120  $\mu$ sec respectively, are shown on Figure 9. It is evident that full initiation of the MDF occurred long before ejection of the sleeve, thus allaying any concern in this regard. As a matter of fact, based on intermediate radiographs, the detonator sleeve did not leave at all prior to 31  $\mu$ sec, during which time the MDF detonation progressed approximately 8 inches.

#### ZIPCORD

Parallel to the developments discussed heretofore, which were prompted by urgent operational needs and thus did not allow for long lead times, other developments were taking place mostly on company-sponsored programs, and resulted in systems known as Zipcord and SUPER\*ZIP.

The two basic drawbacks of unconfined detonating cord were shock and contamination. The magnitude and relative effect of these parameters varied depending on design and circumstances. Many applications could tolerate such a situation. Some applications could not. In an effort to avoid potential problems, steps were sometimes taken to relocate shock-sensitive equipment, or to provide protection by installing a protective gas shield behind the frangible joint (Figure 10). These perennial concerns suggested about eight years ago a design concept which encapsulated the detonating cord initially in a flat metal tube and, subsequently, for reasons of flexibility and weight reduction,

in a polymer tube. The concept, called "ZIP" or "Zipcord"<sup>1</sup>, can be described as follows (Figures 11 and 12): The detonating cord functions in its normal manner. The shock waves and sudden gas evolution and pressure rise cause the outer metal or polymer jacket to expand thus performing work which, in this case, consists of fracturing a frangible joint. After functioning, the integrity of the polymer jacket remains intact, thus all products of combustion are contained. The rate of transfer (and amount) of energy from the cord to the airframe is also attenuated by the work done on the jacket. Further attenuation is obtained through symmetrical design of separation joint, which provides opposing and thus cancelling shock forces. A nonsymmetrical design is shown in Figure 13. Figure 14 shows two strips of movie film, one of a joint separated by a conventional unconfined cord (FLSC), the other by Zipcord. The elimination of debris and gas ejection is obvious. This development work was conducted over a period of several years and lead to systems which were flown successfully in several DOD programs.

#### SUPER\*ZIP

The ZIP design with the polymer jacket had some limitations at high temperatures, i. e. , maintaining the integrity of the jacket when functioned at temperatures in excess of 200°F. In early 1968 another company-funded effort to eliminate this limitation was initiated. Parametric studies coupled with an extensive test program yielded an improved design, named "SUPER\*ZIP". The final design attempted to incorporate as many of the more desirable features of the previous concepts. A cross-section of a joint incorporating "SUPER\*ZIP" is shown in Figure 15. It consists of a symmetrical

---

<sup>1</sup>LMSC PATENT 3373686 "Explosive Actuator"

frangible joint which contains the SUPER\*ZIP assembly, a flattened stainless steel tube with an inner polymer matrix which, in turn, contains two 9-grain HMX MDF cords. Either cord can provide sufficient energy to expand the polymer matrix, round the steel tube and fracture the notched plates on both sides. The second cord, which is incorporated for redundancy, is not affected by the functioning of the first cord and is thus available as a backup, if needed.

A sealed detonator block was also designed to contain all gases. The initiation is with two detonators on the side of the cord, in the manner previously described.

Tests conducted with this assembly at temperatures up to 350°F, were successful with complete containment of gases.

Several successful demonstration tests of the SUPER\*ZIP separation system were conducted using a full scale fairing five foot in diameter and fifteen feet long. A short movie showing such a test (and for comparison an MDF test) will be shown at the end of this presentation.

At present, the system is being incorporated for both longitudinal and circumferential joints in a fairing ten foot in diameter by sixty feet long for an Air Force Program. Due to modular design and weight comparability, this system is readily adaptable to other similar applications.

Shock reductions of approximately three to one can be expected by substituting the SUPER\*ZIP for a conventional detonating cord system (Figure 16). The maximum peak acceleration response was reduced from approximately 275 g's for conventional one cord system to less than 100 g's for SUPER\*ZIP. Both were used on the identical fifteen foot long fairing.

## CONCLUSION

The process of evolution of linear separation systems at LMSC has taken us from the conventional one cord MDF detonating harness as first used twelve years ago (Figure 17) to the two cord MDF system, to the Zipcord, and finally to the SUPER\*ZIP system, which offers significant advantages in shock reduction, gas and debris containment, and high reliability through redundancy. The SUPER\*ZIP system is currently being introduced in a major Air Force program and is being considered for several others, both DOD and NASA. Several fairings using the systems discussed above are shown in Figure 18. In addition other applications are seriously being considered, such as canopy ejections on aircraft.

## MDF (SINGLE SYSTEM)

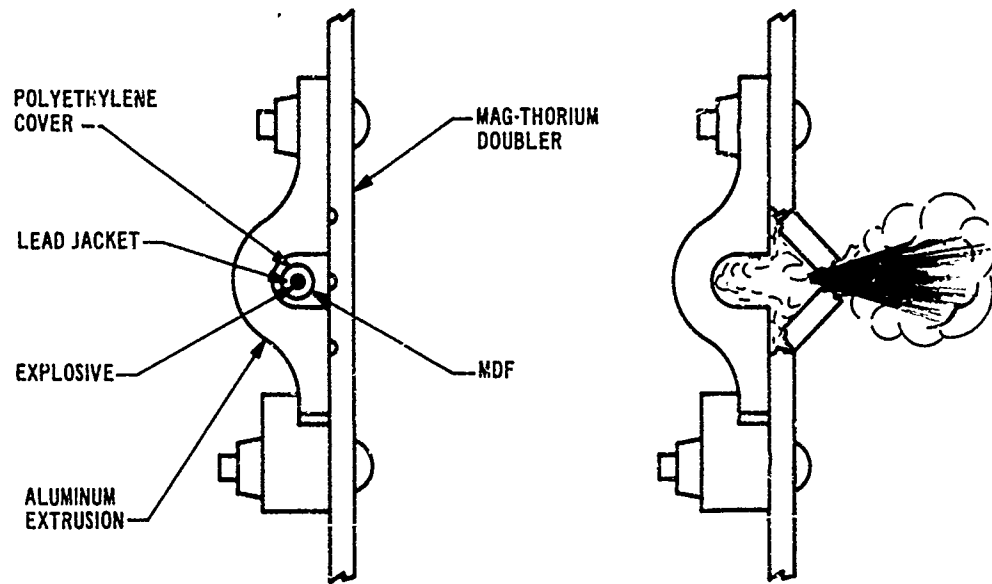


Fig. 1

## MDF EXPLOSIVE SYSTEM

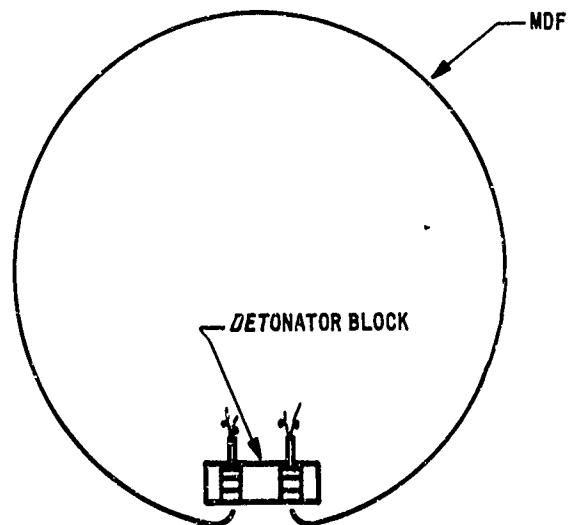


Fig. 2

## FAIRING PYRO SEPARATION SYSTEM

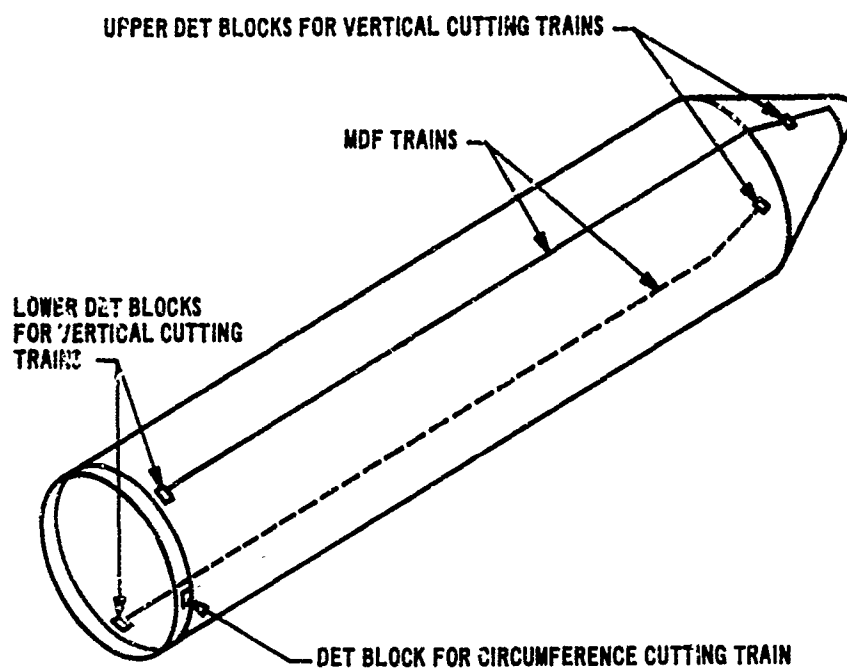


Fig. 3

## VELA FAIRING DETONATOR BLOCK

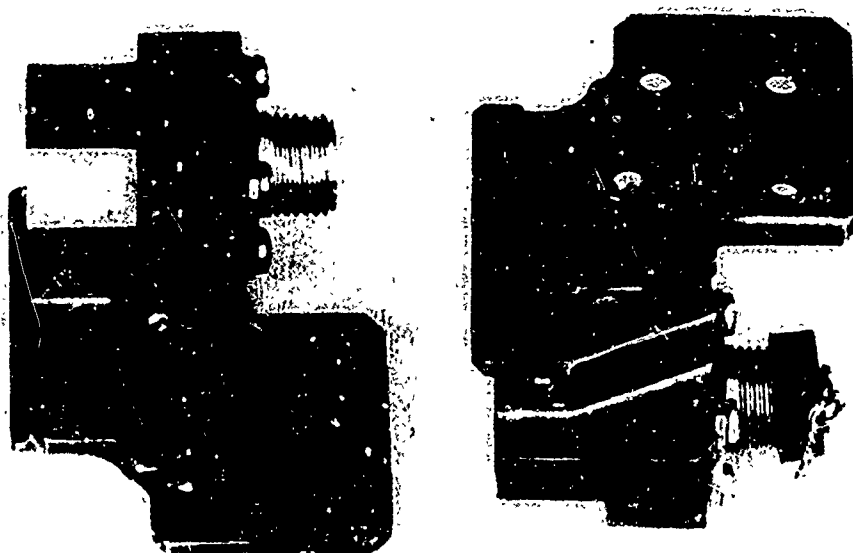


Fig. 4



## FAIRING EXPLOSIVE TRAIN CONFIGURATION

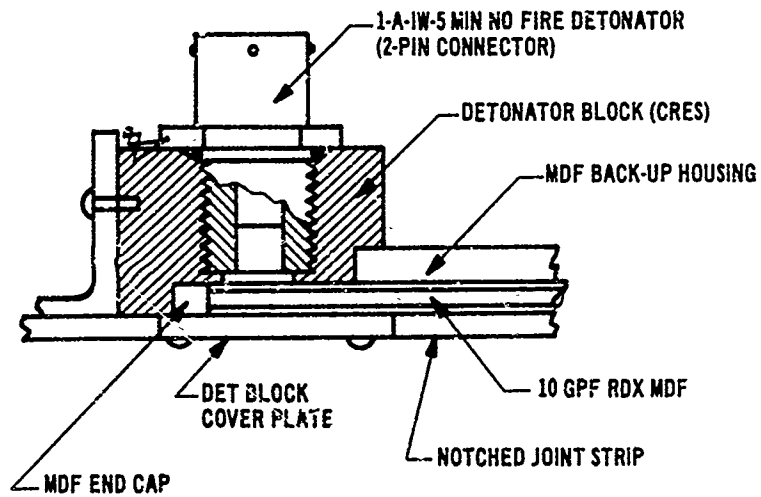


Fig. 5

## MDF REDUNDANT SYSTEM

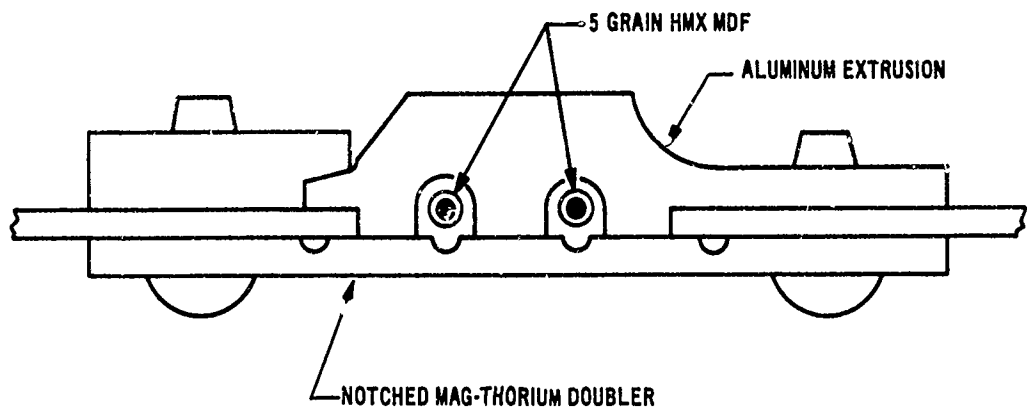


Fig. 6

## BERYLLIUM JOINT

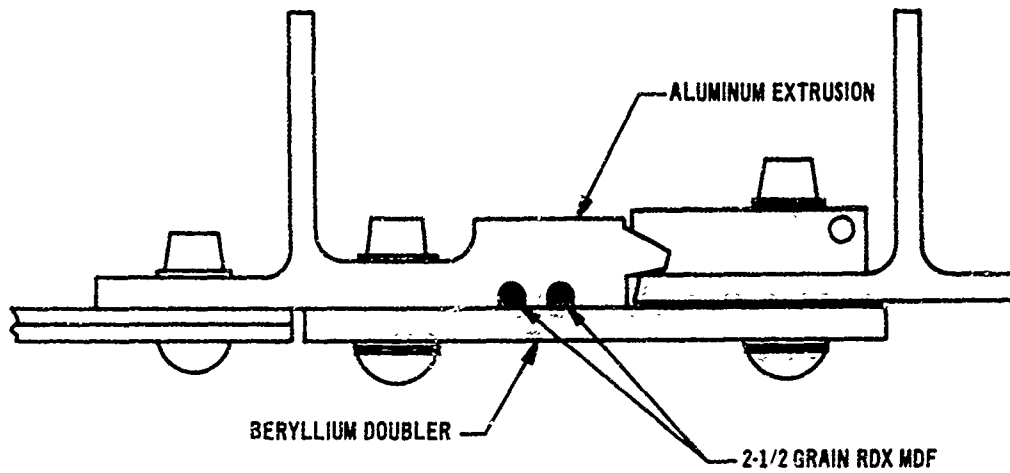


Fig. 7

## DETONATOR

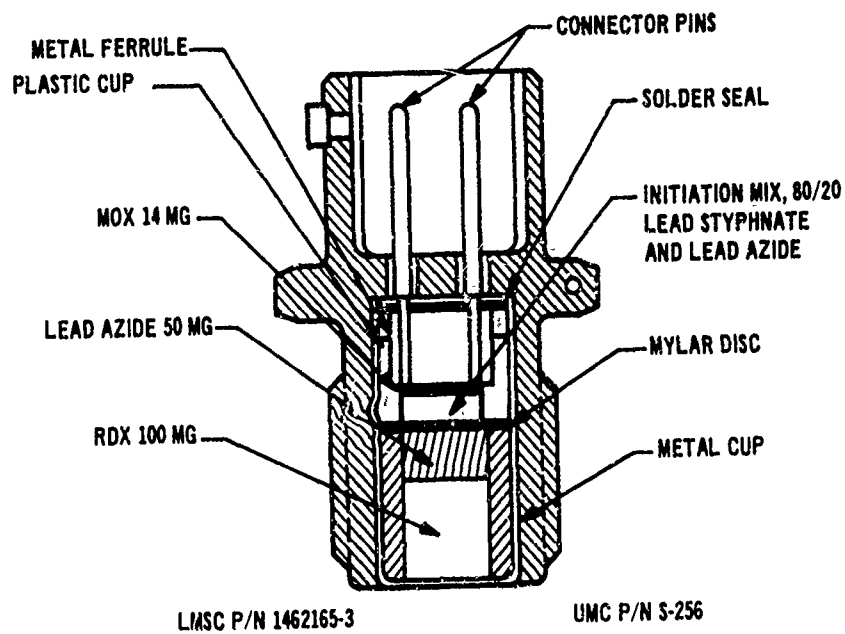


Fig. 8

# FLASH X-RAYS OF MDF INITIATION

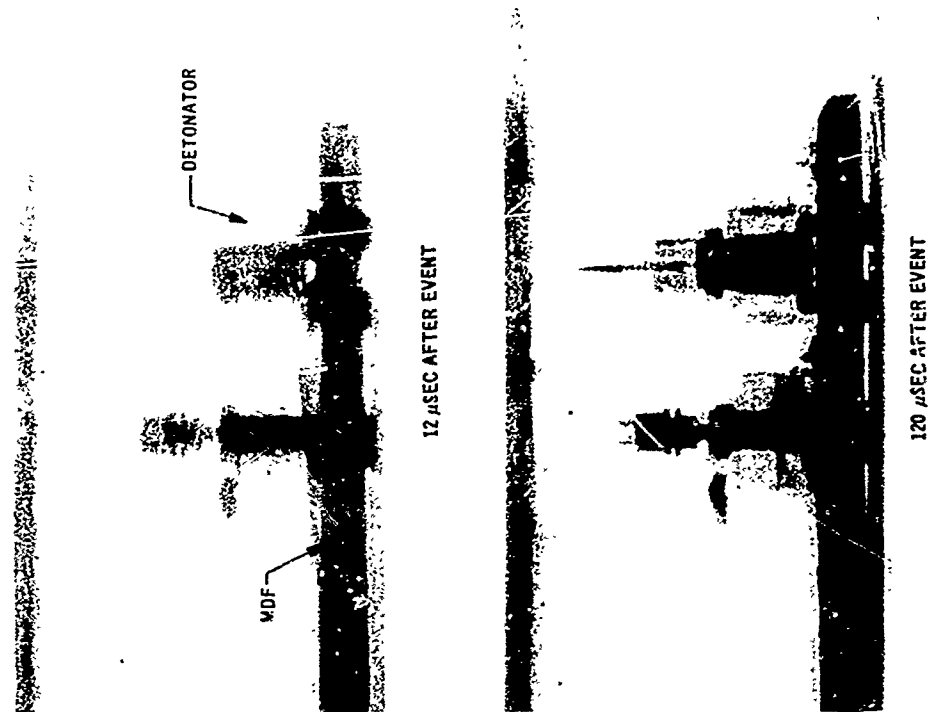


Fig. 9

## VERTICAL JOINT DETAILS TYPICAL BARREL JOINT

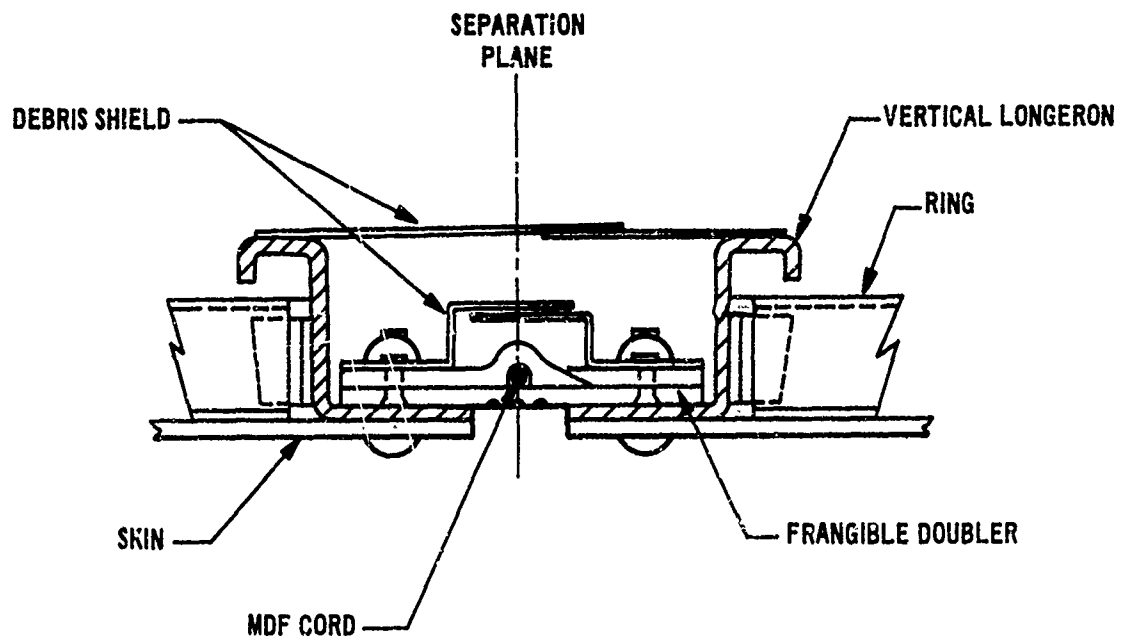


Fig. 10

## SYMMETRICAL ZIP JOINT

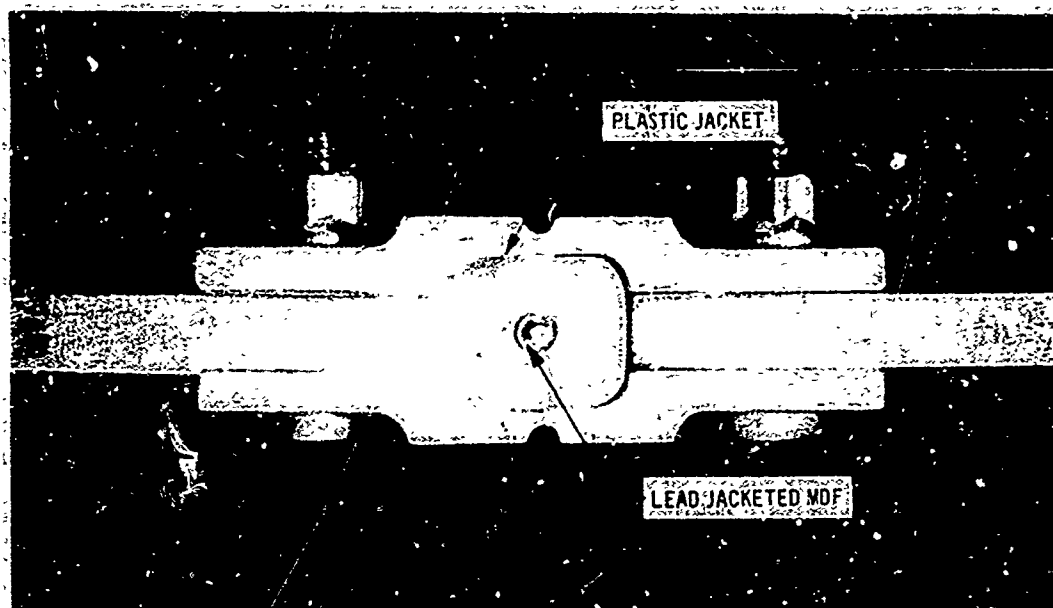


Fig. 11

## SYMMETRICAL ZIP JOINT, POST-FIRE

ZIPCORD REMOVED

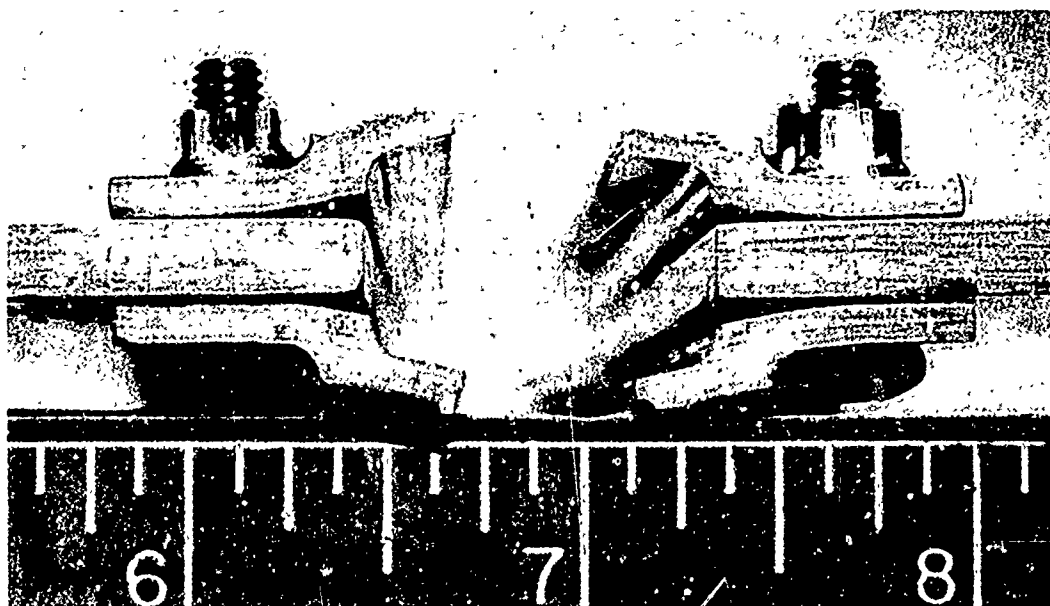


Fig. 12

1-2.18

# NONSYMMETRICAL ZIP JOINT, POST-FIRE

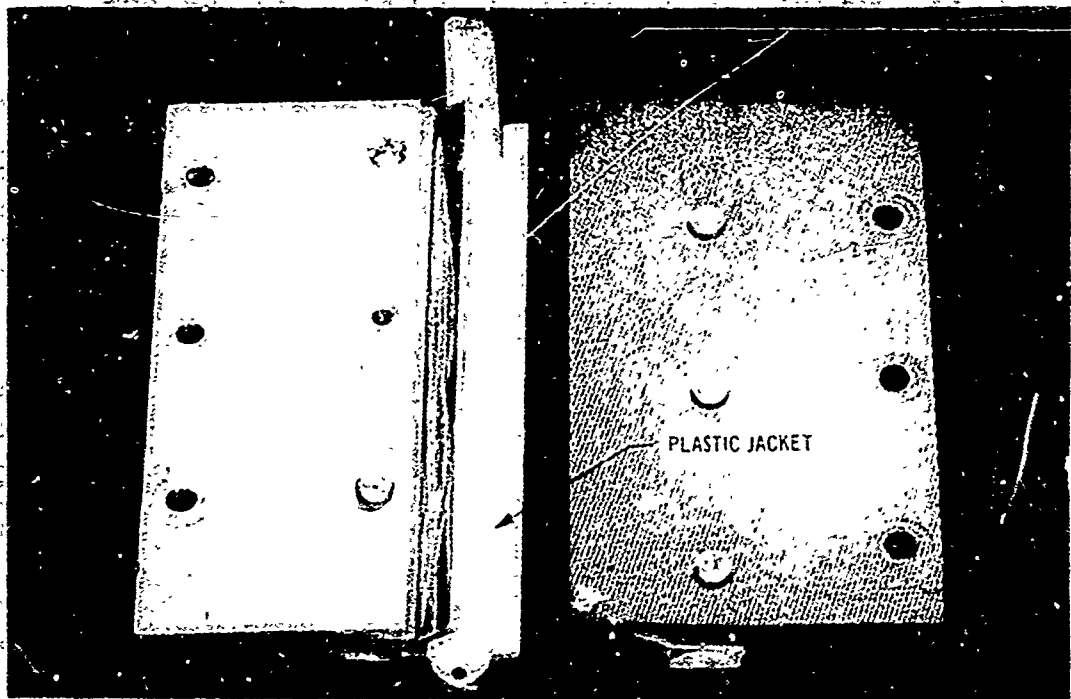


Fig. 13

## COMPARISON OF ZIPCORD TO CONVENTIONAL EXPLOSIVE SEPARATION SYSTEM



Fig. 14

## SUPER • ZIP

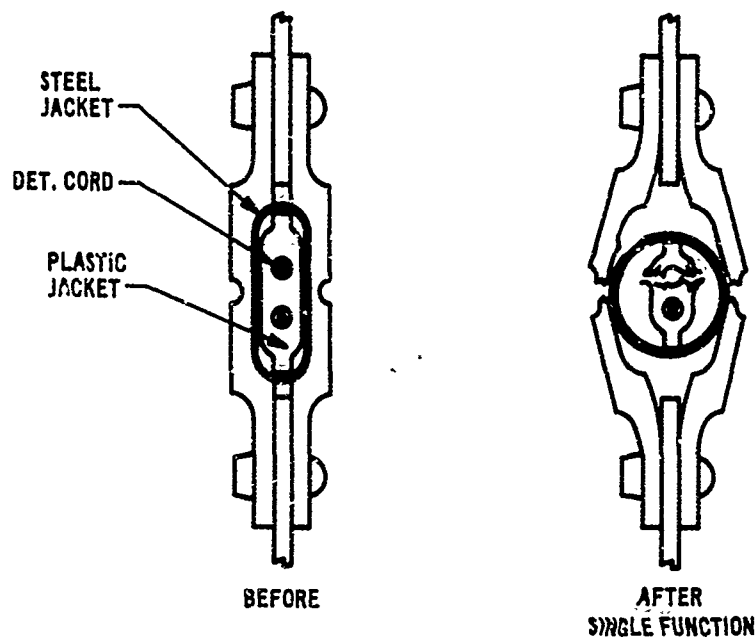


Fig. 15

## SHOCK COMPARISON

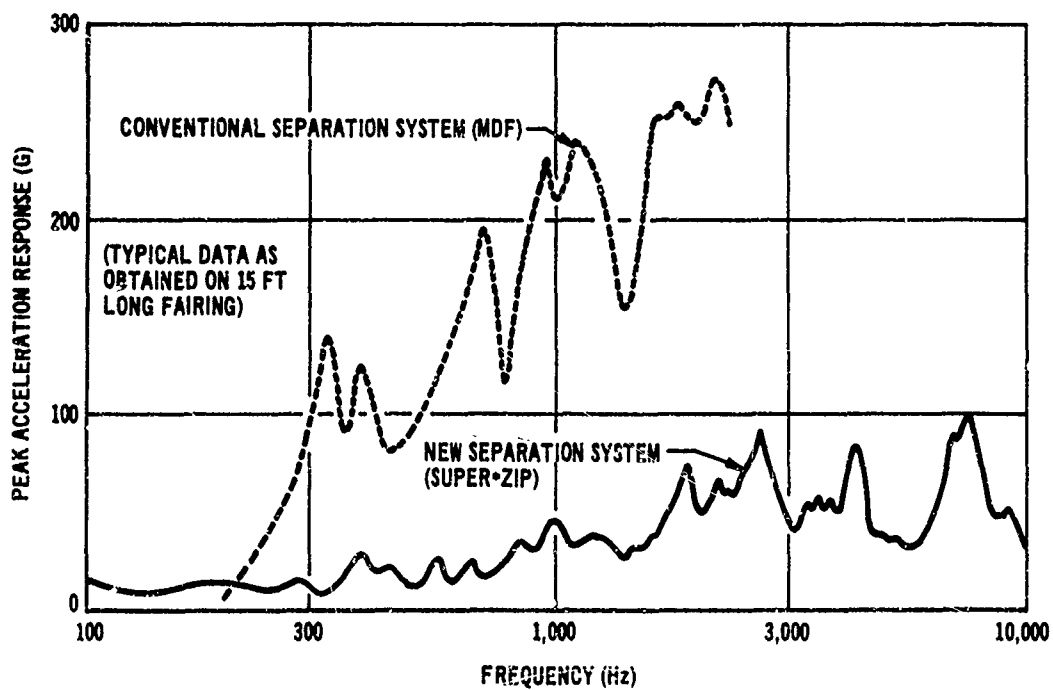


Fig. 16

## EVOLUTION OF LINEAR SEPARATION JOINTS

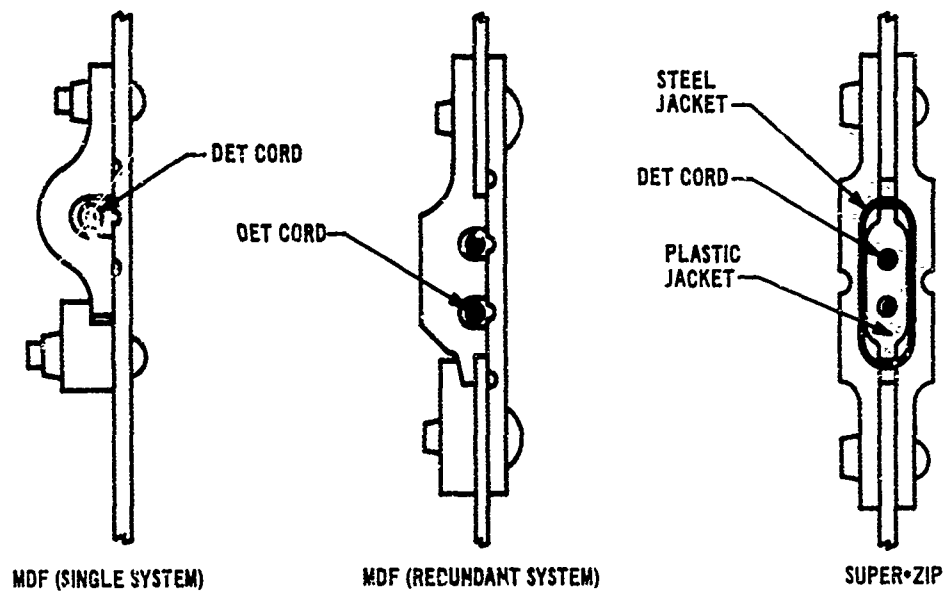


Fig. 17

## CLAMSHELL FAIRINGS

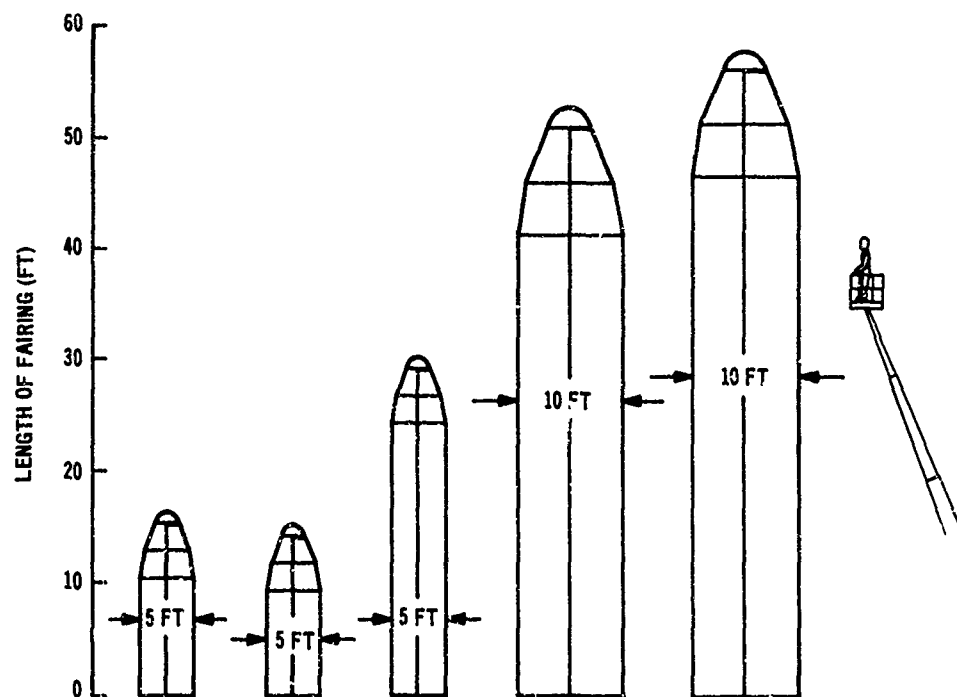


Fig. 18

1-3 A VISUAL MARKER SYSTEM  
FOR A MISSILE

P. K. Salzman

General Dynamics Pomona Division  
Pomona, California

INTRODUCTION

It is often desirable to be able to locate the ground impact point of a missile from positions remote from that site, for relatively long periods of time after impact. One method of doing this is to carry aboard the missile a quantity of pyrotechnic that produces a substantial smoke cloud when deposited in the impact area and ignited. This suggests the kinds of questions that must be answered if a missile sub-system, a "visual marker" system, is to be developed for carrying out the desired sequence of events. That is:

What are the criteria for detecting smoke clouds as a function of distance from the impact site?

How much pyrotechnic is necessary to insure the desired detectability?

What methods of deposition of the pyrotechnic are optimal?

How and when should the deposition be made?

How should the pyrotechnic be ignited?

What physical/chemical properties of the pyrotechnic (i.e., resiliency, burn rate, etc.) and of the delivery system are desired?

By answering these questions analytically and/or experimentally a set of realistic requirements for the system can be developed and preliminary design work begun. These lead into system design and optimization studies followed by feasibility demonstration tests.



This paper discusses the development of a visual marker system for a missile which was carried out in much the manner described. The program culminated in a successful flight test of the final design.

#### OBJECTIVES AND DESIGN CONSTRAINTS

The specific objective of the program was to develop a visual marker (VM) subsystem to provide visual identification of the missile impact location by depositing and igniting sufficient pyrotechnic in the missile impact area to produce dense white smoke. The resulting cloud is to be 90% detectable to the unaided eye for at least three minutes at a slant range of five nautical miles.

Because of prior work and missile system requirements, certain constraints were externally imposed on the system design. They were primarily that the smoke producing agent would be red phosphorous and that the VM system must operate under the missile terminal flight environment; i.e., at impact velocities of from 900 - 2300 ft/sec and in the presence of a detonating warhead (~100 lbs of high explosive). It was further necessary that the VM system require no activation scheme other than warhead detonation (i.e., no electrical/mechanical initiation) and that it be as safe as the warhead itself.

Only limited space was available aboard the missile for the VM system to be stored. This is shown schematically in Figure 1. It was also necessary that the entire VM system be restricted to the free annular volume indicated. Further, in this region of the missile, four fins were attached to the missile body. Any scheme for ejecting pyrotechnic from the missile would have to consider the restrictive effect of these fins (Figure 2).

## TECHNICAL APPROACH AND RESULTS

### Design Concept

A preliminary examination of the system requirements and restrictions and the results of some of the preliminary studies discussed below led to the "square can" design concept illustrated in Figure 3. Here the pyrotechnic is contained in an inner can which is rapidly ejected from the missile by detonation of a sheet of explosive placed between the inner and outer cans. The maximum dimension of the inner can is fixed at the smallest chordal dimension between fins to avoid their restrictive effects during ejection. The inner can protects the pyrotechnic from the detonation products and collimates the pyrotechnic beam to prevent excessive dispersion at ground impact. The outer can is a structural body and seal for the system and provides enough back-up mass (behind the explosive) to help accelerate the inner can to the desired eject velocity.

The ejection explosive is initiated by a detonating cord which is itself initiated by warhead detonation. The outer skin of the missile body is cut open by a linear shaped charge also initiated by the detonating cord.

The red phosphorous based pyrotechnic is saturated with benzene (the casting solvent) to aid in the ignition process which occurs by flame propagation from the ejection explosive and/or warhead fireball to the pyrotechnic surface. Smoke is produced by oxidation of the red phosphorous. A rubbery binder added to the pyrotechnic provides strength and resiliency to the mixture and prevents break-up at ground impact. The remaining materials in the pyrotechnic provide burning rate control.

For the system, the sequence of events is as follows: The warhead detonation initiates the detonating cord. The detonation propagates to a junction point on the VM outer can, which splits the explosive propagation.

One leg goes to a flexible linear shaped charge which cuts the missile skin away in front of the inner and outer can assembly. The other leg goes to the high explosive sheet between the inner and outer cans. The high explosive is initiated by a booster at the end of the detonating cord from the junction. The resulting detonation ejects the inner can from the missile and the associated fireball ignites the pyrotechnic. The inner can, with its pyrotechnic contents ignited, impacts the ground and deploys the pyrotechnic contents.

#### Preliminary Studies

A series of preliminary theoretical and experimental studies were conducted in an attempt to answer some of the questions posed above.

##### 1) Cloud Theory

A theory of cloud formation was developed to relate the number of pyrotechnic pieces and total weight required for a 90% probability of detection at 5 miles as a function of dispersion of those pieces.

The cloud formation assumed is depicted in Figure 4 where  $d_1$  represents the dispersion diameter of the  $N$  slabs of pyrotechnic of weight  $w'$ . The smoke rises at some average velocity  $v$  and for any given burn time has a maximum diameter  $d_2$ . Conservation of mass gives:

$$w_c = f_1 N w' = \left(\frac{\pi}{12}\right) \rho v t_b d_1^2 (1 + \phi_1 + \phi_1^2) \quad (1)$$

where:  $w_c$  = weight of smoke in cloud,  $\rho$  = cloud density,  $v$  = average smoke vertical convection velocity,  $t_b$  = burn time of pyrotechnic,  $\phi_1 = d_2/d_1$ , and  $f_1$  = ratio of mass of smoke produced per mass of pyrotechnic burned.

Cloud detection depends on a number of factors; some are highly subjective. This is illustrated in Figure 5 where a chain linking "detection" and pyrotechnic properties is illustrated. Below each part of the chain are indicated the assumptions made in this study. The essential elements of interest are

indicated by the heavy lines. The relation between detectability, contrast ratio and size is summarized in Figure 6, which is based on theoretical/experimental studies of physiological optics.<sup>1-3</sup> In general:  $C = \text{contrast ratio} = (B_c - B_s)/B_s = B_c/B_s - 1 = I_c/I_s - 1$ , where  $B$  is brightness,  $I$  is intensity and the subscripts  $c$  and  $s$  refer to the cloud and background respectively. For a non-absorbing cloud,  $I_c = I_0 e^{-\gamma l}$  where  $I_0$  is the source intensity,  $l$  is the thickness of the cloud,  $\gamma$  is a coefficient given by  $n\pi a^2 Q_{sca}$  where  $n$  is the number of particles per unit volume,  $a$  is the particle radius and  $Q_{sca}$  is the scattering efficiency. For the background  $I_s = I_0 \beta$  where  $\beta$  is the background reflectance. Combining these with the expression for  $C$ , noting that  $l \approx (d_1 + d_2)/2 = d_1 (1 + \phi_1)/2$ , gives, after rearrangement:

$$n = \ln \left\{ \beta^{-2} (C+1)^{-2} \right\} / (\pi a^2 d_1 (1 + \phi_1) Q_{sca}) \quad (2)$$

Since the pyrotechnic is phosphorous based the main smoke producing reaction gives  $4P + 5O_2 \rightarrow 2P_2O_5$  which is highly hygroscopic;  $P_2O_5 + 3H_2O \rightarrow 2H_3PO_4$ . Consideration of the stoichiometry of the reaction and absorption of water from the air it is possible to show that  $n \approx 1.3 \times 10^{15} \rho$  where it has been assumed that  $2a$ , the droplet diameter, is  $0.1 \mu$ .<sup>4, 5</sup>

Choosing a 90% detectability level the appropriate curve in Figure 6 was fit to an equation of the form  $(C + k_1)^{n_1} (d_1 - k_2)^{n_2} = k_3$ , where  $k_1$ ,  $k_2$ ,  $k_3$ ,  $n_1$  and  $n_2$  are constants.

Within the accuracy of the plot it was found that  $n_1 = 1 = n_2$  and that  $k_1 = 0.4$ ,  $k_2 = 8.0$  and  $k_3 = 0.50$ . Thus:

$$C = 0.4 + 0.5 / (d_1 - 8.0) \quad (3)$$

Considering lateral diffusion it is possible to show that the cloud cone exterior angle is approximately  $78^\circ$ .<sup>6</sup> From this it can be shown that

$$\phi_1 = d_2/d_1 = 1 + v t_b / 4.71 d_1.$$

This, along with the equations for  $n$  and  $C$  can be substituted into Eq (2) and the result solved for  $\rho$ . When substituted into Eq (1), along with the relation for  $\phi_1$  this yields:

$$w_c = f_1 N w' = \frac{v t_b d_1 [1 + (1 + v t_b / 4.71 d_1)^2 / (2 + v t_b / 4.71 d_1)]}{1.3 \times 10^{15} \pi a^2 Q_{sca}} \cdot \ln \left\{ \beta^{-2} (1.4 + 0.5 / (d_1 - 8.0))^2 \right\} \quad (4)$$

Based on pyrotechnic composition and stoichiometry it can be shown that  $f_1 \approx 1.9$ . Assuming  $w' = 35$  gm and  $t_b = 3$  min and noting from the literature that  $v \approx 4.5$  ft/sec,<sup>4</sup>  $Q_{sca} \approx 3.5^7$  and  $\beta = 0.032$  (forest),<sup>3</sup> Eq. (6) can be used to plot  $N$  vs.  $d_1$ . The results are shown in Figure 7 where the total pyrotechnic weight  $N w'$  is also indicated.

The lower bound in Figures 7 (and Figure 6) was chosen by consideration of the other important cloud property shown in Figure 5; viz., size-resolution. As previously indicated, cloud size depends directly on dispersion. Resolution is dependent on the ability of the eye to see objects at long ranges. The relation between resolution  $r$ , range  $R$  and resolving angle  $\alpha$  is given by  $r = R\alpha$ . For  $R = 5$  nautical miles, and  $\alpha = 17-60$  sec,<sup>8</sup>  $r$  is 2.5 - 8.7 ft. Hence a cloud size or dispersion less than  $\sim 6$  ft should not be considered.

## 2) Pyrotechnic Geometry

An analysis was made of pyrotechnic geometry to assure that smoke production would be effectively constant over the entire burn time  $t_b$ . Assuming "thin" rectangular parallelepipeds that burn on the "face-up" side only, the

thickness  $y_0$  is defined by  $y_0 = r_b t_b$  where  $r_b$  is the linear regression rate of the pyrotechnic. Conservation of mass gives  $w' = \rho_p y_0 h_0 l_0$  ( $h_0$  and  $l_0$  are height and length respectively) which in light of the equation for  $y_0$  becomes:  $w' = \rho_p r_b t_b h_0 l_0$  where  $\rho_p$  is the pyrotechnic density. Another relation between  $h_0$  and  $l_0$  is desired to complete the solution. This is found from the requirement that the smoke production rate be essentially constant. Since  $r_b$  is constant it is clear that  $S$ , the burning surface area, must be constant for a constant rate. For a rectangular parallelepiped  $y = y_0 - r_b t$  (burning on one side only),  $h = h_0 - 2r_b t$ ,  $l = l_0 - 2r_b t$  where  $y$ ,  $h$ ,  $l$  are the instantaneous values of thickness, height and length at time  $t$ . Since  $S = 2lh + 2yl + 2yh$  this leads to:

$$S = l_0 h_0 + 2y_0 l_0 + 2y_0 h_0 - 4r_b t (l_0 + h_0 + 2y_0) + 12r_b^2 t^2 \quad (6)$$

The condition for constancy within 100/ $\delta$ % can be shown to be:  $l_0 h_0 + 6y_0 (l_0 + h_0) \geq \delta 4y_0^2$ . Combining this with the equation for  $w'$  leads to the solution:

$$h_0 = \left[ (4\delta\rho_p y_0^3 - w') \mp \sqrt{(4\delta\rho_p y_0^3 - w')^2 - 144\rho_p y_0^3 w'} \right] / 12\rho_p y_0^2 \quad (7)$$

Clearly  $l_0$  is determined from this result and the equation for  $w'$ .

Choosing  $\delta = 46$  (i.e., smoke production constant within 2.2%) and using  $r_b = 0.083$  in/min.<sup>4</sup> and  $\rho_p = 1.76$  g/cc<sup>4</sup> there results:  $y_0 = 0.25$  in,  $h_0 = 2.2$  in =  $l_0$  which defines pyrotechnic geometry.

### 3) Probable Impact Location

An analysis<sup>9</sup> was performed to determine the probable impact point of the VM payload with respect to the missile impact point (miss distance,  $\Delta$ ) as a function of the missile terminal velocity ( $V_m$ ) and dive angle ( $\gamma$ ),

the height of marker ejection ( $h$ ) and the marker ejection velocity ( $V_e$ ). Of concern here is that  $\Delta$  be large enough so that the VM does not go in the hole that the missile produces at impact. It is anticipated that such an event would tend to bury the pyrotechnic pieces and prevent them from burning properly.

The geometry of the situation is shown in Figure 8. Assuming constant velocities (no effective drag over the distances of interest) and straight lines of flight (negligible gravitational effects) it can be shown that

$$\Delta = h (V_e / V_m) \left[ 1 / \sin \gamma (\sin \gamma + (V_e / V_m) \cos \gamma) \right] \quad (8)$$

Calculations for  $h = 100$  ft and  $50$  ft,  $\gamma = 30-60^\circ$  and  $V_m = 900-2300$  ft/sec show that  $V_e$  should be  $200-400$  ft/sec in order to prevent the VM from "going in the hole".

#### 4) Smoke Contrast Measurements

Fundamental to the cloud theory is the criterion for cloud detection expressed as required contrast ratio vs. dispersion (Figure 6). Also the theory predicted the number of pyrotechnic pieces necessary for 90% detectability as a function of dispersion (Figure 7). Accordingly nine tests were performed in which each of 30, 60 and 90 pyrotechnic pieces were burned in 10, 35 and 100 ft diameter circles and the resultant clouds photographed at approximately 3 land miles. The tests were designed on the basis of the theoretical results in Figure 7. Densitometer measurements of the resultant negatives yielded values of contrast ratio which were corrected to 5 nautical miles. The results are shown in Figure 9. These data indicate the surprising result that  $C$  is only slightly decreasing with  $d_1$  for the range considered. In the same way the increase of  $C$  with  $N$  is small and appears to be approaching a limit near  $N = 90$ .

The curve for  $P_0 = 0.9$  from Figure 6 may be superimposed on Figure 9 to show that the desired criterion is minimally satisfied for  $N = 60$  (~5 lbs pyrotechnic) for  $d_1$  between 20 and 40 ft. Comparison of this with the results in Figure 7 shows that the predicted value ( $N \approx 40$  for  $d_1 = 30$  ft) was reasonably close. The difference is probably due to cloud dissipation effects (e.g., wind) neglected in the analysis.

Based on these tests the design goal of the VM system was chosen as "60 pyrotechnic pieces (weighing a total of approximately 5 lbs.) dispersed within a 30 ft diameter circle".

#### 5) Diagnostic Test

Since the VM system is to operate in the vicinity of a warhead the "environment" must be considered severe. The fireball, blast overpressures (considered in a later section) and fragments both from the warhead proper and from accelerated "hardware" within the missile, must all be considered damage mechanisms that are detrimental to any VM subsystem operation.

A detailed knowledge of this "environment" was determined by conducting a diagnostic test on a mockup missile with a live warhead. The test instrumentation consisted of a number of pin probe rasteroscillograph systems. The specific test objective was to determine the operational timing and velocity of damage mechanisms. The instrumentation points and test results are summarized in Figure 10. It was concluded that at some time between 0.83 and 1.64 msec a mass of high-speed (1000-3000 ft/sec) debris impacts the VM location internal to the missile body. Warhead fragments did not appear to be in or near the VM location in this time period.

Probe locations 2 and 20 follow the progress of the detonating cord which is placed next to the warhead and provides the signal for VM operation. Since probe 20 was activated at 0.48 msec from booster initiation (probe 1)



it is clear from the above result, that the VM must expel all its contents out of the missile body in  $(0.83 - 0.48 =) 0.35$  msec to  $(1.64 - 0.48 =) 1.16$  msec. Since the VM space allotment is  $\sim 3$  inches deep (see Figure 1) these times imply a VM ejection velocity  $V_e$  of 700 to 200 ft/sec. By adopting a conservative policy and considering the requirements of the Probable Impact Location analysis, the system design requirement for ejection velocity was chosen as  $V_e \geq 500$  ft/sec.

#### 6) Gurney Constant

In light of the above result and the choice of an expulsion scheme using sheet explosive an experiment was performed to determine  $\alpha$ , the constant in the Gurney equation<sup>10</sup> for the material of interest. The resultant value was  $\alpha = 8000$  ft/sec. The expected ejection velocity of the inner can is directly proportional to  $\alpha$ .

The major conclusions of the preliminary study were that 1) 60 or more pieces of pyrotechnic (35 gm each;  $\sim 5$  lbs total) must be dispersed in 30 ft diameter circle to make the resultant smoke cloud 90% detectable at a slant range of 5 nautical miles, 2) pyrotechnic pieces should be approximately  $0.25" \times 2.2" \times 2.2"$  to insure constant smoke production over the entire burning period, 3) VM ejection velocity should be  $\geq 500$  ft/sec to avoid damage by debris accelerated by the warhead.

#### System Design Studies

In light of the results of the preliminary studies and the design concept chosen, a series of theoretical and experimental studies were conducted to develop a specific set of VM designs.

### 1) Aerodynamic Analysis

An analysis was performed<sup>11</sup> to evaluate drag, impact velocity and flight path for a VM inner can after ejection from the missile. The effect of warhead blast on the trajectories was also considered.

For the design concept in Figure 3, the drag coefficient  $C_D$  vs. Mach number for the VM was computed (to about 15%) and the results used to compute the ballistic coefficient given by:  $B = w_i / C_D A$  where  $w_i$  is the inner can (plus pyrotechnic) weight (assumed to be 10 lbs) and  $A$  is the frontal area. The range of results obtained is shown in Figure 11. The parameters affecting VM impact velocity  $V_i$  are its ballistic coefficient  $B$ , flight distance before impact  $x$  and initial velocity  $V_o$ . The latter quantities are given directly from Figure 8 which shows that:  $V_o = (V_x^2 + V_b^2)^{1/2}$  and  $x = h \csc \left[ \gamma + \tan^{-1} (V_b / V_x) \right]$ .

The solution of the equation of motion for the VM, neglecting gravity gives:

$$V = V_o e^{-\rho x / 2 B} \quad (9)$$

where  $\rho$  is the air density. These results are summarized in Figure 12 for  $h = 75$  ft, a wide range of  $B$ 's and for  $\gamma = 20^\circ$  and  $70^\circ$ . The eject velocity  $V_b$  is assumed to be 500 ft/sec. It is clear that the VM may impact with velocities from ~1000 to 2200 ft/sec. These results define the impact environment suffered by the VM inner can and pyrotechnic and should help to determine the desired physical characteristics of each.

The lift force on the VM inner can tends to curve its flight path from the straight line assumed in Figure 8. Acceleration normal to the marker flight path due to lift is given by  $a = C_L A q / w_i$  where  $C_L$  is the lift coefficient and  $q$  is the dynamic pressure ( $= \frac{1}{2} \rho V^2$ ). Assuming  $a \approx$  constant the error in miss distance  $e_\Delta$  is given by:

$$\epsilon_A = at^2/2 = C_L A \rho (Vt)^2/4 w_1 \leq C_L A \rho (V_{\bullet}t)^2/4 w_1 = C_L A \rho x^2/4 w_1 \quad (10)$$

Assuming  $C_L \approx 1$  and a maximum value of  $x$  (110 ft),  $\epsilon_A$  was computed to be only 6 ft. By comparing Eq's (10) and (8) over the expected range of values of  $V_{\bullet}$ ,  $\delta$  and  $h$  it can be shown that  $\epsilon_A \leq 0.15\Delta$ .

The blast wave from the warhead (~100 lbs of high explosive) will arrive at the (known) marker location approximately 1.0 msec after warhead detonation.<sup>15</sup> Since the marker is activated at 0.48 msec from warhead detonation it is clear that the VM moves only  $500 \times (1.0 - 0.48) \times 10^{-3} = 0.26$  ft (3 in., just clear of the missile skin) before being struck by the blast wave. The velocity increment due to the blast wave is given by:

$\Delta V = (I_R/A) (A/w_1)$  where  $I_R$  is the reflected shock impulse. Based on the known properties of the blast wave<sup>12</sup> and an assumed scaling law for  $I_R$ ,  $\Delta V$  was computed to be only ~60 ft/sec.

## 2) Impact Analysis

A preliminary analysis was performed to estimate the effects of impact on the VM inner can.<sup>13</sup> A set of equations of motion describing the deformation and penetration of the can was proposed. From this, the relations among the velocities in the vertical and horizontal directions, the deformation of the walls and their reaction to internal pressure were shown. The reaction force of the ground upon penetration was taken from an established terradynamic equation. Based on these results and an energy balance it was shown that can failure should occur for impact velocities  $\geq 600$  ft/sec.

## 3) Mechanical Design

Considering the "square can" concept (Figure 3), a number of more detailed VM cans were designed to meet the system requirements developed in the preliminary studies. The parameters varied in the designs were

the outer can back plate and wall thicknesses, the materials and method of attachment of the inner can and inner can top, the inner can top type and the number of ribs (cross-wise) in the inner can.

Outer Can: The outer can is designed primarily to provide sufficient mass behind the explosive to maximize the inner can ejection velocity. In addition, the outer can should provide a hermetic seal for the pyrotechnic. For the former purpose the outer can material was chosen as steel and the back wall thickness fixed at 3/4 in. Since the side walls need only provide structural support and a seal, thicknesses of 1/8" and 1/4" were considered to minimize weight (a maximum VM system weight was imposed on the design).

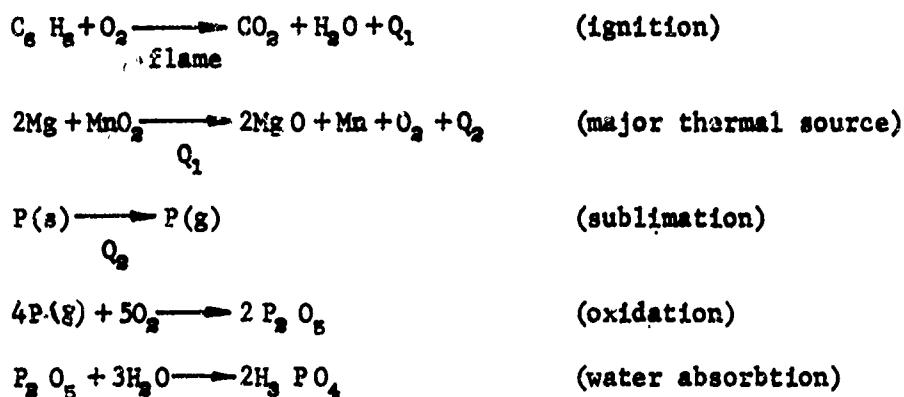
Inner Can: The optimum deposition sequence would be for the inner can to be ejected at the desired velocity, remain intact with the pyrotechnic inside until ground impact, and split open at impact depositing the (burning pyrotechnic) in a 30 ft. diameter circle. This requires that the inner can (and pyrotechnic) physically survive the shock wave and high temperature gas flow associated with detonation of the ejection explosive. Both aluminum and steel inner cans and inner can tops were considered. Since permanent attachments are impractical after pyrotechnic loading, one of the inner can surfaces must be mechanically attached to the rest. Both top and bottom mechanical attachments were considered. For the mechanically attached top surface a number of designs for improved flexural strength were considered including top and bottom waffling,<sup>14</sup> wrap-around lids<sup>14</sup> and counter weighting.

To keep the inner can together cross-wise internal ribs were also considered in the design.

#### 4) Pyrotechnic Development

The pyrotechnic must survive a "severe" environment. The shock wave produced by detonation of the expulsion explosive is of the order of

100 - 200 Kbars ( $1.5 - 3.0 \times 10^6$  psi) and will pass through the pyrotechnic. For purposes of burning rate control it is necessary that this cause a minimum of mechanical damage. At ground impact the pyrotechnic must be ejected from the inner can and land in the near vicinity without gross structural failure. Further, the pyrotechnic must be ignited and remain burning during the whole dynamic sequence. To provide the necessary strength, flexibility and ease of ignition a new pyrotechnic mix was developed.<sup>18</sup> This consisted of a mixture of a well-known composition based on red phosphorous<sup>5</sup> and a casting solvent with good ignition qualities (benzene) cast in a matrix of a Thiokol rubber (for strength and resiliency). The major constituents of the base mix are red phosphorous (smoke producing agent), manganese dioxide (burning rate control agent) and magnesium powder (thermal source). The reaction scheme is as follows:



In general  $Q_2 \gg Q_1$  and is the main thermal source for the sublimation reaction. Most phosphorous oxidation takes place in the vapor phase but some direct reaction with  $\text{MnO}_2$  probably occurs in the solid (liquid?) phase according to:



The Thiokol rubber is not involved in the desired reaction scheme but some burning apparently does take place with  $O_2$  or  $MnO_2$ . It was found that a) before ignition of the magnesium nearly all the benzene is reacted b) about 30 - 35% (by weight) Thiokol rubber (qualitatively) gave the desired physical characteristics and c) control of  $MnO_2$  content controlled the Mg reaction rate and thus the phosphorous sublimation and oxidation reactions (i.e.,  $MnO_2$  is the overall burning rate control agent).

For each of the mechanical designs considered a particular pyrotechnic mixture was considered. Variations were in the  $MnO_2$ , Thiokol rubber and benzene content and the number of pyrotechnic pieces.

#### 5) Impact Test

The pyrotechnic must survive a severe ground impact without structural failure. As previously indicated the ground impact velocity is 1000 - 2200 ft/sec. The inner can also undergoes this impact but structural survival is not required; in fact an inner can failure sufficient to release the enclosed pyrotechnic is desired.

Nine impact tests were performed to determine the effect of the expected ground impact on the developed pyrotechnic and the inner can. This was accomplished by accelerating pyrotechnic samples and a "scaled-down" inner can (containing pyrotechnic) into No. 40 quartz sand using a gas gun. The test set-up used is illustrated in Figure 13. Velocity measurements were obtained from the Hycam camera (5000 frames per second) while the impact was observed with the Millikan camera (500 frames/sec.). The maximum velocity obtained in the test series was ~1100 ft/sec; the gun choked when higher velocities were attempted. It was concluded that pyrotechnic survivability was likely even near the upper end of velocities, but that more data were necessary on inner can impact before an assessment could be made.

## 6) Explosive Tests

The inner can is to be ejected at ~500 ft/sec by the ejection explosive (Figure 3) with minimum damage to the inner can and pyrotechnic. Considering the mechanical design and pyrotechnic types chosen, the design of the sheet explosive was considered in three series of tests.

Parametric Study: A series of 16 tests were performed to determine the effects of material (of the inner can top), gaps (between the explosive and inner can top), perforation of Detasheet, initiation mode and plate thickness (of the inner can top) on the Gurney Constant  $\alpha$  of the Detasheet.

A schematic of the test set-up is shown in Figure 14. Based on Sterne unsymmetrical flat plate theory<sup>16</sup> a specific combination of back-up plate weight N, inner can top weight M, explosive weight C is sufficient to determine the expected inner can velocity divided by  $\alpha$  according to

$$V/\alpha = \left[ (1+x^3)/3(1+x) + (N/M)(M/C)x^3 + M/C \right]^{1/2} \quad (11)$$

where  $x = [C/M + 2]/[C/M + 2N/M]$ . Based on the actual velocity measurements the value of  $\alpha$  associated with Eq. (17) may be computed and compared to the value determined previously.

An analysis of the results showed that the initiation mode, inner can top material and thickness did not affect  $\alpha$  while perforations and gaps did. This is illustrated in Table 1 where the mean value of velocity for similar conditions in the tests is shown.

Table 1  
Effect of Perforation and Gaps on  $\alpha$

	0"	Gap 1/8"	1/4"
Non Perforated Detasheet	7250	--	4530
Perforated Detasheet	5380	5710	4400

The results in Table 1 indicate that the effective value of  $\alpha$  approaches, but is not equal to, the  $\alpha$  for Detasheet itself. Thus the expected reduction in damage to the inner can and pyrotechnic associated with the gap or perforation of the explosive also will result in a decrease in the ejection velocity of the inner can (see Eq. (11)).

Pipe Test: A mock-up VM was loaded and fired to determine the effect of the shockwave generated by the explosive on the developed pyrotechnic. The explosive was a 1/8" in. thick non-perforated sheet of Detasheet. An 1/2" steel back-up plate and a 1/4" Aluminum inner can top were used. The air gap was 1/4". It was concluded that the pyrotechnic would survive shock loading of this magnitude under these conditions.

Can Tests: To develop a feasible VM system design the results of the mechanical design study, the pyrotechnic development and the parametric study must be combined in such a way that the system requirements are met. Accordingly a series of twelve field tests were performed with the mechanical designs and pyrotechnic compositions previously considered and with explosive configurations with varying thicknesses, perforations and air gaps. The measured inner can velocities (280 - 600 ft/sec) were obtained from high-speed camera coverage of the tests. When the can failed, the velocity measured was that of the largest mass of debris. The results indicated that ~100% ignition occurred either if the inner can holds together or the benzene content is ~20%.

From these results it was concluded that several VM systems and designs were feasible in terms of the velocity and dispersion requirements and that to determine the "optimum" design further studies should be performed. However it was concluded that a two ribbed Aluminum inner can with a mechanically attached, wrap-around steel top was superior to the others. This is shown in Figure 15. The holes in the inner can were used to aid ignition.



The major conclusions of the system design studies were that 1) the VM inner can will impact at 1000 to 2200 ft/sec, 2) lift forces and the blast wave from the warhead will not appreciably affect the expected miss distances and velocities of the inner can, 3) inner can failure will probably occur for impacts  $\geq 600$  ft/sec, 4) benzene, the ignition aid in the pyrotechnic, is "burnt off" before ignition of the thermal source ( $\text{Mg} + \text{MnO}_2$ ), 5)  $\sim 30 - 35\%$  (by weight) binder is necessary gives the pyrotechnic the desired physical characteristics, 6) burning rate control can be exercised by control of the  $\text{MnO}_2$  content of the pyrotechnic, 7) the pyrotechnic will survive ground impact at least to 1100 ft/sec, 8) the Gurney constant for the explosive was lowered by perforations in the explosive and gaps between the explosive and the inner can but not by materials, thicknesses and initiation mode, 9) the pyrotechnic will survive the shockwave from the ejection explosive, 10) ignition will be affected if the inner can stays together and/or  $\sim 20\%$  benzene is used in the mix, 11) several VM systems designs considered were feasible in terms of the velocity and dispersion requirements and 12) a particular inner can configuration was superior to the rest; two ribbed Aluminum can with a mechanically attached, waffled, wrap-around steel top.

#### Design Optimization Study

Most of the questions originally posed have been answered in the preliminary or system design studies on a theoretical and/or experimental basis. However the combination of design parameters giving the optimum overall VM system design is not immediately obvious from the results obtained. Accordingly a series of nine tests were performed with variations in the inner can lid, explosive sheet configuration and thickness, initiation scheme, number of pyrotechnic pieces and benzene content of the pyrotechnic. For the inner can two lid lip lengths were chosen to determine if can survivability

could be improved by increasing the inner can and lid overlap. To determine if the inner can velocity could be increased while maintaining inner can lid strength a waffle inside (i.e., the flat surface faces the explosive) configuration was considered. Since the velocities obtained in the can tests were marginal with regard to the requirement an increase in the explosive weight was considered. To help "shape" the inner can lid to minimize dispersion during ejection (in case the inner can failed) the explosive weight was controlled by selectively cutting holes in the explosive. To control the direction of passage of the detonation wave over the inner can lid and thus "shape" it as above, several positions of the initiation points were considered.

Some evidence existed that enough gross breakup of the pyrotechnic occurred at ground impact to substantially increase the number of pieces burning on the ground. To obtain the desired number (~60) after impact, a lesser number of larger pieces was considered in two designs. Benzene content variations were considered to evaluate ignition between 0 and 25%.

An analysis of the test results indicated that an optimum system design would be obtained by the final design parameters shown in Table 2.

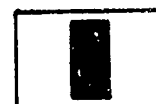
Table 2

Initiation Mode: Initiate at edge of high explosive sheet



Can Choice: Long lip ribbed top plate with 1/16" gap between explosive and top of ribs.

High Explosive: 0.250" explosive sheet with 2" x 4" centered hole. Total explosive weight of 183g.



Mix Choice: Benzene content = 8.0  $\pm$  1.0%. Use 35 large pattern pieces.

It appears that initiation position is not significant and therefore the simplest, most convenient case was chosen. It was clear from the results that the waffle inside was worse than the alternative although the choice between the long and short lip was less obvious. The former was chosen because the

better overall results were obtained in that case. Figure 15 shows the final mechanical design. The center holed Detasheet was chosen because it appeared to "shape" the inner can lid in a desirable fashion while holding down can damage. Since more explosive is involved than in any of the prior designs, the velocity should be closer to the required value. Because of the way in which the pyrotechnic broke up, a smaller number of large pyrotechnic pieces were chosen. An intermediate benzene content was chosen because it appeared to give the highest percent ignition.

#### SYSTEM FEASIBILITY TESTS

Based on the design found in the optimization study four complete systems were produced. The first one was tested to determine if the VM system was "safe"; the second to determine if it would operate successfully in the presence of a high explosive charge simulating the missile warhead; the third to determine if the system would meet the requirements in a static missile with a real warhead; and the fourth to determine if the VM system would meet the requirements under flight conditions with a warhead present.

#### Safety Tests

A series of safety tests were performed to determine the reaction of the completed system to forty-foot drop, fast cook-off, and vibration per MIL E05272C. From the results<sup>17</sup> it was concluded that the VM system remained "safe" through all tests since a) no benzene leakage was detected, b) no significant shifting of internal components was observed, c) no chemical reactions occurred and d) no gross structural failure of the unit were found.

#### "Iron Maiden" Test

The "Iron Maiden" consisted of a crude simulation of a missile consisting of a cylindrical steel shell, a number of bulkheads and 121 lbs of Composition B high explosive. The specific purpose of the test was to evaluate VM per-

formance under static conditions in the presence of a simulated warhead and to check-out certain test parameters for the subsequent test.

The test configuration was chosen so that the VM ground impact angle would be the same as that occurring in an average flight case. From the prior aerodynamic analysis the impact angle was estimated to be  $66^{\circ}$ . For the case of a missile terminal velocity  $V_m$  of zero (i.e., the static case) this angle will be obtained when the missile is tipped upward  $30^{\circ}$ . Because of the possibility of blast wave reflection from the ground interfering with the VM, the center of the "Iron Maiden" was placed 10 ft above the ground. The test set-up is shown in Figure 16. The pyrotechnic description and test results are shown in Table 3. A pilot flying at 10,000 ft AGL at a slant range of about 5 miles observed smoke throughout the test. From a post-test area plot plan it was possible to show that the VM impacted the ground at  $60^{\circ}$  (compared to the predicted value of  $66^{\circ}$ ) and bounced to a position  $\sim 12$  ft from ground zero. The effect of the warhead blast on the VM entry angle appeared to be very small. As expected, the inner can held together although it was extensively dented. The mix survived the impact without significant break-up and was mainly contained within the inner can. This accounts for the relatively long burn time, small dispersion, and high % ignition observed. Since the subsequent environments are considered more severe this "excessive" containment was not considered a problem. It was concluded that the VM could operate successfully in the presence of a "warhead" and that the test set-up used was adequate for the test purposes.

#### "Pole" Test

The "Pole" test consisted of a dummy missile, with a live warhead ( $\sim 100$  lbs of high explosive) hung by ropes from a cross beam on a telephone pole. The purpose of the test was to evaluate VM performance under static conditions with a "real" missile and warhead present. For the same reasons the test

configuration was chosen to be the same as in the "Iron Maiden" test. The test set-up is shown in Figure 17 and the pyrotechnic description and test results are shown in Table 3. A pilot flying the same pattern as before again reported observing smoke throughout the test. From a post-test area plot plan it was shown that the VM ground impact behavior was also essentially the same as in the "Iron Maiden" test.

The inner can held together again, but in this case the pyrotechnic was ejected and dispersed over a large area. This resulted in a shorter burn time.

Since the ignition was essentially complete and the pyrotechnic was not contained, it appears that the warhead fireball contributes to ignition. It was concluded that the VM system could meet the system requirements under static conditions in the "real" missile warhead environment.

#### Flight Test

The ultimate measure of VM system feasibility is demonstration of successful operation (i.e., meeting the system requirements) in a flight test with a warhead present. This certainly represents the most severe test condition and for the present program represented the final step in the development program. The two previous static tests cannot be considered as proof of VM feasibility since both were conducted under restricted conditions (i.e.,  $V_{\infty} = 0$ ).

The pyrotechnic description and test results of the flight test are shown in Table 3. As the ground impact velocity was considerably greater than 600 ft/sec inner can failure and increased pyrotechnic breakup were expected. This led to the shortened burn time. Also, since the percent ignition remained higher than in the static tests the proposed contribution of the warhead fireball to ignition was supported.

The missile launch aircraft pilot observed smoke in several passes over the target throughout the test. Ground observers at approximately 5 miles from the impact site (or about 1 - 2000 ft above the site) observed smoke throughout the test. Post test examination of the impact site showed that the pyrotechnic had not "gone in the hole".

Based on the dispersion and duration data in Table 3 and the observations made, it was concluded that the VM system designed can operate successfully under realistic flight conditions with a warhead present.

An example of VM smoke as seen from the air, is shown in Figure 18 which is an enlargement of one frame from the motion picture coverage of the "Pole" test.

Table 3

Description and Results of "Iron Maiden", "Pole" and Flight Tests

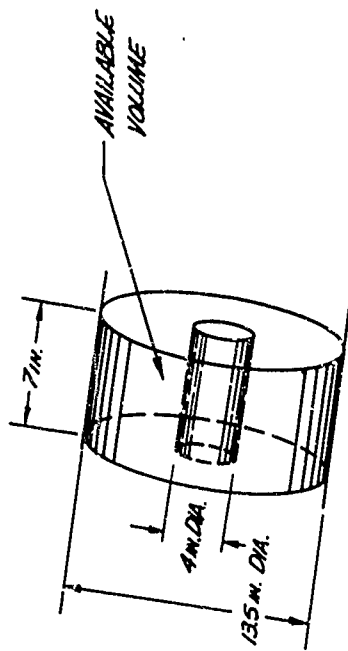
Description		Results								
Test Name	Type	lbs HE Present	Pyrotechnic		Mix Condition	Ignition %	Dispersion	Inner Can Condition	Smoke	
			% Benzene	No. of Pieces					Quality	Duration
"Iron Maiden"	Static	121	9.0	39	5.4	Good	~100	100% ≤ 10 ft	holds	Good 12 min.
	Static	103	9.5	36	5.7	V. Good	~100	85% ≤ 30 ft	holds	V. Good 8 min.
Flight	Dynamic	103	10.0	39	5.9	Fair	~95	85% ≤ 30 ft	fails	Good 6.5 min.

## References

1. "Final Engineering Evaluation Report, Redeye Air Defense Weapon System," Redeye Report No. 67-1, Volumes I and II, USA TEOM Project No. 3-4-0201-01, White Sands Missile Range, 1967 (Confidential Report).
2. N. Kurdyla, "Air Vehicle Visual Detection Probabilities - Results of a Parametric Analysis," Report No. ERR-CL-RAZ-00-184, Canadair Ltd., June 1966.
3. W. E. K. Middleton, "Vision Through the Atmosphere," University of Toronto Press, Canada, 1952.
4. C. Fingerhood, private communication, September 1967.
5. H. Ellern, Military and Civilian Pyrotechnics, Chemical Publishing Company, Inc., New York, 1968.
6. H. Dershin, private communication, September 1967.
7. H. C. Van de Hulst, "Light Scattering by Small Particles," John Wiley & Sons, Inc., New York, 1957.
8. F. Jackson, private communication, January 1967.
9. H. M. Higgins, Internal Memorandum, General Dynamics Pomona Division, Pomona, California, 11 August 1967.
10. J. A. Weeks, "Table of Initial Fragment Velocities Calculated From Gurney and Sterne Formulas for Various C/M Ratios and Explosive Energies," NAVWEPS Report 7592, U.S. NOTS, China Lake, California, December 1960.
11. F. D. Fernandes, "Visual Marker Drag, Impact Velocity and Flight Path," TM No. 6-334-832, General Dynamics Pomona Division, Pomona, California, 26 September 1967.
12. H. T. Goodman, "Compiled Free-Air Blast Data on Bare Spherical Pentolite," BRL Report 1092, Ballistic Research Laboratories, Aberdeen Proving Ground, Maryland, February 1960.
13. C. Riparbelli, Internal Memorandum, General Dynamics Pomona Division, Pomona, California, 22 September 1967.
14. First proposed by P. Studer, October 1967.
15. Developed by J. J. Adams and W. Bock, September 1967.
16. I. G. Henry, "The Gurney Formula and Related Approximations for the High-Explosive Deployment of Fragments," Report No. PUB-189, Aerospace Group, Hughes Aircraft Co., Culver City, California, April 1967.
17. "Visual Marker Safety Tests," Environmental Test Report #1075, Rocketdyne Division, North American Rockwell Corporation, 9 November 1967.



FIGURE 1  
AVAILABLE VOLUME



1-3.26

FIGURE 3  
"SQUARE CAN" DESIGN CONCEPT

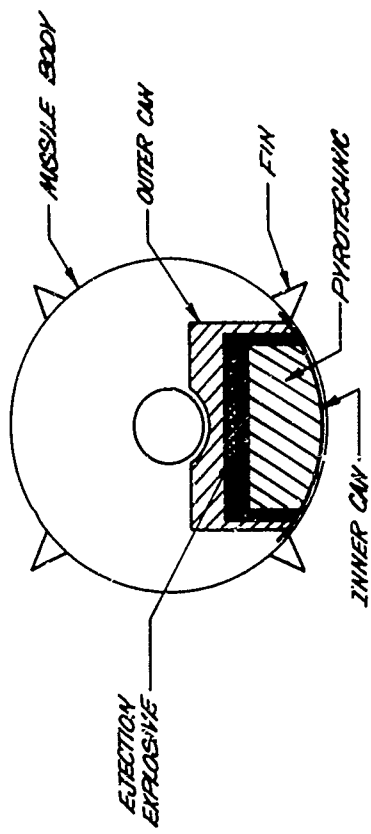


FIGURE 4  
CLOUD FORMATION

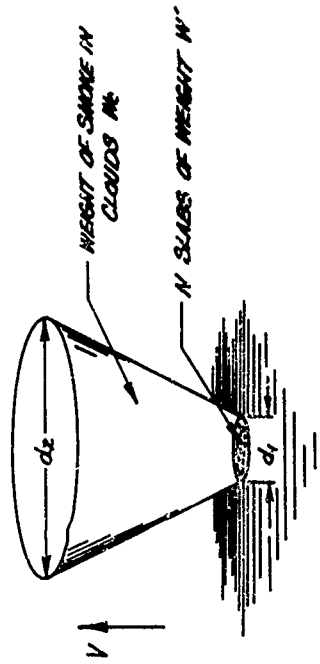
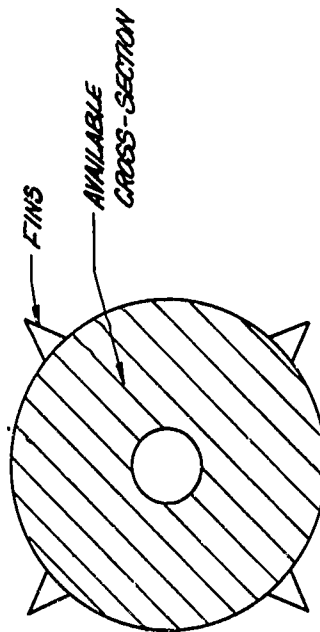
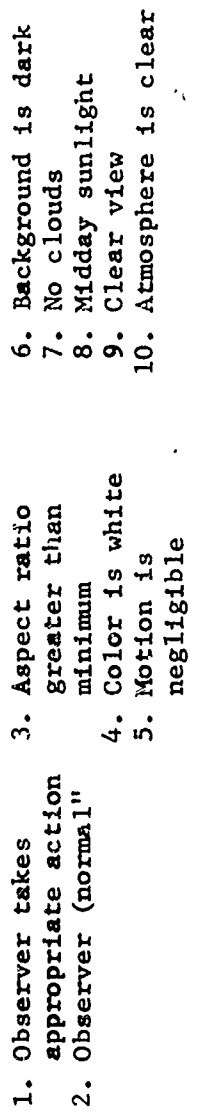


FIGURE 2  
FIN RESTRICTIONS



## Pyrotechnic Properties



**Assume:**

FIGURE 6  
CONTRAST RATIO VS. DIAMETER

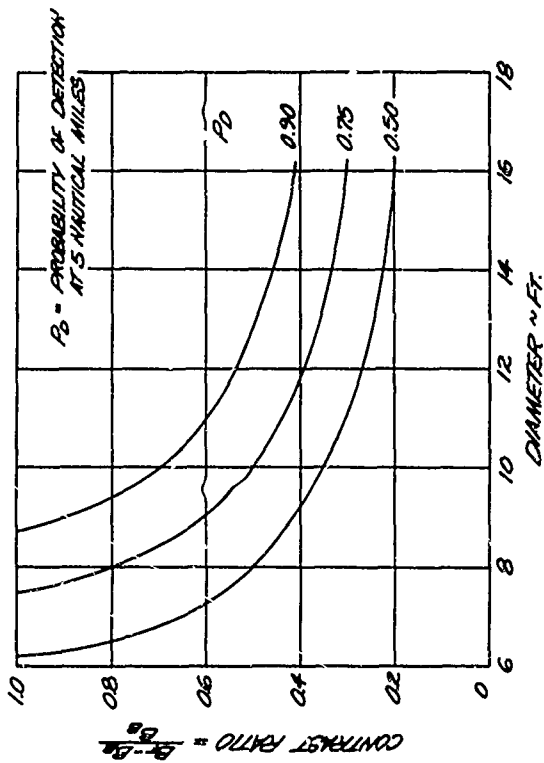
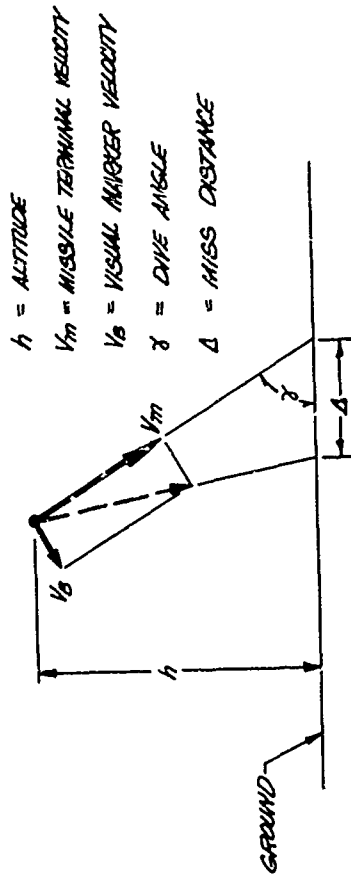


FIGURE 8  
PREDIABLE IMPACT LOCATION



1-3.28

FIGURE 9  
CONTRAST RATIO VS. DISPERSION

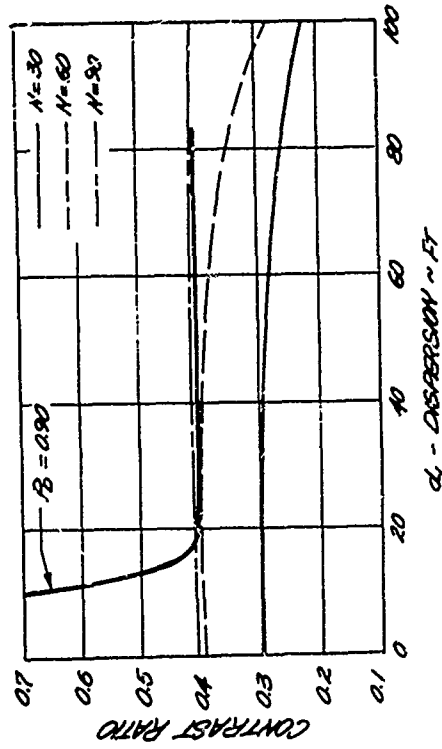


FIGURE 7  
NUMBER OF PYROTECHNIC PIECES VS.  
DISPERSION FOR 90% DETECTABILITY

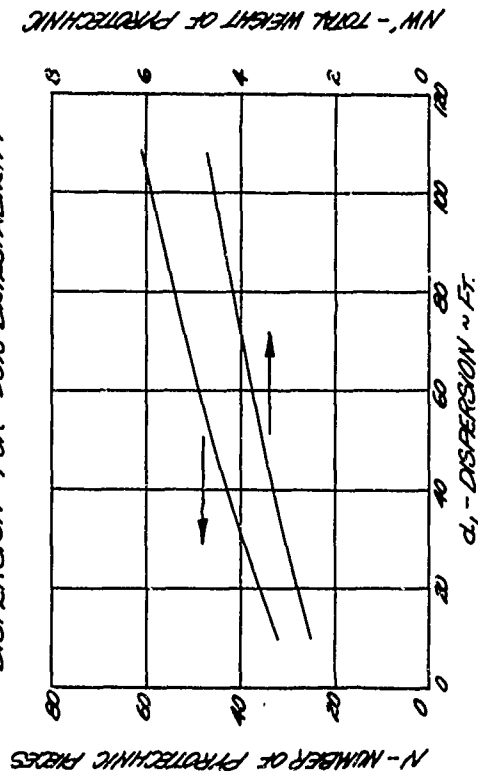


FIGURE 10  
DIAGNOSTIC TEST

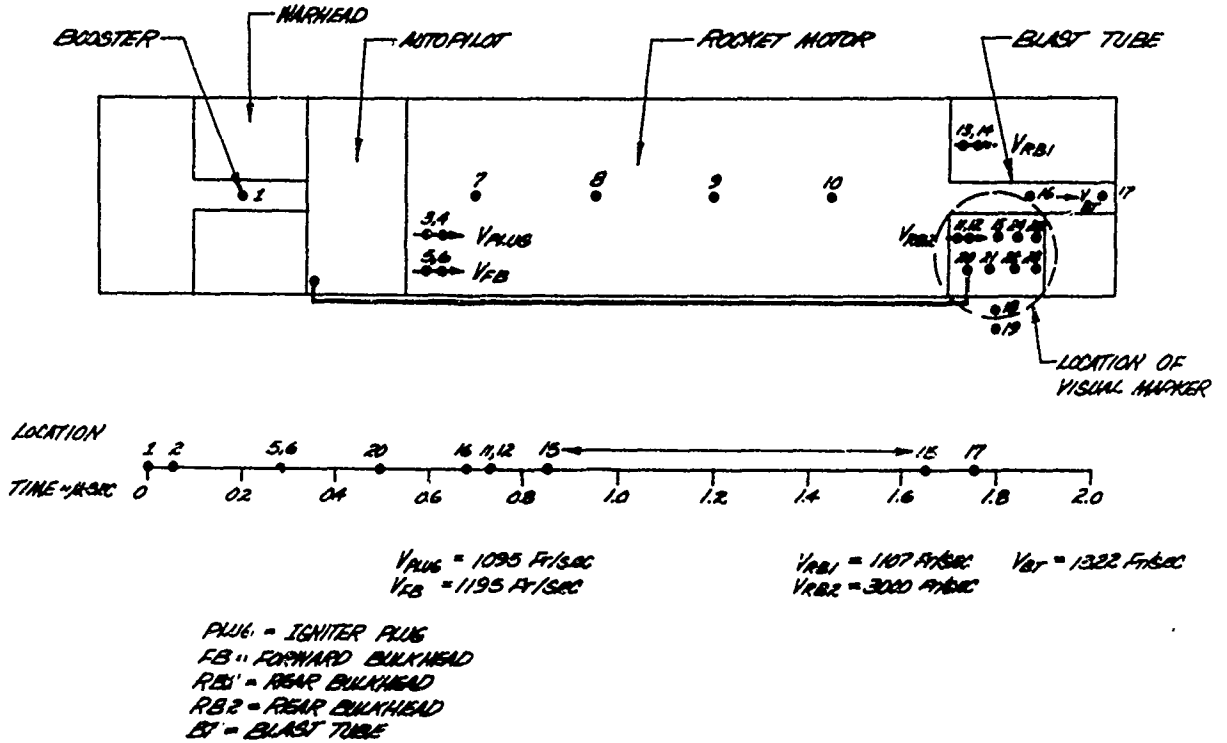


FIGURE 11  
BALLISTIC COEFFICIENT

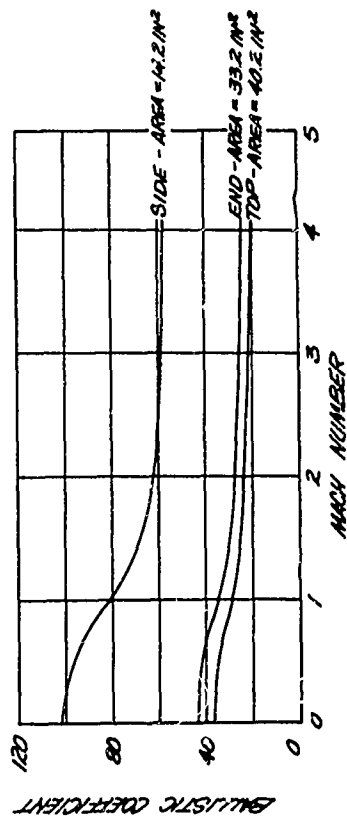


FIGURE 12  
IMPACT VELOCITY

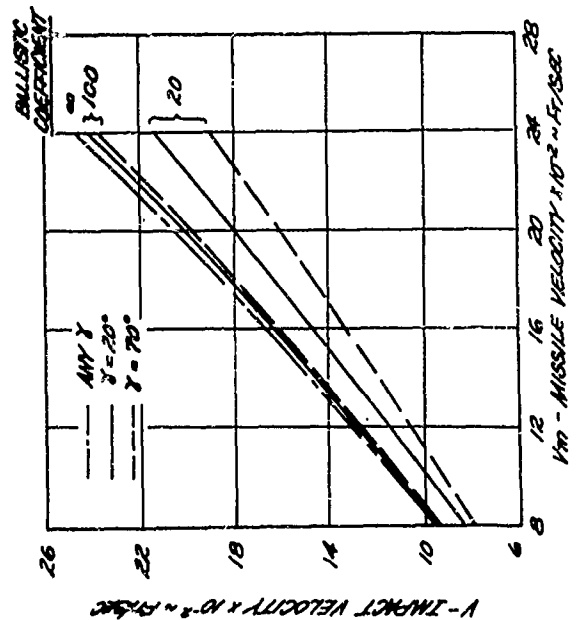


FIGURE 15. FINAL DESIGN



FIGURE 13

TEST SET UP - IMPACT TESTS

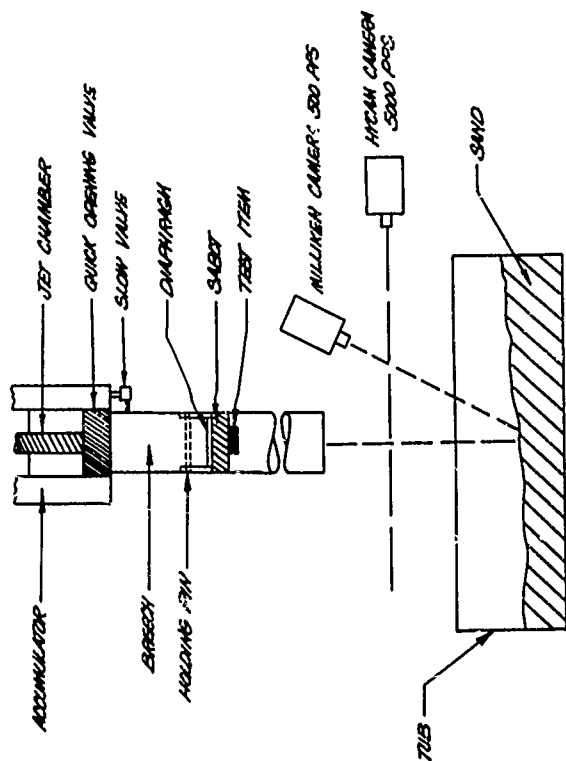
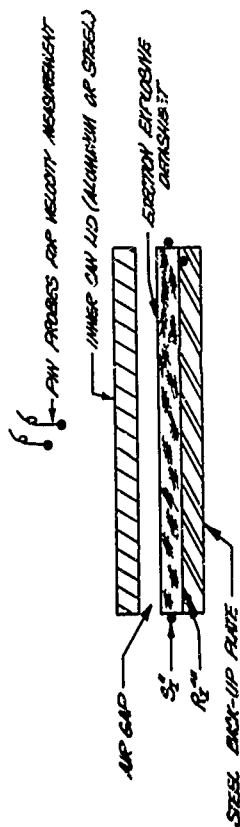


FIGURE 14

TEST SET UP - FRAGMENTATION STUDY



\*  $S_L$  = SIDE INITIATION SITES  
 \*\*  $R_L$  = REAR INITIATION SITES



# 1-4 DEVELOPMENT OF THE SATURN V THRU BULKHEAD INITIATOR

Loyd W. Corwin  
Clarence S. Greenough

North American Rockwell Corp.  
Downey, California

## INTRODUCTION

The Saturn V Launch Vehicle uses an exploding bridgewire design concept employing only secondary explosives to achieve maximum safety from EMR and other stray energy sources. There is a sizeable number of items on the Saturn V which must be initiated however, and using EBW devices directly on all of these would result in a considerable weight penalty due to the firing units. Therefore, CDF (Confined Detonating Fuze) and ordnance manifolds are used as a link between the EBW detonators and the item to be initiated. There are 18 dual initiated solid propellant rocket motors on the vehicle which are used during stage separation to control the ullage in the main propellant tanks and to provide retro thrust. It was therefore necessary to develop an initiator which would ignite these motors while receiving its input from a CDF assembly. Feasibility testing was conducted to investigate methods for accomplishing this objective while overcoming the obvious problem of providing a seal capable of preventing leakage of motor chamber gases back through the expended initiator. Testing quickly pointed to the thru-bulkhead principle as the most practical means of accomplishing this objective.

## BULKHEAD TRANSFER MECHANISM

Inasmuch as post fire leakage thru the expended initiator was believed to be a possible stumbling block, it was elected to use an integral

bulkhead, formed by machining the body directly from bar stock without the use of welding, brazing, or bonding. This involved a substantial amount of machining, of course, and for this reason free machining CRES AISI type 303S steel was selected. Later developments proved this to be an unfortunate choice.

It was believed that, everything else being equal, the greater the sensitivity of the high explosive used in the TBI (thru-bulkhead initiator) the higher the probability of successful detonation transfer while maintaining the structural integrity of the bulkhead. (1,2) As mentioned earlier, only secondary explosives were permitted on the Saturn V, and this ground rule went one step further inspecifying that no explosive more sensitive than PETN could be used. This is admittedly somewhat ambiguous, but since we were looking for the most sensitive explosive permissible, PETN was clearly the only logical choice.

#### Sizing Body and Charge Cavities

Development testing of the TBI began with the sizing of the high explosive charge cavities. The first development tests were performed with the set-up shown in Figure 1. The initiator was required to mate with the standard Saturn V CDF assembly which had not completed development at this time. Therefore, a makeshift CDF assembly consisting of 2.0 grain per foot CDF with a DuPont X-349 primer crimped on the end was used to initiate the donor charge. The CDF assembly was required, by specification, to have an output equal to the DuPont X-349. In an attempt to facilitate production loading, a donor charge carrier was used in conjunction with a thin wafer



of PETN which was pressed directly into the cavity to insure intimate contact with the bulkhead. This arrangement appeared to create more problems than it solved, however, and the carrier was dropped after a few tests. Since shock sensitivity of the receptor charge was very important to reliable functioning of the TBI, the receptor was made as sensitive as possible by pressing the PETN to only 1.0 gm/cc. density. <sup>(3,4)</sup> This also had a "spin'off" advantage in that it softened the output somewhat and therefore, hopefully, would make it easier to get down to a deflagration in the initiator final output.

Only a few tests were required with the set-up of Figure 1 to demonstrate that the 3/4 inch hexagon body would not confine such a large donor charge. Inasmuch as it was required that the **initiator body confine all explosive** effects and retain the CDF assembly after firing, the design was modified to that of Figure 2. The donor charge was drastically reduced from 132 mg to 42 mg and the body size was increased from 3/4 inch hexagon bar stock to 7/8 inch. Also, since cracking at the corners of the cavities had been evidenced, a full radius was used on the cavity bottoms. It should be noted that the authors do not necessarily believe that full radius cavities are the optimum configuration, anymore than we believe that flat bottom cavities are optimum. Full radius cavities permit the use of a thinner bulkhead, however, they also produce a divergent shock wave which, everything else being equal, demands a thinner bulkhead for reliable transfer. It was not the purpose of the program to attempt to optimize this aspect of the design. We did attempt, by appropriate statistical testing, however, to optimize the bulkhead thickness using this basic configuration.

### Sensitivity Tests

Initially, a bulkhead thickness was selected by intuition and a few firings were made with the set-up of Figure 2. This configuration appeared to transfer the detonation properly while meeting all requirements for confinement and an intact bulkhead after firing. It was now necessary to optimize the bulkhead thickness to achieve maximum reliability of transferring the detonation while not jeopardizing the integrity of the bulkhead after firing. This was accomplished by conducting two independent Bruceton tests performed by varying the bulkhead thickness (5) while holding all PETN charge parameters constant. It was hoped that these tests would yield two curves as shown in Figure 3. If the two curves were separated sufficiently so that a bulkhead thickness could be selected which could be shown to be 99.9% reliable, with respect to both propagation and freedom from bulkhead rupture, then our non-optimized bulkhead configuration would be sufficient for our purpose.

The first Bruceton test was performed with thick bulkheads to determine the standard deviation and 50% point for propagation. The test set-up was generally similar to that shown in Figure 2. Ten (10) search units were fired to determine the approximate 50% point, and then 32 specimens were fabricated and fired at ambient conditions. The same procedure was followed using 30 specimens with thin bulkheads. The expended test specimens were pressurized with 8000 PSI hydraulic oil and evidence of leakage was used as the criteria for rupture. The following information in Table I was calculated from the raw data.

TABLE I  
BRUCETON TEST RESULTS

ITFM	BULKHEAD THICKNESS (INCH) (TRANSFER)	BULKHEAD THICKNESS (INCH) (RUPTURE)
(1) 50% Reliable Thickness	0.119	0.036
90% Confidence Limits	$\pm 0.0018$	$\pm 0.0014$
(2) Standard Deviation of 50% Reliable Thickness	0.0032	0.0026
90% Confidence Limits	$\pm 0.00185$	$\pm 0.0015$
(3) 99.9% Reliable Thickness at 95% Confidence	0.102	0.051

Based on these very encouraging results (Figure 4) an optimum thickness of .075 inch was selected and used throughout the remainder of the program.

#### Loading Problems

Sometime after the Bruceton tests were completed two units unexpectedly failed to transfer when initiated at  $-20^{\circ}\text{F}$ . A very laborious failure analysis was performed to determine the exact nature of the failure. Units from the same lot as the failed units were successfully functioned at  $-100^{\circ}\text{F}$  to demonstrate that low temperature in itself did not produce a marginal condition. The upper limit (thick bulkhead) Bruceton test was performed twice at  $-20^{\circ}\text{F}$ ; first with specimens similar to those originally used, and second, with specimens having a low density (1.45) donor. The results of the first test indicated no detectable change from the original ambient Bruceton test, while the low density specimens

yielded a thickness only about .010 inch thinner than the previous results. A number of other more minor investigations were conducted without pointing to any specific cause.

It was eventually concluded, but could not be directly proven, that the cause of failure to transfer was the presence of a small void between the bulkhead and receptor charge. To eliminate this, the donor and receptor cavity surface finish was changed from a 125 micro-inch to a 64 microinch finish and the PETN charges were pressed in two increments rather than one. This appeared to resolve all transfer problems as over 2000 units have now been fired successfully.

#### PRESSURE OUTPUT CHARACTERISTICS

As mentioned previously, the Saturn V uses a number of solid propellant rocket motors encompassing four (4) individual motor designs of varying size and thrust. One type of upper stage motor uses a small non-metallic igniter of limited structural strength, while the second stage ullage motors employ a large pyrogen type igniter. For this reason, NASA's Marshall Space Flight Center had wisely specified, in the early days of the Saturn V program, an EBW initiator having a low pressure, high caloric output. By the time it was decided to develop the TBI, all motors were already under development with the EBW initiator. Therefore, the TBI was required to produce a pressure output envelope generally similar to the EBW initiator. It was required to produce 420 to 800 PSI in a 20.7 cc closed bomb volume with a maximum delay of 8 milliseconds from time of initiation to time of peak pressure. A relatively high thermal

output of 950 calories minimum, which precluded the use of any commonly accepted pyrotechnic mixture, was also specified (Figure 5). Considerable difficulty was encountered in meeting these output requirements.

#### Initial Testing

The first development test specimens with an output charge were fabricated with a configuration as shown in Figure 6. It soon became evident, however, that a grain type charge would not suffice due to its inability to meet the 8 ms delay time. A loose pyrotechnic charge consisting of pyrophoric magnesium and cupric oxide in a stoichiometric ratio was tried next. The configuration (Figure 7) was generally similar to Figure 6, except that the shock attenuator was removed and the pyrotechnic cavity was shortened somewhat. This design solved the long delay problem; however, it was discovered that when sufficient pyrotechnic was used to produce the required 950 calories, the peak pressure was in excess of the 800 PSI allowable. Also, the peak pressure showed excessive unit to unit variability.

The relatively high pressure (1000 PSI) which this design produced was to some extent intriguing, considering that the pyrotechnic itself is gasless. The PETN combustion products and the air in the bomb could account for only 300 to 350 PSI, assuming that these were heated to roughly 2800°K by the burning pyrotechnic. It was therefore assumed that the unexplained pressure was produced by vaporized copper which is, of course, a reaction product when the pyrotechnic burns. On the basis of this, a 3-component pyrotechnic was evaluated.

### Three Component Pyrotechnic

Ferric oxide ( $\text{Fe}_2\text{O}_3$ ) was added to the magnesium-cupric oxide mixture in various ratios to provide a means of controlling the quantity of copper vapor which would be released upon reaction of the mixture. As mentioned earlier, TBI bodies are costly and time consuming to fabricate, so in an effort to expedite the development work, a number of relatively simple EEW test units were fabricated as shown in Figure 8. The sole purpose of these units was to evaluate the 3-component pyrotechnic and determine the proper constituent ratios prior to loading it into TBI type test units.

A few tests were performed with the EEW set-ups, and it was shown that in spite of the incorrect assumption about the copper vapor contributing to the output pressure, the  $\bar{X}$  (average) pressure could indeed be adjusted by adjusting component ratios. Furthermore, the unit-to-unit variability was exceptionally good and well within specification limits. A  $\text{Mg}/\text{Fe}_2\text{O}_3/\text{CuO}$  ratio of 27/35/38 was selected as optimum and a quantity of powder having this composition was blended and loaded into a lot of TBI test specimens. The subsequent test results when these units were fired for p-t trace were far from encouraging.

Not only did the  $\bar{X}$  pressure shift considerably from that which had been experienced with the EEW units, but worse than that, the unit-to-unit variability (scattering) increased a great deal. The latter difficulty was blamed on variability in the output of the receptor charge as opposed to the EEW initiated charge. A series of tests were run to confirm this, but the results were generally inconclusive.

### Fuel-Rich Pyrotechnic

This discouraging turn of events led us to sit down and see what could be done with some theoretical calculations on vapor pressures, condensation rates, and heat transfer rates within the bomb. We were able to show rather conclusively that the copper vapor could not be the constituent contributing to the bulk of the output pressure due to its very rapid condensation rate on the cold bomb walls. The magnesium vapor, on the other hand, due to the mismatch between its mass and the mass of the bomb walls and due to its much lower boiling point could significantly contribute to the pressure output. This is particularly interesting from the standpoint that a high pressure specimen would then be one in which the pyrotechnic reaction did not go to completion, relatively speaking. Accordingly, it was believed that the  $\bar{X}$  pressure could be controlled by blending powders with quantities of magnesium in excess of stoichiometric. It was hoped that this would also help stabilize the reaction in accordance with the Law of Mass Action, in spite of any variabilities in the output of the receptor charge. Some concern was held, however, for the fact that reducing atmospheres in general are not particularly favorable for ignition. (6,7)

A somewhat lengthy series of tests were run with units conforming to Figure 7 and containing Mg/Fe<sub>2</sub>O<sub>3</sub>/CuO pyrotechnic having amounts of magnesium up to as high as 50% in excess of stoichiometric. Analysis of the test results and expended hardware indicated the following:

- (1) the  $\bar{X}$  pressure could be adjusted by varying the magnesium content;
- (2) if roughly 15% of the pressure data were disregarded from any group of firings, the remaining data showed fairly good grouping;
- (3) the specimens which were responsible for the "bad" data could be distinguished by visual examination of the expended bodies.

The 15% disregarded data had the distinct characteristics of excessively high pressure and long delay times. Figure 9 shows a typical normal p-t trace compared to a typical "bad" high pressure trace. Examination of the expended specimen bodies showed an obvious difference in coloration between normal and high pressure units. The pyrotechnic cavities of normal units were reddish brown in color, while the high pressure units were black. It appeared that there was a distinct difference in either the degree to which the reactions had gone to completion, or in the reactions themselves.

#### Calorimeter Studies

In an effort to better investigate the phenomenon, a sodium peroxide type calorimeter was modified to enable firing TBI specimens directly into a special calorimeter bomb. It was also planned to extend this set-up so that a p-t trace could be obtained for each unit fired in addition to measuring the heat output. It was hoped that perhaps some correlation could be found between the heat output and the pressure output. Due to certain equipment problems, this secondary goal was never achieved.

The results of the calorimeter tests were, nevertheless, of considerable interest. Initiators loaded with stoichiometric powders produced expected results, whereas those loaded with powders containing excess amounts of magnesium produced quantities of heat in excess of theoretical. The theoretical values in this case included possible exothermic reactions with closure discs and the oxygen (from air) in the bomb. Several calibrations and other test set-up checks were performed until the probability of experimental error was quite remote. These results appeared then to



basically substantiate what had already been suspected; i.e., the pyrotechnic combustion was erratic and probably susceptible to peculiar side reactions. The tests did little in the way of directly telling us what should be done to correct the problem.

#### Use of Shock Attenuator

Reviewing what had been done since the beginning of the program to achieve proper p-t characteristics, several facts seemed to stand out: (1) no amount of juggling of the pyrotechnic composition or ratios had been really beneficial in solving the erratic combustion problem. (2) stable combustion had been achieved only when the pyrotechnic was ignited by an EBW initiated PETN charge. (3) although variable output of the receptor charge could not be confirmed experimentally, it is obvious from a glance at Figures 7 and 8 that the pyrotechnic is highly shocked by the detonation of the PETN charges. Perhaps the high pressure shock front which precedes the burning front compresses and desensitizes the pyrotechnic, making it especially susceptible to normal variations in receptor output. (8) It therefore appeared logical to separate the PETN and pyrotechnic charges to some degree by use of an intermediate charge or a shock attenuator. One type of shock attenuator had been used in the early days of development in conjunction with bonded grain charges (Figure 6). but unfortunately had been dropped after going to a loose pyrotechnic.

Several types of both shock attenuators and intermediate charges were evaluated and the result was a TBI with an air gap type shock attenuator as indicated in Figure 10. The 25/75, Mg/CuO powder contains magnesium

slightly in excess of stoichiometric. Over 1000 units have now been fired without any abnormal pressures or delay times having been recorded.

#### POST FIRE BULKHEAD LEAKAGE

As mentioned earlier, it is important that the initiator bulkhead not leak after firing as this would permit rocket motor chamber gases to be expelled back thru the initiator. Therefore, by specification, the TBI was required to be subjected to two types of post fire leakage tests. The first test required the expended body to be pressurized with 2500 PSI nitrogen at the output end, while the second test required similar pressurization with 7500 PSI hydraulic oil. Unfortunately, it was assumed early in the program that the 7500 PSI oil test was the more severe of the two. Partially for this reason and partially because of availability of test apparatus, only the hydraulic oil test was performed throughout all but the latter days of development testing. When the first group of expended bodies were finally pressurized with nitrogen at 2500 PSI, it was discovered that approximately one unit in three leaked. The leak rates were quite small, being of the general magnitude of 10 cubic centimeters per minute. Such small leaks could perhaps have been tolerated from a practical standpoint; however, it was felt that an investigation of the problem would have to be undertaken to determine the basic leakage mechanism. Only in this way could the necessary assurance be gained that an unacceptably large leak would not be encountered in the future.

#### Metallurgical Investigation

A number of expended bodies, representing both leakers and non-leakers, were sectioned, polished, and microphotographed. The bulkhead areas  
(9)  
showed the expected twinning and slippage planes. They also showed the

presence of void areas. Further investigation showed that the voids were associated with non-metallic sulphide stringers present in the metal. Sulphur is added to AISI type 303S stainless steel to improve the machining characteristics, and for most normal applications, it has no deleterious effects. <sup>(10)</sup> It appears, however, if leakage in a TBI is important, a body steel should be selected which is relatively free from any type of stringers or inclusions, even though this may result in a sacrifice of other desirable properties.

Although it appeared that a change of body steel would be the most direct method of solving the leakage problem, it was considered undesirable in this particular situation for the following reasons: (1) all testing to date had been performed with type 303S steel and some doubt would be cast on all test results if a different steel were substituted; (2) the new steel, while solving the leakage problem, could possibly introduce a new set of problems; (3) a number of completed initiators were on hand and it was desired to rework them if possible as they were badly needed by the people conducting formal testing on the various solid propellant motors.

#### Shock Wave Trap

A solution to the problem of providing a satisfactory method of rework centered around the idea of reducing the bulkhead damage during firing. Unloaded, unfired bodies were naturally 100% free of leaks. It was hypothesized that a large percentage of the bulkhead damage resulted from the shock wave reflecting from the exterior free surface and collapsing on the bulkhead. If this were indeed the case, the shock wave could be trapped at the free surface and hence prevented from returning to the <sup>(9)</sup> bulkhead area.

The hypothesis was evaluated in the following manner: steel sleeves of .020, .060, and .100 inch wall thickness were press fit onto the cylindrical portion of 30 TBI's. When the units were fired, the resultant compressive shock wave should theoretically encounter no impedance at the steel to steel interface; however, the reflected tension wave would be unable to cross this same interface. The 30 TBI's were fired and no leakage was detected, even with those having sleeves with only .020 inch walls. Based on this somewhat limited sample, the rework method appeared feasible. However, it still remained to determine the optimum sleeve wall thickness. Now all TBI devices, after firing exhibit an expansion of the high explosive charge cavities and an accompanying shrinkage in the bulkhead thickness. This degree of expansion and shrinkage can be used as a convenient yardstick to assess general bulkhead area damage. Figure 11 shows the results of plotting these dimensions versus sleeve thickness. As can be seen, the curves appear to level off at roughly .060 inches. Photomicrographs of the bulkheads tended to confirm this conclusion. Based on this, and certain mechanical considerations, a .060 inch wall sleeve was selected for retrofit of all units.

Hundreds of units have now been produced by this same method and with the design as shown in Figure 12. While the sleeve was successful in reducing both the frequency of the leaks and the size of the leaks by about two orders of magnitude, it did not entirely eliminate the problem, and it was found necessary to permit a leakage rate of 1 cc per minute.

## REFERENCES

1. G. E. Seay and L. B. Seely, Jr., "Initiation of a Low-Density PETN Pressing by a Plane Shock Wave", J. Appl. Phys., vol. 32, No. 6, June 1961. P. 1092.
2. A. W. Campbell, W. C. Davis, J. B. Ramsay, and J. R. Travis, "Shock Initiation of Solid Explosives", Phys. Fluids, vol. 4, No. 4, April 1961. P. 511.
3. Robert H. Dinegar, Richard H. Rochester, and M. S. Millicon, "Effect of Specific Surface on the Shock Sensitivity of Pressed Granular PETN", Los Alamos Scientific Laboratory, Los Alamos, New Mexico
4. Melvin A. Cook, Douglas H. Pack, Lawrence N. Cosner, and William A. Gey, "Instrumented Card-Gap or SPHF-Plate Test", J. Appl. Phys., Vol 30, No. 10 October 1959, P. 1579.
5. H. P. Culling, "Statistical Methods Appropriate for Evaluation of Fuze Explosive-Train Safety and Reliability", Naval Ordnance Laboratory, White Oak, Maryland, 13 October 1953, NAVORD Report 2101.
6. R. F. McAlevy, III, P. L. Cowan, and M. Summerfield, "The Mechanism of Ignition of Composite Solid Propellants by Hot Gases", Presented at ARS Solid Rocket Conference, Princeton, New Jersey, January 1960.
7. Rodney B. Beyer and Norman Fishman, "Solid Propellant Ignition Studies with High Flux Radiant Energy as a Thermal Source", Solid Propellant Rocket Research, 1959. P. 673.

8. D. E. Davenport L. D. Pitts, and J. Gardner, "Improvement of the Ignition System for Simultaneous Ignition of Retro and Ullage Motors on Saturn V." July 30, 1965, NASA Report NAS8-11472.
9. John S. Rinehart and John Pearson, Behavior of Metals Under Impulsive Loads. American Society for Metals, 1954, P. 108 and P. 31.
10. Carl A. Zapffe. Stainless Steel, American Society for Metals, 1949, P. 143.

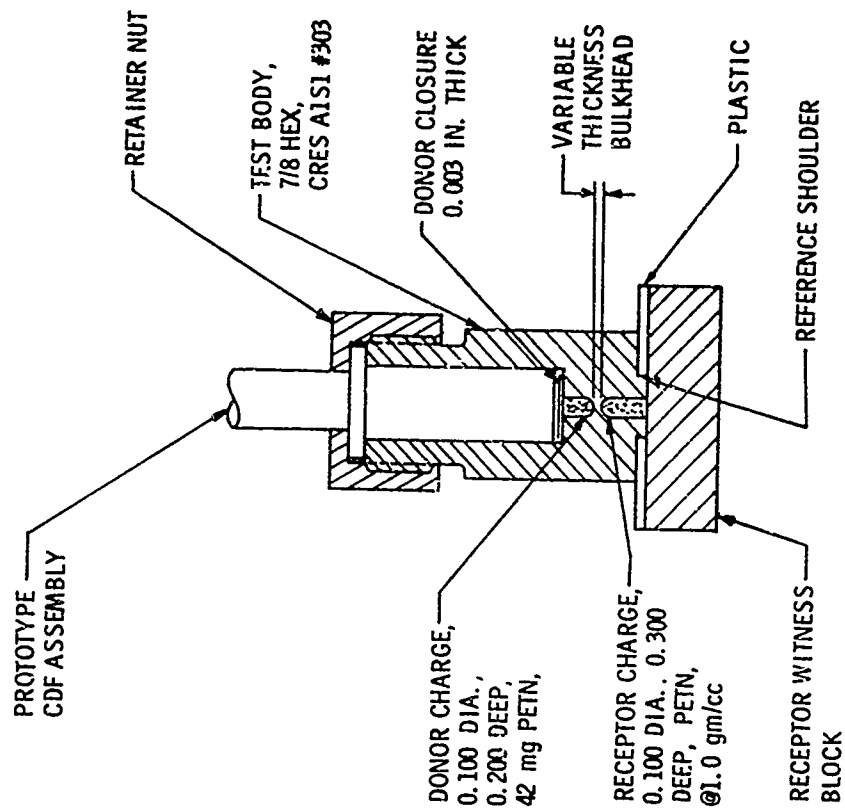
#### ACKNOWLEDGEMENT

The authors wish to thank Dr. D. E. Davenport of Link Ordnance who graciously consented to reviewing the paper for technical and historical accuracy.

#### CONCLUSIONS

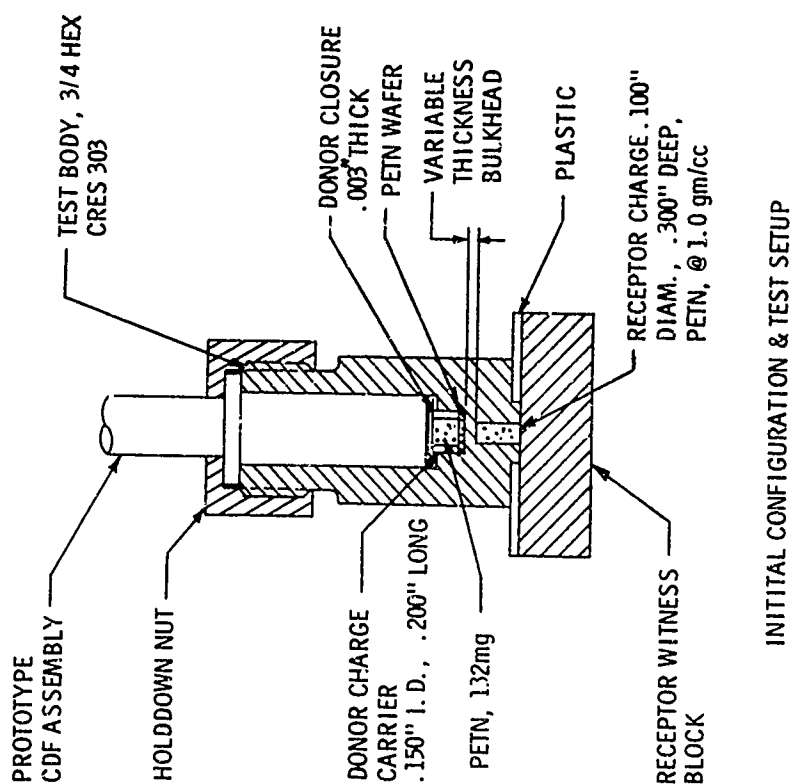
The development program demonstrated that a CDF-TBI system is an entirely practical and reliable means of accomplishing motor ignition. It appears that it is somewhat more difficult to achieve a desired pressure-time profile with a TBI than it is with a conventional initiator. This is probably due to the detonation to deflagration transition which must take place at the high explosive-pyrotechnic interface.

While this program was not successful in completely eliminating the post firing bulkhead leakage, it is believed that this would not be a problem for any future program. The simple expediency of initially selecting any one of the several clean, tough, void-free steels (e.g., type 718) would no doubt preclude any leakage.



SECOND CONFIGURATION & TEST SETUP  
FIGURE 2

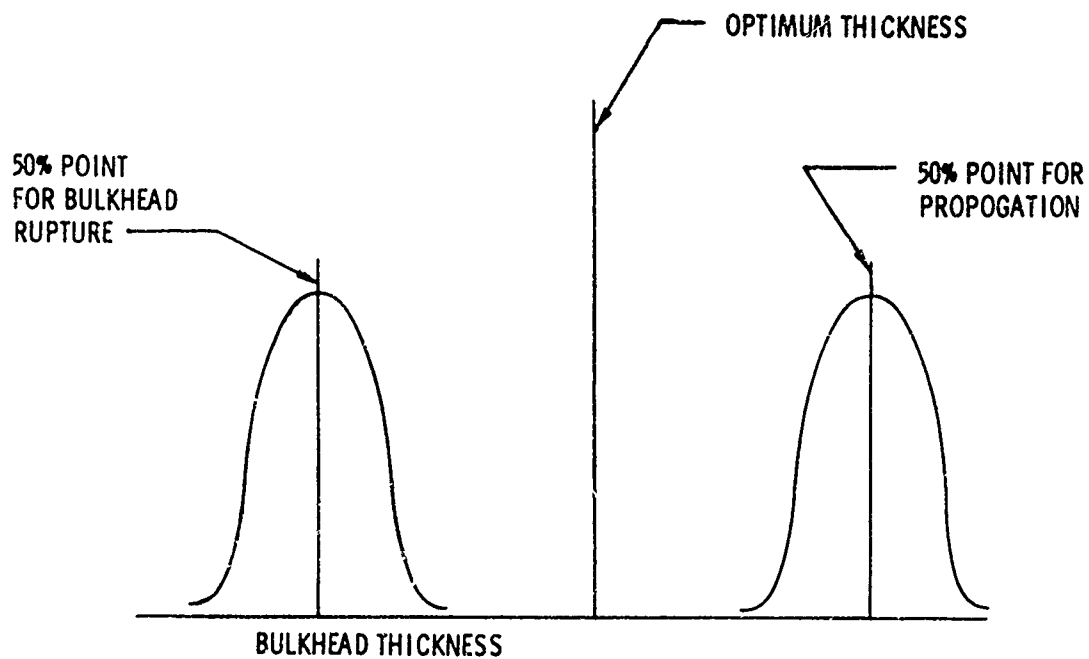
19



INITIAL CONFIGURATION & TEST SETUP  
FIGURE 1

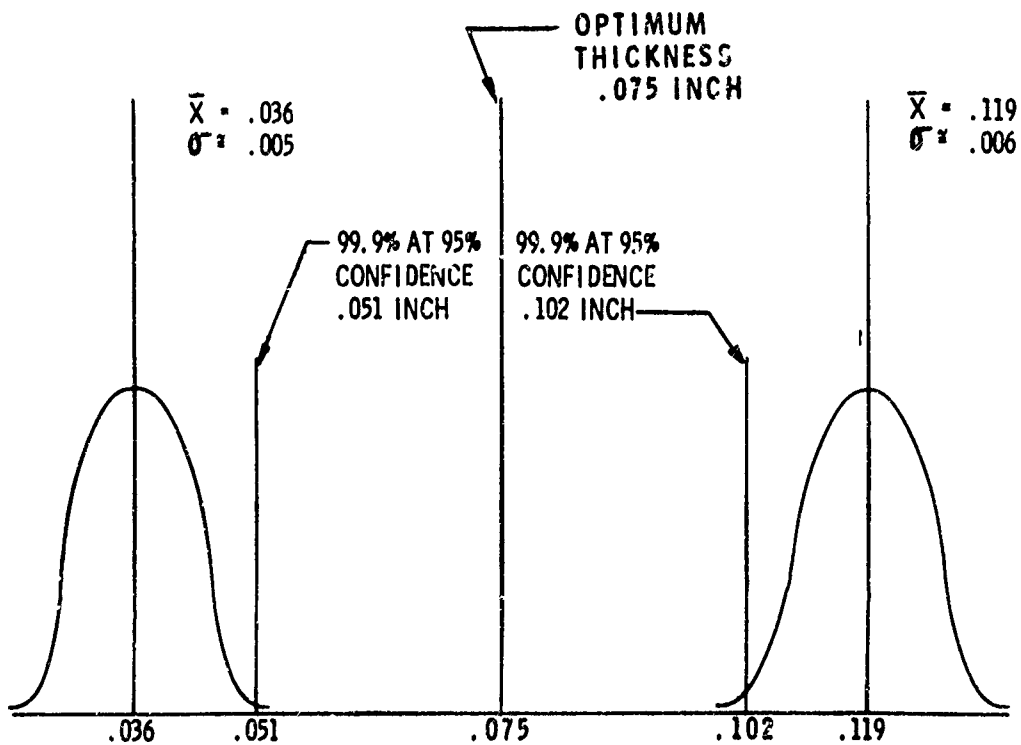
18

1-4.17



ANTICIPATED BRUCETON TEST RESULTS

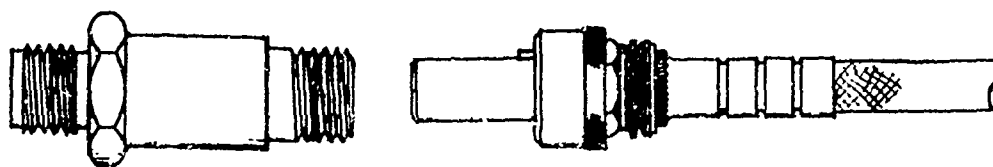
FIGURE 3



BRUCETON TEST RESULTS

FIGURE 4





TBI

MATING CDF ASSEMBLY

REQUIREMENTS:

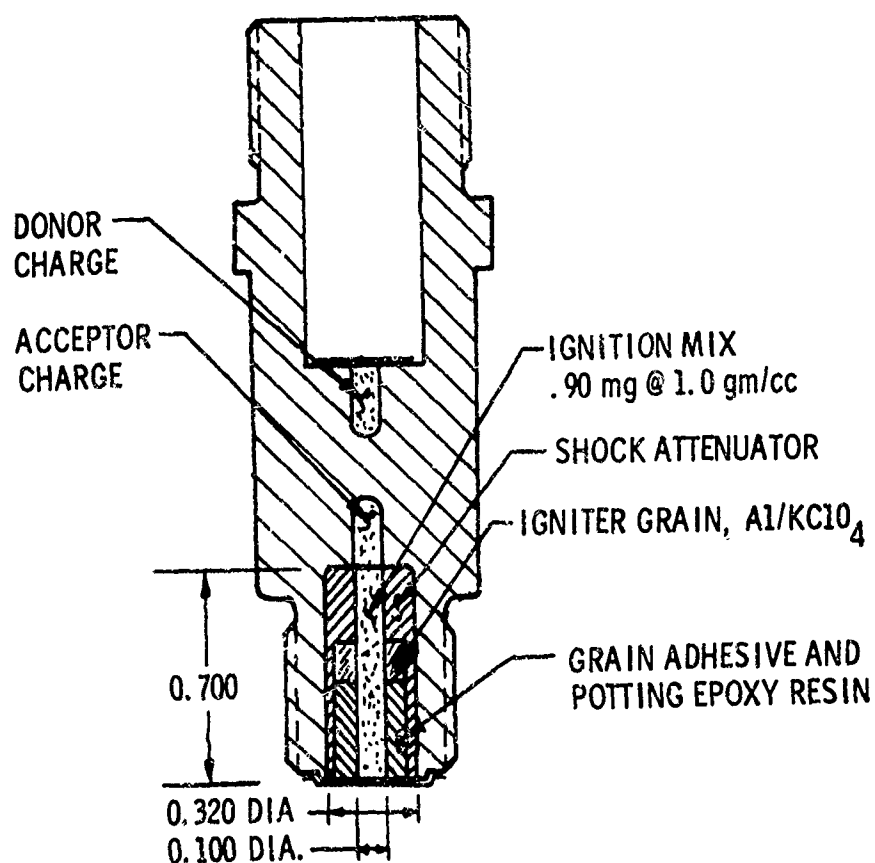
420 TO 800 psig IN 20.7 CC VOLUME

8 ms MAXIMUM DELAY TO PEAK PRESSURE

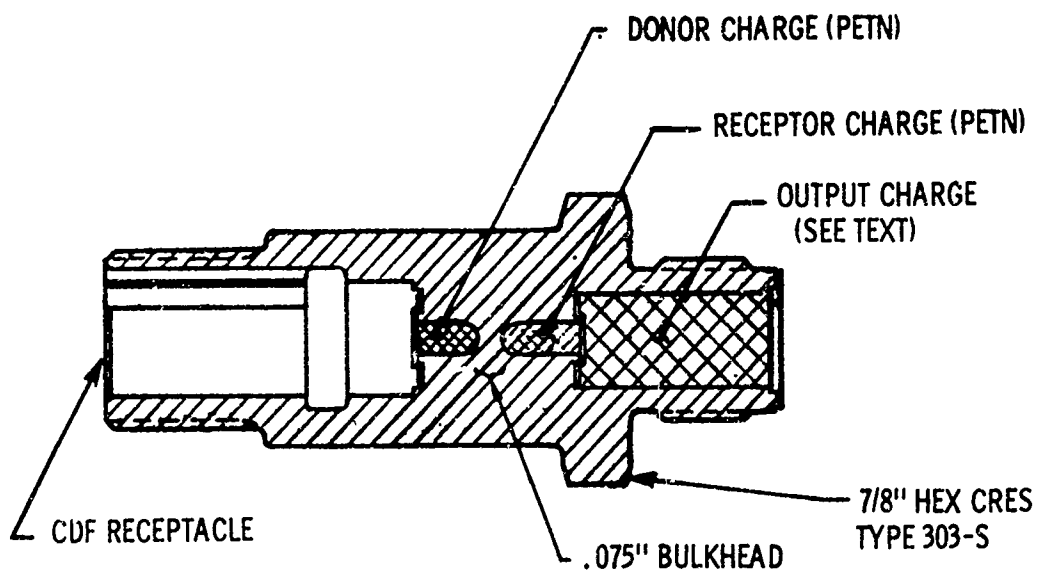
950 CALORIE MINIMUM HEAT OUTPUT

TBI CONFIGURATION AND REQUIREMENTS

FIGURE 5

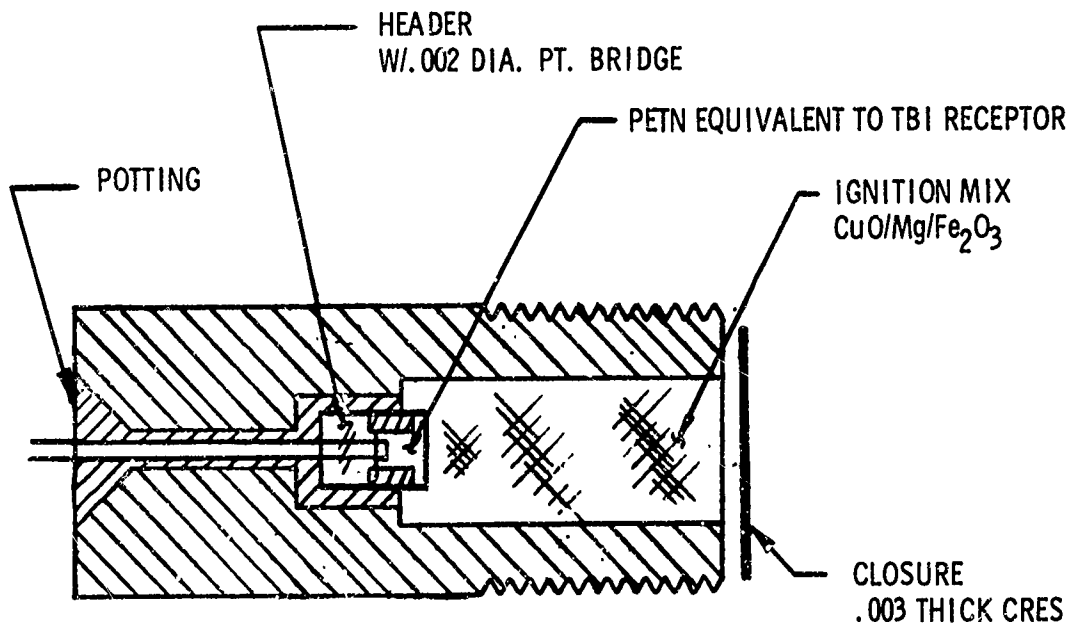


CONFIGURATION OF FIRST DEVELOPMENT UNITS  
WITH AN OUTPUT CHARGE  
FIGURE 6



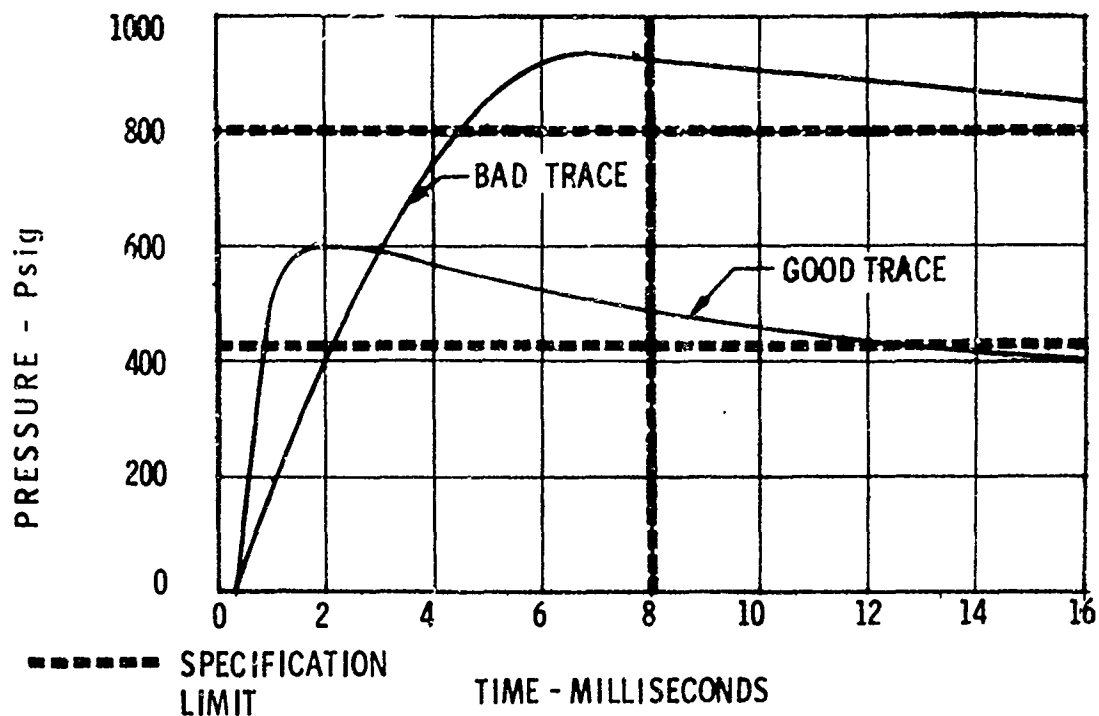
TBI CONFIGURATION USING LOOSE PYROTECHNIC

FIGURE 7



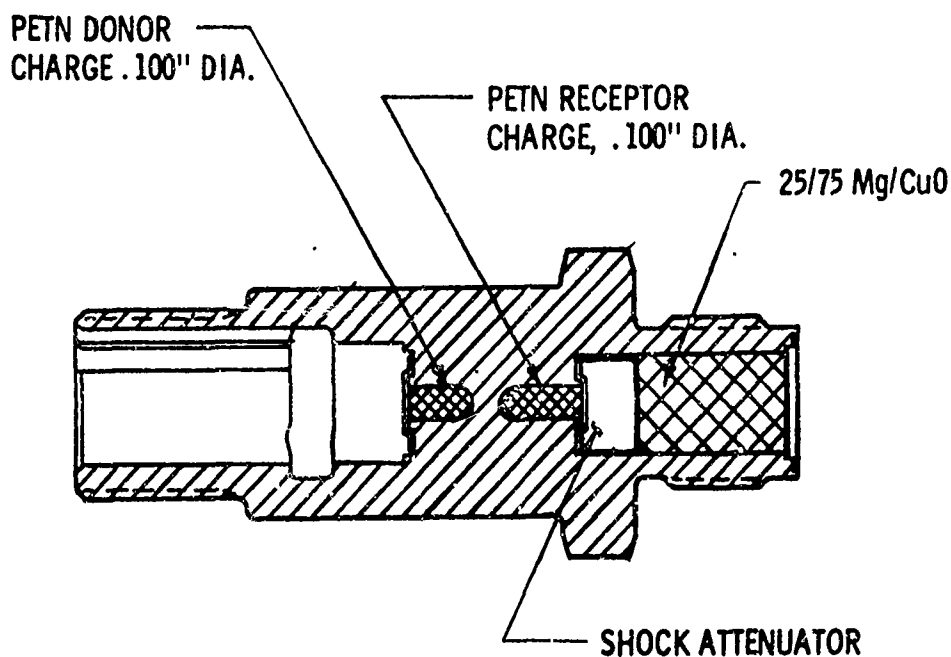
CONFIGURATION OF EBW INITIATED OUTPUT CHARGE EVALUATION UNITS

FIGURE 8

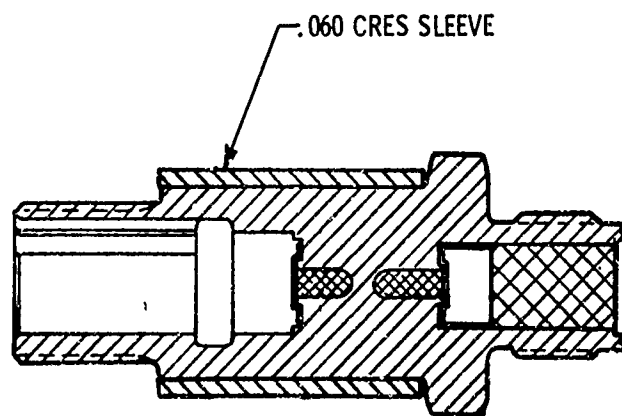
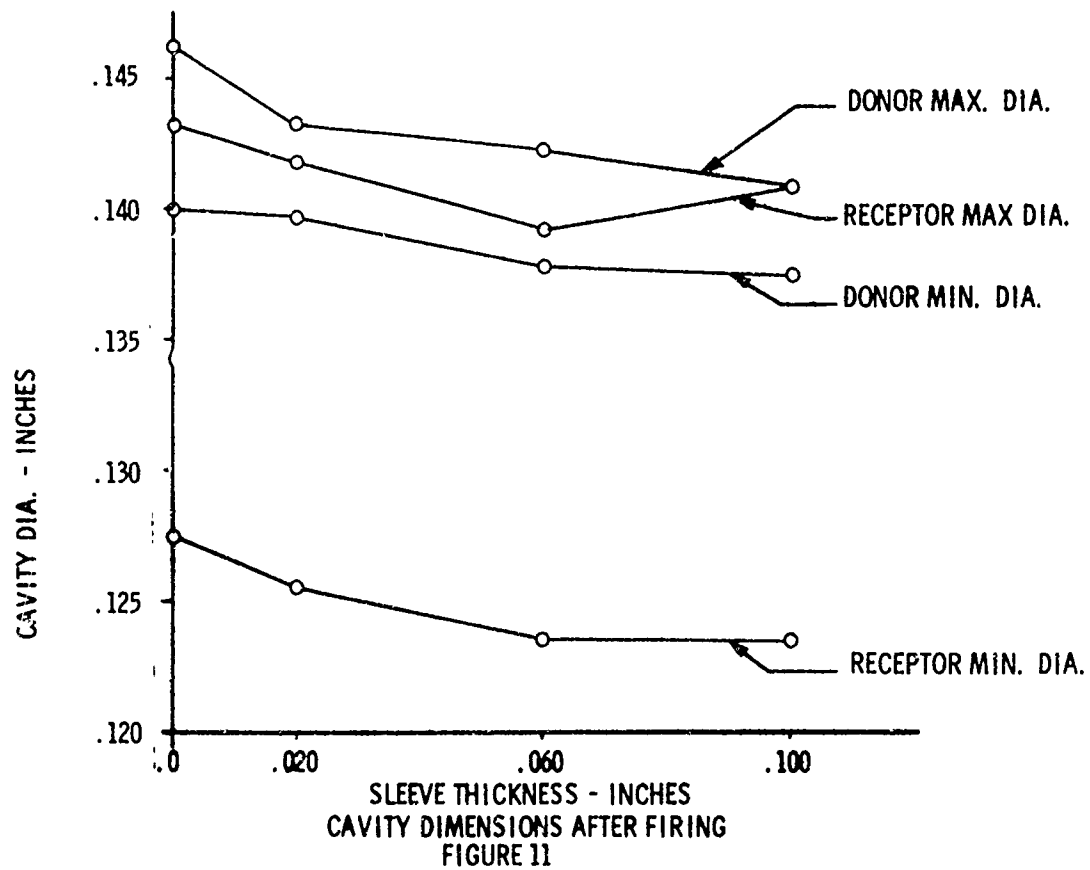


TYPICAL "GOOD" AND "BAD" P-t TRACES

FIGURE 9



TBI CONFIGURATION USING SHOCK ATTENUATOR  
FIGURE 10.



FINAL CONFIGURATION OF TBI

FIGURE 12

## 1-5 A RELEASE MECHANISM FOR STORED HIGH PRESSURE GAS

by

L. G. Bach and L. G. De Grace  
The Bendix Corporation  
Missile Systems Division  
Mechanical Engineering Department

### INTRODUCTION

The mechanism discussed in this paper is a simple, electro-explosively powered release valve for high pressure gas stored in a hermetically sealed container. It was designed to replace two valves used to release two sources of high pressure (2150 and 4150 psi) nitrogen in subsystems of a missile. The replaced valves utilized many elastomeric seals which frequently were sources of leakage. This leakage required a 60 day maintenance and replenishment cycle, causing a constant problem with spare parts and maintenance not only of the missile subsystems, but also of the shipboard high pressure charging equipment.

To eliminate these problems the systems have been modified to provide a minimum service-free period of three years. Development of the release mechanism was the essential key which made this possible. Although two valves were designed, the concept and essential parts are identical for both. The differences are primarily in packaging configuration.

### BASIC REQUIREMENTS

#### Hermetic Seal

Previous investigations indicated that designs utilizing elastomeric seals exhibited sufficient rates of leakage that they could not confidently be used for storage periods of more than 18 months at the required pressure. For

periods greater than this, hermetically sealed storage tanks are necessary.

Therefore, the release mechanism requires a hermetic seal.

#### Instant Release

Missile requirements dictate that the stored nitrogen be released virtually at "first motion" from the launcher. Acceleration sensitive devices are used to detect this motion and to initiate release action. One system was activated by an electrical signal from a "g" switch to a solenoid valve, the other was activated by a direct-acting, acceleration sensitive valve. Activation of the new valve had to be by similar acceleration sensitive devices, and have a total response time of less than 0.2 second.

#### Packaging

Logistics and cost dictated that the new release mechanism could not impose any major redesign of other system or missile parts. While not significant for other applications, two implications of this requirement are of general interest.

Electrical Power Limit:	10 amps per device at 26 vdc
Size:	small (approx. 2 in <sup>3</sup> )
Weight:	low (approx. 1 lb)

#### Contamination

Clearances of 0.0003 to 0.0005 in sliding parts of the systems using the gas, allow virtually no contamination of any kind. Therefore, the release device itself could not be allowed to generate contamination, a potential problem when considering the breaking of a hermetic seal.

## Reliability

Both systems are essential for a successful flight. Therefore, their reliability must be very high. A goal of .999 @ 95% confidence was established.

## DEVELOPMENT

### Initial Considerations

Previous investigations had shown that for single-shot applications such as this one, electro-explosive automatic valve designs are much less complex than mechanically operated valves, due to the high power-to-weight ratio of pressure cartridges. Suitable off-the-shelf valves were sought for this application. Designs examined in detail typically had two objectionable features. Nitrogen release was accomplished by a shear failure of a barrier, rupture of a diaphragm or equivalent devices. These methods of releasing nitrogen can generate possible contamination in the form of small particles. Such contaminants are an unacceptable reliability hazard in this application. The second objection was that one of the subsystems would have required extensive modifications and elastomeric seals would still be needed.

It was decided to attempt to use a rupture tube concept, but to control the rupture process so as to reduce the possibility of objectionable contaminants.

### The Concept

Figure 1 shows the basic elements of the concept which was developed into the final design. An off-the-shelf pressure cartridge is used to power a piston, which strikes the end of the tube causing a tensile fracture at the notch in the tube. The end of the tube folds back about the "hinge", releasing the stored nitrogen. The hinge-notch combination is the key, since it forces the rupture to occur in tension by allowing the piston to produce a bending

moment about the hinge. Tensile failure of the tube at the notch, rather than a shear failure greatly reduces the possibility of generating contamination.

#### Rupture Tube Design

The groove configuration is the critical parameter in the mechanism design. It must withstand the pressure to be stored with the same proof and burst margins as the pressure vessel, yet be capable of consistent fracture with a reasonably low force.

The relationship between notch root thickness and tube burst pressure was determined for Types 304, 321, and 446 stainless steel tubes with 0.291 I. D. nominal. These steels were selected first for welding compatibility with the storage tank materials, and secondly for notch sensitivity. The I.D. was selected to provide the required flow area. Figure 2 shows the basic notch configuration. Burst pressure test data is shown in Figure 3.

As seen in Figure 3, the experimental data showed some variation from the calculated values of burst pressure versus notch root thickness. This was due to variations in the amount of work hardening during machining and varying sharpness of the notch. The calculated values were based on an ultimate tensile strength of 90,000 psi which is approximately the same for the three materials tested. Type 304 stainless was chosen because it provided the cleanest notch fractures.

Based on pressure test and fracture bending moment data, a nominal notch root thickness of 0.0125 inch was selected. This value provided a more than adequate burst pressure of 16,500 psig. The large margin in notch root thickness provides for safety when handling pressurized storage tanks, and allowance for manufacturing tolerances.



The hinge is made by making an indentation in the tube before the notch is machined (see Figure 4). The hinge not only provides a strong point about which the top of the tube bends, but also serves to retain the end of the tube. This eliminates the possibility of contamination being generated by a loose tube-end striking the inner surfaces of the retaining body.

Several tubes were fractured by applying a force to the free end of the tube. Microscopic examination of the fracture area indicated an extremely uniform cutter-like edge on each half with no signs of chipping or slivering of the material. The static moment required to cause the notch to break was found to be approximately 150 inch-pounds, including approximately 10 in-lb to bend the "hinge." The tube was pressurized during the tests. Variations in tube internal pressures between 2000 and 4300 psig did not significantly affect the value of the fracture torque.

Determination of the rupture tube configuration permitted the sizing of the pressure cartridge load and piston effective diameter needed to break the tube in flight.

#### Piston and Firing Chamber Design

The firing chamber and piston designs are based on the desire to utilize a small, standard, inexpensive cartridge to power the device. The prototype piston and chamber configuration are shown in Figure 5.

The chamber had to (1) be strong enough to withstand the required pressures, (2) permit the piston to travel far enough to completely open the tube, (3) retain the piston after firing to prevent it from striking the walls of the device's body, and for safety in the event the device was fired outside the body of the mechanism.

Available space, the limitation on changes to existing hardware, and pressure (structural) safety requirements dictated the following key size relationships:

Notch Tube Lever Arm	$0.381 \pm 0.022$ in.
Active Piston Area	$0.125$ in <sup>2</sup>
Minimum Total Piston Travel	.250 in.
Nominal Chamber Volume	1 cc

The bullet nose of the piston provides a solid, point contact, such as would be obtained from a ball peen hammer. The O-ring prevents the products of the cartridge combustion from entering the nitrogen passages. The conical section of the piston fits into the conical section of the chamber, which acts as a stop for the piston.

#### Pressure Cartridge

An approximation of the piston pressure required to break the notched tube was made by the use of high-pressure-nitrogen/solenoid valve combination to simulate a pressure cartridge. A minimum value of 2400 psi was obtained.

The pressure cartridge selected for the release mechanism activation was supplied by McCormick Selph Associates. The unit is simple in design and similar cartridges are available from several sources. The basic cartridge was developed to produce a pressure of  $3600 \pm 500$  psig in a closed chamber of 2.0 cubic centimeters. The load weight was modified slightly to produce the required pressure for this application. It provides a peak pressure of  $4000 \pm 1000$  psig within 10 milliseconds in a volume of one cubic centimeter, when a minimum firing current of 4.5 amperes is applied. The five minute

minimum no-fire current is 1.0 ampere at 160°F and the 0.050 second sure-fire current is 3.1 amperes at 75°F. The minimum post-firing resistance is specified to be no less than 1000 ohms. The cartridge has demonstrated that it meets these requirements with 99.9% reliability at a 95% confidence level.

Cartridges were also tested for mechanical strength. Four cartridge shells were subjected to a burst pressure test with hydraulic fluid. Failure of the installation O-ring seals of two shells occurred at 9700 psig. The remaining two shells withstood 10,000 psig, the limit of the testing device, for a period of five minutes. Three cartridges were pressurized with nitrogen to 2150 psig. The purpose of this test was to ensure that the cartridge hermetic seal could withstand full systems pressure during special factory test. Visual examination after five minutes at pressure showed no sign of closure failure. Bridgewire resistances measured before and after the test showed no significant change.

## FINAL DESIGN

### Performance Tests

Pressurization system tests utilizing the cartridge activated release mechanism demonstrated satisfactory performance after two minor problem areas were corrected. First, was the inability of the hinge to consistently hold the end of the tube after nitrogen release. This was found to be due to work hardening of the hinge material during fabrication. A simple annealing operation after fabrication eliminated the problem.

The second problem was the inability to consistently develop sufficient energy to rupture the tube, if the piston was positioned against the tube prior to firing. Occasionally this even happened with cartridges having

125% loads. As a result of this finding, the spring clip arrangement shown in Figure 6 was added to the piston. Its function is to position the nose of piston 0.1 inch away from the tube prior to activation. This provides a consistent chamber volume and insures that an impact load will be applied to the tube.

The basis for this solution was a review of the previous nitrogen powered test data. This review showed that in all cases the minimum pressures required for tube rupture were obtained with the piston retracted from the notched tube. Further tests showed that a nominal 0.1 inch separation between the tube and the piston was optimal. The spring clip releases the piston by slipping out of the groove rather than by shearing off. Hence only a small additional load is imposed by the clip.

During the program, 37 system activation tests were made using the pressure cartridge activated release mechanism. The cartridge system has an activation time of approximately six milliseconds, well under the 0.2 second permitted by the prior system acceptance test specification. Activation time was measured from the time current was applied to the cartridge bridgewire to the time the regulator outlet pressure started to rise. No indication of contamination either from the rupture of the tube or products of combustion noted in any of the tests.

#### Environmental Tests

Two complete systems were subjected to the following environmental test program:

- |                        |   |
|------------------------|---|
| 1. Temperature Cycling | 20 cycles: 2 hr. @ -40°F; 2 hr. transition to 160°F; 2 hours @ 160°F; 2 hours transition to -40°F |
| 2. Random Vibration    | 17.4 g's RMS 20-2000 cps; 6 minutes in each of three mutually perpendicular planes                |
| 3. Boost Shock         | 25 g trapezoidal pulse, rise time 0.019 sec. hold time 0.036 second. One longitudinal shock       |
| 4. Handling Shock      | 50 g half sine pulse; 0.011 second period; 1 shock in each direction, mutually perpendicular axes |

After the completion of the environmental tests, each system was given an operational test, using missile circuits to energize the pressure cartridge to show compatibility.

Visual examination of release mechanisms and nitrogen storage tanks of each system made after completion of the performance tests showed that all performance requirements were met.

#### HERO CERTIFICATION

Design data has been submitted for certification that the pressure cartridge ignition circuit is not susceptible to Hazards from Electromagnetic Radiation to Ordnance (HERO). These systems are presently being tested in an overall missile HERO program.

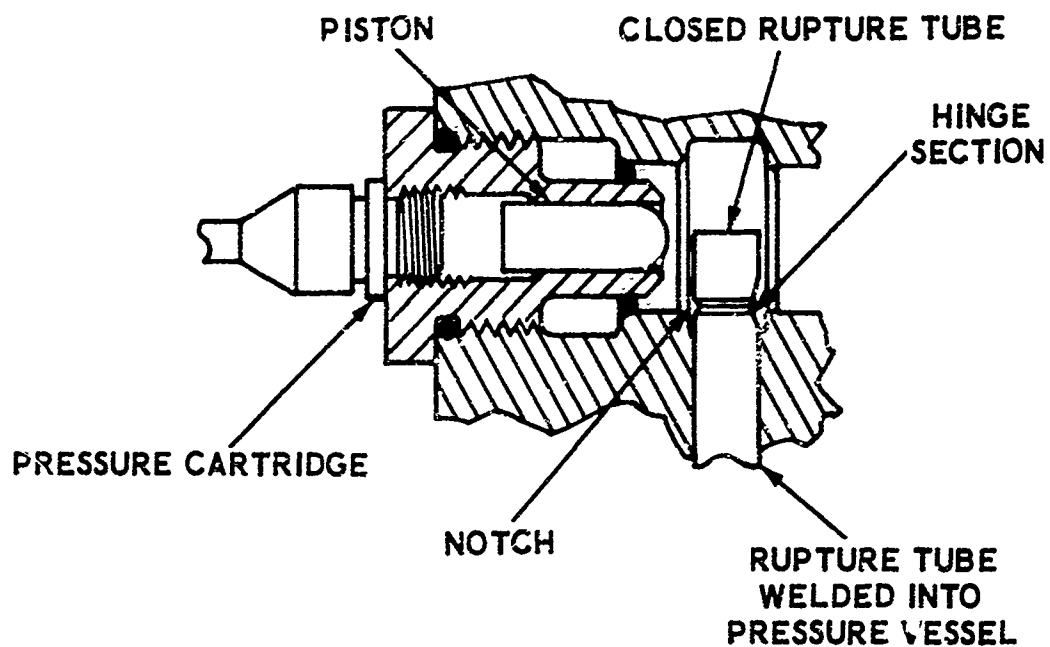


FIGURE 1 - FEATURES OF BASIC CONCEPT

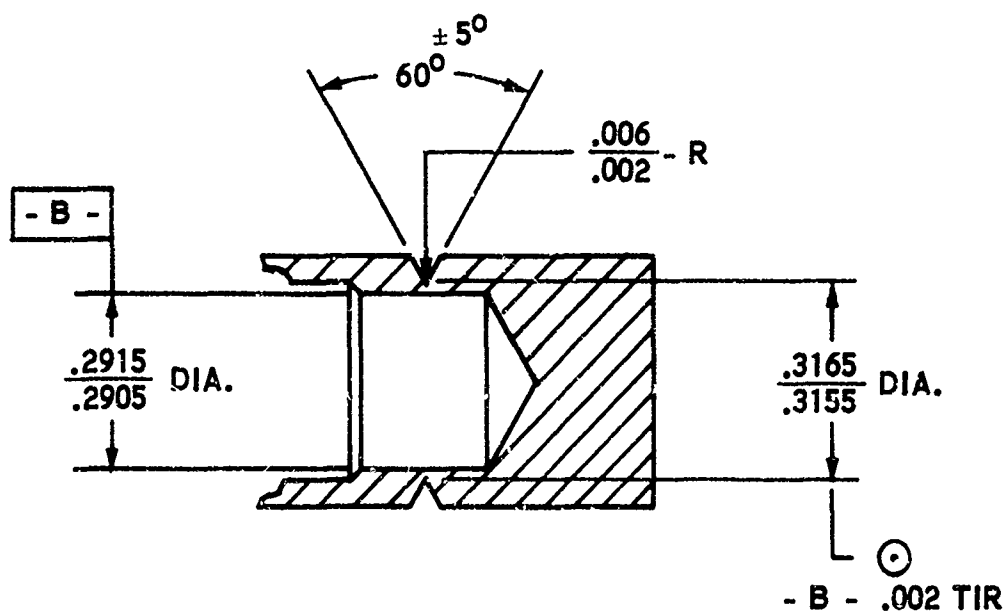


FIGURE 2 - RUPTURE TUBE NOTCH CONFIGURATION

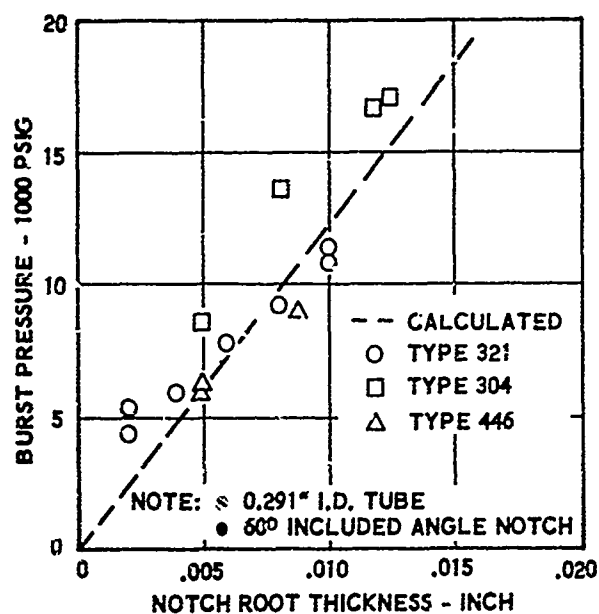


FIGURE 3 - BURST PRESSURE VERSUS NOTCH ROOT THICKNESS

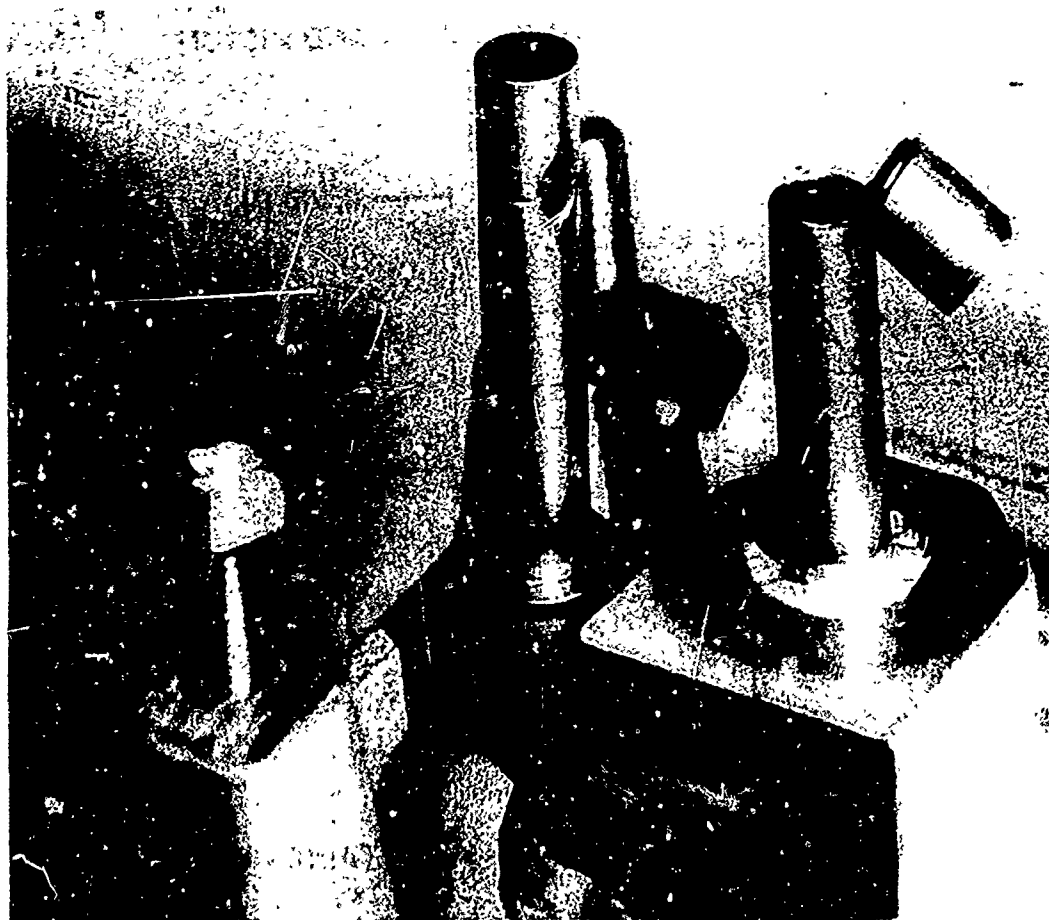


FIGURE 4 - RUPTURE TUBE HINGE IN FIRED AND UNFIRED CONDITION

PISTON TRAVEL, MAX: .250 IN.  
 PISTON AREA, ACTIVE: .125 IN.<sup>2</sup>  
 FIRING CHAMBER VOLUME, MAX: 1 cc

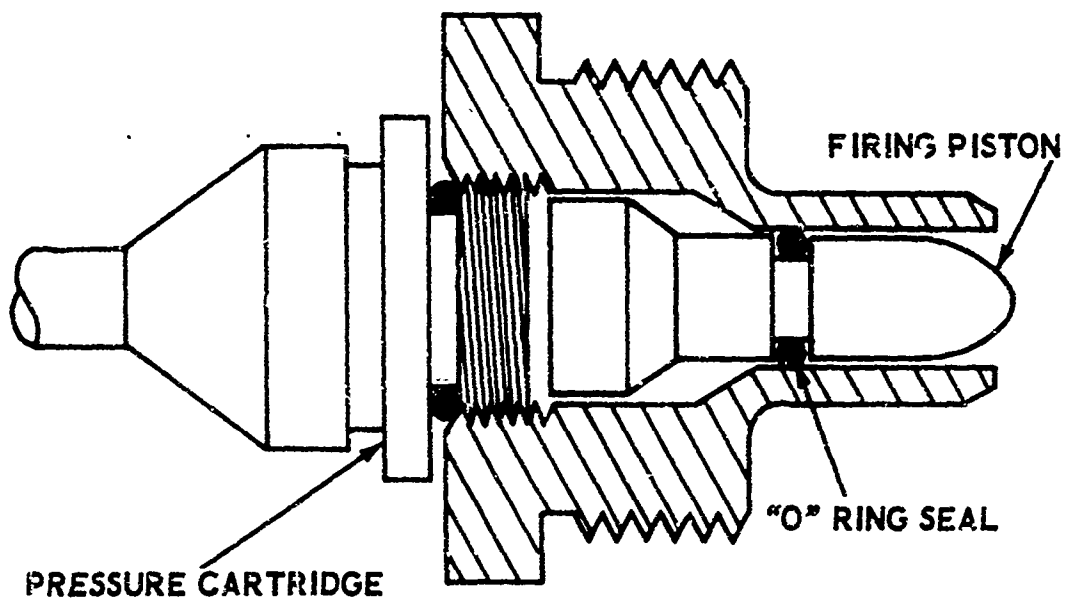


FIGURE 5 - FIRING CHAMBER AND PISTON

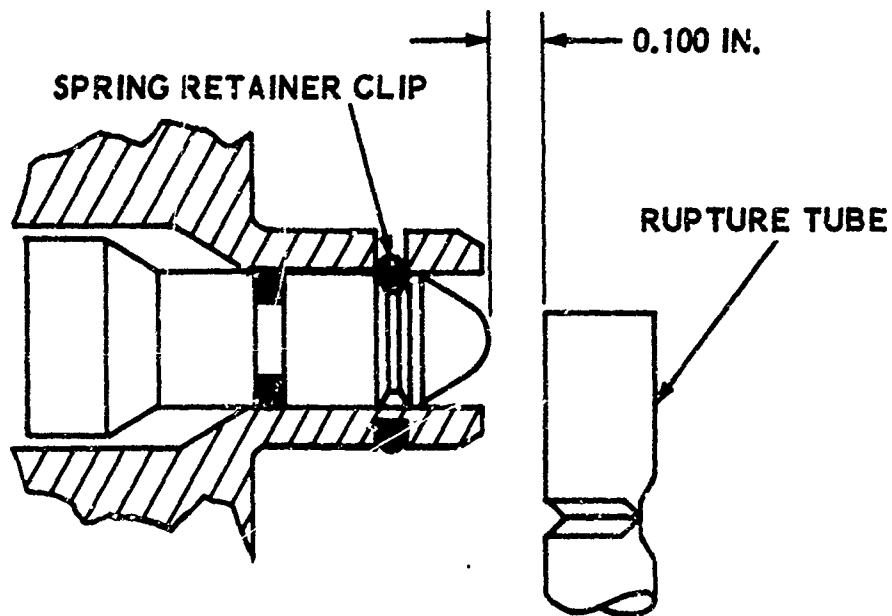


FIGURE 6 - FIRING PISTON AND RETAINER CLIP



## 1-6 VACUUM DEPOSITED THIN FILM BRIDGES IN ELECTROEXPLOSIVE DEVICES

by  
*J.R. Craig, Sandia Corp., O.M. Schroll, Sandia Corp.  
C.E. Simpson, Unidynamics/Phoenix, R. Blackshire, Unidynamics/Phoenix*

### INTRODUCTION

The increasing sophistication of requirements for electro-explosive devices has quite naturally led to an evolving development of manufacturing technology. Of prime importance in this technology is the development and production of new concepts of ignition bridge systems. The subject of this presentation is one of the most promising of these new developments - the Vacuum Deposited Thin Film Bridge. Over the past several years the Sandia Corporation and Unidynamics/Phoenix, a Division of UMC Industries, Inc., have collaborated in the development and production of several types of electroexplosive components employing thin film bridges.

### THEORETICAL CONSIDERATIONS

In designing any bridge system, attention must be given to thermodynamic factors such as the heat transfer from the bridge material to the surrounding media, the available heat sink within the allowable design geometry, and the thermal-time characteristics of the bridge system. In wire and, to a considerable extent in ribbon systems, the major portion of the heat transfer is along the bridge into the contact pins and then into the surrounding media. Relatively little heat is dissipated in other directions because of the small surface area of the wire and the uncertain contact between the wire and its surroundings as it expands during heating. The typically poor thermal conductivity of the explosive surrounding

the wire adds to the problem of heat dissipation. Since wire and ribbon bridges are rigidly constrained only at the welded or soldered end points, thermal expansion and movement occurs during exposure to environments such as thermal cycling or no-fire conditions, resulting in variations of bridge characteristics within a unit and between otherwise similar units.

With a film bridge design, however, the film is strongly bonded in intimate contact with the header and therefore is not subject to such movements. Also, since a film bridge is in more intimate contact with the substrate, heat is dissipated more readily, resulting in a lower temperature gradient and consequently a higher no-fire capability within a given component configuration. No-fire power capabilities of two to three watts can be achieved for electroexplosive devices containing dual film bridges and primary explosives such as lead styphnate or lead azide.

The thermal-time characteristic of the bridge also is of importance since this factor directly determines the bridge efficiency under both no-fire and all-fire conditions. The initial temperature rise rates of both wire and film bridges are equal, both being controlled by the thermal mass of the conductor. However, as more heat is generated, the film temperature rises at a slower rate than that of the wire because the film transfers heat to the substrate faster. This relationship is shown graphically in Figure 1. The effects of a constant

current pulse in a film bridge are very similar to those in a wire/ribbon bridge except that the no-fire power level of the film bridge can be substantially increased, thereby reducing the all-fire/no-fire power ratio and providing a greater design latitude. This is possible because (1) the large surface area of the film and the intimate bond between the bridge and the substrate increase the heat transfer capability, and (2) the heat transfer characteristics of the film are more stable than those of wire or ribbon configurations.

The capacitor discharge firing sensitivity of a film bridge can be varied rather widely. This type of firing pulse is usually delivered in a few microseconds and the sensitivity is primarily a function of the thermal mass of the bridge element since little energy is dissipated in this short time. It is also significant that the capacitor discharge sensitivity is substantially independent of the no-fire capability, which is a function of area and heat transfer characteristics.

#### FILM BRIDGE PARAMETERS

The physical and electrical properties, and hence the functional characteristics of thin film bridges depend on the following parameters: composition of the metal deposited, substrate (header) composition and surface conditions, temperature of substrate, composition and pressure of the bell jar atmosphere

during deposit, and the rate of deposit. The following paragraphs discuss these parameters and point up some general approaches that have been used to achieve production controls.

#### Bridge Material

The process of vacuum deposition is capable of fabricating films from an enormous variety of materials and many have been considered for the ordnance bridge application. Table 1 summarizes an evaluation of several likely candidates.

#### Substrate (Header) Material

Conventional ordnance device header materials (glasses and ceramics) are, in general, suitable for thin film bridges. For one-ampere/one-watt no-fire devices employing primaries such as lead styphnate or lead azide, the bridge area required for a glass substrate is approximately 0.0036 square inch, or 0.045 inch by 0.080 inch. For a ceramic ( $\text{Al}_2\text{O}_3$ ) substrate, the area is approximately 0.0006 square inch, or 0.025 inch by 0.025 inch. Either of these dimensions will fit nicely between 0.040 inch diameter pins on 0.094 inch centers in single or dual bridge designs. The use of a material with high thermal conductivity, such as beryllium oxide, would be required only in a very unusual application.

A polished surface finish is necessary for achieving desirable product uniformity and a high process yield. However, it is not a technical necessity. Surface cracks from grinding and

voids or cracks in ceramic-to-metal braze interfaces are critical defects. Cleanliness is also a critical factor and requires thorough processing.

Units in production at Unidynamics utilize both glass and ceramic substrates. For processing simplification, glass-to-metal seals with flush bridging surfaces are preferred over recessed designs, and separate ceramic substrates to be assembled after bridging are preferred over brazed ceramic headers.

#### Deposition Variables

Several variables are of significance in the vacuum deposition process. Those which are of primary concern are substrate temperature, deposition rate, and residual atmosphere in the vacuum chamber. Substrate temperature affects the mobility of the atoms as they condense onto the surface and largely determines the degree and type of crystalline structure in the metallic film. Deposition rate and residual atmosphere composition and pressure also influence the crystal structure by controlling the absorption of gaseous inclusions into the film during its formation. This controlled inclusion of gas atoms is of considerable importance in determining the electrical properties of the film, e.g., resistivity, temperature coefficient of resistance, and stability.\* The interrelationship of

\*Stability as used here is defined as the percentage change in resistance during a 24 hour anneal at 600° F in air atmosphere or its equivalent.

these variables is complex and not thoroughly understood. Figure 2 illustrates the general nature of the relationship between stability, deposition rate, and substrate temperature at a particular chamber pressure for a chromium film. At a different pressure the pattern will be reshaped. Figure 3 illustrates the relationship between temperature coefficient of resistance, stability, and resistivity.

#### VACUUM DEPOSITION EQUIPMENT

The major equipment used for thin film bridging at Unidynamics is shown in Figure 4. At the far left in the photograph is a laminar flow clean bench for handling clean headers and for header and tooling storage. At the right is a commercial thin film evaporator. The instrument console contains (from top to bottom) a deposit rate controller, vacuum gauge, automatic pressure controller, resistance monitor with manual and automatic shut off, current meters, and a substrate temperature controller. Bridging tooling for one device is shown on the table beside the bell jar.

#### THIN FILM BRIDGE PRODUCTS

Unidynamics/Phoenix has produced a number of electroexplosive devices employing vacuum deposited thin film bridges. The figures on the following pages present design and performance

data for some of these devices, as follows:

Figures 5 and 6 - Detonators

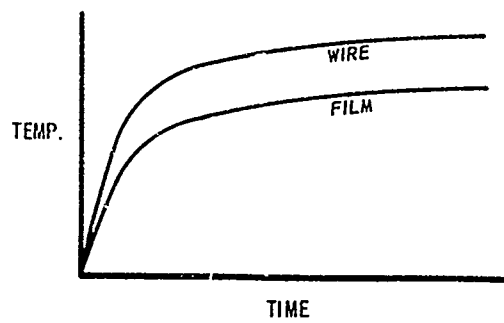
Figure 7 - Squib

Figure 8 - Actuator

In addition to producing these devices, Unidynamics has conducted several thin film programs for special test applications and advanced research.

**TABLE I**  
**EVALUATION RESULTS OF**  
**SEVERAL POTENTIAL FILM BRIDGE MATERIALS**

METAL	EASE OF FABRICATION	MECHANICAL PROPERTIES	CHEMICAL PROPERTIES	RESISTIVITY	TEMPERATURE COEFFICIENT OF RESISTANCE	STABILITY
GOLD	GOOD	GOOD	GOOD	LOW	HIGH	GOOD
PALLADIUM	GOOD	GOOD	GOOD	LOW	HIGH	VERY GOOD
ALUMINUM	GOOD	POOR	GOOD	LOW	HIGH	GOOD
COPPER	GOOD	POOR	POOR	LOW	HIGH	GOOD
SILVER	GOOD	POOR	POOR	LOW	HIGH	GOOD
CHROMIUM	DIFFICULT	GOOD	GOOD	MEDIUM	LOW	GOOD
NICKEL/CHROM.	DIFFICULT	GOOD	GOOD	MEDIUM HIGH	LOW	GOOD
OTHER ALLOYS	DIFFICULT	GOOD	GOOD	LOW TO HIGH	LOW TO HIGH	GOOD
PLATINUM	DIFFICULT	GOOD	GOOD	LOW	HIGH	GOOD
NICKEL	DIFFICULT	POOR	GOOD	MEDIUM	VERY HIGH	GOOD
TANTALUM	DIFFICULT	GOOD	GOOD	MEDIUM HIGH	LOW	GOOD



**FIGURE 1**  
GENERAL TEMPERATURE CHARACTERISTICS  
OF WIRE AND FILM

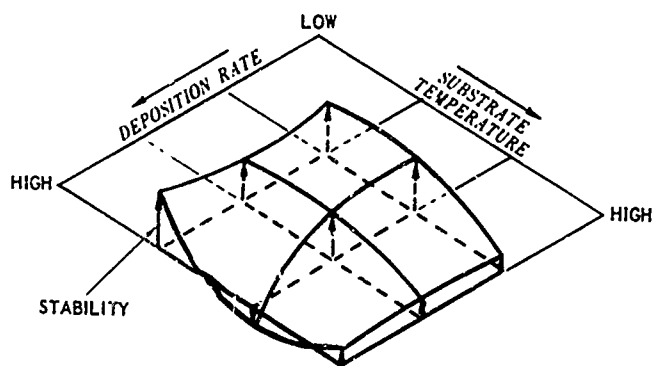


**FIGURE 2**  
RELATIONSHIP OF VARIABLES  
FOR CHROMIUM FILM  
AT A CONSTANT BELL JAR PRESSURE

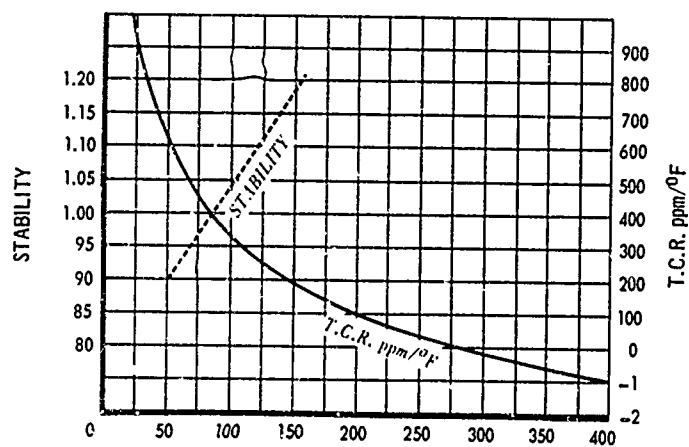


**FIGURE 3**  
GENERAL RELATIONSHIP BETWEEN  
RESISTIVITY, TCR, AND STABILITY





**FIGURE 4**  
**MAJOR VACUUM DEPOSITION EQUIPMENT**  
**IN USE AT UNIDYNAMICS**

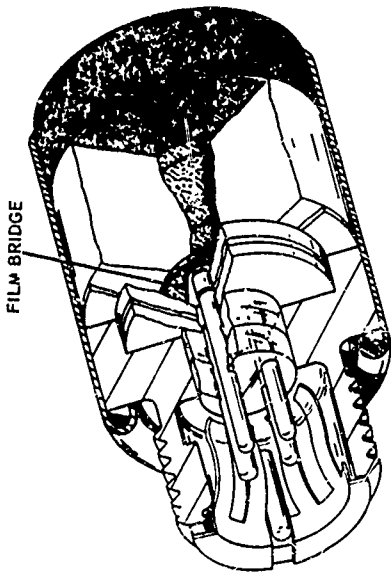


FIGURE 5A  
THIN FILM BRIDGE DETONATOR

MODEL 1107 DETONATOR	
BRIDGE MATERIAL	CHROMIUM
BRIDGE THICKNESS	6,000 Å
BRIDGE GEOMETRY	.023 "L X .025" W
TERMINAL MATERIAL	GOLD
SUBSTRATE MATERIAL	96% ALUMINA
BRIDGE RESISTANCE	1.00 ± .15 ohms
BRIDGE T.C.R.	< 500 ppm/°F
FIRST FIRE EXPLOSIVE	20/80 NLS/LA
NO FIRE: 5 min at 160°F	1.1 AMPERE/1.2 WATT BRIDGE
STATIC DISCHARGE	20 KV FROM 600 pf WITH 500 ohms SERIES R PIN-TO-CASE.
ALL FIRE: 5 amp at -65°F	TYPICALLY 3 MILLISECONDS
5 amp at +165°F	TYPICALLY 2 MILLISECONDS
CAPACITOR DISCHARGE	TYPICALLY 3.6 MICROSECONDS
CAPACITOR DISCHARGE MODE	100 V PEAK, 95% OF 150,000 ERGS IN 3.1 MICROSECONDS.

FIGURE 5B  
THIN FILM BRIDGE DETONATOR

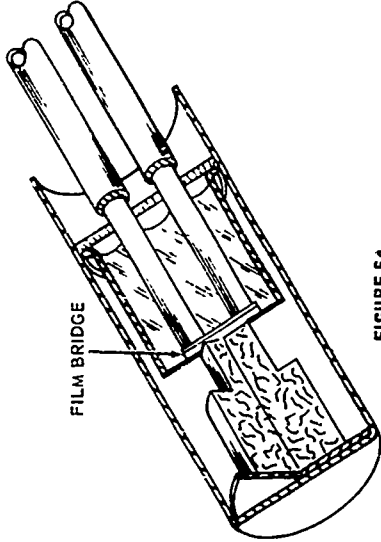


FIGURE 6A  
THIN FILM BRIDGE DETONATOR

MODEL 1104 DETONATOR	
BRIDGE MATERIAL	CHROMIUM
BRIDGE THICKNESS	5,000 Å
BRIDGE GEOMETRY	.055 "L X .080" W
SUBSTRATE MATERIAL	C7052 GLASS
BRIDGE RESISTANCE	1.00 ± .10 ohms
BRIDGE T.C.R.	< 500 ppm/°F
FIRST FIRE EXPLOSIVE	RD 1333 LEAD AZIDE
NO FIRE: 4 min at 160°F	1.0 ampere
30 min at room temp.	1.0 ampere
Static Discharge	20 KV FROM 600 pf WITH 500 ohms SERIES R PIN-TO CASE.
ALL FIRE: 5 amp at 75°F	Typically 2 milliseconds

FIGURE 6B  
THIN FILM BRIDGE DETONATOR

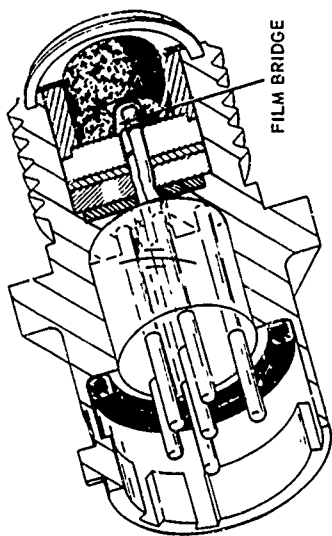


FIGURE 8A  
THIN FILM BRIDGE ACTUATOR

MODEL 5021 ACTUATOR	
BRIDGE MATERIAL	CHROMIUM
BRIDGE THICKNESS	6,000 Å
BRIDGE GEOMETRY	.023" L X .025" W
TERMINAL MATERIAL	GOLD
SUBSTRATE MATERIAL	96% ALUMINA
BRIDGE RESISTANCE	1.00 ± .15 ohms
BRIDGE T.C.R.	<500 ppm/°F
FIRST FIRE EXPLOSIVE	NORMAL LEAD STYPHNATE
NO FIRE: 5 min at 160°F	1.1 amp 1.2 watts/bridge without degradation
72 hrs at room temp.	1.1 amp 1.2 watts/bridge with minor degradation
Static Discharge	20 KV from 600 pf with 500 ohms series R pin-to-case.
ALL FIRE: 5 amp at -65°F	Typically 2.2 milliseconds
5 amp at +160°F	Typically 2.0 milliseconds
3.5 amp at -65°F	Typically 15 milliseconds

FIGURE 8B  
THIN FILM BRIDGE ACTUATOR

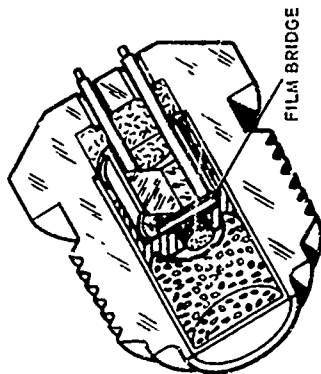


FIGURE 7A  
THIN FILM BRIDGE SQUIB

MODEL 1170 SQUIB	
BRIDGE THICKNESS	CHROMIUM
BRIDGE THICKNESS	5,900 Å
BRIDGE GEOMETRY	.044" L X .080" W
TERMINAL MATERIAL	GOLD
SUBSTRATE MATERIAL	EN-1 GLASS
BRIDGE RESISTANCE	1.00 ± 0.10 ohm
BRIDGE T.C.R.	<500 ppm °F
FIRST FIRE EXPLOSIVE	NORMAL LEAD STYPHNATE
NO FIRE: 5 min at 160°F	1.27 amp
5 min at 75°F	1.40 amp
ALL FIRE: 5 amp at 75°F	Typically 3.5 milliseconds
5 amp at -65°F	Typically 6.2 milliseconds
3.5 amp at -65°F	Typically 22 milliseconds
2.5 amp at -65°F	Typically 81 milliseconds

FIGURE 7D  
THIN FILM BRIDGE SQUIB

## DISCUSSION

Surface finish of the substrate is not critical for deposition of thin film bridges but a smooth surface is desirable to obtain uniform bridge qualities including a tight spread in electrical resistance. Direct deposition has been made on glass and ceramic materials as sealed in a header. The ceramics were first sandblasted to remove scale. The usable yield in this process is less than in the case where surface preparation is made, but the process will work.

Pin connections are made by means of a conductive silver-bearing epoxy cement. While the amine cured epoxies are used in some explosive devices, these amines may have adverse effects on specific explosive materials.

## 1-7 PRESSURE-CONTROLLED

### PROPELLANT-ACTUATED DEVICES

V.W. Drexelius and M.L. Schimmel  
McDonnell Aircraft Company  
St. Louis, Missouri

#### INTRODUCTION

Propellant-Actuated Devices (PAD) are used for aerospace applications to perform a variety of functions including personnel ejection, canopy removal, and parachute deployment. Generally, these units exhibit high-peak breech pressures and associated structural reaction loads. McDonnell Aircraft Company has recently developed a parachute catapult (patent pending) which operates at controlled, uniform pressure (high piezometric efficiency) permitting a significant increase in performance flexibility.<sup>1,2</sup> Prior to this development, the following factors prevented or discouraged a more extensive use of PAD.

- (1) Part of the weight advantage of PAD is offset by the substantial structure required to withstand the impulsive loads.<sup>3</sup>
- (2) A second disadvantage is the relatively long development time normally associated with PAD. Reference (4) details a typical program, employed by Frankford Arsenal, in which a minimum of 24 test firings are made with "boilerplate" models before prototype, or flight weight, evaluation begins. Computer programs for predicting performance have been suggested as a means of expediting PAD design.<sup>5</sup>
- (3) PAD generally must perform satisfactorily over a wide range of ambient temperatures. Thus, the PAD output must be adequate at the lowest operating temperature, while the weight of the device itself as well as that of supporting structure is determined by the pressure and loads associated with the highest operating temperature.

The design principle of the McDonnell pressure-controlled device, which essentially eliminates the above disadvantages, is based on use of crushable honeycomb to control operating pressure within narrow limits. The use of similar honeycomb elements to quantitate explosive output was described at the Fifth Symposium on Electroexplosive Devices.<sup>6</sup> The pressure-controlled PAD design is presently being used for recovery parachute deployment of the F-111 Crew Module, built by McDonnell under contract to General Dynamics Corporation. When incorporated into the Module, the device fulfilled requirements for increasing the velocity of parachute deployment by 50 percent without modifying support structure or increasing catapult operating pressure. Ballistic principles involved are illustrated in the following sections by comparing the design, development, and performance of both the original, conventional F-111 catapult, and the presently employed pressure-controlled catapult.

#### CONVENTIONAL CATAPULT

The initial catapult requirement for the F-111 Crew Module was to deploy a 115-pound recovery parachute at a velocity of 30 ft/sec. The catapult was of conventional design, and its development and performance are described in order to provide a baseline for comparison with the pressure-controlled catapult.

##### Design

Figure 1 illustrates design of the initial F-111 Crew Module catapult. Initiation is accomplished by redundant Shielded Mild Detonating Cord (SMDC) inputs which deflect a deformable firing pin to fire the #49 primer. The primer ignites zirconium, barium chromate ignition material, which in turn ignites black powder for initial pressurization, and 5.5 grams of double base, multiperforated granular propellant, typical of that used in similar catapults. Combustion pressure acts on the head of the inner barrel, and part of the combustion gases is ported through the pressure bleed passage to the annulus between the inner

and outer barrels to enhance snubbing at end of stroke. The inner barrel is attached to a parachute pan which transmits force to the parachute throughout the catapult stroke.

#### Development

The problems encountered during development were typically a result of the wide range of operating temperatures,  $-65^{\circ}$  to  $200^{\circ}\text{F}$ , combined with the requirement for a minimum weight design. Pressure-time curves obtained over this temperature range (Figure 2) illustrate the nature of the problem. When the catapult was fired at  $+200^{\circ}\text{F}$ , a pressure spike of 3000 psi resulted. The design of both the catapult and support structure was based on this value, even though the catapult generally operated below 2000 psi. While the pressure spike could be reduced by increasing the initial free volume, this resulted in unacceptable ignition delays at  $-65^{\circ}\text{F}$ . The curves shown in Figure 2 were considered an optimum trade-off, and the design was released for qualification testing.

#### Performance

Qualification testing consisted of a total of 60 catapult firings, divided between high, low, and ambient temperatures, after exposure to various military environments. These included vibration, shock, temperature cycling, 6-foot drop, humidity, salt spray, and sand and dust. Results of these tests are tabulated in Figure 3.

#### PRESSURE-CONTROLLED CATAPULT

Shortly after qualification testing of the 30 ft/sec catapult, F-111 Crew Module systems tests showed that parachute deployment characteristics were not optimized over the entire escape envelope. Specifically, more rapid parachute opening was desired at "zero-zero" conditions; that is, initiation of the escape system when the Crew Module had no forward velocity and was at ground level. An investigation of various alternative means of accomplishing more rapid parachute opening concluded that minimum redesign and weight penalty would be incurred by

increasing the parachute ejection velocity to 45 ft/sec. However, the required 50 percent increase in velocity is equivalent to a 225 percent increase in catapult energy output. Because Crew Module structure supporting the catapult had already been designed and fabrication begun, it was most desirable not to exceed peak structural loads imposed by the 30 ft/sec catapult. Examination of the pressure-time curves of Figure 2 reveal a moderate piezometric efficiency. If the criteria of no increase in structural reaction loads were to be achieved, the piezometric efficiency of the ballistic system had to be increased. The conventional method of increasing this efficiency includes the selection and/or development of slow-burning propellant to provide a square-shaped pressure-time curve. Generally, this requires a considerable expenditure of time and funds and results in a greater variation in performance over the temperature extremes because of burning rate-temperature sensitivity. Previous work at McDonnell<sup>7</sup> showed that using precalibrated crushable honeycomb elements to measure output of propellant cartridges resulted in combustion taking place at essentially constant pressure, independent of ambient temperature. Accordingly, a honeycomb element with crush characteristics as illustrated in Figure 4, was selected for use in the 45 ft/sec catapult in an attempt to control operating pressure at a level no higher than the maximum experienced with the 30 ft/sec catapult, thus eliminating the need for structural redesign.

#### Design

The pressure-controlled catapult is shown in Figure 5. The design changes required were: 1) increase the cartridge propellant charge, 2) add a honeycomb element and sliding inner piston, and 3) lengthen the inner and outer barrels in order to accommodate the honeycomb element. Pressure control is achieved by crushing of the honeycomb when the pressure above the piston results in a load greater than the honeycomb can withstand. Since, as shown in Figure 4, after initial crippling, the honeycomb crushes at an essentially constant load for



up to 75 percent of its free length, use of the honeycomb within these limits closely regulates catapult pressure.

#### Development

Figure 6 illustrates typical pressure-time curves obtained during extreme temperature test firings of the pressure-controlled catapult. Note the increased piezometric efficiency and resulting absence of the pressure spike previously found in the high temperature firing of the conventional catapult. This eliminated the need for structural redesign. More initial free volume was provided by the design of the sliding inner piston, and the rate of pressure rise is considerably slower than for the conventional catapult. Possibly, incorporation of the honeycomb element eliminates, or at least reduces, the need for initial free volume.

#### Performance

The pressure-controlled catapult was subjected to the same qualification program as the conventional catapult. In this case, however, the required parachute ejection velocity was  $45 \pm 10$  ft./sec. The catapult successfully passed qualification with the performance tabulated in Figure 7. Of particular importance is the evidence that catapult performance showed no statistical difference over the environmental temperature extremes. A significant difference exists in the extent of honeycomb crush and therefore in the energy absorbed by the honeycomb at the three temperatures. These differences may be accounted for by the rates of heat transfer from the combustion gases into the catapult tubes at each temperature. That is, at  $-65^{\circ}\text{F}$ , the rate of heat loss into the tubes is quite high, and there is little excess energy to be absorbed by the honeycomb, while at  $+200^{\circ}\text{F}$ , the rate of heat loss is much less, and more energy is absorbed by the honeycomb. The burning-rate versus temperature sensitivity has also been significantly reduced over conventional applications.

A photograph of the pressure-controlled catapult is shown in Figure 8, and a tabulation comparing it to the conventional catapult is shown in Figure 9.

## OTHER APPLICATIONS OF PRESSURE-CONTROLLED PAD

### Adjustable Output Actuator

Controlling PAD operating pressure with crushable honeycomb provides a degree of flexibility not usually available. For example, Figure 10 illustrates how the output of an actuator may be adjusted by selecting a honeycomb element of the desired crush strength. No change in cartridge is required. At the outset, the cartridge should be sized for the largest expected output requirement. If later system tests indicate that a lower output is required, a weaker honeycomb element can be substituted thereby minimizing redesign, retest, and requalification.

### Regulated Pressure Source

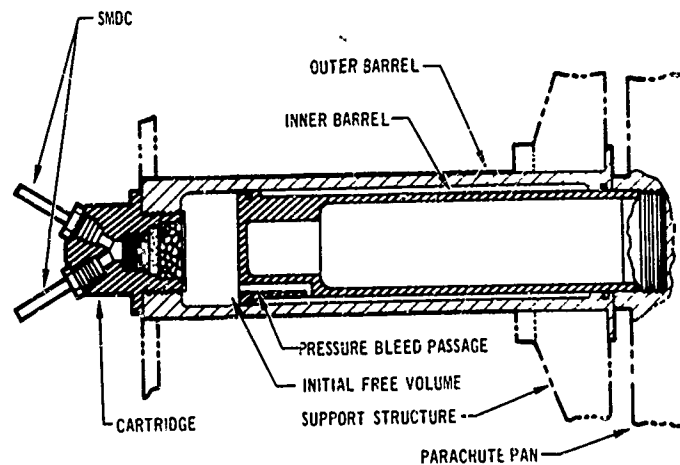
Many aerospace applications require a source of regulated high-pressure gas which is commonly supplied by a pressurized gas bottle equipped with an explosive valve to release the gas and a pressure regulator to deliver the gas at the desired pressure. The design shown in Figure 11 combines the above three functions in a single device which provides regulated gas pressure from a cartridge.

### CONCLUSIONS

- ° The use of crushable honeycomb in PAD provides a means of controlling operating pressure and resulting structural loads within narrow limits.
- ° Ballistics are simplified because the propellant is burned at a constant, predictable pressure.
- ° Output variation at extreme temperatures is reduced or eliminated.
- ° PAD output can be varied by selecting a honeycomb element of the desired strength. No cartridge change is required.
- ° This design technique also may be used to provide a source of regulated gas pressure.

# REFERENCES

- 1 Schimmel, M.L. and Fortenberry, J.D., "Pressure Controlled Propellant Actuated Devices, McDonnell Company Report F145, 15 December 1966.
- 2 Pressure and Load Control for Propellant Actuated Device, U.S. Patent Department Serial No. 679,837, 1 November 1967.
- 3 Christensen, K.C. and Narahara, R.M., "Spacecraft Separation," Space/Aeronautics, July 1966.
- 4 Ordnance Engineering Design Handbook, ORDP 20-270, "Propellant Actuated Devices," July 1961, p. 113.
- 5 Buie, W.F., "Analysis of Striking Propellant Actuated Devices," Frankford Arsenal Memorandum Report M67-19-1, January 1967.
- 6 Schimmel, M.L. and Drexelius, V.W., "Measurements of Explosive Output," Proceedings of the Fifth Symposium on Electroexplosive Devices, June 1967.
- 7 Scott, C.L., "Use of McDonnell Energy Sensor to Measure Output of Power Cartridges," McDonnell Aircraft Corporation Report WR7650, July 1965.



CATAPULT	
LENGTH (IN.)	13.8
OUTSIDE DIAMETER (IN.)	2.4
STROKE (IN.)	9.0
INNER BARREL AREA (SQ IN.)	3.8
CARTRIDGE	
PRIMER	No. 49 (G-11)
IGNITION MATERIAL	0.4 GM. ZIRCONIUM, BARIUM CHROMATE
PROPELLANT	4.7 GM. BLACK POWDER
	5.5 GM. HPSK 5250.95

Figure 1 - Conventional Catapult Design

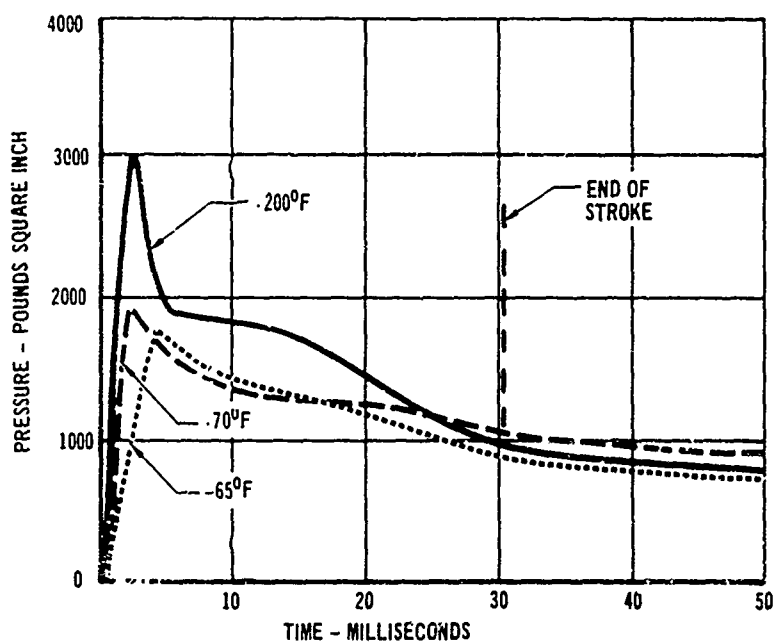


Figure 2 - Conventional Catapult Development Firings

TEMPERATURE (°F)	PARACHUTE EJECTION VELOCITY (FT/SEC)			
	AVERAGE	HIGH	LOW	STANDARD DEVIATION (σ)
-65	27.4	33.3	20.0	4.0
70	29.3	35.9	21.6	3.6
200	30.5	38.3	22.0	4.5

Figure 3 - Conventional Catapult Performance

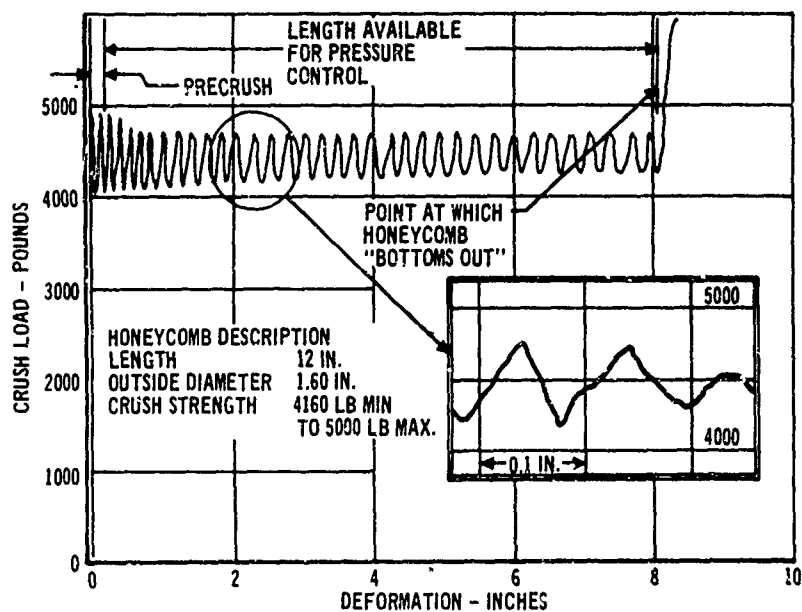


Figure 4 - Honeycomb Crush Characteristics

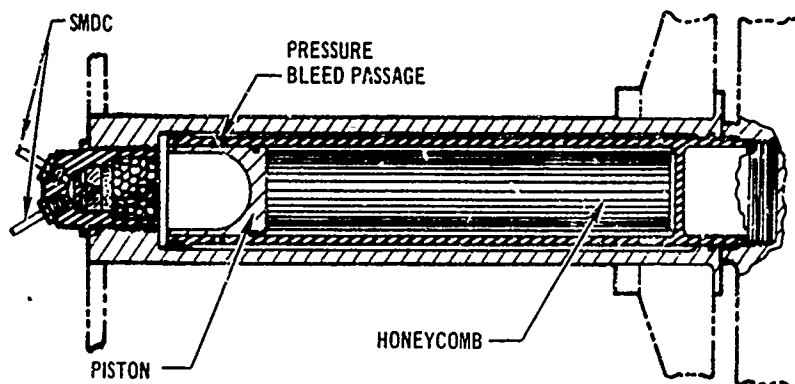


Figure 5 - Pressure-Controlled Catapult Design

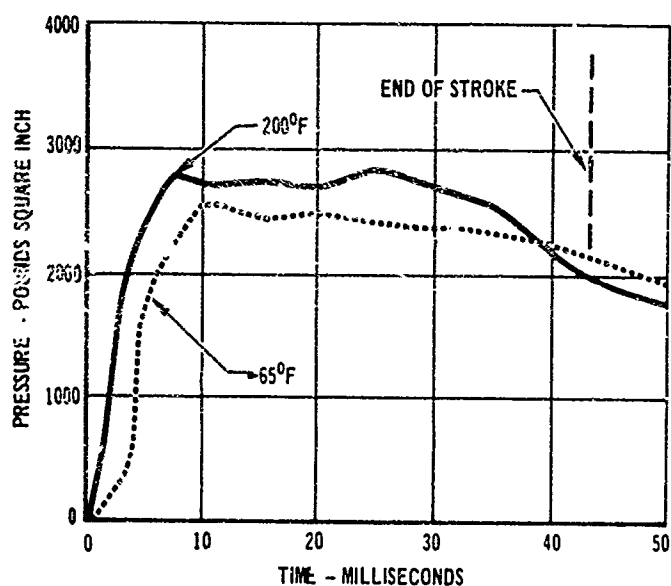


Figure 6 - Pressure-Controlled Catapult Development Firings

TEMPERATURE (°F)	PARACHUTE EJECTION VELOCITY (FT SEC)				AVERAGE HONEYCOMB CRUSH (INCHES)
	AVERAGE	HIGH	LOW	STANDARD DEVIATION (σ)	
-65	44.2	48.5	41.6	2.1	1.0
70	43.4	45.5	37.8	2.1	2.9
200	44.2	47.6	40.4	2.3	6.0

Figure 7 - Pressure-Controlled Catapult Performance

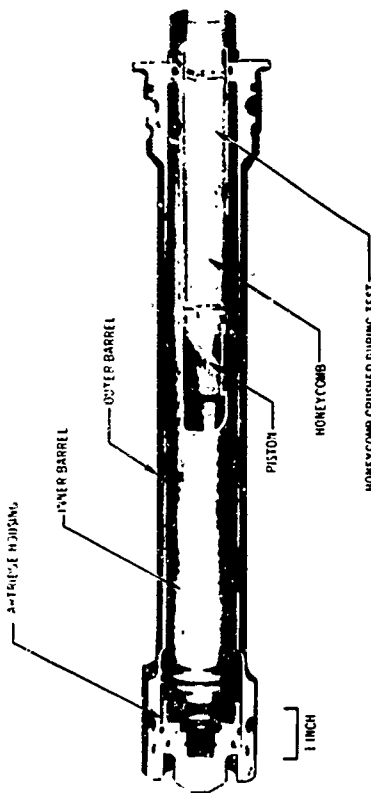
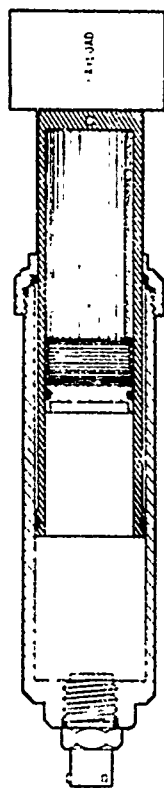


Figure 8 - Pressure-Controlled Catapult



ASSUME EJECTED PAYLOAD - 50 POUNDS  
ACTUATOR STROKE - 30 INCHES

HONEYCOMB CRUSH STRENGTH (LB)	PAYLOAD EJECTION VELOCITY (FT/SEC)
1000	57
750	49
500	40

Figure 10 - Adjustable Output Actuator

	CONVENTIONAL	PRESSURE CONTROLLED
PARACHUTE VELOCITY (FT/SEC)	30	45
ENERGY OUTPUT (FT/LB)	3610	3620
WEIGHT OF PROPELLANT (GRAMS)	10	70
PEAK PRESSURE (PSI)	3050	2700
LENGTH OF CATAPULT (IN.)	13.8	19.5
WEIGHT OF CATAPULT (LB)	3.3	4.6
CATAPULT OUTPUT PER UNIT WEIGHT (FT/LB/LB)	400	765

Figure 9 - Comparison of Conventional Versus Pressure-Controlled Catapult

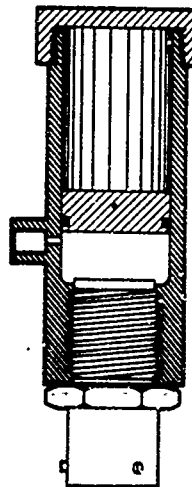


Figure 11 - Regulated Pressure Source

## 1-8 DETACHED ELECTRODE ELECTROEXPLOSIVE DEVICES\*

By D.H. Chamberlain and R.H. Stresau

R. Stresau Laboratory, Inc., Spooner, Wis.

### INTRODUCTION

A "detached electrode electroexplosive device" doesn't look like an electroexplosive device (Figure 1a). It is more like a stab or flash initiated primer or detonator, from which it differs only in that the sensitive-end closure disc is generally thinner and of a high resistivity alloy. By itself it is not an electroexplosive device. Only when it is contacted by an external electrode of suitable design, (Figure 1b) does it assume the properties of an electro-explosive device.

The concept of the detached electrode electroexplosive device was disclosed by the R. Stresau Laboratory to the Naval Ordnance Laboratory, Corona, in November 1964. Interest was expressed at that time but, due to the lack of specific applications, no task was assigned under the then existing contract to reduce the concept to practice.

---

\*Based on work performed for the U. S. Naval Weapons Center, Corona Laboratories, Corona, California under Contract No. N00123-67-C-0508.

A few internally sponsored experiments yielded interesting results, some promising and some discouraging, during 1965, 1966, and 1967.

Toward the end of 1967 a task was assigned by the Naval Weapons Center, Corona Laboratories (successor to the Naval Ordnance Laboratory, Corona) to study the feasibility of extending the concept described above to include stab as well as electrical sensitivity. The results of this investigation are given in Reference 1. The promising results of this investigation led to the assignment of a task to study the feasibility of an application to a specific safety and arming device (of the type commonly referred to as the "Mickey Mouse" safety and arming device because of an imagined resemblance to the watch of that name). This study has been reported in Reference 2.

In late 1968 an "internal arming electric detonator", based on the concept described above, was proposed, and a few experiments have been performed to develop design criteria for such a device.

In this paper an effort will be made to convey the data regarding detonators based on this concept which have been obtained to date.

#### DETONATOR DESCRIPTION

##### Design and Construction

Depending upon the properties desired and the conditions



under which it is to be used, a detonator in accordance with the general concept outlined above might be of any of several designs. However, all of the detonators used in this investigation (except a few which were the subject of very preliminary tests) were of the construction described below.

The typical detonator of this investigation had a case of stainless steel hypodermic needle tubing, one end of which was closed by a very thin disc of stainless steel secured to the case by means of a 360° resistance seam weld. The flash and priming charge, a stab-sensitive priming mix, was loaded directly against the closure disc and the loading completed as shown in Figure 2 and 3. In most experiments, sewing needles were used as combination electrode-firing pins.

Initially, the stab-electric detonator was the small unit shown in Figure 2. This unit proved very interesting, but it was suggested that the detonator be made with dimensions more similar to those of the Stab Detonator M-55. It was then decided to try a unit to fit designs under current consideration, as shown in Figure 3. To obtain a proper weld of the 0.0001 in. stainless steel film to the tubing, ten 300 mfd condensers charged to 290 V were discharged through the detonator-holder electrode (Figure 4) and the brass foil electrode. The unit was

then placed in a die and the stainless foil was punched cleanly from the tube, leaving the end covered. When loaded, the detonator was placed foil end down on a perfectly flat base to preclude tearing of the stainless steel. When loaded, the units are handled gently due to their stab sensitivity.

#### Explosives Tested

Explosive materials tested included RD-1333, PVA lead azide, dextrinated lead azide, silver azide, NOL-130 priming mix, NOL-130 priming mix made with materials of extra fine particle size, RDX, and NOL Varicomps. Descriptions of these materials are as follows:

1. RD-1333 (H) lead azide purchased from Hanley Industries, St. Louis, made in accordance with the recipe of Dr. Taylor. RD-1333, which is made in a carboxy methyl cellulose solution, has properties similar to those of PVA lead azide.
2. RD-1333 (D) lead azide purchased from E. I. DuPont de Nemours & Co. in June, 1967.
3. PVA (polyvinyl alcohol) lead azide purchased from the Olin Mathieson Chemical Co. in July 1960 and certified by that company to be in accordance with MIL-L-3055 (dated 30 Sept. 1945) and amendment #1 (dated 24 March 1952) and E. C. O 23505-S-ANR. Polyvinyl alcohol lead azide is a

patented proprietary preparation of the Olin Mathiesen Chemical Co.

4. Dextrinated lead azide purchased from DuPont in June 1967, and certified by that company to be in accordance with MIL-L-3055 (dated 30 Sept 1945) and E. C. O 23505-S-ANR.

5. Silver azide (H-4) purchased from the Hanley Industries in Nov. 1967. Microscopic examination of this material indicated that its particle distribution is from 2 to 50  $\mu$ .

6. Silver azide (H-1) purchased from Hanley Industries in Aug. 1966, having a particle distribution of less than 2  $\mu$ .

7. RDX (X-334) Type B, Class A, furnished by NOL/White Oak; made at Holston Ordnance Works by the Bachman process.

8. RDX (X-334) Type B, Class E, furnished by NOL/White Oak for general use in connection with work for NOL/Corona. Class E RDX per specification must pass a No. 325 mesh screen. Microscopic examination of this material indicates that its distribution ranges from a few to 44  $\mu$ , which will just pass the No. 325 screen.

9. RDX (E-2) purchased from Canadian Arsenals Limited (their batch E-40) in Aug. 1964. This material is certified to meet the requirements of U. S. Specification MIL-R-00398C (Ord.). Microscope examination shows it to be appreciably

finer than RDX X-177, ranging up to about 25  $\mu$  maximum particle diameter.

10. NOL-130 Priming mix, mixed in accordance with the standard procedure and compositions with the following exceptions:

a. Antimony sulphide-antimony trisulphide, red technical grade, quality control Code #5; Bell Co, Rutherford, N. J.

b. Barium nitrate - Mallinckrodt Analytical Reagent, Mallinckrodt Chemical Works, St. Louis. Meets A. C. S. specifications.

c. Lead Azide - RD-1333 (H) lead azide (see 1. above).

11. NOL-130 extra fine particle size priming mix, mixed in accordance with the standard procedure and compositions as in 11. above, with the following exceptions:

a. The barium nitrate is hand shaken for 20 min, using a U. S. No. 140 sieve. Only the portion passing through the sieve is used.

b. The lead azide is polyvinyl alcohol lead azide that has been milled for 16 hours.

c. The antimony trisulphide is passed through a U. S. No. 325 sieve.

(It is noted that this mixture and procedure did not prove to be more sensitive electrically nor was the stab sensitivity as great as that of the NOL-130 priming mix.)

12. Varicomps, RDX/calcium-stearate binary system explosives furnished by NOL/White Oak for general use in con-

nection with work for NOL/Corona.

13. Lead styphnate, normal lead styphnate purchased from Olin Mathiesen in 1962 and certified to applicable Military specification. Milled 24 hours in a ball mill with glass marbles.

#### EXPERIMENTAL ARRANGEMENTS AND PROCEDURES

##### Pulse Sensitivity Test

Pulse sensitivity determinations were made by means of Bruceton tests (as described in Ref. 3), using the capacitor discharge circuit shown schematically in Figure 5, in which the controlled variable was the voltage to which the capacitor was charged. The mechanical arrangement (Figure 6) consisted of a needle electrode held by a "saw" holding device. In this test a detonator was placed in a brass electrode holder which was placed on a steel witness block. The needle electrode was lowered against the stainless steel top of the detonator. Approximately 8.5 grams were placed on the drill rod section of the needle electrode holder to ensure proper contact. Two types of needle electrodes were used, sewing needles which have a point radius of 1.5 mils and steel phonograph needles which have a point radius of 3 mils.

The experimental arrangement shown in Figure 7 was intended to simulate the safety and arming device colloquially referred to as "Mickey Mouse" and similar to that shown in Ref. 4. In this fixture, leaf spring type electrodes

(Figure 8) were inserted and clamped into position. The rotor was rotated to the armed position and the detonator tested.

The leaf spring electrode (Figure 8) had an adjustable angle ( $\alpha$ ) to which the tip of the electrode could be bent. There were two angles ( $\alpha$ ) to which the electrodes in these tests were adjusted; they were  $45^\circ$  and  $70^\circ$ .

#### Steady State Current Sensitivity

The mechanical arrangement for the steady state current sensitivity tests was the same as that with the pulse sensitivity test (Figure 6). For the steady state tests only sewing needle electrodes were used. A Bruceton test was used in which the current was applied for one minute or such shorter time as it took to fire. It should be noted that the detonator holder and witness block served as heat sinks in these tests.

#### Stab Sensitivity Test

Stab sensitivity determinations also were made by means of Bruceton tests (as described in Ref. 3), in which the controlled variables were weight (0.1 oz) and height. In these tests, a loaded detonator was placed in a Delrin holder, which was placed on a steel witness block (Figure 9) on a Varicomp sample (Figure 10) which was on a witness block. This unit was placed under an electromagnet, the firing needle inserted, and the firing chamber closed.

## RESULTS AND DISCUSSION

### Pulse Sensitivity

Pulse sensitivity was found to vary with flash charge material, input end closure disc thickness, and electrode configuration.

Results of these tests are given in Table 1. Unfortunately, (from the point of view of fundamental research) the experiments which were performed were in groups, each group being directed toward evaluating the applicability of the concept to a specific application. For this reason, as may be noted in Table 1, there was some tendency to change more than one variable at a time. For example, there are no data whereby NOL-130 priming mix can be compared with the lead styphnate or the silver azide flash charges in detonators of the same dimensions. However, it would not be expected that the thermal sensitivity of NOL-130 would be greatly different from that of lead styphnate or silver azide, and in most practical applications the differences in the pulse sensitivity of the detonators loaded with the three explosives tested are essentially equivalent.

The effect of the larger point radius of the phonograph needle electrode was expected to result in a higher threshold energy than was observed with the sharper sewing needle, as might be predicted from Equation 7 of the Appendix. However, as may be noted, it resulted in a more sensitive though more variable combination. It is believed

that a detailed investigation and analysis of the geometry of the contact would yield an explanation of this apparent reversal. It is of interest to note that, when a combination leaf spring electrode such as is shown in Figure 8 is used, the angle between the point and the surface is of critical importance. The results obtained with such electrodes (Figure 8) reported in Table 1 seem to be consistent with Equation 7 of the Appendix.

The energy requirement of detonators with a one mil thick end closure, as may be noted, is over 80 times that of similar detonators with an end closure of 0.1 mil thick rather than 10 times as would be predicted from Equation 7 of the Appendix. The several factors which contribute to this apparent discrepancy are:

1. The Appendix ignores the axial distribution of the current and heat in the end closure disc, assuming a circularly symmetrical distribution.
2. The cooling time of the thicker disc is probably shorter than that of the thin disc, and at the same time the condenser discharge time was increased by a factor of 8 so that heat losses from the hottest spot during the discharge must be appreciably greater.
3. The lower electrical resistivity of the end closure, which serves as a bridge element, increases the importance of series resistance at contacts and elsewhere in the firing circuit.



### Steady State Current Sensitivity

Dimensions of steady state threshold firing current were made for detonators of the dimensions shown in Figure 2 with input end closure disc thicknesses of 0.1 and 1.0 mils. The mean threshold firing current for the detonators with 0.1 mil thick end closure was 0.71 amperes and that for the units with 1.0 mil end closure was 2.55 amperes.

### Stab Sensitivity

The mean stab sensitivity obtained from a 20 shot Bruceton test was 0.093 in. oz with a standard deviation of 0.0128 in. oz. In this test, sewing needles were used as firing pins. This sensitivity (about 20% of the energy requirement of the M-55 detonator) is attributable to the combination of the very thin cover disc and the very small firing pin point. Previous experience with the same priming mix loaded at the same pressure indicates that most of this is the result of the firing pin dimensions, which are smaller than those of the firing pin usually used with M-55. The sensitivity of primers without covers is essentially that of the M-55 and is not affected by the application of covers similar to that in the M-55.

### Applications

Detached electroexplosive devices are smaller and potentially much less expensive than other electroexplosive devices

because of elimination of the "header" or "plugs" through which electrodes are introduced. In addition, since they do not acquire the properties of electroexplosive devices until the electrodes are applied (which can be part of the "arming" process) they are safer against prematurely applied electrical signals than other electroexplosive devices (with the possible exception of exploding bridgewire devices). These properties can be applied in any of a variety of miniaturized fuzes and safety and arming devices such as, for example, the internal arming electric detonator shown in Figures 11 and 12.

Their adaptability as stab sensitive devices makes it possible to use them in applications where a mechanical back-up is desired in an electrical firing system. Such an application is illustrated in Figure 11.

#### CONCLUSIONS AND RECOMMENDATIONS

It may be concluded that detached electrode devices of electrical input characteristics similar to those of existing electroexplosive devices used in ordnance are quite feasible and that such electroexplosive devices have several advantages over other types of electroexplosive devices which should give them a wide range of applicability. The relationship between the characteristics and the dimensions which would be expected to affect them has been shown experimentally to be somewhat more complex than was predicted on the basis of a 2 dimensional model of current

and heat distribution and considerable study will be necessary before such devices can be designed with accurately predicted input characteristics other than those which have been observed and reported herein. A practical design of electrodes and detonators has been demonstrated. It is recommended that detached electrode electroexplosive devices be considered in future designs where electrical initiation of explosives is required. At this stage, it is also recommended that close liaison be established and maintained between fuze designers and those engaged in the design and development of the detonators.

#### REFERENCES

1. Chamberlain, D.H., and Stresau, R.H., "A Stab-Electric Detonator Which is Insensitive Until Armed," Naval Weapons Center Corona Laboratories Report NWCCL-TP 789, Corona, California, February 1969.
2. Chamberlain, D.H., "Adaptation of the EED Synthesis Stab Electric Detonator to an Arming Device," R. Stresau Laboratory Report 68-10-1, Spooner, Wis., 25 October 1968.
3. Statistical Research Group, Princeton University, "Statistical Analysis for a New Procedure in Sensitivity Experiments," (AMP Report 101.1R, SRG-P No. 40, OSRD Report 4040, July 1944).
4. Arming Mechanism Nots Model 56CA, BUWEPS Dwg. No. 2580725.

Table 1. Pulse Sensitivity Test Results

Length (in)	Det. Dia. (in)	Closure Thickness (mils)	Flash Charge Mat'l	Des- crip- tion	Electrode Point Radius (mils)	Angle $\alpha$ (deg)	Threshold Firing Conditions	
							Cap. (mfd)	E.M.F. Energy (volts) (ergs) (log units)
0.100	0.134	0.1	NOL 130	SN	1.5		0.5	27.3 1870 0.06
0.400	0.148	0.1	NOL 130	SN	1.5		0.5	26.5 1750 0.051
0.200	0.050	0.1	lead styph.	SN	1.5		0.5	28.2 1990 0.035
0.200	0.050	0.1	Silver azide	SN	1.5		0.5	30.9 2380 0.021
0.200	0.050	0.1	lead styph.	PN	3.0		0.5	25.8 1870 0.132
0.400	0.148	0.1	NOL 130	Fig 8		45°	0.5	37.8 3560 0.052
0.400	0.148	0.1	NOL 130	Fig 8		70°	0.5	26.0 1690 0.042
0.200	0.050	1.0	lead styph.	SN	1.5		4.0	90.1 163000 0.043

Notes:

NOL 130 - NOL 130 priming mix as described under "Explosives Tested", Item 11.  
lead styph. - Milled normal lead styphnate, Item 11 under "Explosives Tested".  
Silver azide - 2 micron silver azide, Item 6 under "Explosives Tested".

SN - sewing needle PN - phonograph needle Fig 8 - Leaf spring electrode  
(as per Figure 8)

## Appendix

### DISTRIBUTION OF ENERGY IN AN ANNULAR EED FILM-BRIDGE ELEMENT

For single-pin electroexplosive devices, the simplest possible electrode arrangement is coaxial and, where film bridges are to be used, the simplest bridge configuration is that of an annulus connecting the coaxial electrodes. Since, in wire bridge devices, it has been found that the threshold energy requirement is generally proportional to the volume of the bridgewire, it is reasonable to suppose that the general threshold condition for initiation can be expressed in terms of the "energy density" (assuming that the energy is deposited by an electrical pulse of duration short in comparison with the time required for significant redistribution of the resulting heat by conduction or other heat transfer mechanism) in the bridge element. For an annular bridge element of the kind described above, the energy density ( $dq/dv$ , where  $dq$  is the quantity of energy deposited in a differential volume,  $dv$ , of the bridge element) can be estimated as follows:

The total energy delivered to the bridge element is equal to:

$$Q = \int_0^R i^2 dR dt \quad (1)$$

where

$Q$  = energy deposited

$i$  = the instantaneous current

$dR$  = an element of resistance

$dt$  = an element of time

Assuming that the resistivity of the bridge material is constant, the resistance  $dR$  of the circular increment of the bridge element at radius  $r$  and width  $dr$  is given by:

$$dR = \frac{\rho}{2\pi r T} dr \quad (2)$$

where  $\rho$  is the resistivity of the bridge material and  $T$  is the thickness of the bridge element. In terms of the "action integral"  $A = i^2 dt$ , equations (1) and (2) may be combined:

$$Q = \frac{A\rho}{2\pi T} \int_{r_1}^{r_2} \frac{dr}{r} = \frac{A\rho}{2\pi T} \ln \frac{r_2}{r_1} \quad (3)$$

where  $r_1$  and  $r_2$  are smaller and larger radius, respectively.

$$\frac{dq}{dr} = \frac{A\rho}{2\pi T r} \quad (4)$$

and, since  $dv = 2rTdr$ ,

$$\frac{dq}{dv} = \frac{A\rho}{(2\pi r T)^2} \quad (5)$$

For threshold firing conditions, the maximum energy density that at  $r_1$  has a value  $D_e$ , which is a characteristic of the combination of bridge and flash charge materials, is expressed as

$$D_e = \frac{dq}{dv} = \frac{A\rho}{(2\pi r_1 T)^2} \quad (6)$$

$$A\rho = D_e (2\pi r_1 T)^2$$

Substituting in Equation (3),

$$Q_t = 2r_1^2 T D_e \ln \frac{r_2}{r_1} \quad (7)$$

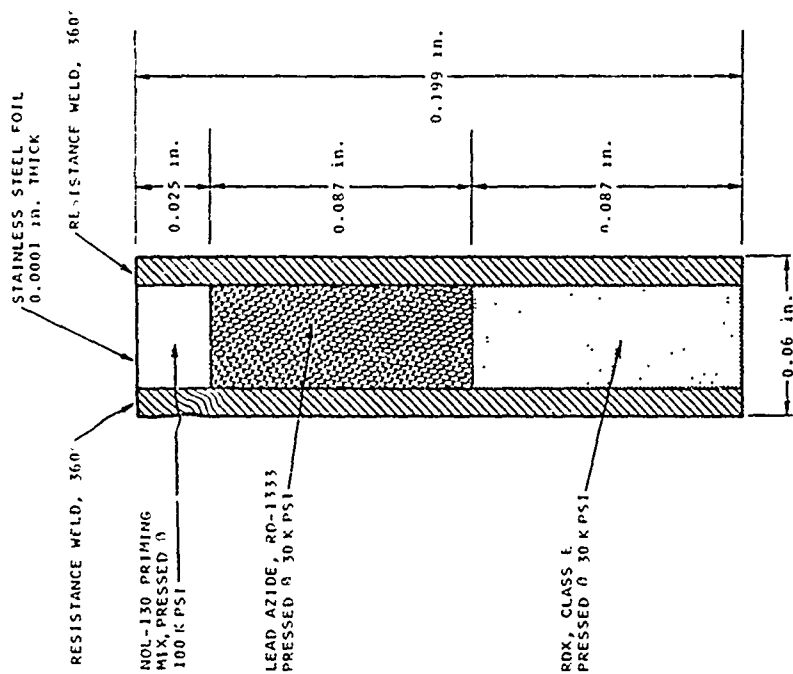


FIGURE 2

INITIAL STAB-ELECTRIC DETONATOR

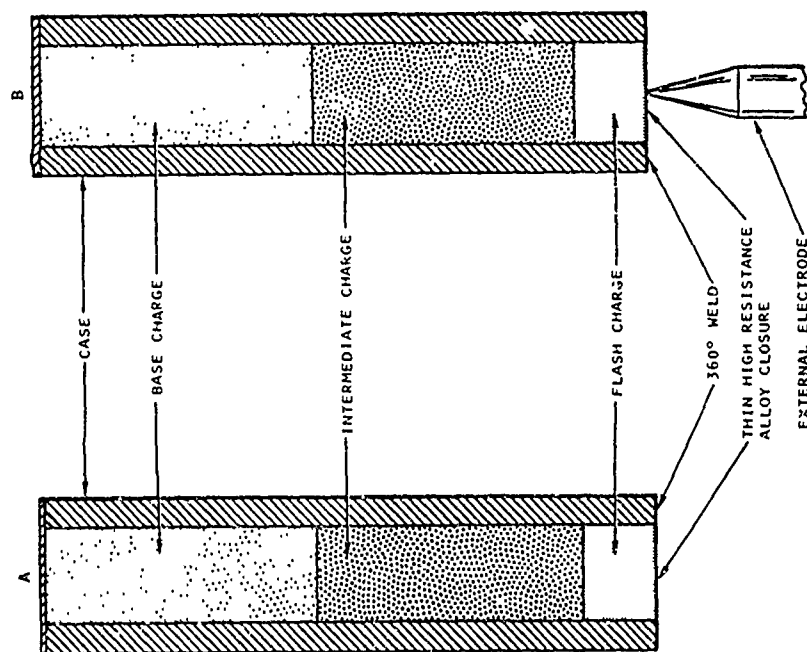


FIGURE 1

DETACHED ELECTRODE ELECTRO-EXPLOSIVE DEVICE

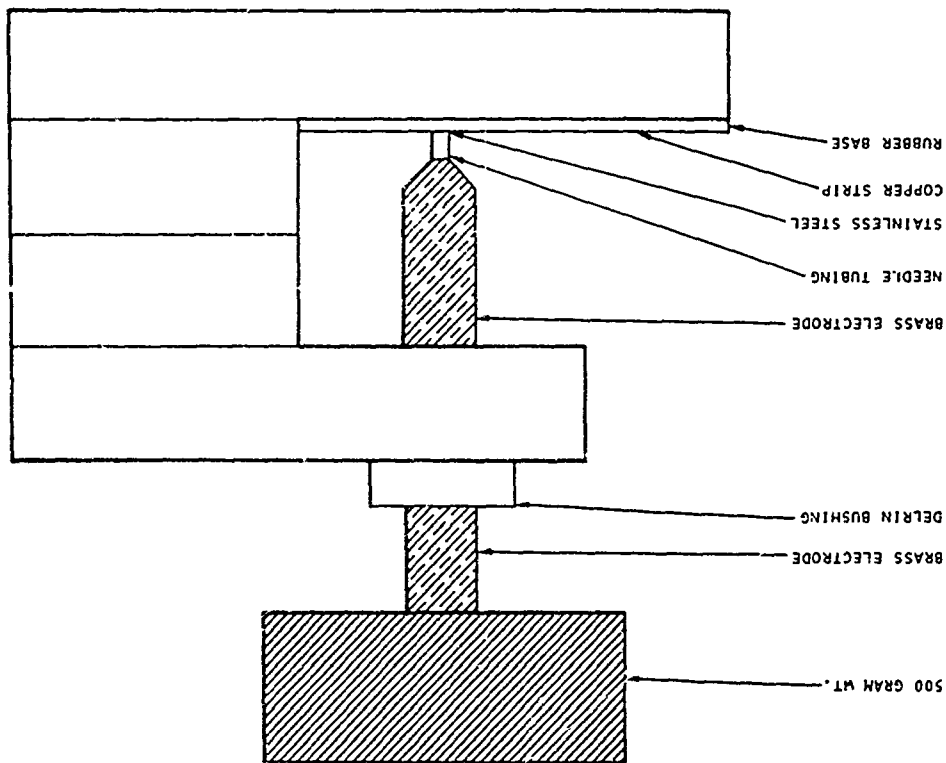


FIGURE 4

DETONATOR WELDER

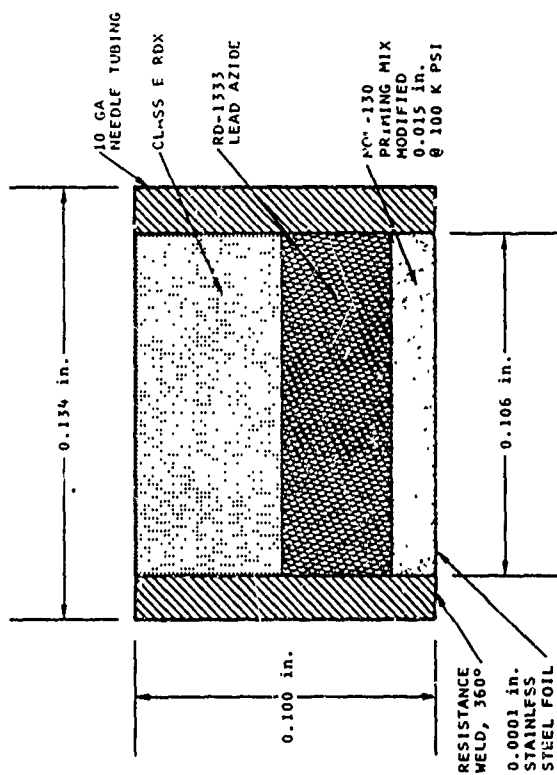


FIGURE 3

STAB-ELECTRIC DETONATOR



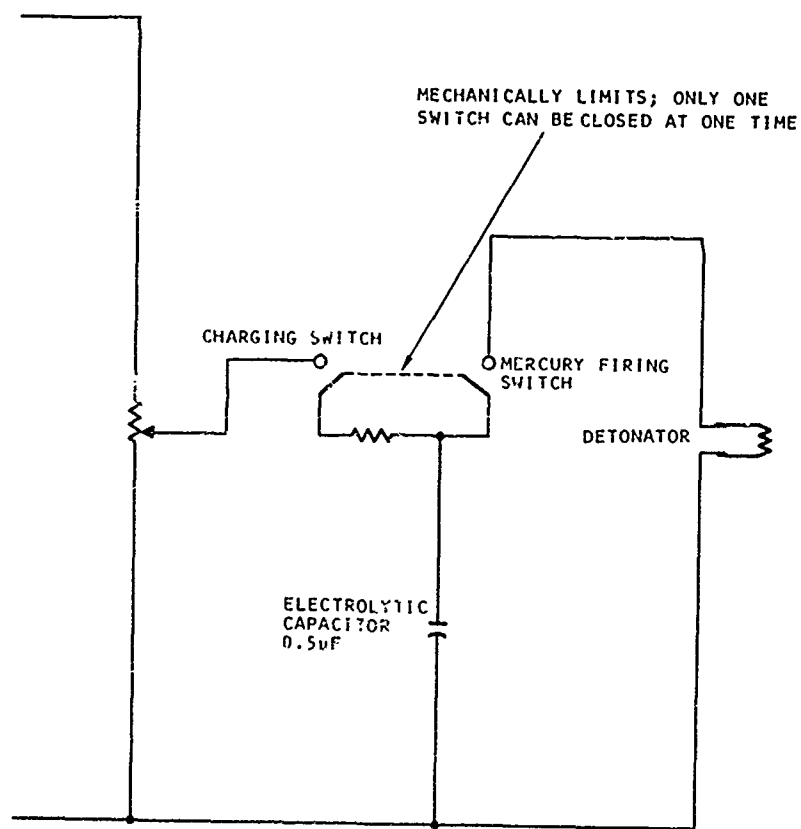


FIGURE 5 PULSE FIRING TEST CIRCUIT

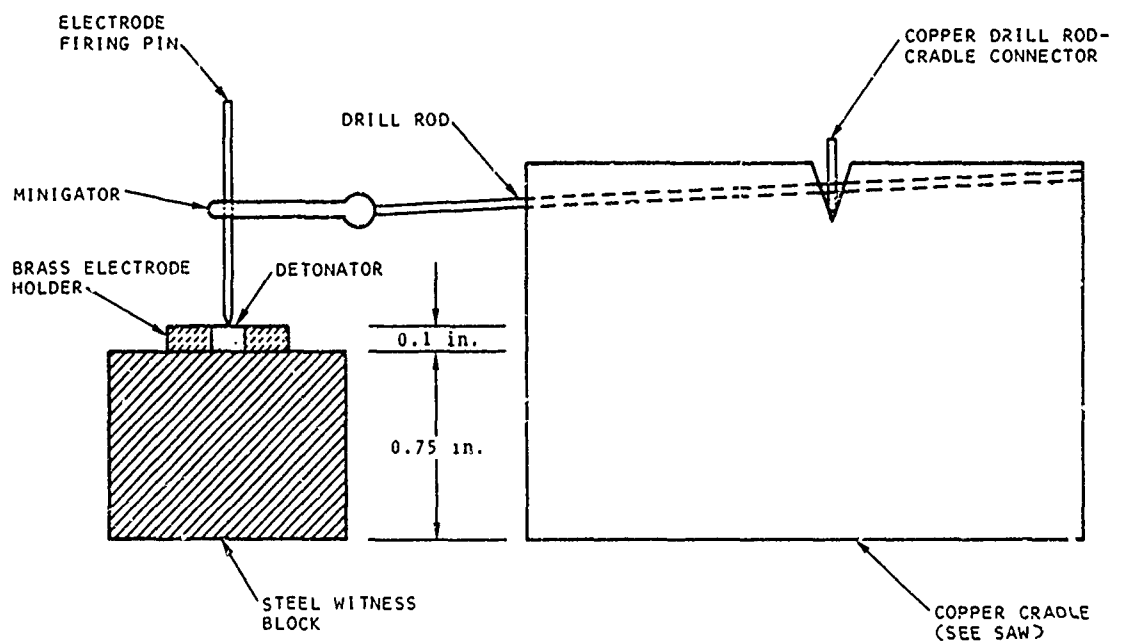


FIGURE 6 ELECTRICAL SENSITIVITY TEST SYSTEM

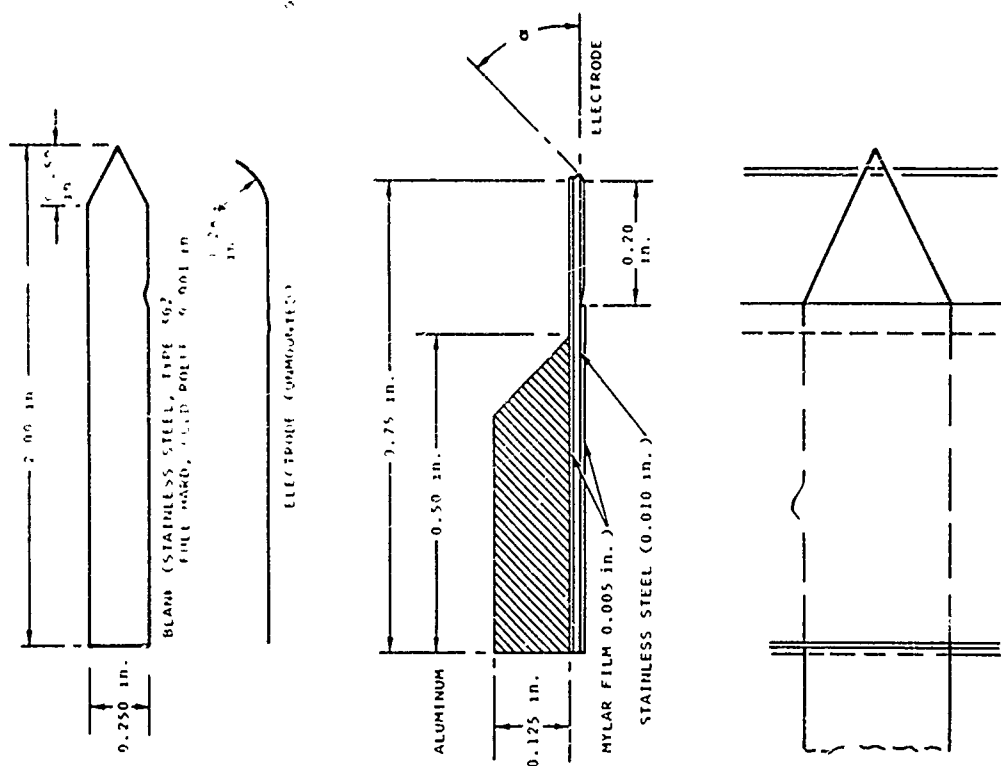


FIGURE 8

EXPERIMENTAL ELECTRODE ASSEMBLY

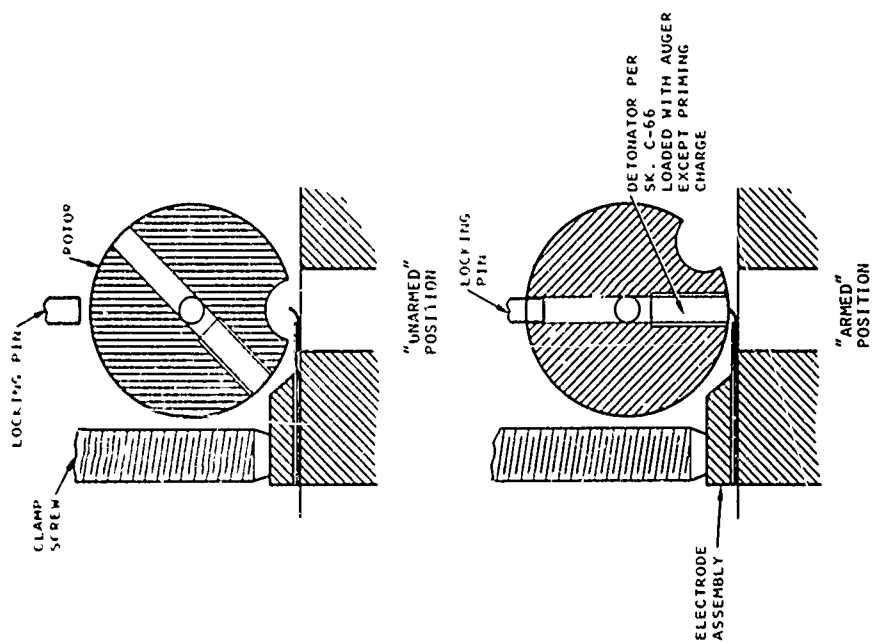


FIGURE 7

"MICKEY MOUSE" TEST FIXTURE (SECTIONAL VIEW)

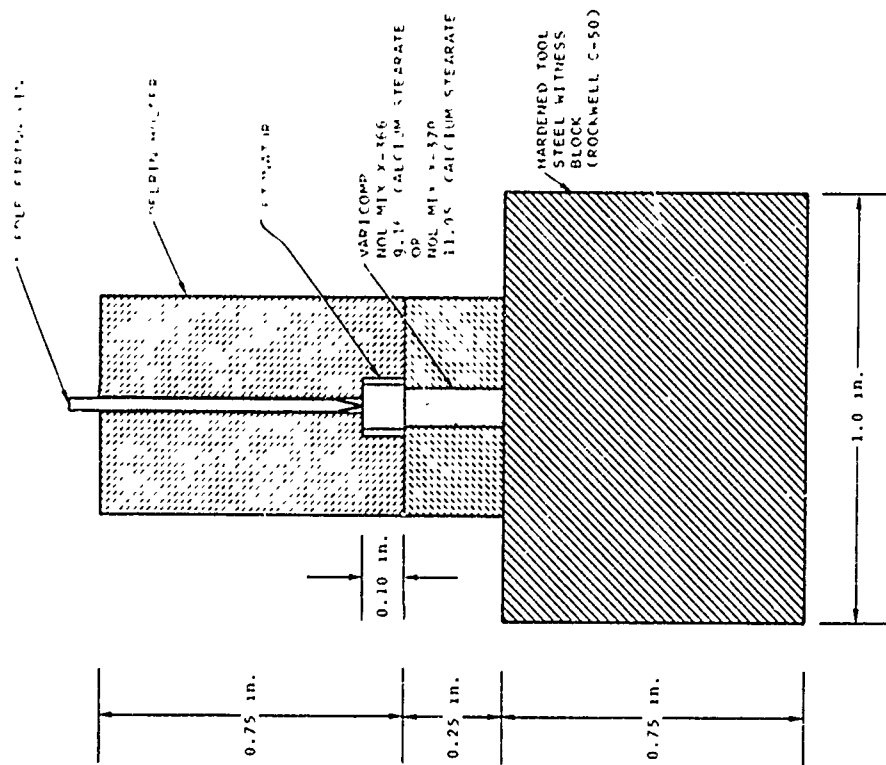


FIGURE 10

VARI COMP OUTPUT TEST SYSTEM

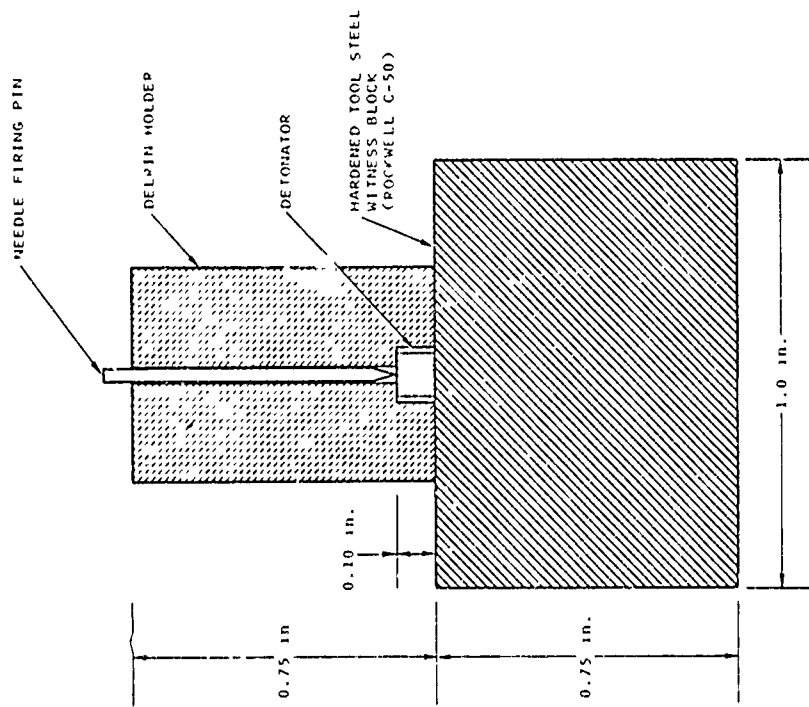


FIGURE 9

SENSITIVITY/DENT OUTPUT TEST SYSTEM

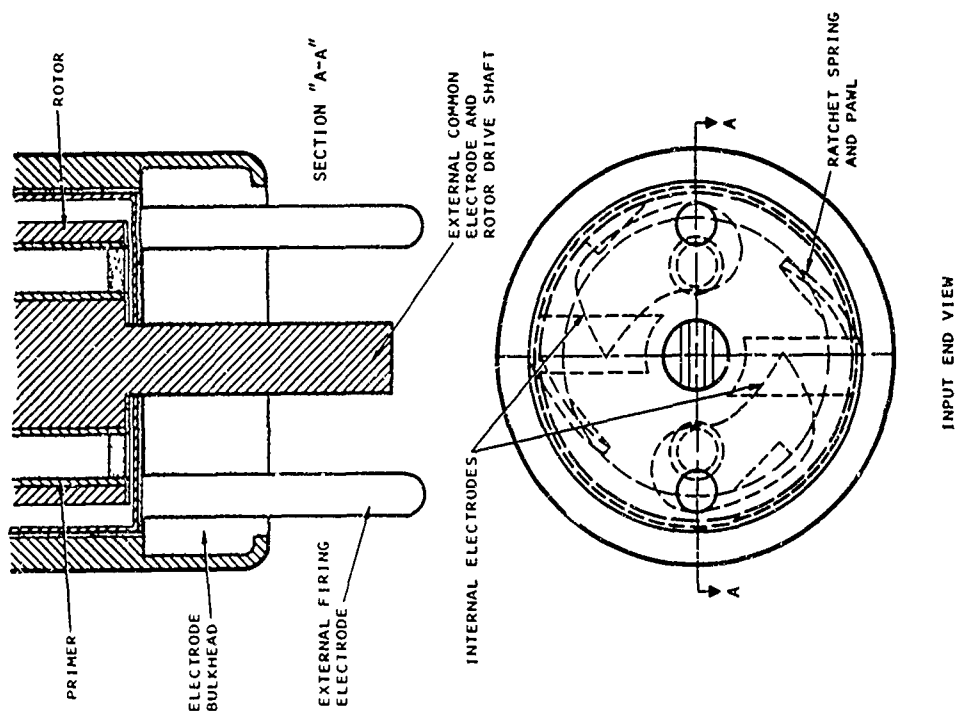


FIGURE 11

INTERNAL ARMING ELECTRIC DETONATOR

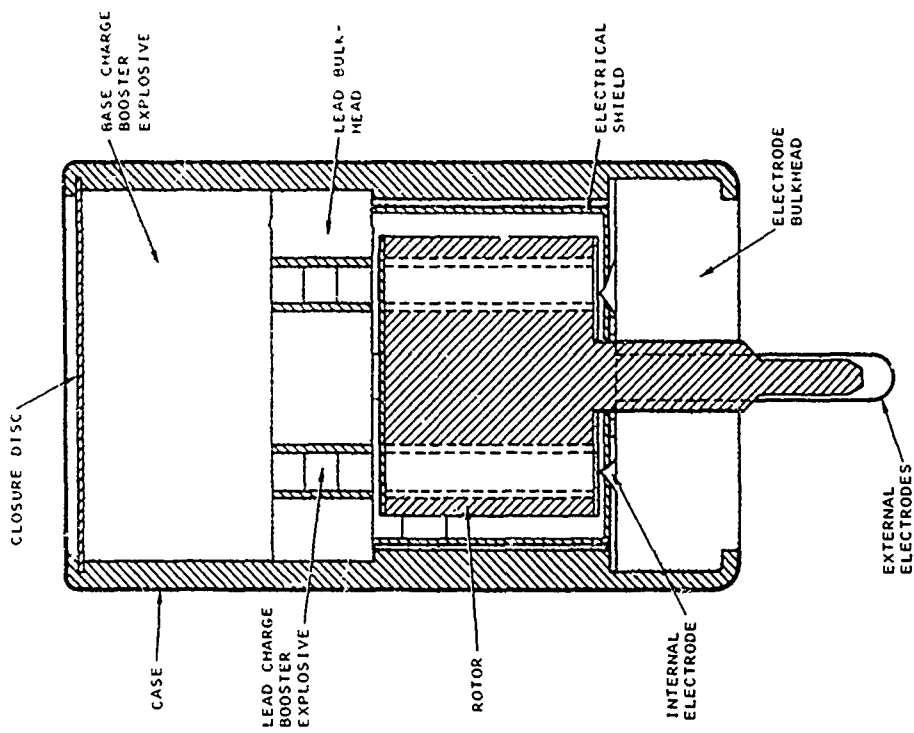


FIGURE 12

INTERNAL ARMING ELECTRIC DETONATOR

# 1-9 DEVELOPMENT AND CHARACTERISTICS OF A LOW-COST DETONATOR FOR PRECISE SYNCHRONIZATION

GIORDANO MELANI  
USA BALLISTIC RESEARCH LABORATORIES  
ABERDEEN PROVING GROUND, MARYLAND 21005

## INTRODUCTION

Explosive tests involving the use of high-speed instrumentation such as framing cameras, streak cameras, and oscilloscopes require detonators to have a functioning time which is reproducible to within about  $\pm 0.1 \mu\text{sec}$ . The detonators must function with this precision when used with various lengths of firing cable. In practice it may be used either singly or in parallel with other detonators, hence, the functioning time should be relatively insensitive to voltage. In addition they must be safe to handle, have a reasonable shelf life, and be as inexpensive as consistent with desired performance.

Prior to 1962, the standard Army detonator M36 met most of the above requirements (except that it had an uncertainty in functioning time of about  $\pm 1.0 \mu\text{sec}$ ). The M36 detonator contained mercury fulminate enclosed in a gilding-metal case. By 1962, the supply of M36 detonators which had been manufactured in 1945 was nearly exhausted and those remaining showed serious deterioration in their performance characteristics.

The M36A1, which contained lead styphnate as an igniter, superseded the M36. However, experience at the Ballistic Research Laboratories (BRL) with M36A1 detonators drawn from Army stock showed their performance to be erratic with variations in functioning time as large as  $20 \mu\text{sec}$ . Since the M36A1 detonators drawn from stock were quoted

at a cost of \$0.31 each, it was assumed that they were manufactured under a large quantity contract. When a sample was tested from a current small production run (see Table 1), the functioning times measured from 4.1 to 7.0  $\mu$ sec giving a range of 2.9  $\mu$ sec. However, the price was in the neighborhood of \$3.50 each in lots of 5,000.

For a period of time, groups at BRL found it necessary to construct exploding bridgewire detonators\* for shots requiring small variations in functioning time. A number of companies were approached to make such detonators on a commercial basis but were either uninterested or else submitted price estimates comparable with the cost of exploding bridgewire detonators made at BRL. A thorough canvas of all possible sources was made to have more M36 detonators manufactured or else to develop a modification of this detonator. The only response came from the Flare-Northern Division of Atlantic Research Corporation at West Hanover, Massachusetts\*\*. This report describes results obtained during the development program and gives functioning-time data for samples of the detonator, designated as ARC NND-211, taken from current production.

#### DEVELOPMENT PROGRAM

##### The Functioning-Time Test

The functioning time of the detonators was determined by using an oscilloscope to measure the time interval between application of the high voltage firing pulse to the detonator and the emergence of the detonation wave from the output end of a plastic bonded RDX booster

---

\*The George Washington Research Laboratory Quarterly Progress Report No. 20, Contract No. DA-18-064-404-CML-163, Project No. 4-04-14-021, Fort Detrick, Frederick, Maryland.

\*\*Mr. Lewis Bettancourt of this company contributed substantially to the developments here reported.

and then subtracting the travel time of the detonation wave through the booster. The high voltage pulse was monitored by means of a Tektronix Type P-6013 capacitive voltage divider (1000:1 attenuation), while the emergence of the detonation wave was detected by means of an ionization probe on the end of the booster as shown schematically in Fig. 1. The probe consists of two double-cotton-covered No. 38 copper wires twisted together and connected to an RC circuit such that when the highly ionized detonation wave emerges it discharges the charged capacitor through the resistor and the voltage across the resistor is displayed on the scope. For good time resolution the signals were displayed on a Tektronix 555 dual beam oscilloscope, and a typical record is reproduced in Fig. 2. The upper beam was used to display both the high voltage firing pulse and the ionization probe signal, the two being mixed by means of a Tektronix Type Z differential amplifier. The lower beam was delayed by an accurately determined time so as to record only the ionization probe signal on a faster sweep, thus allowing a more accurate determination of the time at which this signal occurs.

Due to the sensitivity of the scope to stray electrical impulses, operation of the scope in the immediate vicinity of the high voltage firing unit causes an uncertainty of  $\pm 0.03 \mu\text{sec}$  in the starting time of the lower beam, and the determination of the functioning time is uncertain by this amount.

#### Development

Both the M36 and the M36A1 detonators had an igniter compound

around the bridgewire, followed by a lead azide charge and then by a secondary explosive base charge. Since there was sufficient energy available in the firing circuit at BRL to explode a 2-mil Nichrome wire and initiate powdered PETN directly, it was thought that considerable simplification and improvement could be achieved by eliminating the igniter compound entirely, and using the bridgewire to initiate lead azide directly. The first two tests verified that this approach yielded a reliable functioning time detonator (see Table 2).

These first two lots of ten each were of crucial importance in that they indicated immediately that the concept for this new detonator was feasible. An examination of Table 2 shows that a considerable amount of information was obtained from these two small lots, for in addition to demonstrating feasibility, the data indicate which of two types of lead azide gives the better performance. The range in functioning times (hereafter called the range) is 0.40  $\mu$ sec with Lot No. 1 as compared with 0.15  $\mu$ sec with Lot No. 2, when fired thru 15 ft of RG58A/U coaxial cable with 4  $\mu$ f charged to 5 kV. This same ordering occurred when two detonators were fired in parallel thru 50 ft of RG58A/U cable using 5 kV, giving a range of 0.40  $\mu$ sec for Lot No. 1 versus 0.20  $\mu$ sec for Lot No. 2. In addition, some initial confidence was obtained that the functioning time was not a strong function of voltage, since dropping the voltage from 5 kV to 3 kV resulted in the functioning time increasing from 2.50 to 2.80  $\mu$ sec. Also, firing two detonators in parallel through a single 50 ft cable reduces the voltage delivered to each detonator. When this was done, the functioning time



increased to only 3.08  $\mu$ sec compared to 2.50  $\mu$ sec for a single detonator fired through 15 ft of cable. Finally, a single firing was also made to show that these detonators would function from a low-voltage firing source (6.3 v AC). This test showed that, in addition to being useful for precision work with a high-voltage circuit, these detonators would also be satisfactory for use with a low-voltage battery or hand generator circuit when timing is not critical.

The next four lots of detonators were made using the better lot of lead azide; however, the bridgewire diameter was varied by a factor of 2, from 1.0 mil to 2.0 mils. Each lot contained 10 detonators, all of which were fired singly using 5 kV through 15 ft of RG58A/U cable, so as to furnish enough data for statistical analysis (see Table 3).

It can be seen that both the range and the estimated standard deviation ( $\sigma$ )\* decreased as the wire diameter increased from 1.0 mil to 2.0 mils, with indications that both were leveling out in the range between 1.75 mils and 2.0 mils. Attention is drawn to the single high reading in the 2.0 mil group, which deviates 15  $\sigma$  from the average. At the time, the high reading was attributed to an unknown fault in either the firing or recording circuits.

In the remaining four lots of detonators, which were made using the better lot of lead azide and 1.75 mil bridgewire, the bridgewire was either unplated or gold plated (for ease in assembling), and two different loading pressures were used. Examination of these data, Table 4,

---

\*"Statistical Manual. Methods of Making Experimental Inferences".  
C. W. Churchman. Pittman-Dunn Laboratories, Frankford Arsenal,  
Philadelphia, Pennsylvania, 1951.

shows that there was no great effect from any of these variations. Attention is again called to the single large deviation in Lot 9, cause for which is unknown. The conclusion from these four lots (nos. 7, 8, 9, 10) is that either loading pressure is satisfactory in combination with either unplated or gold-plated bridgewires.

#### Initial Production

After completion of tests on the first 6 lots, a production contract was let for 10,000 detonators. The specifications of this contract covered only the performance of the detonator in its ability to satisfactorily initiate a plastic bonded RDX booster pellet within a certain maximum functioning time (less than 5.0  $\mu$ sec) with close tolerances on the allowable spread in the functioning time distribution.

Sampling for acceptance testing on the production contract was set at 1 percent; but, for the manufacturer's aid and guidance, two pre-production lots of 50 and 51 detonators were tested in their entirety. Results obtained with the pre-production and production lots are illustrated by the graphs in Figures 3, 4, and 5.

As can be seen, these tests were conducted to measure a variety of performance characteristics. But for present purposes, attention is concentrated on all firings of the first pre-production lot through 15 ft of RG58A/U cable at 5.kV as given in Figure 3. It is observed that two detonators had functioning times which deviated by about 3  $\sigma$  from the average.

At the time, it was strongly felt that these long functioning times could be attributed to faults in the firing cable which lowered

the voltage delivered to the bridgewire and hence increased the time required to initiate the lead azide. A second pre-production lot was obtained from the manufacturer who also undertook to improve production controls on this lot. Figure 4 displays the results from this lot. It is evident that the large deviations of the first pre-production lot have been avoided, giving a normal distribution curve with  $\sigma = 0.05 \mu\text{sec}$ .

Results from a production lot of 5,000 are given in Figure 5. Here, it is evident that the sample is quite well represented by a normal frequency distribution with an average =  $2.49 \mu\text{sec}$  and  $\sigma = 0.07 \mu\text{sec}$ . In terms of deviation of individual detonators from the lot average, it can be seen that 50 percent of the lot can be expected to have a deviation of less than  $0.05 \mu\text{sec}$ , 2 out of 100 will have a deviation of  $0.15 \mu\text{sec}$ , while 2 out of 1,000 will have a deviation of  $0.21 \mu\text{sec}$ . The above performance is for single detonators fired from  $4 \mu\text{F}$  charged to 5kV through 15 ft of RG58A/U cable. When the firing voltage is lowered to 3 kV, the functioning time for single detonators through 15 ft of RG58A/U cable increases  $0.2 \mu\text{sec}$  to  $2.7 \mu\text{sec}$ , and if 2 detonators are fired in parallel from a single 50 ft length of RG58A/U with  $4 \mu\text{F}$  charged to 5 kV, then the functioning time increases approximately  $0.7 \mu\text{sec}$  to  $3.2 \mu\text{sec}$ .

#### Current Production

Further improvements in the detonator have been made since its initial development. The DC current which it will withstand has been increased, and it has been designed to be immune to electrostatic discharges from the human body\*.

\*"Electrostatic-Insensitive Detonator for Precise Synchronization", Boyd C. Taylor, this Symposium.

Also, experience has been gained in manufacturing and in production quality control of the item. The end result is that the detonator has exhibited a consistently reliable performance to date. Figure 6 is the functioning time distribution of a random sample from a current production contract. It is obvious that production control is excellent and that the distribution is a normal one.

Dimensions, cost, and functioning times of the current model are listed in Table 5.

#### SUMMARY

The need for, and development of, a reliable and inexpensive detonator for precise synchronization have been described. The ARC-NND-211 detonator which resulted from this program presently costs \$1.895 each in lots of 15,000. It has a functioning time of 2.42  $\mu$ sec, with an estimated standard deviation of .045  $\mu$ sec when fired through 15 ft of RG58A/U coaxial cable from a 1  $\mu$ F capacitor charged to 5 kV. This functioning time is not highly sensitive to voltage since lowering the voltage by a factor of 10 to 500 v increases the functioning time by only a factor of 2 to 5.58  $\mu$ sec. In addition, the detonator can be fired from a low voltage source such as a hand gun.

This detonator utilizes many of the components and techniques developed for the Army M36A1 detonator, and consequently, benefits from this source. The main departure from the M36A1 construction is the use of a heavier bridgewire, which when either electrically heated or exploded, initiates the lead azide directly. An additional departure was made from M36A1 specifications in that the present detonators

were not made subject to the environmental tests that are required for acceptance of the M36A1.

Further development of this detonator to render it immune to electrostatic discharges from the human body is described in a companion paper\*.

TABLE 1

Detonator : M36A1  
Source : Flare-Northern Division  
Voltage : 3 kV  
Capacitance: 4  $\mu$ F

Functioning Time ( $\mu$ sec)	Deviation ( $\mu$ sec)
4.1	-1.3
4.7	-0.7
4.9	-0.5
5.1	-0.3
5.4	0.0
5.5	+0.1
5.8	+0.4
5.9	+0.5
7.0	+1.6
Average:	5.4
$\sigma$ :	.8
Range :	2.9

\* "Electrostatic-Insensitive Detonator for Precise Synchronization",  
Boyd C. Taylor, this Symposium.

TABLE 2

Detonator : Experimental, Lots 1 & 2  
 Source : Flare-Northern Division  
 Voltage : Various  
 Capacitance: 4  $\mu$ F

	Functioning Time ( $\mu$ sec)	Deviation ( $\mu$ sec)	Firing Conditions
<u>Lot 1:</u>	2.8	---	3 kv, 15 ft RG58A/U
	2.3	-0.2	5 kv, 15 ft RG58A/U
	2.5	0.0	5 kv, 15 ft RG58A/U
	2.5	0.0	5 kv, 15 ft RG58A/U
	2.7	+0.2	5 kv, 15 ft RG58A/U
	2.9	-0.2	5 kv, 50 ft RG58A/U 2 Dets in Parallel
	3.0	-0.1	5 kv, 50 ft RG58A/U 2 Dets in Parallel
	3.1	0.0	5 kv, 50 ft RG58A/U 2 Dets in Parallel
	3.3	+0.2	5 kv, 50 ft RG58A/U 2 Dets in Parallel
<u>Lot 2:</u>	---	---	6.3 v (AC), Fired O.K.
	2.8	---	3 kv, 15 ft RG58A/U
	2.5	-0.10	5 kv, 15 ft RG58A/U
	2.55	-0.05	5 kv, 15 ft RG58A/U
	2.65	+0.05	5 kv, 15 ft RG58A/U
	2.65	+0.05	5 kv, 15 ft RG58A/U
	3.1	-0.05	5 kv, 50 ft RG58A/U 2 Dets in Parallel
	3.1	-0.05	5 kv, 50 ft RG58A/U 2 Dets in Parallel
	3.1	-0.05	5 kv, 50 ft RG58A/U 2 Dets in Parallel
	3.3	+0.15	5 kv, 50 ft RG58A/U 2 Dets in Parallel

TABLE 3

Detonator: Experimental, Lots 3, 4, 5 & 6  
 Source : Flare-Northern Division  
 Voltage : 5 kv  
 Circuit : 4  $\mu$ f Low Inductance Firing Unit, 15 ft RG58A/U Cable

Functioning      Deviation  
 Time ( $\mu$ sec)      ( $\mu$ sec)  
Lot 3, 1.0-mil Bridgewire:

2.42	-.07
2.46	-.03
2.46	-.03
2.48	-.01
2.50	+.01
2.50	+.01
2.50	+.01
2.52	+.03
2.54	+.05
2.56	+.07

Average: 2.49  
 $\sigma$  : .04  
 Range : .14

Lot 5, 1.75-mil Bridgewire:

2.60	-.03
2.60	-.03
2.60	-.03
2.62	-.01
2.62	-.01
2.62	-.01
2.62	-.01
2.62	-.01
2.64	+.01
2.64	+.01
2.68	+.05

Average: 2.63  
 $\sigma$  : .02  
 Range : .08

Functioning      Deviation  
 Time ( $\mu$ sec)      ( $\mu$ sec)  
Lot 4, 1.5-mil Bridgewire:

2.46	-.07
2.51	-.02
2.52	-.01
2.52	-.01
2.54	+.01
2.54	+.01
2.54	+.01
2.54	+.01
2.58	+.05
2.58	+.05

Average: 2.53  
 $\sigma$  : .03  
 Range : .12

Lot 6, 2.0-mil Bridgewire:

2.60	-.07
2.62	-.05
2.64	-.03
2.64	-.03
2.64	-.03
2.66	-.01
2.66	-.01
2.66	-.01
2.66	-.01
2.66	-.01
2.94	+.27

Average: 2.67	If Discard High Reading: Average: 2.64
$\sigma$ : .10	$\sigma$ : .02
Range : .34	Range : .06

TABLE 4

Detonator: Experimental, Lots 7, 8, 9, & 10  
 Source: Charge-Portner Division  
 Voltage: 5 kV  
 Load: 4  $\mu$ F, Low Inductance Firing Unit with 15-ft RG58A/U Cable

Time ( $\mu$ sec)	Deviation ( $\mu$ sec)	Functioning Time ( $\mu$ sec)	Deviation ( $\mu$ sec)
Lot 7, Gold Plated, Low Pressure: *		Lot 8, No Plating, Low Pressure: *	
2.50	-.03	2.52	-.04
2.50	-.03	2.52	-.04
2.51	-.02	2.52	-.04
2.51	-.02	2.53	-.03
2.51	-.02	2.53	-.03
2.51	-.01	2.56	.00
2.53	.00	2.60	+.04
2.57	+.04	2.60	+.04
2.58	+.05	2.61	+.05
		2.62	+.06
Average: 2.53		Average: 2.56	
$\sigma$ : .03		$\sigma$ : .04	
Range : .08		Range : .10	
Lot 9, Gold Plated, High Pressure: *		Lot 10, No Plating, High Pressure: *	
2.46	-.12	2.53	-.02
2.50	-.08	2.53	-.02
2.53	-.05	2.53	-.02
2.54	-.04	2.54	-.01
2.56	-.02	2.54	-.01
2.58	.00	2.55	.00
2.59	+.01	2.55	.00
2.61	+.03	2.56	+.01
2.84	+.26	2.58	+.03
Average: 2.58		Average: 2.55	
$\sigma$ : .10		$\sigma$ : .02	
Range : .38		Range : .05	

OMITTING 2.84:

Average: 2.55      Average: 2.55  
 $\sigma$  : .05       $\sigma$  : .02  
 Range : .13      Range : .05

\*Loading Pressure: Final charge density is varied by this method.

TABLE 5

# DETONATOR MND-211

## DIMENSIONS, COST, AND FUNCTIONING TIMES

Diameter (in.)	0.285
Length of Body (in.)	0.532
Lead Length (in.)	6.0
COST, each for 15,000 Production Run	\$1.895
Functioning Time ( $\mu$ sec):	
Single Detonator, 15 ft RG58A/U, 1 $\mu$ F at 5 kV	2.42 $\sigma$ = .045
Single Detonator, 15 ft RG58A/U, 1 $\mu$ F at 3 kV	2.63 $\sigma$ = .079
Two Detonators in Parallel from Single Lead of 50 ft RG58A/U, 4 $\mu$ F at 5 kV	3.2



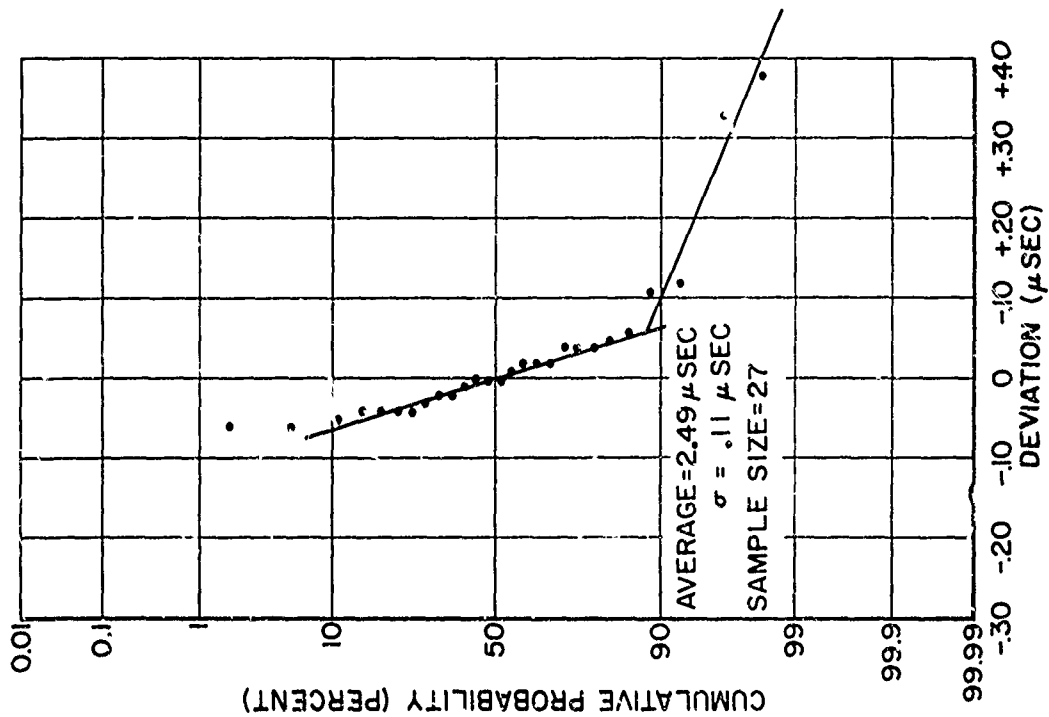


FIGURE 3-FUNCTIONING TIME DISTRIBUTION OF FIRST PRE-  
 PRODUCTION LOT

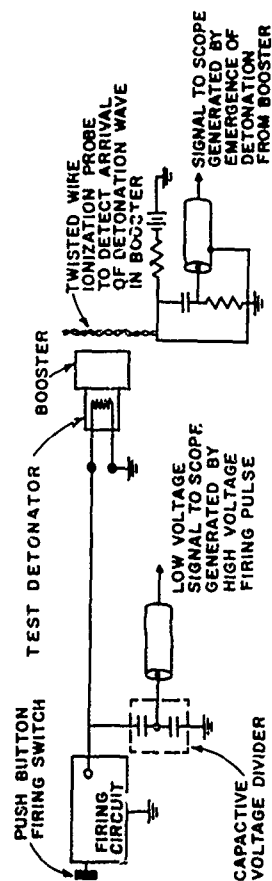
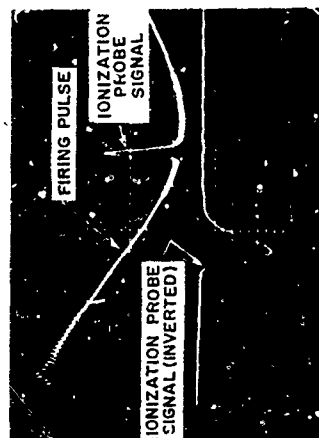


Figure 1 Schematic of Functioning - Time Test Circuits.



UPPER BEAM AT .5  $\mu$  SEC / CM  
 TO DISPLAY BOTH FIRING PULSE AND  
 EMERGENCE OF DETONATION FROM  
 BOOSTER.

LOWER BEAM AT .2  $\mu$  SEC / CM  
 WITH START DELAYED 3.6  $\mu$  SEC  
 FROM START OF UPPER BEAM TO  
 GIVE EXPANDED DISPLAY OF  
 ARRIVAL OF IONIZATION PROBE SIGNAL

Figure 2. Oscilloscope Traces From Functioning - Time Test.

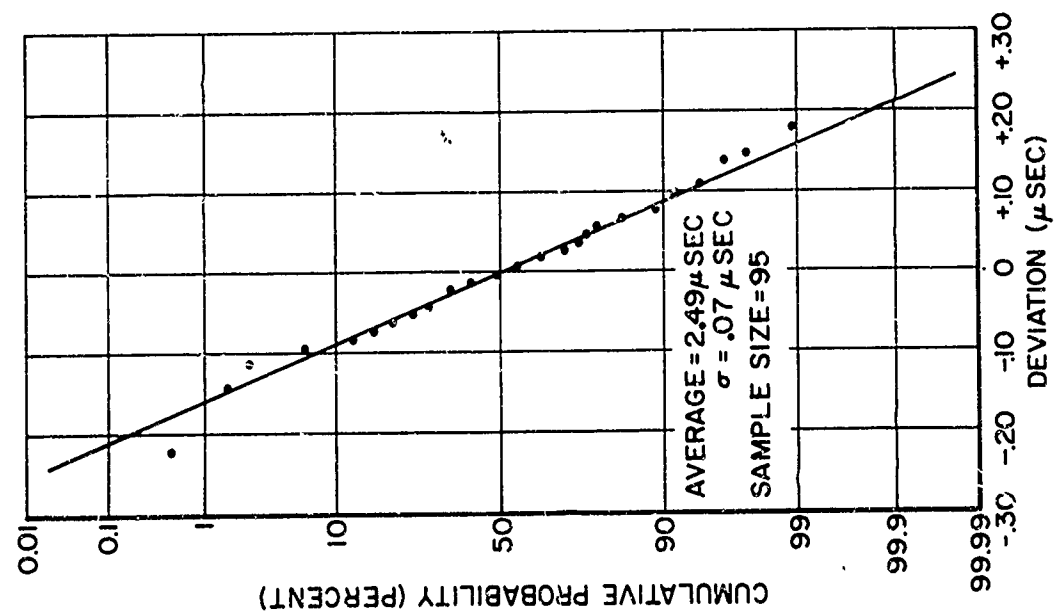


FIGURE 5 - FUNCTIONING TIME DISTRIBUTION OF SAMPLE FROM PRODUCTION RUN OF 5000.

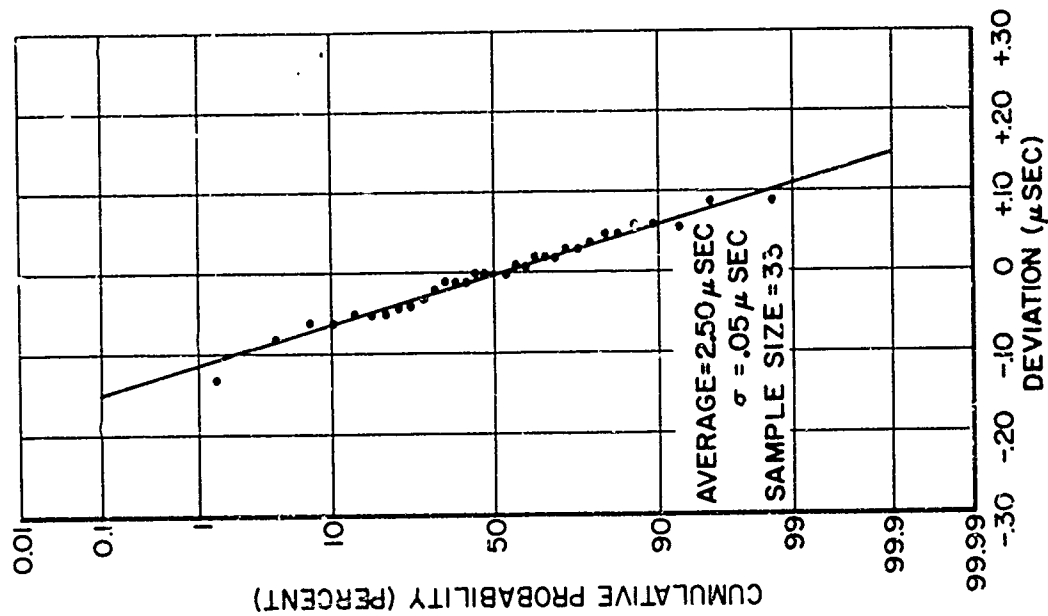


FIGURE 4 - FUNCTIONING TIME DISTRIBUTION OF SECOND PRE-PRODUCTION LOT.

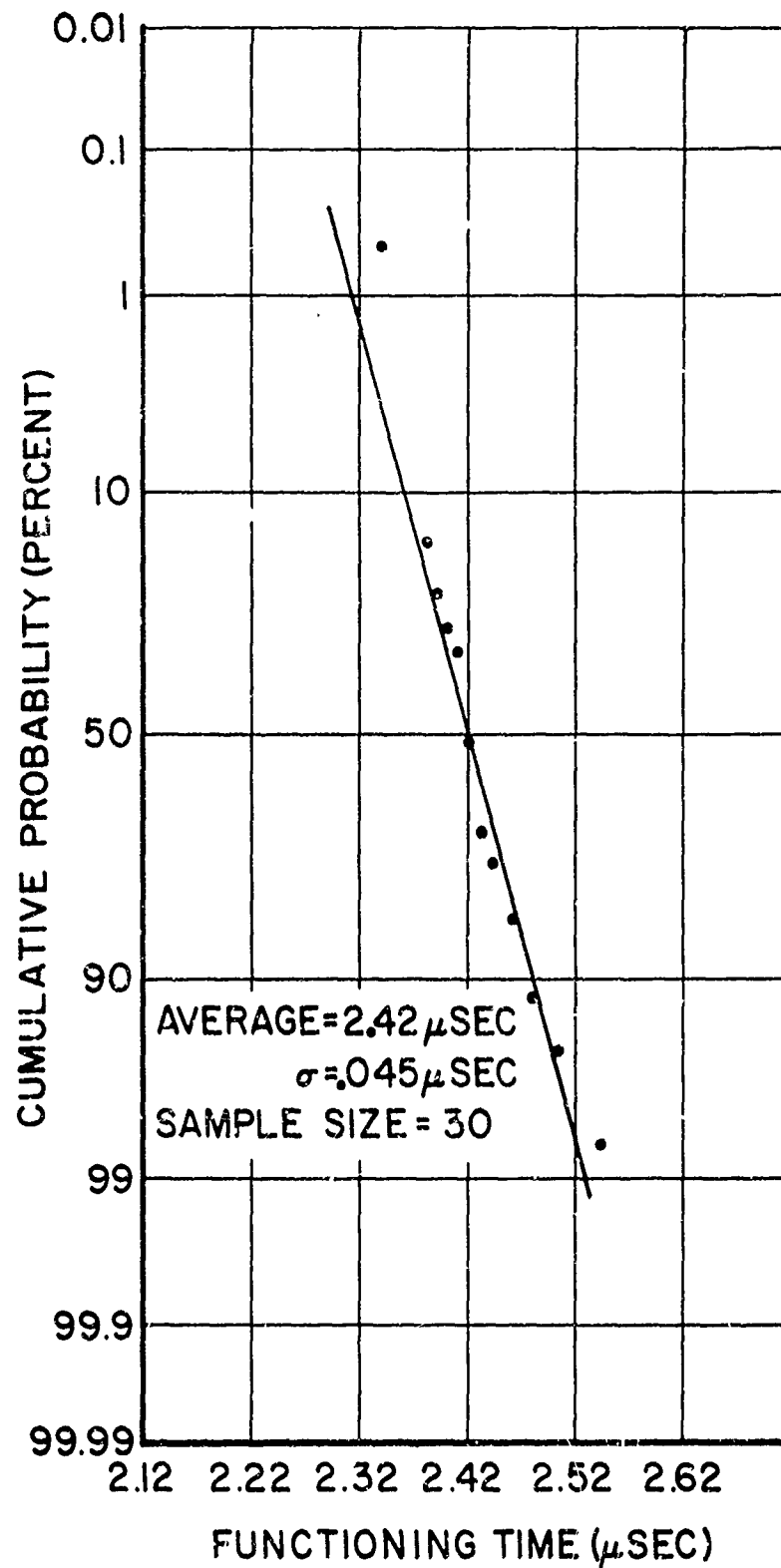


FIGURE 6- FUNCTIONING TIME DISTRIBUTION OF  
CURRENT PRODUCTION LOT.

1-9.15

# 1-10 ELECTROSTATIC-INSENSITIVE DETONATOR FOR PRECISE SYNCHRONIZATION

BOYD C. TAYLOR  
USA BALLISTIC RESEARCH LABORATORIES  
ABERDEEN PROVING GROUND, MARYLAND 21005

## I. INTRODUCTION

By request of a user of the initial distribution\* of the Atlantic Research Corporation NN-D-211 detonator (ARC-211) the sensitivity of these detonators to accidental electrostatic spark discharges was examined and the current design of the ARC-211 was developed. Since the problem of static electricity hazard to detonators is not a simple one, the investigation of this hazard was expanded to include considerable detail, only part of which is reported here.

This investigation was organized to answer two basic questions relevant to the electrostatic spark hazard to detonators. (1) What is the source of the danger? and (2) How can the danger be minimized? The answers to these questions produced by this investigation can be grouped as follows:

- (1) What is source electrostatic spark hazard to detonators?
  - (a) Electrostatic charge (energy) accumulated on human body.
  - (b) Sensitivity of detonator to this energy
    - 1) Across bridgewire
    - 2) Bridgewire to case
- (2) How can electrostatic spark hazard be minimized?
  - (a) By operator following established safety procedures
  - (b) By decreasing the sensitivity of detonator to electrostatic energy.

\*"Development and Characteristics of a Low-Cost Detonator for Precise Synchronization", Giordano Melani, this Symposium.

1) Across bridgewire

2) Bridgewire to case

The present paper is concerned primarily with the solution (2)(b) above, "decreasing the sensitivity of detonator to electrostatic energy."

In the author's opinion, many laboratories and installations located in normally humid regions have had so little trouble from static electricity in the past that their personnel have not become familiar with the electrostatic spark sensitivity of commonly used electric detonators, and have tended to forget or neglect safety procedures to protect against this hazard. However, operations using electro-explosive devices are now being conducted under many unusual conditions, both in the field and in the laboratory, where static accumulation is possible. Furthermore, such unusual conditions seem to be growing in number.

In addition, the use of synthetic fiber clothing is increasing, and in many cases this clothing will readily generate static electricity if it is untreated for static suppression. For instance, as shown by repeated tests, if an ungrounded individual removes a plastic raincoat, he acquires sufficient electrostatic energy to immediately initiate an M36A1 detonator. Explosive setups are becoming more complex and exotic, with considerable use of static generating plastics. There are many situations where personnel making the setup and detonator hookup can be out of physical contact with an electrical earth ground unless this point is kept constantly in mind.

## II. RESULTS

### A. Sensitivity of Detonators to Static Electricity

# 1. Tests with Static Electricity from Human Body and from Equivalent-Circuit for Human Body.

To convey some idea of the sensitivity of ARC-211 and M36A1 bridgewire type detonators to static energy stored on a human body and discharged from this body to the detonator by means of an air spark, the results in Table 1 are presented. For these particular experiments, shown in Fig. 1, the subject was insulated from a 2 ft sq aluminum ground plate by 0.25 in. thick polyethylene plus leather soled shoes. The capacitance to ground of the subject, measured by a Kay-Lab Micro-Miker Model 402A operating at 1 MHz, was 150 pF. Electrical contact to the subject was by means of a 1 x 1 1/2 in. metal plate strapped to mid-forearm and connected by wire to a 1/2 in. diameter metal rod held in the hand. The subject was charged to a positive high potential by bringing the metal rod into contact with a terminal connected to the high voltage power supply through a 33 MΩ resistor, voltage on this terminal was indicated by an electrostatic voltmeter. The subject was then discharged to the detonator by quickly moving the metal rod about 2 in. to another terminal connected by insulated cable to the detonator. The two cables connecting the detonator to the apparatus were 6 ft lengths of insulated core of RG58A/U coaxial cable, with the measured capacitance between cables being 50 pF. Three pulses were applied to the detonator at each voltage level until either the detonator fired or withstood three pulses of 20 kV, the maximum voltage used in these tests.

Usually in testing detonators for sensitivity to static discharges from the human body, the human body itself is not used, but instead it

is approximated by an equivalent circuit consisting of a capacitor and a resistor in series. Various values for the circuit constants, as well as for the maximum voltage of the accumulated static charge, are given by different investigators. For the limited purpose of this paper, the equivalent circuit consisted of a 500 pF capacitor charged to 20 kV maximum with a zero ohms series resistor. This combination was an extremely conservative one in that it delivered much more energy to a low resistance bridgewire than would an actual human body charged to the same voltage. Results obtained with this circuit are shown in Table 2.

As for the problem of establishing a realistic equivalent circuit for the human body, several considerations should be mentioned. First, there is the problem of measuring the dynamic resistance of the human body for a high-voltage discharge (generally to one hand). This resistance differs greatly from the value of 5,000 ohms or so accepted for electrocardiographic recording. Second, there is the problem of specifying the resistance of the air spark which is the means by which the energy stored on the human body is transferred to the detonator. Third, there is the difficulty of determining how to treat the possibility that the electrostatic energy stored on the human body might be transferred first to some intermediate object and then to the detonator. If the dynamic resistance of this intermediate object is appreciably lower than that of the human body, this process can result in delivering sufficient energy to initiate the detonator in circumstances where it could not be initiated by a direct discharge from the human body.

As noted in Table 2, the human body equivalent circuit was discharged by means of a 5C22 hydrogen thyatron switch tube which has

TABLE 1  
SENSITIVITY OF DETONATORS TO STATIC ELECTRICITY  
FROM HUMAN SUBJECT

		CHARGING VOLTAGE (kV)							
		2.5	5.0	7.5	10.0	12.5	15.0	17.5	20.0
ARC-211 original design	CASE TO BW		000	X					
			000	000	X				
			000	0X					
			000	000	X				
			000	000	X				
	ACROSS BW								000
									000
									000
									000
									000
ARC-211 current design	CASE TO BW								000
									000
									000
									000
									000
	ACROSS BW								000
									000
									000
									000
									000
M36A1	CASE TO BW		000	X					
			000	X					
			000	X					
			000	000	X				
			000	X					
	ACROSS BW		000	X					
			000	000	X				
			000	X					
			000	X					
			000	X					

- NOTES: 1. 0 indicates "no-fire" to single voltage pulse.  
X indicates "fire" to single voltage pulse.  
BW = bridgewire
2. Human subject standing w/shoes on 0.25" thick polyethylene on 2 ft. square aluminum ground plate measured 150 pF.
3. Electrical connection between charged subject and detonator lead was by air spark to a 0.5" diameter rod held in hand with a wire connecting the rod to a 1.5 square inch metal plate strapped to middle of forearm.
4. Capacitance between the two leads (6 ft. length each) of insulated core of RG58A/U cable connecting to the detonator was 50 pF.
5. Positive pulse applied to case with BW grounded.



TABLE 2

SENSITIVITY OF DETONATORS TO STATIC ELECTRICITY  
FROM EQUIVALENT CIRCUIT FOR HUMAN BODY  
(500 pF IN SERIES WITH ZERO OHMS)

		CHARGING VOLTAGE (kV)							
		2.5	5.0	7.5	10.0	12.5	15.0	17.5	20.0
ARC-211 original design	CASE TO BW	000	X						
		000	X						
		000	X						
		000	00X						
		000	X						
	ACROSS BW	000	000	000	000	000	000	000	000
		000	000	000	000	000	000	000	000
		000	000	000	000	000	000	000	000
		000	000	000	000	000	000	X	
		000	000	000	000	000	000	000	000
ARC-211 current design	CASE TO BW	000	000	000	000	000	000	000	000
		000	000	000	000	000	000	000	000
		000	000	000	000	000	000	000	000
		000	000	000	000	000	000	000	000
		000	000	000	000	000	000	000	000
	ACROSS BW		000	000	000	000	000	000	000
			000	000	000	000	000	000	000
			000	000	000	000	000	000	000
			000	000	000	000	000	000	000
			000	000	000	000	000	000	000
M36A1	CASE TO BW		000	00X					
			000	0X					
			X						
		000	X						
		000	X						
	ACROSS BW		X						
			X						
			X						
			X						
			X						

- NOTES: 1. 0 indicates "no-fire" to single voltage pulse.  
X indicates "fire" to single voltage pulse.  
BW indicates bridgewire.
2. Pulse was generated by discharge of 5C22 hydrogen thyatron switch tube.
3. Capacitance between the two leads (6 ft. length each) of insulated core of RG58A/U cable connecting to the detonator was 50 pF.
4. Negative pulse applied to case with BW grounded.

appreciable dynamic resistance during a short duration pulse. To further test the current design ARC-211 detonator, a 20 kV pulse was generated by discharging the human body equivalent circuit by means of a vacuum switch and this pulse was applied between the bridgewire leads and the cable. The pulse was of negative polarity and the case was grounded. A total of 30 units were tested in succession, each subjected to 3 pulses of 20 kV each, and none detonated.

The energy stored by a 500 pF capacitor charged to 20 kV is 0.1 joule or 1,000,000 ergs. If this circuit is discharged across the detonator bridgewire by means of a vacuum switch, then most of this energy is delivered to the bridgewire and the detonator will fire. When this same circuit is discharged by a 5C22 switch tube, the energy divides between the dynamic resistance of the tube and the resistance of the bridgewire with the result that insufficient energy reaches the bridgewire to fire the detonator.

## 2. Discussion of Results of Tests with Static Electricity.

These tests reveal the following about the sensitivity of these detonators to static from the human body and from the equivalent circuit.

(1) Sensitivity to static electricity from the human body (Table 1).

### (a) Case to bridgewire mode

1) The sensitivity of the original design of the ARC-211 was about equal to that of the M36A1, both being in the neighborhood of 7.5 kV, which is not a high voltage for accidental static electricity accumulation.

2) The current design of the ARC-211 successfully withstood the maximum voltage of 20 kV.

(b) Across bridgewire mode

1) Both the original design and the current design of the ARC-211 withstood the maximum voltage of 20 kV.

2) The M36A1 was fired by static charge of 7.5 kV, which, again, is not a high voltage.

(2) Sensitivity to static electricity from human body equivalent circuit (500 pF in series with zero ohms Table 2).

(a) Case to bridgewire mode

1) Again, the original design of the ARC-211 and the M36A1 are about equal; both fired at about 5.0 kV with this circuit.

2) The current design of the ARC-211 was not fired by the maximum voltage of 20 kV.

(b) Across bridgewire mode

1) The ARC-211 was insensitive to static pulses across the bridgewire. The original design had one fire at 17.5 kV while four withstood 20 kV, and the current design lot of five withstood the maximum voltage of 20 kV.

2) The M36A1 fired at 5.0 kV in this test, which is not a high voltage for accidental static electricity accumulation.

B. Current Design of ARC-211

Discussions on methods to reduce the static sensitivity of the original design of the detonator\* resulted in two possible methods both

---

\*Private communication, Mr. Patrick Cannon, Flare Northern Division

of which were simple and inexpensive. Subsequent tests at Ballistic Research Laboratories (BRL) showed both methods to be effective, in that they render the detonator insensitive to a series of five static discharges from a 500 pF capacitor charged to 20 kV applied between the case and bridgewire. Both methods depend on establishing a conducting path between one of the bridgewire leads and the metal case, so as to limit the potential difference that can exist between these two structures during a static discharge and hence reduce the possibility of an electric spark occurring in the interior of the detonator. Of course, the most direct method of establishing this conducting path would be a metal link from one bridgewire lead to the metal case. However, this would require a major change in the manufacturing process and increase the cost appreciably, so other methods were sought. One method is the use of a conductive epoxy applied between one bridgewire lead and the case after the detonator had been assembled and crimped. Since this conductive epoxy is difficult to apply quickly and precisely, the author determined by test that another method using flexible conductive paint\* was more suitable. After the conductive paint has dried, it is given a coating of insulating varnish which serves to protect it. However, the conductive paint patch remains visible through the varnish and this serves to identify electrostatic insensitive detonators of current design.

An interesting and useful result from these tests is that the conductive path established by the paint is fully effective in protecting the detonator even when the continuity of the path suffers small breaks.

\*Silver Micropaint, Type SC-13, Micro-Circuits Company, New Buffalo, Michigan (Possible Alternatives not investigated).

The results in Table 3 show that the conductive paint offered full protection whether its initial resistance was high or low. In most cases, application of five pulses from a 500 pF capacitor charged to 20 kV served to open the path, but the protection afforded by the paint was not affected. In a separate test, solvent was used to remove all visible traces of the paint, but the particles which remained on the surface apparently offered a preferred path for voltage breakdown, and still served to protect the detonator against static discharges.

Table 3. Performance of Conductive Paint in Protecting ARC-211 Detonators Against Static Electricity\*

<u>Resistance of Paint (ohms)</u>		<u>Effect of Test on Detonator</u>
<u>Before</u>	<u>After</u>	
2	open	did not fire
2	open	did not fire
10	open	did not fire
11	open	did not fire
36	0.7	did not fire
40	open	did not fire
90	open	did not fire
120	0.4	did not fire
150	open	did not fire
2300	open	did not fire

The effectiveness of this conductive path in protecting the detonator against a static discharge applied between case and bridge-wire is also shown in Tables 1 and 2 when one compares the results for ARC-211 original design and current design, both samples being from production lots.

\*Note: Test consisted of applying five pulses between bridgewire and case from 500 pF (charged to 20 kV) in series with zero ohms discharged by 5C22 hydrogen thyatron.

### C. Functioning Time of Current Design of ARC-211

The functioning times of the ARC-211 detonator as it is currently manufactured are tabulated in Table 4 along with the charging voltage and size of energy storage capacitor.

Where the functioning time distribution exhibits relatively small dispersion, the average functioning time, estimated standard deviation, and sample size are tabulated. In other cases, only the raw data are tabulated.

Attention is called to the fact that the functioning time of this detonator is relatively insensitive to firing voltage. Lowering the voltage from 5000 V to 500 V, a factor of 10, results in only approximately doubling the functioning time, from 2.42 to 5.58  $\mu$ sec. The detonator is usable at voltages as low as 6 V and at this level its functioning time is approximately 500  $\mu$ sec.

Specifications require that the detonator withstand 0.5 amp DC for one minute, and survive 5 pulses from a 500 pF capacitor in series with zero ohms discharged by a vacuum switch. The capacitor being charged to 20 kV and the pulses being applied between the shorted bridge-wire leads and the detonator case.

Table 4. Functioning Times of ARC-211 Detonators  
Fired thru 15 ft of RG58A/U Coaxial Cable

Voltage	Capacitor	Functioning Times ( $\mu$ sec)	
5000	1 $\mu$ F	2.42	
		$\sigma = .045$	
		N = 30	
3000	1 $\mu$ F	2.63	
		$\sigma = .079$	
		N = 10	
500	1 $\mu$ F	5.58	
		$\sigma = 0.37$	
		N = 5	
300	1 $\mu$ F	7.8	16.4
		11.2	55.6
		11.4	
6	battery	470	530
		510	640
		520	

Note:  $\sigma$  = estimated standard deviation  
N = sample size

### III. CONCLUSIONS

1. The objective of designing and manufacturing an inexpensive detonator immune to static electricity and suitable for precision synchronization has been met. Two direct tests, one using the human body and the other using a very conservative equivalent circuit for the human body (of 500 pF in series with zero ohms), have shown that the ARC-211 of current design is immune to static electricity from the human body up to at least 20 kV.

2. The technique of using conductive paint to establish a path to harmlessly dissipate a static electricity discharge from the human

body to an electric detonator has been developed and the value of this technique has been successfully demonstrated in production lots of the ARC-211 of current design.

3. The desirable low-voltage characteristics of the detonator have been retained, and it will function reliably down to 6 volts.

4. These investigations have revealed the complexities of establishing a realistic equivalent circuit for actual electrostatic discharges from the human body. When the very conservative equivalent circuit of 500 pF in series with zero ohms is used, the safety margin is over-designed in some cases. It is felt that more consideration should be given to the problem of specifying a more realistic human body equivalent circuit and incorporating it into military specifications.



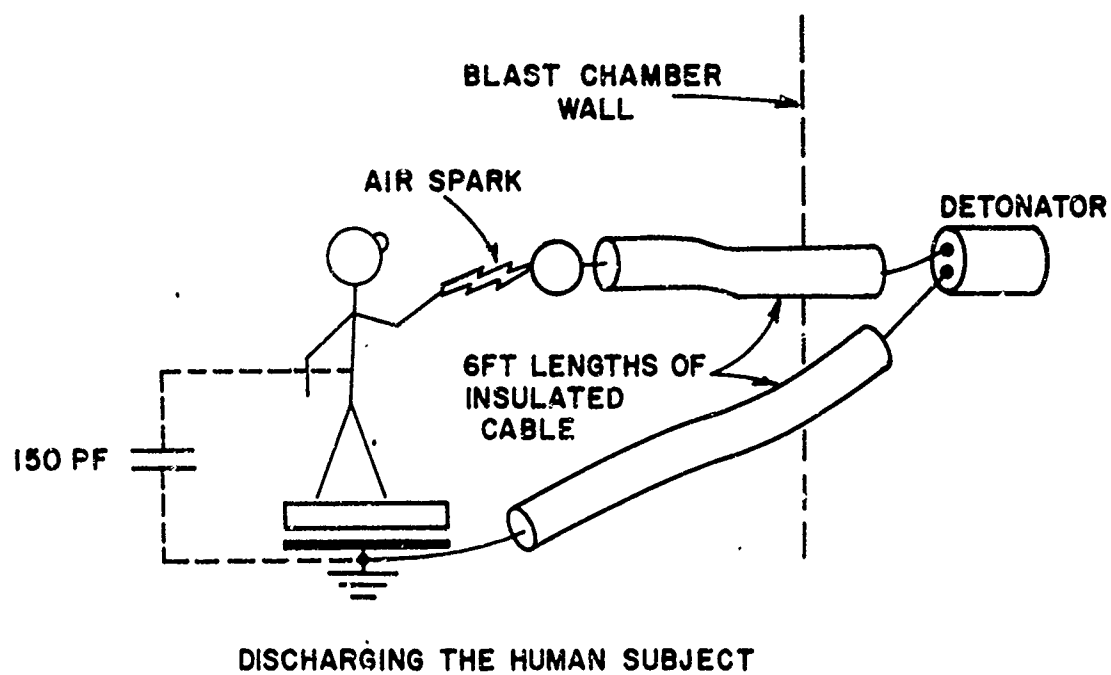
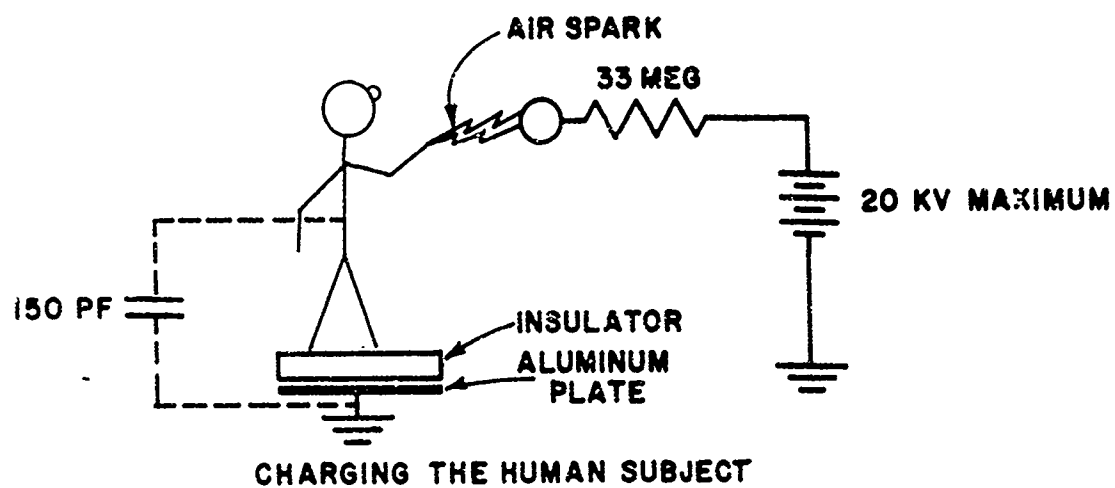


Figure 1. Detonator Tests With Static From Human Subject.

## 1-11 FURTHER ADVANCES IN MICROCIRCUIT BRIDGE TECHNOLOGY

D. N. GRIFFIN

PELMEC DIVISION  
QUANTIC INDUSTRIES, INC.  
SAN CARLOS, CALIFORNIA

### INTRODUCTION

This paper is a sequel to the paper presented at the Fifth Annual Symposium two years ago entitled "A Microcircuit Bridge for High Reliability Electro-explosive Devices". In the previous paper detailed information was presented on the design, fabrication, and performance characteristics of the Pelmec Microcircuit Bridge (MCB). Since that time several MCB configurations have been developed and are incorporated in a series of electro-explosive devices that have been qualified and are already in production. The purpose of this paper is to provide a brief description of the various microcircuit bridges and their applications.

### REVIEW

The Pelmec Microcircuit Bridge is based on thick-film technology as contrasted with thin film bridges of the type usually produced by vacuum deposition. I will not attempt to describe the advantages and disadvantages of the various types of bridges since this was covered in the previous paper.

The Pelmec MCB consists of a moly-manganese film approximately 1 mil thick sintered onto an alumina ceramic substrate.

Microcircuit bridge design and process details were given in the previous paper and are also covered by U.S. Patent No. 3,334,205.

The basic MCB design configuration is shown in Figure 1. The bridge itself consists of the necked-down portion in the middle of the pattern approximately .002 inches wide by approximately .020 inches long. This portion of the pattern controls the functioning characteristics of the bridge since it is here that a hot spot develops when the firing current is applied followed by burnout of the bridge. The remaining portions of the pattern consist of the attachment points to the connector pins and resistance leads from the attachment points to the microcircuit bridge. This design approach allows one to vary bridge circuit resistance and function time independently since total circuit resistance can be varied by changes in the resistance leads without change in the bridge itself. This design freedom is shown graphically in Figure 2 in which several of the different development configurations of the Microcircuit Bridge are shown.

Figure 3 shows the construction steps involved in attachment of the connector pins to the header and to the bridge. After sintering of the moly-manganese bridge, a nickel oxide paint is applied in the area of the pins and is also sintered in a reducing atmosphere to form a nickel coating. The connector

pins are then attached by riveting as shown in the middle view, after which a brazing alloy is applied and the part is furnace brazed. As shown in the top view, the brazing alloy flows and forms a bond between the connector pins and the bridge, wetting the bridge only in the area that is covered by the nickel coat. The brazing operation simultaneously forms a high-strength hermetic seal between the ceramic header and the pins, and an electrical connection between the pins and the bridge.

The MCB header shown in Figure 3 was used in the Pelmec Model 1353 Initiator that was described in the previous paper. This initiator was the first of a series incorporating the micro-circuit bridge in an all-ceramic configuration as shown in Figure 4. The Model 1353 Initiator consists of the alumina ceramic header and a ceramic cup containing the pyrotechnic charge. The header and cup are sealed with a filled epoxide high-temperature resin that provides a hermetic seal that has been temperature cycled from  $-300^{\circ}$  to  $+600^{\circ}\text{F}$  without failure. Because of the all-ceramic design the initiator is non-magnetic and provides a high degree of electrical isolation, as well as resistance to temperature cycling limited only by the pyrotechnic materials and the epoxide seal. The use of alumina ceramic instead of plastic materials for electrical isolation of the pyrotechnic cavity also provides improved heat dissipation, and consequently better no-fire characteristics. The Model 1353 Initiator was developed as a thermal battery

initiator, and can be used by itself or with a metal can closure to provide a faraday shield. For most applications the can is considered to be superfluous since the initiator is usually installed in a metal housing in its final assembly.

#### NEW DEVELOPMENTS

In the two years that have elapsed since the last symposium microcircuit bridges have been developed to meet several specific applications. The various configurations are shown in Figure 5. The header at the top of the figure contains a 1-amp/1-watt/.4-ohm bridge that was incorporated in the Model 1353 Initiator just described. The three headers shown in the middle of the figure all contain 1-amp/1-watt/1-ohm bridges, the first two consisting of equivalent bridges on different size headers, and the right hand header containing a dual-bridge configuration. The header shown at the bottom of the figure carries a 5-amp/1.5-watt/.06-ohm bridge. Applications for these various header configurations will be described briefly in the following figures.

#### High Energy Initiator

Figure 6 shows the construction of the Pelmec Model 1435 High Energy Initiator. This item was developed for motor ignition in the Air Force Short Range Attack Missile (SRAM), and it has been qualified and is in production. The High Energy Initiator utilizes a .06-ohm bridge that will withstand 5 amperes direct current on 1.5 watts for five minutes without firing. The

reliable all-fire current is 10 amperes dc for 10 milliseconds. The initiator is an all-ceramic design similar to the Model 1353 Initiator except that the ceramic case is longer to contain a larger output charge. A two-conductor shielded cable is attached to the initiator which is enclosed in a metal can. The wire braid shield on the cable is grounded to the can to provide a complete electrical shielding of the initiator and its wire leads. The initiator output charge is 175 mg of  $\text{BKNO}_3$  which develops a nominal pressure of 650 psi in a 9-cc chamber volume.

#### Detonator

A one-amp/one-watt/one-ohm detonator has also been developed for a destruct system for SRAM. This detonator, Peltec Model 1471, is shown in Figure 7. The basic construction of the detonator is similar to the high energy initiator except that a one-ohm microcircuit bridge is utilized. The high explosive charge is pressed into a metal sleeve which is contained in the ceramic cup together with the initiating elements of the pyrotechnic train as shown in the figure. The completed ceramic detonator is enclosed in a metal can in accordance with the customer requirements. For many applications the ceramic detonator could be used by itself since it is normally installed in a metal housing in which case the metal can is superfluous. The detonator output charge consists of 125 mg. of HMX, initiated by Lead Azide, and produces a nominal dent of .025-inches in the steel block dent test.

### Gas Generator

Figure 8 shows a gas generator that was also developed for SRAM for use in pumping electrolyte into a battery system. The generator utilizes dual 1-ohm microcircuit bridges having 1-amp/1-watt no-fire and 3.5 amp all-fire capability. This design utilizes a 4-pin glass-to-metal seal. Three wire leads are employed with one lead common to one leg of each of the two bridges. In this case the ceramic header is utilized as a heat sink and a carrier for the microcircuit bridges with the glass-to-metal seals providing the external hermetic and high pressure seal. The gas generator output will displace a nominal volume of 5500 cubic centimeters of fluid.

### Pressure Cartridges

The Pelmec Model 1464 Pressure Cartridge is shown in Figure 9. This cartridge is a large-volume low-cost item in use on a Viet Nam type weapon system. The cartridge is a 1-amp/1-watt no-fire device utilizing a 1-ohm microcircuit bridge on a ceramic header. Because of the low cost requirement of the application several novel design features have been incorporated. The ceramic header with wire leads attached is encapsulated in molded plastic as shown in the figure. The plastic also forms a cup on the face of the header that is loaded with the initiating elements of the pyrotechnic charge. The header sub-assembly is then pressed into the cartridge body together with an O-ring. This configuration provides high-pressure environmental seal that will withstand pressures in excess of 20,000 psi.

The header subassembly is in effect an electric match that provides its own high pressure seal and is readily adaptable to other applications.

The 1-amp/1-watt single and dual bridged headers shown in the previously described designs have also been incorporated into standard two-pin and 4-pin cartridges as shown in Figure 10. These cartridges also incorporate a glass-to-metal seal on the connector pins and are available with 1/2-inch, or larger, mating threads.

#### CONCLUSIONS

The brief descriptions of the various electro-explosive devices given in this paper show that the Pelmec microcircuit bridge has been reduced to practice and has been incorporated in a complete EED product line. Superior electrical characteristics of the microcircuit bridge have been demonstrated, as well as its applicability to large-volume low-cost production.



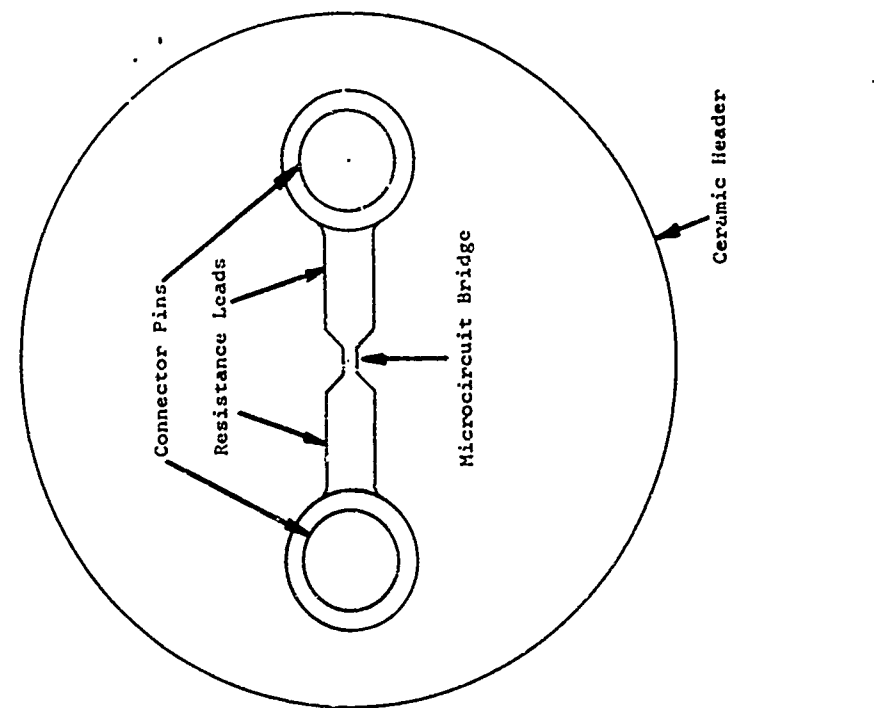


FIGURE 1 - Basic Microcircuit Bridge Design Configuration

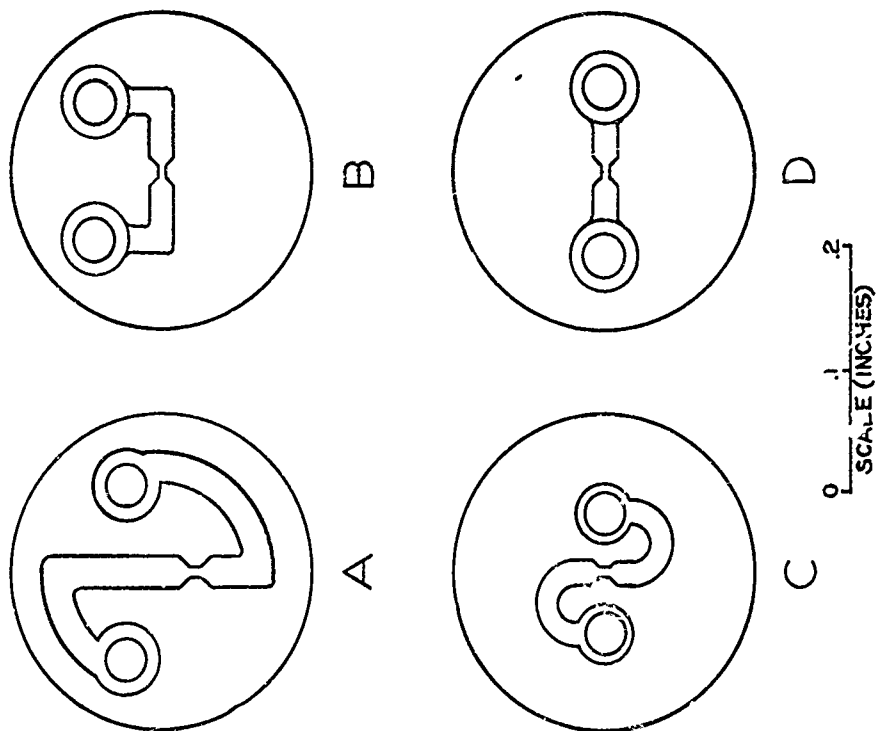


FIGURE 2 - Microcircuit Bridge Designs

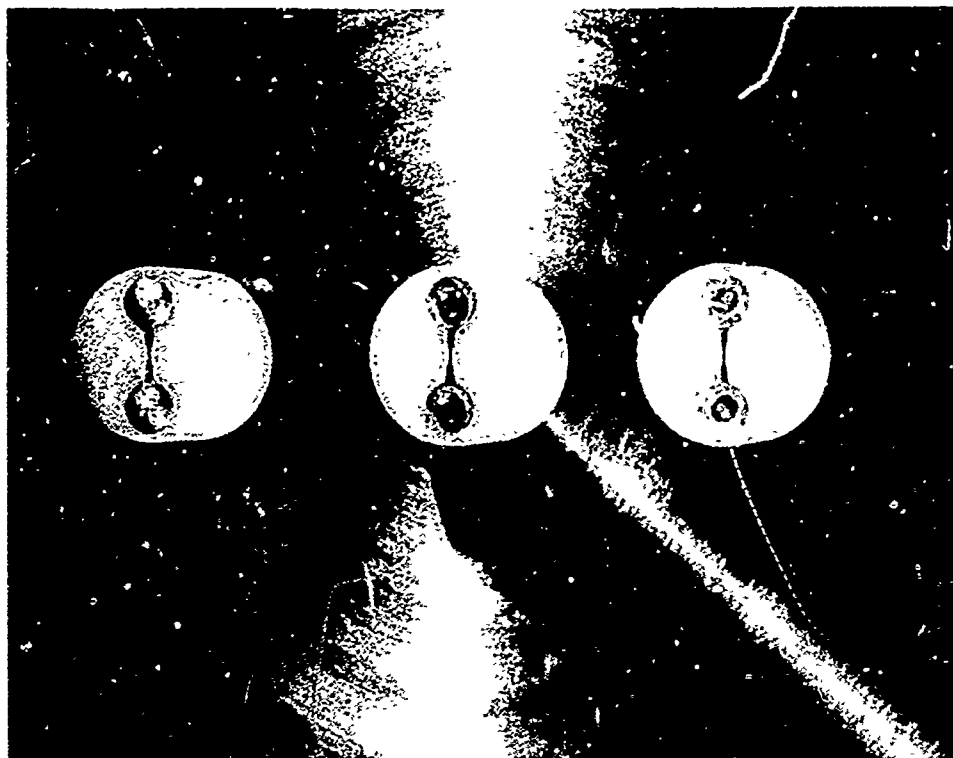


FIGURE 3 - Model 1353 Initiator Header with 0.4-ohm MC Bridge

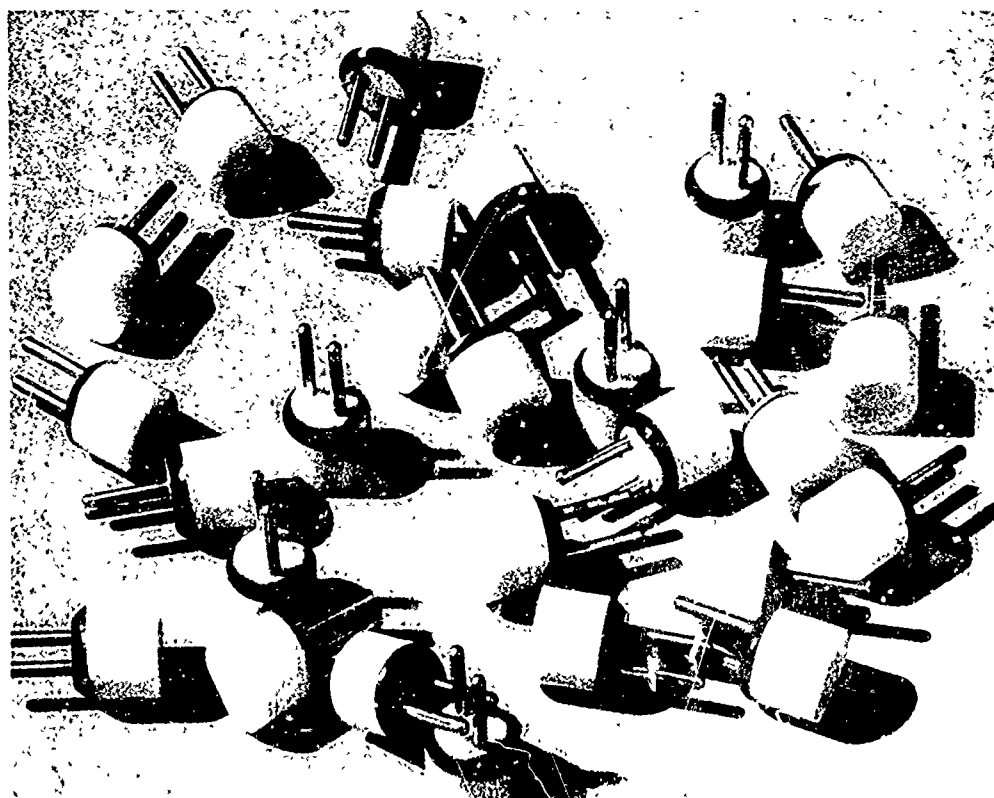


FIGURE 4 - Peltec Model 1253 Initiator

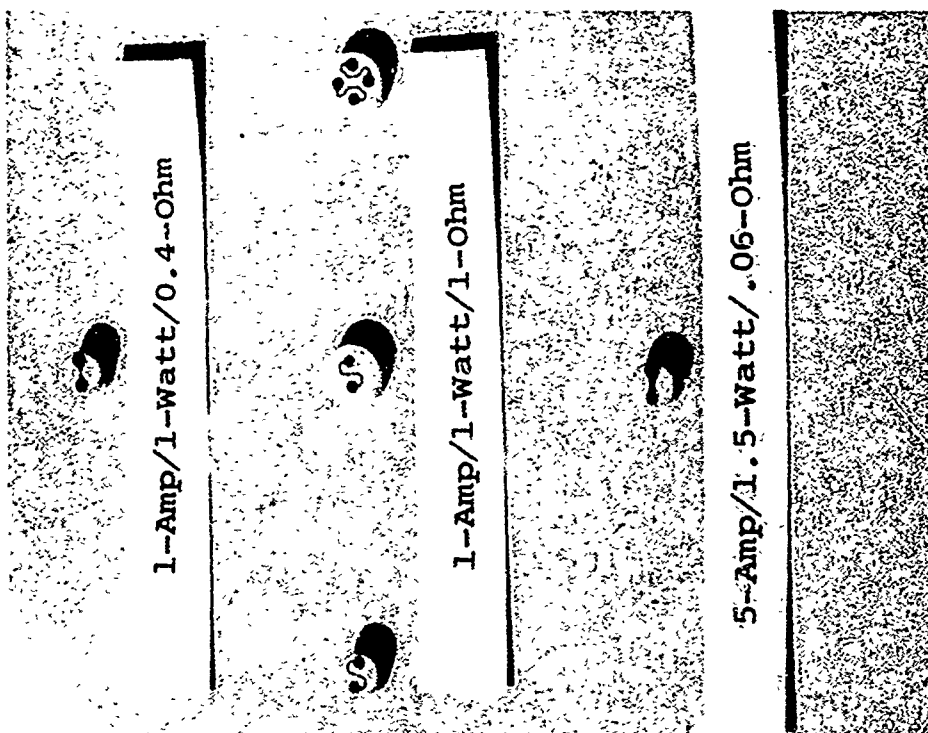


FIGURE 5 - Peltec Microcircuit Bridge (MCB) Headers

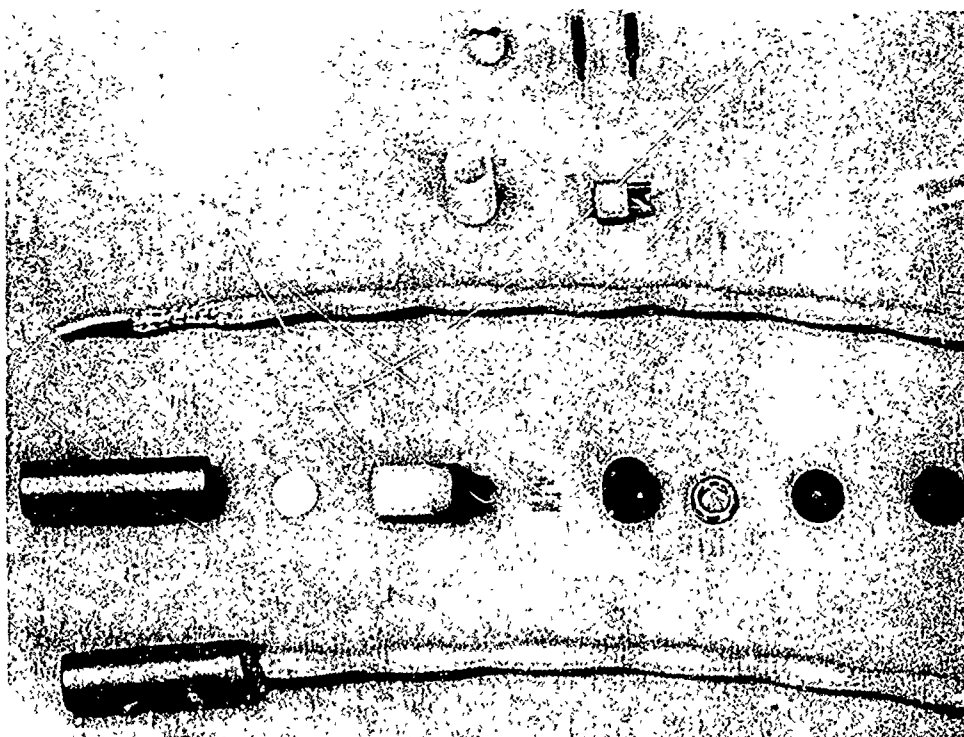


FIGURE 6 - Model 1435 High Energy Initiator

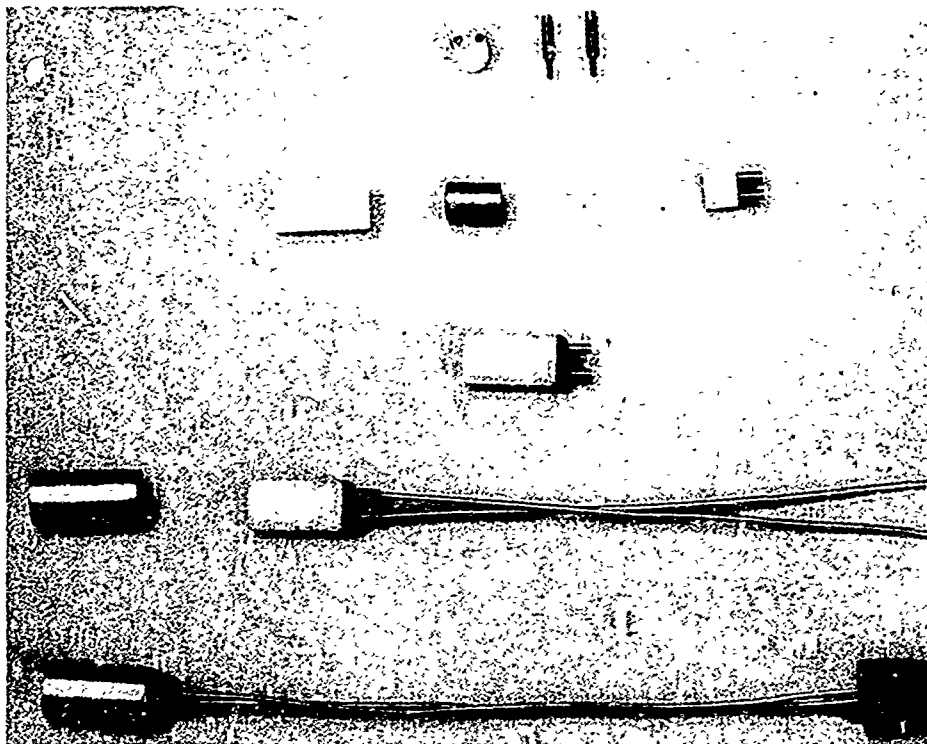


FIGURE 7 - Model 1471 Detonator

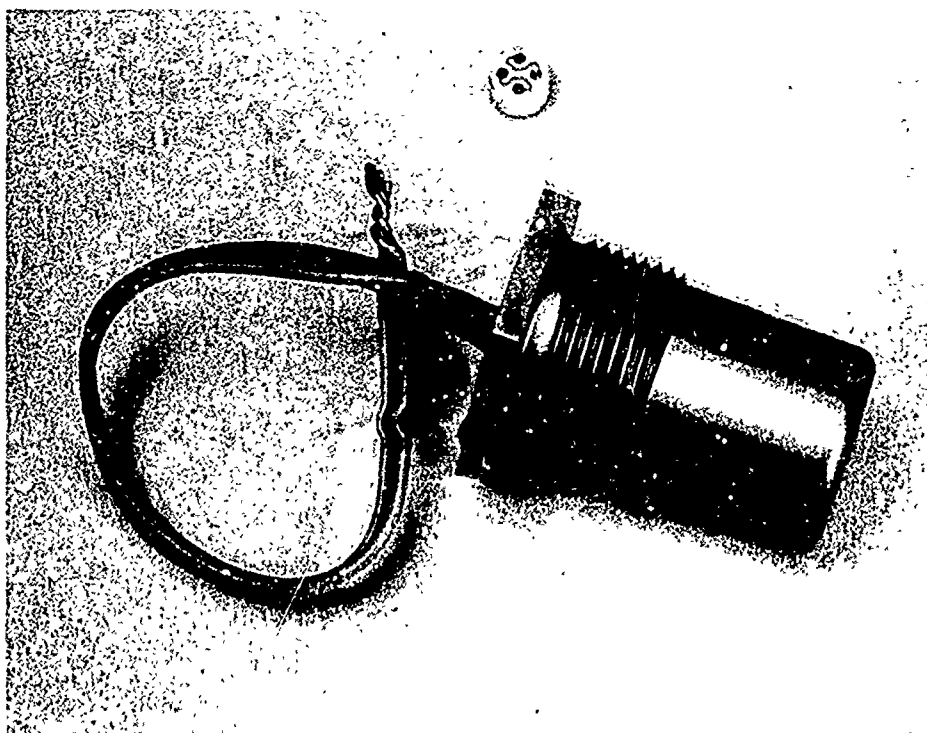


FIGURE 8 - Model 1473 Gas Generator

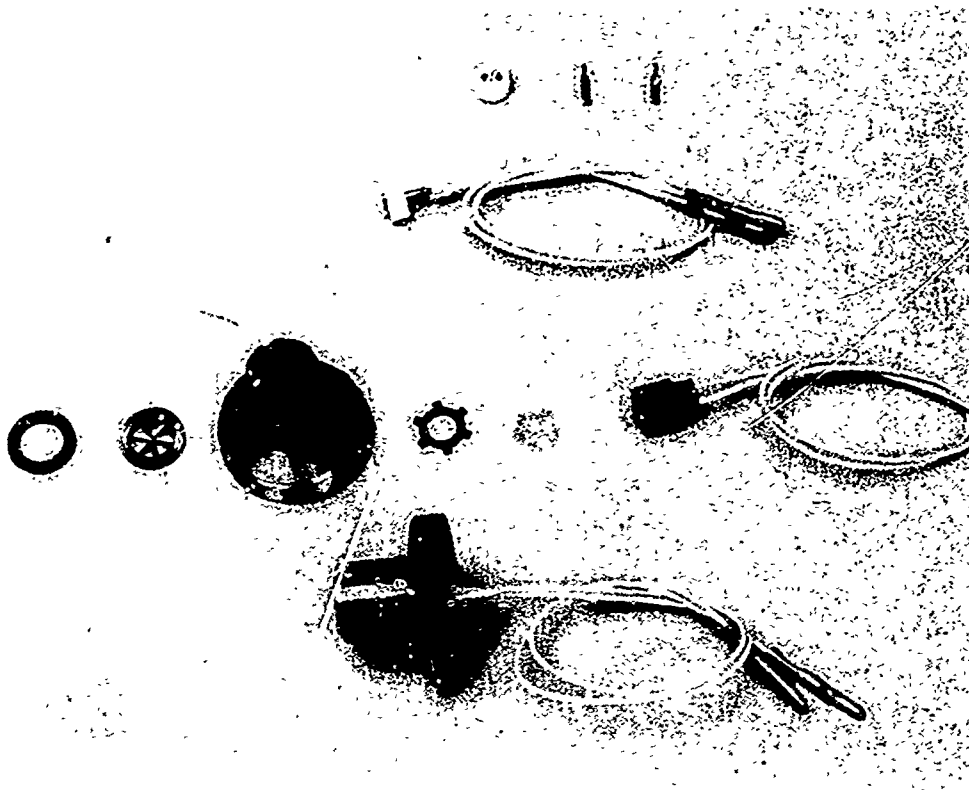


FIGURE 9 - Model 1464 Pressure Cartridge

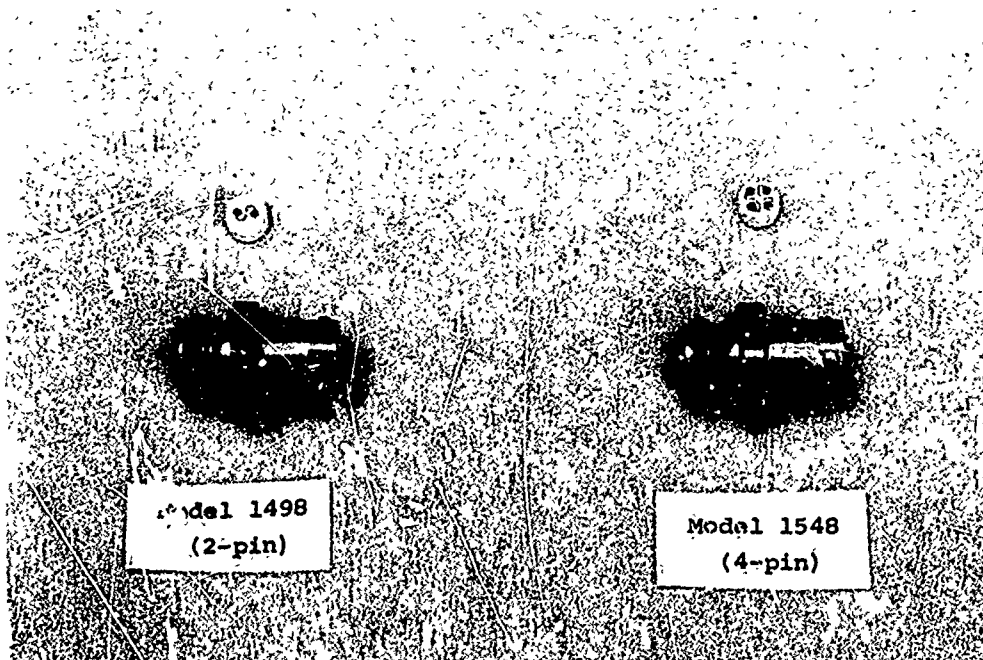


FIGURE 10 - Model 1498 and Model 1548 Pressure Cartridges

1-12 DEVELOPMENT OF AN ORDNANCE CIRCUIT RF FILTER  
P. F. MOHRBACH, D. J. MULLEN

1. INTRODUCTION

In October, 1968 The Franklin Institute Research Laboratories (FIRL) entered into a contract with Martin-Marietta Corporation for the development of an ordnance circuit RF filter. In essence this filter was to be built into the backshell of a standard Bendix type connector with 4 pins using minimum space and was to produce a worst case power attenuation of 40 dB from 100 MHz to 10 GHz. In addition a number of other design criteria were stated which included a series resistance of less than 0.2 ohms, a shunt resistance of at least 50 megohms, a current capacity of 20 amperes for 100 milliseconds duration, an RF power dissipation capacity of 20 watts for 5 minutes in both pin-to-pin and pins-to-case and degradation of the rise time, 10% to 90% amplitude, of the normal firing pulse no greater than an increase of 2 milliseconds. In addition, the design was to consider the normal space flight environments although FIRL would not test for most of these.

After consideration of many types of RF filters we chose an absorptive type, as opposed to one which depends on reflection. The basic RF unit of the attenuator is shown in Figure 1. The constraints upon this unit are as follows:

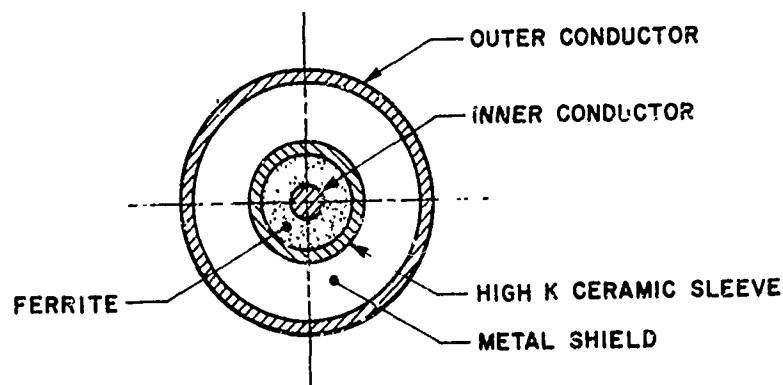


Figure 1. Basic Ferrite Attenuator

- a) The ferrite must be of a special type exhibiting large RF losses at high frequencies.
- b) The high dielectric constant (K) ceramic sleeve is primarily included to provide insulation resistance and block the low resistance shunt path between the two conductors. The value of K should be greater than 1000 and the thickness of the sleeve should be no greater than 20 mills.
- c) The metal shield is to prevent leakage of RF around the ferrite-ceramic complex.
- d) Good electric bonding is critical at all interfaces.

The final design was constructed with 5 of the basic units assembled on each pin to obtain the necessary attenuation, and the metal shield was carried along the entire length of the stacks to improve heat dissipation. This complete assembly is shown in Figure 2.

## 2. TEST RESULTS

The prototype units were constructed for evaluation. The physical characteristics of these filters were as follows:

Nominal length including backshell	1-3/4 inches
Nominal length over leads (no backshell)	1-7/16 inches
Maximum diameter	-11/16 inches
Weight (including backshell)	-20 g/0.7 oz.
(without connector)	-10.5 g/0.37 oz.
External finish	Iridite
Series resistance through leads	-less than 0.007 ohms
Shunt resistance between pins (measured at 500 volts)	-greater than 5000 megohms

### 2.1 Worst Case Attenuation

Worst case attenuation is the minimum dissipative loss that one can obtain from a unit under any input and output conditions. Methods for determining this loss vary with frequency and magnitude of the loss, but a typical system of the type used for the majority of our measurements is shown in Figure 3.

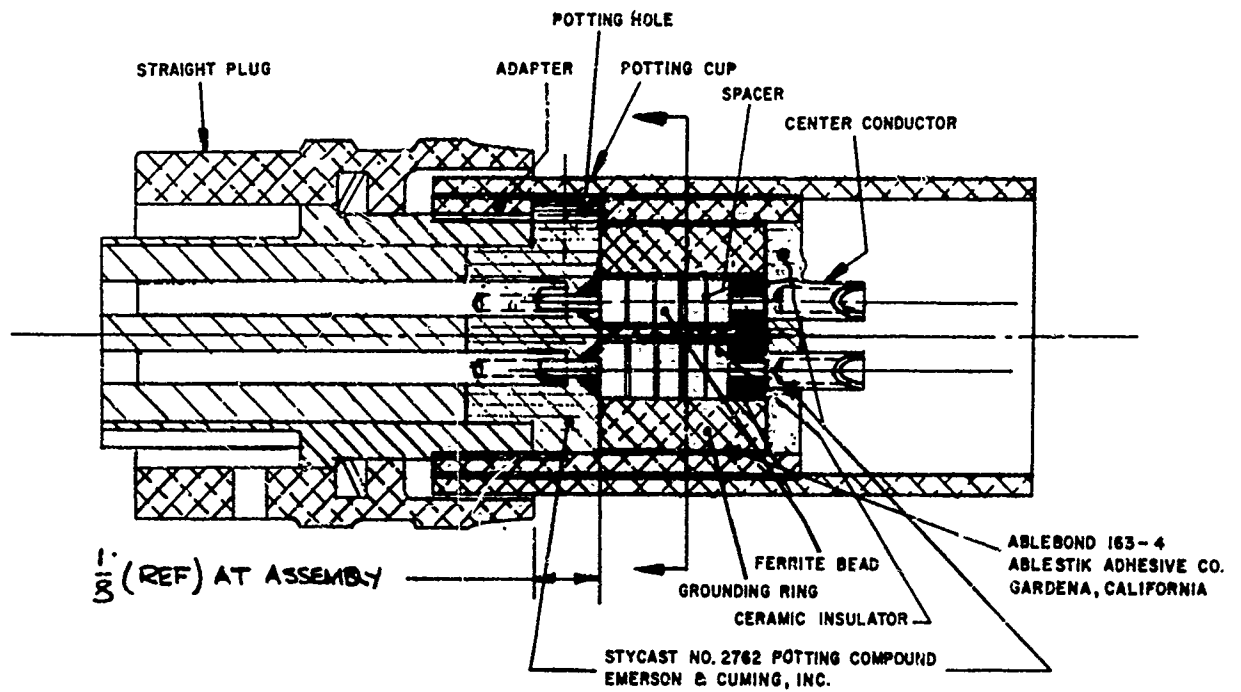


Figure 2. Connector - RF Filter Assembly

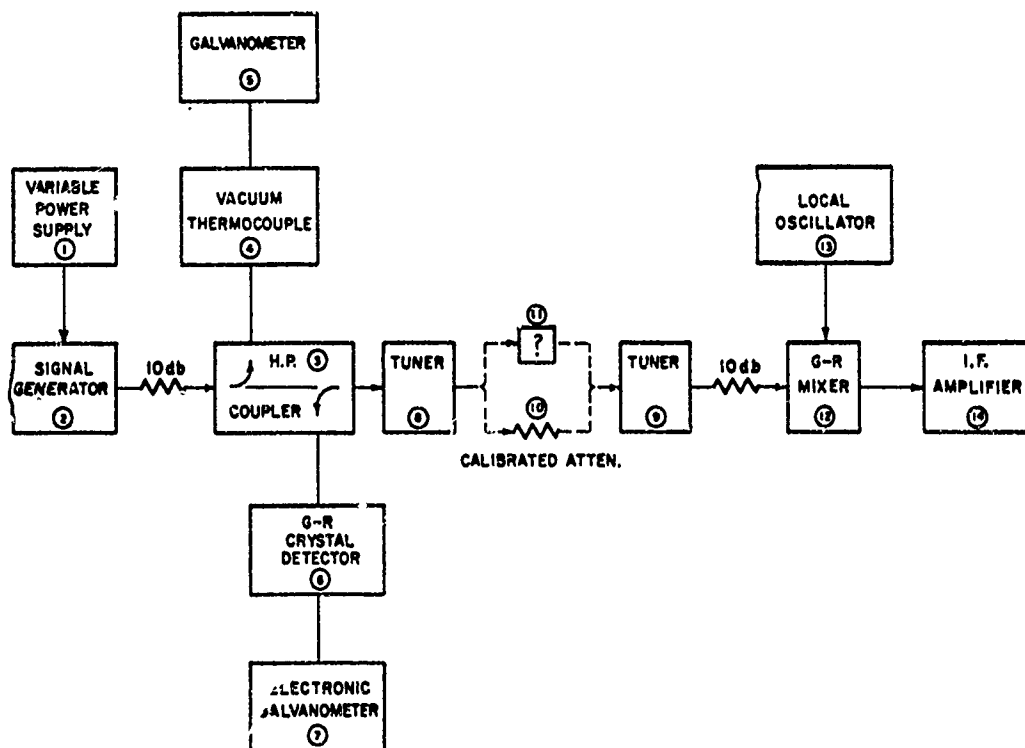


Figure 3. High Frequency Attenuation Test Set-Up



Tables 1 lists the  $dB_{wc}$  values obtained on a typical leg of one of the prototype filters at several discrete frequencies. Note that from 10 MHz on down we can only state that the values are less than 10. This is a function of the system resolution. Also at 9000 MHz values are stated to be greater than 35 dB. This value (35 dB) represents the dynamic range of the equipment at this frequency. Actual dB values for the filter are probably much larger.

## 2.2 Terminated Power Loss (TPL)

Terminated Power Loss is the measurement of minimum dissipative loss that a device can produce if its output is terminated in a known impedance. This measurement is frequently valid for filters used in ordnance circuits since such filters are frequently terminated in an explosive device. It should be noted, however, that it is the terminating impedance that must be held constant if the laboratory measurement is to be related to an actual application.

All the measuring systems for determination of  $dB_{wc}$  can be easily modified to measure TPL if the termination impedance employed is small in relation to 50 ohms, the characteristic impedance of the laboratory measuring systems. In our measurements disc resistors in feed through mounts with the disc placed across the line were used as terminations. The results on one of the prototype filters for terminations of 0.5, 1.0 and 5.0 ohms are shown in Table 2.

## 2.3 Degradation of Firing Pulses

To determine the effect of the filter on normal firing pulses a constant current pulse of 9 amperes amplitude and 100 milliseconds duration was applied to one leg of each filter. The Franklin Institute Research Laboratories FILUP was used to supply the pulse. The output of the filter was terminated in a high power, non-inductive, one ohm resistor. The input pulse and the output pulse were observed on a Tektronix 551 Dual Beam Oscilloscope using Type K plug-in units. The results are shown on Figure 4. These photographs are of course subject to interpretation, but even a harsh analysis of the figures indicated very little effect on the rise time of the pulse or its amplitude.

Table 1

WORST-CASE ATTENUATION  
FILTER #46

Room Temperature

<u>Freq.</u> (MHz)	<u>Leg</u>	<u>dB</u>	<u>Freq.</u> (MHz)	<u>Leg</u>	<u>dB</u>	<u>Freq.</u> (MHz)	<u>Leg</u>	<u>dB</u>
0.1	A	<10	50	A	36	5000	A	>60
	B	<10		B	37.5		B	>60
	C	<10		C	36.0		C	>60
	D	<10		D	36.5		D	>60
0.5	A	<10	100	A	48	9000	A	>35
	B	<10		B	50		B	>35
	C	<10		C	48		C	>35
	D	<10		D	50.6		D	>35
1.0	A	<10	200	A	58			
	B	<10		B	58			
	C	<10		C	56			
	D	<10		D	59			
2.0	A	<10	500	A	>60			
	B	<10		B	>60			
	C	<10		C	>60			
	D	<10		D	>60			
5.0	A	<10	700	A	>60			
	B	<10		B	>60			
	C	<10		C	>60			
	D	<10		D	>60			
10.0	A	<10	900	A	>60			
	B	<10		B	>60			
	C	<10		C	>60			
	D	<10		D	>60			
30.0	A		2000	A	>60			
	B			B	>60			
	C			C	>60			
	D			D	>60			

Table 2  
TERMINATED POWER LOSS (dB)  
FILTER #45

Room Temperature

Freq. (MHz)	Leg	0.5Ω (dB)	1.0Ω (dB)	5.0Ω (dB)	Freq. (MHz)	Leg	0.5Ω (dB)	1.0Ω (dB)	5.0Ω (dB)
0.1	A	19.1	15.2	2.0	100	A	57	61	54
	B	19.6	16.3	6.1		B	62	62	59
	C	8.0	4.9	1.8		C	57	58	55
	D	7.5	5.3	1.1		D	56	56	53
0.3	A	5.7	5.2	2.5					
	B	6.5	2.5	2.0					
	C	11.3	4.0	2.0					
	D	1.5	2.8	0.8					
0.5	A	3.0	1.1	0	200	A	>60	>60	>60
	B	3.6	3.4	0		B	>60	>60	>60
	C	3.0	.4	0		C	>60	>60	>60
	D	3.2	1.1	0		D	>60	>60	>60
1.0	A	6.9	5.1	1.7	500	A	>60	>60	>60
	B	7.0	5.2	1.9		B	>60	>60	>60
	C	6.5	4.5	1.7		C	>60	>60	>60
	D	6.9	4.5	2.0		D	>60	>60	>60
3.0	A	15.2	12.6	6.7					
	B	15.2	12.6	6.7					
	C	15.3	12.0	6.5					
	D	15.0	12.8	6.8					
5.0	A	14.4	11.6	5.8	700	A	>60	>60	>60
	B	14.3	11.7	5.3		B	>60	>60	>60
	C	14.0	11.7	5.7		C	>60	>60	>60
	D	19.5	16.9	10.8		D	>60	>60	>60
10	A	17.9	15.4	9.7	900	A	>60	>60	>60
	B	17.5	15.2	9.2		B	>60	>60	>60
	C	17.3	14.5	9.2		C	>60	>60	>60
	D	21.3	18.6	13.1		D	>60	>60	>60
30	A	32.5	29.6	26.4	2000	A	>60	>60	>60
	B	32.7	29.0	25.8		B	>60	>60	>60
	C	32.6	29.3	26.1		C	>60	>60	>60
	D	34.2	26.1	27.9		D	>60	>60	>60
50	A	42	42	40					
	B	41	41	40					
	C	38	37	36					
	D	36	36	35					

NOTE - PULSE : 9A  
100 ms

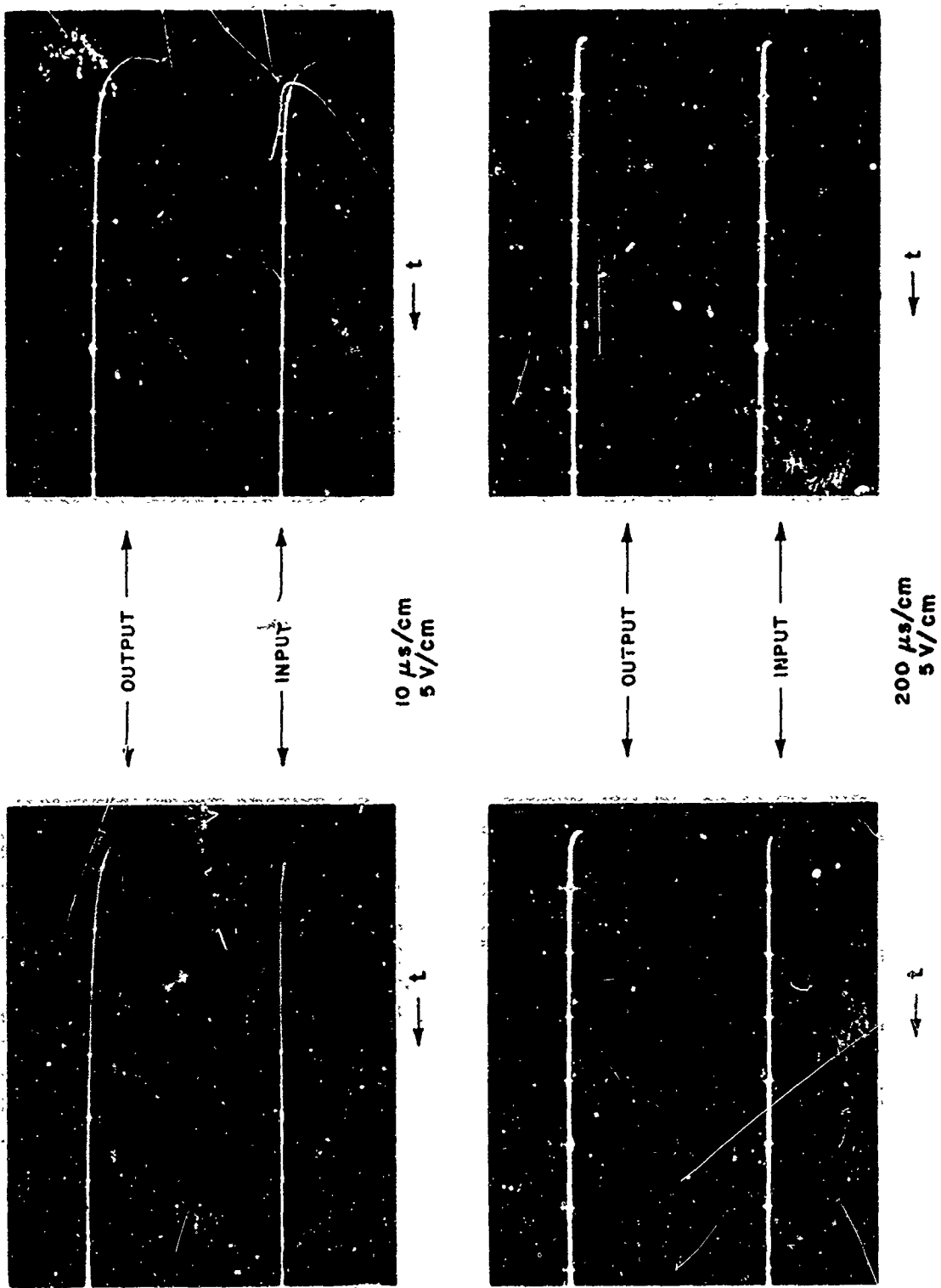


Figure 4. Degradation of Firing Pulse

As a further check on this phase of the filter's effect on firing pulses, ten McCormick-Selph pressure cartridges manufacturer's P/N: PD6050129-505, received from Martin-Marietta Corporation were connected in turn to the output of the filter and the standard firing pulse of 9 amperes amplitude, 100 milliseconds duration was applied to the input of the filter. All units fired and the functioning times are shown in Table 3.

#### 2.4 Current Capacity

For this evaluation the same setup as used in Section 2.3 was used except that the pulse had a 20 ampere amplitude for 100 milliseconds. Prior to exposure to this pulse the resistance between the center conductor of the filter and the case was greater than 5000 megohms. There was no change in this value following the application of the pulse.

Table 3  
FUNCTIONING TIMES OF MC CORMICK SELPH PRESSURE CARTRIDGES  
P/N PD 6050129

<u>Pressure Cartridge No.</u>	<u>Functioning Time (milliseconds)</u>
0013422	1.764
0013446	2.360
0013445	2.228
0013444	1.747
0013443	2.201
0011963	1.628
0011964	2.472
0011962	1.944
0011965	1.919
0013022	<u>1.720</u>
Average Functioning Time	1.998

## 2.5 RF Power Capacity

The purpose of this test was to determine the response of the filter when 20 watts of RF was dissipated in the filter for a period of 5 minutes. A special mount was constructed to permit RF power to be delivered to the input of the filter and still provide a minimum heat sink on the filter. The *output* of the filter was unterminated. Neither FIRL #45 nor FIRL #46 was used in this test. A thermocouple was attached to the surface of the filter near the input end. A frequency of 5400 MHz was used since it was the only frequency of the indicated test frequencies which could deliver sufficient power. However, it was felt that this high frequency would also represent the most severe test for the filter. The results are shown in Table 4.

The filter was then tested to destruction to determine the failure mode. The same test set up was used. At 25 watts/215°C and at 30 watts/260°C some smoke was found inside the test chamber but shunt resistance and attenuation remained unchanged. At 35 watts/305°C the rubber that held the pins in the connector protruded about 1/8 inch from the end of the connector. However, measurements of shunt resistance and attenuation still indicated no significant change. At 40 watts/330°C, the test was terminated at 1 minute. By this time the rubber had completely cleared the connector and measurements of attenuation could no longer be made since the filter had essentially come apart. Measurements of shunt resistance were as follows:

a) Pins-to-Case Resistance

Leg B - 5k  $\Omega$

Leg C - 4k  $\Omega$

Leg D - 4k  $\Omega$

Leg A - 200k  $\Omega$

b) Pins-to-Pin Resistance

A to C - 200k  $\Omega$

C to D - 200  $\Omega$  (intermittent)

A to D - 2M  $\Omega$

Table 4  
RF POWER CAPACITY OF FIRL #47

<u>RF Power</u> <u>(watts)</u>	<u>Surface</u> <u>Temperature</u> <u>°C/°F</u>
0	27°/80°
7.5	75°/165°
15	145°/292°
20	200°/390°

Shunt Resistance before and after all tests - >5000 megohms  
Approximate attenuation at 100 MHz before and after all tests - 50 dB.

Failure analysis indicated no specific point of failure in the filter. The only conclusion that could be reached is that overall destruction occurred at this level and any circuit containing the filter would have to be considered nonoperative and failure cataclysmic.

## 2.6 Impedance Measurements

Because it was felt to be of considerable interest in the long range view, impedance measurements were made on one of the filters. This data is shown in Table 5. This data was obtained with the following:

- a) General Radio Type 1606A or 916A RF Bridge - 0.4 to 60 MHz
- b) General Radio 821-A Twin - Tee Bridge - 1 to 30 MHz
- c) General Radio 1607A Transfer Function and Immittance Bridge - 25 to 1500 MHz

## 2.7 Temperature Tests

During the design phase on the filter, attenuation was checked at -50°C/-60°F and +100°C/212°F. Results at that time indicated an approximate loss of 10 dB at -50°C and little or no change at 100°C. There is nothing in the final design that should change that data. Tests were started on one of the prototype filters and the tests showed that at a temperature of 100°C, attenuation at 50, 100 and 200 MHz showed no significant change in attenuation over ambient conditions. However, difficulties arose at 900 MHz and readings as low as 47 dB were observed.

Table 5  
IMPEDANCE MEASUREMENTS ON FILTER NUMBER 46

<u>Freq.</u> (MHz)	<u>Leg</u>	<u>Z<sub>11</sub></u> (Ω)	<u>Z<sub>22</sub></u> (Ω)
1.0	A	7.4 - j68.0	7.2 - j68.0
	B	6.0 - j58.0	6.2 - j58.0
	C	13.1 - j74.0	12.5 - j72.0
	D	5.5 - j68.0	5.7 - j68.0
5.0	A	10.0 - j10.0	10.0 - j7.0
	B	7.4 - j9.4	8.7 - j8.1
	C	7.8 - j13.0	11.0 - j8.0
	D	8.4 - j9.0	8.1 - j8.6
10.0	A	13.0 - j6.1	15.5 - j1.4
	B	12.4 - j4.1	14.0 - j3.8
	C	11.0 - j5.9	17.5 - j1.4
	D	13.5 - j4.8	13.3 - j3.6
30.0	A	1.9 - j5.7	14.4 - j1.4
	B	8.0 - j5.3	9.0 - j3.4
	C	7.9 - j5.6	18.6 - j2.8
	D	8.1 - j5.8	9.6 - j3.3
50.0	A	6.9 - j3.3	9.0 - j0.32
	B	7.05 - j3.9	8.2 - j0.53
	C	6.94 - j3.1	18.6 - j1.4
	D	7.07 - j3.3	16.6 - j0.55
100	A	4.0 + j1.0	12.0 + j4.5
	B	4.0 + j0.5	5.5 + j7.0
	C	4.5 + j1.0	14.0 + j4.0
	D	5.0 + j1.0	6.0 + j6.0
200	A	4.0 - j6.0	10.5 - j14.0
	B	4.0 + j5.5	5 + j17.0
	C	4.0 + j6.0	11.5 + j14.0
	D	4.0 + j6.0	5 + j16.5
500	A	3.0 + j19.0	12.5 + j45.0
	B	3.5 + j17.0	7.5 + j47.0
	C	2.0 + j18.0	13.0 + j40.0
	D	4.0 + j18.5	6.5 + j44.0
700	A	4.5 + j26.0	21.0 + j62.0
	B	3.0 + j24.0	15.0 + j75.0
	C	4.0 + j25.0	24.0 + j63.0
	D	5.0 + j25.0	18.0 + j77.0
900	A	4.96 + j32.0	72.0 + j93.0
	B	3.0 + j30.0	72.0 + j120.0
	C	3.0 + j31.0	67.5 + j84.0
	D	2.0 + j33.0	52.5 + j120.0



However, the main feature was highly erratic readings. A return to ambient temperatures and shifting to other legs still produced very erratic results.

This phenomenon has been observed in the past and we believe is associated with the connector. The connectors of this type when they have gone through a hundred or so connections and disconnections seem to produce erratic results on RF determinations at frequencies above 500 MHz. The full reason for this has not been determined and is in fact not even proven except by frequent observation.

As a quick check, however, a special version of the filter was made up with a single 5 bead stack using identical materials and material interfaces as in the backshell filter but mounted in a fixture with regular RF connectors. This special filter measured greater than 60 dB attenuation at 900 MHz both at ambient and 100°C. All testing on the backshell filters was halted at this point.

### 3. SUMMARY AND CONCLUSIONS

The present filter designed to fit into the backshell of a standard ordnance connector appears to meet all of its specifications of a physical and electrical nature. In its present form, the filter elements themselves add approximately 1/2 inch of length to the system and overall size including the connector and provisions for attaching and potting the input cable is approximately 1-3/4 inches. The weight added by the filter for each explosive device is approximately 10 grams. Series resistance, that is the resistance from the input of the filter to the output of the connector, is less than 0.007 ohms while the pins-to-case resistance is greater than 5000 megohms. Worst case attenuation is greater than 40 dB from 100 MHz to 10 GHz and this level is apparently maintainable over a temperature range of -50°C to +100°C. Although data on this point is somewhat limited, the filter shows no significant deterioration of a normal firing pulse of 9 amperes delivered for 100 milliseconds. Currents of 20 amperes delivered for 100 milliseconds have shown no detectable effect on any parameter of the filter. The filter has absorbed 20 watts of RF without any detectable effect on characteristics. No specific failure mode has been established so far

at any of these required conditions; however, at the level of 35 to 40 watts absorbed in the filter, at which time temperatures of 500 to 600°F can be expected on the surface of the filter, failure occurs and must be assumed at this time to catalytic.

On the cautionary side, several points might be made, however. For example, when and if 20 watts of power are absorbed in the filter, surface temperatures can rise as high as 300°F with internal temperatures even higher. How much heat could be transferred forward to the explosive element and what the effect would be is not known at this time. This temperature is for a filter with minimum heat sinking, however, and the temperatures could vary greatly depending on heat sinking. Such techniques as the addition of cooling fins to the filter could greatly reduce overall temperature.

Little information exists at this time on the long term stability of the filter. Similar filters which we have built in the past have shown no significant shift in attenuation or resistance parameters over a period of several years, but the particular combination of materials and construction in this filters are unique and aging must be considered.

There is also the continuing evidence of some degradation of high frequency attenuation (500 MHz and above) as a function of aging and temperature cycling which is not completely resolved. We have some reason to believe that part or all of what we observe can be traced to wear and tear in the connector, but this has not been clearly established.

Finally there is the problem of surviving the other environmental tests. We do not expect any serious problem on this, but the tests must still be conducted.

## ABSTRACTS - SESSION TWO

### 2-1 The Second Law Applied to Pyrotechnic Systems

J.H. McLain

Thermodynamic considerations are recommended as an effective screening tool in the development of pyrotechnic formulations. Use of maximum value of the heat of reaction is suggested to determine free energy and the maximum equilibrium constant for "gasless" delay mixes that enter into nearly isentropic solid-solid reactions. For some reversible reactions, crude approximations of the temperature of reaction reversal show good agreement with calculated and experimental values in the literature. A suggested application toward improving the emissivity of illuminant mixes is made as a result of these "temperatures of reversal".

### 2-2 Statistical Scanning Study of Explosive End Fittings

R.R. Sullivan,  
S.A. Moses, and G.R. Compton

The results of a study to evaluate end fittings for a confined detonating fuse are reported. Two different modifications of three end fitting designs (called *protruding*, *stepped*, and *conical*) are discussed on the basis of the results of a statistical scanning test program. The end fittings are evaluated as both donor and acceptor charges. This report includes an account of the effects of using Class 2 and Class 4 pentaerythrite tetranitrate and loading pressures of 5, 10, and 20 kips per square inch. The material and thickness of potential end caps are likewise examined, along with the results of tests performed to determine whether assembly procedures degrade the detonating characteristics of the fittings.

### 2-3 Interior Ballistics of High-Low Propulsion Systems

Otto K. Heiney

A first order high-low interior ballistic formulism is developed and theory correlated with experiment. The high-low ballistic concept consists of burning propellant in a high pressure plenum and venting combustion products in a controlled manner through nozzles during and subsequent to propellant burn. The results of the analysis indicate that while the high-low phenomenon is outwardly similar to conventional interior ballistic theory the response is fundamentally different in many respects. Experimentally determined chamber and combustion plenum pressure time traces are compared to analytic digital computer predictions determined for an 11-inch parachute deployment mortar currently under development.

### 2-4 Nomographical Solution of Electro-Explosive Device Firing Time Equation

D. Peckham,  
D.E. Davenport

A review of existing solutions for the electroexplosive device design problem is given. Rosenthal's solution is expanded and refined to permit the prediction of firing data strictly from blueprint data. A set of nomographs is presented to permit the rapid, easy solution of the new set of equations. The new solution is compared against firing data with excellent results.

### 2-6 Quantitative Predictions of EED Firing Characteristics

D.E. Davenport

Previous papers have presented a mathematical model dubbed STATE (Space, Time and Temperature Evaluation) for predicting the behavior of EED's based only on physical, thermal and electrical characteristics of the components. The formulation has been shown to be very good for predicting the change in functioning characteristics of a device with variation of parameters such as bridgewire geometry or temperature coefficient of resistivity. The present paper shows the quantitative agreement between the model and experimental results in time-to-fire and no-fire level predictions.

2-7P Electrical and Thermal Considerations in the Design of Electroexplosive Devices

*R.H. Stresau*

This paper is a heuristic discussion of effects of reaction kinetics, states of aggregation, and parameter distribution as they affect initiation characteristics. The discussion is largely concentrated in the area of hot bridgewire devices but includes some mention of film bridge devices.

2-8 The Development of a Fixed Gap, Electrostatic Spark-Discharge Apparatus for Characterizing Explosives

*L.J. Montesi*

The sensitivity of explosives to electrostatic spark discharges is of major concern to personnel working with explosives and explosive components. To meet the need for a simple and reproducible apparatus that could easily be built and used to obtain comparable results, new apparatus was designed. By following the construction specifications and operating instructions, it should be possible now for independent laboratories to obtain comparable results. The apparatus developed uses a fixed gap of 0.050, a capacitor of 0.01 mfd, a line resistance of 100 ohms, and a point-to-plane spark discharge.

2-9 Experiments in Measurement of Output Energy of Electroexplosive Devices Through Metal Deformation

*S. Barron,  
E.G. Pierson*

Two experimental methods for the measurement of the output energy of EED's through metal deformation have been employed. One method covers relatively slow burning charges to medium brisance devices while the other is restricted to the range of brisance explosives. The brisance type of explosive was tested with a modified version of the lead block Trauzl apparatus. The second procedure involving equipment referred to as the Conax Energy Monitor has been used in place of the pressure bomb for engineering evaluation and quality assurance testing of relatively slow burning to medium-high brisance devices.

2-10 Use of Neutron Radiography for Visual Non-Destructive Examination of Ordnance Components

*C.R. Wilson and  
W. Breakey*

Neutron radiography has been utilized by Ordnance manufacturers, NASA and DOD agencies for visual non-destructive examination of critical ordnance devices for about two years. Several such uses are discussed in this paper along with the benefits attained by using neutron radiography. The present status of neutron radiography is defined and future growth is expected to be significant. This paper also discusses the fundamentals of neutron radiography inspection and explains the similarities and differences between x-ray radiography and neutron radiography.

2-11 Non-Destructive Testing of Apollo CSM Spacecraft Ordnance Devices by Neutron Radiography

*W.H. Knight and A.L. Hitchens,  
N.M. Ewbank and G. Gigas*

Non destructive testing of Apollo CSM (Command and Service Module) spacecraft ordnance devices has been accomplished by indirect and direct neutron radiography using a 1 megawatt swimming pool reactor source. These examinations have shown discrepant loading, internal debris and contamination. A process specification has been developed for neutron radiographic testing and a certification program for n-radiographic film readers has been established. This method has proven to be an extremely powerful technique for analysis and portends much promise in the future development of new electroexplosive devices.

2-12 Through-Bulkhead Initiator Design Margin Study

*William B. Freeman*

Through-bulkhead initiator explosive trains (RDX) were studied in a parametric test program which included relative measurements of donor output, shock attenuation through steel bulkheads, and shock sensitivity of acceptor charges. Detonation velocity versus column length was investigated in donor and acceptor charges. Data are presented and test methods are described.

2-13 Dynamic Output Characterization of Thrusting Type Pyrotechnic Devices

*J.L. Lilly*

Laboratory test procedures and equipments have been developed for performance characterization of thrusting type pyrotechnic devices. Work diagrams are developed to characterize the output of devices and compared to space vehicle application work diagrams to establish base line design margins. These work diagrams can then be used for assessment of reliability models and degradation patterns of these devices due to storage, changing environments, and vehicle aging, etc.

2-14 Instrumentation Control Charts

*S. Denskey*

Control charts have become traditional tools in controlling a process through the statistical evaluation of the product parameters or dimensions. By considering the test measurements of 'one shot' devices as a process, these control charts can be effectively used to control the test instrumentation as the test is being conducted. The sequence of events leading to the present group of charts is discussed.

2-15P Information Sources for Explosives and Pyrotechnics

*Gunther Cohn*

The great bulk of current technical information makes it difficult to keep posted. For this reason, this paper reviews briefly the useful information sources in the field of explosives and pyrotechnics. Updating the paper included in the Proceedings of the Fifth Symposium of Electroexplosive Devices, it includes: (1) Mission houses, (2) Government manuals, (3) Commercial publications, (4) Symposium proceedings, and (5) R&D programs.

2-16P Explosive Detonator Shock Testing for Impact Sensors

*Joseph Robin Klein*

No abstract.

## 2-1 THE SECOND LAW APPLIED TO PYROTECHNIC SYSTEMS

J. H. McLain  
W. Alton Jones Professor of Chemistry  
Washington College, Chestertown, Md.

Due to the increased requirements for performance brought about by the exigencies of their use the development of pyrotechnic formulations and end items have placed the pyrotechnics engineer under some extreme pressure.

Under these pressures it is not surprising sometimes that basic thermodynamic considerations are either overlooked or neglected. This is not true in the successful developments or they would not be successful but altogether too much time and energy has been expended on empirical investigations of candidate formulations which are doomed from the outset because they are opposed to the laws of chemistry.

Perhaps this situation arises because there are few if any specific examples of application of these laws to pyrotechnics in the literature. It is possible too that the concept of entropy has been taught by the Carnot Cycle or the methodological approach rather than the chemical approach which stresses its chemical probability and degree of randomness nature. Qualitative though this may

be, it is essential to applications to these problems.

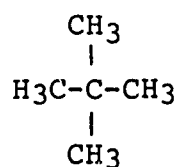
The second law,  $\Delta G = \Delta H - T\Delta S$ , states that the trend toward equilibrium in any system under given conditions requires a maximum increase in entropy i.e., randomness while maintaining a minimum free energy.

Two general applications of this law are

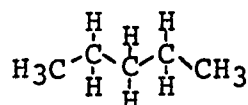
(1) Melting Point and Symmetry

Organic chemists have used with some success an empirical rule which states that the greater the symmetry of a compound the higher is its melting point. This is not strictly true as can be seen from the following but is quite useful.

Compare two isomeric pentanes



neo-pentane



n-pentane

at a temperature well below the melting point of either, which for n-pentane is  $143^\circ\text{K}$  and for neo-pentane is  $256^\circ\text{K}$ . As heat energy is added to the solid the system in keeping with the dictates of the 2nd. Law must gain as much randomness as possible maintaining a minimum free energy. Thus neo-pentane

because of its nearly spherical symmetry can achieve randomness with very little expansion of the lattice by undergoing solid state rotation, whereas nearly linear n-pentane in order to achieve a similar freedom must expand its lattice to such an extent that the lattice collapses and melting occurs. Thus the melting of the neo-pentane can be successfully postponed until a much higher temperature. If the liquids are heated still further of course boiling occurs and the substances pass into the highest entropy state of all i.e. gaseous. If there is little structure in either the liquid or the gas the boiling points of the isomers\* should be approximately the same and the melting point-symmetry rule is quite accurate. However a better way of picturing this process is by measuring the liquid temperature range ( $T_b - T_m$ ) of a substance because if a solid is so symmetrical that it can obtain all the degrees of freedom that it would possess as a gas it will postpone melting almost up to its boiling point.

Some illustrations of this effect are:

<u>Substance</u>	<u><math>T_b - T_m</math></u>
neo-pentane	29.5°
n-pentane	26.°

---

\* Troutons Law  $S_v = \frac{H_v}{T_b} = \text{Constant.}$



<u>Substance</u>	<u>T<sub>b</sub> - T<sub>m</sub></u>
octane (2,2,3,3 tetra methyl butane)	4.3 °
n-octane	182. °
butyl chloride tertiary	77. °
n-butyl chloride	209. °
ortho dichloro benzene	197. °
para dichloro benzene	121. °
cyclohexane	74.5 °
cyclohexene	187. °
cyclohexadiene 1,3	178. °
benzene	74.6 °

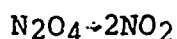
(2) All spontaneous polymerization reactions are exothermic.

The concept of entropy as a measure of randomness is illustrated very clearly by this application.

All polymerization reactions can be written in a general form as  $n(A - A) \rightarrow [-A-A-A-A-]_{n/2}$  in the course of which the molecules are tied together and the degree of randomness is decreased markedly.

Thus in the equation  $\Delta G = \Delta H - T\Delta S$  the  $\Delta S$  term must be negative and when multiplied by the negative temperature coefficient becomes positive. Yet if the reaction is to go the  $\Delta G$  term must be negative and this can be true only if  $\Delta H$  is negative or exothermic. Thus any and all polymerization reactions must be exothermic.

The converse of this is of course that decomposition reactions are either endothermic or in the case of azides et al explosive. Some examples --



### Pyrotechnic Applications

#### Solid-Solid Reactions

Similar to the polymerization application it can be seen that if two solids react to give two solids that the change in randomness or  $\Delta S$  approaches 0.\* Thus the  $T\Delta S$  term in  $\Delta G = \Delta H - T\Delta S$  approaches zero and  $\Delta H$  must be negative in order for the reaction to proceed.

The "gasless" delay mixes are very nearly isentropic and for this reason the free energy and of course the equilibrium constant are almost entirely determined by the  $\Delta H$  term. It can be expected then that the maximum

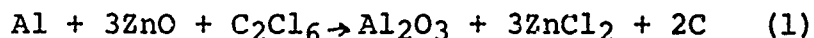
---

\* The only difference from zero depends upon the  $C_p$  of the reactants and products and this is almost negligible by reason of the additivity of the heat capacities of the atoms making up the simple states. (Kopps Rule)

heat of reaction will in fact determine the  $\Delta G$  and the maximum equilibrium constant i.e. stoichiometry. Heat of reaction has been used based on this principle to determine stoichiometry of pyrotechnic reactions. <sup>1,2</sup>

### Reversible Reactions

In the development of the HC, Type C Smoke Mix early in 1942 <sup>3</sup> it was observed that the stoichiometric mix based upon the following equation



was much too hot (melting the grenade can body), too fast and too dark in color due to the carbon product. It proved to be possible to utilize the reversible reaction



to whiten the smoke and because this reaction is endothermic, decrease the total heat output decreasing the reaction temperature and increasing the burning time. The net effect of using this reaction, inasmuch as the zinc produced by it can react with more hexachlorethane,

- 
- (1) Spice, J. E. and Stavely, L. A. K. JSCI 68 348 (1949)
  - (2) McLain, J. H. Ind. & Eng. Chem. submitted for publication
  - (3) McLain & McBerty TDMR CWS Tech Command "Development of HC type C Filling for the MB Grenade" (1942)

if it is provided in the formulation, to make more carbon to make more zinc and so on, is to decrease the aluminum content. Thus burning times and depth of color could be controlled by aluminum content.

Reaction (2) is fairly widely known inasmuch it is this reaction which is used in zinc smelting. There are others that are similar to it however that are less widely known and the source of some confusion in the flare industry.

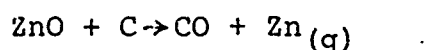
Application of the 2nd. Law shows that the enthalpy term and the entropy term are clearly opposed so that although the reaction

$$\text{Zn}_{(s)} + \text{CO}_{(g)} \rightarrow \text{C}_{(s)} + \text{ZnO}_{(s)} \quad (3) \quad \Delta H = - 57.1 \text{ kcal}$$
proceeds at ambient temperatures there will be some temperature at which the  $T\Delta S$  term will outweigh the  $\Delta H$  and cause the reaction to reverse.

Explicitly in  $\Delta G = \Delta H - T\Delta S$  the reaction represented by equation (3) has  $\Delta H = - 57.1 \text{ kcal}$ . The  $\Delta S$  term is negative because the reactants are gaseous and the products are two solids thus randomness decreases. The  $- T\Delta S$  term therefore must be positive. As the temperature is increased the  $T\Delta S$  contribution increases much more rapidly than the  $\Delta H$  term decreases therefore there will be a tem-

perature at which the  $T\Delta S$  overcomes the exothermic heat term.

Short of an exhaustive plotting of  $\Delta G$  vs  $T$  plots worthwhile approximations can be made. For example in this same system



$\Delta H$  obtained from heats of formation and the heat of sublimation of Zn is  $57.1 + 31.0 = 88.1$  kcal. The  $S^\circ$  values are\*

CO	= 47	cal./mole-degree
ZnO	= 11	cal./mole-degree
C	= 4	cal./mole-degree
Zn <sub>(g)</sub>	= 38	cal./mole-degree

$\Delta S^\circ$  for the reaction as written is 70 cal./mole-degree.

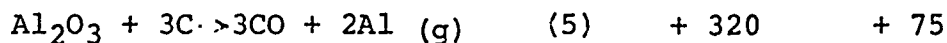
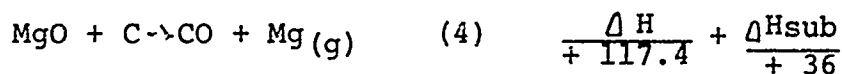
This  $\Delta S^\circ$  would require a temperature of  $\frac{88100}{70} = 1260^\circ\text{K}$  or  $987^\circ\text{C}$ .

Although this is a very crude approximation because the  $\Delta S^\circ$  and the  $\Delta H^\circ$  are not the same at the higher temperatures, it will be seen later that good agreement with experiment and with more refined calculations is obtained.

---

\* Handbook of Chemistry and Physics 43rd. Edition  
Chemical Rubber Publishing Company Cleveland, Ohio

There are two more reactions of importance to pyrotechnics that should be discussed.



$S^\circ$  values are  $\text{MgO} = 6.4$  cal./mole-degree

$\text{Mg (g)} = 35.5$  cal./mole-degree

$\text{C} = 4.$  cal./mole-degree

$\text{CO} = 47.$  cal./mole-degree

$\text{Al}_2\text{O}_3 = 12.$  cal./mole-degree

$\text{Al (g)} = 39.3$  cal./mole-degree

$\Delta S^\circ$  for equation (4) = 72 cal./mole-degree

$\Delta S^\circ$  for equation (5) = 195 cal./mole-degree

Calculated temperature of reversal for equation

(4) = 2130° K or 1857°C

Calculated temperature of reversal for equation

(5) = 2410° K or 2137°C

Upon checking in Mellor<sup>4</sup>, Bodenstein and Schubart<sup>5</sup> are quoted as measuring the temperature at which a mixture

---

(4) Mellor, J. W. "A Comprehensive Treatise on Inorganic and Theoretical Chemistry" Longmans, Green & Co., London

(5) Bodenstein, M. and Schubart, F., Zeit. Elektrochem. Soc. 5, 207 (1904)

of zinc oxide and carbon is converted into zinc vapor and carbon monoxide as 1030°C which is in good agreement with the 1022°C cited by W. McA. Johnson.<sup>6</sup>

Also in Mellor, Kowalbe and Grenfell<sup>7</sup> found that MgO is reduced to Mg by carbon at 1950°C.

Dannatt and Ellingham<sup>8</sup> have published a plot of  $\Delta G^\circ$  vs temperature a part of which is reproduced in Figure 1 of this paper. Temperatures of reversal can be read from the intersections of the  $C + \frac{1}{2}O_2 \rightarrow CO$  plot and the metal-metal oxide system concerned.

Values from the D & E plot, those calculated in this paper and the experimental values are summarized in Table I below.

TABLE I

Reaction	Temperature of Reversal		
	D&E Plot	Calc this paper	Exp't'l
$ZnO + C \rightarrow CO + Zn$	960	987	1025
$MgO + C \rightarrow CO + Mg$	1850	1857	1950
$Al_2O_3 + 3C \rightarrow 3CO + 2Al$	2100	2137	----

- 
- (6) W. McA. Johnson, Trans. Amer Electro Chem Soc. 5 207 (1904)  
 (7) O. L. Kowalbe and D. S. Grenfell *ibid* 27 221 (1915)  
 (8) C. W. Dannatt and H.J.T. Ellingham, "The Physical Chemistry of Process Metallurgy", Discussions of the Faraday Society, No. 4 (1948) p. 130.

Dannatt and Ellingham state <sup>9</sup> "Although carbon is able to reduce the oxides of even the most reactive of metals if sufficiently high temperatures are employed, the disadvantages of operation at very high temperature may lead to alternative reducing agents being preferred." For example, the C - CO line intersects the Mg - MgO line at 1850° C thus above this temperature MgO can be reduced by carbon to give CO and magnesium vapor. "This process presents special difficulties (for smelting) owing to the tendency for the reverse reaction  $\text{Mg}_{(g)} + \text{CO} \rightarrow \text{MgO} + \text{C}$  to occur during the cooling of the gases unless the temperature is brought down very rapidly below the boiling point of the magnesium by 'shock' cooling . . . ."

#### Applications

There are several applications that can be made from the combination of the D & E plot and the calculation of the temperature of reversal such as approximation of a missing  $\Delta S^\circ$  or  $\Delta H_{\text{sub}}$ .

Of more immediate interest to the technology however is that in illuminating flare mixes based on Mg,  $\text{NaNO}_3$  and Laminac mixtures the  $\text{C} + \text{MgO} \rightarrow \text{CO} + \text{Mg}$  reaction can and does play an important role at the temperatures of the burning flare. In as much as this reaction is highly endothermic it causes the temperature of the reaction to be decreased and affects the light emission of the flare adversely. It points very strongly to using some other binder than a carbonaceous material.

There is another interesting point from the D & E

---

(9) Ibid p. 138.



plot. As can be seen the Al -  $\text{Al}_2\text{O}_3$  line intersects the Mg - MgO line at about  $1650^\circ\text{C}$  and this would predict that Al would reduce MgO at this temperature or higher.

Conclusions are that the quick and easy calculation using "hand book" data is quite sufficient to enable the engineer to determine whether or not the temperatures that obtain in a reacting system are sufficient to allow reversal of the reaction under study and that the data obtained are of practical use to the design engineer.

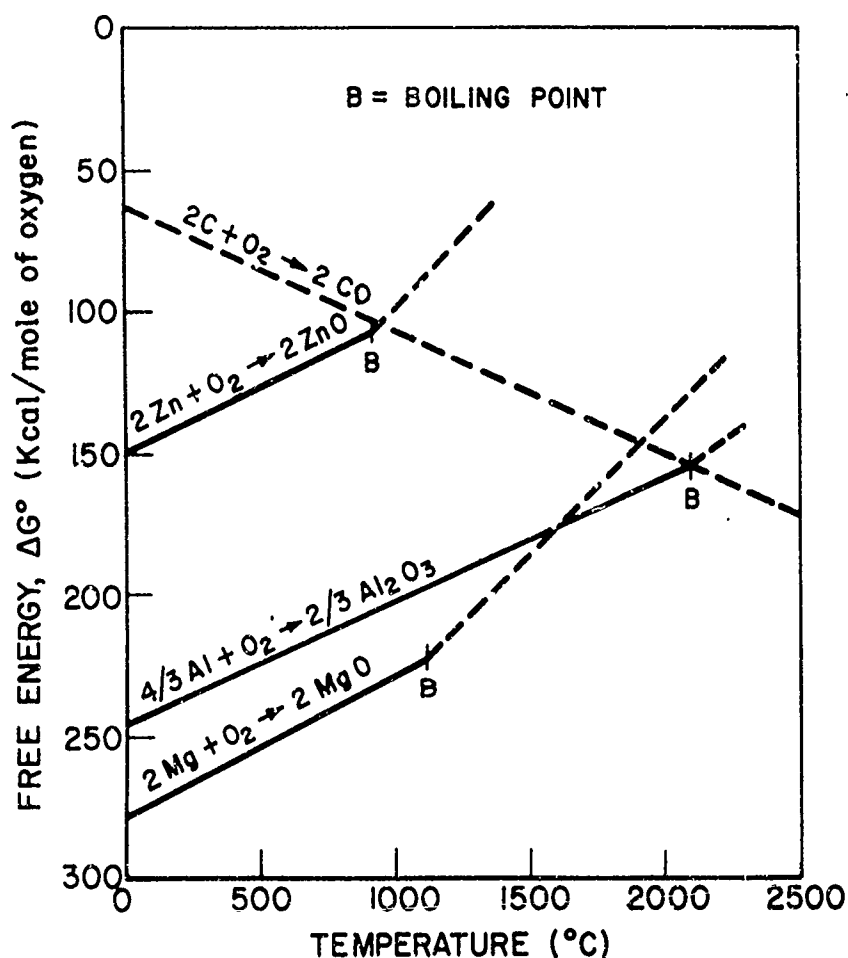


Figure 1. Standard Free Energy of Formation of Oxides:  
Variation with Temperature

## 2-2 STATISTICAL SCANNING STUDY

OF

### EXPLOSIVE END FITTINGS

By: R. R. Sullivan, S. A. Moses, and G. R.  
Compton, McDonnell Douglas Astronautics  
Company, Western Division

#### ABSTRACT

The results of a study to evaluate end fittings for a confined detonating fuse are reported. Two different modifications of three end fitting designs (called protruding, stepped, and conical) are discussed on the basis of the results of a statistical scanning test program. The end fittings are evaluated as both donor and acceptor charges.

This report includes an account of the effects of using Class 2 and Class 4 pentaerythrite tetranitrate and loading pressures of 5, 10, and 20 kips per square inch. The material and thickness of potential end caps are likewise examined, along with the results of tests performed to determine whether assembly procedures degrade the detonating characteristics of the fuse.

#### INTRODUCTION

This paper describes a statistical test program evaluating three different explosive end fitting designs for use on the Spartan missile being manufactured by the McDonnell Douglas Astronautics Company, Western Division, under contract to Bell Telephone Laboratories, Inc.\*

Explosive transfer systems with mild detonating fuse (MDF) or confined detonating fuse (CDF) are used extensively in aerospace vehicles. In these systems, initiation of one end of the detonating fuse will, in turn, transfer

\*The work described was accomplished under Contract DA-30-069-AMC-333(Y), Purchase Order 601312, December 1967 through March 1968.

the detonation to the other explosive devices. If this fuse must be installed in several individual sections or lengths, it is common practice to cap each end with an explosive end fitting to assure reliable initiation across any intervening gap.

Since the first usages of CDF and MDF at MDAC-WD in the late 1950's, various design concepts for end fittings have evolved. The first design was developed for programs that were the building blocks for the Spartan missile.

At the onset of the Spartan program, a missile-age old dilemma developed: Should the program minimize testing by utilizing the tried and proven "flight qualified" designs, or should the latest "state-of-the-art" designs be modified to meet the Spartan missile constraints? After consultation with industry and customer experts, it was decided to proceed using the flight qualified designs. Basically, the design consisted of 2 grain-per-foot PETN MDF confined in fiberglass overwraps and capped with a metal end fitting containing 2 grains of PETN for a booster. The MDF was allowed to protrude into the booster charge in the end cap to provide maximum contact with the PETN.

During the fall of 1967, flight qualified CDF end fittings failed to meet reliability test requirements as measured by their ability to propagate from fitting to fitting across an overtolerance air gap. Figure 1 shows a typical failure of the acceptor fitting. With this fitting, the PETN pressed into the end cavity apparently detonated abnormally. The 2 grain-per-foot CDF detonated for a distance of about 2 1/2 inches before dying out. After several of these failures, it was decided to change the design of the end fitting. The new design was based on highly successful work performed by the McDonnell Aircraft Corporation, St. Louis and the U.S. Naval Ordnance Laboratory, White Oak, Maryland, in developing CDF end fittings for the

Full capsule escape system. Although that system uses explosives that are more difficult to initiate than the PETN used in the Spartan, it was reasoned that the same design techniques could successfully be employed with the more sensitive explosive.

Both the old (protruding) and new (conical) designs are shown in Figure 2. It should be noted that these end fittings may be either donor or acceptor charges. When acting as a donor, the PETN is initiated by detonation of the CDF lead. When acting as an acceptor, the output from the donor will jump a gap and initiate the PETN which will, in turn, initiate the CDF lead. The changed design resulted in a rather spectacular increase in the ability of the donor charge to initiate an acceptor across an air gap. As shown in Figure 3 with the protruding design, failures occurred at somewhat under a two-inch air gap. With the conical design firing down a steel tube, some successes were achieved with gaps as great as 23 inches. Factors influencing this improvement were investigated in a parametric test program.

#### Mistreatment of Confined Detonating Fuse

As a prelude to testing different end fitting designs, it was desirable to determine if the CDF itself could have contributed to any of the problems encountered during the gap-jumping tests. Could an adverse effect result from the various manufacturing and handling procedures during assembly of CDF or MDF into the end fittings? For these tests, it was decided to deliberately mistreat the CDF or MDF to a much greater degree than was believed likely to occur during its assembly into the end fittings. It was reasoned that if these mistreated samples detonated satisfactorily, problems with the fuse could be discounted.

The effect of crimping a steel sleeve to the CDF was investigated for the first series of tests. End fittings are normally crimped to the CDF with the steel sleeves being indented to an outside diameter of 0.313 inch. For these tests, five of the specimens were crimped in the normal manner and an additional five were indented to an outside diameter of 0.275 inch which was the smallest diameter that could be formed with the fixture used for this purpose.

The test samples were X-rayed and it was determined that this extra crimping did not crack or deform the lead sheath surrounding the PETN core. The fuse samples were then placed on aluminum witness plates and detonated. Examination of these witness plates indicated that the excessive crimping did not appear to affect the detonation.

In a like manner, tests were made to determine the effect of nicking approximately halfway through the lead sheath with a razor blade, of kinking the MDF into a tight loop, and kinking followed by a straightening operation. In addition, tests were performed to determine whether the detonation would be adversely affected when MDF was first confined in a steel tube and then passed from this confined condition to an unconfined state. All these treatments are indicated in Figure 4.

All the test samples were X-rayed and detonated in contact with aluminum witness plates. In no case could any adverse effect be noted.

Although it appears that CDF and MDF can be badly mistreated without affecting the detonation, it would be unrealistic to relax any of the quality control or inspection procedures established for handling these materials.

### Discussion of End Fitting Designs

The statistical evaluation test program of the explosive end fittings was designed to provide information on the importance of a relatively large number of parameters. To keep the program to a reasonable size, only three basic designs, as shown in Figure 5, were evaluated with the following items maintained constant throughout the program:

1. The type of explosive: PETN.
2. The volume to be filled with explosive: 0.046 cubic inch ( $75.5 \times 10^{-3}$  cc).
3. The outer diameter of the steel end fitting: 0.250 inch.
4. The diameter and length of that portion of the explosive load which was closest to the end discs: 0.165 diameter by 0.165 length.

As the total explosive volume was the same in the three designs, this meant that the "doughnut" surrounding the protruding MDF, the small cylinder in the stepped fitting and the truncated cone in the conical design also contained equal volumes of explosive.

The basic designs were modified in some tests so that the explosive could be loaded into the cavity by one of two different methods. With some fittings designated "without cup" the PETN was pressed directly into the hollow end cavity in two increments. The metal disc was then bonded onto the end of the fitting. These are shown in Figure 5.

With other fittings, a cup was fabricated by bonding an end disc to a hollow cylinder and this was loaded with the main portion of the charge. A second charge was pressed into the small cavity in the end of the fixture and the

two parts were then mated together. This latter method of loading is indicated in Figure 6. With fittings loaded in this manner, any air gap that occurred could be between the explosive increments. With the fittings without a cup there is a possibility of a thin air gap, no more than 0.002- or 0.003-inch thick between the explosive and the disc because of the bonding material around the edge of the disc.

All designs were evaluated as both donor and acceptor charges in a series of tests that will be discussed.

#### Donor Dent Block Tests

Two types of donor dent block tests were performed. The first of these was to evaluate the interface between the MDF and the pressed PETN and for this series the length of the PETN output charge was reduced from 0.165 to 0.080 inch. This was done so that if a non-stable or low order detonation occurred at the MDF-PETN interface, it would have less opportunity to build up into a high order detonation in the short length provided. If a nonstable detonation did occur, it would not make as deep a dent as a stable detonation.

In general, these dent tests were performed in a manner similar to standard tests described in MIL STD 331 with two major exceptions:

1. The donors and dent blocks were placed in the special test fixture shown in Figure 7. This was done to attempt to gain information relating the depth of dent to the transmitted energy as determined by movement of the linear potentiometer. Unfortunately, no usable information was gained from this part of the experiment.

2. The fittings were fired without the use of confining sleeves.

These were omitted to eliminate any variation in dent due to differences in the fit of these sleeves.

A thin film of silicone grease was applied to the output end of all charges. This eliminated the possibility of an air gap in that region and also allowed the shock to be transmitted more uniformly into the dent block.

The raw results of these dent block tests are shown in Figure 8. This figure also illustrates the type of testing that was used to obtain maximum parametric data with minimum tests. Each cell contains only two data points yet for any one parameter, such as the 10 Ksi loading density, there are 12 individual test points. Using analysis of variance techniques, the effect of that parameter can be determined as can any interaction between parameters. An examination of these results show that in all probability, non-stable detonations occurred with Class 4 PETN at the 5- and 10-Ksi levels with the protruding design. When evaluated by analysis of variance techniques at the 99% confidence level, the following results were noted with these half-length fittings:

1. The stepped design appears to be the best of the three, especially when loaded with Class 4 PETN.
2. The protruding design may result in a non-stable detonation in the PETN output charge.
3. On an across-the-board basis there is little to choose between Class 2 and Class 4 PETN. This is also true when only the stepped and conical designs are compared.



4. With both classes of PETN, a loading pressure of 20 Ksi gives significantly better results than lower loading pressures.

The second type of donor dent block test was to evaluate the output of the various designs with full-length donors. The procedure was similar to that used for the half-length charges employed for the MDF/PETN interface tests.

The various parameters that were evaluated are shown in Figure 9 which also gives the results of the dent tests. The figure also illustrates another method used to minimize testing by factoring the matrix. The effect of using full length charges was completely evaluated using the conical design. The protruding and stepped designs were only spot-checked to see if the results varied grossly from the conical.

As expected, these full length donors produced deeper dents than the half-length charges utilized for previous tests. However, as with the half-length donors, the most significant test finding was the inferior results obtained with the protruding design. In general, the results of the output tests indicated the following:

1. Both the stepped and conical designs are superior to the protruding design.
2. There are no significant differences between the stepped and conical designs.
3. There is no significant difference between the two classes of PETN.

4. With Class 2 PETN, a loading pressure of 20 Ksi appears to give better results than lower loading pressures, although the sample was too small to show significance. With Class 4 PETN, the 20-Ksi loading pressure does not produce significantly better results than loading at 10 Ksi, even though both pressures show better results than loading at only 5 Ksi.

From the results of donor tests, it was concluded that there did not appear to be much choice between the stepped or conical end fitting designs or between Class 2 and Class 4 PETN. However, because of the greater difficulty in handling the fine-grained Class 2 material, it was recommended that Class 4 PETN loaded at 20 Ksi be considered for donor charges for future designs.

#### Donor Fragment Pattern Tests

The ability of a donor end fitting to initiate an acceptor across a relatively wide air gap (for example, 1 inch or more) is directly related to the energy and concentration pattern of the fragments produced by the donor end disc or cap. This fragment pattern was examined by firing various donor end fittings into a plexiglas target as shown in Figure 10. As indicated, the MDF lead attached to the donor was detonated by a commercial blasting cap. Detonation of the donor charge broke up the end disc and projected it against the target. The depth of penetration of the major fragment and the approximate size of the major crater were then measured.

The parameters investigated and the results of the fragment pattern tests are shown in Figure 11. The diameter values shown are those of craters made by fragments after breakup of the end disc and do not indicate the concentration of the pattern.

The diameter of the largest individual craters made by fragments from aluminum end discs ranged from 0.02 to 0.12 inch as these discs were fractured into a large number of small pieces. Even some of the 0.006-inch thick steel discs were badly fractured with crater diameters ranging from 0.10 to 0.38 inch. This last diameter is actually greater than that of the end disc and represents the impact area of at least three major fragments.

The most significant finding from the fragment pattern tests was that end discs made from 0.006-inch thick stainless steel were definitely superior to those made from thinner steel and aluminum. Figure 12 shows representative targets impacted by a 0.003-inch thick aluminum, by a 0.003-inch thick steel, and by a 0.006-inch thick steel end disc. With each target, the pattern was accentuated by darkening the surface pits.

As can be seen, the thin aluminum broke up into perhaps 500 to 1,000 particles, each producing only a shallow crater. The 0.003-inch thick steel disc broke into 25 to 30 fragments, any one of which contained far greater impact energy than the fine fragments from the aluminum disc.

Only eight out of fourteen of the 0.006-inch thick steel discs produced the concentrated pattern shown in Figure 12. The fragments from these specimens penetrated the target to a depth of between 0.050 and 0.106 inch, whereas discs of the same thickness which broke into a greater number of fragments penetrated to a depth of between 0.038 and 0.060 inch. The fact that some of these discs broke up extensively indicates that the optimum thickness of steel end disc may be greater than 0.006 inch.

It is suspected that with end discs of the same material and thickness, the breakup pattern is controlled by the shape of the detonation wave at the interface as well as by relatively small variations in the smoothness of the disc surface. One well-known technique for projecting an explosively driven disc without breaking it up is to form the disc into a shallow dome with the convex side toward the explosive. Although this technique was not evaluated during the test program, it is suggested for installations in which a donor must detonate an acceptor across an air gap of two inches or more.

Unfortunately, the penetration data from the tests under discussion were so scattered that no precise conclusions could be drawn regarding the relative merits of loading pressure or design. It is interesting that in this limited series of tests the protruding design with a 0.006-inch end disc performed as well as the stepped and conical designs. However, there is not sufficient evidence to select this design over either the stepped or conical design.

Also of interest is the apparent superiority of the conical no-cup design over the conical cup design. It is suggested that this superiority is related to the small air gap that may exist between the explosive and the end disc with the no-cup design.

As mentioned previously, it is possible that a small gap exists in this region because of the thickness of adhesive around the edge of the end disc. Such an air gap would attenuate the shock wave passing into the disc resulting in less breakup and greater target penetration. The use of similar shock-attenuating devices is a technique sometimes used to control the fragmentation from explosive warheads.

#### Acceptor Dent Block Tests

Depending upon the separation distance of the donor and acceptor charges, the acceptor may be initiated by high velocity fragments, impinging hot gases, transmitted shock or possibly a combination of these mechanisms. For the acceptor tests described in this section, an attempt was made to gain information on the effect of initiation under various conditions. The tests were performed using the dent test fixture previously described but in each case the donor charge was of the stepped cup design. Each donor incorporated a 0.006-inch steel end disc and each was loaded with Class 2 PETN pressed at 10 Ksi.

One third of the tests were made with an 0.0625-inch thick plastic barrier between the donor and acceptor. This barrier stopped (or delayed) the hot gases and fragments and thereby allowed the acceptors to be initiated by shock. An additional third of the tests were made with a two-inch air gap between the donor and acceptor so that initiation was the result of impact

by high velocity fragments. The final third of the tests were made with an 0.150-inch air gap between donor and acceptor. For this group, the acceptor was probably initiated by a combination of shock, hot gases and fragments.

As was the case with some of the donor tests described earlier, the acceptor charges were only half as long (i.e., 0.080 inch) as a normal charge. Again, these short-length charges enabled stable detonations to be distinguished more easily from non-stable detonations. Also, for these acceptor tests, the metal components were cut off at the point where the PETN-MDF interface would normally occur. This cut off face was placed in contact with the dent block after a thin film of silicone grease had been spread over the end to ensure contact with the surface of the block. The three test conditions are shown in Figure 13. The results of the acceptor dent tests are summarized in Figure 14.

Probably the most interesting and unexpected result from this series of tests was the formation of consistently more shallow dents when the acceptor was initiated across a two-inch air gap. There appear to be at least two possible explanations for this phenomenon:

1. The acceptor was initiated by a weak air shock ahead of the fragments and, as a result, a non-stable detonation occurred.
2. More probably, the fragments penetrated some distance into the explosive before initiating it and the shallower dents are a result of initiating shorter columns of explosive.

In either case, the weaker output must be taken into account when a Bruceton-type sensitivity test is performed in which the air gap is the variable, and this adds one more complicating variable to such a test.

Another interesting and unexpected test result was that the conical design without cup gave significantly better results than the same design with cup. Again, it should be pointed out that there is the possibility of a small air gap between the explosive and end disc in the no-cup design and this may have a bearing on the better performance. If an explosive is initiated by rapid compression and heating of entrapped gas either in, or between, the explosive crystals as has been postulated, it is entirely possible that the thin air gap in the no-cup design is heated rapidly by shock wave or fragment impact so that initiation occurs very near the surface. This would result in a longer column of explosive being detonated and, consequently, a deeper dent. Other results of the acceptor tests indicate the following:

1. The thickness or material of the end disc is not statistically significant over the range tested.
2. The significance of the class of PETN is questionable.
3. There is no significant difference between the stepped design and conical design, with cup.
4. The significance of the pressing pressure is questionable.

#### CONCLUDING REMARKS

The results of the statistical scanning tests just described may be summarized as follows:

1. The performance of end fitting donor charges is significantly improved by use of 0.006-inch-thick stainless steel end caps rather than caps of thinner steel or aluminum. The thicker steel caps result in a concentrated pattern of high-velocity fragments which should initiate reliable detonation of the donor charges over an air gap of several inches.

2. Even though fragment concentration and impact energy are improved by use of a steel end cap, a half-length acceptor initiated by high-velocity fragments has less output energy than one initiated by shock. It is probable that this effect would not be noticed with full-length acceptors; nevertheless, because of this unexpected phenomenon, a statistical gap-jumping (Bruceton) test may not be a satisfactory method of estimating the reliability of end fittings.
3. If the donor and acceptor end fittings *are* to be the same design, either the conical or stepped design is satisfactory and the choice of which to use may be made on the basis of manufacturing cost. Either of these designs is better than the protruding design.
4. For donor or acceptor end fittings, either Class 2 or Class 4 PETN pressed at 20 Ksi is equally satisfactory. However, Class 4 is easier to handle than Class 2 and should be selected for this reason.
5. The procedures now used to assemble CDF into the end fittings appear to have no effect on the detonation characteristics of the fuse. However, the present level of control and inspection should not be relaxed.
6. Design of a thin, low-density gap between the explosive and the fitting end cap should be considered. With a donor, this gap may help produce a more concentrated fragment pattern. With an acceptor, the gap may eliminate the reduced effectiveness of fragment initiation noted in 2, above.



7. The analysis of variance technique may be used to obtain significant information about many parameters and parameter interactions without expending excessive test parts.

#### BIBLIOGRAPHY

1. M. L. Schimmel and B. Kirk, "Study of Explosive Propagation Across Air Gaps", Report B331, McDonnell Aircraft Company, St. Louis, Mo., 1964.
2. "Fuze and Fuze Components, Environmental and Performance Tests for", Military Standard 331, January 1966.
3. L. D. Hampton, "Effect of the Hardness of the Steel Used Upon the Results of the Steel Dent Test of Detonators", NAVORD Report 3983, Naval Ordnance Laboratory, 1953.
4. R. H. Stresau and W. M. Slie, "Application of the Steel Plate Dent Test to the Quality Control of the Mark 63 Detonator", NAVORD Report 3879, Naval Ordnance Laboratory, 1953.
5. J. N. Ayres, "Standardization of the Small Scale Gap Test Used to Measure the Sensitivity of Explosives", NOL (NAV WEPS7342), Naval Ordnance Laboratory, 1961.
6. O. L. Davies (Editor), "The Design and Analysis of Industrial Experiments", Hafner Publishing Company, New York, 1960.
7. "Ordnance Explosive Train Designers' Handbook", NOLR 1111, Naval Ordnance Laboratory, 1952.
8. F. P. Bowden and A. D. Yoffe, "Initiation and Growth of Explosive in Liquids and Solids", Cambridge University Press, 1952.
9. S. A. Moses and G. R. Compton, "Spartan Detonating Fuse End Fittings, Statistical Test Report", DAC-61629, Douglas Missile and Space Systems Division, June 1968.
10. MIL-P-387, Pentaerythrite Tetranitrate (PETN), January 9, 1957.

## FAILURE EXPERIENCED IN GAP-JUMPING TESTS

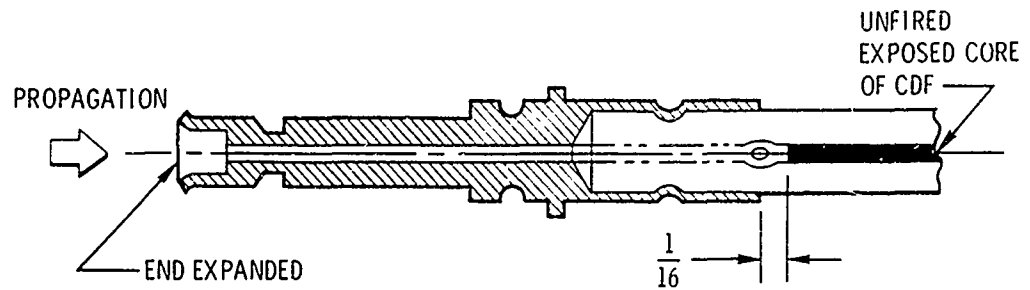


FIGURE 1

## EXPLOSIVE END FITTINGS

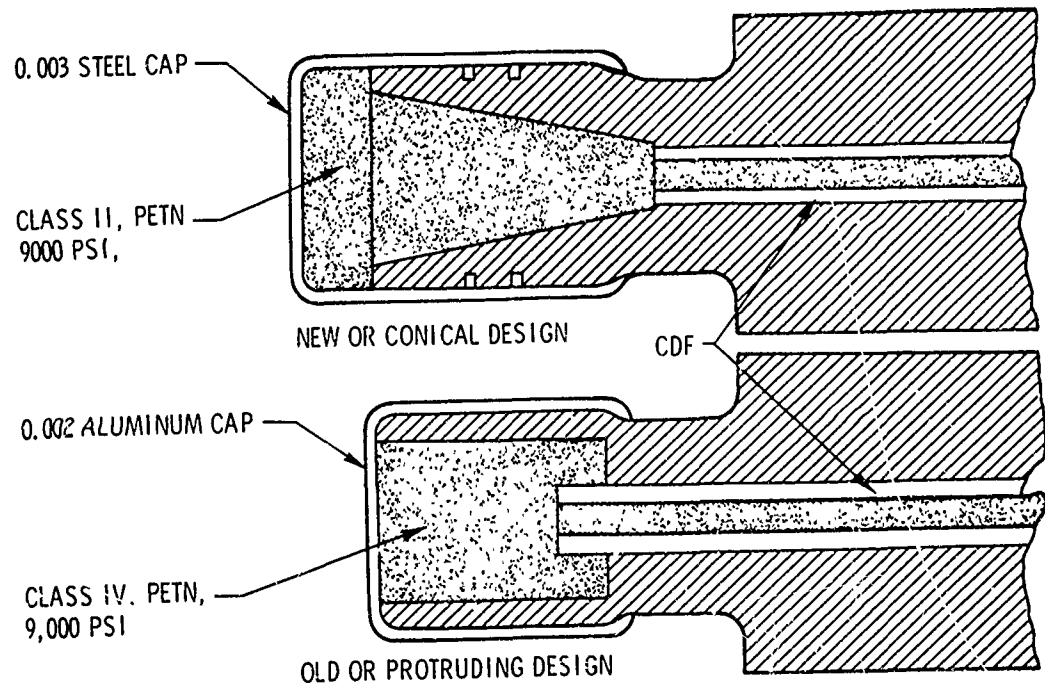


FIGURE 2

## GAP JUMPING TEST RESULTS

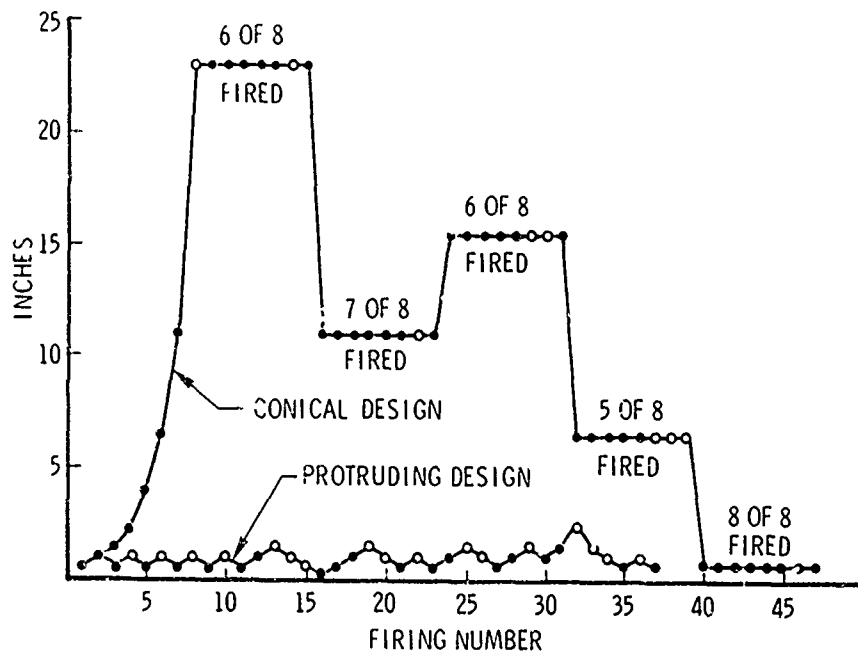


FIGURE 3

## MISCELLANEOUS CDF TESTS

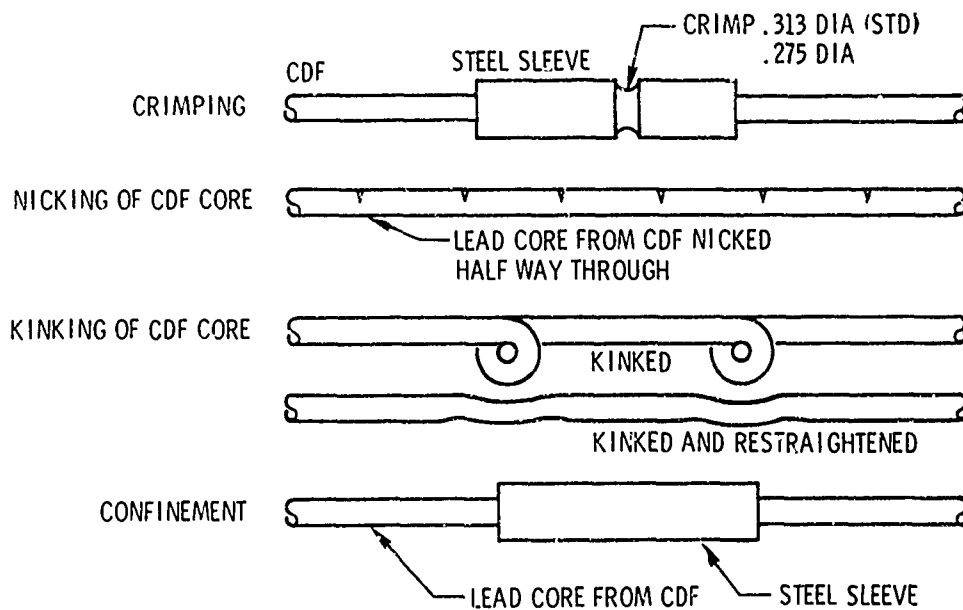
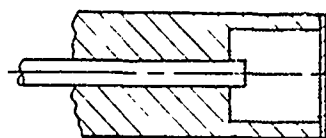


FIGURE 4

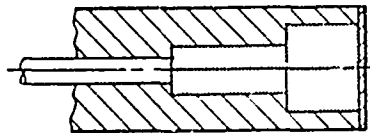
## END FITTINGS FOR TEST PROGRAM

### PROTRUDING END FITTING



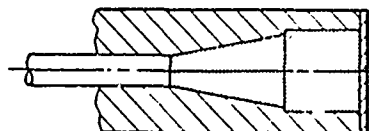
END OF MDF MACHINED. PETN PRESSED  
IN CAVITY. END DISC BONDED IN PLACE  
CAVITY: .165 DIA X .213

### STEPPED END FITTING



PETN PRESSED INTO CAVITY IN TWO INCREMENTS.  
END DISC BONDED IN PLACE  
LARGE CAVITY: .165 DIA X .165  
SMALL CAVITY: .078 DIA X .200

### CONICAL END FITTING

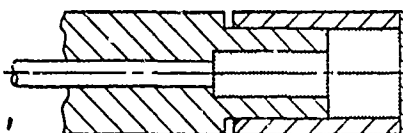


PETN PRESSED INTO CAVITY IN TWO INCREMENTS  
END DISC BONDED IN PLACE  
LARGE CAVITY: .165 DIA X .165  
CONICAL CAVITY:  $\begin{cases} .056 \text{ DIA} \\ -20^\circ \text{ X } .160 \end{cases}$

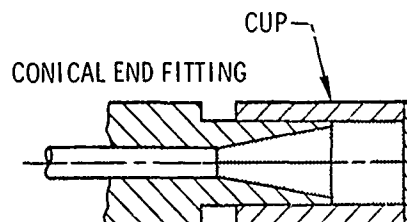
FIGURE 5

## END FITTINGS (WITH CUP) FOR TEST PROGRAM

### STEPPED END FITTING



PETN PRESSED IN SMALL CYLINDRICAL  
CAVITY AND INTO CUP, THEN  
PARTS MATED



PETN PRESSED INTO CONICAL CAVITY  
AND INTO CUP, THEN PARTS MATED.

FIGURE 6

# DENT TEST FIXTURE ASSEMBLY

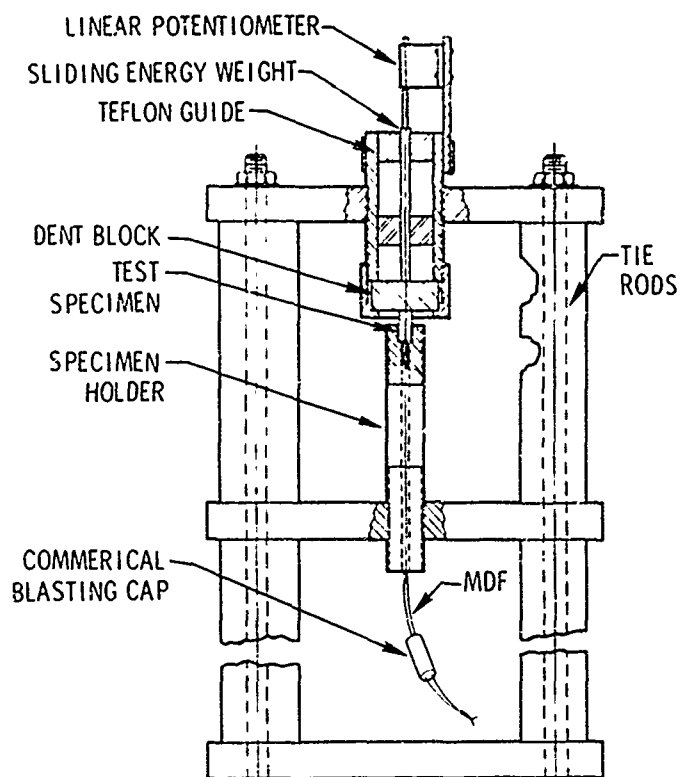


FIGURE 7

## RESULTS OF MDF/PETN INTERFACE, DONOR TESTS\*

TYPE OF DESIGN	CLASS 2 PETN			CLASS 4 PETN		
	5 KSI	10 KSI	20 KSI	5 KSI	10 KSI	20 KSI
PROTRUDING	18, 19	22, 21	26, 27	10, 9	7, 23	23, 22
STEPPED (NO-CUP)	25, 25	28, 26	25, 26	19, 26	31, 31	32, 32
CONICAL (NO-CUP)	27, 26	18, 21	29, 27	21, 22	21, 26	27, 28

\* MEASUREMENTS OF DENT DEPTH X 10<sup>3</sup>

FIGURE 8

2-2.20

## RESULTS OF DONOR OUTPUT, DENT TESTS\*

TYPE OF DESIGN	CLASS 2 PETN			CLASS 4 PETN		
	5 KSI	10 KSI	20 KSI	5 KSI	10 KSI	20 KSI
PROTRUDING	-	32, 30	-	-	26, 21	--
STEPPED (WITH CUP)	-	36, 35	-	-	34, 33	-
CONICAL (WITH CUP)	29, 30	36, 33	40, 42	29, 30	39, 33	36, 37

\* DENT DEPTH MEASUREMENTS  $\times 10^3$

FIGURE 9

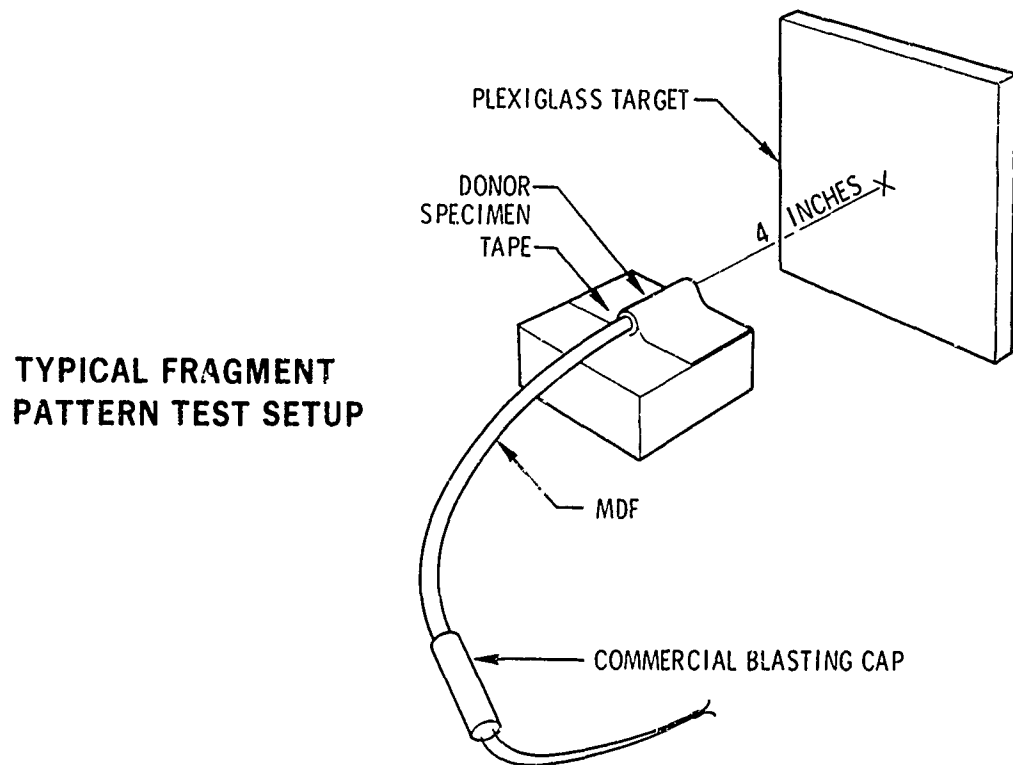


FIGURE 10

2-2,21

## RESULTS OF DONOR FRAGMENT PATTERN TESTS

TYPE OF DESIGN	STEEL END DISC					ALUMINUM END DISC			
	.003 IN.		.006 IN.			.003 IN.		.006 IN.	
	10	20	5	10	20	10	20	10	20
PROT.	—	—	—	83	48	0	5	—	—
	—	—	—	*	(	(	(	—	—
STEPPED (WITH CUP)	—	—	—	85	48	9	6	—	—
	—	—	—	*	*	(	(	—	—
CONICAL (NO CUP)	53	53	—	—	—	—	—	23	31
	(	(	—	—	—	—	—	(	(
CONICAL (WITH CUP)	40	24	53	60	98	5	9	24	20
	(	(	(	*	*	(	(	(	(

1. ALL CLASS 2 PETN

2. VALUES = DEPTH (IN.  $\times 10^3$ )

3. \* = CONCENTRATED FRAGMENT PATTERN

4. ( = MANY SCATTERED FRAGMENTS

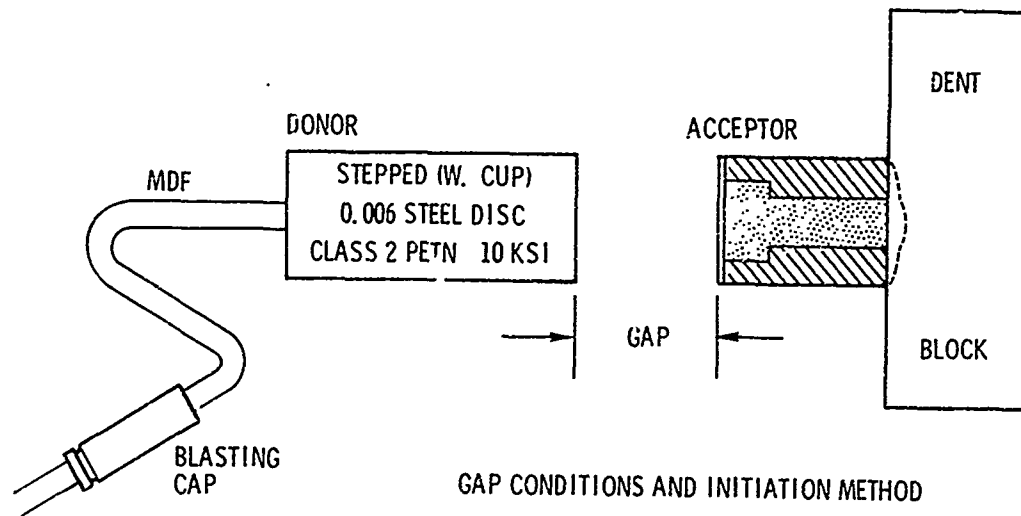
FIGURE 11.

## TYPICAL PLEXIGLASS TARGETS FOR FRAGMENT TESTS



FIGURE 12.

## ACCEPTOR, DENT BLOCK TESTS



### GAP CONDITIONS AND INITIATION METHOD

1. 0.15 AIR (SHOCK, HOT GAS, FRAG.)
2. 0.0625 PLEXIGLAS (SHOCK)
3. 2.0 AIR (FRAG.)

FIGURE 13.

## RESULTS OF ACCEPTOR DENT BLOCK TESTS

END DISC MATL.		STEEL						ALUMINUM			
THICK		.003		.006				.003			
CLASS PETN		2	4	2		4		2		4	
DESIGN	GAP	20 KSI	20 KSI	10 KSI	20 KSI	10 KSI	20 KSI	10 KSI	20 KSI	10 KSI	20 KSI
PROT.	AIR .15							20	21	21	23
	PLAS1/16							24	25	24	23
	AIR 2.0							12	16	14	17
STEPPED (W. CUP)	AIR .15			20	26	24	24			23	24
	PLAS1/16			22	23	24	26			22	24
	AIR 2.0			NF	16	18	17			20	22
CONE. (W. CUP)	AIR .15	26	27	22	24	23	25	25	25	24	23
	PLAS1/16	26	24	23	24	26	24	24	29	26	25
	AIR 2.0	12	21	17	18	17	15	17	19	17	19
CONE. (NO CUP)	AIR .15			23	27	32	29	28	26		
	PLAS1/16			22	25	25	25	33	27		
	AIR 2.0			24	19	18	20	20	18		

1. ALL DONORS: STEPPED (W. CUP); .006-IN. STEEL, CLASS 2, 10 KSI

FIGURE 14.



## 2-3 INTERIOR BALLISTICS OF HIGH-LOW PROPULSION SYSTEMS\*

Otto K. Heiney

Jet Propulsion Laboratory

Pasadena, Calif.

### I. INTRODUCTION

The basic interior ballistic problem of a conventional propellant-actuated system is to determine the energy release and corresponding pressure generation by the burning of propellant in a variable volume. This volume is a function of an initial chamber volume plus an additional volume exposed by the movement of a piston whose motion is a known function of its mechanical response characteristics and the force exerted on its face.

In contrast, the high-low system shown in Fig. 1 has a fixed-volume, high-pressure combustion chamber coupled to a variable-volume lower-pressure action chamber where the payload is accelerated.

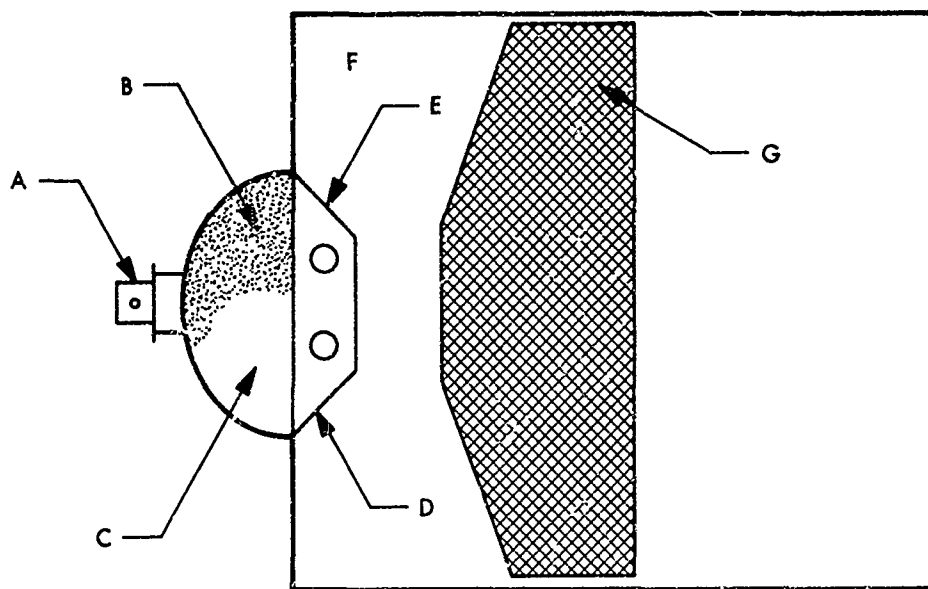


Fig. 1. High-low system

\*This paper presents the results of one phase of research carried out at the Jet Propulsion Laboratory, California Institute of Technology, under Contract No. NAS 7-100, sponsored by the National Aeronautics and Space Administration.

The sequence of events of operation is as follows (see Fig. 1):

- (1) Squib (A) fires into the closed high-pressure combustion chamber (C) and ignites the disk propellant (B).
- (2) The burning of the propellant flakes further increases the pressure until the nozzle closure diaphragm (D) fails.
- (3) This allows gases to vent through nozzles (E) into the working chamber (F), where the gases accelerate the payload (G) to the desired velocity.

This high-low system allows the combustion and acceleration processes to be uncoupled, because subsequent to the establishment of choked flow in the nozzles, the chamber pressure is independent of projectile motion. The blow-out nozzle closure eliminates any ignition problem by allowing the buildup of high pressure before initiating nozzle flow. The resulting penalty associated with the use of dual chambers is a slightly increased heat loss in the system.

Because of the interdependence of the various parameters in the high-low system, closed-form solutions are unobtainable. Thus, the basic analytic results are contained in Eqs. (8) and (21) in a form specifically tailored for machine computation.

Section II presents a mathematical model of the high-low ballistic process and Section III discusses the technique applied to accelerate and launch a parachute to be used as an aerodynamic deceleration system, a planetary landing vehicle.

## II. ANALYSIS

The solution for the pressure history in both the combustion and working chamber, and therefore for the projectile motion as well, requires the coupling

of state equations with a mass flow boundary condition. This effectively allows the processes to be considered as independent in the quasi-steady state-type analysis.

The equation of state for the combustion chamber is:

$$PV_c = mRT \quad (1)$$

also

$$F_P = R T_o \quad (2)$$

where  $F_P$  is the impetus of the propellant, having units of specific energy (ft-lb/lb) and is similar to the  $c^*$  of rocket propellants

$$c^{*2} = \frac{RT_o}{\Gamma^2} \quad (3)$$

with

$$\Gamma^2 = \gamma \left( \frac{2}{\gamma + 1} \right)^{\frac{\gamma + 1}{\gamma - 1}} \quad (4)$$

where  $\Gamma$  is a flow factor and a function of the combustion products of the propellant.

Then

$$\frac{dP_c}{dt} V_c = \frac{dm_c}{dt} F_P \quad (5)$$

with  $V_c$  being the combustion chamber volume less the volume displaced by the unburned propellant.

The mass balance in the chamber is a function of the input due to propellant combustion decreased by the outflow through the nozzles

$$\frac{dm_c}{dt} = \frac{dm_P}{dt} - \frac{dm_N}{dt} \quad (6)$$

$$\frac{dm_P}{dt} = \rho_P r S_B \quad (7)$$

with  $r$  being determined as a function of pressure by a tabular look-up routine and the burning surface a function of charge weight and propellant web.

$$S_B = \frac{2}{\rho_P w_0} C_W$$

where  $C_W$  is the initial charge weight less the weight of unburned propellant lost through the nozzles. This can be approximated to be a small fraction of the gas flow, such as is done in recoilless rifle ballistics.

The expression for the rate of nozzle mass flow is that used for rocket ballistics (Ref. 1) and is as follows:

$$\frac{dm_N}{dt} = \frac{P_c A_T}{c^*} \quad (8)$$

The propellant loss term can be most effectively defined as a fraction of the gas nozzle flow such that

$$\frac{dm_L}{dt} = \xi \frac{dm_N}{dt}$$

Equations (5), (7), and (8) then provide a solution for the high-pressure side of the device whose operation is independent of phenomena occurring on low-pressure side.

The solution for the low-pressure or action side of the device is through a standard gun ballistic approach similar to that given in Ref. 2. An additional term is required in the energy balance for the high-low system, however. This is to account for the work accomplished by the gases in driving the ambient air from the device. In a conventional gun with a small bore and very high pressures, this effect may be neglected. In a high-low system with relatively large bores and low pressures, this effect must be considered.

The energy balance for the low-pressure side will be

$$E_1 = E_2 + E_3 + E_4 + E_5$$

where

$E_1$  = energy put in system by nozzle flow of combustion gases

$E_2$  = translational energy of piston

$E_3$  = heat loss to walls

$E_4$  = energy required to accelerate unburned propellant and combustion gases

$E_5$  = energy required to remove ambient air from bore

To account for heat loss in the combustion chamber, a new impetus value is defined where

$$F_B = (1 - \phi) F_P \quad (9)$$

which implies that

$$T_O' = (1 - \phi) T_O$$

Then, at any point in the ballistic cycle, with  $A$  = cross section of bore,  
 $V_p$  = initial low pressure volume, and  $X$  = distance from  $X_0$  to piston base,  
 Eqs. (1) and (2) give

$$P_P(V_P + AX) = m_c F_B \frac{T}{T_0} \quad (10)$$

The Chemical energy transported will be

$$E_1 = m_N C_V (T_0' - T) \quad (11)$$

The translational energy of payload will be

$$E_2 = \frac{1}{2} m_B V^2 \quad (12)$$

The heat loss of the gases is proportional to the distance traveled, which  
 (Ref. 3) is roughly proportional to the square of the velocity. This heat loss  
 can then be approximated

$$E_3 = \frac{1}{2} \beta m_a V^2 \quad (13)$$

Using a Kent form solution (Ref. 5) with high-velocity modifications  
 (Ref. 4) for the energy contained in the accelerating gases and unburned pro-  
 pellant, it is approximated that

$$E_4 = \frac{1}{2} \frac{C_W}{g\delta} V^2 \quad (14)$$

with  $\delta = 3$  at low velocities and increasing at high velocities as the density dis-  
 tribution becomes less uniform. This effect, and the variation of  $\delta$  with pay-  
 load velocity, is covered in Ref. 4.

An effective mass may then be defined as

$$m_a = m_B + \frac{C_W}{g\delta} \quad (15)$$

Due to the relatively large bore area associated with the high-low system, the expansion work must be considered; this is typically ignored in a conventional gun system. This expansion work is:

$$E_5 = P_o AX \quad (16)$$

Then

$$E_2 + E_3 + E_4 + E_5 = (1 + \beta) \frac{1}{2} m_a V^2 + P_o AX \quad (17)$$

The term  $\gamma$  is defined by

$$(\gamma - 1) = \frac{R}{C_V} = \frac{F_B}{C_V T_o} \quad (18)$$

Then, from Eqs. (11), (17), and (18)

$$m_N F_B \left( \frac{1 - T}{T_o} \right) = \frac{1}{2} (\gamma - 1)(1 + \beta) m_a V^2 + P_o AX \quad (19)$$

The temperature ratio is eliminated by the introduction of the equation of state to give the basic ballistic equation

$$P_P (V_P + AX) = m_N F_B - (\gamma - 1)(1 + \beta) \frac{m_a}{2} V^2 - (\gamma - 1) P_o AX \quad (20)$$

Because a differential form of the above equation is more convenient for incremental computation, differentiating Eq. (20) gives

$$\frac{dP_p}{dt} (V_p + AX) = \frac{dm_N}{dt} F_B - (\gamma - 1)(1 + \beta) m_a \frac{dV}{dt} \frac{dX}{dt} - PA \frac{dX}{dt} - (\gamma - 1)P_o A \frac{dX}{dt} \quad (21)$$

Equation (8) provides the high-pressure-chamber-to-low-pressure plenum coupling relationship by defining the mass flow

$$\frac{dm_N}{dt} = \frac{P_c A_T}{c^*}$$

Values for the three factors  $\phi$ ,  $\beta$ , and  $\xi$  are necessary for the use of the above algorithm. These factors will vary within a small range depending upon the nature of the system used. The term  $\phi$  is the heat loss in the high-pressure chamber and is expressed as a function of total energy available. The term  $\beta$  is the heat and friction losses on the low-pressure side and is expressed as a fraction of the payload kinetic energy. The term  $\xi$  is propellant lost unburned from the high-pressure plenum and expressed as a percentage of the nozzle gas flow. Reasonable values will be as follows:

$$0.02 \leq \phi \leq 0.1$$

$$0.35 \leq \beta \leq 0.75$$

$$0.05 \leq \xi \leq 0.15$$

An application of this analysis to the design and development of an 11-in. parachute mortar is covered in Section III.



### III. PARACHUTE MORTAR BALLISTIC DESIGN

An alternate method for soft-landing an instrument capsule on a planet, other than the retromotor, is an aerodynamic deceleration system, or parachute. This approach, while less elegant than a retromotor, offers promise of high reliability, light weight, and considerable cost savings. The following describes the initial stages of a research effort designed to provide a ballistic technology base for the future development of directly mortared aerodynamic deceleration systems. Because of the large bulk and relative light weight of a parachute, standard interior ballistic systems are inadequate and the high-low approach must be used.

The initial heavyweight hardware used for prototype parachute mortar simulation and analytic ballistic verification is as shown in Fig. 2. The high-pressure chamber is illustrated with a sterilizable squib as well as with a high-pressure piezometric pressure transducer. The low-pressure plenum also has a Kistler fast-response crystal pressure transducer. The base of the fiberglass sabot that supports the parachute, is shown immediately above the high-pressure chamber.

A simulated parachute pack in its protective sabot is presented in Fig. 3. Also shown in the figure is the heavy steel launch tube and shear-off muzzle cover. On the left is the combustion chamber and nozzle plate with brass blow-out diaphragm and sterilizable squib. The gas obturation device used on the fiberglass sabot is a simple O-ring which proved adequate for the prevention of blowby.

The ballistic properties of the device are presented in Table 1.

These design parameters were determined by optimizing the theoretical high-low interior ballistic computer program which was designed from the mathematical model of the thermodynamic processes discussed in Section II.

Table 1. Shot Characteristics

Item	Ballistic properties
Propellant type	M-10
Propellant web	0.0018
Chamber volume	50 in. <sup>3</sup>
Plenum volume	4.5 in. <sup>3</sup>
Charge weight	16 gm
Payload weight	25 lb
Muzzle velocity	135 ft/sec

A correlation between experimental and theoretical pressure time histories for the combustion chamber is shown in Fig. 4. The figure shows the experimental data and theoretical analysis are in agreement at the start and at the end of the ballistic cycle. A degree of difference is noticed in the center portion of the firing. This is caused by the fragmentation of a fraction of the propellant grains during combustion and by lack of simultaneity of nozzle plug release. These effects both imply an initial higher pressure followed by earlier web burnout and subsequent lower pressures. These effects are apparent on the experimental data plot. In general, however, the correlation is certainly adequate for optimization of ballistic design.

The parachute mortar shown in Fig. 3 has been successfully fired several times with a dummy parachute, and once vertically with an operational chute. Future firings will be with flightweight rather than heavyweight hardware.

The high-low concept lends itself to a wide variety of applications because of its significant inherent flexibility. Fixing a payload weight, bore diameter, and propellant type, an infinity of pressure time histories is possible by altering the two chamber volumes, nozzle area, and propellant web. This

provides not only the ability to alter the peak of the pressure time trace, but also to reshape it completely. The pressure time history can be progressive, regressive, neutral, or in possession of dual peaks. Associated with this flexibility is the capability of operating the low-pressure action chamber at pressures at which conventional gun propellants will not burn reliably and reproducibly.

#### IV. CONCLUSIONS

The high-low interior ballistic technique has been sufficiently investigated to provide a technological base for the development of any required propellant-actuated device to accelerate large-caliber, lightweight projectiles. The thermodynamics and kinetics of the phenomena have been mathematically modeled and computer-coded. A prototype parachute mortar system has been designed, fabricated, and successfully tested. Should any future mission effort require a parachute deceleration system, or other bulky package deployment, a proven methodology is available.

#### NOMENCLATURE

$A$	bore area
$A_T$	nozzle throat area
$C_W$	initial propellant charge
$c^*$	characteristic velocity of propellant gases
$C_V$	specific heat of combustion products
$F_P$	impetus of propellant
$F_B$	recovered impetus of propellant
$g$	acceleration due to gravity
$m_a$	effective propelled mass

$m_B$	payload mass
$m_c$	mass in high-pressure chamber
$m_L$	propellant lost
$m_N$	propellant gas transported through nozzles
$m_P$	propellant burned
$P_c$	chamber pressure
$P_P$	plenum pressure
$P_o$	ambient pressure
$R$	gas constant
$r$	burning rate of propellant
$S_B$	propellant burning surface
$T$	gas temperature
$T_o$	flame temperature
$T_o'$	recovered flame temperature
$V$	payload velocity
$V_c$	chamber volume
$V_P$	plenum volume
$X$	payload travel
$\beta$	bore heat loss
$\phi$	chamber heat loss
$\xi$	propellant loss factor
$\gamma$	specific heat of propellant gases
$\delta$	density distribution factor
$\rho_P$	propellant density
$\omega_o$	propellant web
$\Gamma$	flow factor

## REFERENCES

1. Huggett, C., Bartley, C. E., Mills, M., "Solid Propellant Rockets," Princeton University Press, New Jersey, 1960.
2. Heiney, O. K., "The Interior Ballistics of Closed Breech Guns," AFATL Report 67-42, Eglin Air Force Base, 1967.
3. Hirschfelder, Kershner, and Curtiss, "Interior Ballistics." Reports A-142 and A-180, National Defense Research Council, Office of Science and Research Development, U. S. Government, Vols. I and II, February and April 1943 (Declassified).
4. Heiney, O. K., "A New Computer-Oriented Formulism for Gun Ballistics," Proceedings 3rd ICRPG-AIAA Solid Propulsion Conference, Vol. I, 3-5 June 1968 (Confidential).
5. Kent, R. H., "Some Special Solutions for the Motion of the Powder Gas," Physics, Vol. 7, 1936.

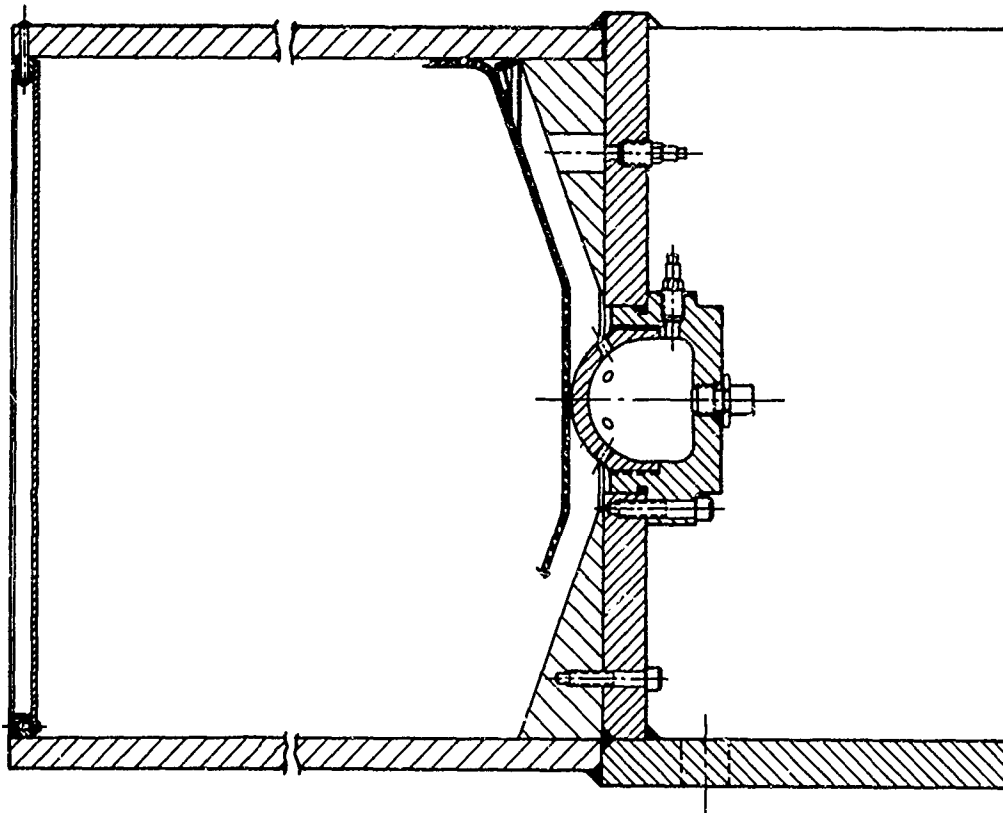


Fig. 2. Parachute mortar section



Fig. 3. Parachute mortar components

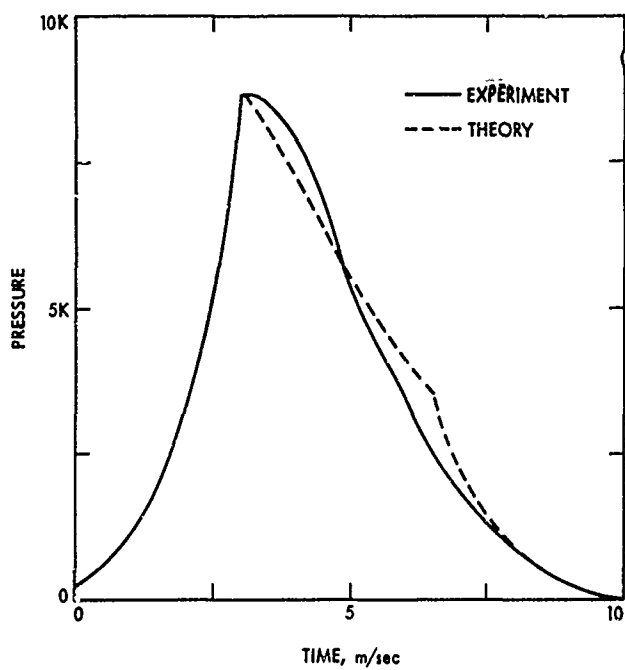


Fig. 4. Combustion chamber pressure-time plot

## 2-4 NOMOGRAPHICAL SOLUTION OF ELECTRO-EXPLOSIVE DEVICE FIRING TIME EQUATION

By

Herbert D. Peckham, Gavilan College and Donald E. Davenport,  
Singer-General Precision, Inc. Advanced Products Division Link Group.

### ABSTRACT

A review of existing solutions for the electro-explosive device (EED) design problem is given. Rosenthal's solution is expanded and refined to permit the prediction of firing data strictly from blueprint data.

A set of nomographs is presented to permit the rapid, easy solution of the new set of equations. The new solution is compared against firing data with excellent results.

### I. INTRODUCTION

#### A. Present Theoretical Knowledge of Electro-Explosive Devices

The widespread utilization of electro-explosive devices in aerospace applications has given rise to new requirements of reliability and theoretical knowledge. The manufacturer of such devices is faced with the problem of predicting device performance on the basis of incomplete experimental evidence, and of almost no understanding of the physics of the explosive-electrical interface. Since such predictions often involve considerable financial risks to the manufacturer and may involve serious time delays to the buyer, the case for a theoretical tool to permit valid prediction of EED characteristics is obvious.

The industry is in need, then, of an EED "equation-of-state". Such an equation, or equations, should involve only the basic design parameters, and should enable the designer to accurately predict how the device will respond to an electrical stimulus before the device is constructed. An additional need for an equation of state is to generate a theoretical knowledge of the physical processes taking place. Such an understanding will inevitably lead to optimum designs both in terms of reliability and of performance.

The objective of this paper is to develop a valid, simple EED equation of state. Then, a set of nomographs will be constructed to permit the rapid solution of the equations.

#### B. Exact Solutions Available

There are several very good solutions to the basic problem. These solutions represent different approximations to the true electro-explosive interface, and according to the accuracy of the model, are characterized by rather involved computer solutions.

A good solution in closed form has been developed by Davenport (References 1 and 2). This solution stems from a basic approach outlined by Carslaw and Jaeger (Reference 3). The solution accounts for the temperature dependence of bridgewire resistance and gives good predictions of temperature versus time subsequent to a specific electrical stimulus. A computer is required to handle the solution. The differential equation which describes the model is:

$$\rho c' (\pi r^2 dx) \frac{dT}{dt} = K \left[ \left( \frac{dT}{dx} \right)_x - \left( \frac{dT}{dx} \right)_{x+dx} \right] \pi r^2 - (2 \pi r dx) \left[ H (T - T_0) \right] + \frac{I^2 R_0 (1 + \alpha T) dx}{4.186 \lambda} \quad (1)$$

In equation (1)

- $\rho$  = density of the bridgewire material, gm/cm<sup>3</sup>
- $c'$  = heat capacity of the bridgewire material, cal/gm°C
- $r$  = radius of bridgewire, cm
- $x$  = distance along the bridgewire, cm
- $T$  = temperature of the bridgewire, °C
- $t$  = time, sec
- $K$  = thermal conductivity of the bridgewire material, cal/cm sec°C
- $H$  = radial heat transfer coefficient, cal/cm<sup>2</sup> sec °C
- $T_0$  = initial temperature of the system, °C
- $I$  = current flow, amps
- $R$  = bridgewire resistance, ohms
- $\lambda$  = length of the bridgewire, cm



This equation describes a constant current model. The equation can be put in the form

$$\frac{dT}{dt} = \kappa \frac{d^2T}{dx^2} - \nu (T - T_0) + a$$

where

$$\kappa = \frac{K}{\rho c'} \quad a = \frac{I^2 R_0}{4.186 c' r^2 \pi \rho \lambda} \quad (2)$$

$$\text{and } \nu = \left( \frac{2 H}{c' r \rho} - \frac{I^2 R_0 \alpha}{4.186 c' r^2 \pi \rho \lambda} \right)$$

The solution in closed form which yields temperature as a function of position and time, taking  $T_0 = 0$  is:

$$T = \frac{a}{\nu} \left[ 1 - \frac{\sinh x \sqrt{\frac{\nu}{\kappa}} + \sinh (\lambda - x) \sqrt{\frac{\nu}{\kappa}}}{\sinh \lambda \sqrt{\frac{\nu}{\kappa}}} \right] - \frac{4a}{\pi} \sum_{n=1}^{\infty} \left[ \frac{\sin (2n-1) \pi x}{\lambda} \right] \frac{e^{-t \left[ \nu + \frac{\kappa (2n-1)^2 \pi^2}{\lambda^2} \right]}}{(2n-1) \left[ \nu + \frac{\kappa (2n-1)^2 \pi^2}{\lambda^2} \right]} \quad (3)$$

Equation (3) gives excellent results if accurate values of all the parameters are known. The only disadvantage is that the solution is in a form which is fairly difficult to interpret and requires a computer. This solution will be utilized to refine the simplified solution which is the objective of this paper.

Another solution has been described by Massey (Reference 4). This solution is not given in closed form, and is a good deal more complicated than Davenport's, requiring a numerical computer solution. This solution gives temperature as a function of time, distance along the bridgewire, and radial distance from the bridgewire axis. Because of its complexity, this solution will not be discussed further in this paper.

### C. Rosenthal Solution

The simplest solution to the problem and the one which has had the most widespread recognition was developed by Rosenthal (Reference 5) in conjunction with the U. S. Naval Ordnance Laboratory. His is a "lumped parameter" model described by the equation:

$$c \frac{dT}{dt} + \gamma T = I^2 R \quad (4)$$

where

$c$  = heat capacity of the bridgewire

$\gamma$  = energy loss rate per degree C from the bridgewire.

Other parameters are as previously defined.

If one assumes  $c$  and  $\gamma$  are constants, Equation (4) can be solved easily for the solution

$$T = \frac{I^2 R}{\gamma} \left( 1 - e^{-\frac{\gamma}{c} t} \right) \quad (5)$$

Several methods have been suggested by Rosenthal and others for the empirical determination of  $\gamma$  and  $c$ . The fact that the device must be in existence before the empirical determination of  $\gamma$  and  $c$  can be accomplished is a serious disadvantage. There are other serious problems in the model itself which will be discussed in detail. The Rosenthal solution is given here since it is the point of departure for the refined solution which is the subject of this paper.

## II. AN EXPANDED FIRST ORDER SOLUTION

### A. The Rosenthal Equation

The differential equation describing the lumped parameter model utilized by Rosenthal has already been given (Equation 4). Several comments should be made regarding this equation.

First, the power generation term on the right side of the equation makes no provision for the variation of the resistance,  $R$ , with temperature. The fact that this is a serious omission can be seen easily. If the bridgewire is nichrome, with a temperature coefficient of resistivity of 0.0001, and the required temperature is  $300^{\circ}\text{C}$  (a reasonably good value for lead styphnate) the final resistance is 1.03 times the initial resistance. Taken by itself an error of 3% does not seem serious. However, as will be developed later, this does have significance in firing times. If the bridgewire is tungsten with a temperature coefficient of resistivity of 0.0045, the final resistance is 2.35 times the original resistance!

The first change, then, will be to replace  $R$  in Equation (4) by  $R_0 (1 + \alpha T)$ .  $R_0$  is the initial resistance at ambient temperature,  $T$  is the temperature change measured from ambient, and  $\alpha$  is the temperature coefficient of resistivity of the bridgewire material. Ayres (Reference 6) has discussed the factor  $\alpha$  in the analysis of EED's with the Rosenthal equation.

The second change in Equation (4) concerns the temperature. Implicit in the first order, lumped parameter approach is the assumption that the entire bridgewire is at the same temperature. Davenport has calculated the ratio of  $\bar{T}/T_{\text{max}}$  utilizing the temperature distribution given in Equation (4).  $\bar{T}$  is the average temperature of the bridgewire and  $T_{\text{max}}$  is the maximum bridgewire temperature. The ratio  $\bar{T}/T_{\text{max}}$  can vary from 1 to as low as 0.70, depending upon the bridgewire material and configuration, and the time after current is applied. Thus, this ratio is time dependent, and must be accounted for in the differential equation. It is extremely important to note at this point that if we use a single temperature to characterize the entire bridgewire as is done in Equation (4), this temperature must be  $\bar{T}$ . On the other hand, the temperature which determines the initiation of the explosive is  $T_{\text{max}}$ . This situation will be accounted for in subsequent sections.

## B. Introduction of Basic Design Parameters

Making the substitution  $R_0 (1 + \alpha \bar{T})$  for  $R$  and recalling that  $\bar{T}$  is the temperature which characterizes the entire bridge-wire, Equation (4) becomes

$$c \frac{d\bar{T}}{dt} + \gamma \bar{T} = I^2 R_0 (1 + \alpha \bar{T}) \quad (6)$$

The term  $\gamma$  in Equation (6) contains two terms. One is the radial loss related to  $\bar{T}$ , the other is the longitudinal loss and is related to  $T_{\max}$ .

Equation (6) can be put in the form

$$c \frac{d\bar{T}}{dt} + \gamma' \bar{T} = I^2 R_0 \quad (7)$$

where

$$\gamma' = (\gamma - I^2 R_0 \alpha) \quad (8)$$

Equation (7) is the same form as Equation (4). The solution is immediately seen to be

$$\bar{T} = \frac{I^2 R_0}{\gamma'} (1 - e^{-t/t_c}) \quad (9)$$

$$\text{where } t_c = c/\gamma' \quad (10)$$

The next task will be to "de-lump" the "lumped parameters"  $c$  and  $\gamma$ . As utilized to this point in the industry,  $c$  and  $\gamma$  are determined empirically from tests on the device. What is desired here is to express these parameters in terms of basic design information.

The first term,  $c$ , is the easiest to examine. It is simply the "effective" heat capacity of the bridgewire and can be expressed as

$$c = \frac{N \omega \lambda \rho c'}{j} \quad (11)$$

where N is a factor introduced to take advantage of information from Davenport's solution

$$\begin{aligned}\omega &= \text{cross sectional area of bridgewire, cm}^2 \\ j &= 0.2389 \text{ cal/joule}\end{aligned}$$

The other factors are as previously defined in Equation (1). For the present, N will remain undefined but will be discussed in detail in the next section.

The other "lumped parameter"  $\gamma$ , is simply the sum of the specific energy loss rates through the two ends, and through the lateral surface of the bridgewire. These specific energy loss rates can be described by:

$$\gamma = \left( \frac{2M\omega K}{\lambda} + H p \lambda \right) \frac{1}{j} \quad (12)$$

where M is a factor which will generate the proper temperature gradient at the ends of the bridgewire. This factor will be discussed and defined in the next section.

$p$  = bridgewire perimeter, cm.  
Other factors are as previously defined.

We note the fact that M and H are both time dependent. However, for the purposes of this report, they will be assumed constant. In fact, the reason for introducing N in the heat capacity term was to correct for this.

#### C. Use of Information From Exact Solution

Recall the solution given by Equation (9) is in terms of  $\bar{T}$ . Of course, what is desired is the solution in terms of  $T_{\max}$  since this is the temperature which controls initiation of the primer material. Define  $\delta$  to obtain a simple approximation to convert the form, one can proceed as follows:

$$\delta = \bar{T}/T_{\max}$$

By using Equation (3) with  $t = \infty$ , Davenport was able to calculate the steady state value of  $\delta$ . This is

$$\delta = \frac{1 + \frac{1 - \cosh(\mu\lambda)}{\frac{\mu\lambda}{2} \sinh(\mu\lambda)}}{1 - \operatorname{sech}\left(\frac{\mu\lambda}{2}\right)} \quad (13)$$

where

$$\mu = \sqrt{\frac{Hp}{\omega K}} = \sqrt{\frac{\nu}{\kappa}} \text{ if } \alpha \text{ is assumed } 0,$$

where

$p$  = BW perimeter

$\omega$  = BW cross section area

It is known, however, that  $\delta$  is actually time dependent. Three facts are known. First at  $t = 0$ ,  $\bar{T}/T_{\max} = 1$ . Second, at  $t = \infty$ ,  $\bar{T}/T_{\max} = \delta$ . Third, the ratio changes rapidly initially and asymptotically approaches  $\delta$  as  $t$  approaches  $\infty$ . Thus, a function is required which will generate this behavior. It would seem that the same functional relation which describes the variation of temperature with time would be appropriate. Such a function which has the desired characteristics is:

$$\frac{\bar{T}}{T_{\max}} = \left(1 + (1 - e^{-t/t_c}) (\delta - 1)\right) \quad (14)$$

Equation (14) can be solved for  $\bar{T}$  and used to introduce  $T_{\max}$  into the solution given by Equation (9). The result is

$$T_{\max} \left(1 + (1 - e^{-t/t_c}) (\delta - 1)\right) = \frac{I^2 R_o}{\gamma'} (1 - e^{-t/t_c})$$

If this equation is solved for  $t$ , the time to reach  $T_{\max}$ , the result is

$$t = -t_c \ln \left[ 1 - \frac{T_{\max}}{\frac{I^2 R_o}{\gamma'} - T_{\max} (\delta - 1)} \right] \quad (15)$$

Equation (15) is the desired solution. The only remaining task is to define N in Equation (11) and M in Equation (12). N will be defined first.

Empirically, it has been found that  $N = 2.24 \delta$  (16) gives a good fit to the data. In Davenport's solution, a constant factor of 2 gave the best fit to the data instead of  $2.24 \delta$ . This matter should be investigated in the future.

Now M must be defined. The temperature gradient at the ends of the wire can be computed from Davenport's solution (Equation 3) by assuming  $t = \infty$  and evaluating  $dT/dx$  at  $x = 0$ . Experience shows that this approximation is reasonable for times other than  $t = \infty$ . If this is done, the result is

$$\left. \frac{dT}{dx} \right|_{\substack{x=0 \\ t=\infty}} = \frac{a}{\nu \lambda} \left\{ \mu \lambda \left( \frac{\cosh(\mu \lambda) - 1}{\sinh(\mu \lambda)} \right) \right\} \quad (17)$$

The heat which flows out the ends of the wire according to Equation (17) is

$$\Delta Q = 2 \left. \frac{dT}{dx} \right|_{\substack{x=0 \\ t=\infty}} \omega K$$

According to the first order model, the heat flowing out the ends of the wire is

$$\Delta Q = 2 \frac{M \omega K}{\lambda} \bar{T}$$

M is defined such that these two terms are equal. Therefore

$$2 \left. \frac{dT}{dx} \right|_{\substack{x=0 \\ t=\infty}} \omega K = 2 \frac{M \omega K \bar{T}}{\lambda}$$

solving for M, the following relation is obtained:

$$M = \frac{\lambda}{1} \left. \frac{dT}{dx} \right|_{\substack{x=0 \\ t=\infty}} \quad (18)$$

$$\text{Define } \beta = \left( \frac{\cosh(\mu\lambda) - 1}{\sinh(\mu\lambda)} \right) \text{ in Equation (17)} \quad (19)$$

$$\text{Then } \left. \frac{dT}{dx} \right|_{\substack{x=0 \\ t=\infty}} = \frac{a}{\nu\lambda} (\mu\lambda) \beta \text{ which, when substituted in}$$

Equation (18) gives the definition of M.

$$M = \frac{a}{\nu} \left( \frac{\mu\lambda}{\beta} \right) \beta \quad (20)$$

Now, the problem is to evaluate M in a fashion that will produce a useable solution. The question, then, is the ratio  $a/\nu$ .

If in Davenport's solution, see Equation (2), the approximation  $\alpha = 0$  is made, the result is:

$$a = j \frac{I^2 R_o}{\rho c' \omega \lambda}, \text{ and } \nu = \frac{4H}{\rho c' d}$$

From this the ratio below can be obtained:

$$\frac{a}{\nu} = j \frac{I^2 R_o d}{4\omega\lambda H}$$

If the approximation  $\alpha = 0$  is made in Equation (9) and we let  $t = \infty$ , we obtain

$$I^2 R_o = \bar{T} \gamma$$



If this is substituted in the ratio  $a/\nu$  above, the result is

$$a/\nu = j \frac{\bar{T}_Y}{H\rho\lambda}$$

But

$$\gamma = \left( 2 \frac{M \omega K}{\lambda} + H\rho\lambda \right) \frac{1}{j}$$

Also, if  $\alpha = 0$   $H\rho = \mu^2 \omega K$  (see Equation 13)

Making these substitutions and solving for M, the value can be obtained as follows:

$$M = \frac{(\mu\lambda)^2}{\frac{\mu\lambda}{\beta} - 2} \quad (21)$$

Equation (21) was tried in the solution and it was found that for significant temperature coefficients of resistivity, a good data fit was not obtained. This should not be too surprising, since it was formulated from equations which assumed  $\alpha = 0$ . Therefore, an extremely pragmatic approach will be taken to correct equation (21) for  $\alpha$ . Since the energy generation is proportional to R, and since R increases as  $(1 + \alpha T_{\max})$ , it might be reasonable that a better approximation would be to assume that the leakage increases by the same factor. A simple correction would be to multiply M by  $(1 + \alpha T_{\max})$ . Note that  $(1 + \alpha T_{\max})$  is used for simplification purpose rather than the correct form  $(1 + \alpha \bar{T})$ .

Therefore

$$M = \frac{(\mu\lambda)^2}{\frac{\mu\lambda}{\beta} - 2} (1 + \alpha T_{\max}) \quad (22)$$

This was found to give a good data fit.

#### D. Discussion of Approximations

A number of assumptions, and approximations have been made to this point. These should be discussed in light of the stated objective of this paper. Recall the objective was to produce a simple solution which works -- one that does not become lost in complexities. What has happened is that first order corrections have been applied to Rosenthal's original equation. In working towards the values of M and N, the same corrections have often been ignored. However, M and N are themselves first order corrections, so the neglected corrections are second order. It is felt that this is valid in light of the stated objectives.

The validity of the approximations must be judged in terms of how well the new equation works. This is not to say that further investigations into the equation should not be made, merely that a good, working, first step has been obtained.

#### E. Recapitulation of Expanded First Order Solution

The solution, expressing firing time in terms of the other parameters is:

$$t = -t_c \ln \left[ 1 - \frac{T_{\max}}{\frac{I^2 R_0}{\gamma'} - T_{\max}(\delta - 1)} \right] \quad (23)$$

where

$$t_c = c/\gamma' \quad (24)$$

$$c = \frac{2.246 \omega \lambda \rho c'}{j} \quad (25)$$

$$\gamma' = \left( 2 \frac{M \omega K}{\lambda} + H p \lambda \right)^{\frac{1}{j}} - I^2 R_0 \alpha \quad (26)$$

$$M = \frac{(\mu\lambda)^2}{\frac{(\mu\lambda)}{\beta} - 2} (1 + \alpha T_{\max}) \quad (27)$$

$$\delta = \frac{1 + \frac{1 - \cosh(\mu\lambda)}{\frac{\mu\lambda}{2} \sinh(\mu\lambda)}}{1 - \operatorname{sech}\left(\frac{\mu\lambda}{2}\right)} \quad (28)$$

$$\beta = \frac{\cosh(\mu\lambda) - 1}{\sinh(\mu\lambda)} \quad (29)$$

$$\mu = \sqrt{\frac{Hp}{\omega K}} \quad (30)$$

Equations (23) through (3) can be solved for the desired results. In these equations

- $t$  = firing time at constant current, sec
- $c$  = "effective" heat capacity of bridgewire, joules/ $^{\circ}\text{C}$
- $\rho$  = density of bridgewire material, gm/cm<sup>3</sup>
- $c'$  = specific heat of bridgewire material, cal/gm $^{\circ}\text{C}$
- $\lambda$  = length of bridgewire, cm
- $j$  = mechanical equivalent of heat = 0.2389 cal/joule
- $\omega$  = cross section area of bridgewire, cm<sup>2</sup>
- $K$  = thermal conductivity of bridgewire material, cal/sec cm $^{\circ}\text{C}$
- $H$  = radial heat transfer coefficient cal/sec cm<sup>2</sup> $^{\circ}\text{C}$
- $I$  = constant firing current, amperes
- $R_0$  = ambient resistance of bridgewire, ohms
- $\alpha$  = temperature coefficient of resistivity of bridgewire material,  $^{\circ}\text{C}^{-1}$
- $T_{\max}$  = increase in temperature above ambient required for initiation of explosive,  $^{\circ}\text{C}$
- $p$  = perimeter of bridgewire, cm

### III. A NOMOGRAPHICAL SOLUTION

#### A. Motivation for a Nomographical Solution

Equation (23) through (30) give the refined, simplified solution to the basic problem. If a more accurate solution is

required, and a computer is available, Davenport's solution can be used. There is certainly nothing to prevent the designer from using the equations developed in this paper in their present form, however, nomographs have been constructed to solve these equations. It is felt that there are compelling reasons for using this approach.

The typical values of the factors in Equation (23) through (30) are such as to make a power of ten mistake very likely. Nomographs make it much less likely that this type of mistake will occur. Most engineers like to use nomographs for this reason.

The nomographs are constructed to permit a reasonably rapid analysis of a particular design. Most important however, is that the effect of parameter variation can be seen clearly using nomographs. This is difficult using the raw equations. It is possible therefore, for the designer to acquire a "feel" for the problem which will enable rapid answers to be obtained as to how to meet specific specification requirements, or indeed if the requirements can be met.

If the problem is particularly important and merits the investigative effort, the nomographs can be used to get a solution, which can itself be subjected to computer refinement using Davenport's solution.

#### B. Rearrangements of Solution to Facilitate Nomographical Solution

The solution given in Equations (23) through (30) will now be adapted to the specific case of a round bridgewire.

Equation (30) defines  $\mu$ . The argument of the hyperbolic functions in Equations (26) through (29) is  $\mu\lambda$ . Thus, the first step is to develop this. If the substitutions

$$p = \pi d \text{ and } \omega = \pi \frac{d^2}{4}$$

are made in Equation (30), and the expression is multiplied by  $\lambda$  the result is:

$$\mu\lambda = \lambda \left( \frac{4H}{Rd} \right)^{1/2} \quad (31)$$

where  $d$  = bridgewire diameter, cm

and other parameters are as previously described.

Next, Equation (27) must be put in the form to permit  $M$  to be obtained. To simplify the expression, the substitution below will be used.

$$A = (1 + \alpha T_{\max})$$

Equation (27) is in suitable form for nomographic solution

$$M = \left[ \frac{(\mu\lambda)^2}{\frac{(\mu\lambda) \sinh(\mu\lambda)}{\cosh(\mu\lambda) - 1} - 2} \right] A \quad (32)$$

The substitution  $\omega = \frac{\pi d^2}{4}$  together with the definition of  $\delta$  is used in Equation (25) to obtain

$$c = 2.24 \frac{\pi}{4j} d^2 (\rho c') \lambda \left[ \frac{1 + \frac{1 - \cosh(\mu\lambda)}{\frac{\mu\lambda}{2} \sinh(\mu\lambda)}}{1 - \frac{1}{\cosh(\frac{\mu\lambda}{2})}} \right] \quad (33)$$

The next problem is to evaluate  $\gamma'$  as given in Equation (26). Making the substitution

$$\omega = \frac{\pi d^2}{4} \quad \text{and} \quad p = \pi d$$

The result is

$$\gamma' = \left( \frac{\pi}{2j} K \frac{d^2 M}{\lambda} \right) + \left( \frac{\pi}{j} H \lambda d \right) - (I^2 R_O \alpha)$$

This can be put in the form

$$\gamma' = \xi + \Phi - \Theta \quad (34)$$

where  $\xi = \frac{\pi}{2j} Kd^2 \frac{M}{\lambda}$  (end leakage)

$$\Phi = \frac{\pi}{j} H\lambda d \text{ (radial leakage)}$$

$$\Theta = I^2 R_0 \alpha \text{ (excess energy input because of temperature coefficient)}$$

In the event that  $R_0$  must be calculated, it can be derived from the equation

$$R = \frac{4}{\pi} \frac{\rho' \lambda}{d^2} \quad (35)$$

where  $\rho'$  = bridgewire material resistivity, ohm cm

Once  $\gamma'$  is known the solution can be carried to Equation (23). Two substitutions will be used:

$$\psi = \frac{I^2 R_0}{\gamma'} \quad (36)$$

$$\text{and } \Omega = -T_{\max} \left[ \left( \frac{1 + \frac{1 - \cosh(\mu\lambda)}{\frac{\mu\lambda}{2} \sinh(\mu\lambda)}}{1 - \frac{1}{\cosh(\frac{\mu\lambda}{2})}} \right) - 1 \right] \quad (37)$$

Now use the substitutions

$$\beta' = \psi + \Omega$$

$$\text{and } \tau = \frac{t}{t_c}$$

Equation (23) can be put in the form

$$T_{\max} = \beta' (1 - e^{-\tau}) \quad (38)$$

From Equation (38)  $\tau$  can be obtained. The final equation required to reach  $t$  is

$$t = \frac{\tau \cdot c}{\gamma'} \quad (39)$$

The new set of equations solved by nomographs will be repeated here for convenience

$$\mu\lambda = \lambda \left( \frac{4H}{Kd} \right)^{1/2} \quad (40)$$

$$M = \left[ \frac{\frac{(\mu\lambda)^2}{\cosh(\mu\lambda) - 1}}{\frac{(\mu\lambda) \sinh(\mu\lambda)}{2} - 1} - 2 \right] A \quad \text{where } A = (1 + \alpha T_{\max}) \quad (41)$$

$$c = 2.24 \frac{\pi}{4j} d^2 (\rho c') \lambda \left[ \frac{1 + \frac{1 - \cosh(\mu\lambda)}{\frac{\mu\lambda}{2} \sinh(\mu\lambda)}}{1 - \frac{1}{\cosh(\frac{\mu\lambda}{2})}} \right] \quad (42)$$

$$\xi = \frac{\pi}{2j} K d^2 \frac{M}{\lambda} \quad (43)$$

$$\Phi = \frac{\pi}{j} H \lambda d \quad (44)$$

$$R_o = \frac{4}{\pi} \frac{\rho' \lambda}{d^2} \quad (45)$$

$$\Theta = I^2 R_o \alpha \quad (46)$$

$$\gamma' = \xi + \Phi - \Theta \quad (47)$$

$$\psi = \frac{I^2 R_o}{\gamma'} \quad (48)$$

$$\Omega = - T_{\max} \left( \frac{1 + \frac{1 - \cosh(\mu\lambda)}{\frac{\mu\lambda}{2} \sinh(\mu\lambda)}}{1 - \frac{1}{\cosh(\frac{\mu\lambda}{2})}} - 1 \right) \quad (49)$$

$$\beta' = \psi + \Omega \quad (50)$$

$$T_{\max} = \beta' (1 - e^{-\tau}) \quad (51)$$

$$t = \frac{\tau C}{\gamma'} \quad (52)$$

With the exception of Equations (47) and (50), a set of nomographs is presented which will solve the system of Equations (40) through (52).

#### C. Discussion of Nomographs

The nomographs solving the set of equations (40) through (52) are contained in Appendix A. They are presented in the same order as the equations above. There are two nomographs (10A and 10B) for Equation (51) depending upon whether  $\tau$  is - or +. In all the nomographs, the instructions are self-explanatory. A work sheet to assist in the computation follows the nomographs in Appendix B. Its use is also self-explanatory.

### IV. COMPARISON OF NOMOGRAPHICAL SOLUTION WITH EXPERIMENTAL RESULTS

#### A. General Discussion of Solution Characteristics

Several comments should be made concerning solutions utilizing the nomographs. In the approximation used in the nomographical solution  $H$  should not be dependent upon the bridge-wire. As a first trial,  $H$  will be considered constant, independent of bridgewire diameter. Subsequent investigations may indicate that refinements in the treatment of  $H$  will be required.

For a given explosive,  $T_{\max}$  is an explosive constant, and should not depend upon bridgewire material.

#### B. Data Utilizing Platinum Bridgewires

Figure 1 shows the comparison between the theoretical nomographical solution and experimental firing data. The value of  $T_{\max}$  is  $300^{\circ}\text{C}$  and  $H$  is 0.150. As can be seen, the agreement between theory and experiment is excellent.

#### C. Data Utilizing Nichrome Bridgewire

Figure 2 shows the comparison between theory and experiment for nichrome bridgewire. As for platinum,  $H = 0.150$ ,  $T_{\max} = 300^{\circ}\text{C}$ , with the exception of the 1 mil wire, the agreement is excellent. The question of instrumentation accuracy arises for very short firing times (less than 1 millisecond) and needs to be investigated further.



#### D. Comparison of Nomographical to Davenport's Solution

The nomographical solution has been compared to Davenport's solution obtained with a computer. The agreement is very good for both nichrome and platinum. The agreement justifies the approximations that were made in the development of the nomographical solution. The excellent agreement with experimental data verifies that a valuable and accurate new tool has been derived.

#### E. Sample Nomograph Solutions

In order to provide the reader with a known solution, sample calculations are presented in Appendix B for several bridgewire current combinations. As one becomes experienced with the use of the nomographs a complete function time current curve should be generated in less than 30 minutes for a given header configuration.

#### DISCUSSION

The discussion brought out the fact that the firing temperature of 300°C had been fitted empirically and that different firing temperatures would give different firing times. Mr. I. Kabik of NOL cited their previous work with the MK I Squib where 500°C gave them very good agreement between calculated and experimental results using Prof. Rosenthal's equations. Rosenthal too solved the equations in two ways, one of which took into account the thermal coefficient of resistivity. This work was discussed at previous EED Symposia.

#### BIBLIOGRAPHY

1. Davenport, D. E. "Theoretical Approach to 1 Amp/1 Watt, No-Fire Ordnance Designs," IEEE Aerospace Technical Conference and Exhibit, June 1965
2. Davenport, D. E., "Temperature Coefficient of Resistivity Effects on 1A/1W No-Fire Initiators, Proceedings of the Fifth Symposium on Electroexplosive Devices, Franklin Institute, June 13-14, 1967.
3. Carslaw, H. S. and S. C. Jaeger, "Conduction of Heat in Solids", 2nd Edition, Oxford at the Clarendon Press.
4. Massey, J. M. Jr., "A Heat Transfer Model Study of the Hot Wire Initiator, NWL Report 1919, 1964.
5. Rosenthal, Louis A., "Electro-Thermal Equations for Electro-explosive Devices", NavOrd Report 6684, August 15, 1959.
6. Ayres, J. N., "Comments on the Temperature Coefficient of Resistance As Used in Wire Bridge Electro-Explosive Device Analysis", NOLTR 61-154.

TABLE I Values of H

Case	K	D	3	2	1	0.15
1	.001		.10	.15	.15	.70
2	.0075		.08	.12	.12	.50

$$K = \text{cal/cm}^2/\text{cm/sec}/^\circ\text{C}$$

$$D = \text{B/W diameter (in mils)}$$

Case (1) Flush B/W on Glass - organic primary, e.g., styphnate

Case (2) Suspended B/W - organic primary, e.g. styphnate.

TABLE II

B/W Primary	Pt, Ag, Au, $\alpha = .0039$	Molybdenum Tungsten $\alpha = .0035$	Kovar $\alpha = .0033$	Nichrome $\alpha = .0001$
Pb Styphnate (n or basic) $T_{\text{max}} = 300^\circ\text{C}$	2.20	2.05	1.99	1.03
Pb Azide $T_{\text{max}} = 400^\circ\text{C}$	2.60	2.4	2.32	1.04

$$A = (1 + \alpha T_{\text{max}})$$

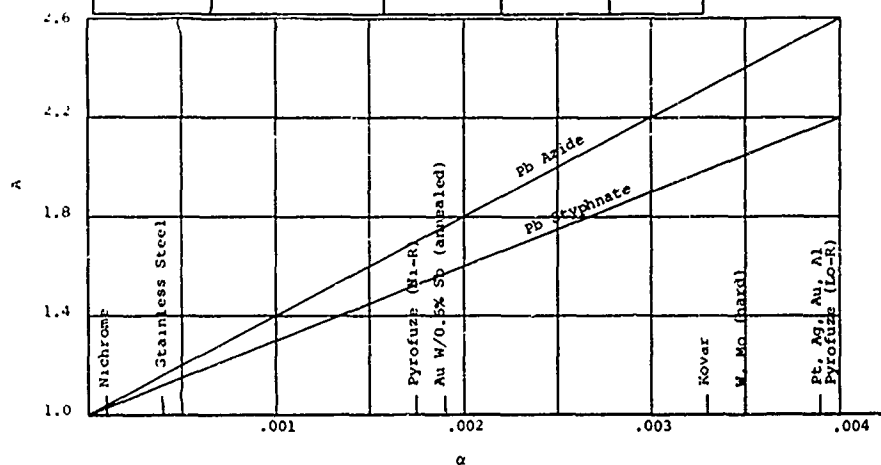
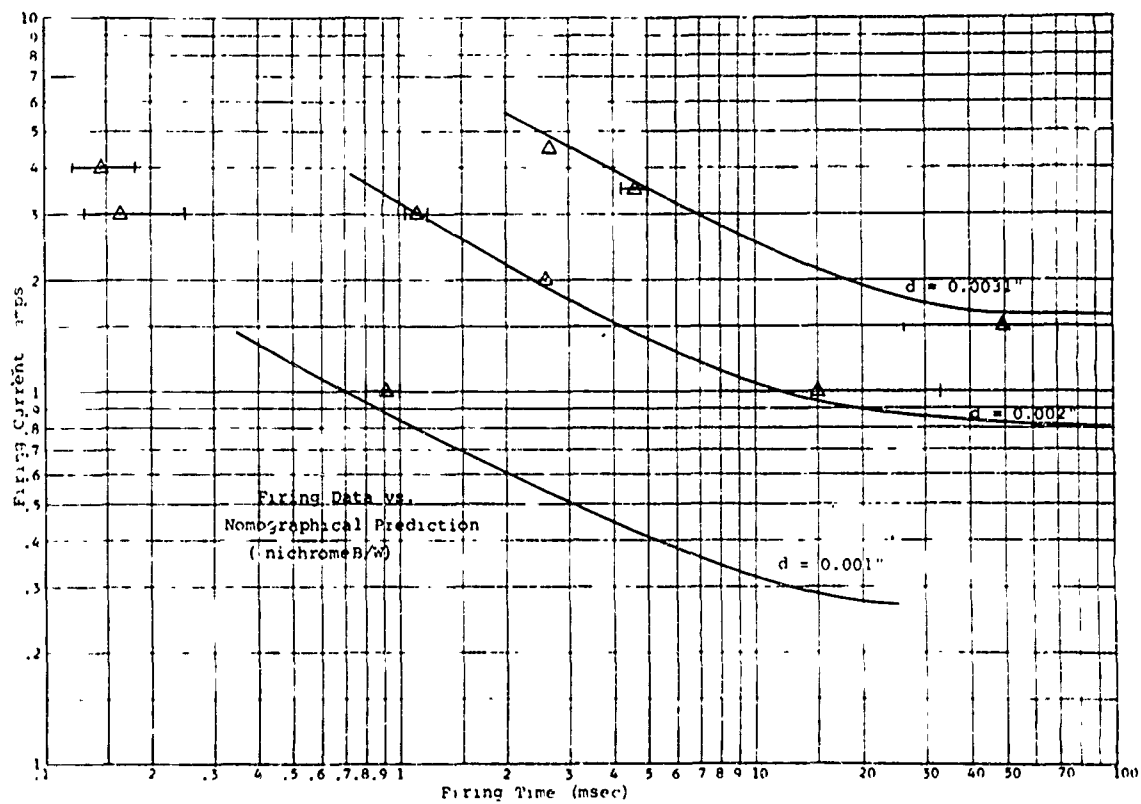
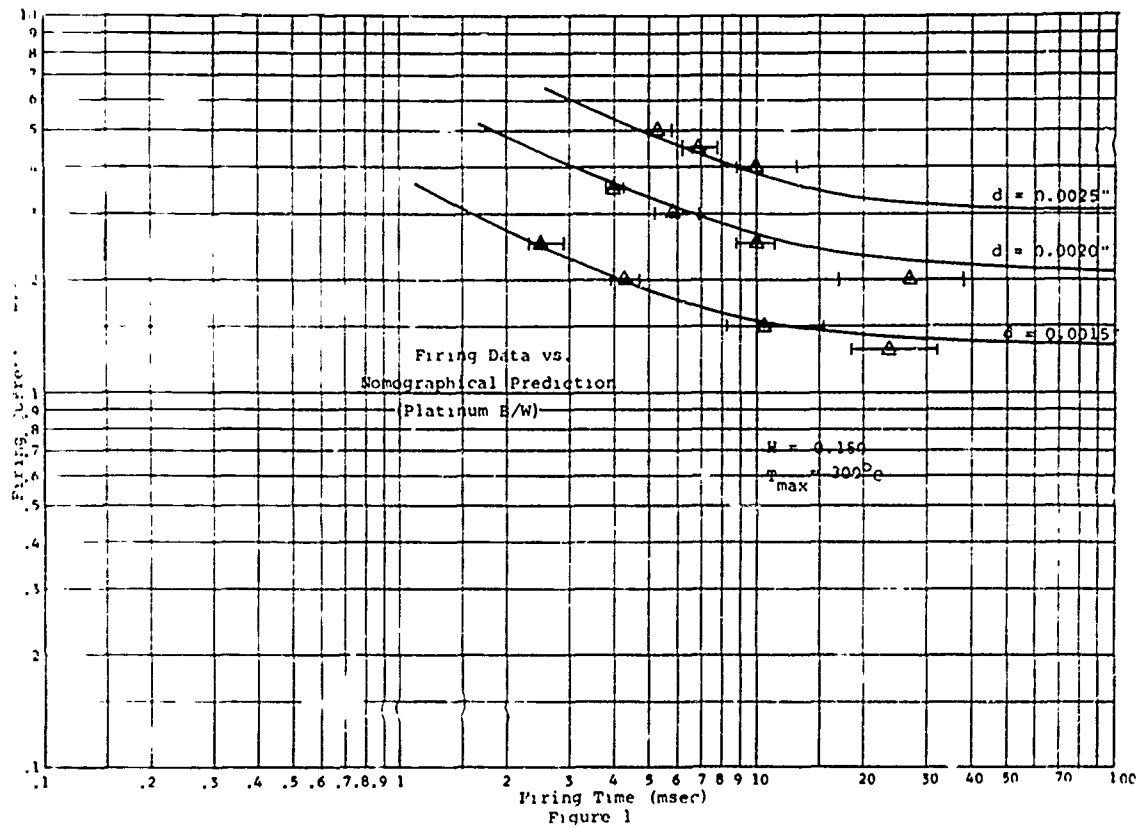


TABLE III

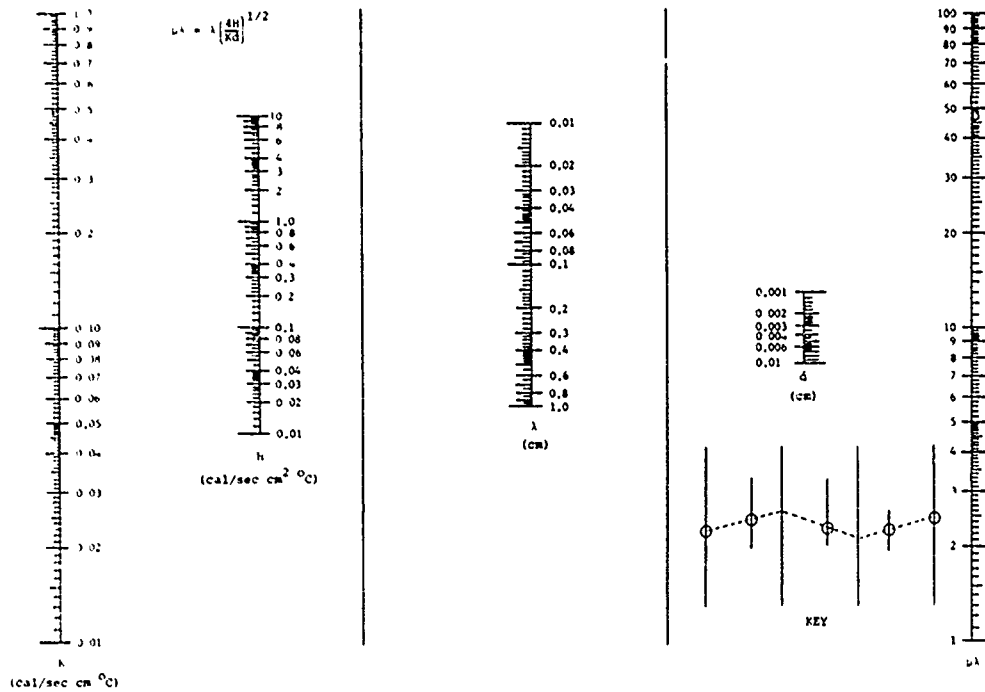
	$\rho \text{ C}'$	Resistivity $\rho' \mu\text{cm}$	Temperature Coefficient $\alpha$
Au (hard)	.602	2.24	.0038
Au (annealed)	.602	2.23	.0039
Pt (hard)	.669	11.62	.0032
Pt (annealed)	.669	11.47	.0033
Mo (hard)	.674	6.98	.0036
Mo (annealed)	.674	5.15	.0047
0.6% Sb-Au (hard)	.601	2.63	.0033
0.6% Sb-Au (annealed)	.601	4.49	.0019
Ag (hard)	.596	1.58	.0036
Ag (annealed)	.596	1.50	.0038
Kovar (hard)	.879	54.8	.003
Kovar (annealed)	.879	48.8	.0033
Nichrome V (hard)	.900	113.0	.0001
Nichrome V (annealed)	.900	104.7	.0001
Pyrofuze (Hi-R)		10.30	.00175
Pyrofuze (Lo-R)		4.65	.0039

 $\rho$  = density in gm/cc $\text{C}'$  = heat capacity in cal/gram $\rho'$  = resistivity in  $\mu\text{cm}$  $\alpha$  = temperature coefficient of resistivity

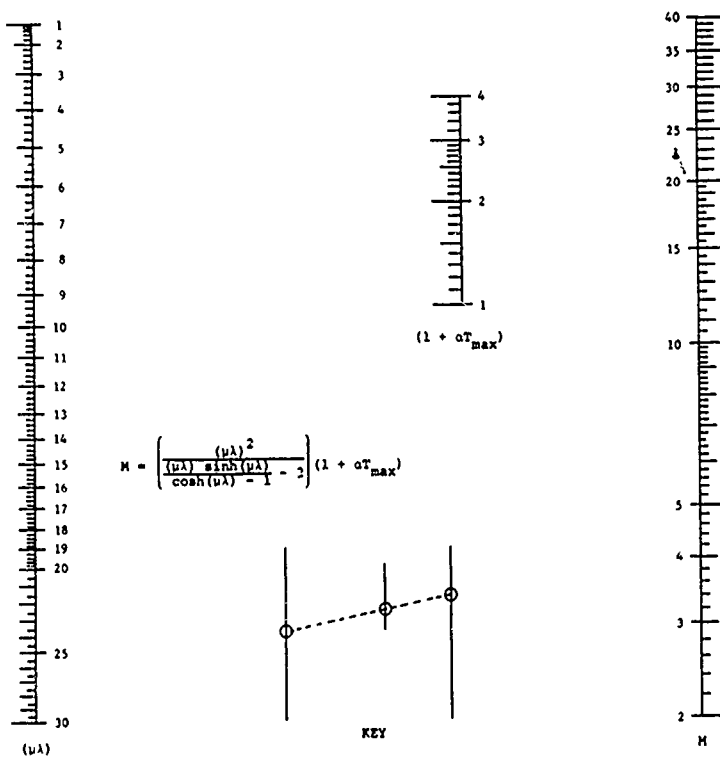
2-4,20



APPENDIX A  
Nomographs 1 - 11

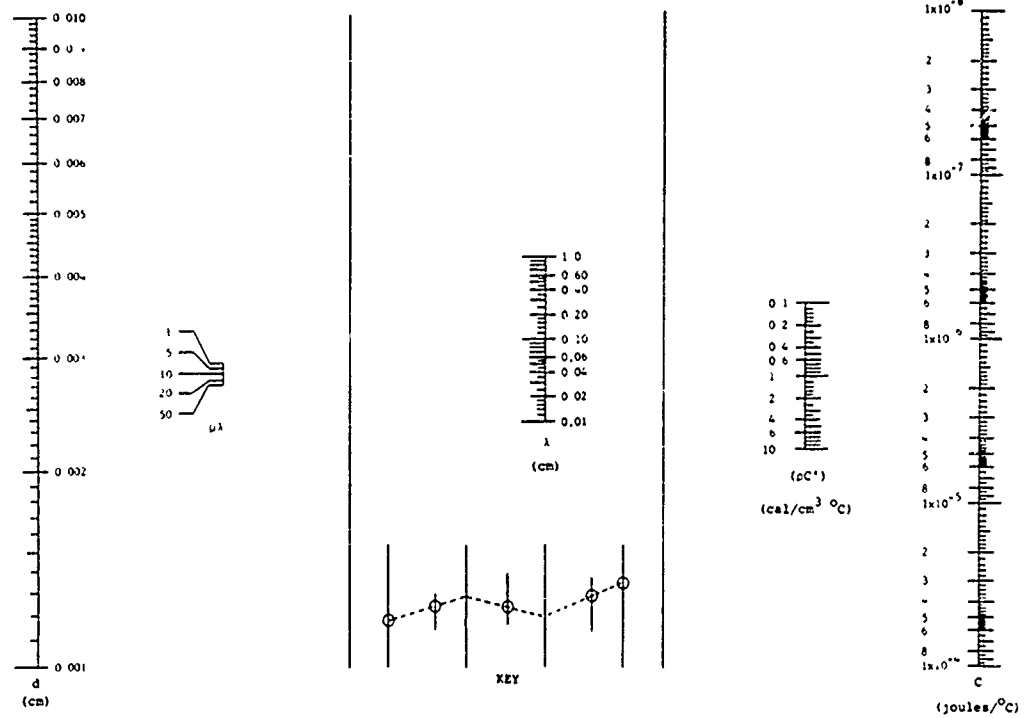


Nomograph 1

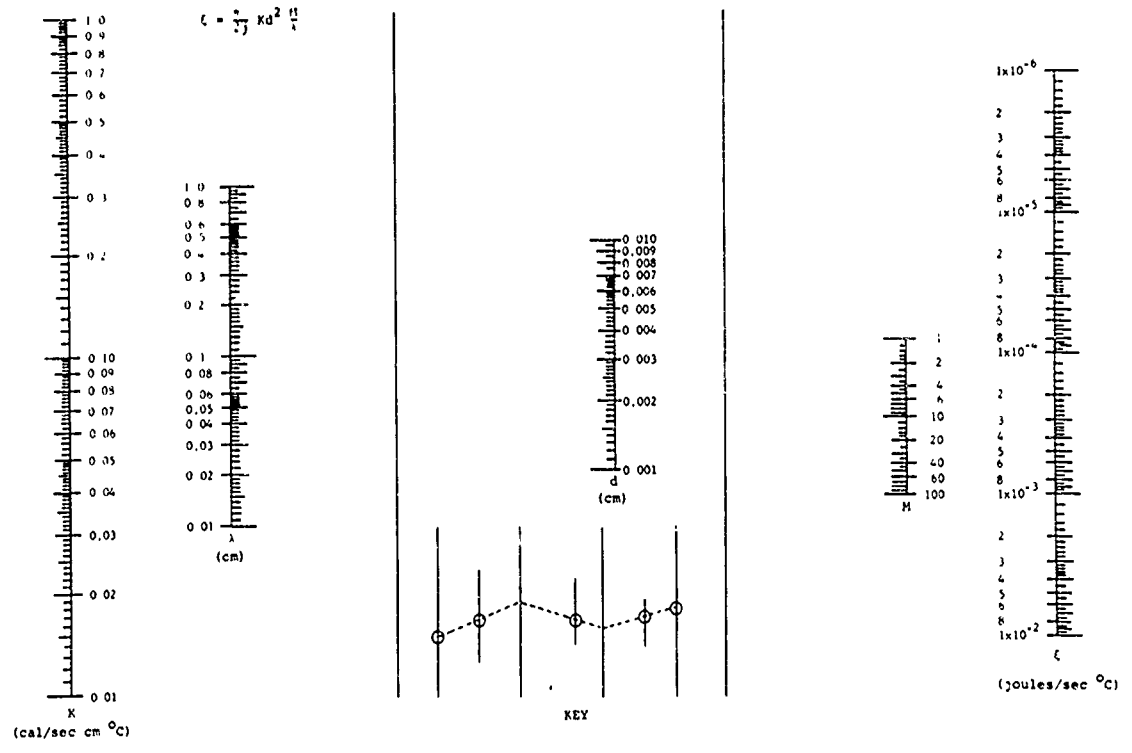


Nomograph 2

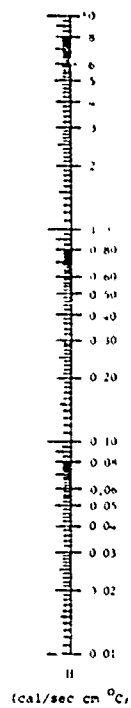
$$C = 1.12 \frac{\pi}{\lambda^2} d^2 (\rho C^*) \lambda \left( \frac{1 + \frac{1 - \cosh(\nu \lambda)}{\nu \lambda} \sinh(\nu \lambda)}{1 - \frac{1}{\cosh(\frac{\nu \lambda}{2})}} \right)$$



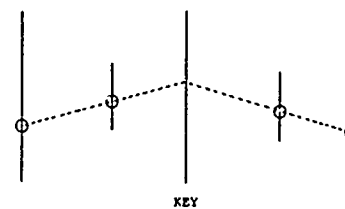
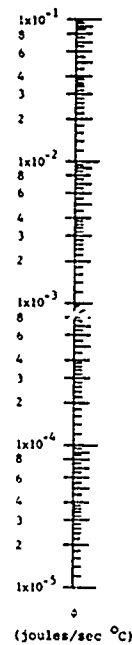
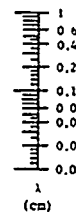
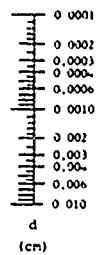
Nomograph 3



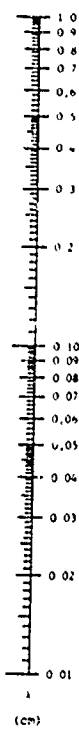
Nomograph 4



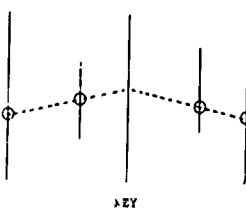
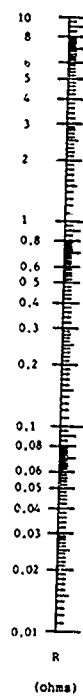
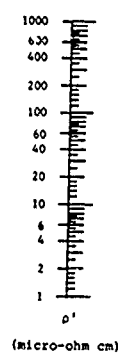
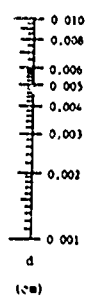
$$q = \frac{P}{A} \text{ W/m}^2$$



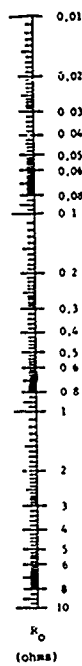
Nomograph 5



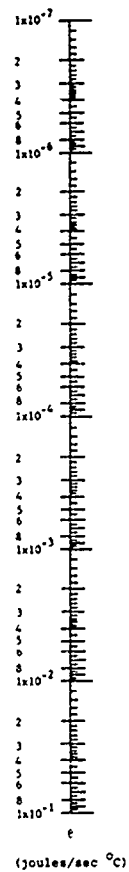
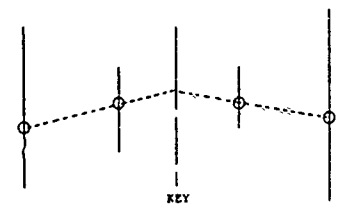
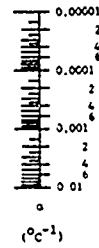
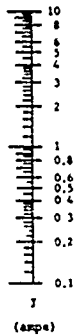
$$R = \frac{4}{d^2} \left( \frac{P}{A} \right)$$



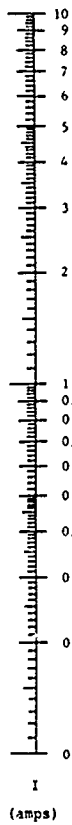
Nomograph 6



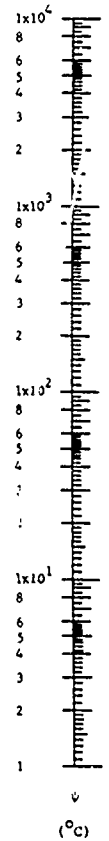
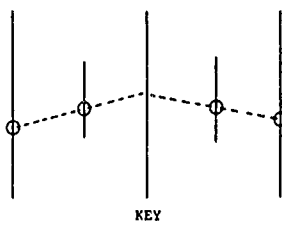
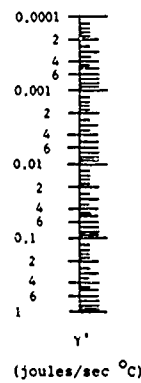
$$\theta = I^2 R_O \alpha$$



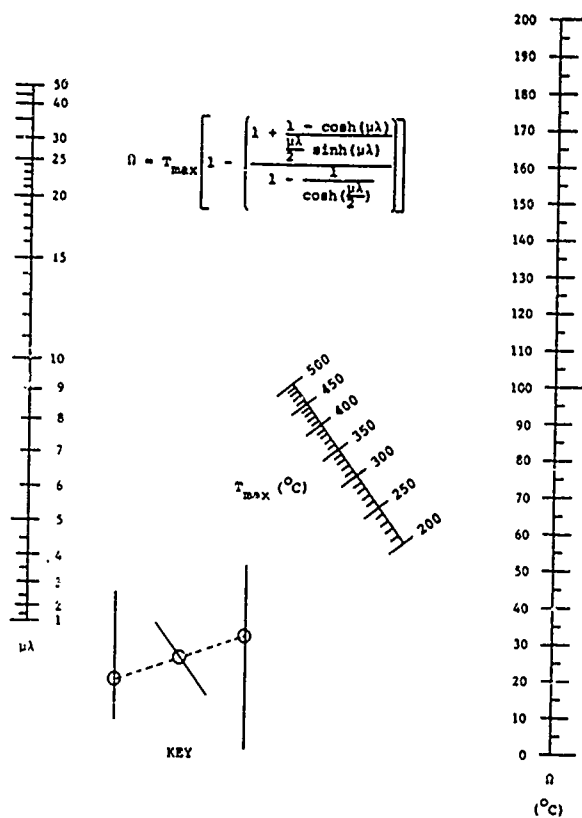
Nomograph 7



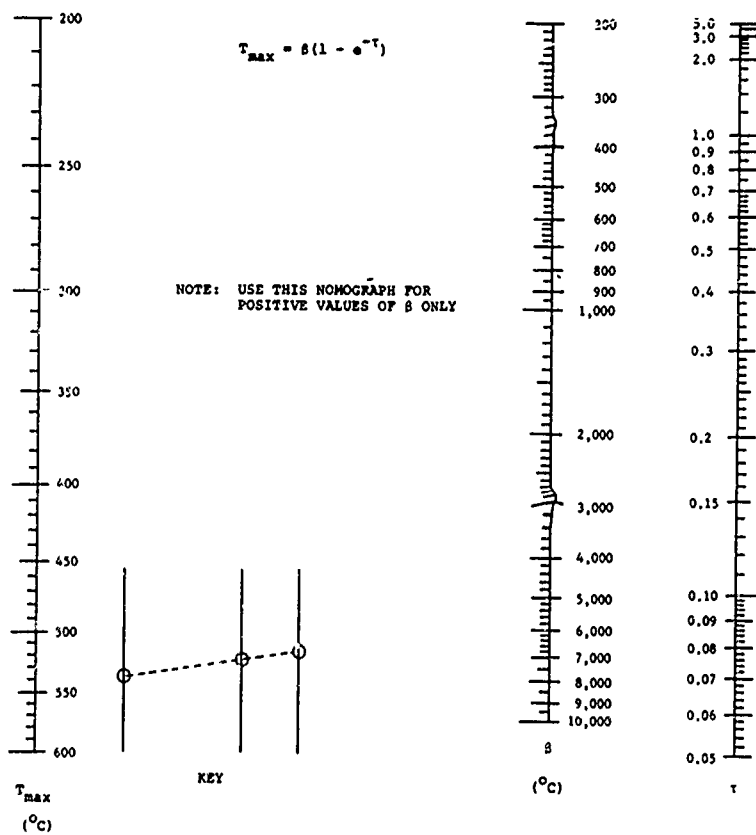
$$\psi = \frac{I^2 R_O}{Y'}$$



Nomograph 8  
2-4.25

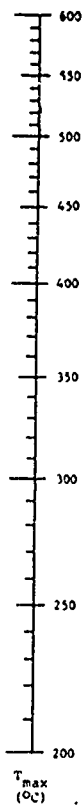


Nomograph 9



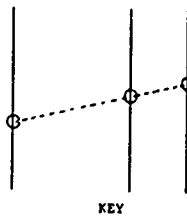
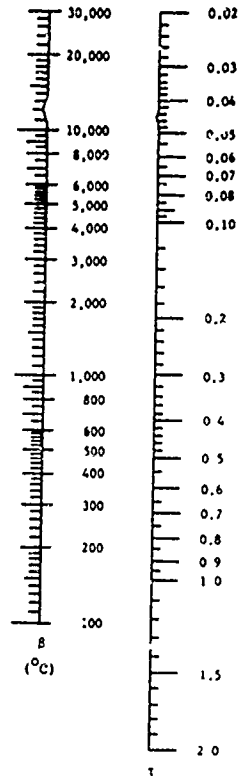
Nomograph 10A



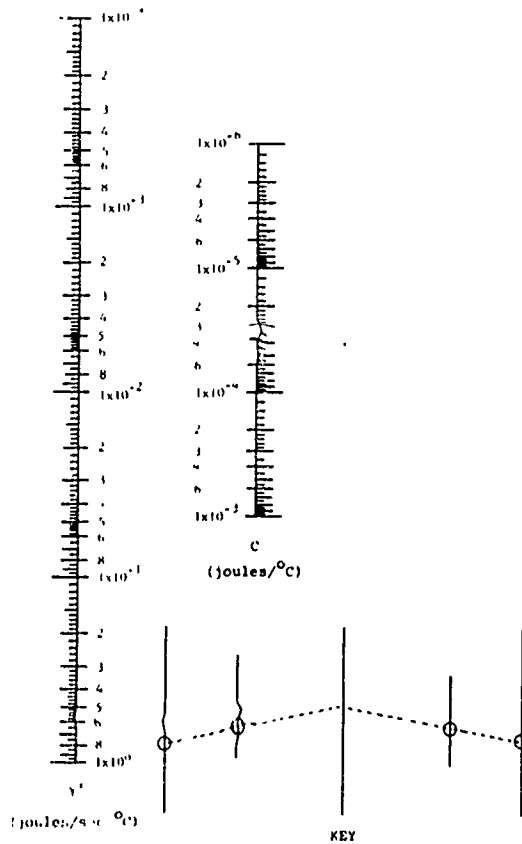


$$T_{max} = \beta(1 - e^{-T})$$

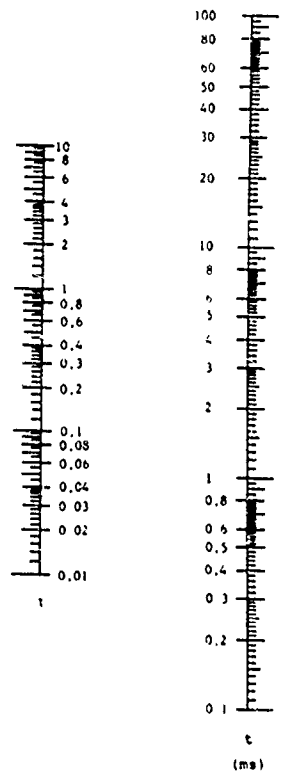
NOTE: Use this nomograph for negative values of  $\beta$  only



Nomograph 10B



Nomograph 11  
2-4, 27



(Sample Nomographs)

Page 1 of 1

W. S. KATZ, JR. PAS-411

PSYCHOL. LITER.

[illegible]

- |          |  |
|----------|--|
| $\sigma$ | thermal conductivity of bridgewire ( $\text{cal/cm}^2\text{sec}^\circ\text{C}$ ) |
| $\alpha$ | radial leakage constant (see Table I)  |
| $l$      | length of bridgewire (cm)  |
| $r$      | radius of bridgewire (cm)  |
| $\beta$  | bridgewire temperature coefficient term (see Table II)                           |
| $\rho$   | resistivity of bridgewire ( $\text{cal/cm}^2\text{sec}^\circ\text{C}$ )          |
| $\rho_0$ | resistivity of bridgewire  |

BIBLIOGRAPHIC WORKSHEET

Page 2 of 2

B/S	PRINL	III ADLR
-----	-------	----------

1	$t = I^2 R_0 t$	Excess energy generation	$R_0$ $I(S)$ $a(9)$						
	$I = S \cdot V = Y'$		$\theta$ $Y'$						
2		synthetic $I_e$	$I$ $R_0$						
	$I = \frac{I^2 R_0}{Y'}$		$Y'$ $\psi$						
3		$(I_{max} - T)$	$\mu$ $I_{max}(10)$ $\beta$						
	$\mu \cdot \beta = \beta$		$\beta$						
10	(A) or (i)	time to fire in holding times	$I_{max}$ $\beta$ $\tau$						
11	$t = \text{Time to fire (msec)}$		$Y'$ $C$ $\tau$ $t$						
	Constant firing current (amperes)	$I$							

- (8)  $I$  = current (amperes)  
(9)  $\alpha$  = temperature coefficient of resistance of bridgewire  
(10)  $T_{\max}$  = ignition temperature of explosive

2-6 QUANTITATIVE PREDICTIONS OF EED  
FIRING CHARACTERISTICS

By

D. E. Davenport and Herbert Reynolds

SINGER

Ordnance Products

INTRODUCTION

In previous papers 1, 2, and 3 the author has presented a simple theory for calculating the performance of an EED given only the physical dimensions and thermal properties of the materials to be used in the design. This theory has the virtues that it enables the prediction of performance of an initiator before it is built and also enables one to predict how small variations in the geometry or materials of construction during production will affect the performance of the initiator. Since the application of the theory was somewhat tedious without a computer, more recent work with H. Peckham <sup>(4)</sup> has reduced the solution to a series of nomographs which are presented in another paper at this symposium.

The remarkable fit to experimental data which the theory has been able to give was all the more remarkable because of some of the approximations which were incorporated which were known to be matters of expediency at best. They provide a real limitation to the theory since it is hazardous to apply the theory outside the regions where these approximations have been tested. It is the purpose of this paper to present a more detailed theory which removes the worst of these approximations. The paper shows that the more accurate approximations are simple to handle, given

- 
- (1) IEEE Symposium - Houston, 1965,
  - (2) Fifth EED Symposium on Electroexplosive Devices
  - (3) EED Symposium - Tarbes, France 1968 - Designing EED for Space  
by D. E. Davenport and L. D. Pitts
  - (4) A Theoretical Description of a Radial Heat Transfer Coefficient  
by Herbert D. Peckham, Gavilan College

a computer, and that they eliminate the empirical nature of the solution. These more accurate solutions also fit available data quite well over a wide range of bridgewire materials and geometries.

As presented in the original papers, the basic approach is to consider the actual header geometry shown on Figure 1, reduced to a simple symmetric geometry, as shown in Figure 2. One considers the electrical leads (pins) as infinite heat sinks, since their temperature will rise only negligibly in the normal 1 to 100 millisecond time-to-fire. Then (Reference 5a) the heat balance equation may be written as:

$$\rho c (\pi r^2 dx) \frac{\partial T}{\partial t} = K \left[ \left( \frac{\partial T}{\partial x} \right)_x - \left( \frac{\partial T}{\partial x} \right)_{x+dx} \right] \pi r^2 - (2\pi r dx) [H(T-T_0)] + \frac{I^2 R dx}{(4.186) (\lambda)} \quad (1)$$

In this equation:

$\rho$  = density of the bridgewire material, gm/cm<sup>3</sup>

$c$  = heat capacity of the bridgewire material, cal/gm/°C

$r$  = radius of bridgewire, cm

$x$  = distance along the bridgewire, cm

$T$  = temperature of the bridgewire, °C

$t$  = time, in seconds

$K$  = thermal conductivity of the bridgewire material, cal/cm<sup>2</sup> sec °C/cm

---

(5) Carslaw, H. S. and S. C. Jaeger "Conduction of Heat in Solids" Second Edition Oxford Press (a) Pages 149-150, (b) Eqn 13.7 (6)

H = an effective radial heat transfer constant

$T_0$  = initial temperature of the system, °C

I = current flow, amperes

R = bridgewire resistance, ohm

$\lambda$  = length of the bridgewire, cm

In the solution of this equation, (1), the power input,  $I^2 R$ , may be written as  $I^2 R_0 (1 + \alpha T)$  to include the effect of the temperature coefficient of resistivity of the bridgewire,  $\alpha$ .

In this equation the term on the left hand side of the equals sign is the rate of heat storage in the bridgewire, the first term on the right hand side is rate of the longitudinal heat leakage out the ends of the wire. The second term on the right hand side is a linearized representation of the rate of heat leakage radially from the wire and the last term is the rate of heat generation within the wire. It is quite simple to generate an analytical solution for this equation for the constant current (or constant power) case by assuming that H is constant (i.e. independent of time). Then the equation may be written as:

$$\frac{\partial T}{\partial t} = k \frac{\partial^2 T}{\partial x^2} - \nu (T - T_0) + a \quad (2)$$

where  $k = \frac{K}{\rho c}$ ;  $a = \frac{I^2 R_0}{4.186 \text{ cr}^2 \pi \rho \lambda}$

and  $\nu = \frac{2 H}{c r \rho} - \frac{I^2 R_0 \alpha}{4.186 \text{ cr}^2 \pi \rho \lambda}$

The solution for the temperature distribution as a function of time and space (taking  $T_0$  to be 0) is

$$T = \frac{a}{\nu} \left[ 1 - \frac{\sinh x \sqrt{\frac{\nu}{k}} + \sinh (\lambda - x) \sqrt{\frac{\nu}{k}}}{\sinh \lambda \sqrt{\frac{\nu}{k}}} \right] - \frac{4a}{\pi} \sum_{n=1}^{\infty} \frac{\left[ \sin \frac{(2n-1)\pi x}{\lambda} \right] e^{-t \left[ \nu + \frac{k(2n-1)^2 \pi^2}{\lambda^2} \right]}}{(2n-1) \left[ \nu + \frac{k(2n-1)^2 \pi^2}{\lambda^2} \right]} \quad (3)$$

This equation expresses the temperature distribution along the bridgewire as a function of time and, with the proper choice of constants, will predict the temperature distribution quite accurately during the first 100 milliseconds when our approximation of infinite heat sinks for the pins at the ends of the bridgewire holds.

The major difficulties with the solution are that it requires use of a constant value of  $H$  (while it should be a time varying function) and that in order to make the solution fit experimental results it requires a value for the specific heat of the bridgewire material that is approximately twice that of the real material. It was suspected that these two deviations from the real world were intimately related and so it was decided to investigate the development of a solution which did not have these shortcomings. What was desired was a solution which incorporated  $H$  as the proper function of time and the specific heat with its proper value to fit the experimental data.

#### H AS A FUNCTION OF TIME

As can be seen from equation (1) the radial heat leakage term is represented as the product of three terms (a) the surface area,  $2\pi r dx$ , of an incremental length of the wire (b) the difference in temperature between that of the wire,  $T$ , and the initial

temperature,  $T_o$ , and (c) a constant, H. One may discover the nature of H by comparing it with the form of the equation in a bit more conventional form

$$\begin{aligned} \text{Rate of Leakage} &= (\text{Area}) (\text{thermal conductivity}) (\text{temperature gradient}) \\ &= (2\pi r dx) (K) \left( \frac{\partial T}{\partial r} \right)_{r=a} \end{aligned} \quad (4)$$

where K is the thermal conductivity of the material surrounding the bridgewire and the temperature gradient is evaluated at the surface of the bridgewire (i.e.  $r=a$ ).

Thus, comparing the radial leakage term in (1) with (4) one can say that H may be written as

$$H = \frac{K}{T - T_o} \left( \frac{\partial T}{\partial r} \right)_{r=a}$$

If the initial temperature is considered to be zero (or one considers T to represent the increase in temperature), this may be written as

$$H = \frac{K}{T} \left( \frac{\partial T}{\partial r} \right)_{r=a}$$

Thus H may be defined in terms of the wire temperature and the temperature gradient at the wire surface.

The equations for the values of the temperature and the temperature gradient at the surface of an infinitely long wire as a function of time were derived by Herbert Peckham (Reference 6) from the development by Carslaw and Jaeger (Reference 5b). The equations resulting were:

- 
- (6) A Theoretical Description of a Radial Heat Transfer Coefficient  
Internal Link Report

$$T \Big|_{r=a} = \frac{2}{\pi^3} \frac{Q\alpha^2}{K} \int_0^\infty \frac{(1 - e^{-\chi u^2 t/a^2})}{u^3 \Delta(u)} du$$

$$\frac{\partial T}{\partial r} \Big|_{r=a} = - \frac{2}{\pi^3} \frac{Q\alpha}{Ka} \int_0^\infty \frac{(1 - e^{-\chi u^2 t/a^2})}{u \Delta(u)} du$$

$$\Delta(u) = \left[ u J_0(u) - \alpha J_1(u) \right]^2 + \left[ u Y_0(u) - \alpha Y_1(u) \right]^2$$

where "a" is the radius of the bridgewire in cm

Q is the power input (which cancels from the ratio)

$\alpha = 2 \pi a^2 \rho c/S =$  twice the ratio of the heat capacity of a volume of surrounding material to the heat capacity of a like volume of the wire.

K is the thermal conductivity of the surrounding material in cal/cm<sup>2</sup>sec °C/cm

$\chi$  is K/ $\rho c$  for the surrounding material

t is time in seconds

and the thermal conductivity of the wire is considered infinite so that the temperature is uniform across the diameter. The only variable which depends upon the material of the bridgewire is  $\alpha$  and since its effect on the results was negligible over the range of  $\alpha = 1/5$  to  $\alpha = 5$ , the solution was evaluated for  $\alpha = 1/2$ .



In order to compute these integrals numerically, it is helpful to first transform them to integrals over a finite domain. This transformation is easily accomplished by introducing the variable defined by

$$Z = \frac{1}{1+u}$$

then,

$$I(\alpha, R) = \frac{-2\alpha}{\pi^3} \int_0^1 f(Z) dZ = \frac{Ka}{Q} \left. \frac{\partial T}{\partial r} \right|_{r=a}$$

$$J(\alpha, R) = \frac{2\alpha^2}{\pi^3} \int_0^1 g(Z) dZ = \frac{Ka}{Q} T \Big|_{r=a}$$

where,

$$f(Z) = \frac{1}{\left(\frac{1-Z}{Z}\right) \Delta\left(\frac{1-Z}{Z}, \alpha\right)} \frac{e^{-R\left(\frac{1-Z}{Z}\right)^2}}{\frac{1}{Z^2}}$$

$$g(Z) = \frac{1}{\left(\frac{1-Z}{Z}\right)^3 \Delta\left(\frac{1-Z}{Z}, \alpha\right)} \frac{e^{-R\left(\frac{1-Z}{Z}\right)^2}}{\frac{1}{Z^2}}$$

A useful method for numerical integration is Simpson's rule which for a given partition

$$0 = Z_0 < Z_1 < \dots < Z_n = 1$$

with

$$Z_i - Z_{i-1} = h, \quad (i=1, 2, \dots, N)$$

states that

$$\int_0^1 f(Z) dZ = \frac{h}{3} [f(Z_0) + 4f(Z_1) + 2f(Z_2) + \dots + f(Z_n)] + O(h^5)$$

with a similar expression for g.

The only apparent difficulty in using this method is that of computing f and g at the end points of (0,1). These points, however, are not singular points for in (3; app. A) it is shown that

$$f(0) = \pi/2, f(1) = 0$$

$$g(0) = g(1) = 0$$

Thus, once the formulas given in (4, pp. 369-370) for computing the Bessel functions are borrowed, it is a simple matter to obtain numerical values for the integrals I and J, and hence for the function H.

The resulting numerical solution for H was fit with a series of line segments as the simplest composite to use for inserting H as a function of time into the problem. The line segments were:

$$H = \left(\frac{K}{a}\right) 1.345 \left(\frac{\kappa t}{a}\right)^{-.4679} \quad .01 \leq \left(\frac{\kappa t}{a}\right) \leq 0.1$$

$$H = \left(\frac{K}{a}\right) 1.460 \left(\frac{\kappa t}{a}\right)^{-.4323} \quad 0.1 \leq \left(\frac{\kappa t}{a}\right) \leq 1$$

$$H = \left(\frac{K}{a}\right) 1.460 \left(\frac{\kappa t}{a}\right)^{-.3649} \quad 1 \leq \left(\frac{\kappa t}{a}\right) \leq 10$$

$$H = \left(\frac{K}{a}\right) 1.088 \left(\frac{\kappa t}{a}\right)^{-.2372} \quad 10 \leq \left(\frac{\kappa t}{a}\right) \leq 100$$

wire appears to be simply surrounded by explosive for the region of interest. On the other hand if the wire is pressed hard against the substrate so that it may even be flattened a bit, the thermal conductivity of the substrate becomes important.

Now that we have an expression (or actually a series of expressions) for  $H$  as a function of time we may return to the differential equation and insert these time dependent values for  $H$  and see how we have changed the behavior of our equation.

#### IGNITION TEMPERATURE AS A FUNCTION OF TIME

A second correction to the equation which can be simply included is to consider that the ignition temperature as a function of time rather than taking it to be constant as in our previous papers. The major difficulty is in establishing the correct values which should be used.

The equation actually gives us the temperature of the bridgewire as a function of time, and the assumption is made that the ignition occurs when the hottest point on the bridgewire reaches some critical temperature. If there is no "inert surface film" of low thermal conductivity between the bridgewire and the explosive, then the critical temperature should correspond to the temperature at which the reaction rate becomes very rapid.

Following the example of Friedman, (Reference 7), Enig (Reference 8) and others, one might assume an Arrhenius type relationship, so that a plot of the logarithm of ignition time versus  $1/T$  gives a straight line. Then using the ignition time versus temperature data obtained for times of the order of 1 to 100 seconds, one may estimate the temperatures appropriate for 1 to 100 milliseconds.

- 
- (7) A General Thermal Explosion Criterion. Application to Initiation by Imbedded Wires, M. H. Friedman, The John Hopkins University
  - (8) Approximate Solutions in the Theory of Thermal Explosions for Semi-infinite Explosives, By J. W. Enig

A second approach is to attempt to measure the ignition temperatures as a function of time in the millisecond region by using a very small bridgewire with a large temperature coefficient of resistance. The resistance of the bridgewire as a function of time as it is heated by the electrical current, gives a smooth curve which has a shape that is dependent on the current. At ignition there will be a significant "knee" in the curve as the energy from the decomposition of the explosive also contributes to the heating of the bridgewire and thus to its resistance increase. The presence of the "knee" becomes quite predominant when the bridgewire is of the order of 0.1 to 0.2 mils in diameter.

From the increase in the bridgewire resistance at the time the "knee" appears, the average bridgewire temperature can be calculated. Based on the above model a calculation of the maximum bridgewire temperature may be made from the average temperature. This is the ignition temperature for the observed ignition time.

At the present time it cannot be claimed that either of these methods is very accurate because of the scatter in the observed data on which the predictions are based. Our observations for basic lead styphnate, which most of our experiments used, showed only that the  $1/T$  vs  $\log t$  plot could be considered consistent with our millisecond ignition time observations. Therefore, we have used the  $1/T$  plot to get a consistent set of ignition temperatures versus times. The values selected are given in Table I.

#### CONSTANT VOLTAGE AND CAPACITANCE FIRING PREDICTION

Finally, it should be noted, that since the solution is to incorporate time dependent parameters, it can also handle the case of a time varying current,  $I$ , which results for the constant voltage and the capacitor firing cases. This gives the solution

a true generality in its application and requires only a few simple modifications to provide for the input parameters necessary to calculate the current function.

#### THE SOLUTION WITH TIME DEPENDENT PARAMETERS

With the introduction of the time dependent parameters of  $H$ ,  $I$ , and the ignition temperature, one can no longer obtain a simple analytic solution such as equation (3). One resorts, instead, to a numerical method which can be simply carried out on a computer.

The given initial-value problem represented by equation (1) is a classic example of a non-linear parabolic type that can be integrated numerically by the method of finite differences, or some variation thereof. One simple process consists of replacing the analytic derivatives by finite difference expressions which are simply numerical approximations for the derivatives. A recursion formula can then be developed which will allow numerical calculations to take place over a lattice of mesh points starting with the given boundary and initial conditions. The lattice cannot be arbitrary but must be chosen such that the numerical solution is stable and an accurate representation of the theoretical solution while at the same time it must render the computation time feasible. Fortunately, this procedure has proved to be quite adequate in regard to these items for the initial value problem considered here.

This method of replacing the analytic derivatives by corresponding finite difference expressions, is as follows:

Letting

$$\frac{\partial T}{\partial X} = \frac{T(x, t + \Delta t) - T(x, t)}{\Delta t}$$

$$\frac{\partial^2 T}{\partial X^2} = \frac{T(x + \Delta x, t) - 2T(x, t) + T(x - \Delta x, t)}{\Delta x^2}$$

where  $\Delta x$  and  $\Delta t$  are small increments of the variables  $x$  and  $t$ . In view of the definition of partial differentiation, this process is certainly feasible if  $\Delta x$  and  $\Delta t$  are small enough.

Now, let  $N$  be a positive integer and let  $\Delta x$  be chosen such that there exists a positive integer  $M$  for which  $M\Delta x = L$ . Then a lattice of mesh points (or grid) can be defined whose coordinates  $x, t$  have the form,

$$\begin{aligned} x &= m\Delta x & m &= 0, 1, \dots, M \\ t &= n\Delta t & n &= 0, 1, \dots, N \end{aligned}$$

If  $T(m\Delta x, n\Delta t)$  is denoted by  $T_m^n$ , the difference expressions may be written

$$\frac{\partial}{\partial t} T(m\Delta x, n\Delta t) = \frac{T_m^{n+1} - T_m^n}{\Delta t}$$

$$\frac{\partial^2}{\partial x^2} T(m\Delta x, n\Delta t) = \frac{T_{m+1}^n - 2T_m^n + T_{m-1}^n}{\Delta x^2}$$

and the initial condition becomes,

$$T_m^0 = 0 \quad \text{for } m = 0, 1, \dots, M$$

$$T_0^n = T_M^n = 0 \quad \text{for } n = 0, 1, \dots, N$$

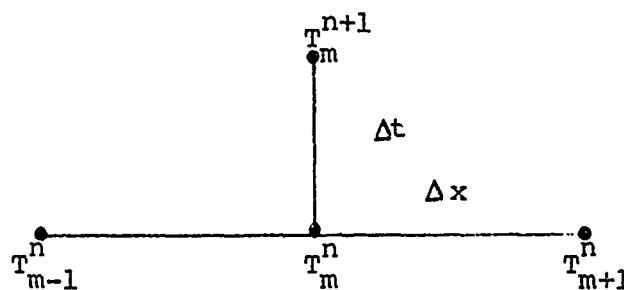
Substitution of these expressions in the differential equation with a slight rearrangement of terms yields, at the point  $(m\Delta x, n\Delta t)$ ,

$$\begin{aligned}
T_m^{n+1} &= \left[ 1 - \frac{2\Delta t}{\Delta x^2} \kappa + \Delta t \nu(n\Delta t) \right] T_m^n \\
&+ \kappa \frac{\Delta t}{\Delta x^2} (T_{m+1}^n + T_{m-1}^n) \\
&+ \Delta t \mu(n\Delta t, T_m^n)
\end{aligned}$$

This equation is called a finite difference equation and in functional notation is of the form.

$$T_m^{n+1} = \chi(T_{m-1}^n, T_m^n, T_{m+1}^n)$$

The recursive nature of this relation is clear and is illustrated in the following scheme:



For given  $n$ , three successive values of  $T$ , viz.,  $T_{m-1}^n$ ,  $T_m^n$ ,  $T_{m+1}^n$ , will allow the prediction of a fourth,  $T_m^{n+1}$ . Thus, starting with the initial conditions given above, a solution can be generated over the entire lattice -- the accuracy, of course, being contingent on the choice of  $\Delta x$  and  $\Delta t$ .

In using this method of numerical approximation, one should also keep in mind the stability criterion for differential equation of the form,

$$\frac{\partial T}{\partial t} = \kappa \frac{\partial^2 T}{\partial x^2}$$

In (9; pp. 475-476), it is shown that for this partial differential equation, the finite difference scheme is stable provided that

$$x \frac{\Delta t}{\Delta x^2} \leq \frac{1}{2}$$

This inequality should be used only as a guide for the more general equations considered in this paper.

The finite difference equations given above have been programmed for all three (cases) modes in FORTRAN IV for use as a study tool on the IBM 360/30, 44 PS system. The functions  $\mu$  and  $\nu$  are computed as follows:

1. Constant voltage case, (Voltage = E)

$$\nu(n\Delta t) = -\frac{2H(n\Delta t)}{\rho cr}$$

$$\mu(n\Delta t) = \frac{aE^2}{1 + \alpha T_n^m}$$

where

$$a = \frac{1}{4.186 \pi cr^2 \rho \lambda R_0}$$

2. Capacitance firing (Voltage  $E_c$  on capacitance C with a parasitic resistance  $R_1$  in series)

$$\nu(n\Delta t) = \frac{-2H(n\Delta t)}{\rho cr}$$

$$\mu(n\Delta t) = \frac{aE(n\Delta t)^2}{1 + \alpha T_n^m}$$

---

(9) Garabedion P. R. Partial Differential Equations, John Wiley and Sons, Inc. N. Y. 1964



where,

$$E(n\Delta t) = E((n-1)\Delta t) \sqrt{1 - \frac{2\Delta t}{C(R_o + R_1)}}$$

with

$$E(0) = \frac{Ec}{1 + R_1/R_o (1 + \alpha \bar{T})}$$

and

$$a = \frac{1}{4.186 \pi cr^2 \rho \lambda R_o (1 + \alpha \bar{T})}$$

### 3. Constant current (I)

$$\nu(n\Delta t) = \frac{2H(n\Delta t)}{\rho cr} - a\alpha$$

$$\mu(n\Delta t, T_n^m) = a = \text{constant}$$

$$a = \frac{I^2 R_o}{4.186 \pi cr^2 \rho \lambda}$$

## COMPARISON OF THEORY WITH EXPERIMENT

In order to compare the predictions of this modified theory with actual data, a series of measurements were made on a glass header with a bridgewire length of 0.19 cm. The bridgewire material and the bridgewire diameter were varied over the normal range that one would expect to encounter in EED designs. The explosive was limited to basic lead styphnate applied as a slurry in a 0.050 inch deep cup and then dried.

The time-to-fire measurements were made with a photocell which responded to the light output from the surface of the explosive. These times will differ from ignition times by the time required for the reaction zone to travel approximately 0.050 inches.

In the case of the 0.15 mil tungsten wire the bridge-wire length was only 0.025 inches (0.062 cm) and the slurry thickness was less than 0.010 inches since a different header was used. The presence of the "knee" in the curve gave confirmation of the ignition times for this small diameter wire and agreed quite well with the light output from this thin slurry layer.

The data shown in Figures 4 , 5, and 6 show the measured firing times as a function of current over nearly a decade in firing current for each wire diameter. The three fitted curves for each wire diameter were calculated from the theory using three different values for the assumed thermal conductivity of the environment around the bridgewire.

It is seen that for nichrome (which has a very small thermal coefficient of resistance) the curve based on a thermal conductance,  $\chi$ , of  $0.0003 \text{ cm}^2/\text{sec}$  fits quite well for all three wire diameters except in the region of very short firing times. The disagreement at the short firing times may simply indicate that the ignition time is 0.1 to 0.2 milliseconds shorter than that measured by the photocell because of the thickness of the slurry. Each of the experimental points represents 3 to 5 measurements which fall within the symbol except when a bar is incorporated extending beyond the symbol.

In the case of platinum bridgewire which has an intermediate resistivity but a high temperature coefficient of resistivity, the agreement is qualitatively correct but the data for the 2.5 mil case in particular seems to fall above the curves throughout its length. That is the firing times are all about 50% longer than predicted by the curve. For the other two curves the data falls within 10 - 20% of the theoretical curve.

Going to a material of high conductivity and high temperature coefficient of resistivity such as aluminum results in the data in Figure 7 . In this case, it was anticipated that there might be an appreciable "inert film of low thermal conductivity" on the surface of the wire in the form of  $\text{Al}_2\text{O}_3$ . No such effect is indicated by the limited data obtained.

Finally, going to a very small diameter and very short bridgewire we have the data on the 0.15 mil diameter tungsten bridgewire presented in Figure 6 . Here the data becomes quite sensitive to the value assumed for the thermal conductivity of the material around the bridgewire. Again, however, the value of  $0.0003 \text{ cm}^2/\text{sec}$  for the thermal conductance fits very well, over the limited range of measurements. (Experiments showed no units fired at 0.09 amps and limited measurements at 0.2 amps indicated a firing time less than 0.1 millisecond.)

#### DISCUSSION

The good correlation between theory and experiment when the constant value of  $H$  is replaced by a properly time varying function and the proper value of the specific heat of the bridgewire is inserted rather than the empirically doubled value, indicate that the theory is quite well based. The remaining disagreement observed in the case of the larger size platinum wire suggests that there may still be deficiencies in the theory details which need to be included. The most obvious omission is that of the temperature drop encountered at the surface of the wire which heat transfer people are wont to ascribe to thermal resistance at the interface.

The lack of any well defined theory for predicting thermal resistance at the interface would mean that such a correction would have to be introduced more or less empirically and would thus become another adjustable constant which could raise doubts about validity of the rest of the theory. Furthermore,

it would appear less likely to find such a phenomenon at the surface of an inert material like platinum than the more reactive nichrome, aluminum or tungsten. Perhaps extension of the measurements to much larger bridgewire diameters such as 5 to 10 mils would help sort out the effect.

It would be of interest to repeat these measurements with other explosives such as normal lead styphnate, lead azide, silver azide, KDNBF and other primaries which have different ignition temperatures and buildup times. These measurements are underway at our laboratories at this time.

#### APPLICATIONS

The two primary uses for such a theory is to be able to rapidly design an initiator to be able to meet any specified all-fire times or no-fire levels and then to be able to predict the sensitivity of the design to various manufacturing variables such as resistance range or thermal coupling of the bridgewire. We presently have the model programmed for the computer for all three cases (constant current, constant voltage and capacitance discharge) and can run off a series of data on any selected geometry in little more than the time that it takes to get access to the computer. This proves to be of a great deal of assistance to the design engineer when other than proven designs are called for.

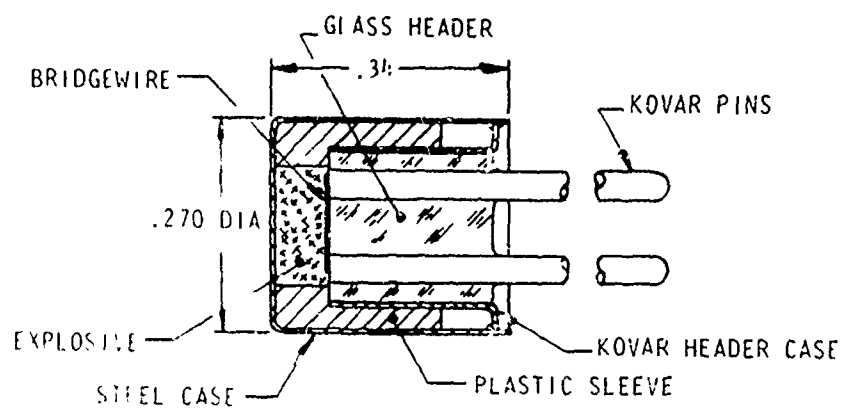
The other major use for the theory is in making possible nondestructive testing of initiators for their all-fire level. This measurement, called the thermal coupling test (TCT), depends for its application on the bridgewire having a significant thermal coefficient of resistance. Then from the measurement of the resistance increase of the bridgewire caused by a low level current pulse, the theory enables the prediction of the current level which would be required to reach the firing temperature within

the required function time. The presence of gaps around the bridgewire, moisture in the bridgewire mix or other changes in the thermal conductance environment of the bridgewire are readily detected.

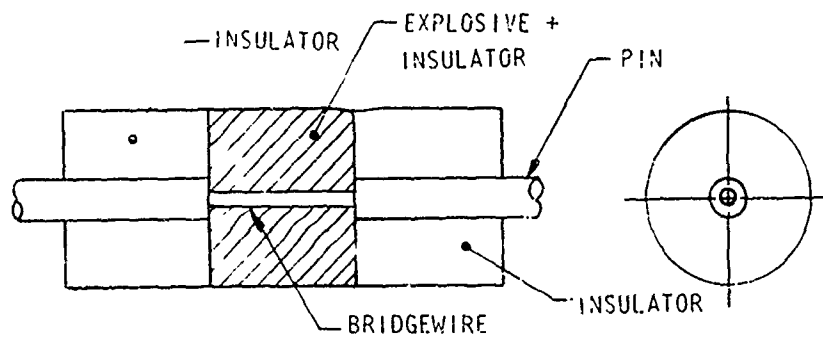
Using the TCT technique one can appreciably narrow the functioning range of a given group of detectors. The selection is limited to thermal coupling effects, of course, and would not necessarily find defects such as degraded explosive or a nick in the bridgewire unless the effect was large enough to be reflected in the average thermal response. The method has a major advantage over any other technique in that it can be applied to an individual initiator without any specific historical data on the specific initiator. Thus, it shows real promise as a field monitoring technique as well as a production monitoring technique.

TABLE I TIME TO FIRE vs TEMPERATURE FOR BASIC LEAD STYPHNATE

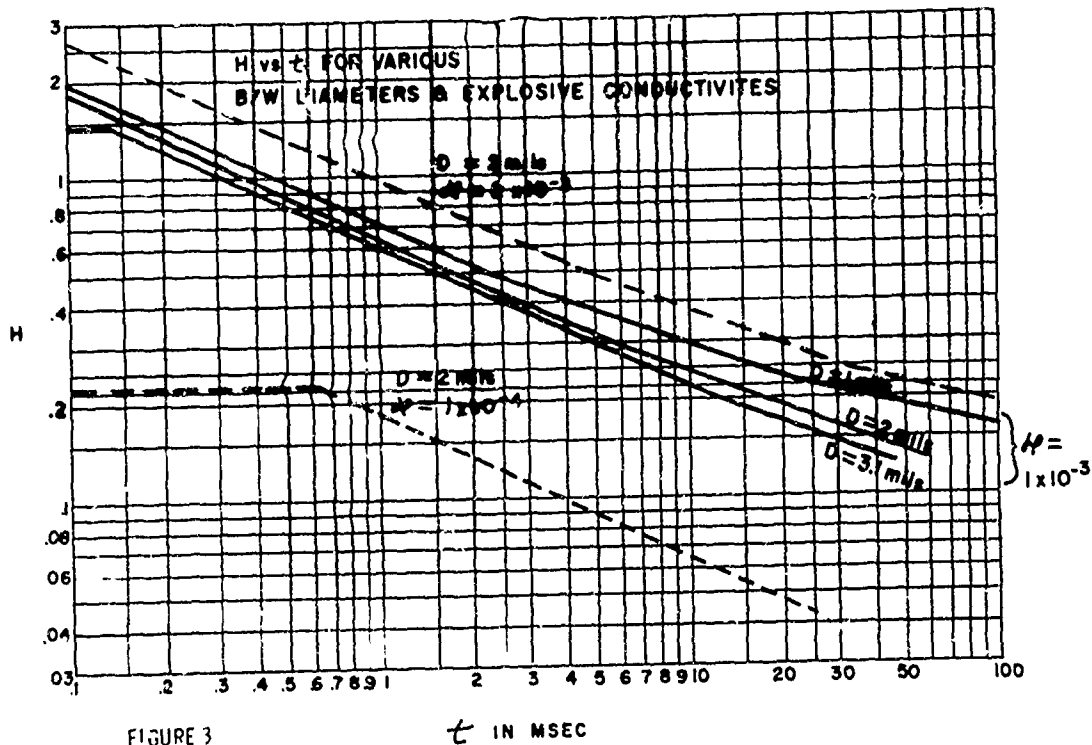
Time		Temperature
10	sec.	275°C
1	sec.	300°C
0.1	sec.	325°C
0.01	sec.	355°C
.006	sec.	360°C
.004	sec.	365°C
.002	sec.	375°C
.001	sec.	385°C
.0005	sec.	400°C
.0002	sec.	415°C
.0001	sec.	425°C



TYPICAL SMALL INITIATOR DESIGN FIG. 1



IDEALIZED INITIATOR CONFIGURATION FIG. 2



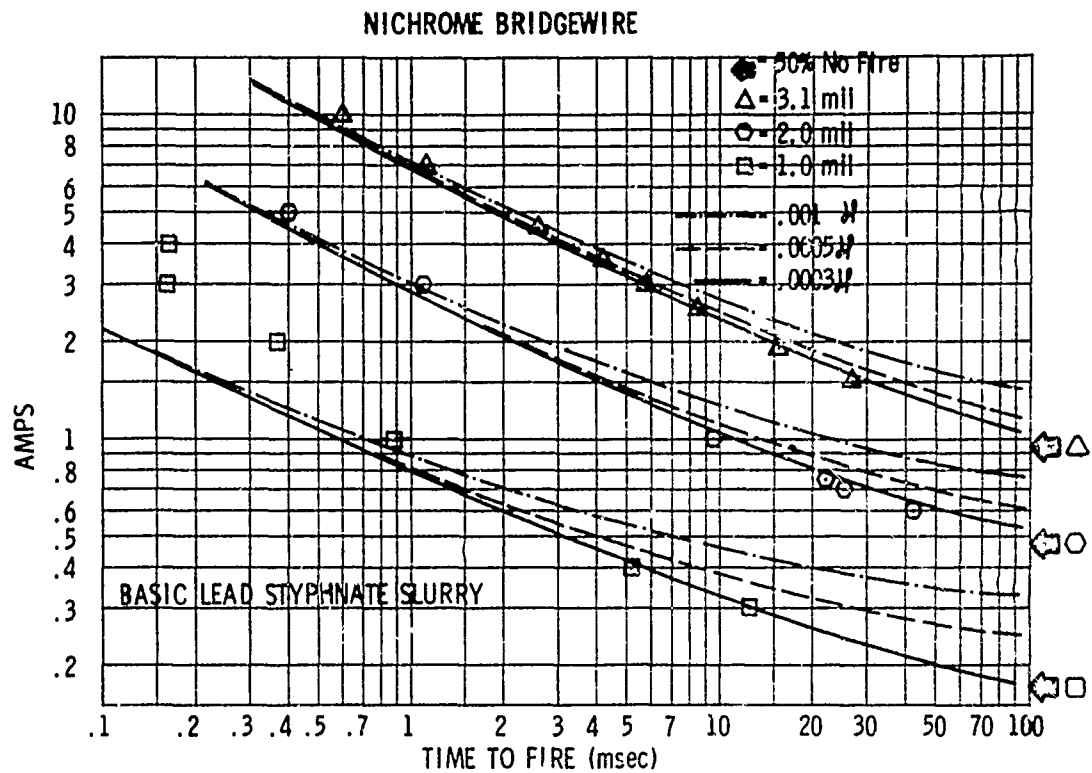


FIGURE 4 COMPARISON OF THEORY WITH EXPERIMENT

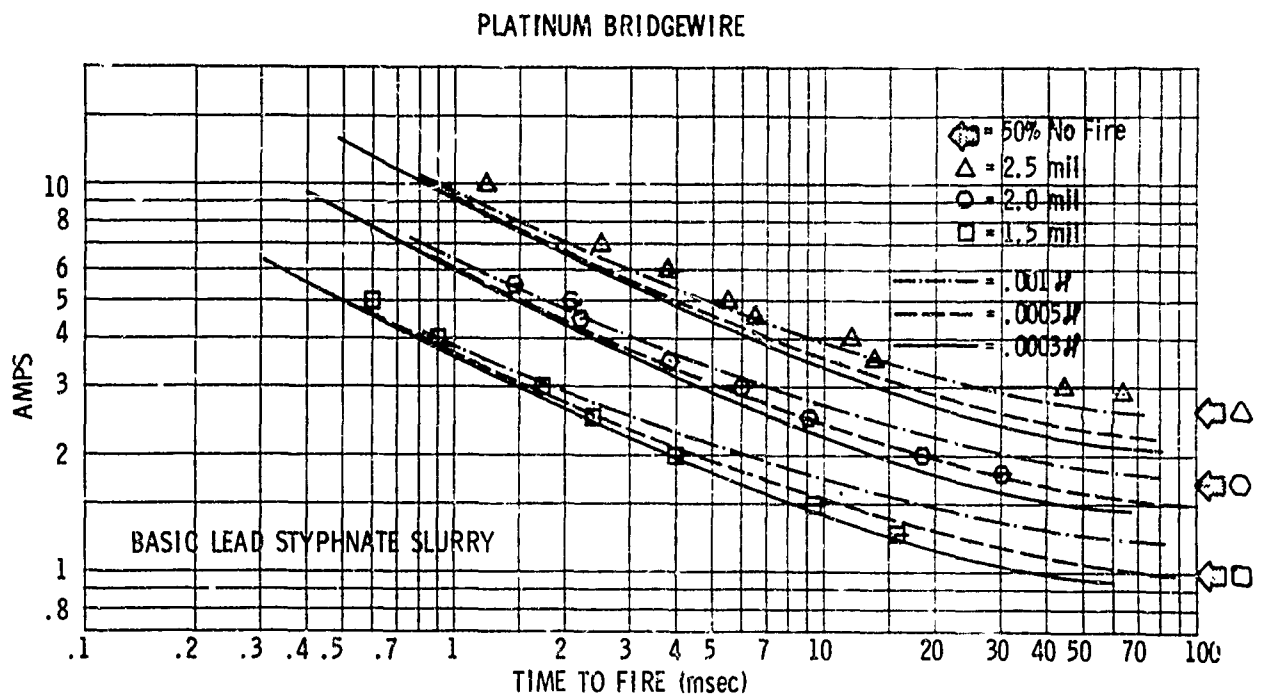


FIGURE 5 COMPARISON OF THEORY WITH EXPERIMENT

TUNGSTEN BRIDGEWIRE  
0.15 mil

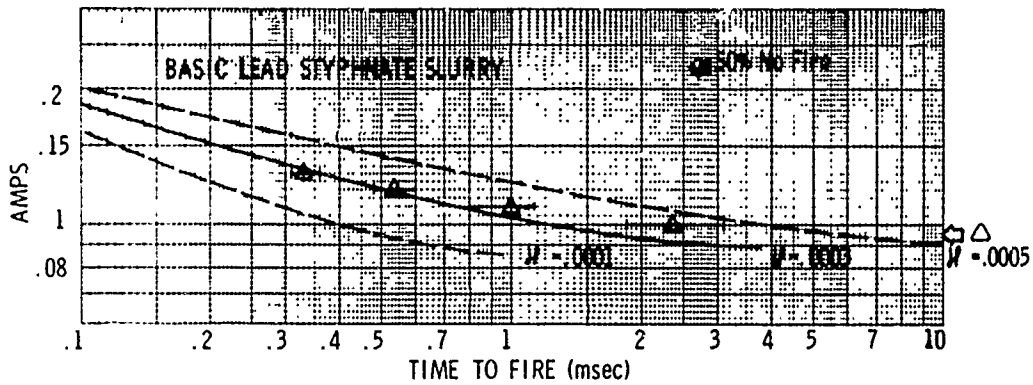


FIGURE 6 COMPARISON OF THEORY WITH EXPERIMENT

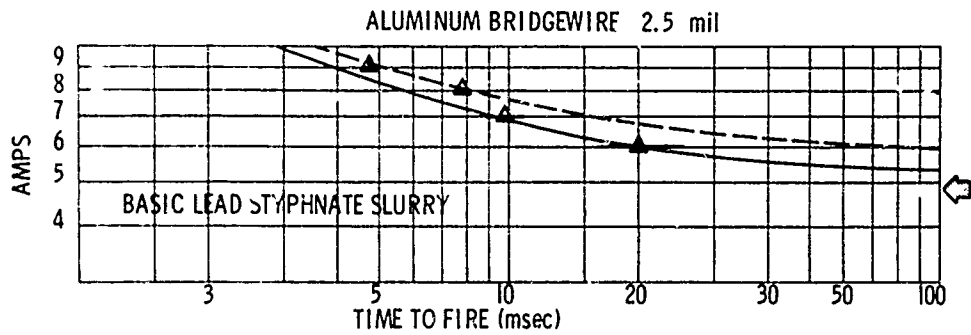


FIGURE 7 COMPARISON OF THEORY WITH EXPERIMENT

50% No Fire

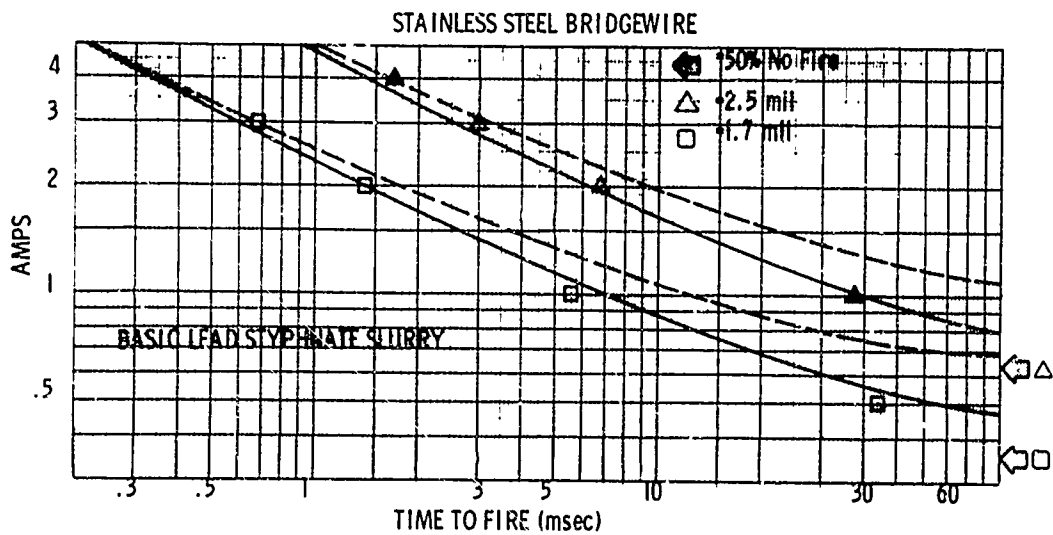


FIGURE 8 COMPARISON OF THEORY WITH EXPERIMENT



# ERRATA SHEET

Page 6 Note K is for materials around bridgewire  
Not the K of Equation (1)

Page 8  $R = \frac{\chi t}{a}$

$Z_1$  instead of Z, in  $0 = Z_0 < Z_1 < \dots < Z_n$

Page 9 References

(3; app. A)

Reynolds, H. B., "Numerical Intergration of Certain Improper Intergal Families Occurring in Heat Studies", LIS/5560/HBR-ER-1, Singer-General Precision, Link Information Sciences Sunnyvale, California, January 1969

(4, pp. 369-370)

Abramowitz M., and I. A. Stejan, "Handbook of Mathematical Function AMS 55", National Bureau of Standard, Washington, D. C., 1966

Page 11 Figure 3 -  $\chi = 1 \times 10^{-3}$  for 3 solid curves

Page 15 Final paragraph -  
This method of replacing the analytic derivatives by corresponding finite difference expressions, is as follows:

Letting

$$\frac{\partial T}{\partial x} = \frac{T(x, t+\Delta t) - T(x, t)}{\Delta t}$$

$$\frac{\partial^2 T}{\partial x^2} = \frac{T(x+\Delta x, t) - 2T(x, t) + T(x-\Delta x, t)}{\Delta x^2}$$

Page 16

Second paragraph should read -

Now, let  $N$  be a positive integer and let  $\Delta x$  be chosen such that there exists a positive integer  $M$  for which  $M\Delta x = L$ . Then a lattice of mesh points (or grid) can be defined whose co-ordinates  $x, t$  have the form, ----

Bottom of the page - subscripts are incorrect, equation should read

$$T_0^n = T_M^n = 0 \text{ for } n = 0, 1, \dots, N$$

Page 17

$\chi$  of first equation is really a of Equation (2) page 4

$\Delta x$  should be  $\Delta x$

Page 18

Reference (7; pp. 475-476) should be listed as Reference 9

Pages 18 and 19, the "a" should be " $a^1$ " to distinguish from previous a of Equation (2).

$$1) \quad \nu(n\Delta t) = \frac{-2H(n\Delta t)}{\rho c r}$$

Page 19

First three equations,  $R_0$  should be replaced by  $R_0(1+\alpha\bar{T})$  where  $\bar{T}$  is the average temperature.

Page 20

First paragraph, first sentence - 0.015 mil should read 0.15 mil.

## 2-7P ELECTRICAL AND THERMAL CONSIDERATIONS IN THE DESIGN OF ELECTROEXPLOSIVE DEVICES\*

Heuristic Discussions of Effects of Reaction Kinetics,  
States of Aggregation, and Parameter Distribution as  
They Affect Initiation Characteristics

by R. H. Stresau

### INTRODUCTION

Considered qualitatively, an electroexplosive device is quite simple. The "bridge," an electrical resistor of small dimensions which is surrounded by an explosive or pyrotechnic, is heated electrically to a temperature which will result in ignition of the explosive or pyrotechnic. Efforts to derive rigorous quantitative equations whereby the behavior of such devices may be predicted reveal that such systems are in fact quite complex. A complete rigorous analysis would have to account for geometric configuration of the bridge system and surrounding explosive or pyrotechnic, thermal contact with the surroundings, reaction kinetics of the explosive or pyrotechnic (including effects of the state of aggregation and intimacy of mixture) heat transfer processes in the pyrotechnic (also as affected by the state of aggregation and intimacy of mixture partition of heat loss between radial and axial components), thermal coefficients of electrical resistivity and thermal conductivity, as well as the effects of imperfections which may be inherent results of manu-

\*Based in part on work performed for the U. S. Naval Weapons Center, Corona, California under Contract No. N00123-67-C-0508.

facturing processes. A set of equations accounting for all of these variables would be impressive but relatively useless in view of the lack of much of the data which would be necessary for its application. The acquisition of the necessary data would require an effort substantially exceeding the total of all activities now engaged in explosive device research and development. In recognition of these difficulties, various investigators engaged in such work have derived equations based on simplifying assumptions and from empirical considerations of experimental data. These equations have proven to be quite useful to designers and others concerned with EEDs. However, as with all equations derived from simplifying assumptions or empirical considerations, they are in danger, which increases with continuing successful operation of being accepted as rigorous derivations of fundamental laws. Such acceptance can result in promulgation of unrealistic specifications and in the rejection of devices and design concepts which, though entirely satisfactory from any practical consideration of safety or functional characteristics, may not behave "normally" (that is in accordance with the accepted equations). The blind acceptance of such equations also results in considerable wasted effort in attempts to develop devices beyond the range of applicability of the equations.

In the present report, consideration will be given to some

of the factors which have been ignored in most mathematical considerations of EEDs. Where quantitative calculations are not yet available, an effort will be made to make heuristic predictions of the effects of factors which have not been included in mathematical characterizations.

#### EQUATIONS (PUBLISHED)

An equation which has served as the starting point by many investigators considering thermal ignition of explosives is the general heat flow equation to which is added an "Arrhenius term" to account for the contribution of heat to the system which results from the decomposition of the explosive:

$$K \nabla^2 T = \rho c \frac{dT}{dt} - \rho Q Z e^{\frac{-E}{RT}}$$

where

K is thermal conductivity

$\rho$  is density

C is specific heat

Q is heat of reaction

Z is a statistical frequency factor

R is the gas constant

E is the activation energy

To the author's knowledge, no analytical solution of this equation (1) has been attained. Numerical solutions have been obtained for a number of special cases.<sup>1 & 2</sup> In addition, experimental data has been obtained which supports the general applicability of the relationships implied in

equation 1 to the initiation process<sup>3, 4, 5</sup>, in one case<sup>5</sup> applied to wire bridge EEDs. Some of the implications of these relationships with respect to the design and to the prediction of the behavior of EEDs will be discussed further on in this report.

The equation which has been used most widely in recent years in the characterization of EEDs is that which is referred to as the "Rosenthal equation"<sup>6</sup>:

$$C_p \frac{d\theta}{dt} + \gamma\theta = P(t) \text{ --- (2)}$$

where

$C_p$  is the heat capacity of the bridge system

$\theta$  is the temperature rise above ambient

$t$  is time

$\gamma$  is a heat loss factor

$P(t)$  is time dependent power input

This equation has been used quite successfully to characterize the input properties of a variety of electric initiators, some of them under a wide range of conditions. However, its use of lumped heat capacity and heat loss factor, as well as the assumption of a constant threshold temperature for initiation can lead to a considerable degree of confusion if the equation is taken literally as a fundamental statement. Some of these difficulties will be discussed further on in this paper.

In Reference 9 equations are derived for the calculation of heat loss factors of bridge wire/flash charge systems

of several idealized spatial configurations. Those which are believed to be of particular interest are the following: for a "long bridgewire" (assuming cylindrical symmetry and the homogeneous explosive and ignoring end effects):

$$P_r/\theta = \gamma_r = \frac{2 Lk}{\ln D_2/D_b} \quad \text{--- (3)}$$

where

$P_r$  is the total heat flux through the surface

$\theta$  is the temperature difference between a bridgewire of diameter  $D_b$  and a concentric cylinder heat sink of internal diameter  $D_2$

$\gamma_r$  is a "heat loss factor"

$L$  is the length of the cylinder (and the bridgewire)

$k$  is the thermal conductivity of the flash charge material

For a "short bridgewire" assuming terminals to be "perfect" heat sinks and radial heat loss to be negligible:

$$\gamma_a = \frac{8k_b \rho}{R_b} \quad \text{--- (4)}$$

where

$k_b$  is the thermal conductivity of the bridgewire material

$\gamma_a$  is the axial heat loss factor

$\rho$  is the resistivity of the metal of the bridgewire

$R_b$  is the resistance of the bridgewire

For a film bridge on a thermally conductive substrate (assuming the substrate to be large in all dimensions concerned with the effective film bridge):

$$P_s / \theta_m = \gamma_s = k_p \sqrt{2A} \text{ - - - - - (5)}$$

where

$P_s$  is the total heat flux in a spherically divergent flow

$\theta_m$  is the maximum temperature rise

$\gamma_s$  is the heat loss factor

$k_p$  is thermal conductivity of the substrate

Equations 3- 4, and 5 have been found to be quite useful in the prediction of performance of EEDs. Of course, some account must be taken of the deviation of real initiators from the idealized configurations and conditions assumed in their derivation. One such deviation is that bridge wires are generally neither "short" nor "long" but somewhere in between. In a bridgewire in which both the axial and radial components of the heat loss factor are significant  $\gamma_a$  can be represented by the equation:

$$\gamma_a = \frac{4AK_w \pm 2 \sqrt{4A^2K_w^2 + AK_wK_rL^2}}{L} \text{ - - - (6)}$$

where

$A$  is the cross section area of the wire

$K_w$  is the thermal conductivity of the wire metal at any point along the wire

$K_r$  is the radial heat loss factor per unit length

$L$  is the length of the wire

$\gamma_a$  is the axial component of the heat loss factor

The radial component of the heat loss factor ( $\gamma_r$ ) can be represented by the equation:

$$\gamma_r = K_r \left( L - \frac{8AK_w}{3\gamma_a} \right) \text{ - - - - - (7)}$$



Equation 7 has been simplified for tractability but Reference 7 shows it to be applicable and also gives the derivation of Equations (6) and (7).

#### DISCUSSION

Equations 3 through 7 are for hot bridgewire devices. They have proven to be quite useful in predicting the performance of hot bridgewire electroexplosive devices used in conjunction with the assumption of a constant "ignition temperature" for any given flash charge material. It has also been found that the assumption of a constant "ignition temperature" is quite useful in predicting the minimum firing energy requirement for a pulse fired unit when combined with the assumption that the energy of the pulse is all used to heat the bridgewire uniformly throughout its volume. However, it turns out that the ignition temperature which must be assumed to predict energy requirement under pulse firing conditions may be two or three times as high as that required to predict steady state characteristics using Equations 3 through 7. For example, steady state bridgewire temperatures to fire lead styphnate with a half mil bridgewire are close to  $500^{\circ}$  while bridgewire temperatures necessary under pulse firing conditions are close to  $1000^{\circ}$ .<sup>5</sup> It should be pointed out that these temperatures are based on both theoretical calculations and experimental data which are in good agreement. The reason for this apparent discrepancy is not difficult to assign qualitatively on the basis

of simplistic models. A self propagating reaction may be expected to occur at any time when heat is liberated by the reaction within a "reaction nucleus" faster than it could be dissipated therefrom. In the case of a pulse fired detonator, these conditions must be established within the very short time that the bridgewire is hot, whereas under steady state conditions the temperature of the bridgewire is maintained while heat can accumulate in a relatively large reaction nucleus. In the region around the larger reaction nucleus, the "steady state" condition implies equilibrium heat flow with much flatter thermal gradients than exist in the region surrounding a bridgewire suddenly heated by a short pulse. As a result, the effective "heat loss factor" for the suddenly pulsed bridgewire is much higher than that for the same bridge-wire under steady state conditions. As the result of the higher heat loss factor and smaller reaction nucleus around a bridgewire heated by a short pulse, the reaction rate must be much higher (requiring a higher temperature) than that in the larger reaction nucleus, with a smaller heat loss factor around a bridgewire heated by a steady current.

If solutions of Equation 1 were available for both the "steady state" and pulse fired cases, they might be expected to agree quite quantitatively with the experimental data, as they have in relating pulse energy requirements to bridgewire dimensions and activation energies of flash

charge explosives. It is suggested that a good computer program (similar to Enig's<sup>10</sup> for marginal shock initiation of high explosives) in which Equation (1), with appropriate boundary conditions for a hot wire EED, is solved for a variety of combinations of detonator design and electrical input parameters would contribute greatly to the understanding of this type of device. Lacking the resources for such a program, an effort will be made to draw some qualitative implications from Equation (1) and the principles it expresses.

Equation 1 expresses the following principles:

1. That in any differential volume of material, the product of the heat capacity and the rate of temperature rise is equal to the sum of the net rate of heat flow into the volume and the rate at which heat is evolved due to chemical reaction in the volume.

2. That, at any point, the rate of heat flow is proportional to the temperature gradient.

3. That the rate at which heat is evolved is an exponential function of temperature of the Arrhenius type. This equation, or simpler equations based on similar considerations, have formed the basis for many quite successful interpretations of thermal sensitivity data<sup>3, 4</sup> and theoretical considerations of the initiation process.<sup>1, 2</sup> The following discussion, though non mathematical, is an effort to consider the hot wire initiation process in

these terms.

If a pulse is short enough, it may be tentatively assumed to heat a bridgewire before it has time to lose a significant quantity of heat to surrounding material. Based on this tentative assumption, the temperature rise is given by the energy delivered to the wire divided by its heat capacity. If, as implied in Equation 1, it is assumed that heat transfer is proportional to the gradient and the heat transfer coefficient of the flash charge explosive, which is in good thermal contact with the bridge-wire, the foregoing implies a finite temperature change in a zero thickness of explosive and, thus, an infinite temperature gradient and heat flow rate. This infinite temperature gradient and heat flow rate is, of course, the initial condition. The infinite heat flow rate results in an infinite rate of change of the gradient and, thus, after any finite time, the heat flow rate is also finite. In an effort to obtain a quantitative idea regarding the rate at which the bridgewire temperature and the heat loss rate from the bridgewire vary with time, a few numerical calculations were made for a typical electro-explosive device. The device considered was one of the general type which includes the Mk 70, Mk 71, M36, and M48, as well as numerous others which have threshold firing energies of the order of 4000 ergs. The bridge-wire of such a typical detonator is about 1/2 a mil in

diameter by perhaps 40 mils long. The heat capacity of the wire itself is about 4 ergs per degree Centigrade so that, at its threshold firing energy, the temperature is about  $1000^{\circ}$  (if the temperature distribution is assumed to approximate that for a steady state, with the outer diameter ( $D_2$  of Equation 3) varying with time in such a manner that the quantity of heat necessary to establish the temperature gradient in the explosive is equal to that which has been lost by the bridgewire). It turns out that the proportional quantity of the bridgewire heat, which has been lost to the explosive, is approximately equal to the proportional excess of the effective  $D_2$  over the bridgewire diameter, where these proportional quantities are small compared with one. That is to say, when  $D_2$  is 1.1 times the bridgewire diameter ( $D_b$ ), approximately one tenth of the heat in the bridgewire has been transferred to the explosive. At this same time, the heat flow rate from the bridgewire to the explosive in a typical detonator of the kind discussed above is calculated (using Equation 3) to be about 3 watts (or 30 ergs per microsecond). At this heat flow rate, it would take over 10 microseconds for the bridgewire to lose 10% of its initial heat to the explosive. Of course, the heat flow rate before this time is very much higher so that the time required to attain this condition would be appreciably less than that calculated on the basis

of a constant heat loss rate, but after only 1% of the heat of the bridgewire had been lost the heat loss rate would have been only 300 ergs per microsecond, at which rate it would take over a microsecond to lose another 9% of its heat. These calculations thus indicate that a loss of 10% of the initial bridgewire heat to the surroundings would take place in between 1 and 10 microseconds. A corollary indication is that it is quite feasible to construct circuitry which will deliver a pulse short enough to heat the wire to the threshold temperature for initiation of typical flash charge explosive in a time sufficiently short that the heat loss of the bridgewire during the pulse is negligible compared with other errors and random and systematic variables inherent in the testing of electroexplosive devices.

Again referring back to Equation 3, it may be seen that the inverse relationship between  $D_2$  of that equation and the heat loss factor is such that when  $D_2$  is 1.1 times  $D_b$ , the heat loss factor is approximately 50 times that when  $D_2$  is equal to 50 times  $D_b$  (a typical ratio under steady state conditions for EEDs of this general design). The calculations are thus reasonably consistent with the general experience that detonators of this class will fire on about 1/10 of an ampere and about 50 milliwatts. For detonators which meet the one watt, one ampere, no-fire criterion,<sup>12</sup> much higher heat loss factors are necessary.

Where such large heat loss factors are attained by using large bridgewires, the heat capacity of the bridge increases almost in proportion to the heat loss factor so that the times required to attain a given proportional relationship of the kind discussed above may be expected to be of the same order of magnitude. On the other hand, where an effort is made to retain the pulse sensitivity of detonators of the characteristics discussed quantitatively above while increasing the heat loss factors sufficiently to meet the one watt, one ampere, no-fire criterion, the times, of course, are very much shorter, and there is some question as to whether circuits of the kind ordinarily used in the firing of detonators will deliver the threshold firing energy before a very significant amount of heat has been lost from the bridgewire to the surroundings. In partial answer to this question, it has been found experimentally<sup>11</sup> that detonators with flash charges of lead styphnate to which thermally conductive materials, such as aluminum or graphite, have been added, have very nearly the same pulse sensitivities as similar detonators with flash charges of pure lead styphnate, although the heat loss factors and steady state firing power requirement of detonators with flash charges of the thermally conductive mixture may be many times those of detonators with pure lead styphnate flash charges.

Equation 2 includes a heat loss factor ( $\gamma$ ) which is presumed to be a constant for each electroexplosive device. As the foregoing discussion indicates, the heat loss factor is anything but constant, varying inversely with the time after the bridgewire has been heated electrically. One result of this is the substantially higher bridgewire temperatures required for pulse initiation than are required for initiation by a steady current. Ayres<sup>13</sup> has noted that "heat loss factors," as calculated from alternating current measurements by the third harmonic analysis,<sup>14</sup> are higher than heat loss factors of the same detonators, as measured by direct current techniques. This is to be expected on the basis of the foregoing. While the effective or apparent heat loss factor tends to decrease with time after the application of an electrical pulse, the effective or apparent heat capacity of the bridge tends to increase with time, as more and more of the explosive material is heated.

As has been mentioned earlier in this report, the bridgewire temperature required for pulse initiation is appreciably higher than that for steady current initiation. This was attributed to the very much larger heat loss factor and smaller reaction zone of the bridge system of an initiator under pulse initiated conditions than under steady state conditions. The smaller reaction nucleus around a smaller bridgewire also results in a require-



ment for a higher initiation temperature as bridgewire diameters are decreased.<sup>5, 15</sup> This effect has been quantitatively verified to fit a solution of Equation 1. A general solution of Equation 1 due to Gamow and Finkelstein<sup>1</sup> predicts that the natural logarithm of a linear dimension should be approximately proportional to  $E/2RT_c$  where  $T_c$  is the critical temperature for initiation. Plots of data relating reciprocals of temperatures associated with threshold firing conditions to logarithms of bridgewire diameters yielded straight lines, the slopes of which reduced to activation energies which agreed within 1% or so with values for the same explosives (lead styphnate, mercury fulminate, and lead azide) obtained by entirely different techniques by Henken and McGill.<sup>4</sup> This agreement continues to be very persuasive evidence of the applicability of Equation 1 to electroexplosive devices.

A rather interesting question is raised by the successful applications of both Equation 1 and Equation 2 to EED initiation processes. If the use of distributed parameters and reaction kinetics as expressed in Equation 1 yields variable heat capacity, heat loss factor, and threshold temperature for initiation for the same EED, why does Equation 2 with its lumped parameters and fixed values of heat capacity, heat loss factor, and "ignition temperature?" A partial answer to this question is

probably the built in compensation of some of these variables when the quantities are determined on the basis of either destructive or non destructive tests of initiators rather than by calculations using equations similar to Equations 3 through 7. If, for example, the heat capacity of the bridge system is determined using the third harmonic technique, the value obtained would generally be expected to be appreciably higher than that of the bridgewire itself since at the frequencies used in this technique there would be sufficient time for appreciable heat transfer from the bridge to the surrounding explosive. If this larger heat capacity were used in the calculation of the threshold firing temperature from the threshold firing energy a considerably lower temperature would be calculated than would result from the use of the heat capacity of the bridgewire itself. From the practical point of view as a user of an EED, it really doesn't make much difference whether the threshold energy for pulse firing heats a larger quantity of material to a lower temperature or a smaller quantity of material to a higher temperature.

Although calculations beyond the scope of this paper would be needed to demonstrate it, it seems probable that the right combination of materials and dimensions would result in an EED for which the interaction of the

effects of distributed parameters upon heat flow and those of reaction kinetics upon threshold firing characteristics produces the same hyperbolic relationship between threshold firing energy and power as would be predicted by Equation 2 (with heat capacity ( $C_p$ ) and heat loss factor ( $\gamma$ ) calculated from experimentally determined firing characteristics). It is not obvious, however, that such a relationship applies generally, even to the idealized systems which form the basis of most theoretical calculations. It seems quite clear that real EEDs with their complex configurations (as compared with the idealized systems used in most calculations), non-homogeneous materials, discontinuities of thermal conductivity and specific capacity, and thermal coefficients of many of the important quantities, in addition to the effects of distributed parameters, and reaction kinetics, would generally be expected to have much more complex input characteristics (in terms of the response to stimuli which are intermediate between the short pulses for which the energy requirement approaches its minimum and those which approximate "steady state" conditions) than would be predicted by solutions of Equation 2.

The success of Equation 2 in predicting the behavior of at least one type of initiator<sup>6</sup> over a broad range of input conditions, has inspired confidence in its general applicability to EEDs. Two results of such

confidence should be guarded against; (1) the tendency to obtain sufficient data for a new device to determine a heat loss factor and heat capacity and depend upon the equation to predict behavior under all other conditions, (2) the tendency to characterize an initiator as "abnormal" if it does not behave as predicted by Equation 2. The first of these tendencies could, of course, result in a hazard, if an initiator accepted on this basis turned out to be more sensitive than predicted for some set of conditions to which it was exposed. Failures are less likely, because system development usually includes establishment of reliability under intended conditions of use.) The second tendency could easily lead to the rejection of a device or concept which would have proven quite useful if given more realistic consideration.

#### SUMMARY AND CONCLUSION

Equations derived with the help of simplifying assumptions have contributed greatly to the understanding of the behavior of electroexplosive devices and are extremely useful in their design evaluation and in the prediction of such behavior. It can, however, be a serious mistake to lose sight of the assumptions which have been made in the derivation of such equations and to look upon them as infallible and completely realistic representation of the

conditions which result from the application of an electrical signal to an electroexplosive device. It can be useful, while using equations based on simplified models, to consider, qualitatively, the effects of the assumptions in terms of more general equations (which it may be impractical to solve, quantitatively, for the devices under consideration).

#### REFERENCES

1. Finkelstein, R. J., and Gamow, G., "Theory of the Detonation Process, Navord Report 90-46, Navy Dept., Bureau of Ordnance, 20 April 1947.
2. Bowden, F. P., and Yoffe, A. D., "Initiation and Growth of Explosion in Solid Explosives," The Syndics of the Cambridge University Press, Bentley House 1, London.
3. Wenograd, Joseph "The Behavior of Explosives at Very High Temperatures," Proceedings of Third Symposium on Detonation, (Princeton University) ONR Symposium Report, ACR-52, Vol. 1, p. 61, 26-28 Sept, 1960.
4. Henkin, H., and McGill, R., "Thermal Sensitivity of Explosives," J. Ind. and Eng. Chem. 48, 1090 (1956).
5. Kabik, I., Stresau, R. H., and Hampton, L. D., "Firing Characteristics of Electric Initiators Made by the Spray-metal Process," NOLM 10771, U. S. Naval Ordnance Laboratory, White Oak, Silver Spring, Maryland, dated 30 March 1952.
6. Kabik, I. B., Rosenthal, L. A., and Solem, A. D., "The Response of Electroexplosive Devices to Transient Electrical Pulses," Paper No. 18, Proceedings of Electrical Initiator Symposium, 1960, held at the Franklin Institute, Philadelphia, 29, 30 November 1960, (F-A2446).
7. Austing, J. L., Kennedy, J. E., Chamberlain, D. H., and Stresau, R. H., "A Heat Transfer Study of Hot Wire Ignition of a Metal-Metal Oxide Mixture," Paper No. 3, Proceedings of the Fifth Symposium on Electroexplosive Devices, 13, 14 June 1967.

8. Davenport, D. E., "Temperature Coefficient of Resistivity Effects on 1A/1W No-Fire Initiators," Paper No. 3, Proceedings of the Fifth Symposium on Electroexplosive Devices, 13, 14 June 1967.
9. Stresau, R. H., "Electrical and Thermal Considerations in the Design of Electroexplosive Devices," U. S. Naval Ordnance Laboratory, Corona, California, Navweps Report 8839, 30 June 1966.
10. Enig, Julius W., "Growth of Detonation From an Initiating Shock," U. S. Naval Ordnance Laboratory, Silver Spring, Maryland, Paper presented at Third Symposium on Detonation, James Forrestal Research Center, Princeton University, September 26-28, 1960.
11. Stresau, R. H., Petersen, R., and Chamberlain, D., "Electric Detonators for Navy Guided Missile Applications--Experimental Studies of Four Concepts," Paper No. 3.4, Proceedings of the Fifth Symposium on Electroexplosive Devices, held at the Franklin Institute, June 13-14, 1967.
12. MIL-L-23659 (WEP) "Military Specifications, Initiators, Electric, Design and Evaluation of," March, 1963.
13. Private communications, J. N. Ayres, Naval Ordnance Laboratory, White Oak
14. Rosenthal, L. A., "The Harmonic Generation Technique for the Determination of Thermal Characteristics of Wire Bridges used in Electro-Explosive Devices," NAVORD Report 6691 Ad 231918, 9 Sept 1959.

2-8 THE DEVELOPMENT OF A FIXED GAP ELECTROSTATIC  
SPARK DISCHARGE APPARATUS FOR CHARACTERIZING  
EXPLOSIVES

Louis J. Montesi

U. S. Naval Ordnance Laboratory  
White Oak, Silver Spring, Maryland 20910

1. The Navy is in the process of preparing a military standard for booster type explosives. This standard contains a series of tests which if passed will qualify the explosive as a booster explosive. There are eight tests proposed (see Figure 1) one of which is the sensitivity of the test explosive to electrostatic spark discharges. The development of the apparatus for conducting the electrostatic spark discharge test is the subject of this paper.
2. A simplified and reproducible electrostatic spark discharge apparatus has been developed. It has been described in the set of Navy drawings covered by LD SE/SK 7062. The apparatus has been used successfully for screening explosives, particularly for distinguishing between the primary explosives and booster type explosives. The development program consisted of several phases:
  - (a) Construction of a prototype model for parameter investigations
  - (b) Testing of explosives and comparison of results with those obtained on the existing NOL/ERDE electrostatic spark discharge apparatus<sup>1-6</sup>

(c) Documentation of apparatus

(d) Fabrication of a second apparatus by a machine shop solely from the documentation

(e) Repetition of explosive sensitivity testing using the second electrostatic discharge apparatus and comparison of results with results previously obtained from the first model and, (f) Development of test procedures and operating instructions for specifications.

3. The test procedure is now being documented, and it is believed that independent laboratories (by following specified construction procedures and operating instructions) will be able to arrive at comparable results. This has not been the case until now, because the various apparatuses constructed by different test facilities and the test procedures used, differ greatly and are not well defined.

4. The first model of the electrostatic discharge apparatus built is shown in Figure 2. It consists, mainly, of a variable high voltage power supply, an electrostatic voltmeter, a discharge circuit, and a variable gap electrode arrangement (Figure 3). This apparatus was used to investigate the effect on sensitivity of such parameters as capacitor size, circuit resistance, electrode gap size, and charge voltage.



5. Ideally, we had hoped to build an apparatus which, with a particular gap, capacitor, and potential would initiate sensitive primary and secondary explosives, but which would fail to initiate insensitive secondary explosives when the same gaps, capacitors, and potentials were used. It should be mentioned, and probably stressed, that the apparatus was to be developed to determine the relative static spark sensitivity of explosives and not absolute energy values. Therefore, the apparatus was developed with simplicity and reproducibility in mind, not efficiency of energy transfer. The apparatus developed, indeed, does have energy transfer losses. We tried to minimize these losses but only to the degree that the apparatus not become complex and expensive.

6. The proposed military standard previously referred to will establish criteria for the testing and acceptance of explosives for use beyond a fuze interrupter. Since safety is of major concern a fire was assumed in all our tests if the explosive gave the slightest indication of reaction.

The factors used to determine reaction were:

- (a) emission of smoke
- (b) charring
- (c) burning or explosion

7. From our investigation of the apparatus parameters mentioned previously, the following apparatus details were arrived at:

- (a) a fixed electrode gap of 0.050
- (b) a capacitor of 0.01 mfd
- (c) a test voltage of 10,000 volts
- (d) a fixed line resistance of 100 ohms

With these conditions, we found that the primary explosives were initiated with a few thousand volts, and the secondary explosives could not be initiated with 15,000 volts. This wide separation was ideal for categorizing explosives as primary or booster type as needed for the proposed military standard.

8. During the development program, we found that:

(a) with smaller gaps, larger capacitors, or smaller line resistances, the separation between fire potentials for primary and booster explosives was considerably reduced.

(b) with larger gaps, smaller capacitors, and larger line resistances, the voltage required for initiation of the test explosives was increased to a level where special insulating techniques would be required to minimize losses and arcing.

9. In the electrical circuit used in the first experimental model, a Jennings' RE-6B vacuum relay switch was used to transfer the energy to the test explosive. This switch was found to have satisfactory energy transfer characteristics. The capacitor employed was a General Electric 0.01 mfd, high voltage, low inductance, energy storage discharge capacitor

for oscillatory discharges. The spark was discharged through a series resistor of 100 ohms, which was used to minimize line changes that can occur and which normally would affect the discharge characteristics. A microswitch was used to energize the Jennings' switch to allow for subsequent charging and discharging of the capacitor across the air gap. The discharge characteristics are those of a point to plane discharge (See Figure 4). A phonographic needle was used as the upper electrode, and a steel cylinder ( $3/4$ "diameter x  $3/4$ "length) was used as the base electrode. A phenolic sleeve was glued onto the base electrode to contain the test explosive.

10. The fire/no-fire voltage of the explosives tested on the prototype apparatus are given in Table 1. Also shown in Table 1 are the results of these same explosives tested on the NOL/ERDE electrostatic test apparatus (reference 1-6). This NOL/ERDE electrostatic apparatus is a duplicate of the electrostatic apparatus used at the Explosive Research and Development Establishment located at Waltham Abbey, England. The NOL/ERDE apparatus was fabricated by Dr. Wyatt when he was in residence at NOL as a visiting research scientist. Unlike the fixed gap apparatus the ERDE apparatus has a moveable arm electrode assembly arrangement. The discharge (point to plane) occurs when the stored potential is sufficient

to jump the diminishing gap of the approaching electrodes. (See Figure 5). The details of this apparatus are given in the references cited.

11. Both apparatuses, in general, show a distinct increase in the potential (volts) required for the firing of secondary explosives. The fixed gap apparatus shows a larger increase, but does not provide fine ordering of the explosives within each category (i.e., primary or secondary). Some differentiation into broader sensitivity classes can be obtained, if one desires, by selecting several test potentials, for example 5000 or 10,000 volts. Test explosives could then be labeled very sensitive, sensitive, and insensitive. In addition to the explosives listed in Table 1, a large number of metal/oxidant type mixtures was also tested on both apparatuses and the sensitivity ordering obtained was comparable.

12. Based on the results obtained in the development part of this program, a second test set was fabricated from the documentation and drawings prepared during the first part of the program. A number of additional safety features not on the original model were incorporated into this design. This second test apparatus is shown in Figures 6 through 10. A schematic of the electronic circuit used in the static discharge test set is shown in Figure 11. Few problems were encountered during the fabrication of this model by an independent source.

13. When the second model was completed in the shops, a number of explosives were retested and the results obtained were comparable to the previous results obtained with the first apparatus. (See Table 2)

14. The last part of the program consisted of developing test procedures for the military standard. This draft is so far only proposed and might not be the final test procedure. Basically, the test consists of running a series of shots at one test level. The actual number of shots depends on the results obtained, i.e. the ratio of the fire/number tested as the test progresses. Satisfactory performance is achieved if no more than 0/20, 1/35, or 2/43 fires are observed. From binomial statistics, these values give an expected no fire probability value of 0.86 at 95% confidence level. Three fires disqualifies the explosive as a booster material.

15. In closing I would like again to emphasize the need for having one standard, simple, but yet reproducible static discharge test set for testing explosives. Generating minimum no-fire energy values on different apparatuses is not important. These values are good only for the apparatus with which such data were generated, and can easily be misused. What is important is knowing whether the explosive material you are working with is "sensitive" to electrostatic spark discharges, and to be able to compare data with and use data from other laboratories. The test set developed and described within will, I believe, be capable of filling this need.

16. The Navy recognizes this needs, and as a result, is working in the direction of standarizing these tests for the military specification on qualifying booster explosive. A joint Army-Navy-Air Force group will also consider the proposed standard for Department of Defense use.

#### REFERENCES

1. P. W. J. Moore, J. F. Sumner, R. M. H. Wyatt, "The Electrostatic Spark Sensitiveness of Initiators, Part I", ERDE Report No. 4/5/56.
2. Part II, "Ignition by Contact and Gaseous Electrical Discharges", ERDE Report No. 5/5/56, Confidential.
3. P. W. J. Moore, Part II, "Modification of the Test to Measure the Electrostatic Hazard under Normal Handling Conditions", ERDE Report No. 22/5/56, Confidential.
4. D. B. Scaife, Part IV, "Initiation of Explosion by Spark Radiation", ERDE Report No. 9/5/59, Restricted.
5. R. M. H. Wyatt, Part V, "Further Study of Ignition with Metallic and Antistatic Rubber Electrodes," ERDE Report No. 24/R/59, Confidential Discreet.
6. R. M. H. Wyatt, "The Electrostatic Spark Sensitivity of Bulk Explosives and Metal/Oxidant Mixtures (U)", NAVORD Report 6632, 1 Jun 1959, Confidential.

TABLE 1  
COMPARISON OF EXPLOSIVE SENSITIVITY

Explosive*	Minimum No Fire Potential (volts)	
	ERDE/NOL <sup>(1)</sup>	Fixed Gap <sup>(1)</sup>
Normal Lead Styphnate (Milled)	Sensitive (0.001 mfd)	2,500 (0.001 mfd)**
Basic Lead Styphnate	Sensitive (0.001 mfd)	3,000 (0.001 mfd)**
Poly-vinyl lead azide	Sensitive (0.001 mfd)	2,500 (0.001 mfd)**
Dextrinated lead azide	1,000	2,000**
Tetracene	1,500	3,000**
LMNR	7,500 (2)	15,000 (2)
LMNR (Milled)	7,500 (2)	15,000 (2)
Ammonium Perchlorate (A.P.)	7,500 (2)	15,000 (2)
A.P./Wax (80/20)	7,500 (2)	15,000 (2)
A.P./Al (90/10)	2,500	2,500
PETN	7,000	15,000 (2)
RDX	7,000	15,000 (2)
HNS IB	3,500	14,000
HNS II	4,000	-
DIPAM	4,000	15,000 (2)
TETRYL	7,500 (2)	15,000 (2)
TETRYL/GRAPHITE	-	15,000 (2)
TETRYL/GRAPHITE (-325)	7,000	15,000 (2)

\*Materials tested are regular explosive materials as used by the Navy.

(1) Unless otherwise specified, the following conditions exist:

Apparatus	NOL/ERDE	Fixed Gap
Capacitor	0.01 mfd	0.01 mfd
Increment Voltage	500 volts	500 volts below 5000; 1000 volts above 5000
Voltage Maximum	7500 volts	15,000 volts
Electrode Gap Size	Diminishes	0.050

(2) No fires observed at this level, no trials were made above this level.

\*\*No spark discharge occurred at this level, fires observed above this level.

TABLE 2  
COMPARISON OF RESULTS FROM BOTH FIXED GAP  
ELECTROSTATIC MODEL

Explosive	Model #1 No Fire Potential	Model #2 Test Potential (volts)		
		5000	10,000	15,000
Normal Lead Styphnate (Milled)	2,500 (0.001 mfd)*	Fired	Fired	NT <sup>(1)</sup>
Basic Lead Styphnate	3,000 (0.001 mfd)*	Fired	Fired	NT
PbN <sub>6</sub>	2,000*	Fired	Fired	NT
A.P./Al (90/10)	2,500	Fired	Fired	NT
Tetracene	3,000*	Fired	Fired	NT
PETN	15,000	NT	Failed	Failed
RDX	15,000	NT	Failed	Failed
LMNR (Milled)	15,000	NT	Failed	Failed
Tetryl (Pure)	15,000	NT	Failed	Failed
HNS-IB	14,000	NT	Failed	Failed
DATB	15,000	NT	Failed	Failed

\*No spark discharge occurred at this level, fires observed above this level.

(1) N.T. - Not tested at this level.



## **Fig. 1 SENSITIVITY TESTS FOR QUALIFYING BOOSTER EXPLOSIVES**

- 1. IMPACT TEST**
- 2. BON FIRE (THERMAL) TEST**
- 3. HOT WIRE TEST**
- 4. VACUUM THERMAL STABILITY TEST**
- 5. SMALL SCALE GAP TEST**
- 6. ELECTROSTATIC SPARK SENSITIVITY TEST**
- 7. FRICTION TEST**
- 8. FLYING PLATE TEST**

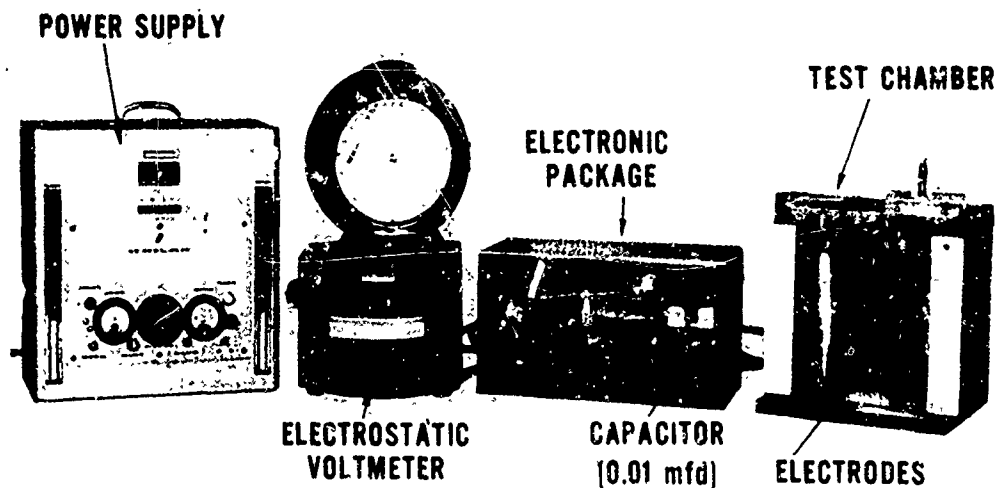


**FIG. 2 FIXED GAP ELECTROSTATIC DISCHARGE  
APPARATUS, MODEL #1**

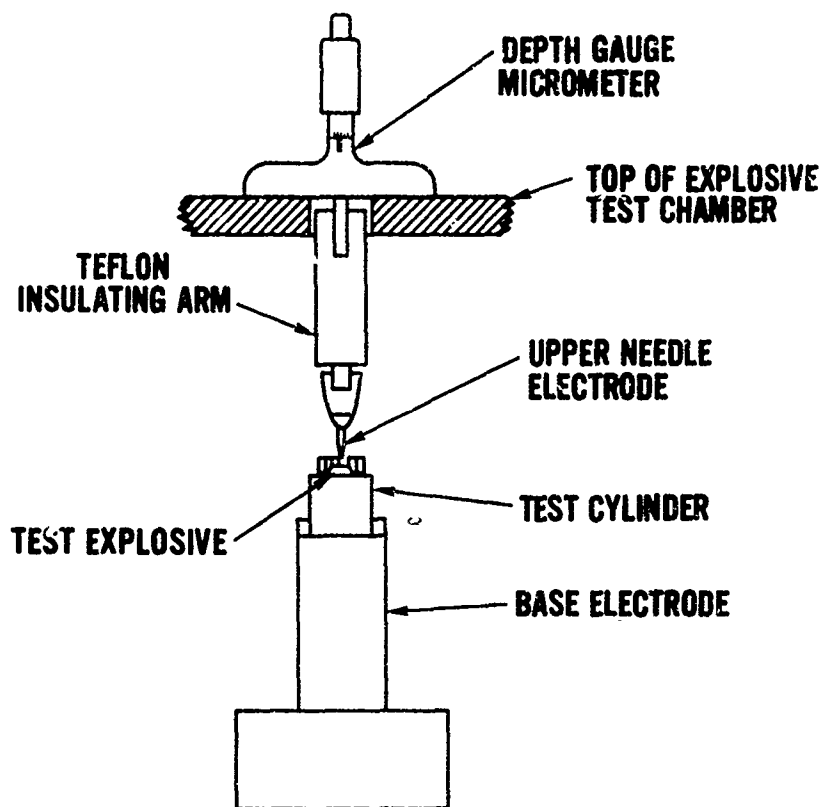


**FIG. 3 ELECTRODE TEST ARRANGEMENT, MODEL #1**

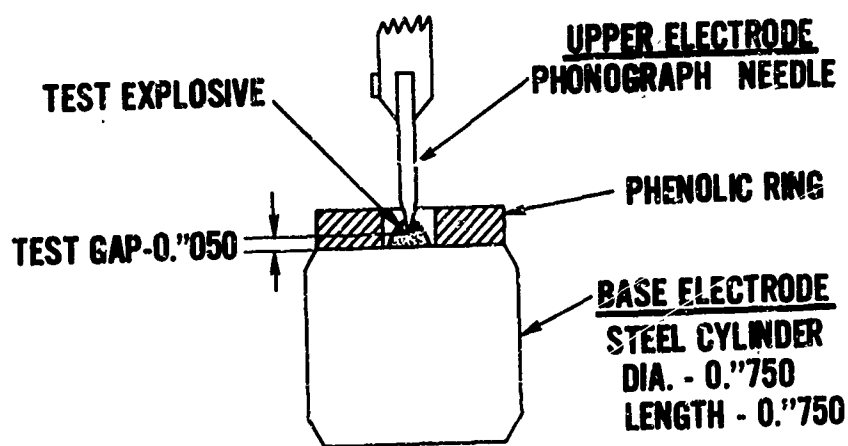


**FIG. 4 ELECTRODE ARRANGEMENT-FIXED GAP  
ELECTROSTATIC DISCHARGE MODEL #1**

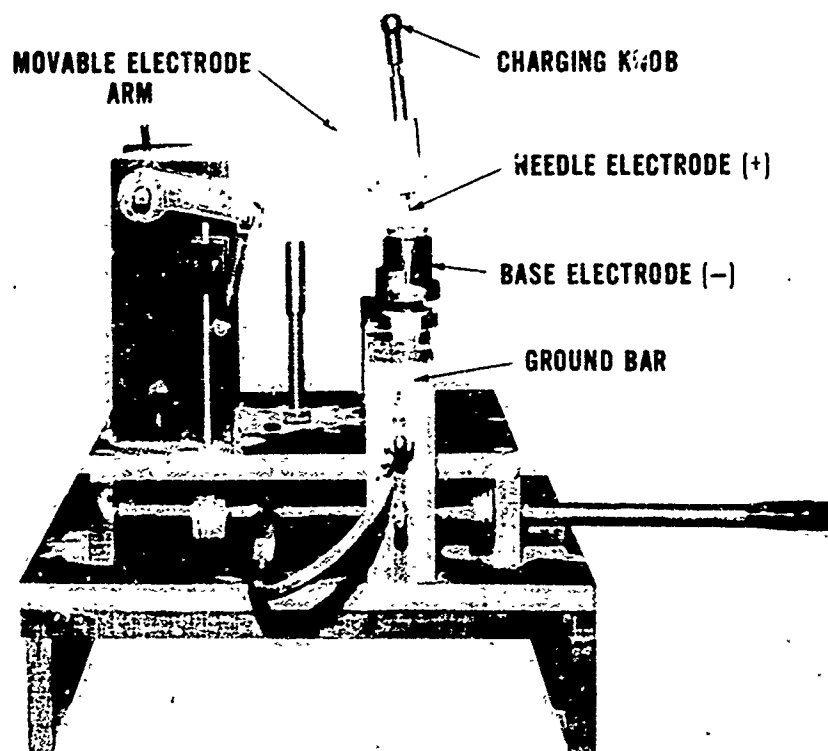


**FIG. 5 NOL/ERDE-ELECTROSTATIC  
DISCHARGE TEST - ELECTRODE ASSEMBLY  
(SIDE VIEW)**

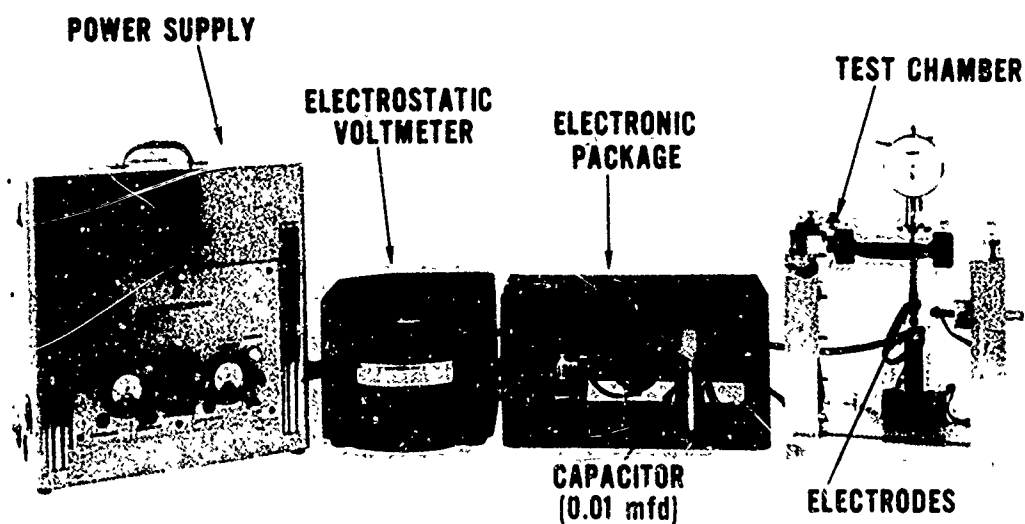


**FIG. 6 FIXED GAP ELECTROSTATIC DISCHARGE APPARATUS-MODEL #2**

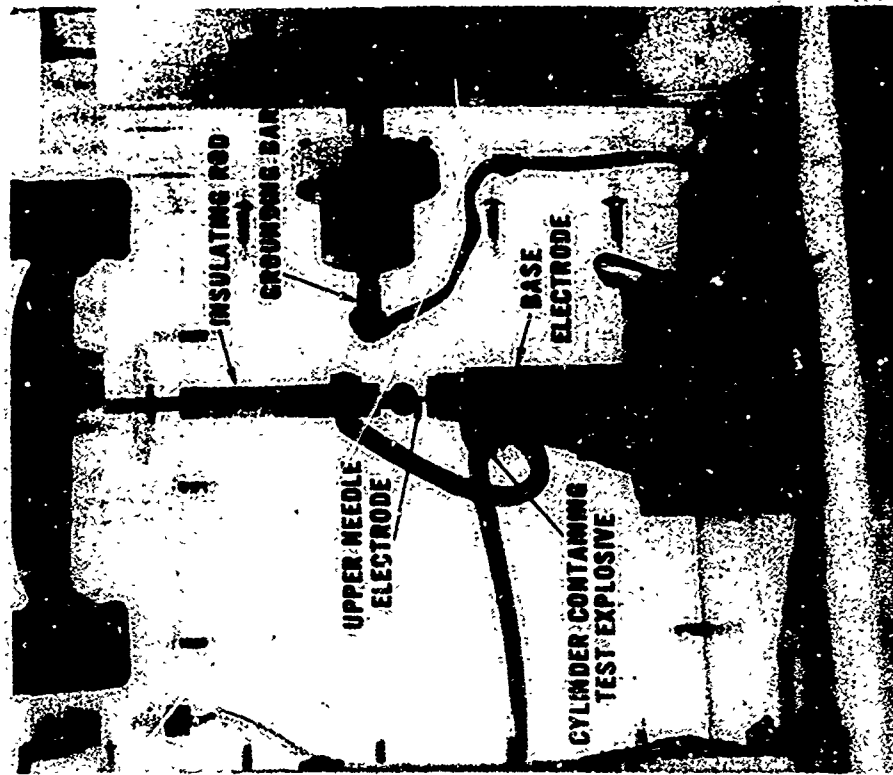


FIG. 8 ELECTRODE ARRANGEMENT  
FOR FIXED GAP APPARATUS

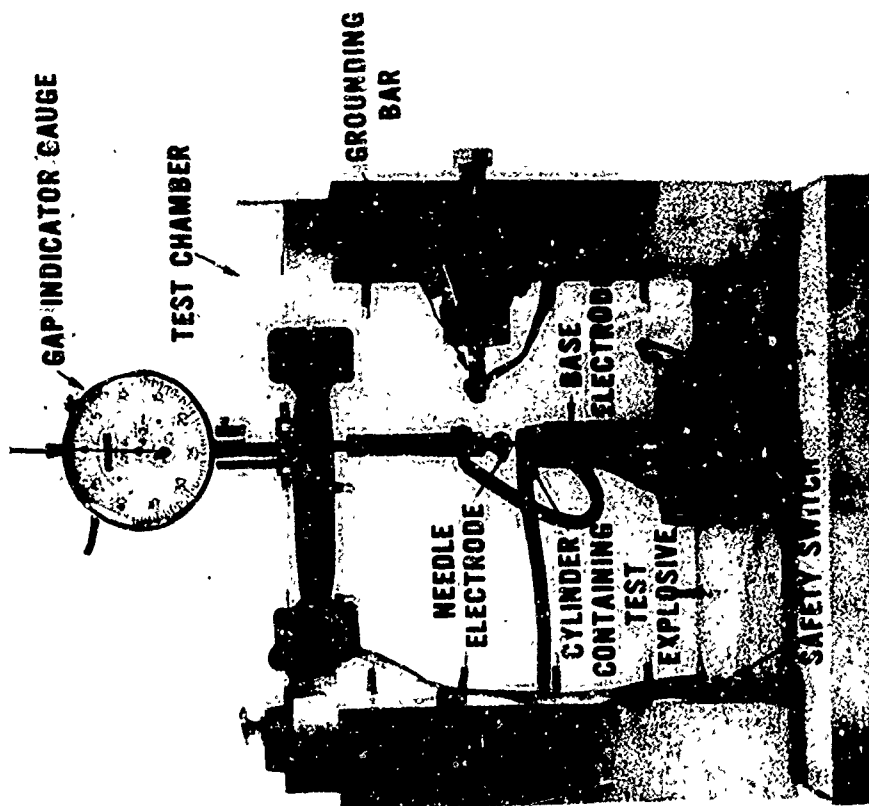
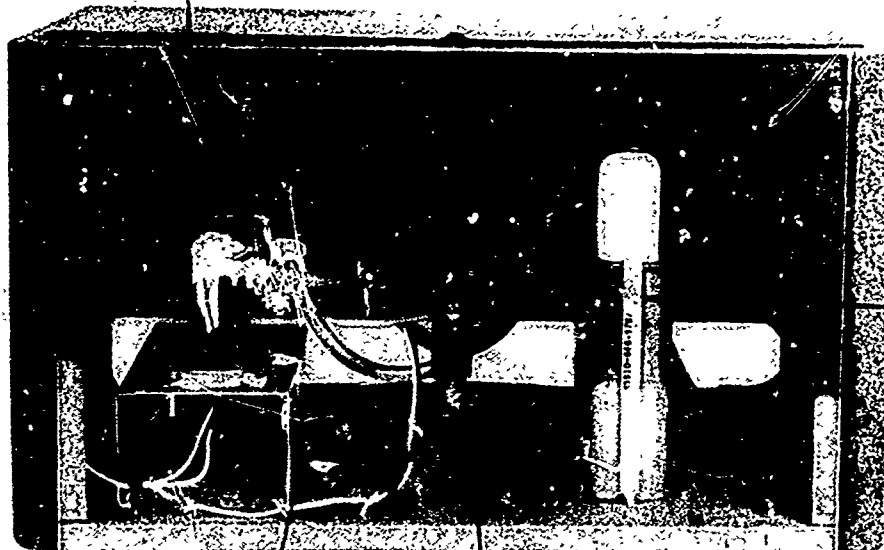


FIG. 7 EXPLOSIVE TEST CHAMBER

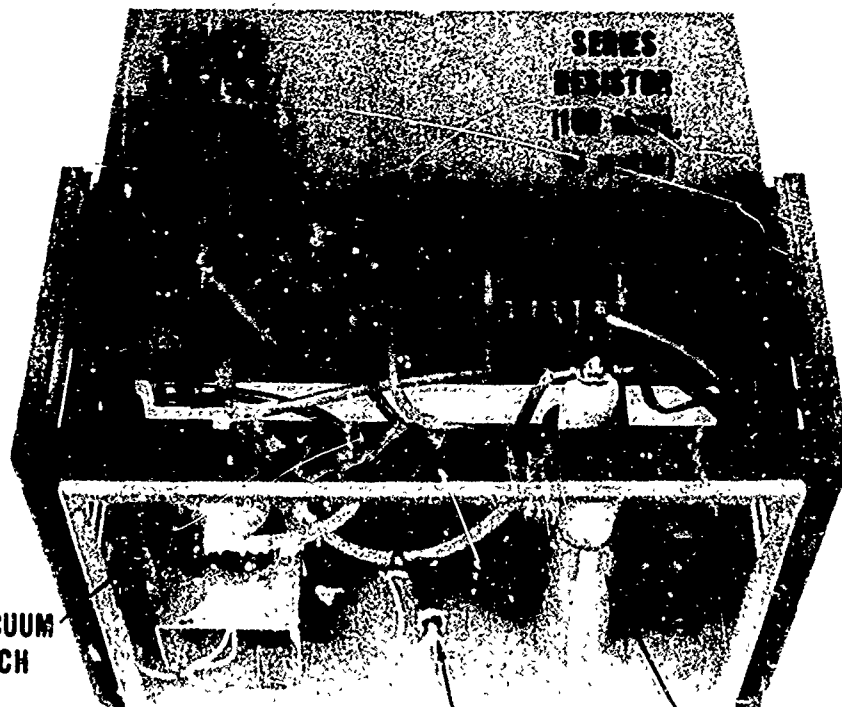
JENNINGS VACUUM  
RELAY SWITCH



CAPACITOR  
(0.01 mfd)

CHARGE LIGHT MICRO SWITCH

FIG. 9 ELECTRONIC PACKAGE (FRONT VIEW)



SERIES  
RESISTOR  
(100 OHMS)

JENNINGS VACUUM  
RELAY SWITCH

MICRO SWITCH

CAPACITOR  
(0.01 mfd)

FIG. 10 ELECTRONIC PACKAGE (TOP VIEW)



2-9 EXPERIMENTS IN MEASUREMENT OF  
OUTPUT ENERGY OF ELECTRO-EXPLOSIVE  
DEVICES THROUGH METAL DEFORMATION

BY

\*DR. S. BARRON AND EDWARD G. PIERSON  
CONAX CORPORATION, BUFFALO, NEW YORK

INTRODUCTION

The search for a reliable and economical means of measuring energy output of explosives and electro-explosive devices (E.E.D.) seems to be endless. Such measurements are desirable not only from the viewpoint of quantitative evaluation of given weights and types of explosives, but also with regard to uniformity in quality control. When explosives are manufactured in quantity lots, it would be beneficial to have a simple inexpensive method of controlling their consistency.

Conax Corporation has for many years used a considerable number of E.E.D.'s in electro-explosive operated devices, such as valves and *actuators*. A photograph of a combination valve, involving four explosive operations, is shown in Figure 1.

Until recently, the pressure bomb with its piezo-electric transducer had been used at Conax to evaluate the consistencies of burning rates of various EED's. The pressure bomb is subject to a number of irregularities. Confinement has a marked effect on the burning rate of explosives and consequently the resulting peak pressure. Trans-

\*Professor of Chemistry: S.U.N.Y. College at Buffalo-Consultant to  
Conax Corporation

ducers rated at 75,000 psi statically may not survive the shock accelerations associated with pressures of 20,000 psi.

In addition, under certain conditions we have found that two statically calibrated transducers pressurized from the same bomb cavity were widely divergent in their readings. Unless two transducers agree in their dynamic readings, little credence can be given to their accuracy.

Therefore Conax Corporation realized the need for improved test methods and hence engaged in two sets of experiments to find more acceptable methods of testing our E.E.D.'s. These experiments both involved metal deformation. One was centered around the Trauzl lead block application while the other involved a projectile penetrating its target.

A search was made of the published literature pertinent to our applications. It is described below. The lead block method was first selected because of published recommendations for its use in the measurement of brisance.

#### LITERATURE SURVEY-PRIOR ART

Two properties are usually considered in relating the effectiveness characteristics of explosives. One is the brisance or shattering power as distinguished from total work capacity. The other is power of an explosive determined by the rate at which heat energy is liberated. The total work capacity of an explosive is a function of the total



available heat liberated at the instant of detonation. Tests such as sand, plate dent, lead block, and fragmentation measure the brisance of the explosive charge. The calorimetric bomb measures the heat of explosion in a manner similar to that used to determine heat of combustion without further addition of oxygen. The heat of explosion is expressed in calories per gram and hence represents useful work capability.

At this point, we will review some of the published data on the matter of energy measurement of explosives as they relate to subject experiments.

As recently as 1963, V. J. Menichelli<sup>1\*</sup> stated that evaluating the output of explosives and explosive components, and in particular, measurement of output, is most difficult. Because parameters of temperature and pressure exist for such short periods (nanoseconds), elaborate, costly, sensitive equipment is required and hence analyses have yielded to the measurement of destructive or damage effects from explosives. He cites typical tests such as the bent nail, lead disc, steel dent, sand bomb, compressed springs, shearing rods, movement of mass through some distance, the pressure bomb test, etc. But he points out that until more work is performed on understanding the mechanism of initiation in fixed geometries, it is likely that output testing will follow the same approaches of the past.

Lothrop and Handrick<sup>2</sup> performed several studies which had as their objectives the relationships of performance of explosives with

---

1\* Superscript numbers refer to the bibliography at the end of this paper.

structural composition. Of particular interest is the use of "oxygen balance" in measuring the power of explosives. The term, oxygen balance relates to the percentage of oxygen required for the complete conversion of the carbon and hydrogen present in explosives to carbon dioxide and water. A zero balance would indicate that exactly the proper amount of oxygen was present, a negative balance would indicate insufficient oxygen, a positive balance would indicate that excess oxygen was available. It is of interest here to note how this phenomena is evaluated through the use of the lead block test and the ballistic mortar test. These data are shown clearly in Figures 2 and 3 respectively. The Trauzl lead block test in their report is described as a classical method and depended on measurement of the expansion created in a block of pure lead by a given weight of explosive under confinement. Since "power and brisance vary concomitantly", they stated that their separation is not of great importance as long as caution governs such data as an absolute measure of power. The ballistic mortar test is considered to be uncomplicated by brisance (unlike the lead block test). Deference is made to the ballistic mortar method because the work of expansion is measured in absolute mechanical units. The results of both of these methods are granted to be useful, and as might be expected, the lead block data are much more extensive for reasons of economy. Of their 13 graphs of test results showing power and brisance as affected by oxygen balance, 9 were plotted from lead block data, 3 from ballistic

mortar data, and I used the sand crush test data.

Rinehart and Pearson<sup>3</sup>, state that the lead block test measures the distension effect of a given weight of explosive when detonated under moderate confinement in a standardized lead cylinder. The increase in chamber volume is used as the measuring value. Some data for comparison of brisance, and relative power measured by the ballistic pendulum, and Trauzl lead block tests are shown in Table 1.

Cook<sup>4</sup> applies various fundamentals to the reliability of ballistic mortar and Trauzl-block methods "which comprise the only methods of strength determination that have yet been used to any appreciable extent in commercial explosive technology". He states that the ballistic mortar is not a reliable method for determining field strength of high explosives, but does show good reproducibility, and that theoretically, the Trauzl block provides an excellent measure of available energy (power). He recommends the lead block for a reliable determination of available energy under high loading density. In other words, the mortar is limited because of shattering effects and care must be exercised in testing explosives with regard to both their type and amount to be tested.

The Aerospace Ordnance Handbook<sup>5</sup> states that testing of aerospace ordnance is a specialized technology within the broad field of ordnance. The accuracy and adequacy of the test depend primarily on the equipment used to perform the test. For example, in the case of a squib, many factors enter into the measurement of peak pressure, wave shape, and rise time, such that the transducer it-

self becomes a most important variable. (This bears out our above remarks regarding simultaneous use of two transducers).

A more recent method of energy measurement has been developed by McDonnell Aircraft Corporation<sup>6</sup> (now McDonnell-Douglas) through the use of a honeycomb cartridge. They state that their Energy Sensor measures the output of explosives via the amount of crush of a honeycomb element. "It measures the explosive output of detonators, squibs, and power cartridges, and bears a linear relationship to energy output". Individual honeycomb sensing elements are calibrated prior to use and outputs are obtained in inch-pound, mechanical work units.

An extensive analysis of the lead block Trauzl method was performed by Gordon, Reed, and Lepper<sup>7</sup> in conjunction with their experiments using this method. In the standard Trauzl test, 10 grams of explosive, together with a detonator, are placed in a well in a cylindrical block of lead, covered with sand, and fired. The net expansion thereby ensuing is used as a measure of energy. The many results obtained with explosives are compared to TNT as a standard. Since the temperature of the block at the time of firing is the major effective variable, it can be seen that precisely controlled tests are readily accomplished.

#### EXPERIMENTS WITH THE LEAD BLOCK

Since diazodinitrophenol (DDNP) is a "high" or detonating ex-

plosive exhibiting good brisance characteristics, it was selected for the base charge in the lead block tests. Three nominal weights were used; i.e. 60 mg, 120 mg, and 170 mg. The ignition mix for each charge weighed about 80 mg and was composed of potassium chlorate, lead styphnate, and some DDNP.

Attempts were made to manufacture lead spheres for these tests; a diameter of 3 inches was selected similar to that in reference 7. An aluminum mold was constructed in two halves to accommodate the lead pouring. However a considerable amount of difficulty was encountered in that after each cooling, deep wells would form in each sphere at the fill location. It was then decided to change to lead cylinders. Thereupon, cylindrical lengths of commercial lead of 2.5" diameter were utilized and were cut into sections 2.5 inches in length each. (See photograph, Figure 4). This greatly simplified the problem.

Holes (0.29" diameter) were drilled centrally into each cylinder to a depth of 1.25 inch. Each block was numbered and the volume of its drilled hole measured by water displacement, and recorded.

Tests were conducted by inserting each charge into the drilled hole of the lead cylinder and sealing it by pouring 1.3 grams of sand over the charge. The unit was then placed in the test cell and fired with the loading end up, using a uniform firing current. After each firing, the volumes of the expanded holes were again measured by water displacement and the net (increased) volumes recorded. A cutaway of the cylinder showing the effect of the detonation of a

120 mg charge can be seen by referring to Figure 4 again.

From these tests, the standard deviations were calculated for the three classes of charge weights and the results were plotted in terms of frequency distribution versus net volume for the three base charge weights of 60 mg, 120 mg, and 170 mg, in Figures 5, 6, and 7 respectively.

The frequency distribution curve of Figure 5 shows that a mean net volume of  $\bar{x}$  of 2.210 ml. was obtained for the 60 mg. charges, nine such tests having been made. It further indicates that 68% of the net volumes based on  $1\sigma$  fall between values of 2.175 and 2.245 ml. The 95% spread between  $\pm 2\sigma$  falls within  $\pm 3.16\%$  of  $\bar{x}$ .

The frequency distribution curve drawn from the results of tests on the 120 mg charges is shown in Figure 6. The mean net volume,  $\bar{x}$ , is 3.47 ml. Seven tests were performed with this weight of charge. The value of  $1\sigma$  here is  $8.7 \times 10^{-2}$  ml. and hence 68% of the values can be expected to fall between 3.383 and 3.557 ml. The 95% spread based on  $2\sigma$  falls between 3.296 ml. and 3.644 ml. and is within  $\pm 5\%$  of  $\bar{x}$ .

The data obtained from testing ten 170 mg charges are plotted in Figure 7. The mean net volume,  $\bar{x}$ , is 5.05 ml. The value of  $1\sigma$  is  $3.7 \times 10^{-2}$  ml. and hence 68% of the charges can be expected to have net volumes between 5.013 and 5.087 ml. Based on  $2\sigma$ , it can be expected that 95% of the net volumes will fall between 4.976 ml. and 5.124 ml. which are within  $\pm 1.4\%$  of  $\bar{x}$ .

These results show that good consistencies have been obtained

with the lead blocks when measuring sample lots of explosives with high brisance characteristics.

## EXPERIMENTS WITH THE CONAX ENERGY MONITOR

### EQUIPMENT

A second group of experiments in EED energy measurements conducted at Conax Corporation employed a projectile and its deformable metal target. This device, shown in Figure 8, is known as the Conax Energy Monitor hereinafter referred to as the CEM. Its operation closely simulates the manner in which EED's are used to power Conax explosive-operated devices with their high metal-to-metal interference fitted rams. The high interference fit provides minimum initial volume confinement which promotes faster burning of the explosive charge with resultant higher peak pressures. Referring again to Figure 8 it can be seen that the assembled device consists of brass projectile, aluminum monitoring disc, gun barrel, anvil, body and EED test specimen.

The important factors in this design other than low cost are: - -

- (1) The uniform flared sealing lip which provides initial resistance to breakaway movement of the projectile until a high rate of combustion is well established. (The breakaway force required is 363 pounds or 4,700 psig pressure).
- (2) Control of the initial void volume between seated projectile

and EED is held to  $.003 \pm .0006$  cu. in.

- (3) Vydux dip lubrication of the brass projectile and the 17-4 PH hardened gun barrel minimizes frictional losses as the projectile moves one inch thereby increasing the confining gas cavity by .0769 cubic inch. (The frictional energy required to compress the 0.321 diameter flare while moving one inch through the 0.313 in. diameter gun bore approximates 2-1/3 foot-pounds when measured with a load cell and recorded on an X-Y plotter.) Tests of samples of Vydux in a pressure bomb demonstrated that this lubricant added very little fuel effect to the combustion.
- (4) Uniform hardness of the brass projectile is assured when the major flare diameter produced by a 2,000 lb. load transmitted through the 0.672" diameter ball, as shown in Figure 9, falls in the range of 0.320 - 0.325".
- (5) The 6061 aluminum alloy monitoring discs are annealed to produce a deflection of 0.120 inches when Vydux lubricated and pressed with a 2,000 pound force between two 1/4" diameter ground and polished steel balls. By maintaining proper hardness of the projectile and the monitoring disc, the ratio of their respective metal deformations is constant.
- (6) Recoil energy conservation is achieved by firmly fastening the anvil to the gun barrel by means of the body member. Any acceleration of the anvil is toward the projectile. Therefore, maximum deformation of the monitoring disc results without the need for massive anvil and gun barrel components.



## TESTING

EED energy testing with the CEM is simple and direct. It is simple in that only a 1/4" steel ball and a 1" micrometer are required to measure the resultant deformation of the monitoring disc. It is direct in that by referral to a conversion chart, equivalent foot-pounds of energy versus deformation can be obtained. The energy is calculated from the equation  $1/2 mv^2$ .

Figure 10 shows how the steel ball establishes a firm, repeatable position in the fired disc cavity for an overall micrometer reading. The micrometer readings before and after firing, while allowing for the 0.250" ball diameter, yield a differential which becomes the penetration measurement.

Data for the conversion chart was obtained from 14 EED firings. EED's with six different loadings were used. Included were extremes of the lowest and the most powerful units. The projectiles were carefully weighed prior to each firing. Velocity measurements were desired immediately prior to impact. A special CEM which differs from the device described above only by virtue of an increased body length was used in order to measure velocity over a greater distance. See Figure 11 which shows both the latter and the standard device.

After the projectile leaves the gun barrel in the special device, it travels 1-1/4" before impact on the disc. In this 1-1/4" of free travel are located two parallel nichrome contact wires, one-inch apart, to be broken by the projectile. Initially 0.003" diameter

when installed, they are drawn in tension so as to be of uniform resistance (just below their breaking point). Teflon guide bushings were used to maintain the 1" exact spacing. The breaking of the wires when contacted by the projectile applied sequential pulses to an Atec microsecond counter to produce a time differential.

These velocity measurements were used to calculate energy as stated above. These energy values with their related penetration measurements were then plotted on log-log graph paper to produce the straight line conversion chart shown in Figure 12.

### CONCLUSIONS

In plotting the straight line conversion chart, based on metal deformation, projectile mass, and velocity measurements, it appears that there may be some discrepancies in our wire break method of velocity measurement. One of the 14 points for this chart could have been in error by 5-1/2% in microsecond timing. All others were well within 2-1/2% of anticipated velocity based on penetration correlations. The curve should not be extended in either direction without additional velocity measurements.

Improvement in the microsecond timing might be possible by the use of laser beams and photodiodes in place of the tensioned wires. A counter capable of 1/10 microsecond increments would have been desirable when it is realized that the one microsecond pulser can produce better than a 1% possible error when the total count time is as

low as 86 microseconds. The possible effects of errors due to timing can be minimized statistically by increasing the number of tests used to establish the conversion chart.

It should be noted that the energy values shown on the conversion chart do not include the 2-1/3 foot-pounds of energy dissipated by the projectile as friction and deformation of the flare diameter while travelling in the gun barrel.

Portability of the equipment permits power output tests to be run with safety and uniformity at any location. Once the conversion chart has been prepared there is no need for any instruments other than the micrometer.

Brisance of the explosive is not a requisite for the EED's used in this device. It can be applied to deflagrating or detonating charges within structural strength limitations. The maximum energy that the 0.6 inch thick monitoring disc can accept is 350 foot-pounds.

More data *on* EED behavior can be obtained using this equipment or a modification of same if electronic instrumentation is added. For example, if it is desired to measure the time from application of firing current to initial projectile movement, an accelerometer can be attached to the gun barrel and its output, together with the firing current, can be recorded with an oscilloscope. With more elaborate instrumentation, the history of projectile acceleration with respect to both time and projectile travel can be measured.

### SUMMATION

For comparison purposes, a frequency distribution chart has also been prepared for the CEM using the 170 mg base charge primers employed in the Trauzl lead block tests. See Figure 13. We can now compare the relationship between the  $2\sigma$  and  $\bar{x}$  values for the two methods of test in which milliliters have been displaced in the Trauzl block test and depth of penetration as well as foot-pounds of energy are the related units in the CEM.

In the former test, the  $2\sigma$  deviation represents 1.4% of  $\bar{x}$  (ml.) while in the CEM, this ratio is calculated to be 3.76%.

A frequency distribution curve has been plotted as Figure 14, for the data obtained from firing 37 samples in the CEM. They were taken from five different manufacturing lots which accounts for the higher sigma value; 120 mg. charges were used.

Table 2 has been prepared below to make some further comparisons of the two methods of test. It compares DDNP primers at three different weight loadings. The ratios of the energies calculated in foot-pounds using the CEM device is precisely in agreement with the ratio of the total weights of the explosive charges while the ratios of the net displacements shown in the Trauzl lead block tests fall off rapidly as the charge weights decrease.

This indicates that the lead block tests depend upon brisance effects and that not all of the charge exerts a detonating force. On the other hand, these data show that the CEM utilizes all of

the available charge, regardless of its nature, and hence becomes a more valuable device for our purposes. The lead block tests would appear to be more appropriate for evaluation of large charge weights of detonatable materials and not for small EED's.

A photograph of some of the stocked components of the CEM, such as projectiles, monitoring discs, and replacement gun barrels, presently used in our tests, is shown in Figure 15.

#### REFERENCES

1. Menichelli, Vincent J., "A Review of Explosive Testing Output," Proceedings of Electric Initiator Symposium, The Franklin Institute Laboratories for Research and Development, (1963).
2. Lothrop, Warren C., and Handrick, Richard G., "The Relationship between Performance and Constitution of Pure Organic Explosive Compounds," Chemical Reviews, 44, Page 419 (1949).
3. Rinehart, John S. and Pearson, John, Explosive Working of Metals, Pergamon Press, The MacMillan Co., N. Y. (1963).
4. Cook, Melvin A., The Science of High Explosives, Reinhold Publishing Corporation, (1958).
5. Pollard, Frank B., and Arnold, Jack H., Aerospace Ordnance Handbook, Prentice-Hall, Inc. (1966).
6. McDonnell Aircraft Corporation, Measurement of Explosive Output Report E206, 15 November 1965.
7. Gordon, William E.; Reed, Everett F.; Lepper, Bessie A.; "Lead Block Test for Explosives," Industrial and Engineering Chemistry, Vol. 47, No. 9, Page 1794 (Sept. 1955).

#### DISCUSSION

Explosives used were on the propellant side (low explosives) rather than high explosives.

TABLE 1 EFFECTS OF HIGH EXPLOSIVES (REF. 3)

(ANON, MILITARY EXPLOSIVES, TM 9-1910, TO 11A-1-34,

DEPARTMENTS OF THE ARMY AND AIR FORCE, WASHINGTON, D. C. (APRIL 1955) )

EXPLOSIVE	BRISANCE MEASURE BY			RELATIVE POWER FROM BALLISTIC PENDULUM TEST (% TNT)	RELATIVE POWER FROM TRAUZI LEAD BLOCK TEST (% TNT)
	SAND TEST (% TNT)	PLATE DENT TEST (% TNT)	FRAGMENTA- TION OF SHELL (% TNT)		
TNT	100	100	100	100	100
Ammonium nitrate	-	-	-	-	56
50/50 Amatol	81	-	82	122	124
Composition A-3	107	126	150	132	-
Composition B	112	131	139	133	130
Composition C-3	112	114	133	126	115
Composition C-4	117	115	-	130	-
Explosive D	78	-	99	98	-
Haleite	109	121	134	136	122
50/50 Pentolite	114	121	131	126	122
52/48 Picratol	94	100	102	100	-
Picric Acid	101	107	-	109	103
PETN	129	127	-	145	170
RDX	124	131	-	150	170
Tetryl	114	-	121	128	129
70/30 Tetrytol	111	117	117	120	-
Torpex	122	120	126	134	131
80/20 Tritonal	97	93	91	124	

TABLE 2 COMPARISON OF DATA OBTAINED FROM THE  
LEAD BLOCK AND CEM TESTS

DIAZO PRIMERS			TRAUZL LEAD BLOCK TESTS		CEM TESTS FOOT-POUNDS	
BASE CHARGE MG.	TOTAL CHARGE MG.	% OF TOTAL CHARGE  250 MG. = 100%	ML. DISPLACE.	% OF ML. DISPLA- CEMENT  5.05 ML. = 100%	FOOT- POUNDS, 1/2 MV <sup>2</sup>	ENERGY %  182 FT-LB. = 100%
170	250	100	5.05	100	182	100
120	200	80	3.47	68.7	144	79.2
60	145	58	2.21	43.8	106	58.2

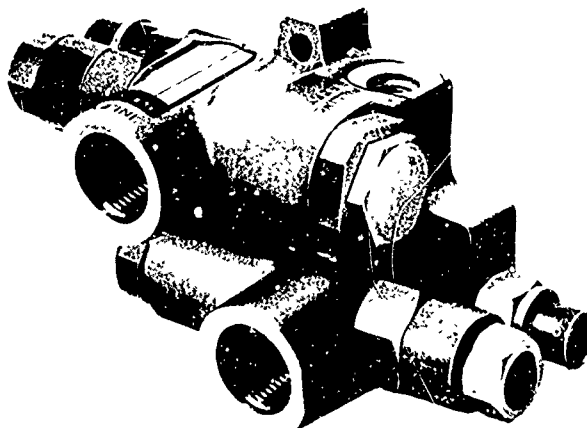


FIGURE 1: CONAX COMBINATION VALVE WITH  
FOUR EXPLOSIVE ACTUATORS

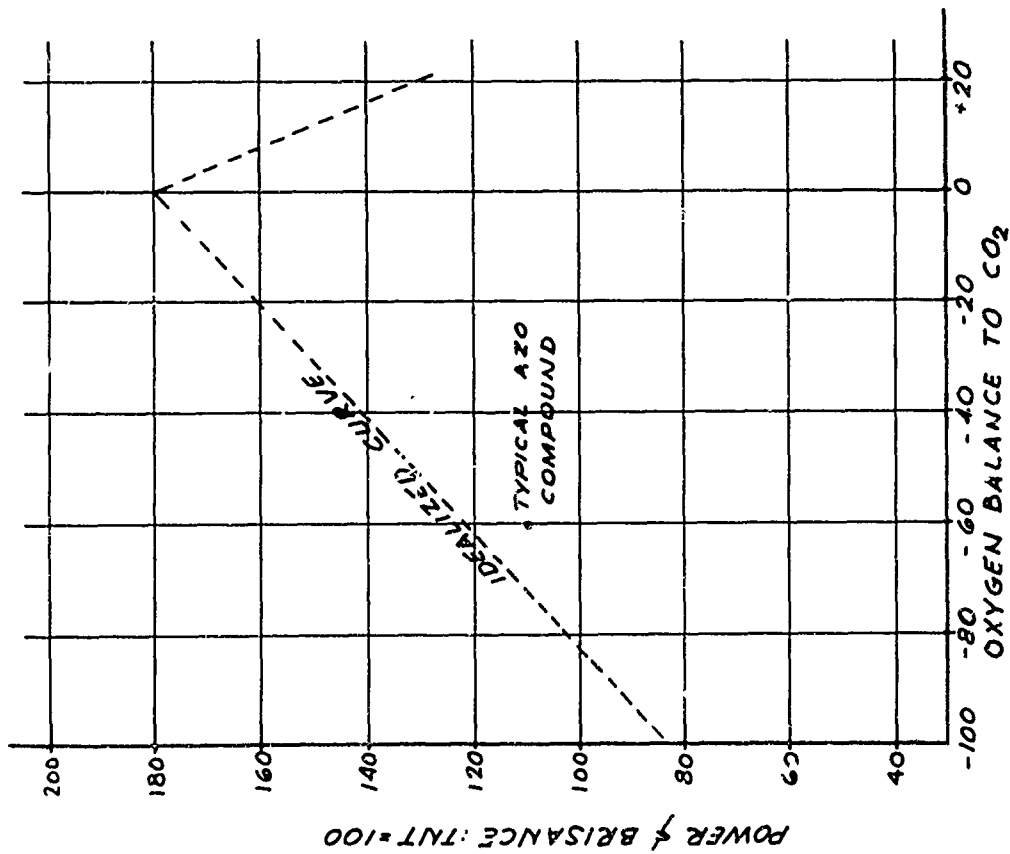


FIGURE 2: EFFECT OF OXYGEN BALANCE USING LEAD BLOCK TESTS (REF.3)

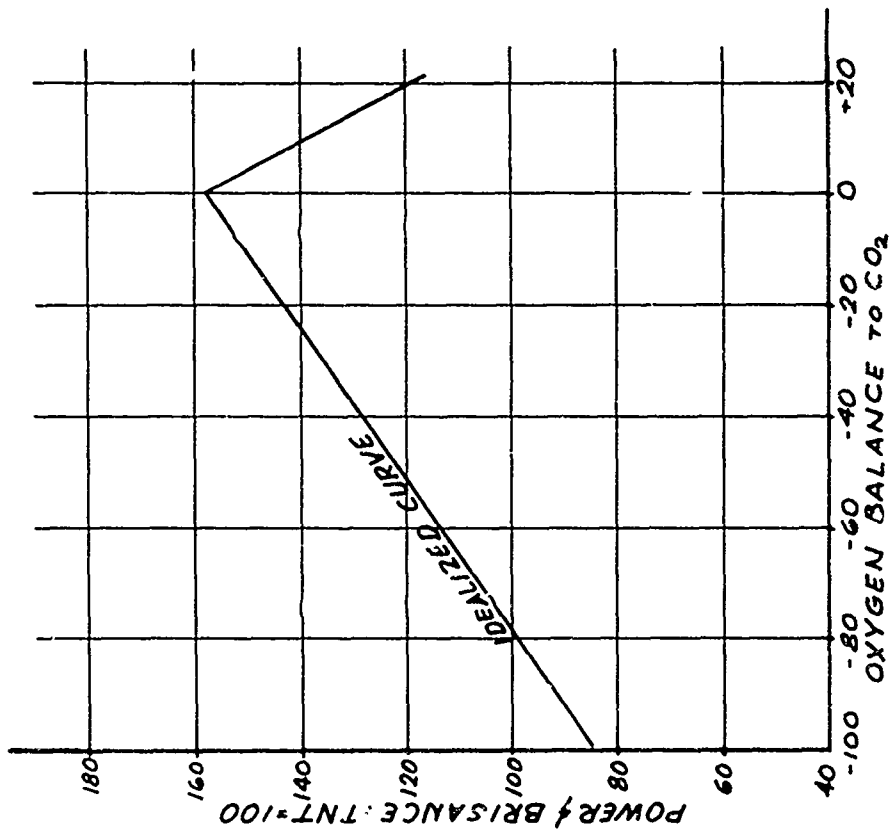


FIGURE 3: EFFECT OF OXYGEN BALANCE ON POWER & BRISANCE OF EXPLOSIVES USING BALLISTIC MORTAR (REF 3)



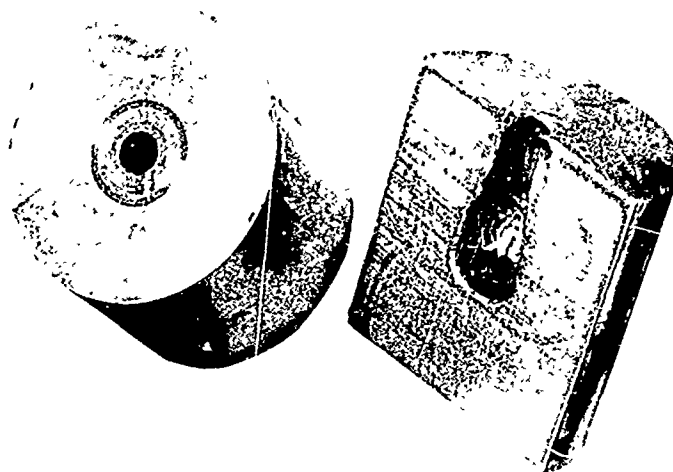


FIGURE 4: LEAD CYLINDER BEFORE FIRING AND CUTAWAY AFTER FIRING A 120 M9 CHARGE

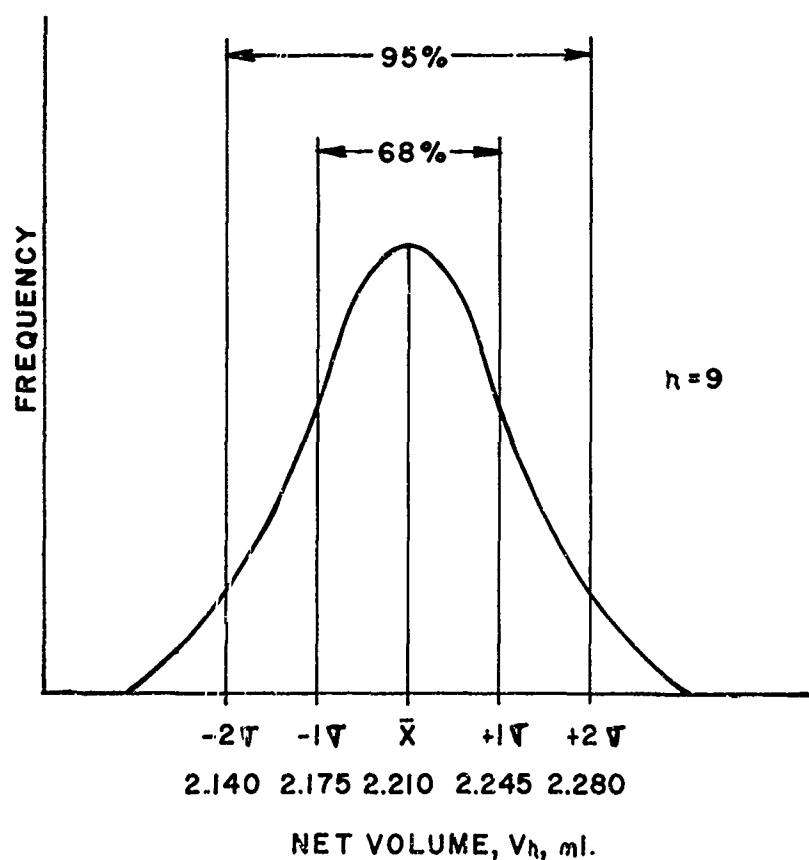


FIG. 5 FREQUENCY DISTRIBUTION CURVE FOR 60 M<sub>g</sub>. CHARGES (LEAD BLOCK TEST)

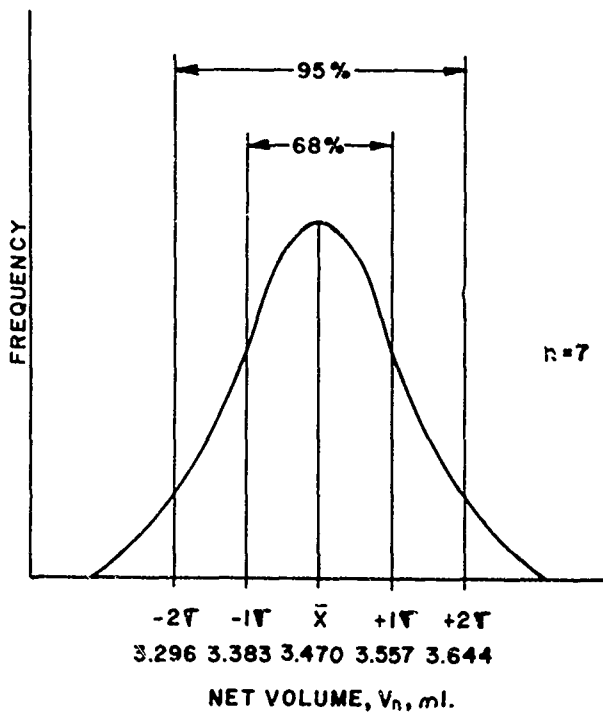


FIG. 6 FREQUENCY DISTRIBUTION  
CURVE FOR 120 mg. CHARGES  
(LEAD BLOCK TEST)

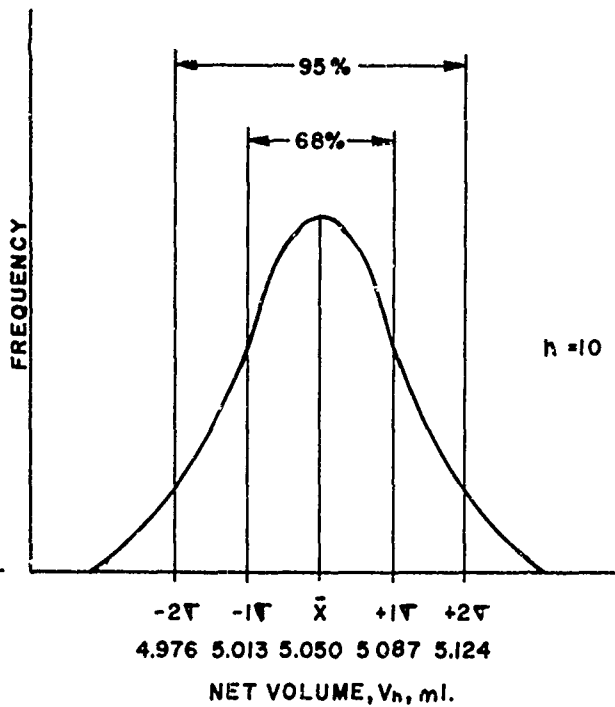


FIG. 7 FREQUENCY DISTRIBUTION  
CURVE FOR 170 mg. CHARGES  
(LEAD BLOCK TEST)

## CONAX ENERGY MONITOR (CEM) FOR CARTRIDGES

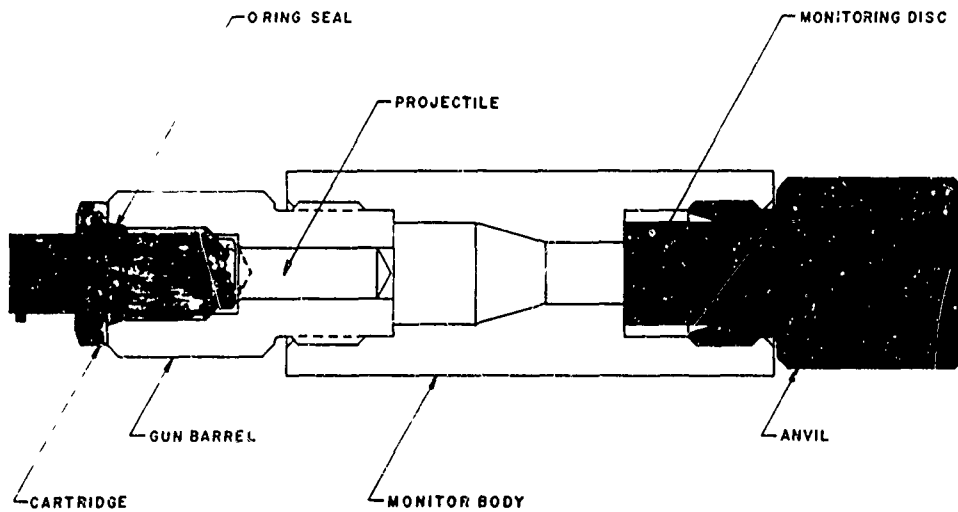
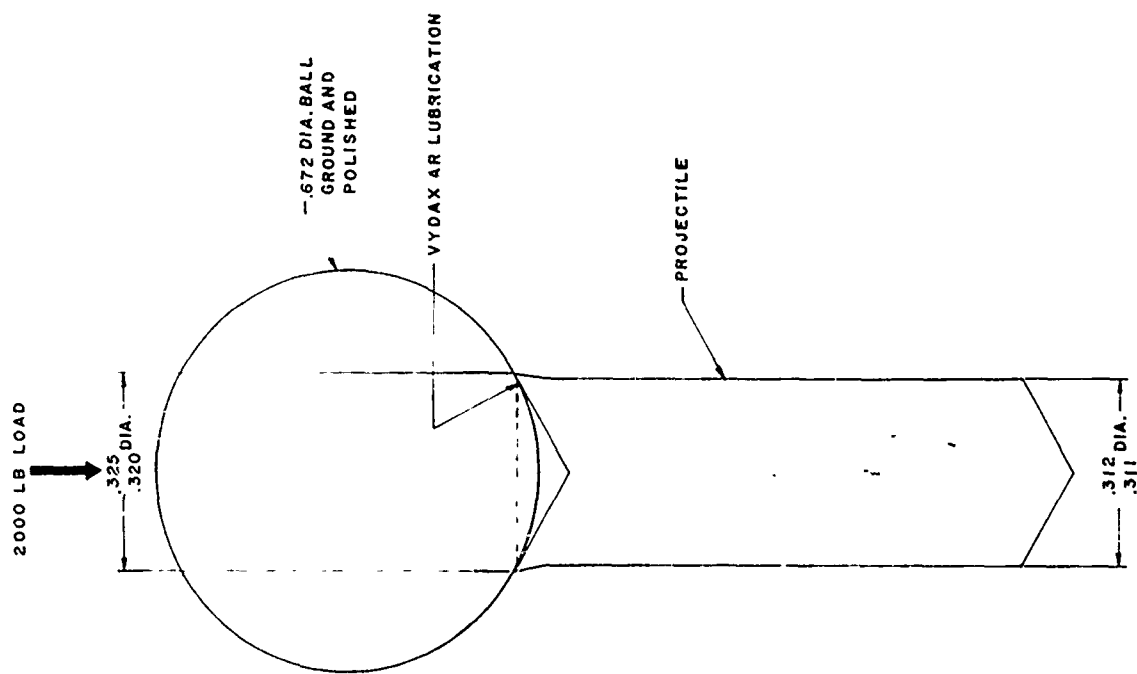
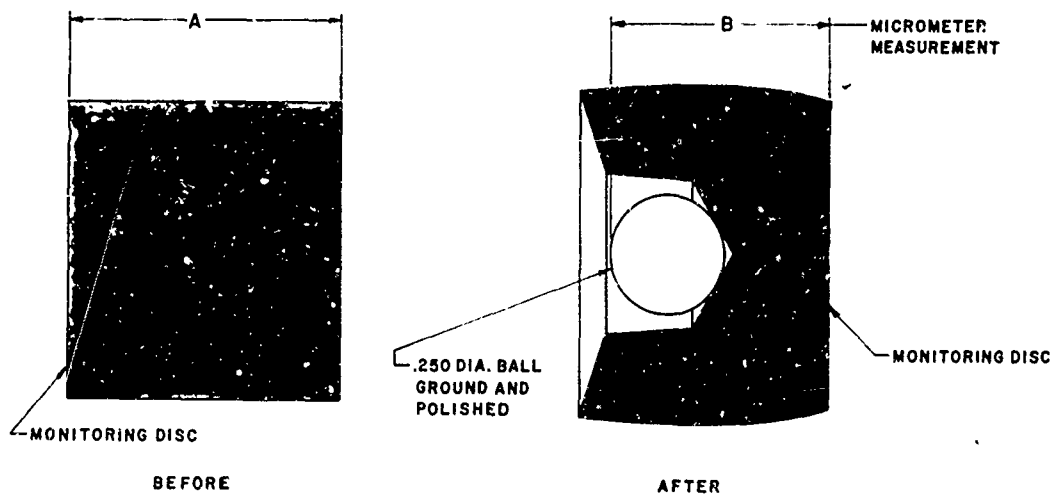


FIG. 8



BALL FLARING OF PROJECTILE  
FIG. 9

### MICROMETER MEASUREMENTS BEFORE & AFTER DEFORMATION OF DISC



$$\text{PENETRATION} = A + .250 - B$$

FIG. 10

2-9.21

# CEM CONVERSION CHART

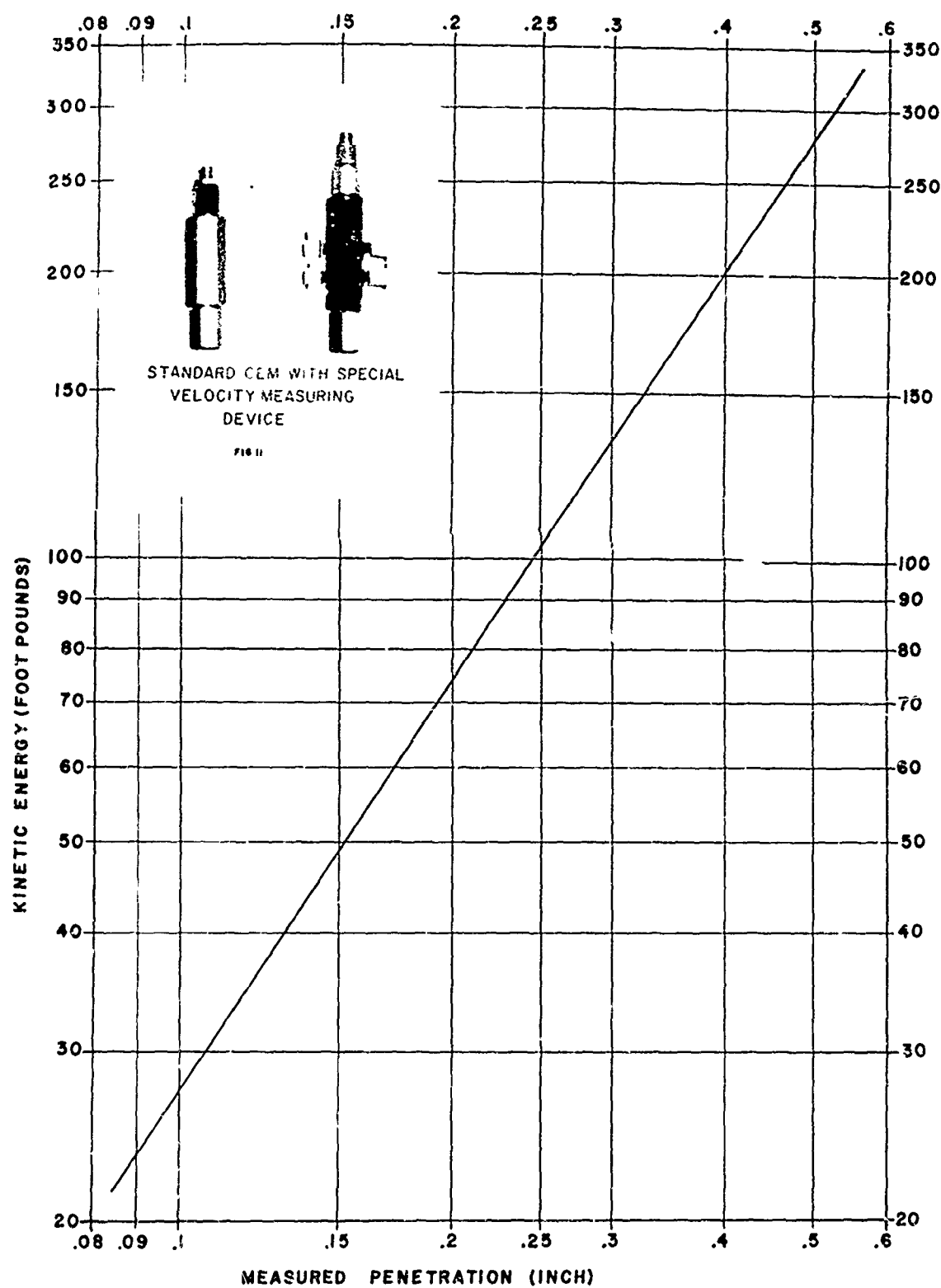
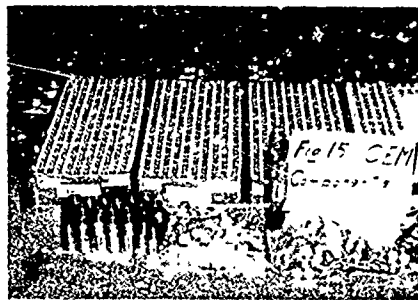
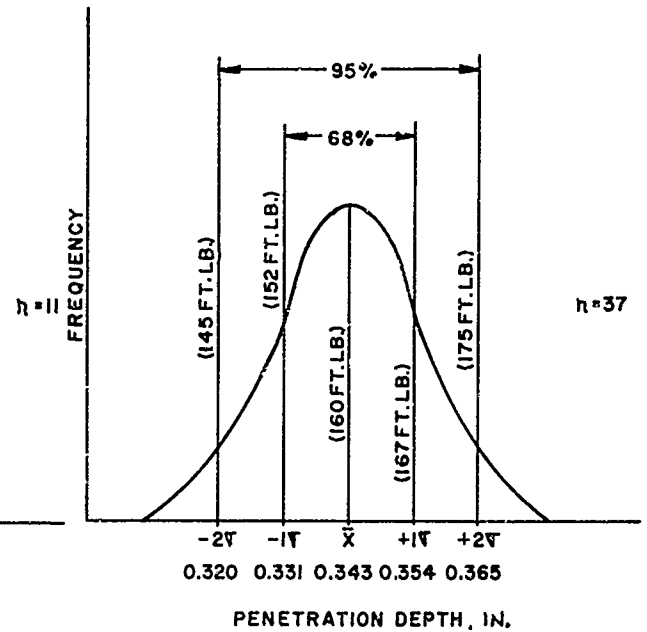
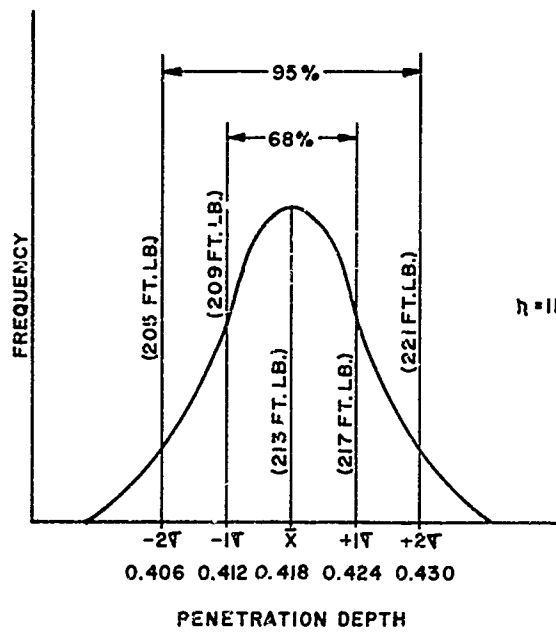


FIG. 12



## 2-10 USE OF NEUTRON RADIOGRAPHY FOR VISUAL NON-DESTRUCTIVE EXAMINATION OF ORDNANCE COMPONENTS

C. R. Wilson, General Electric Co.  
W. P. Breakey, McCormick Selph Corporation

### NEUTRON RADIOGRAPHY

This presentation describes the use of neutron radiography for visual non-destructive examination of ordnance devices. Before beginning, we will cover briefly, "just what is neutron radiography?" To do this, I will compare it with x-ray radiography. As you all know, x-rays are absorbed by objects at a rate depending on the density and thickness of the object. The denser and thicker the object, the more difficult it is to pass x-rays through the object. An x-ray negative, therefore, allows the inspector to view on film the density and thickness variation of the object.

Neutron radiography is quite different from x-ray radiography. To explain this difference, I will introduce you to a less known physical property of matter called cross section. You are probably more familiar with such physical properties as melting point, freezing point, density, etc. Cross section is similar to these basic properties of matter and all elements have a cross section just as all elements have a density. Cross sections of elements are in units called barns, which vary randomly and are completely independent of the density. It is this less known property of matter that makes neutron radiography different from x-ray radiography, thus a neutron beam is attenuated by an object at a rate depending on the cross section and thickness of the object and this rate of attenuation is independent of the object's density.

Figure 1 shows some common elements and compares x-ray attenuation rates with neutron beam attenuation rates to demonstrate just how different these two radiographic techniques are.

Notice that neutron attenuation rates are truly independent of density. For example, hydrogen, the least dense of all elements, attenuates neutron orders of magnitude better than lead or tungsten, which are among the heaviest elements. Also note, x-ray absorption rates vary about a factor of 30 from the lightest to the heaviest elements, whereas neutron beam

attenuation rates vary about a factor of 2000. This unique capability allows neutron radiography to image broad changes in materials and produces a negative with wide ranges of contrast.

To further compare x-ray radiography with neutron beam radiography, let's look at some actual radiographs.

Figure 2 shows radiographs of a toy train. Notice how well the dense metal components show up in the x-ray such as the steel track, the lead weights in the engine and coal car, and the steel wheels. On the other hand, these features are less dominant in the neutron radiograph, but notice how clearly nylon gears, rubber traction rings on drive wheels and the plastic engine structure stand out — items difficult or impossible to distinguish except in a neutron radiograph.

The basic mechanical process for taking a neutron radiograph is similar to that for x-ray radiography. The object to be radiographed is placed in a well collimated neutron beam. The neutrons are attenuated at different rates depending on the type of material present and its thickness. The resultant image is recorded on conventional x-ray film using either an indirect or a direct transfer foil screen. At our facility, General Electric Vallecitos Nuclear Center, we use both methods, but prefer the direct gadolinium transfer foil because of the inherent better resolution capability of this technique and the very low gamma field in the neutron beam. General Electric Company was the first commercial supplier of Neutrography\* Service and are leaders in this new technique. Our facility routinely produces very high resolution radiographs, 14" x 17" in size. Figure 3 shows the typical resolution that can be achieved at our facility. The slide is greatly enlarged and these small holes are about 0.7 mils in size.

The use of neutron radiography as an inspection tool in the ordnance industry is becoming a standard practice where zero defects are of paramount importance. At present, NASA and DOD either require or are investigating the requirement of neutron radiography inspection of ordnance components on critical programs and components.

\* Service Mark of the General Electric Company.

## USES OF NEUTRON RADIOGRAPHY AT McCORMICK SELPH

McCormick Selph, headquartered in Hollister, California is a supplier of a wide variety of ordnance components for many critical NASA, DOD and commercial *contracts*. They have put neutron radiography to effective use in establishing standards and assuring zero defect products. McCormick Selph, as a leader in this field, has selected the following slides to illustrate the many uses of neutron radiography they have adopted.

Figure 4 shows three time delays. The housing in this case is aluminum. Of particular interest is the small gap (shown by the light line) between the lead azide and lead styphnate charge in the unit at the left. This gap is also visible in an x-ray provided the unit is in the center of the beam and lined up properly. The center unit, however, shows a contaminant, probably epoxy (shown by the dark line) between the same two charges. This defect would have appeared as a small gap in an x-ray. The unit at the right is part of a failure analysis study made by McCormick Selph on this unit. Shown here is the result of a low yield detonation, which burned out the explosive in the transfer charge and silver sheath MDF, but failed to have enough force to rupture the shell and transfer over the gap to the next transfer charge. Other items shown in this figure are lead sheath Small Column Insulated Delay (SCID), which are the looped objects near the center of the device. Notice how well the explosive core is imaged compared to the lead sheath. Also shown are "O" rings and other hydrogenous substances in the parts.

Figure 5 shows several transfer connectors. In this particular figure, the units on top have been purposely contaminated with stearic acid. The bottom unit shows stearic acid contamination which is just barely visible on the tip of the transfer charge at the far right.

Figure 6 shows McCormick Selph's press pressure standards. The standards are arranged in groups of two and are arranged as follows, starting from the left:



<u>Pair Number</u>	<u>Press Pressure, psi</u>
1	25,000
2	20,000
3	15,000
4	10,000
5	5,000
6	2,500

As this figure indicates, the explosive density in ordnance components can be visually checked by neutron radiography. We reduced the information in this figure to densitometer readings and plotted this against press pressure and as shown on the graph in Figure 7, we received a fairly smooth curve which is quite steep at the higher press pressures and then leveling at the very low press pressures. The slight scattering of data is probably due to our difficulty in making an exact center line reading on these cylindrical samples.

It is also possible to use neutron radiography to determine the moisture content of explosive mixes. We were unable to prepare standards and reduce the data for presentation at this time, but we are confident moisture can be detected by this technique. It won't be possible, however, to tell the difference between press pressure and moisture as both will appear the same on a neutron radiograph.

Figure 8 shows McCormick Selph's Through Bulkhead Initiator (TBI). The units at the left have been loaded in the normal fashion with a ram pressure of 363-373 pounds force. The output explosive mix is a Ti/CuO mix and is not visible in a neutron radiograph because of its low neutron attenuation properties. The units in the center are loaded with the same amount of explosive, but in this case, the ram pressure is 400-410 pounds force. As you can see, the cavities are not completely full and it is obvious the mix has a much higher density than in the units at the left. The unit at the right is loaded in the normal way and in this particular unit, we loaded the output cavity with a 99% Ti/CuO - - - 1% GdO mix so the charge would be visible in the neutron radiograph. As shown, this slight addition of 1% gadolinium oxide (GdO) is ample to give a strong indication of the presence of this mix.

We calculated that as little as 0.5% GdO addition could be used successfully to image this mix in the TBI. Gadolinium oxide is quite inert and acts and looks much like alumina but has a higher density. The small additions needed to provide an image in a neutron radiograph should have little or no effect on the function of the device. Short and long term tests should probably be conducted to prove this point.

Figure 9 shows several pieces of nominal 8 grain/ft lead sheath SCID. Notice that the lead appears as a faint outline in the neutron radiograph and the powder core is readily visible. The two top SCID lines have been purposely drilled out on both ends and residual powder in this area can be seen clinging to the lead walls. The powder in the middle unit was completely drilled out and then attempts were made to fill it again to demonstrate the appearance of a low density load. As shown, the low density areas are clearly visible in this neutron radiograph. The second unit from the bottom is the control unit and the bottom unit shows what appears to be a void in the explosive core. This is actually a lead plug and hence, is not visible in the neutron radiograph. High energy x-ray inspection, however, would have picked up this type of contamination.

Figure 10 shows several samples of a simulated severance assembly booster with a ferrel cavity and booster cavity. These samples with purposely induced defects made by McCormick Selph, were radiographed with both x-rays and neutrons for comparative purposes. All the built-in gap defects are visible in the neutron radiographs whereas only a few are just barely visible on the x-ray radiograph.

Figure 11 shows several detonators made by McCormick Selph for the Saturn Vehicle. The detonator at the left has been left unloaded as a control unit. The two detonators at the right are loaded units included for comparison purposes. Note the difference in shading between the loaded and unloaded units. The fourth unit, SN 2119, was the subject of a failure analysis study. The failed unit shows a large void in the prime charge cavity which is the area indicated by the arrow LC. The void in the failed unit gave an indication prior to opening the unit that the bridgewire had

burned with sufficient energy to expel the prime charge, even though the detonator case was completely intact. Also visible is a crack in the phenolic prime charge cup as indicated by the vertical arrow.

### SUMMATION

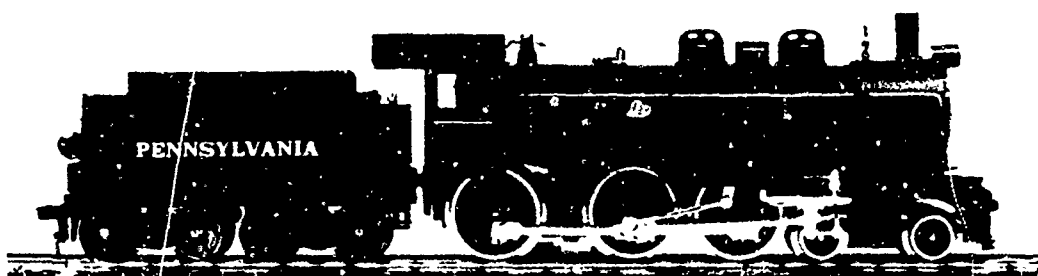
The use of neutron radiography as a failure analysis tool as well as a production inspection method has proven invaluable in many, many cases as it allows the investigator an opportunity to observe the internal details of a part prior to cutting into the unit and risking the loss of vital information.

Neutron radiography as a visual tool for nondestructive examination of ordnance components is becoming more a standard practice every day. We have shown here today some of the many places where McCormick Sulph has put this new tool to work to assure their customers of zero defect components.

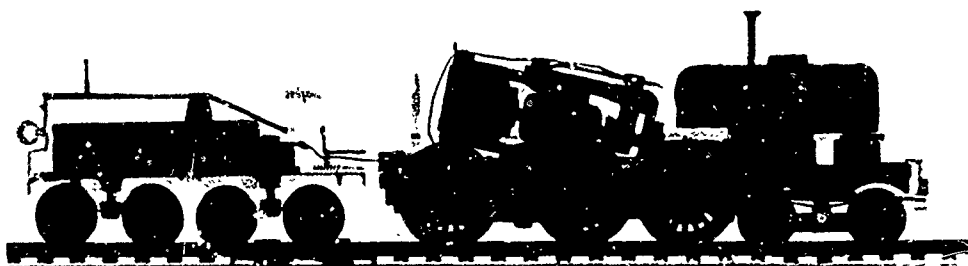
Figure 1. Absorption Coefficients

<u>Element</u>	<u>X-Ray</u>	<u>Neutron Beam</u>
Hydrogen	0.280	48.5
Beryllium	0.131	0.50
Boron	0.138	24.0
Aluminum	0.156	0.036
Titanium	0.217	0.119
Iron	0.265	0.141
Nickel	0.310	0.213
Copper	0.325	0.095
Zirconium	0.710	0.047
Silver	1.05	0.24
Cadmium	1.09	11.2
Gadolinium	2.08	84.0
Tungsten	2.88	0.058
Lead	3.50	0.034

FIGURE 2



PHOTOGRAPH  
HO SCALE LOCOMOTIVE



X-RADIOGRAPH



NEUTROGRAPH  
(GENERAL ELECTRIC SERVICEMARK)

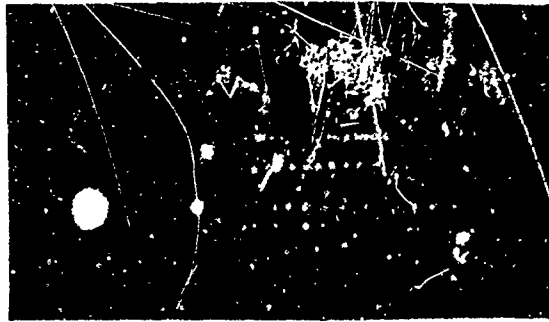


FIGURE 3

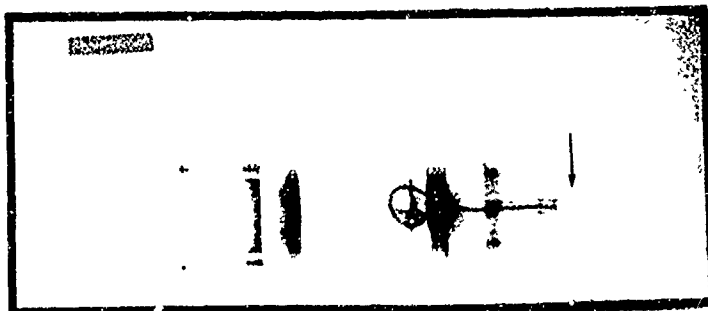
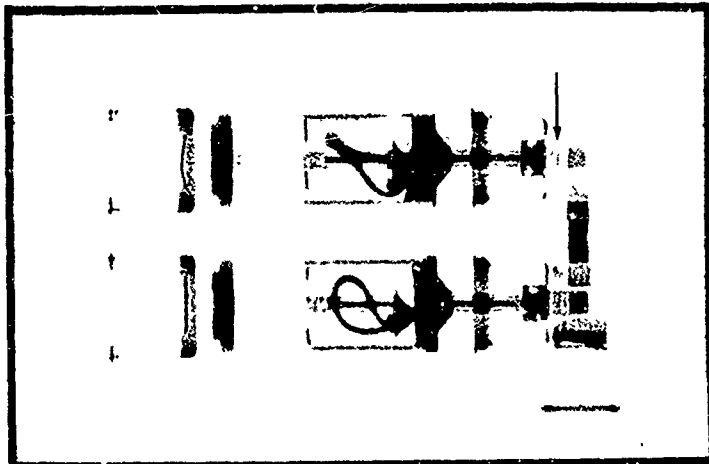
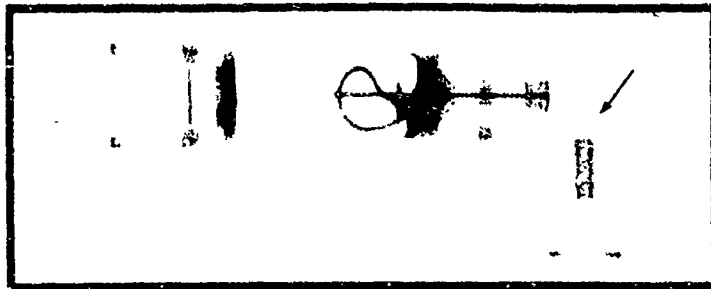


FIGURE 4

2-10.8

FIGURE 5

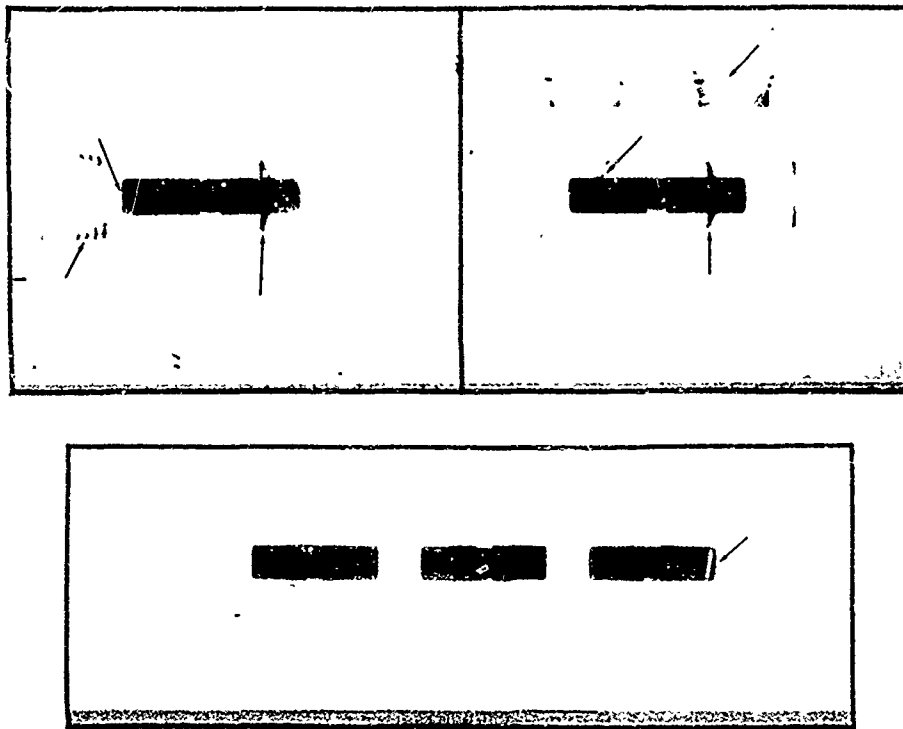


FIGURE 6

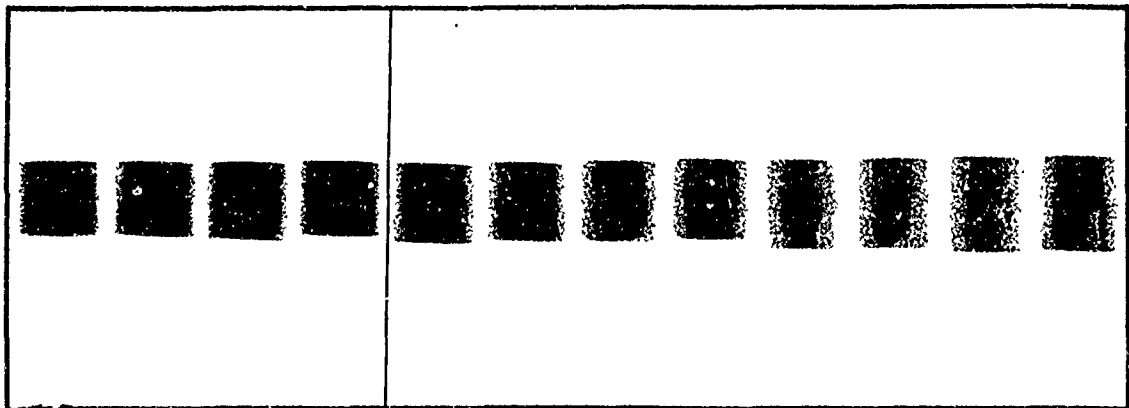


FIGURE 7.

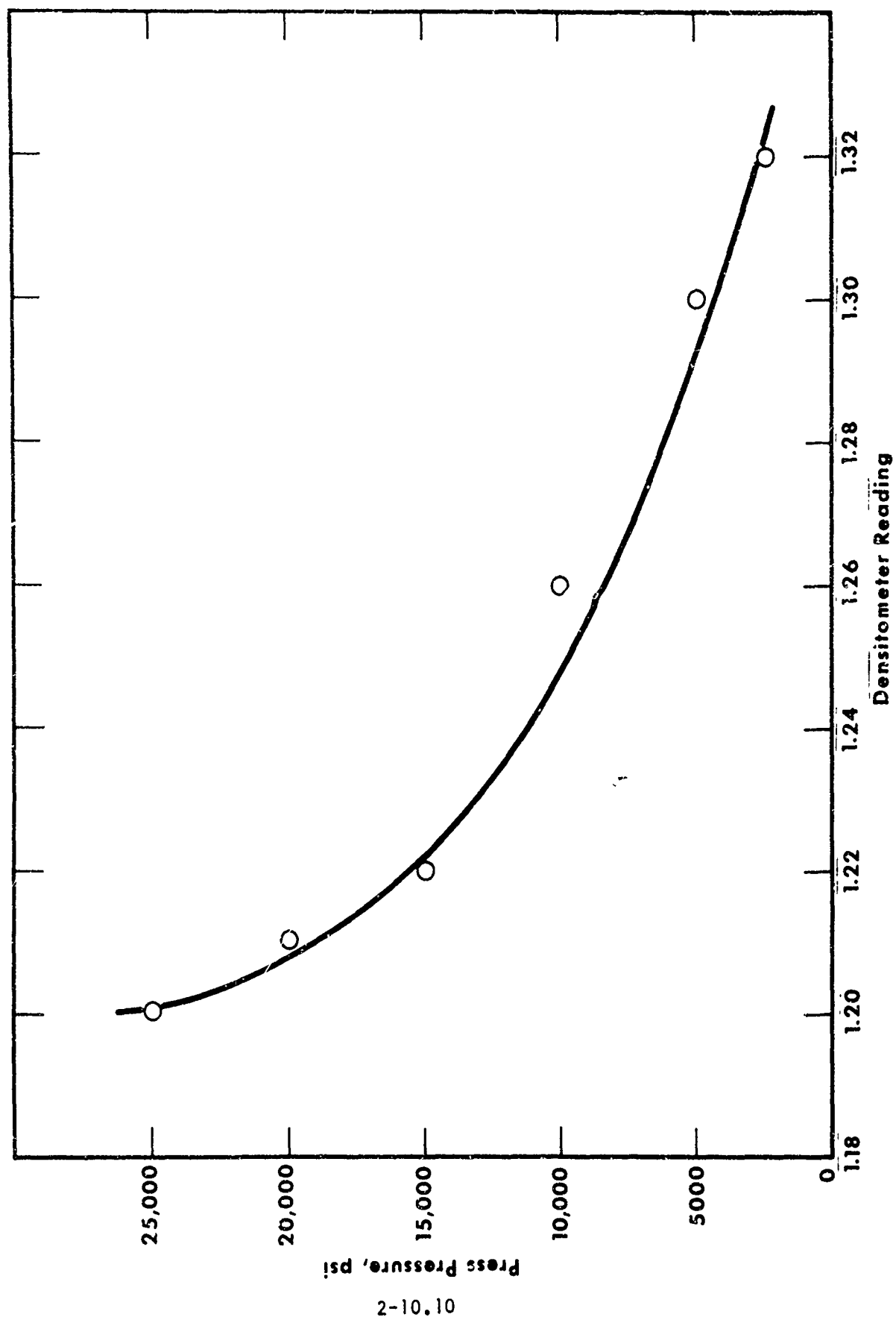


FIGURE 8

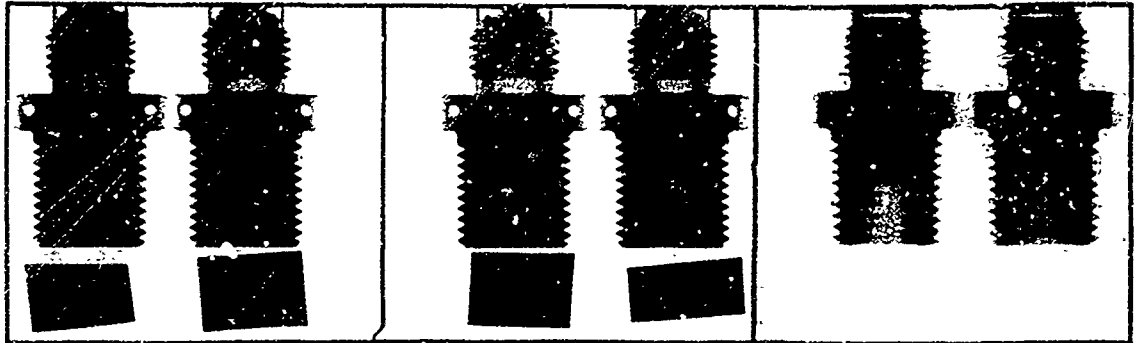


FIGURE 9





FIGURE 10

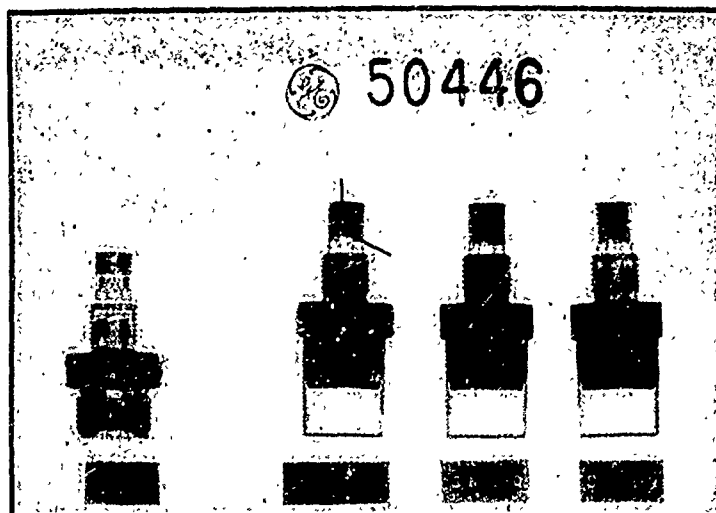


X RAY-RADIOGRAPH



NEUTRON RADIOGRAPH

FIGURE 11



## DISCUSSION

It is difficult to explain why certain materials tend to be opaque to neutrons and others nearly transparent. The property is a physical one like the freezing point of water. Presently, there is no answer to the reasons for neutron absorption; there may be some day.

The energy level required to produce damage in semi-conductors is on the order of  $10^{10}$  neutrons/sq cm/second.

Neutrons are collimated by pin holes most often, but tubes are also used. Neutrons are produced in a nuclear reactor. Neutron radiography produces almost one-to-one size scales on film plates and in this respect the technique is superior to those of X-rays which are of diverging beam.

Stop motion neutron radiography is being worked on by Mr. Charles Porter at Oregon State. Currently the facilities described cannot produce stop motion.

2-11 NONDESTRUCTIVE TESTING OF APOLLO CSM SPACECRAFT ORDNANCE DEVICES  
BY NEUTRON RADIOGRAPHY \*

W. H. Knight and A. L. Hitchens

Space Division

A Division of North American Rockwell Corporation

Downey, California

N. M. Ewbank and G. Gigas

Atomics International

A Division of North American Rockwell Corporation

Canoga Park, California

Nondestructive testing of Apollo CSM (Command and Service Module) spacecraft ordnance devices has been accomplished by indirect and direct neutron radiography using a 1 megawatt swimming pool reactor source. These examinations have shown discrepant loading, internal debris and contamination. A process specification has been developed for neutron radiographic testing and a certification program for n-radiographic film readers has been established. This method has proven to be an extremely powerful technique for analysis and portends much promise in the future development of new electroexplosive devices.

---

\* Work supported in part by the National Aeronautics and Space Administration.

## INTRODUCTION

Neutron radiography is a relatively new analytical and inspection technique rapidly gaining in variety and scope of applications, especially by the aerospace industry and defense contractors. It is new enough that standards of nomenclature, technique, and reporting methods have not yet been prepared, although it is anticipated that in the near future standardization will be initiated in the American Society for Testing and Materials (ASTM),<sup>(1)</sup> or the American Society for Non-destructive Testing (ASNT). For the present purposes of this paper then, we will use Webster's New International Dictionary (Second Edition) unabridged definition of radiography. Thus, (neutron) "radiography is the art, practice, or act of making pictures produced upon a sensitive surface, as of a photographic plate, by some form of radiation other than light," and, in this example, the radiation is produced directly or indirectly by the interaction of an uncharged particle of mass slightly greater than the proton with some material. The picture produced will, of course, be a negative, that is the density of the image will be inversely proportional to the absorptivity of the material located between the neutron beam and the sensitive surface.

## NEUTRON RADIOGRAPHY

Where the internal details of various materials or components are of interest, and where other non-destructive (NDT) methods such as ultrasonics, liquid penetrant, thermal examination, magnetic particle, and eddy current are unable to provide the inspection desired, radiography is a general technique considered. Neutron radiography has become an important complement

---

(1) Neutron Radiography Standardization Through the use of the American Society for Testing and Materials Facilities.

to the more common x-radiography (x-ray) technique. There is a marked difference between the electromagnetic (x-ray) and neutron attenuation characteristics of certain elements (and in most elements comprised of several isotopes there is a wide variation of neutron attenuation characteristics of isotopes within the element), this is one reason why neutron radiography (n-ray) results in vivid images with good resolution in many cases where x-ray cannot be used effectively.

In its general approach, n-ray inspection is very similar to x-ray inspection. The basic physical properties of the various elements result in a significant difference between the effectiveness of these two approaches when examining certain combinations of elements and materials. Although the mass absorption coefficients of different elements for x-rays generally increase directly proportional to the atomic number, the coefficients for thermal neutrons show no such proportionality, rather a "shotgun" pattern in a mass absorption vs atomic number plot can best describe this relation. The variation of neutron absorption coefficients for isotopes of the elements may be illustrated by considering the properties of the element uranium. For Uranium-238 the coefficient is approximately 0.02, while the coefficient for the uranium isotope that is commonly used for nuclear fuel, Uranium-235, is 1.9. Thus, the ability to differentiate between the isotopes of uranium can be very important in the nuclear ordnance area. In normal ordnance it serves as an example of an approach that might be useful in developmental studies.

Attenuation of electromagnetic radiation (x-rays) is determined largely by the electron density of the material being examined. In most applications of a practical nature, the x-rays undergo a scattering reaction with the atomic orbital electron cloud. The density of a material is, in general,

directly proportional to the electron density; therefore, x-ray attenuation is also proportional to the density of the material. Neutrons undergo two main types of reactions with atomic nuclei: absorption (capture) and scattering. The mass absorption coefficient for neutrons is thus a function of both the scattering and capture probabilities for each element. Hydrogen has the highest scattering coefficient, while some isotopes of boron, cadmium, samarium, and gadolinium have unusually high neutron capture probabilities. For this reason, hydrogenous or boron-containing materials can be delineated by n-rays from other elements in many cases where x-ray practices are inadequate. It is thus possible to delineate a hydrogenous (organic) or borated explosive sealed in a metallic container and to project an image of the explosive having excellent resolution and contrast, thereby distinguishing between the charge material, the imperfections therein, and its container. Current n-ray films do not as yet have the apparent crispness of x-rays because the organics are not normally machined as are the metallic portions that are revealed by x-rays and the films available are optimized for x-ray techniques. It appears that for certain converters the bulk of the n-ray image may not penetrate the entire depth of an x-ray emulsion. As a production technique, neutron radiography is in its infancy (~ 3 years) and extensive improvement in the areas of portability, speed and resolution can be expected.

The first step in preparing for n-ray examination of a new material or set of devices is to perform a preliminary analysis of the method and exposure combination most likely to achieve the specific goal desired. Among the many factors to consider during this step are whether to use the direct or indirect method of obtaining the image. Both direct and indirect method is normally used for production work at AI.

With the direct method, a cassette is made containing (from front to back) an opaque cover of aluminum or magnesium, an x-ray film with the emulsion on the back side, and a converter foil all sandwiched in a light-tight container. Gadolinium is one of the better converters for this purpose. The foil is exposed to the differentially absorbed neutron beam and serves as a converter screen, emitting radiation which exposes the film. The cover plate is transparent to the beam and has no measurable effect on the beam. The x-ray film scatters some of the beam but the scattering is rather uniform over the film and does not seriously affect the image. The neutron beam alone will not produce an identifiable image on the film in the time of the normal exposure. The gamma beam (x-ray) associated with the neutron beam does leave an image, therefore the final image is a combination due to x-rays and n-rays. Because of this x-ray component, films produced by this method give the illusion of being sharper than the indirect method produced films.

For the indirect method, non-prompt emitting converter foils are placed in the differentially absorbed and scattered neutron beam (which scattering is caused, of course, by the specimen in the beam prior to the foil). After a suitable exposure of a few minutes the irradiated converter foil may be transported to a dark room and exposed between two films. This part of the technique is known as auto-radiography, in which process the films are exposed by the differential radiation pattern emitted by the converter foil. Thus in the indirect method the film is not exposed to neutrons or the "noisy" environment associated with the interfering gamma radiation in the neutron exposure flux. The indirect method is the only method known for the radiography of radioactive specimens and is the method employed for the majority of the ordnance work at AI.

If neutron radiography is to be an industrially practical reality from a time and cost standpoint, a high-flux source of well-collimated thermal neutrons with preferably a low gamma (or x-ray) background is required. A thermal neutron is an uncharged particle with a very low energy (about 0.025 electron volts at room temperature). At the present "state of the art" only a reactor can provide the population of neutrons required for routine examination of parts in a practically realistic time scale. Several good facilities for performing neutron radiography are located at AI. The Shield Test and Irradiation Reactor (STIR) located in the Santa Susana mountains in California is the reactor normally used for high volume inspections. A cutaway view of the reactor is given in Figure 1.

Neutrons are born in the fission process with a high energy level (usually over one million electron volts) and are called fast neutrons. Absorption coefficients of the elements for fast neutrons form a curve very similar to that for x-rays; therefore, fast neutrons are not generally effective in discriminating between the various elements. The fast neutrons are 'slowed down' by passing through a material such as pure carbon that will reduce the energy of the neutrons with only minor reduction of neutron population. A certain amount of collimation takes place in this operation. The amount of thermalization can be determined in a number of ways. One of the easiest and least expensive methods uses a determination of the cadmium ratio. Cadmium effectively absorbs all neutrons with an energy of less than 1.0 ev with little effect on higher energy neutrons. Two gold foils are exposed to the neutron beam and one of the two is wrapped in cadmium (a soft metal). The radioactivity levels of the two foils are counted and the ratio of counts is termed the cadmium ratio. The higher the ratio the greater is



the population of the thermal neutrons. The cadmium ratio of the neutrons provided at the target by the STIR averages around 10.

The high power level of STIR and the attendant high thermal flux permits exposures of large radiographs, either singly or in sets, in short-time periods. The reactor is capable of operating steady state at a power level of one megawatt, but a typical exposure of 5-10 minutes is made at the 400 kilowatt operating level since this results in a thermal neutron flux of about  $4 \times 10^6$  neutrons per squared centimeter per second at the target area.

The test vault in which the exposures are made is about 40 ft by 20 ft by 30 ft high. The rack of specimens being exposed can be positioned perpendicular to the neutron beam as shown in Figure 2. For small Apollo ordnance devices, 10-20 sets of devices are normally exposed simultaneously, each set mounted on an 11-inch by 14-inch plate. Separate mounting devices are used for larger specimens such as Apollo explosive trains (ten or twelve feet in length).

#### PROCESS SPECIFICATION

The production work performed at AI is entirely North American Rockwell work in support of the NASA Apollo program. Preliminary engineering work was performed to provide input for the preparation of a process specification that could be used as a guide by both engineering and quality and reliability assurance groups.<sup>(2)</sup> The possibility of damage to the explosive was also

---

(2) MA-0222-0003A, "Neutron Radiographic Inspection of Apollo Ordnance," A. Hitchens and P. Reese, Space Division, North American Rockwell, 12214 Lakewood Blvd., Downey, California 90241.

investigated and found in general to be no problem of consequence. (3,4)

The specification, North American Rockwell, MA-02222-0003, covers the procedures for neutron radiographic inspection of Apollo ordnance devices to provide additional assurance that the pyrotechnic mixture is present and properly oriented and uniform from sample-to-sample. Specifications for ordnance equipment, handling storage, inspection procedures, and repackaging were already in effect.

The above specification also covers the details, limitations, and assignment of responsibilities relative to the actual neutron exposure. Full traceability is required. Numbers and letters as required to maintain lot and serial traceability (as required per component specification-part number, serial number, lot number and manufacturer's code number) must be identified with the test article to permanently identify the test article with the radiographic plate.

The integrated neutron flux per exposure by specification must not be greater than  $10^{10}$  neutrons/cm<sup>2</sup> per exposure and gamma exposure dose must not exceed  $10^3$  roentgens per exposure as measured by instrumentation whose calibration is traceable to National Bureau of Standards certification. If more than one exposure is made, the total exposure for explosive components and devices must not exceed  $3 \times 10^{10}$  neutrons per square centimeter and  $3 \times 10^3$  roentgens of gamma or x-ray.

- 
- (3) Atomics International Internal Letter from N. M. Ewbank dated October 4, 1967, "Review of Radiation Effects on Explosives as Related to Neutron Radiography."
- (4) Trip Report by N. M. Ewbank, "Symposium on Radiation Effects on Propulsion Systems and Explosives, February 7, 8, and 9, 1968 at Lockheed Palo Alto Research Laboratory."

Two positive prints of the neutron radiographs are obtained; however the radiographs are not exposed for a printing optimum density. Quality Control inspection interpretation is made on the neutron radiographic negative and the Quality Control personnel require a dense negative. The prints which are limited to about 10 per cent of the density scale range of a film are used in a data pack to show the engineer at the installation point that the part has been neutron radiographed and inspected. It had been observed that engineers and technicians do not look at negatives; while they do look at prints. A major problem during the first half-year was keeping enough rejected prints available to satisfy souvenir hunters.

#### INSPECTION CERTIFICATION

A film interpreter certification program was initiated at both AI and the North American Rockwell Corporation Space Division (SD). After long hours of discussion among research, engineering, production, and quality assurance groups, it was decided that the most important qualification for a film interpreter was a past history of performance as an inspector (x-ray) with demonstrated flexibility to adapt to the peculiarities of neutron radiography. Past experience with ordnance would be helpful because at that time acceptance/rejection gauges had not been developed for neutron radiography. At the present time these are slowly evolving. It was agreed that the interpreters would have to be trained in the nuclear aspects of this relatively new procedure. The book, "Neutron Radiography" by Harold Berger, Elsevier Publishing Company, Amsterdam, 1965, was used as the basic text (actually the only text available). Instruction was a cooperative effort of the ordnance group, reactor operations group and research group. Instructions covered about a four-month period and achievement testing was

performed, both at AI and SD. By the end of this period the engineering studies had been completed and we were ready for routine inspection of Apollo ordnance.

## INSPECTION RESULTS

### 1. Discrepant Loading

The ability of n-ray quality control inspection to verify the presence of explosive loading non-destructively, as well as the ability to assess discrepancies in the loading such as voids or inclusions, explosives outside of design areas, etc. is readily apparent from the viewing of the radiographs, Figures 3 through 7. In practice, considerations of high cost and schedule impact make it inadvisable to radiograph the subject again at  $\pi/2$  orientation to preclude any possible error due to anomalies in film, printing or development. A discrepancy in loading may take the form of a discontinuity between initiator and other charges. In practice, engineering gauges must be set up and used to set a lower limit on acceptability standards to avoid excessively high rejection ratios.

### 2. Non-Explosive Discrepancies

It may occur in practice that a foreign inclusion may be present in, or a non-explosive supporting material may be absent from a region of interest in an explosive device. Or, as mentioned under the previous section, the discrepancy may involve a discontinuity (sometimes as a separation) between parts or separation in the same continuous entity as shown in Figures 8 and 9. Such non-explosive discrepancies are not difficult to locate in presently supplied ordnance devices due, in part, to the sensitivity of the neutron inspection techniques. Sometimes residual protective greases applied by a device case supplier are not thoroughly removed by the manufacturer loading the device; such irregularities are easily seen in the radiograph. Other

discrepancies involving epoxy, silver solder, sealants or "O" ring materials are also vividly apparent.

#### CONCLUSIONS

That neutron radiography can be a most effective tool for the non-destructive inspection of explosive devices has been well substantiated here by example. Present day production facilities can use neutron radiography where the requirements of high reliability can justify the attendant costs involved. A suitable large reactor facility operating at high capacity can minimize these costs. In the area of research and development for the explosives industry the utility and value of this technique cannot be overestimated.

As has been mentioned in this paper, state-of-the-art improvements in sources, converters, detectors and display systems will make neutron radiography a tool of increasing power, utility, and scope for the future.

### SHIELD TEST AND IRRADIATION (STIR) FACILITY

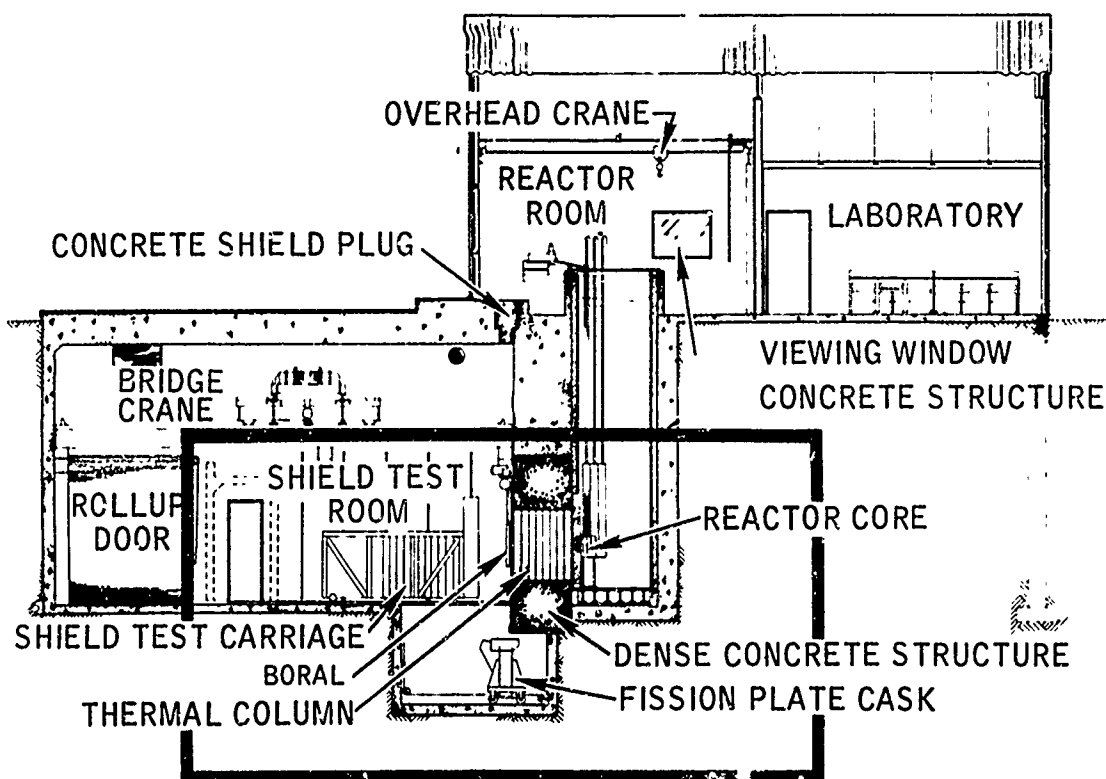
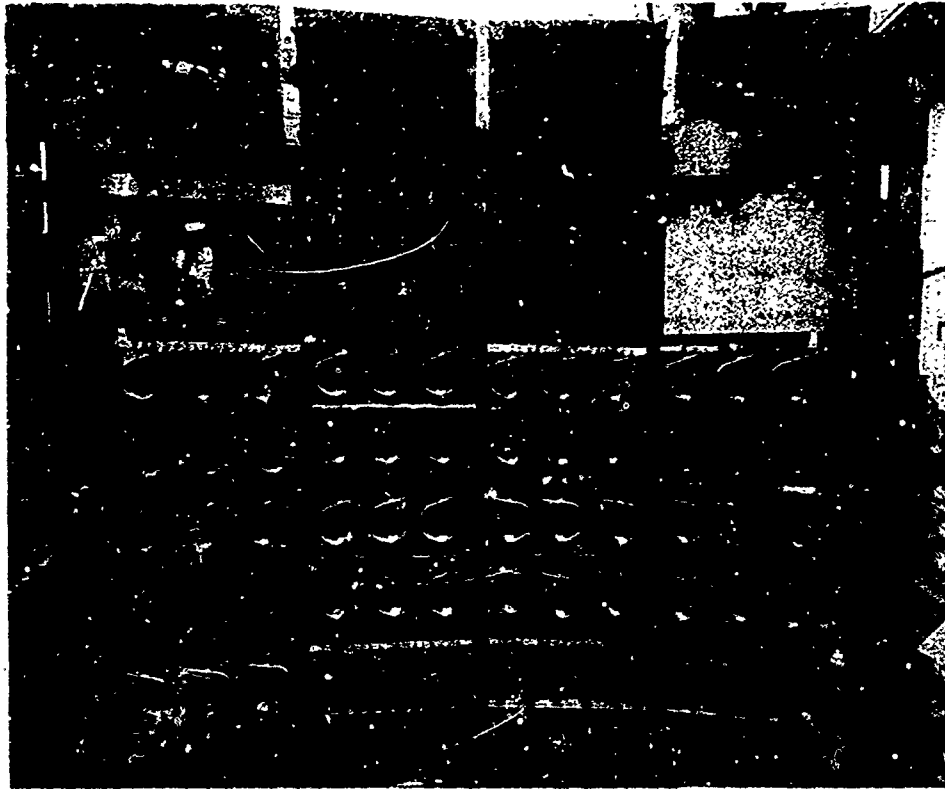


Figure 1



SPECIMEN EXPOSURE TEST RACK  
Figure 2

## NEUTRON RADIOGRAPHY OF SOLID ROCKET MOTOR FUEL

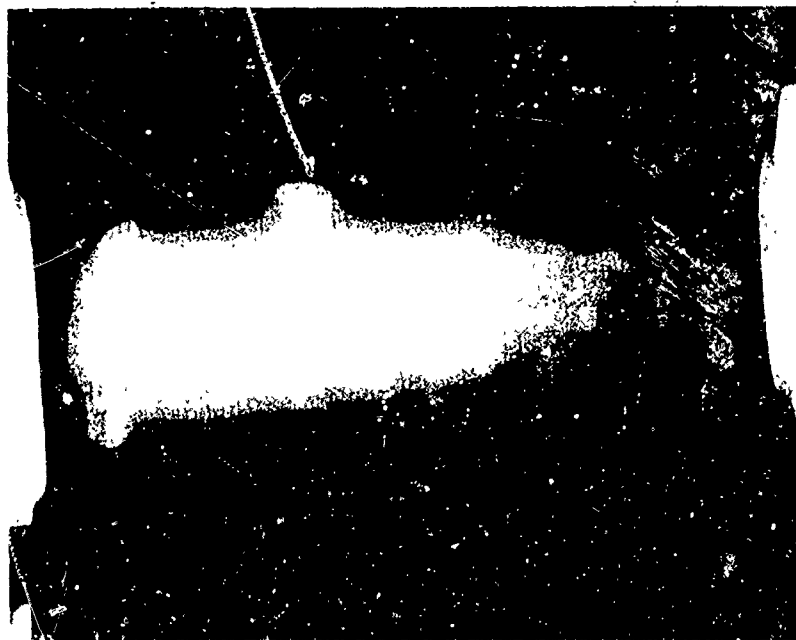


Figure 3

2-11,12

# ENLARGED NEUTRON RADIOGRAPH OF EXPLOSIVE DECOUPLER

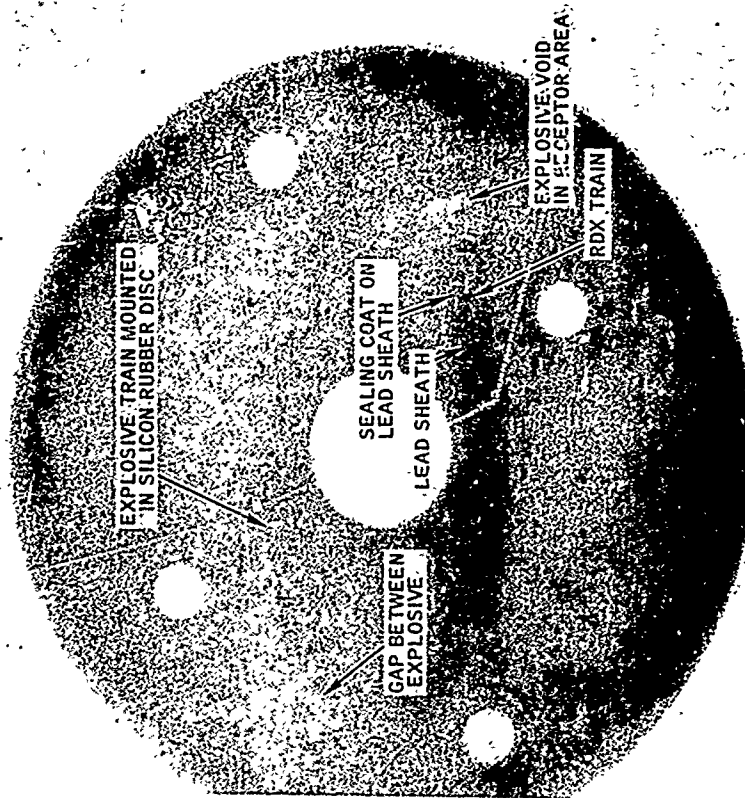


Figure 5

# POSITIVE RADIOGRAPHS OF CONFINED DETONATING CORD BOOSTER END ASSEMBLY

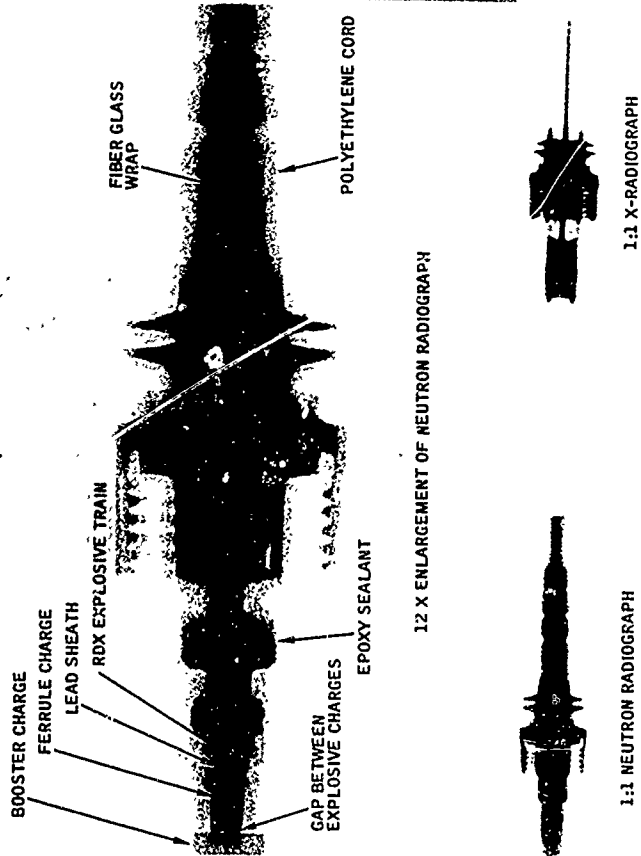


Figure 4

## COMPARATIVE RADIOGRAPHS OF AMMUNITION

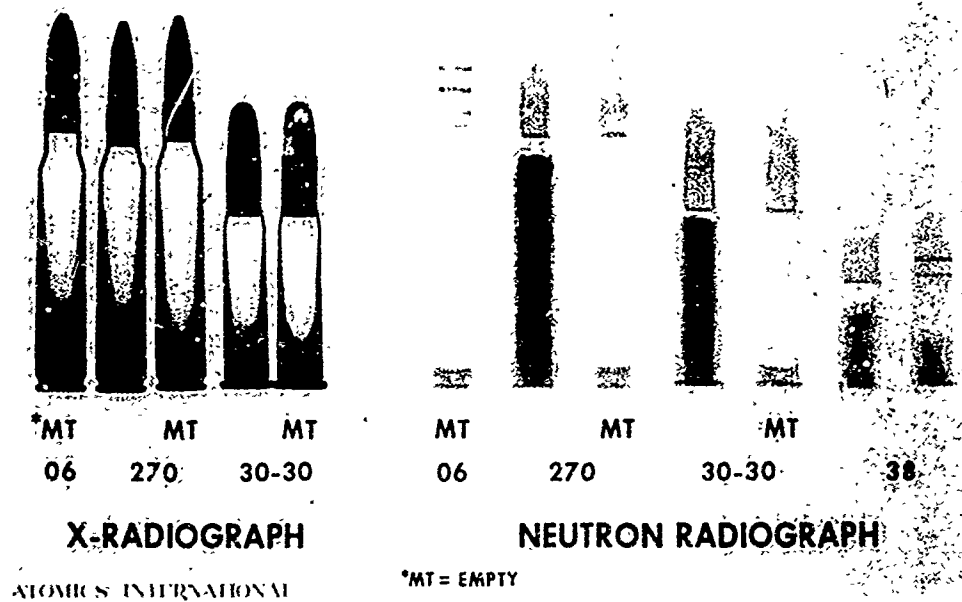


Figure 6

## NEUTRON RADIOGRAPH OF COLT 45 AUTOMATIC

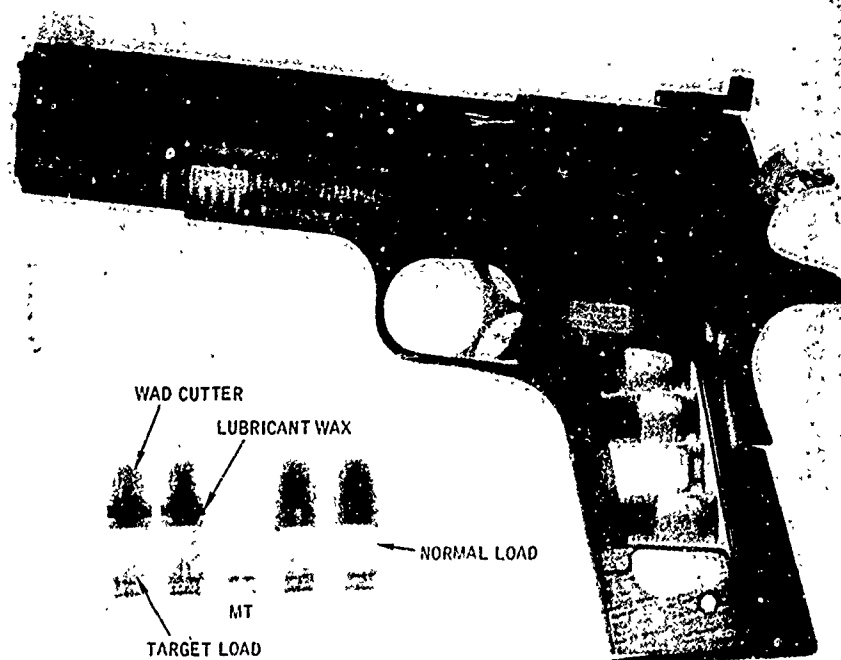


Figure 7

2-11.14



# COMPARATIVE RADIOGRAPHS OF EXPLOSIVE COUPLER

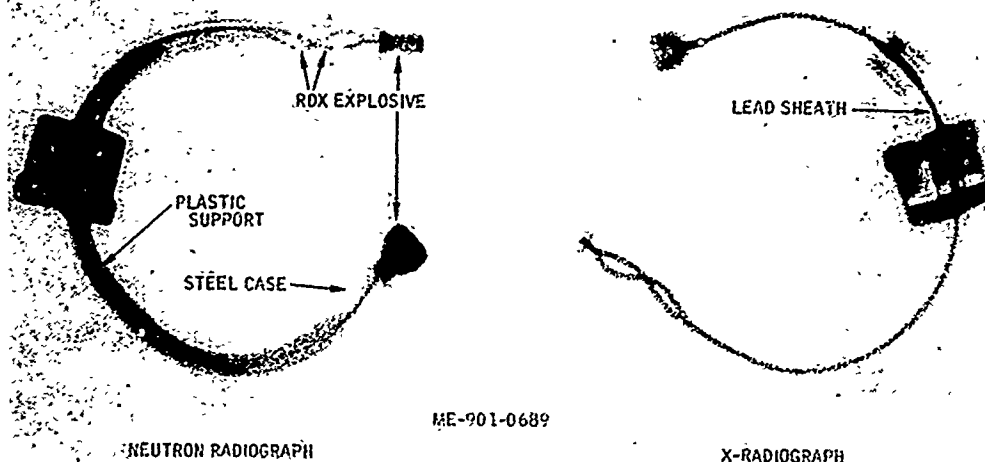


Figure 8

# POSITIVE NEUTRON RADIOGRAPH OF EXPLOSIVE COUPLER

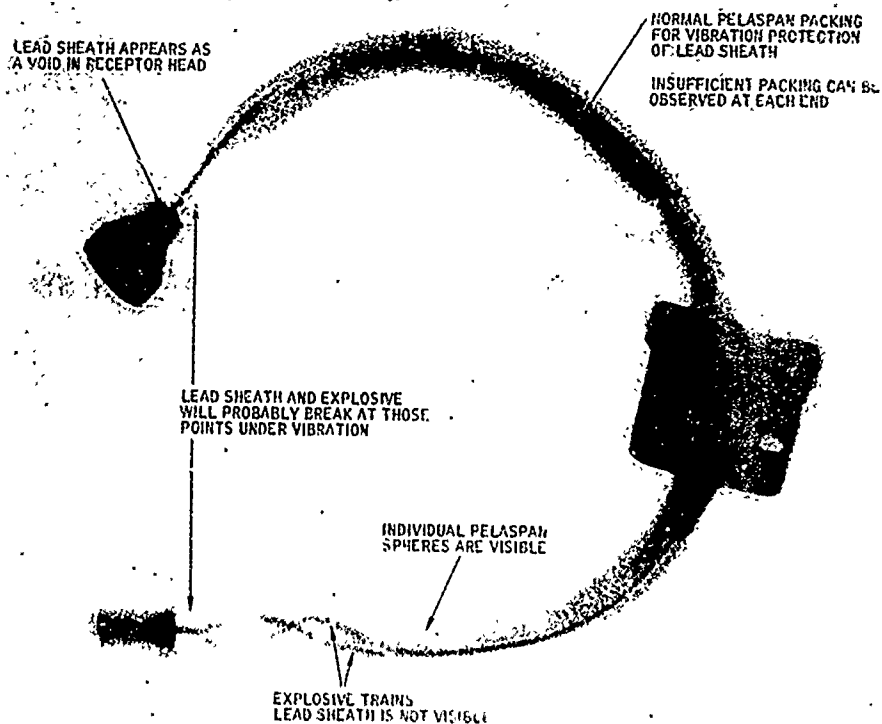


Figure 9  
2-11.15

## DISCUSSION

In order to reduce costs it was suggested that a portable neutron source be considered. This suggestion was countered with the statement that pictures can be made with radioisotope or accelerator sources but the quality of pictures taken in this manner suffers.

The time required for taking pictures with a typical radioactive source may be as long as six hours. Large volume of work can make neutron radiography cost comparable to X-ray.

The motor cycle sequence was made using indium. Gadolinium foil has been used earlier but has been abandoned in favor of indium because of costs.

It was mentioned that NASA has neutron radiographed about 90% of the parts used on Apollo. Such things as voids in foam used to back up MDF could be detected using this technique. The use of neutron radiography was highly recommended.

It was further added that detonator faults were readily detected by neutron radiography that could not be seen using conventional X-ray methods.

## 2-12 THROUGH-BULKHEAD INITIATOR DESIGN MARGIN STUDY

WILLIAM B. FREEMAN

ORDNANCE DEPARTMENT

MARTIN MARIETTA CORPORATION

ORLANDO, FLORIDA

### INTRODUCTION

The design reliability of a through-bulkhead initiator explosive train was studied from data gathered in a parametric test program. The initiator is shown in figure 1 and consists of: 1) an RDX donor charge which is initiated by an exploding bridgewire; 2) a steel body containing a bulkhead which passes the shock output of the detonating donor charge without rupturing; 3) an RDX acceptor charge which is initiated by the shock passed through the bulkhead; and 4) an output charge which is initiated by the acceptor charge and is used for ignition of solid propellant. The reliability of such a design hinges on the margin that the shock transmitted through the bulkhead exhibits when compared to the shock sensitivity of the acceptor charge. The design margin study described in this paper was precipitated by a number of random failures that occurred in a series of several hundred initiator firings. These failures to transfer detonation through the bulkhead were not related to fabrication errors, contamination, or environmental conditioning. The study shows that the original design, which had been formulated on an intuitive basis, was definitely marginal. However, the study also shows that highly reliable designs can be formulated if correct tests are conducted to establish an adequate energy balance between the shock transmitted through the bulkhead and the sensitivity of the acceptor charge.

### GENERAL APPROACH

The through-bulkhead initiator concept<sup>\*</sup> was broken down into three elements (donor, bulkhead, acceptor) as shown schematically in figure 2. The conditions at each of the two interfaces between the elements were studied by conducting three series of tests which produced relative measurements of:

- 1 Donor charge output;
- 2 Shock attenuation through steel bulkheads;
- 3 Shock sensitivity of acceptor charges.

The program included approximately 450 firings. The effects of changes in charge length, density, RDX particle size, bulkhead thickness, bulkhead material, and acceptor charge diameter were studied.

Throughout this paper, test results and interface condition are expressed in terms of "pressure". It must be emphasized that this is an arbitrary use of a term to conveniently define a shock pulse entering or leaving the interface under consideration. The pressure values shown were computed from approximations based on steel dent test results or on copper crusher gage compression calibrations. As such, the values are highly dependent on the test method and the absolute values may not compare well with pressure readings obtained by other methods. However, the values are adequate for the purpose of the overall study program because they are only used to show the relative effects of variations in the explosive trains which were tested.

Detonation velocity versus column length was investigated in RDX donor charges initiated by an exploding wire and in RDX acceptor charges initiated by through-bulkhead shock. A resistance wire technique was used and continuous plots of reaction front position versus time were obtained. These plots were used to determine the minimum column length required to reach stable conditions in the donor and acceptor elements.

<sup>\*</sup>McCormick Selph Associates, Inc., holds U.S. Patent 3,238,876 entitled "Method for Through-Bulkhead Shock Initiation."

## EXPERIMENTAL PROGRAM

### 1. Donor Charge Output

Pressure generated by donor charges were established from steel dent test data. The general arrangement for each donor charge test is shown in figure 3. All charges studied were 0.175 inch diameter columns with high density sections pressed in steel confining sleeves by a one increment stop-loading technique. Charge weights were held within plus or minus one milligram of the desired weight. The low density section (adjacent to the bridgewire) of each charge was loaded to a density of 0.9 g/cc with 62 milligrams of EBW grade RX which has a specific surface area of 4150 cm<sup>2</sup>/gram. The bridgewire used for initiation in each test was gold with a diameter of 0.0015 inches and a length of 0.040 inches. The following variables were studied in the high density section of the donor charge:

- 1 RDX grade (specific surface area)  
1270 cm<sup>2</sup>/g, 4150 cm<sup>2</sup>/g, 4650 cm<sup>2</sup>/g
- 2 Charge length, .090, .125, .175 inches
- 3 Loading density, 1.55, 1.65 g/cc.

High density sections loaded in two increments were also tested but results were not significantly different from the single increment tests.

Dent blocks were grade 1020, ASTM A108 steel, Rockwell hardness B70 to B95; dents resulting from detonation of the donor charges were measured according to MIL-STD-316.

For each possible combination of variables, six test shots were fired and the resulting dent values were averaged for use in the pressure approximation. The average dent value for a particular set of variables was converted to detonation velocity using an empirical relationship (figure 4)

taken from the U. S. Army Explosive Charge Design Handbook <sup>(1)</sup>. These velocities were used in the approximation <sup>(2)</sup>

$$P_d = .00987 P \frac{D^2}{4}$$

where:

$P_d$  = detonation pressure, atmosphere

$\rho$  = density, g/cc

$D$  = detonation velocity, meters/second

to estimate the equivalent donor charge output pressure.

Results are shown in figure 5, which is a series of plots of donor charge output pressure,  $P_d$ , versus the length of the high density donor charge section. A separate curve is shown for each RDX grade and loading density. These plots constitute the reference data that will be used in the bulkhead attenuation measurements.

Based on the results of the donor charge tests, four charge designs spaced through the range of pressures observed were selected for use in determining shock attenuation characteristics of bulkhead materials. The designs selected were:

Charge design, <u>High density section</u>	<u><math>P_d</math>, K bar</u>
1.55 g/cc .175 x .090 4650 cm <sup>2</sup> /g	90
1.65 g/cc .175 x .090 1270 cm <sup>2</sup> /g	104
1.55 g/cc .175 x .175 4650 cm <sup>2</sup> /g	121
1.65 g/cc .175 x .175 1270 cm <sup>2</sup> /g	146

## 2. Shock Attenuation Through Steel Bulkheads

Pressure transmitted through a steel bulkhead and entering the interface between the bulkhead and the acceptor charge was determined by detonating a donor charge on one face of a bulkhead and measuring the resulting compression of a copper crusher gage in contact with the opposite face of the bulkhead. The general arrangement for each of these tests is shown in figure 6. Test bulkheads were slipfitted into steel alignment tubes and were supported by a steel sleeve on the downstream face of each bulkhead. Donor charges were prepared as described in the preceding section and then were pressed to contact the upstream side of each bulkhead. Each loaded alignment tube was installed in a holding fixture and a copper crusher gage was adjusted and supported to contact the downstream face of the bulkhead. The following bulkhead materials and thicknesses were tested:

<u>Material (Stainless Steel)</u>	<u>Thickness, inches</u>
Type 302	.125, .150, .170
17-4 PH, H1150 heat treat	.125, .150, .170
17-4 PH, H900 heat treat	.125, .150

Each combination of material and thickness was tested with all four of the donor charges selected in the donor charge output tests described above. For each possible combination of variables, six test shots were fired. Copper crusher gages were 0.2225 inch diameter x 0.400 inch cylinders purchased from Olin Mathieson Chemical Corporation. Tarage table 326 furnished by Olin Mathieson, relates permanent deformation to incident pressure. After each test firing, the compressed length of the crusher

gage was measured and the corresponding pressure value from the Tarage table was recorded as  $P_t$ , the pressure transmitted through the bulkhead. Values for each set of variables were averaged and the standard deviation was calculated.

The transmitted pressure data ( $P_t$ ) were plotted against various arbitrary functions of donor charge output and bulkhead thickness for each material in a cursory search for a near straight line transfer function. The relationship finally chosen was a plot of  $P_t$  versus  $\frac{P_d^{1/3}}{t}$  where:

$P_t$  = pressure entering bulkhead/acceptor interface, pounds per square inch

$P_d$  = donor charge output pressure (pressure entering the donor/bulkhead interface), Kilobars

$t$  = bulkhead thickness, inches.

Results for type 302 stainless steel bulkheads are shown in figure 7 and are typical of results obtained with all of the steels tested. For each set of variables, an average value of  $P_t$  is plotted along with a plus and minus three sigma spread. Because no gross differences were noted among the three materials, data points were combined, disregarding material difference.

Straight lines were fit to the data, resulting in the overall transfer function shown in figure 8 which relates pressure transmitted through a stainless steel bulkhead to donor charge output and bulkhead thickness.



### 3. Shock Sensitivity of Acceptor Charges

Sensitivities of two acceptor charge designs were determined by Bruceton testing with fixed (0.175 inch diameter) RDX donor charges and incrementally varying bulkhead thickness. Knowing the output of the donor charge and the thicknesses of the bulkheads, the through-bulkhead transfer function (figure 8) was used so that the sensitivity of each acceptor charge design could be expressed in terms of  $P_t$ , which has been defined as the pressure transmitted through the bulkhead and entering the bulkhead/acceptor interface. The general arrangement for each of these tests is shown in figure 9. Acceptor charges were pressed into steel confinement bushings by a one-increment stop-loading technique. Charge weights were held within one milligram of the desired weight; pressed charges were flush with both ends of each bushing. Bulkheads were slip fitted into steel alignment tubes. The close fit between the bulkhead and alignment tube prevented blow-by from the donor charge. Acceptor and donor charges were inserted into the alignment tubes and were pressed to contact opposite faces of each bulkhead. Each loaded alignment tube was positioned on an aluminum witness plate so that the downstream face of the acceptor charge was in contact with the plate. In this position the acceptor bushing supported the bulkhead. After each firing, a dent in the aluminum plate was used as the "Go" criterion to indicate that the acceptor charge had been initiated.

All donor charges had high density sections loaded with 1270 cm<sup>2</sup>/g RDX pressed to a density of 1.65 g/cc in a .175 x .175 column. Donor charge output tests described above have established that the output ( $P_d$ ) of this design is 146 Kbar.

The shock pressure ( $P_t$ ) incident on the acceptor charges was varied on successive tests in the Bruceton series by varying the bulkhead thickness in 0.01 inch increments. Unfortunately, this does not correspond to a uniform increment on the  $P_t$  scale. Nevertheless, the Bruceton calculations were made in terms of  $P_t$  (from transfer function, figure 8, using  $P_d = 146$  Kbar and  $t$  = test bulkhead thickness) rather than in terms of the bulkhead thickness. Judgement was exercised in selecting the values of increments for use in the standard deviation calculations.

The shock sensitivity of an acceptor charge design is identified as  $P_a$  which is defined as the shock pressure corresponding to the 50% firing point in the Bruceton test. Thus the terms  $P_a$  and  $P_t$  have the same units and they can be compared to each other on the same relative scale.

Bruceton test data and calculations are shown in tables 1 and 2. Acceptor charge designs which were tested are described below along with their sensitivity values.

	<u>Configuration A</u>	<u>Configuration B</u>
Design		
RDX grade	4150 cm <sup>2</sup> /g	1270 cm <sup>2</sup> /g
Loading density	.97 g/cc	.97 g/cc
Dimensions	.055 x .250 dia.	.219 x .125 dia.
RDX weight	42 mg	42 mg
Shock Sensitivity (K psi, relative scale)		
$P_a$ (50% firing prob)	31.9	23.9
$P_a + 3$ (99.87% firing prob)	51.6	25.2
$P_a - 3$ (0.13% firing prob)	17.1	22.5

#### 4. Detonation Velocity Versus Column Length

Reaction front velocity (deflagration or detonation) in each element of a typical through-bulkhead initiator explosive train was determined by a method based on work described by Pitts <sup>(3)</sup>. The initiation of low density explosive charges by relatively weak shocks begins with a deflagration phase during which the velocity of the reaction front increases. It accelerates until reaching the stable velocity characteristic of the detonation phase. The test charges were similar to the: 1) low density section of the donor charge; 2) high density section of the donor charge; and 3) acceptor charge, except that the columns were long enough to ensure that each test charge would reach detonation velocity. Each test charge was initiated by the method used to initiate it in the actual initiator design (e.g., the acceptor test charge was initiated through a bulkhead).

The experimental arrangement is shown in figure 10. High resistance wires were placed along the inside walls of brass cylinders. The wires, which were 0.0012 inch diameter nichrome (450 ohms per foot) with enamel insulation, were shorted to one end of the brass cylinder but were insulated from the cylinder along the length to be studied. After the wire was installed in a test cylinder, the explosive was loaded to the desired density by stop-loading in 0.250 inch increments. Final length of the explosive column was 1.188 inches in each test.

A constant current was applied through the high resistance wire to the brass cylinder during each test. As the reaction front progressed through the explosive column, the wire was progressively shorted to the cylinder.

Thus, effective resistance, and consequently the voltage, was a function of reaction front position at any given time. This change in voltage with time was presented on an oscilloscope which was triggered by the electrical pulse to the exploding bridgewire which initiated the explosive train. Velocities and stabilization conditions were determined from the oscilloscope traces. In the case of the low density donor charge section and also in the acceptor charge test, the stabilization distance was confirmed by distinct changes in the expansion and fracture patterns in the brass cylinders. Complete fragmentation of the cylinders used in the high density donor section tests prevented a similar comparison for that element.

Oscilloscope traces for each explosive train element are shown in figure 11. Results are summarized in table 3. All charges tested required a run of 0.17 to 0.20 inches to reach steady detonation conditions. Only one grade of RDX, 4150 cm<sup>2</sup>/g, was tested.

#### DESIGN ANALYSIS

The data gathered in the experimental program permit a straightforward analysis of the design margins in a family of RDX loaded through-bulkhead initiators. The margin of  $P_t$ , the pressure transmitted through the bulkhead, over  $P_a$ , the pressure required for acceptor charge initiation, is the critical area from a reliability standpoint. In addition, the length of the acceptor charge should allow the reaction front to build to stable detonation velocity to insure reproducibility.

Figure 12 summarizes the analyses of two designs. Configuration A is the design shown in figure 1; configuration B is a proposed high-reliability design based on observations in the experimental program. The interface

conditions are shown in terms of pressures on arbitrary scales as defined in the experimental program. The donor charge output pressure,  $P_d$ , for each design was determined from figure 3; the pressure transmitted through the bulkhead was determined from figure 8 and the acceptor charge sensitivity,  $P_a$ , corresponds to the Bruceton test data for that particular charge design. The ratio of  $P_t$  to  $P_a$  for each design is indicative of reliability.

	$\frac{P_t}{P_a}$
Configuration A	0.97
Configuration B	1.45

Thus, configuration B shows a large margin of  $P_t$  over  $P_a$  and this design is considered reliable. Test history of configuration A confirms the low reliability indicated by a  $P_t/P_a$  ratio of less than unity.

Design reliability can also be evaluated from figures 13 and 14. Here, the Bruceton test data for the acceptor charge is plotted on probability paper as firing probability versus pressure transmitted through the bulkhead,  $P_t$ . The plus and minus 3 sigma values of  $P_t$ , taken from figure 8 for a given donor charge design and bulkhead thickness, can be evaluated against the pressure required to produce a given firing probability. This technique shows (figure 13) that configuration A is unreliable even with the highest  $P_t$  values probable in that design. Figure 14 shows that configuration B should be highly reliable even with the lowest value of  $P_t$  probable in that design.

The acceptor charge length of configuration A is 0.055 inches. According to the velocity tests in the experimental program, this is considerably less than the column length required to build velocity to stable conditions in the acceptor charge. Configuration B acceptor charges are long enough to achieve steady detonation; this was confirmed by the deformation patterns observed in the acceptor charge confinement bushings during sensitivity test.

### CONCLUSIONS

A series of tests requiring simple instrumentation provided sufficient data to estimate the performance of a family of RDX loaded through-bulkhead initiators. Acceptor charge sensitivity values are referenced to an arbitrary standard. The usefulness of the data can be expanded by testing other acceptor charges or other explosives and referencing the data to the same standard copper gage compression scale. The type evaluation presented, or its equivalent, should be imperative for any through-bulkhead initiator design if good reliability and a sound design basis are desired. The type of testing which has been described also should be used to determine the acceptability of various explosive material lots which may be used during the manufacturing life of a particular design.

The experimental program confirmed that the shock sensitivity of RDX is significantly affected by its specific surface area. The relationship of donor charge diameter to acceptor charge diameter also influences acceptor charge sensitivity.

Obviously, more sophisticated instrumentation methods such as streak cameras, quartz transducers, etc., could be used to perform the same types of tests with greater accuracy. However, the evaluation program which has been described was designed to provide a general understanding of the through-bulkhead detonation transfer mechanism with a minimum of capital investment.

### REFERENCES

- 1 AMCP-706-379, "Explosive Charge Design - Engineering Design Handbook, "U. S. Army Munitions Command, Picatinny Arsenal, Dover, N.J.
- 2 Cook, M. A., "The Science of High Explosives," Reinhold Publishing Company, New York, 1958.
- 3 Pitts, L. D., "Electrical Probe Technique for Measurement of Detonation and Deflagration Velocities," Fourth Symposium on Detonation, ACR-126, Office of Naval Research

# DISCUSSION

Post-fire pressure requirements for TBI are 5000 psi of nitrogen with no noticeable leakage under water. It was mentioned that the final design had a 0.150 inch wall, considerably thicker than earlier models. Some fissures were evident after metallographic working and polishing that extended about 1/3 of the wall thickness; none have ever penetrated the wall.

Similar tests have been made over a number of years using units with no acceptor charge. The same incipient spall line and no blow throughs.

TABLE 1 BRUCETON TEST RESULTS  
ACCEPTOR CONFIGURATION "A"

JUNIOR: 146 KBAR

ACCEPTOR: .055 x .250 Dia., .97 g/11, 4150 cm<sup>2</sup>/g RDX

BULKHEAD THICKNESS: Variable

Bulkhead thickness (t)	P <sub>t</sub> PSI	Firing Number																		N <sub>x</sub>	N <sub>o</sub>	i	1N	1 <sup>2</sup> N
		1	2	3	4	5	6	7	8	9	10	11	12	13	14	15	16	17	18					
0.150	35.0													x		x		x		3	0	4	12	48
0.160	33.0	x									x		o		o		o		o	2	4	3	6	18
0.170	31.0	o	x							o	o									1	3	2	2	4
0.180	29.3			x					o											1	1	1	1	1
0.190	27.7				x	o														1	1	0		
0.200	26.4					o															1			
																				8				
																				N				
																						21		71
																						A		B

x = acceptor initiated  
o = acceptor not initiated

P<sub>t</sub> increment = 2.0 from P<sub>t</sub> = 29 to 35

= 1.5 from P<sub>t</sub> = 26 to 29

$$\bar{P}_a = 27.7 + 2.0 \left( \frac{A}{N} - \frac{1}{2} \right) = 31.9 \quad (50\% \text{ Firing probability})$$

$$+\sigma = 1.62 (2.0) \left( \frac{NB-A^2}{N^2} + .029 \right) \quad -\sigma = 1.62 (1.5) \left( \frac{NB-A^2}{N^2} + .029 \right)$$

$$+\sigma = 6.57$$

$$-\sigma = 4.93$$

$$+3\sigma = 19.7$$

$$-3\sigma = 14.8$$

$$\bar{P}_a + 3\sigma = 51.6 \quad (99.87\% \text{ firing probability})$$

$$\bar{P}_a - 3\sigma = 17.1 \quad (0.13\% \text{ firing probability})$$

TABLE 2 BRUCETON TEST RESULTS,  
ACCE.TOR CONFIGURATION "B"

DONOR: 146 KBAR

ACCE.TOR: .219 x .125 Dia, .97 g/11, 1270 cm<sup>2</sup>/g RDX

BULKHEAD THICKNESS - VARIABLE

Bulkhead thickness (t) (inches)	P <sub>t</sub> KPSI									N <sub>x</sub>	N <sub>o</sub>	1	1N	1 <sup>2</sup> N
		1	2	3	4	5	6	7	8					
0.210	25.0	x		x						2	0	1	2	2
0.220	24.0				x		x			3	0	0		
0.230	23.0		o			o		o		0 5 N	3		2 A	2 B

x = acceptor initiated  
o = acceptor not initiated

P<sub>t</sub> increment = 1.0

$$\bar{P}_a = 24.0 + 1.0 \left( \frac{A}{N} - \frac{1}{2} \right) = 23.9 \quad (50\% \text{ Firing probability})$$

$$\sigma = 1.62 (1.0) \frac{(NB - A^2)}{N^2} + .029$$

$$\sigma = .44 \quad (\text{standard deviation})$$

$$3\sigma = 1.32$$

$$\bar{P}_a + 3\sigma = 25.2 \quad (99.87\% \text{ firing probability})$$

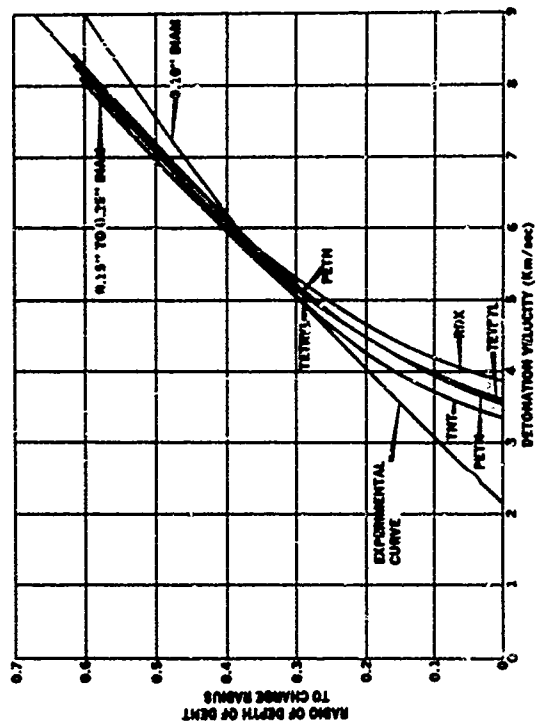
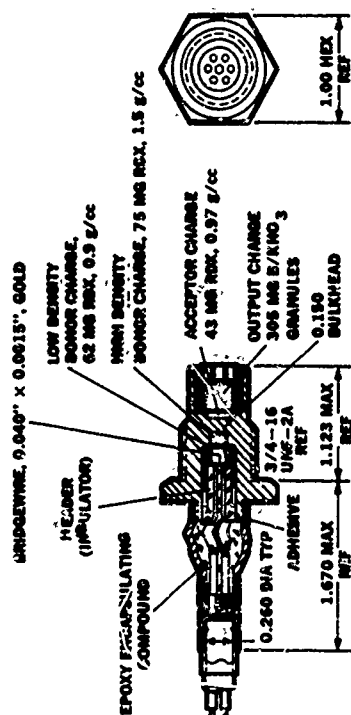
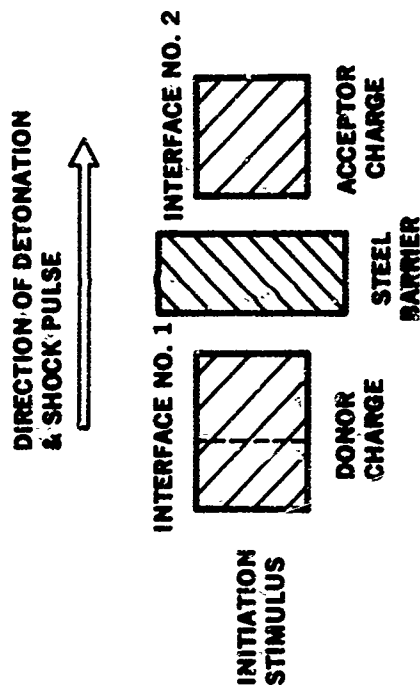
$$\bar{P}_a - 3\sigma = 22.5 \quad (0.13\% \text{ firing probability})$$

TABLE 3

Velocity Test Results

Charge	Density RDX (g/cc)	Initiation Method	Stable Velocity (Meters Sec)	Length To Reach Stable Velocity (in)	Configuration "A"	
					Design Length (in)	Velocity At Design Length (Meters/Sec.)
Low Density Donor Section	0.9	Exploding Wire	5,620	0.20	0.175	5,100
High Density Donor Sect.	1.55	Low Density Donor Sect.	7,800	0.17	0.125	5,130
Acceptor	0.97	Donor, Thru Bulkhead	5,640	0.18	0.055	2,600





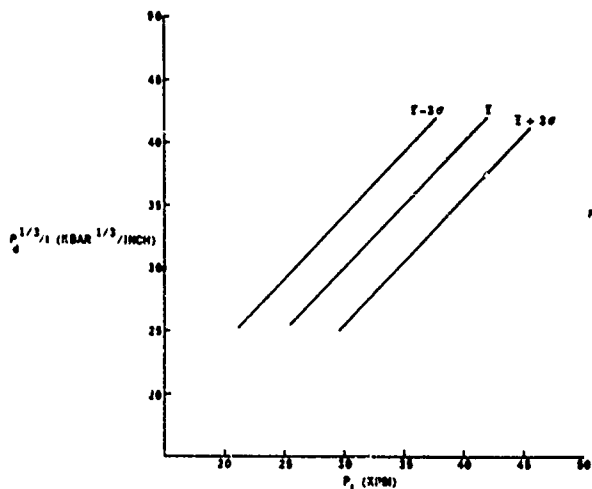


Fig. 6 - Transfer Function - Shock Attenuation Through Stainless Steel Bulkheads

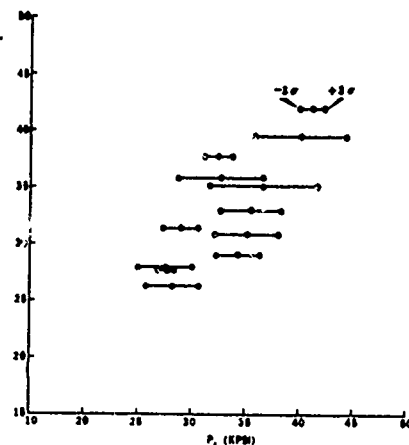


Fig. 7 - Attenuation Data, Type 302 Stainless Steel Bulkhead

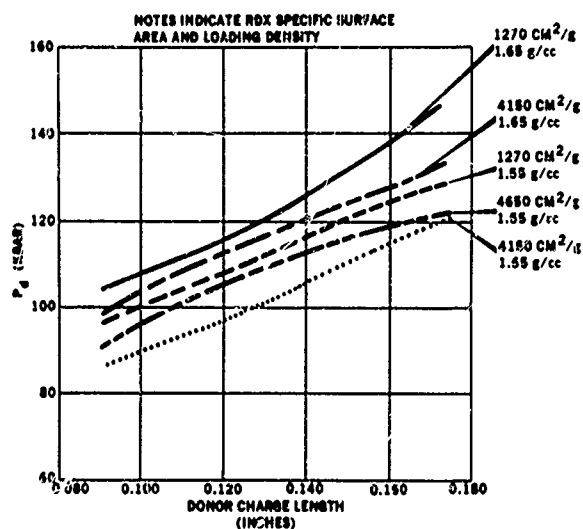


Fig. 8 - Output Pressure From 0.175 Inch Diameter RDX Charges in Steel Confinement

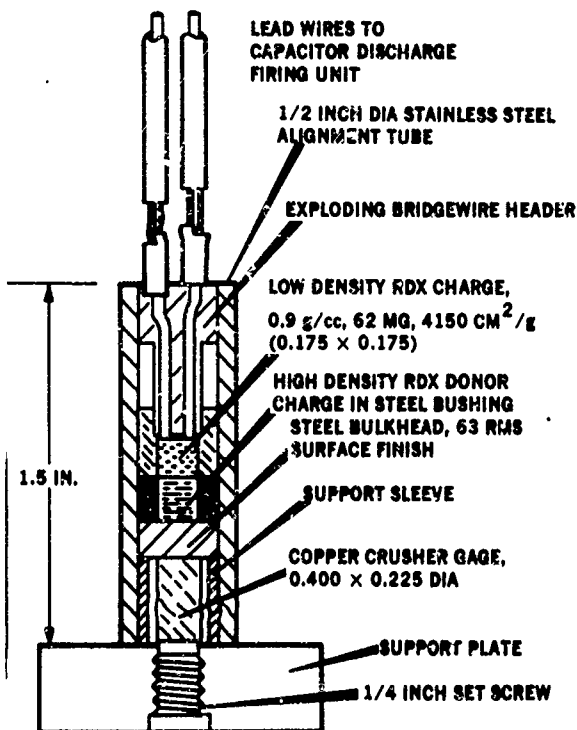
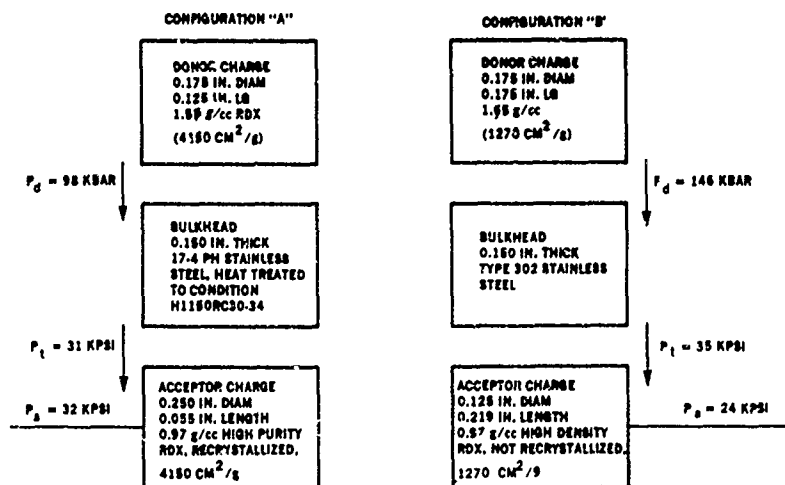


Fig. 6 - Bulkhead Attenuation Test Arrangement



PRESSURE VALUES ARE TAKEN FROM THE RELATIVE SCALE OF THE PARAMETRIC TESTS.

Fig. 12 - Comparison of Through-Bulkhead Elements

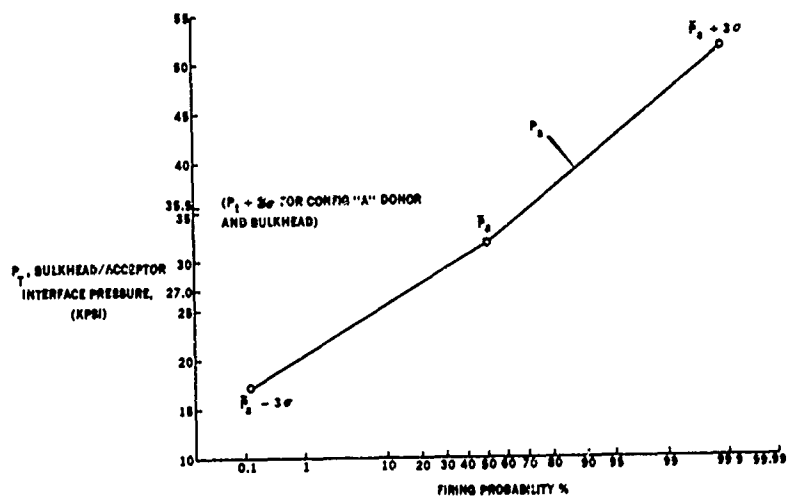


Fig. 13 - Sensitivity of Config. "A" Acceptor

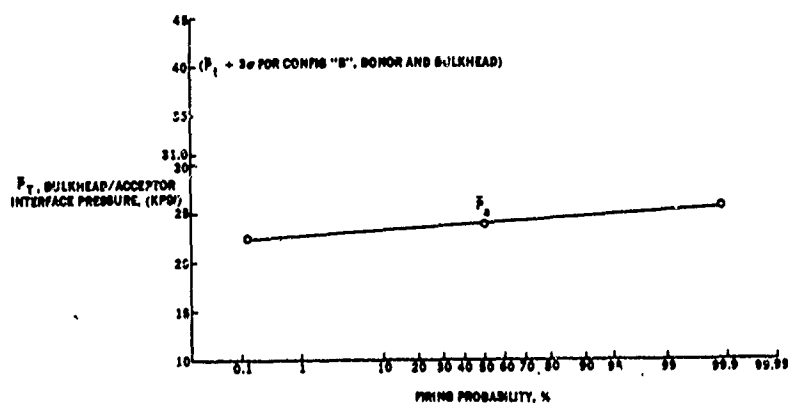
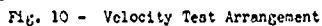
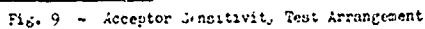


Fig. 14 - Sensitivity of Config. "B" Acceptor



C) ACCEPTOR CHARGE  
(0.37 g/cc, 4150 CM<sup>2</sup> /g RDX)  
INITIATED THROUGH 0.150  
STAINLESS STEEL BARRIER BY  
98 KBAR DONOR CHARGE

2-12.18

## 2-13 DYNAMIC OUTPUT CHARACTERIZATION

OF

### THRUSTING TYPE PYROTECHNIC DEVICES

J. L. LILLY

General Electric Company  
Space Systems Organization  
King of Prussia, Pennsylvania

#### SUMMARY

The high output to size/weight ratio of explosively powered thrusting devices make them very attractive for many spacecraft applications. The inherent "single shot" characteristic of these devices, however, puts a great premium on intelligent application and particularly on realistic applications testing. It is very important if high reliability is to be attained to characterize the interfacing mechanisms as well as the thrusting component. A realistic testing program must, therefore, consider the dynamics of how the output of the thrusting components is developed and equally important how the energy developed is used in the particular spacecraft application.

#### INTRODUCTION

Many explosively actuated components may be classified as thrusting type devices in that the core element of the mechanism is a driven piston. By this definition piston motors, dimple motors, pin pullers, bolt cutters, cable cutters, valve actuators, separating nuts, separating bolts, etc. may be all classified as thrusting type devices.

At General Electric Space Systems Organization we want to demonstrate by test the design margin or lack thereof built into each spacecraft explosive powered thrusting device application. It is also desirable to determine the design margin with as few tests and expenditure of explosive components as practical. To accomplish these ends test equipment and procedures have been developed for measuring the output capability of thrusters and how much of this output is used for a specific application, hence the title of this paper Dynamic Output Characterization of Thrusting Type Devices and Applications.

### THRUSTING DEVICE CHARACTERIZATION

Generally speaking, the output testing and evaluation of these thrusting components follows the sequence described hereinafter. The testing described assumes the structural compatibility and safety of the thrusting actuator and its explosive cartridge has already been established by analysis and test.

- \* Determine the opposing load required to stall the thrusting piston at end of designed stroke and mid-stroke positions.
- \* Determine maximum thrust developed for the following test conditions.
  - . Piston stalled in zero stroke position
  - . Piston stalled at end of designed stroke position
  - . Piston stalled in a mid-stroke position
- \* Determine reaction loads for the thrusting device fired under no load condition.

### THRUSTING DEVICE OUTPUT EVALUATION

- \* Evaluate thruster output data for compliance with component design requirements.
- \* Evaluate effects/impact of stall thrusts, stall loads and no load reaction data obtained on design of interfacing mechanisms and equipments.
- \* Adjust thruster output characteristics as necessary by either modification of the actuator or by adjustment of the power cartridge explosive charge.
- \* Fire a control sample of thrusting devices for the record to confirm stall thrust and loads data.

The testing described above is performed in a thruster test stand schematically illustrated in Figure 1. The test stand is basically similar to one developed at Frankford Arsenal for testing Propellant Actuated Devices which is described in Ordnance Engineering Handbook ORDP 20-27. A photograph of the Space Systems Thruster Test Stand is shown in Figure 2. The output of the load cell and the displacement transducer are recorded usually on a dual beam oscilloscope or a recorder as thrust

vs. time and displacement vs. time. A typical scope picture is illustrated in Figure 3. From this data curves of (thrust vs. stroke) and (thrust vs. time) can be directly plotted and supplied to the mechanisms and structural design engineers.

#### THRUSTING DEVICE TEST EVALUATION

Since starting this type of thruster evaluation at Space Systems a number of interesting problems have been uncovered. You will recall that a prerequisite to this testing program was that the thruster/squib structural compatibility be established. During stall thrust testing we have blown pins in both glass and ceramic headers, ruptured both cartridge cases and thruster casings, extruded "O" rings and collapsed piston rods. During no load testing numerous pistons have not been retained in the thruster as specified. Therefore, it is highly recommended that all test stands include enclosures for thrusters undergoing test.

Data developed on this test stand has been useful in many ways. It has for instance been used to:

- . Develop data for adjusting the initial free volume in actuators to modify thrust for quick fix situations.
  - . Ascertain capability of alternate thrusters and their compatibility with existing mechanisms.
  - . Establish lot to lot device output variations for a single vendor or multiple vendors.
  - . Establish qualification of new or alternate vendors to produce specified output characteristics.
  - . Verify device output after long periods of storage for flight certification
- Table I for example shows output for a linear actuator thruster at the beginning and after a 2 year storage period.

- . Certify that two lots of rod cutters by different manufacturers, one fabricated in 1963 and the other in 1968 had the same output. The cutter was modified by replacing the blade with a piston of the same weight as shown in Figure 4 for these tests. The results are tabulated in Table II and clearly show the rod cutters have the same output capability.

In summary the thruster test stand for dynamic output characterization of thrusting type devices has proved to be an extremely useful tool for:

- . Developing thruster design data
- . Trouble shooting failures
- . Surveillance of manufactured items
- . Surveillance of aging and storage
- . Recertification of lots
- . Ascertaining design margins

#### SPACECRAFT APPLICATIONS

All too often the ordnance engineer is faced with an incompatibility of the ordnance device and the interfacing mechanisms and structures. More often than we may like to admit the component design loads and operating environments are intuitive engineering estimates based on limited static and environmental analyses and tests. Reliable and trouble free spacecraft applications must be based on firm information. Therefore, ordnance applications testing and characterization must logically follow device and component testing.

#### ORDNANCE APPLICATIONS TESTING

Applications testing must simulate as closely as possible actual spacecraft conditions. It is not enough merely to simulate conditions and fire go - no go type of tests. At Space Systems testing must provide monitoring and measurement devices to adequately evaluate the performance of the ordnance powered subassembly. During a functioning test we must not only find out how much of the available energy is used up but also the manner in which it was used. A further requirement is to ascertain the effects



of thruster and mechanism reaction loads on the structure and associated equipments. Testing sequences can and will vary to suit certain mechanisms but in general may follow this typical sequence.

\* Determine by test the effect of thruster firing on mechanism and structure for the following test conditions.

- . Mechanism locked in zero stroke position
- . Mechanism locked at end stroke position
- . Mechanism placed in mid-stroke position
- . Mechanism placed in position so thruster completes stroke under no load.

\* Determine thrust and/or reaction vs. time for each of the mechanism positions listed above.

\* Determine shock pulses in associated structure for each test where practical

\* Determine thrusting device load vs. time for each test where practical.

\* Fire control same tests with mechanism loads set at 50%, 100% and 150% of predicted spacecraft loads.

\* Determine how much of the available thruster output is used for each test.

\* Evaluate structural integrity of the spacecraft application

\* Determine design margins for the spacecraft application

The test equipment required to perform spacecraft applications testing must of necessity be peculiar to each application. This equipment and the results obtained may be best explained by citing an example of testing accomplished.

#### LINEAR ACTUATOR (PIN PULLER) APPLICATION

The pin puller illustrated in Figure 5 was developed to meet the following requirements.

- . Stroke - 0.5"
- . Pull Pin Diameter - 0.25"
- . Peak Thrust - 1200 lbs.
- . Application - pull pin 0.3 inches against a constant side load of 1500 lbs. applied in double shear

The pin puller was first tested in the previously described thruster test stand and determined to have the output capabilities shown in Figures 6 and 7. For evaluating the spacecraft application as a pin puller the test stand illustrated schematically in Figure 8 was designed and used. In this test stand load cell A is used to record the side load applied to the pin while load cell B records the pull load as the pin is pulled through the clevis/tongue assembly and the stroke is monitored by a linear transducer. With this data available thrust vs. stroke and thrust vs. time plots can be developed and compared to the previously determined output capabilities of the pin puller. The average pin puller output used to pull the pin under a 1500 lb. side load is plotted in Figures 6 and 7. The excess capability of the pin puller is readily evident. Tests were also performed with 150% overloads and with various lubricants and clevis/tongue materials. In the tests just described the pin puller setup used was not designed to release the tongue from the clevis. Subsequent tests were performed with a short pin which released the tongue from the clevis for evaluation of the release function. Further testing is currently being planned to evaluate thrust and pull load on clevis and tongue assemblies that have been assembled under load for long periods of time and have been subjected to various environments.

With the many small and rugged load cells available to the pyrotechnic engineer today dynamic testing of explosive powered devices and mechanisms is quite feasible in most applications. The data obtained therefrom is invaluable in:

- \* Developing mechanisms design data
- \* Trouble shooting failures
- \* Surveillance of manufactured items
- \* Surveillance of aging and storage
- \* Ascertaining applications design margins
- \* Certifying ordnance equipment for flight

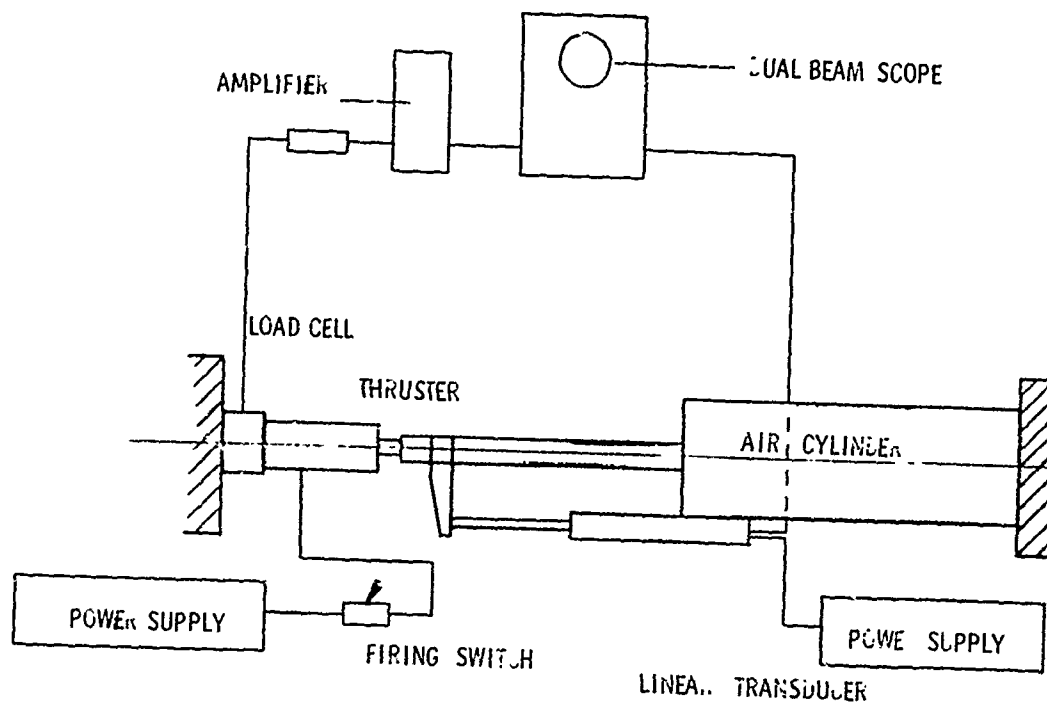
LINEAR ACTUATOR (THRUSTER)  
OUTPUT TESTS

TABLE 1

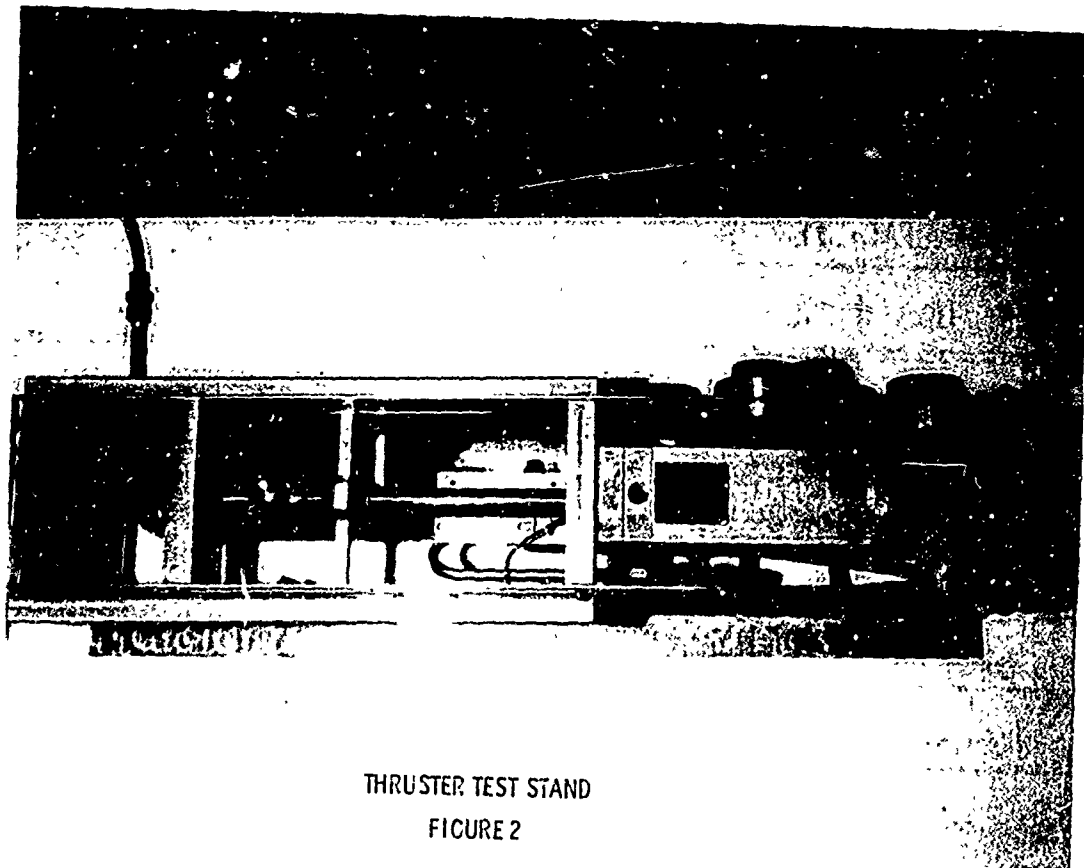
1966		1968	
TEST NO.	WORK (IN LBS.)	TEST NO.	( WORK IN LBS. )
1	287	1	302
2	293	2	316
3	285	3	293
4	301	4	296
5	286	5	285

ROD CUTTER OUTPUT TESTS

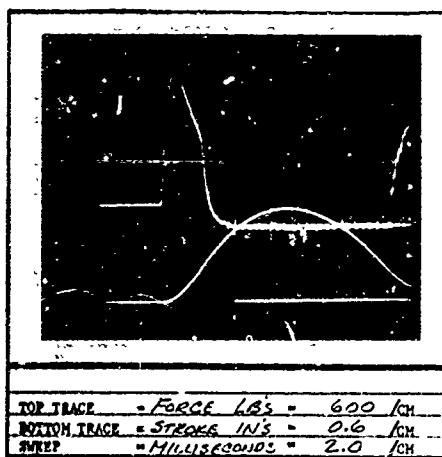
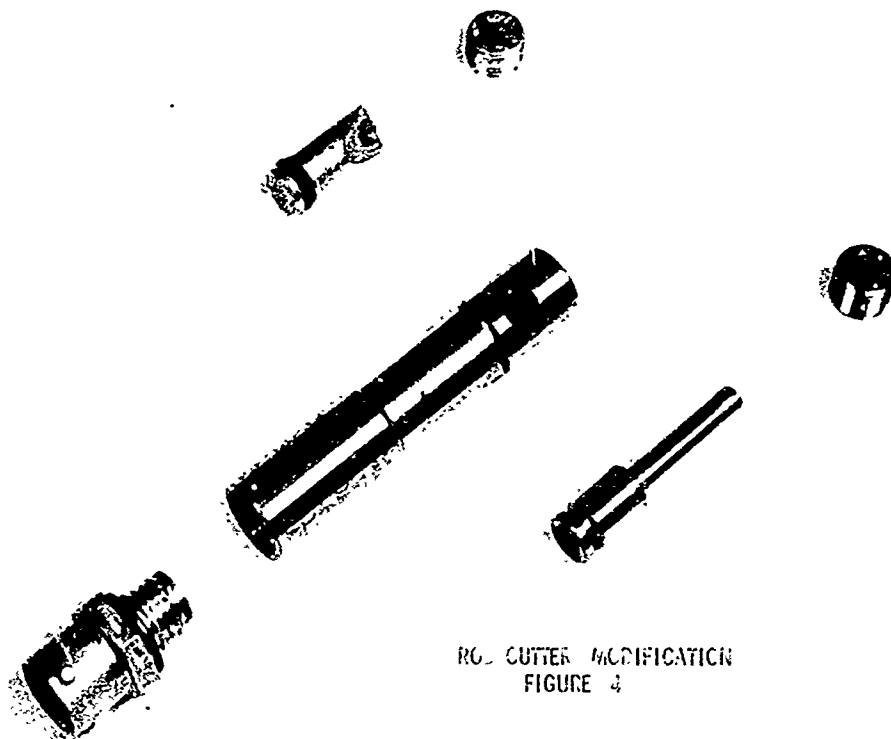
MANUFACTURER A		MANUFACTURER B	
TEST NO.	WORK (IN LBS.)	TEST NO.	WORK (IN LBS.)
69-7	1200	69-6	1140
69-9	1180	69--8	1060
69-11	1130	69-10	1130
69-13	1170	69-12	1090
69-15	1190	69-14	1050



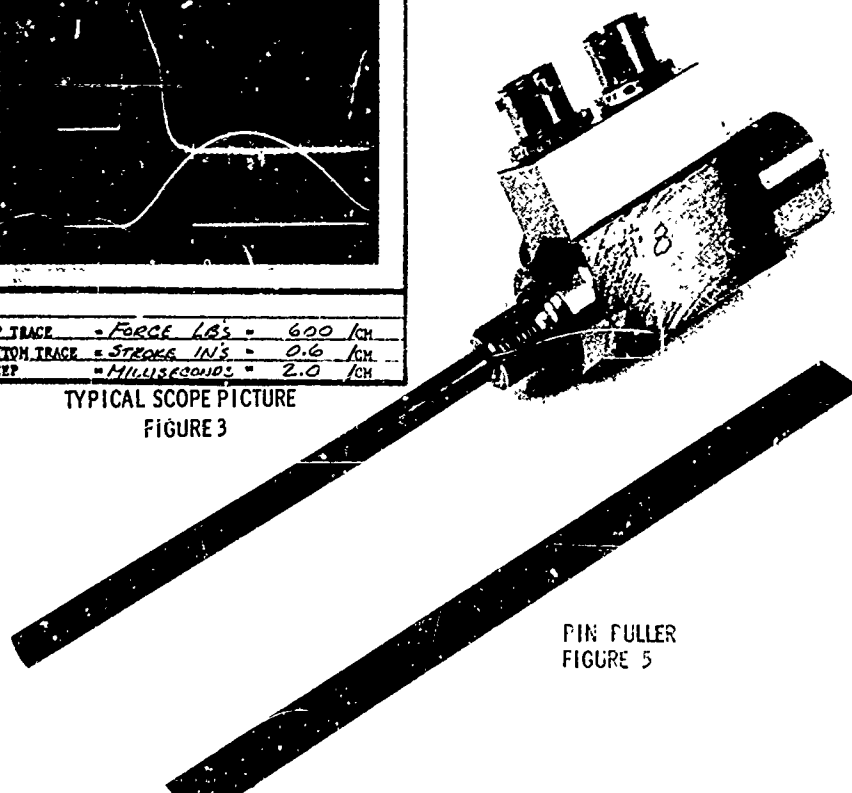
THRUSTER TEST STAND  
FIGURE 1



THRUSTER TEST STAND  
FIGURE 2



TYPICAL SCOPE PICTURE  
FIGURE 3



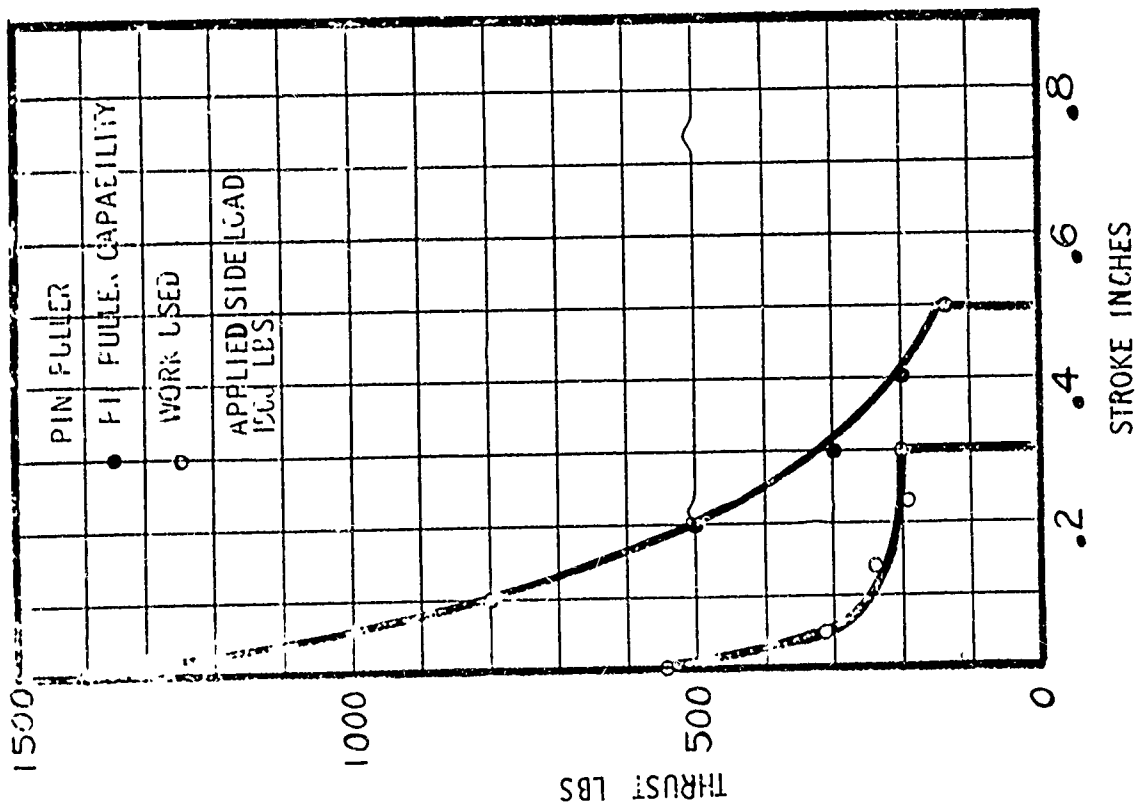


FIGURE 6

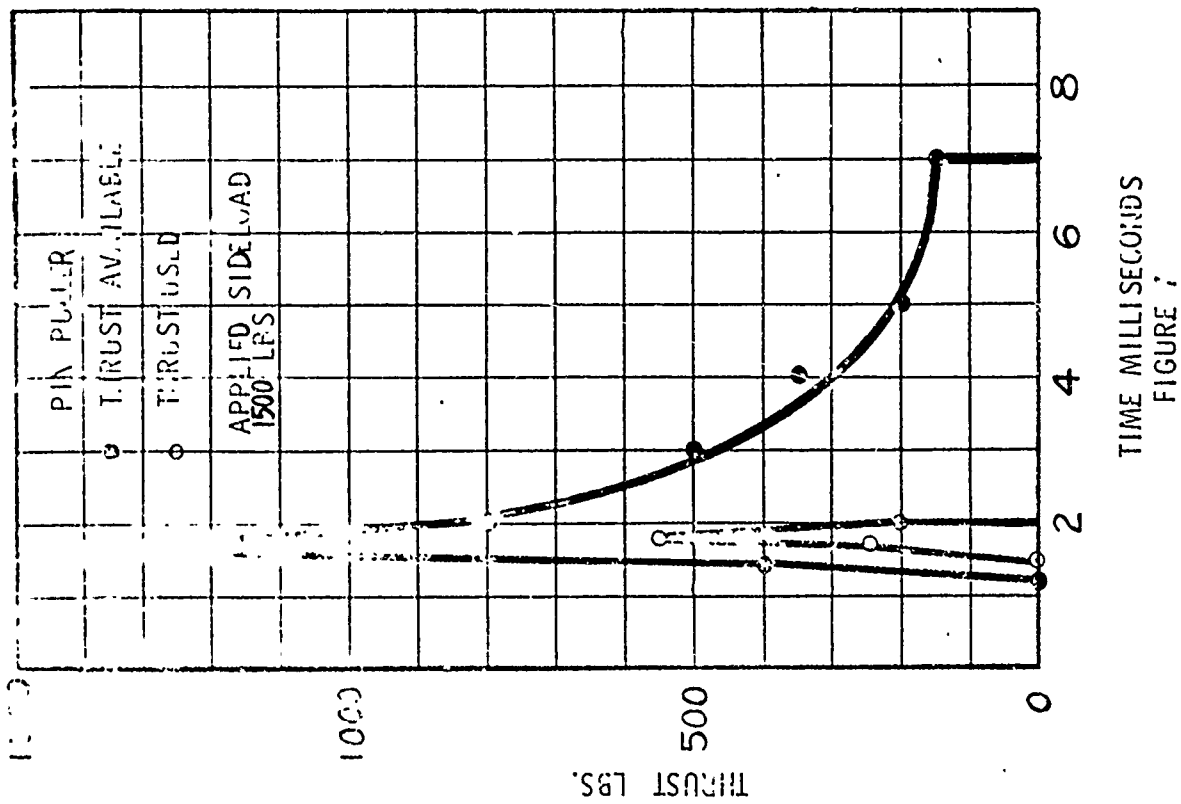
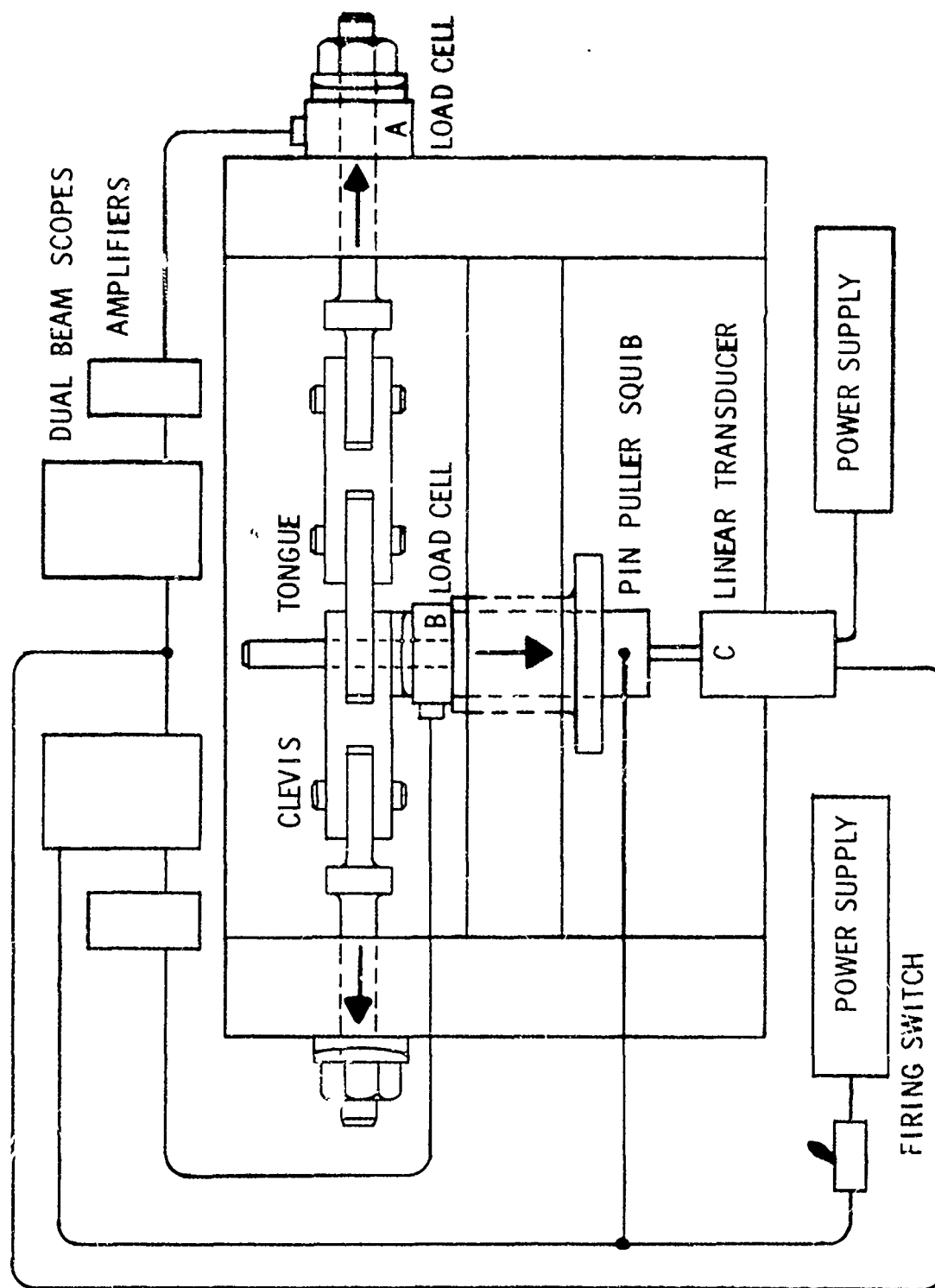


FIGURE 7



PIN PULLER TEST STAND  
FIGURE 8

## DISCUSSION

A note of caution was added concerning the need for intelligent use of systems such as this where inertial, fictional, and force loading are mixed. Excessive cylinder inertia, it was pointed out, could *make* a good device look bad.

The problem of accurate presentation of pressure in the presence of shock loading was brought out. This problem became evident when two gauges were used in a single chamber; they disagreed. The *speaker* claimed the loss of one pressure crystal as the only problem evident to him in three years of testing.



## 2-14 INSTRUMENTATION CONTROL CHARTS

S. DEMSKEY

### GENERAL ELECTRIC COMPANY - RE-ENTRY SYSTEMS

#### 1.0 Summary

This paper describes the evolution, interpretation and application of statistical control charts for evaluating instrumentation performance during the testing of ordnance devices.

Three charts are used, and they are:

1. The range (R) chart
2. The difference (d) chart, and
3. The average ( $\bar{X}$ ) chart.

When the test statistic, R or d, falls on or outside the control limits, an assignable cause of variation in instrumentation performance is inferred. Thereupon, corrective action is taken which complies with standard control chart procedures. With the  $\bar{X}$  chart, however, the test statistic is expected to be outside the control limits and corrective action is taken when more than half of the  $\bar{X}$  values fall inside the limits.

Thus the most desirable situation occurs when the R and d charts are "in statistical control" and the  $\bar{X}$  chart is "out of statistical control", which results in a firm balance between control and sensitivity.

If the measurement process falls out of control or loses sensitivity, then the instrumentation failure is assumed to have an assignable cause and the test is stopped

to find the cause. If one considers the high cost of some "one shot" devices, then the cost effectiveness of the recommended control chart applications is quite high.

## 2.0 Introduction to Control Charts

Traditionally, statistical control charts have been used for controlling a mass-production manufacturing process. Engineering wise, a process could be defined as a set of operations performed by people and machines which modifies the original material and increases its economic value. Statistically speaking, however, a process is quantified by the confidence interval of a statistic. For purposes of illustration, let us consider the statistic known as the mean.

For a standard  $\bar{X}$  chart

$$CL's = \bar{\bar{X}} \pm 3 S/\sqrt{n} = \bar{\bar{X}} \pm A_2 \bar{R}$$

where

CL's are the confidence limits of  $\bar{\bar{X}}$ , the grand mean and the confidence interval is defined by either  $3 S/\sqrt{n}$  or  $A_2 \bar{R}$ ,

where  $S$  is the standard deviation

$n$  is the individual group sample size

3 represents the normal deviate associated with a confidence value of 0.9973 or the complementary risk of 0.0027.

$\bar{R}$  is the average range which when multiplied by  $A_2$  a control factor, yields the confidence interval.

The range calculation is preferred because of the simpler calculations.

Now, let us compare process control limits obtained from a control chart and the specification limits which are ordinarily of greater concern to engineers.

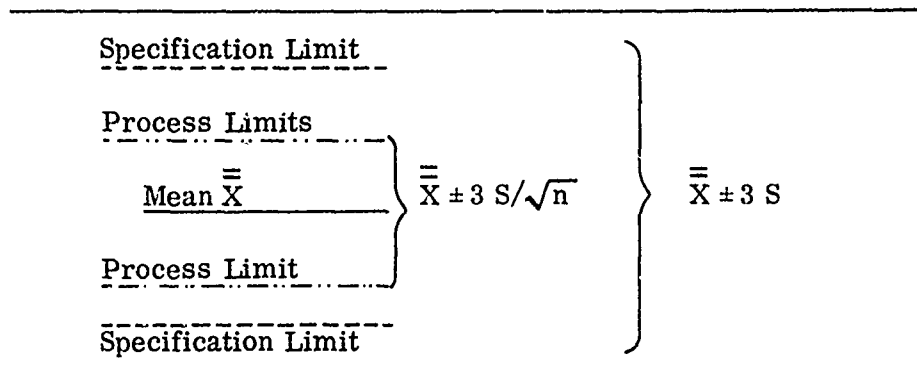


Figure 1. Comparison of Specification Limits and Process Limits

It is apparent that specification limits are much wider than process limits and the degree of exceedance depends on the individual group sample size. From the operational point of view, the plotted value of the average which falls on or outside the process control limit is a signal for possible corrective action. In other words, time and/or options are still open for correcting the process so that the values of the individual units (whose values comprise the mean) will continue to remain within specification limits.

From the statistical point of view, the mean is a preferred statistic because of its robustness; that is, the distribution of averages is normally distributed, regardless of the distribution of the individual units.

By considering the measurement of "one shot" devices as a process, the control chart can be effectively applied to control the test instrumentation as the test is being conducted and as each test unit is fired.

3.0 Evolution of Control Charts for Instrumentation

The question that arises, however, is why we are concerned with this application. The story begins several years ago when the two channel readings straddled an extremely tight specification for total impulse of a rocket.

This situation led to an Instrumentation Variation Analysis because of Reliability/Confidence (R/C) requirement on the parameter. The effect of the Instrumentation Variation Analysis always leads to an increased R/C estimate as will now be shown. The basic reliability formula, assuming a normal distribution is

$$K = (SL - \bar{X})/S$$

where SL is the specification limit  
 $\bar{X}$  is the calculated mean  
S is the calculated standard deviation

The higher the calculated K, the higher the R/C estimate and the smaller the S, the larger the K.

The effect of the magnitude of S may be demonstrated. Let us imagine that we have test fired four motors and have used two instrumentation channels (C1 and C2) to measure the total impulse.

S/N	C1	C2	d
1			d <sub>1</sub>
2			d <sub>2</sub>
3			d <sub>3</sub>
4			d <sub>4</sub>
$\bar{X}$	$\bar{X}_1$	$\bar{X}_2$	
S	S <sub>1</sub>	S <sub>2</sub>	

Since each unit yielded a single value of total impulse, then any difference  $d$ , that is observed must be due obviously to a response difference in the instrumentation. If we cover up the C2 and  $d$  columns, then it is also intuitively reasonable that the calculated standard deviation,  $S_1$ , reflects not only the motor variation but also includes some instrumentation variation.

By using only one channel, there is no direct method of separating these two effects. By using two or more channels, however, it is possible to separate and estimate the contribution of each of these factors. This is seen, briefly, in the following formula.

$$S^2_{\text{total}} = S^2_{\text{Instrumentation}} + S^2_{\text{hardware}}$$

The diagram illustrates the relationship between the total standard deviation squared ( $S^2_{\text{total}}$ ), the instrumentation standard deviation squared ( $S^2_{\text{Instrumentation}}$ ), and the hardware standard deviation squared ( $S^2_{\text{hardware}}$ ). The equation  $S^2_{\text{total}} = S^2_{\text{Instrumentation}} + S^2_{\text{hardware}}$  is shown at the top. Below the equation, three arrows point downwards from each term. From  $S^2_{\text{total}}$ , an arrow points to the text "by direct calculation". From  $S^2_{\text{Instrumentation}}$ , an arrow points to the text "by subtraction". From  $S^2_{\text{hardware}}$ , an arrow points to the text "by subtraction".

Now since the standard deviation for the hardware,  $S_H$ , must be less than the total standard deviation  $S_T$ , then

$$\left[ K_H = (SL - \bar{X})/S_H \right] > \left[ K_T = (SL - \bar{X})/S_T \right]$$

It follows, therefore, that the R/C estimate for  $K_H$  is greater than that for  $K_T$ .

After this type of analysis resolved the problem to everyone's satisfaction, the design engineer asked if I could develop a statistical control chart; its purpose would be to alert us to the problem as the test was being conducted, rather than becoming aware of the problem after the test was completed.

This question led to the development of two of the three control charts described, namely the R and d charts.

The range, R, chart is used to measure and control the degree of consistency between the two (or more) channels.

The difference, d, chart is used to measure and control the degree of bias in the two channel readings, i.e., the tendency for one channel to yield higher readings more frequently than the other channel.

In its first application, the R chart detected a saturated transducer when the fourth motor in a test series was fired. Subsequently, the R chart was again useful when a post mortem analysis detected a poor reading; in this test, an oscilloscope and a digital counter were used as redundant instrumentation. The interesting factor that emerged at this time was that, contrary to expectation, the "outlier" was obtained from the digital counter.

The final chart,  $\bar{X}$ , was developed as a result of testing pressure cartridges. Again, the objective was to obtain a preliminary R/C estimate from development tests. The data was presented in three groups A, B, and C. The parameter considered was peak pressure. In group A, the units were subjected primarily to ambient environments and no periodic calibrations were made. Group B consisted of units which had been used for sensitivity tests which have no effect on the peak pressure; also static calibration measurements were made after the firing of every fifth unit. Group C consisted of units exposed to temperature extremes and again static calibration tests were conducted after every fifth unit.

The subsequent application of the analysis of variance to estimate the instrumentation variation necessitated the rejection of the Group A data. The reason was that the statistical mean square for the instrumentation was greater than the statistical mean square for the hardware. If the sensitivity of the instrumentation was to be an order of magnitude better than the hardware, then the situation would be the reverse.

The control charts,  $R$  and  $d$ , were then calculated for the Group A data as a post mortem. The results were that all the values fell inside the control limits. The only indication of a problem was a "run" of eight values on the  $d$  chart. It then became apparent that a control chart analogous to the  $F$  test in the analysis of variance would be useful. This is the  $\bar{X}$  control chart. Although this chart parallels the analysis of variance, it requires an inverse interpretation. With the standard control charts,  $R$  and  $d$ , a point falling on or outside the control limits signals a non-uniform condition. With the  $\bar{X}$  chart, a point on or outside the control limit parallels a significant  $F$  test and is indicative of instrumentation sensitivity necessary to discriminate between the test units.

When the Group A data (no periodic calibration) is subjected to the  $\bar{X}$  chart, all the values fall inside the control limits. Thus, the use of control charts would have detected the lack of instrumentation sensitivity very quickly as the test was being conducted. When the Group B and C data (periodic calibrations) are subjected to the  $\bar{X}$  control chart analysis, most of the values fall on or outside the control limits. The three control charts provide a firm balance between control and sensitivity.

In addition to the interpretive difference for the  $\bar{X}$  chart, another difference exists with the instrumentation control charts; it is the fact that the control limits are based on the cumulative sample size, thus a decision is possible very shortly after testing begins. Under standard control chart procedure, 20-25 subgroups under normal operation conditions are necessary to estimate the centerline and control limits before the process can be evaluated.

#### 4.0 Conclusion

The procedures, multiplication factors for simplifying calculations and sample forms are given in the Appendix; it will eventually become an independent document for implementing these procedures.

Our experience indicates that this application of statistical control charts is a useful supplement to standard calibration procedures. The reason is that the instrumentation is constantly being evaluated during the entire test, thereby preventing costly error and delay.



APPENDIX

GUIDE MANUAL FOR USE OF  
INSTRUMENTATION CONTROL CHARTS

1.0 Objective and Summary

This report provides statistical control chart procedures for destructively tested hardware which are applied as the test is being conducted.

Control charts have become traditional tools in controlling a process through the statistical evaluation of the product parameters or dimensions. By considering the test measurements of "one shot" devices as a process, these control charts can be effectively used to control the test instrumentation as the test is being conducted. The data used are the duplicate values obtained from redundant instrumentation which are customarily used to assure that at least one observation be retained for each.

The charts and their control objectives are as follows:

1. The range R, chart is used to measure and control the degree of consistency between the two redundant instruments.
2. The difference, d, chart is used to measure and control the degree of bias in the two redundant readings, i. e., the tendency for one unit to read higher more frequently than the other unit.
3. The average  $\bar{X}$  chart is used to measure and control the degree of sensitivity, i. e., the capability that differences between the redundant instruments' readings should be smaller than the differences between the hardware units.

Interestingly, the desired situation occurs when the R and d charts are "in statistical control" and the  $\bar{X}$  chart is "out of statistical control", which results in a firm balance between control and sensitivity.

If the measurement process falls out of control or loses sensitivity, then the instrumentation is assumed to have an assignable cause and the test is stopped to find the cause. If one considers the high cost of some "one shot" devices, then the cost effectiveness of the recommended control chart applications is quite high. When calibration firings are available, control charting of this information dovetails to assure even a higher degree of control over the test measurement process.

## 2.0 Data Collection and Reporting (DCR)

The following requirements add to, but do not cancel or modify, any other DCR requirements.

Each unit test fired should be identified in submitted data sheets by:

1. Date
2. Instrumentation (e. g. , transducers) serial number
3. Test condition - temperature level, etc.

Data for each static calibration should be identified similarly by:

1. Date
2. Instrumentation serial number
3. "R" step level, etc.

Copies should be included in the Test Report.

Factors are given (Enclosure 1) which reduce most of the calculation effort. Also provided are sample charts and data forms which may be copied. See Enclosure 3.

One question which may arise is, why the Control Chart multiplication factors have not been preprinted on the data forms. The reason is missing data, "out of control" results, etc. Some comfort may be had when it is realized that the major effort is required with the first 20 units. At this point, the control limits should be established and the already simplified calculations are reduced even more.

### 3.0 Statistical Control Charts

Since lost data from destructively tested equipment is irreplaceable, redundant or redundant types of instrumentation are commonly used in industry to assure that at least one observation is obtained for each firing. Although this procedural objective is obviously worthwhile, it does not extract the maximum available value from the data.

By considering the sequence of test measurements as the output of a manufacturing process, then statistical control charts can be an effective means of assuring reliable measurements while the test is being conducted; this contrasts with the post mortems which cannot associate a suspect measurement with either the hardware or the

instrumentation. If we consider the cost of some destructively tested hardware, i. e., rockets, electro-initiators, then the cost effectiveness of the statistical control charts becomes high.

### 3.1 Relationship of Control Charts to Measurement Objectives

The measurement objectives of any test may be defined in terms of consistency, bias-free and sensitivity. Their definitions are:

Consistency — capability of redundant instrumentation to provide differences between readings which are constant and within random variation as controlled by the R chart.

Bias-free — capability of redundant instrumentation to provide the differences between readings which yield an average value of zero, within random variation.

Bias exists when one instrument always yields higher readings than the other. This is controlled by the d chart.

Sensitivity — capability of redundant instrumentation to yield differences between readings which are smaller than the differences of the hardware being tested. This is evaluated by the  $\bar{X}$  chart.

### 3.2 Comparison of Control Chart Methods — Instrumentation vs. Standard

The use of redundant instrumentation actually creates two sources of measurement variation ( $V_m$ ):

1.  $V_B$  or  $S_B^2$  is the variance due to the differences between the redundant instruments, i. e., between channel variation.
2.  $V_W$  or  $S_W^2$  is the variance due to the difference between repeated measurements of the same instrument, i. e., within channel variation.

When testing destructively tested hardware, it is obvious that only  $V_W$  can be measured, at the present state of the art, from static calibration tests. When dynamic calibration tests become available, the present procedures will be improved and updated.

Since only  $V_B$  is available, it is defined as the experimental error for instrumentation performance.

All control chart instructions which follow are based on sub-group sizes of two units, although extension to any number is easy.

The confidence levels given are at the 95% (5% type I or alpha risk) level instead of 99.73% ( $3\sigma$ ) limits; although  $3\sigma$  limits are economically reasonable with a consumer goods, mass production process, these instrumentation procedures are concerned with short runs under R&D conditions.

Since testing of destructively tested devices will not ordinarily permit sufficient test data for calculating initial values of the control lines, as required by standard variables charts, the values of the control lines and limits are calculated from a cumulative sample size (Reference 1).

If control charts are applied to static calibration data, then a sequence for applying and interlacing two control charts is given in Enclosure 2; that is, the Calibration/Instrumentation (C/I) chart is used to supplement the Hardware/Instrumentation (H/I) chart. The instructions in Enclosure 2 are self-explanatory. Another alternative would be the Difference Control Charts given in Reference 2.

#### 4.0 Control Chart Procedures for Between Channel Variation

Step by step instructions for calculations follow in the next section.

#### 4.1 Control Chart Calculations

The combined data and calculation sheet is given as Enclosure 4A. The control chart form is given as Enclosure 4B and should be adjacent to the data form in actual operation.

The following explain the columns given in the data form by column number:

1. Line — line number — for convenient reference purposes
2. f — Degrees of freedom; also the cumulative number of tests with two redundant units only.
3.  $X_1$  — Datum or reading for channel #1
4.  $X_2$  — Datum or reading for channel #2
5. R or d — The calculated difference between  $X_1$  and  $X_2$  with sign; a plus (+) sign is not written, but if  $d = (X_1 - X_2)$  is negative, the minus sign is recorded. The test unit value without the sign (+ or -) is recorded on the R chart and with the sign recorded on the d chart.
6.  $|\Sigma R|$  — the sum of the absolute values of the R or d values
7.  $\bar{R}$  --  $\Sigma R$  / divided by the cumulative number of hardware units tested.  $\bar{R}$  is the centerline of the R chart.
8. Sum  $X_1 + X_2$  — self explanatory
9.  $\bar{X}$  — Sum  $(X_1 + X_2)$  divided by 2 or any other number of redundant data. The unit  $\bar{X}$  is recorded on the  $\bar{X}$  chart.

Columns 9., 10. and 11. are used to calculate the cumulative average. Ordinarily, the cumulative sum would be obtained and then divided by the cumulative number of observations; this, however, would lead to an inconvenient large number of digits in the cumulative sum, so the infrequently used calculations of columns 10., 11. and 12. are given to calculate the cumulative average  $\bar{\bar{X}}$ . See Enclosure 3 for the derivation.

10.  $-\Delta \bar{X} = \bar{X}_i - \bar{\bar{X}}_{(i-1)}$  i. e., the difference between the present units average ( $\bar{X}_i$ ) and the previous cumulative average ( $\bar{\bar{X}}_{(i-1)}$ ).
11.  $\Delta \bar{X}$  is divided by the cumulative number of units tested ( $n_i$ ).
12.  $\bar{\bar{X}}_i$ , the cumulative average is obtained by adding  $\Delta \bar{X}/n_i$ , algebraically to the previous cumulative average  $\bar{\bar{X}}_{(i-1)}$ . The term "algebraically" is emphasized because the difference may be positive or negative.  $\bar{\bar{X}}_i$  is the centerline of the  $\bar{X}$  chart.
13. F #3 is the control chart multiplication factor for the  $\bar{X}$  chart given in Enclosure 1.
14. F #3 ( $\bar{R}$ ) is the product of F #3 (Step 13) and  $\bar{R}$  (Step 7). It is the confidence interval for the  $\bar{X}$  chart.
15.  $LCL(\bar{\bar{X}})$  is the lower control limit of the  $\bar{X}$  chart. Its value is  $\bar{\bar{X}} - F \#3 (\bar{R})$
16.  $UCL(\bar{\bar{X}})$  is the upper control limits of the  $\bar{X}$  chart. Its value is  $\bar{\bar{X}} + (F \#3) (\bar{R})$
17. F #1 is the control chart multiplication factor for the R chart given in Enclosure 1.

18.  $UCL(\bar{R})$  is the upper control limit for the R chart. Its value is the product of F #1 (Step 17) and  $\bar{R}$  (Step 7).
19. F #2 is the control chart multiplication factor for the d chart given in Enclosure 1.
20. CI is the confidence interval for the d chart. Since it is added to and subtracted from a theoretical value of 0, the "no-bias" condition, it is also the upper and lower confidence limit for the d chart. Its value is the product of F #2 (Step 19) and  $\bar{R}$  (Step 7).
21. Comments are recorded as necessary on the chart.

#### 4.2 Control Chart Interpretation

1. As soon as the calculations are completed for each unit, plot these unit values, i. e., R, d and  $\bar{X}$  on the appropriate chart for comparison with the centerlines  $\bar{R}$ ,  $\bar{d}$  and  $\bar{X}$  and, more important, with the statistical control limits.
2. If any of the R or d values fall on or outside the control limits, then an assignable cause of variation has been detected (with an  $\alpha$  or 5% risk, of course). The test should be stopped and if the cause is diagnosed, corrective action should follow.
3. If more than half of the averages fall inside, then a lack of sensitivity has been detected and corrective action is required.

This statistical result parallels the application of an analysis of variance although the signal for corrective action is opposite to that of standard control chart procedures as exemplified by the R and d charts. The statement is often made that "our instrumentation is an order of magnitude" more precise than the hardware, and the  $\bar{X}$  chart can



support this contention. It would seem reasonable, however, to take any remedial action with this chart starting with the third test unit, because of the size of the F #3 factor.

4. Periodically, exactly the same readings are obtained with both channels and "out of control" results will manifest themselves in subsequent R charts but obviously not in the  $\bar{X}$  charts. In this case, some judgment must be used for test continuance. It is also possible that if too many false signals of "out of control" or "lack of sensitivity" occur, this to be indicative that the instrumentation system is more stable than our experience would indicate. In this case, justification should be made and the two-sided 2% (one-sided 1%) alpha limits should be used. In no case, however, should the two-sided 0.27% (0.147% one-sided) alpha, or more lenient limits, be used.
5. If no assignable cause can be found after the control charts signal a problem, it is recognized that schedules might force a continuance of testing. The risk taken under this course of action is obvious. If schedule permits, then the application of the Calibration/Instrumentation Control Chart is recommended per Enclosure 2. Also advisable under these conditions would be more frequent static calibration runs.
6. When test conditions are changed, caution will have to be used. For example, if gas generators have been subjected to 70°F and 160°F temperatures, we can expect the  $\bar{X}$  to show a shift if we test the 70°F units first and follow up with the 160°F units. The R and d charts should not necessarily detect a shift but they

could. When control chart shifts are associated with this cause, then the calculations will have to start at the beginning.

### 4.3 Formulas for Control Chart Factors

Since it is assumed that an insufficient number of hardware units for test will be tested for obtaining standard values of  $\bar{X}$ ,  $\bar{R}$  and their respective control limits, only the formulas for cumulative sample sizes (Reference 1) will be given. Also, "standard" formulas will be given for control charts based on static testing.

#### 4.3.1 Control Charts — Modified for Cumulating Sample Size

##### Range Chart

$$\begin{aligned} CL_R &= \left[ 1 \pm t_{\alpha/2}(d_3, d_2) \right] \bar{R} = \left[ 1 \pm t_{\alpha}(0.8525/1.128) \right] \bar{R} \\ &= \left[ 1 \pm 0.756 t_{\alpha/2} \right] \bar{R} \end{aligned} \quad \text{(formula 1)}$$

##### d Chart

$$\begin{aligned} CL_d &= 0 \pm \left[ t_{\alpha/2}(1.41) (\bar{R}/d^*_2) \right] \\ CI_d &= 0 \pm \left[ 1.41 (t_{\alpha/2})/d^*_2 \right] \bar{R} \end{aligned} \quad \text{(formula 2)}$$

##### $\bar{X}$ Chart

$$CL_X = \bar{X} \pm (t_{\alpha/2} \bar{R}/d^*_2) \left[ \frac{1}{m.n.} + \frac{1}{n} \right]^{1/2} = \bar{X} \pm (t_{\alpha/2}/d^*_2) \left[ \frac{m+1}{2m} \right]^{1/2} \bar{R} \quad \text{(formula 3)}$$

#### 4.3.2 Control Charts — Standard

The formulas that follow are applicable to the C/I Charts wherein at least 20 static test runs can be performed conveniently before the actual hardware units are test fired. If an R stepping procedure is used, that is a range of weights is used, then the difference between the standard value and the response value can be used.

Given 20 sets of data with 2 observations each, the control limits at 95% confidence (2-sided) are:

##### Range Chart

$$UCL_R = D_4 (0.975) \bar{R} = 2.48 \bar{R} \quad (\text{formula 4a})$$

$$LCL_R = D_4 (0.025) \bar{R} = 0.00 \bar{R} \quad (\text{formula 4b})$$

##### d Chart

$$\begin{aligned} CL_d &= 0 \pm t_{(0.025)} (2S^2)^{1/2} = 0 \pm (1.96) (1.414) \left(\frac{\bar{R}}{d_2}\right) \\ &= 0 \pm \left[ \frac{2.77}{1.128} \right] \bar{R} = 0 \pm 2.45 \bar{R} \end{aligned} \quad (\text{formula 5})$$

##### $\bar{X}$ Chart

$$\begin{aligned} CL_{\bar{X}} &= \bar{\bar{X}} \pm t_{\alpha/2} S/\sqrt{n} = \bar{\bar{X}} \pm t_{\alpha/2} (\bar{R}/d_2^*) \sqrt{n} \\ &= \bar{\bar{X}} \pm \bar{R} \left[ t_{\alpha/2} / (1.414 d_2^*) \right] \\ &= 1.23 \bar{R} \end{aligned} \quad (\text{formula 6})$$

#### 4.4 Supplementary Control Chart Methods

In order to sharpen up the discriminating capability in predicting and diagnosing process shifts, various supplementary techniques are applied; with the following methods, the plotted points do not even have to fall on or outside the control limits.

Perhaps the best known supplementary technique is the "run" or successive number of points above or below the mean.

##### 4.4.1 "Runs"

The use of 7 consecutive points is the "run" boundary, generally used in the control of a mass production consumer goods process. Considering the "run" length and its associated alpha risk,

<u>Run Length</u>	<u>Alpha</u>
7	0.0078
6	0.0156
5	0.0312
4	0.0625

it is reasonable to reduce the length for an R&D measurement process. The value of 5 is recommended as a warning limit but 6 is designated as an action limit.

##### 4.4.2 "Yardstick"

A supplementary technique which is optional for instrumentation control charts, but is worthy of mention, is known as the "yardstick". See Reference 1.

A "yardstick" is defined as the minimum difference between two successive points which is associated with random or sampling variation. In other words, if the vertical distance between two successive points ( $\bar{X}$ ,  $d$ , or  $R$ ) is equal to or greater than the length of the "yardstick", then this is equivalent to an out-of-control point, that is, a process shift is predicted. As in the application of "run" theory, both points under consideration may be inside the control limits.

#### Range - $Y_R$

$$1. \quad f_y = 0.9 (n-1) (m) = 0.9 (1) 2 = 1.822 \approx 2.$$

$$2. \quad S_R = \bar{R} (D_4 - 1)/3 = \bar{R} (3.267 - 1)/3 = 2.267 \bar{R}/3 = 0.756 \bar{R}$$

$$3. \quad S_R^- = S_R \text{ (as number of ranges per group is 1)}$$

$$4. \quad Y_R = \text{twice half interval} - 2 Z 0.05 S_R^-$$

$$= 2 (3.05) (0.756) \bar{R} = 4.61 \bar{R} \quad (\text{formula 7})$$

#### Means

$$1. \quad S_X = \bar{R}/d*2$$

$$2. \quad S_X^- = S_X/\sqrt{n} = S_X/1.4$$

$$3. \quad \bar{Y} = \text{twice half interval} = 2 Z 0.05 \bar{X} = 2 (3.05) S_X^-$$

$$= 6.1 \frac{S_X}{1.41} = 4.31 \frac{\bar{R}}{d*2} = \left(\frac{4.31}{d*2}\right) \bar{R} \quad (\text{formula 8})$$

## 5.0 Other Methods

The preceding techniques can be deviated from, provided prior approval is obtained from the responsible development engineer and statistician. Other techniques which have been recently developed and which could be acceptable are geometric moving average and cumulative sum charts.

### ENCLOSURE 1 (1/1)

#### R MULTIPLICATION FACTORS BY FORMULA NO. (F#)

#### FOR TWO REDUNDANT INSTRUMENTS

No. Groups, $\frac{m}{m}, \text{ for } n=2$ $m=f$	$t_{\alpha/2}$ ( $\alpha = 0.05$ )	$d_2^*$	F#1		F#3	F#2	F#8
			$1-0.756 t_{\alpha/2}$	$1+0.756 t_{\alpha/2}$	$\frac{t_{\alpha/2}}{d_2^*} \left[ \frac{m+1}{2m} \right]^{1/2}$	$\frac{1.41 t_{\alpha/2}}{d_2^*}$	$\frac{4.31}{d_2^*}$
1	12.706	1.41	0.00	9.61	9.02	12.72	3.06
2	4.303	1.28	0.00	4.25	2.91	4.74	3.37
3	3.132	1.23	0.00	3.41	2.12	3.65	3.50
4	2.776	1.21	0.00	3.10	1.81	3.23	3.56
5	2.571	1.19	0.00	2.94	1.67	3.05	3.62
6	2.447	1.18	0.00	2.85	1.59	2.93	3.65
7	2.365	1.17	0.00	2.79	1.53	2.85	3.68
8	2.303	1.17	0.00	2.74	1.48	2.78	3.68
9	2.262	1.16	0.00	2.71	1.45	2.75	3.72
10	2.228	1.16	0.00	2.68	1.42	2.71	3.72
11	2.201	1.16	0.00	2.66	1.41	2.68	3.72
12	2.179	1.15	0.00	2.65	1.40	2.68	3.75
13	2.160	1.15	0.00	2.63	1.38	2.65	3.75
14	2.145	1.15	0.00	2.62	1.38	2.65	3.75
15	2.131	1.15	0.00	2.61	1.35	2.61	3.75
16	2.120	1.15	0.00	2.60	1.34	2.59	3.75
17	2.110	1.15	0.00	2.60	1.34	2.59	3.75
18	2.101	1.15	0.00	2.59	1.33	2.58	3.75
19	2.093	1.15	0.00	2.58	1.32	2.57	3.75
20	2.086	1.15	0.00	2.58	1.31	2.55	3.75
$\infty$	1.960	1.13	0.00	2.48	1.23	2.45	3.81

Note (1):  $d_3/d_2 = 0.8525/1.128 = 0.756$

Note (2): For standard control charts, i. e., at least 20 "runs" are performed and the factors used are those for  $f = \infty$

## ENCLOSURE 2 (1/1)

### PROCEDURE FOR COMBINING INSTRUMENTATION CONTROL CHARTS, TEST HARDWARE (H/I) WITH THE STATIC CALIBRATION (C/I) CHARTS

Sequence Number	Instrumentation Control Charts		Comments	
	Calibration (C/I)	Hardware (H/I)	If all points are in control	If point is out of control
1	a) 10 consecutive measurements (20 pairs)	----	1) Set up standard values for C/I charts	A) <u>re: Setting up C/I chart.</u> Reject and recalculate averages & limits
2	----	a) Unit #1	2) Start H/I charts	B) <u>re: H/I Chart.</u> Stop
3	----	b) Unit #2	3) Continue H/I charts	testing and try to identify
4	----	c) Unit #3	4) Continue H/I charts	and correct cause. If
5	----	d) Unit #4	5) Continue H/I charts	cause is not apparent, go
6	----	e) Unit #5	6) Continue H/I charts	to C/I chart.
7	b) 2 measurements	----	7) Continue C/I chart	C) <u>re: C/I Chart.</u> STOP
				calibrating and try to
				identify and correct
				cause. If cause is not
				apparent continue with
				calibration measurements
				until value reaches mean
				or a point on other side
				of centerline before pro-
				ceeding to hardware
				testing. There may be
				a carryover due to dyna-
				mic response of hard-
				ware.
8	----	f) Unit #6	8) Continue H/I chart	
9	----	g) Unit #7	9) Continue H/I chart	
10	----	h) Unit #8	10) Continue H/I chart	
11	----	i) Unit #9	11) Continue H/I chart	
12	----	j) Unit #10	12) Continue H/I chart	
13	c) 2 measurements	----	13) Continue C/I chart	
...	...	...		
...	...	...		

## ENCLOSURE 5

### REFERENCES

1. H. Hotelling, "Multivariate Quality Control . . ." in Techniques of Statistical Analysis, ed. Eisenhart, Hastay and Wallis, McGraw-Hill 1947.
2. A. J. Duncan, "Quality Control and Industrial Statistics" R. D. Irwin, Inc. 1959.

# ENCLOSURE 3 (1/1)

## DERIVATION OF FORMULA FOR CALCULATING CUMULATIVE MEAN ( $\bar{\bar{X}}$ )

(Note: Since  $X_1$  and  $X_2$  refer to data of redundant instrumentation, the value for each unit tested is referred to as  $\bar{X}$ , whereas the cumulative average for n units tested is referred to as  $\bar{\bar{X}}$ ).

$$1. \quad \bar{\bar{X}}_{i-1} = \sum_{i=1}^{(n-1)} \bar{X}_{i-1} / n_{i-1}$$

$$2. \quad \bar{\bar{X}}_i = \sum_{i=1}^n X_i / n_i$$

$$3. \quad (n_i) \bar{\bar{X}}_i = \sum_{i=1}^{(n-1)} \bar{X}_{i-1} + \bar{X}_i$$

$$4. \quad \bar{X}_i = n_i \bar{\bar{X}}_i - \sum_{i=1}^{(n-1)} \bar{X}_{i-1}$$

$$5. \quad \bar{\bar{X}}_{(i-1)} = \sum_{i=1}^{(n-1)} \bar{X}_{(i-1)} / n_{(i-1)}$$

$$6. \quad \bar{X}_i - \bar{\bar{X}}_{(i-1)} = n_i \bar{\bar{X}}_i - \sum_{i=1}^{(n-1)} \bar{X}_{(i-1)} - \frac{\sum_{i=1}^{(n-1)} \bar{X}_{(i-1)}}{n_{(i-1)}}$$

$$7. \quad = n_i \bar{\bar{X}}_i - \sum_{i=1}^{(n-1)} \bar{X}_{(i-1)} \left( 1 + \frac{1}{n_{(i-1)}} \right)$$

$$8. \quad n_i \bar{\bar{X}}_i = \left[ \bar{X}_i - \bar{\bar{X}}_{(i-1)} \right] + \sum_{i=1}^{(n-1)} \bar{X}_{(i-1)} \left( \frac{n_{(i-1)} + 1}{n_{(i-1)}} \right)$$

$$9. \quad \text{but } n_{(i-1)} + 1 = n_i \text{ and}$$

$$10. \quad n_i \bar{\bar{X}}_i = \left[ \bar{X}_i - \bar{\bar{X}}_{(i-1)} \right] + \sum_{i=1}^{(n-1)} \bar{X}_{(i-1)} \left( \frac{n_i}{n_{(i-1)}} \right)$$

$$11. \quad \bar{\bar{X}}_i = \frac{[\Delta \bar{X}]}{n_i} + \frac{\bar{\bar{X}}_{(i-1)} (n_i)}{n_i}$$



# ENCLOSURE 4A. CONTROL CHART CALCULATION FORM

Program  
Equipment Tested  
Parameter Measured

Calculations for Data  
Table

Line		f	X <sub>1</sub>	X <sub>2</sub>	R or d	Σ  R	Σ X <sub>1</sub> + X <sub>2</sub>	$\bar{X}$	$\bar{X}-\bar{X}$	$\frac{\Delta \bar{X}}{f_i}$	$\bar{\bar{X}}_i$	re: $\bar{X}$ Chart				re: $\bar{R}$ Chart		re: $\frac{d}{F\#2} \pm CI$		
												F#3	F#3 (R)	LCL	UCL	F#1	UCL	F#2	±CI	
1		2	3	4	5	6	7	8	9	10	11	12	13	14	15	16	17	18	19	20
2																				
3																				
4																				
5																				
6																				
7																				
8																				
9																				
10																				
11																				
12																				
13																				
14																				
15																				
16																				
17																				
18																				
19																				
20																				
21																				

# CONTROL CHART, R, d AND $\bar{X}$

Line	Program Equipment Tested Parameter Measured	Control Charts for Data		Notes
		R Chart	D Chart $\bar{X} + 0.0$	
1				
2				
3				
4				
5				
6				
7				
8				
9				
10				
11				
12				
13				
14				
15				
16				
17				
18				
19				
20				
21				
22				
23				
24				
25				

## 2-15P. INFORMATION SOURCES FOR EXPLOSIVES AND PYROTECHNICS

*by*

Gunther Cohn  
The Franklin Institute Research Laboratories

The great bulk of current technical information makes it difficult to keep posted. Each year it becomes a greater chore to keep abreast of new publications, or for that matter, of old ones that have been updated.

For this reason, this paper reviews briefly the useful information sources in the field of explosives and pyrotechnics. Updating the paper included in the Proceedings of the Fifth Symposium on Electroexplosive Devices (at The Franklin Institute, June 1967), it is again arranged by information sources, even though the type of information they furnish is mixed: some furnish data, some publish documents, some answer questions. The reader will certainly find it rewarding to become familiar with any of the sources listed that he has not dealt with in the past. This is not only a good way to learn about what is currently available but also to keep abreast of planned documents.

### 1. THE MISSION HOUSES

No review of information sources would be complete if it would not start with the government agencies whose mission calls for R&D in the area of interest: the mission houses. Defense, NASA, and AEC all have agencies that are responsible for a particular piece of hardware or for research in the area of explosives and pyrotechnics. The advantage of going to the mission house is that they (1) have people who can answer a question or who can direct you to a place where the answer can be found, (2) have good technical libraries stocked with documents in their field, and (3) publish reports, catalogs, indexes, and other documents of current interest. The best starting point is to consult your own librarian. She should be thoroughly familiar with all of the standard sources and should know ordering procedures.

## 2. GOVERNMENT MANUALS

The government is still the most prolific publisher. Defense, as well as NASA and AEC publish formal manuals for their material. Most series have their own index for easy searching. The recent and planned manuals are:

- *Military Explosives*, Department of the Army and Air Force, TM9-1300-214 (Army) or TO 11A-1-34 (AF), November 1967.

This comprehensive manual has been completely updated from the 1955 edition. It is a useful reference for general and technical information on military explosives and propellants. Among the subjects covered are descriptions, properties, tests, handling methods, theory, and use. Bibliography, index, 270 pages.

- *Properties of Explosives of Military Interest*, Army Materiel Command, Engineering Design Handbook, AMCP 706-177, March 1967 (AD-814 964).

This handbook listing the properties of explosives that are of interest to the military has been enlarged, updated, and revised. Formerly with 80 entries, the new edition lists 110 explosive compounds and mixtures. Tabulated data include sensitivity to friction, impact, heat; performance characteristics or effectiveness in weapons; physical and chemical properties; methods of preparation, synthesis or manufacture. References.

- *Explosive Trains*, Army Materiel Command, Engineering Design Handbook AMCP 706-179, March 1956, AD-462 254.

This text on explosive trains was written as an aid to ammunition designers. It covers fundamental principles of explosive reactions and theory, design considerations of all the diverse explosive elements including main charges, and related considerations of environment, fabrication, and evaluation. Glossary, references, index.

- *DOD Contractors' Safety Manual for Ammunition, Explosives and Related Dangerous Materials*, Dept. of Defense, DOD 4145.26M, October 1968. Super. Documents, \$1.50.

Primarily written to cover the provisions for DOD contractor operated plants, it serves well others who purchase, ship, or handle ammunition, explosives, and related dangerous material. Both mandatory (*shall, must*) and advisory (*should, may*) rules are covered. The healthiest chapter deals with manufacturing: processing, assembly, and disassembly of ammunition and explosives. Definitions, references, index, 180 pages.

- *Navy Transportation Safety Handbook*, Naval Ordnance Systems Command, OP 2165, Fifth Edition, Vol. 1, November 1968; Vol. 2, February 1969.

This handbook deals with the transportation of ammunition, explosives, and other dangerous articles. Volume 1 covers administrative requirements, preparation for shipment, procedures for inspection, safety regulations, disposal and other instructions. Volume 2 is a tabulation of standard ammunition shipped.

- *Fuzes*, Army Materiel Command, Engineering Design Handbook, AMCP 706-210, Revised. In publication: Fall 1969

Prepared as an aid to ammunition designers, this handbook presents both theoretical and practical fuze data. Extensive changes were made to update this volume from the 1960 original. Illustrations and test data of sample ammunition items were brought up to date. The treatment of electric fuze actions was greatly enlarged and new chapters were included on design considerations and guidance. Glossary, references, index.

- *Fuze Catalog*, Dept. of Defense, Military Handbook 137. In publication: Fall 1969.

This catalog is a complete revision and update of the Army, Navy, Air Force Fuze Catalog published in 1959. A complete store of military and technical information of all fuzes and fuze explosive components (both standard and developmental), it covers detailed design and performance characteristics. Three volumes, 1500 data sheets (classified).

- *Explosives and Explosive Devices*, by Gunther Cohn, National Aeronautics and Space Administration, Technological Survey NASA-SP- . In publication: Fall 1969.

This critical review was written to inform industry of NASA's contribution to modern technology in this field. Covered are explosive devices, low and high explosives, incendiaries, and related materials. Because most of today's devices are electrically initiated, the survey also covers power sources, instrumentation, circuits, and prevention of radio-frequency hazards. Glossary, references, manufacturers' list, 66 pages.

- *Design of Ammunition for Pyrotechnic Effects*, Army Materiel Command, Engineering Design Handbook, Part Four, AMCP 706-188. In publication: Summer 1970.

A practical engineering reference for the design of pyrotechnic ammunition, it emphasizes terminal effects and engineering aspects. This handbook is one of a five-part series, the other volumes having already been published: Part One: Theory and Application (AMCP 706-185), Part Two: Safety, Procedures and Glossary (AMCP 706-186), Part Three: Properties of Materials Used in Pyrotechnic Compositions (AMCP 706-187), Part Five: Bibliography (AMCP 706-189).

- *Hardening Weapon Systems Against RF Energy*, Army Materiel Command, Engineering Design Handbook, AMCP 706-235. In publication: Spring 1970.

This handbook describes the design techniques that will help protect the weapons system against radio-frequency energy, static electricity, and lightning. Design techniques are illustrated for a variety of subsystems. Glossary, references, index.

### 3. COMMERCIAL PUBLICATIONS

In recent years, manufacturers' catalogs have improved greatly. They now contain worthwhile technical information, performance data, and other useful notes. Catalogs are available from the manufacturer for the asking. Why not send for them? There are also a couple new books and periodicals.

- *Military and Civilian Pyrotechnics*, Herbert Ellern, Chemical Publishing Co., Inc., New York, 1968, \$15.

This volume serves both as a primer for newcomers and as a general reference handbook. Considerably updated over the first edition (1961), it enlarged civilian (commercial) aspects including matches, fireworks, thermite, spontaneous ignition. Glossary, references, pyrotechnic formulations, index, 464 pages.

- *Chemical Warfare, Pyrotechnics and the Fireworks Industry*, by T.F. Watkin et al, Pergamon Press, Long Island City, N.Y. 1968.

This small but valuable contribution is divided into three parts which correspond to the three divisions of the title. Part I evaluates chemical warfare from its introduction into battle in 1915 through its future potential. It gives a detailed account of the nerve gases and problems associated with them. 110 pages.

- *Radio Frequency Energy, A Potential Hazard in the Use of Electric Blasting Caps*, Institute of Makers of Explosives, 420 Lexington Ave., New York, N.Y. 10017, Safety Library, Publication No. 20.

This booklet is designed to give the commercial blaster an appreciation of the hazards associated with initiation of electric blasting caps by RF energy and guidelines which should permit safe operation when in close proximity to RF sources. The booklet contains tables of safe distances and data on common RF sources.

- *American Pyrotechnist*, Max P. Vander Horck, Editor, 6359 Wunderlin Ave., San Diego, Calif. 92114. \$5/year.

An educational and information publication for all fireworks enthusiasts, this monthly publication is dedicated to the advancement of safety, skill, and artistry in pyrotechnics through communications. Twelve pages/issue, started January 1968.

- *explosives and pyrotechnics*, Gunther Cohn, Editor, The Franklin Institute Research Laboratories, Philadelphia, Pa. 19103. \$15/year.

This monthly newsletter covers explosives, pyrotechnics, and their devices. Designed as an information network to serve all those interested in the field, it covers new developments, publications, events, and reader contributions on explosive technology, safety, circuitry, handling, and related information. Four pages/issue, started January 1968.

#### 4. SYMPOSIUM PROCEEDINGS

To date we have held at The Franklin Institute five symposia on Electric Initiators and two HERO Congresses on (Hazards of Electromagnetic Radiation to Ordnance). These meetings were sponsored by various military agencies and each was attended by over 300 representatives of government and industry. Their proceedings serve as a review of the state of the art. Copies may be obtained from the Defense Documentation Center. A (U) indicates that the proceedings are classified Confidential.

<u>Proceedings</u>	<u>Date</u>	<u>DDC No.</u>
1st Proceedings Electric Detonators	Sept. 1954	AD-066 001
2nd Proceedings Electric Initiators (U)	Sept. 1957	AD-153 579
3rd Proceedings Electric Initiators (U)*	Nov. 1960	AD-323 117
4th Proceedings Electric Initiators	Oct. 1963 (U) Oct. 1963	AD-350 150 AD-440 764
5th Proceedings Electroexplosive Devices**	June 1967	---
1st Proceedings HERO Congress (U)*	May 1961	AD-326 263
2nd Proceedings HERO Congress	May 1963 (U) May 1963	AD-342 306 AD-417 172

*\*Summarized in "Electric Initiators: A Review of the State of the Art," by Gunther Cohn, The Franklin Institute Research Laboratories, Report LM-A2357-12, November 1961 (AD-266 014).*

*\*\*Order from The Franklin Institute Research Laboratories, Philadelphia, Penna. 19103, \$10.*

## 5. R&D PROGRAMS

We at The Franklin Institute Research Laboratories have been engaged in research relating to explosives and pyrotechnics for over twenty years. We would be pleased to talk with you if you need further details. Contact Mr. E.E. Hannum, Manager, Applied Physics Laboratory, 215/448-1236. The following are a few samples of our efforts with EED's.

- *Prediction of Pyrotechnic Performance.* For Picatinny Arsenal.

Data from experiments with magnesium/sodium nitrate flares were organized for computer retrieval. Relationships determined between composition parameters and output characteristics can then be used to predict the performance of similar compositions. (C1881)

- *Sensitivity of Carbon Bridge Detonator to RF Energy.* Commercial project.

The occasional premature functioning of electric fuzes on an assembly line was investigated to pinpoint the problem. A thorough RF evaluation of the carbon bridge indicated the difficulty to lie in both the sensitive electric detonator and the energy source. No mishaps have occurred after recommended changes in procedures were instituted. (C1985).

- *Estimation of the Peak Output Voltages of TV Antennas Due to Lightning.* Commercial project.

The peak output voltage of typical TV receiving antennas due to lightning strokes was analyzed to determine the effect of lightning on circuit transistors. The electric field response was plotted. (C2137)

- *Computation of RF Hazards.* For NASA

Methods were examined for analyzing the potential RF susceptibility to electrical components and systems used in typical space vehicles. The result was a compilation of the computational and analytic methods for analyzing RF hazards as well as the philosophy, applicability, and limitation of this approach. (C2210)



## 2-16P EXPLOSIVE DETONATOR SHOCK TESTING FOR IMPACT SENSORS

Author: Joseph Robin Klein \*

Operation: Re-entry System Department  
3198 Chestnut Street  
Philadelphia, Pennsylvania

### INTRODUCTION

A problem involved in the design of inertial switches for use as impact sensors is the duplication of the acceleration to be experienced by the switch and switch response to this acceleration. When the inertial switch is to be used to sense impact in an impact fuzing system the overall problem is increased in that the switches response time is an added factor to the success of the fuzing mode. In addition, the actual characteristics of the switching operation must be determined to ensure compatibility of the switch and related circuitry. Chatter and contact bounce become important factors in design or selection of an inertial switch. To assure switch performance that will satisfy the fuzing systems requirements, it is imperative that the switch in question be subjected to the closest approximation of the actual shock expected at impact.

### PROBLEMS OF PRESENT TEST METHODS

Heretofore, the testing of impact switches has been divided into two techniques; (1) the individual switch in the laboratory and (2) the complete fuzing system in the field or in flight. The least expensive of these two methods is the testing of the individual switch with standard laboratory test equipment. Although there are many laboratory methods and shock application test machines that can be used for this purpose, they are limited to relatively slow shock applications and

\* The author is now employed as a Senior Engineer at Fairchild Space and Defense Systems, Copiague, New York.

small magnitude shock levels. Most laboratory shock machines are limited in their applications to about 3000 g's, with a minimum pulse width of 200 microseconds whereas many impact shocks experienced by present day vehicles exceed the 3000 g, 200 microsecond shock pulses.

The second testing technique has been used in order to determine impact switches response to shocks realistic of those experienced in actual usage. This has involved field tests using a rocket driven sled to create the higher accelerations and faster applications of acceleration with time. Usually this involves the installation of the switches in simulated vehicles, a costly and lengthy procedure. Other tests have involved a projectile which is fired into a simulated structure containing the switch.

Today's usage of impact switches demands greater reductions in response times; in addition it has been necessary to not only test to a specific threshold, g level, but also to define the rate of application of the shock, the  $dg/dt$  value. For example, in one application an inertial switch was required to operate after experiencing a shock loading of 350 g's applied at the rate of 500 g's/microsecond. Since this degree of shock loading is out of the range of present shock machine capability, a new test method was pursued. The goal was a new test method which would permit reliable and economical testing of inertial switches subjected to multiple and varied shock inputs. Such a test method was determined and employed.

#### DETONATOR TESTS - APPROACH

The approach that was chosen was the use of high energy detonators to deliver the high shock levels at the rapid rate required. These detonators, or blasting caps, consist of a sealed metal or plastic shell in which there is an explosive

charge and a plug element with a bridge wire for electrical initiation. An initial series of exploratory tests were run in which two types of high energy detonators were fired against a fixture. The two detonators used were the Dupont E-77 and E-96 detonators containing 3.2 grains of PETN and 4.1 grains of RDX respectively. A piezoelectric accelerometer mounted on the fixture measured the shock input delivered by the detonators. The E-77 detonator provided initial  $dg/dt$  rates of 175 to 250 g's/microsecond with peak acceleration up to 2500 g's. The E-96 detonator with its larger charge supplied  $dg/dt$  rates up to 850 g's/microsecond with peak g levels exceeding 3250 g's before the accelerometer trace exceeded the limits of the simple instrumentation.

#### TEST PROCEDURE

As this preliminary series showed that the detonator tests were a feasible approach, a series of tests were run on three inertial switches. These inertial switches are a normally closed switch. One contact is held against a stationary contact by magnetic and spring force. When the acceleration on the contact's mass overcomes the combined magnetic and spring forces, the two contacts will separate and the circuit will open. The three switches had thresholds of 700, 1000 and 1500 g's. Four different detonators of increasing energy output were used in the tests. Illustration 1 shows the test setup and electrical circuitry used. The detonators were mounted on a steel plate in contact with an aluminum cylinder. At the opposite face of the cylinder, a piezoelectric accelerometer and an inertial switch were mounted equidistant from the center of the cylinder. The cylinder was suspended as a pendulum, two feet from the center of rotation. In order to obtain simultaneous time records of the shock output and inertial switch opening, the accelerometer and inertial switch outputs were fed into the two channels of a dual beam oscilloscope. The light output, or flash, of the exploding detonator was

detected and used to trigger both traces of the oscilloscope.

The detonators used to generate the shock loads were the Dupont E-94, E-77, E-1B (8), and E-3B detonators. They were selected according to the quantity of explosive contained in order to vary the shock input and the magnitude of the acceleration produced. Due to the rapid damage of the steel plate from the detonators, a new plate was used for each shot.

The last series of tests involved the firing of a particular detonator, the Dupont E-1B (8), against twenty inertial switches in order to determine spread of response times from switch to switch and thus be able to predict with greater confidence the response times of all switches of the particular design. In addition, the repeated tests with the same detonator would show to what extent the shock input could be held constant for a given detonator.

#### TEST RESULTS

Several terms were used to describe the resultant accelerometer traces in the tests. A typical accelerometer trace is shown in Illustration 2. There is a time lag from detonation (start of trace) to the first acceleration recorded. This is the time required for the shock wave to travel the length of the aluminum rod to the accelerometer. The accelerometer trace usually showed a slight acceleration and then the full shock four to five microseconds later. This first vertical deflection of the accelerometer is felt to be the action of the steel cover plate coming into full contact with the cylinder as a result of the detonator shock. It is of sufficiently small energy that its effect can be ignored. Therefore, for  $dg/dt$  computations, the average slope of the initial large digression from the zero acceleration was used. The inertial switch response time was defined as the time from the initial major trace deflection to switch opening.

The series of tests that were run on the varied threshold switches and several detonators showed some interesting relationships. In several cases, relatively fast response times were observed for comparatively low initial and/or peak accelerations. The rate of increase of acceleration ( $dg/dt$ ) seems to have been the primary factor governing the response time of the switches rather than initial or peak accelerations. This is evidenced by an examination of Graph 1 which shows response time as a function of  $dg/dt$  until it approached a minimum response time band. Similar results could be shown for the other switches although more energy or higher  $dg/dt$  values would be required to produce a similar curve. Table 1 lists the  $dg/dt$  values from the four types of detonators to indicate the range of shock inputs delivered by the various types. As shown in this table, consistent  $dg/dt$  values of 300 g's/microsecond or greater could be obtained by using the E-1B (8) or E-3B detonators.

The final series of test involved during one type of detonator (E1B 8 ) against two groups of switches, each group containing ten switches. In addition to determining the variability of response time from switch to switch, this series of tests gave data on over 200 firings of the E-1B (8) detonator. Graph 2 shows the distribution of the resulting  $dg/dt$  value. Although there were ten firings that resulted in  $dg/dt$  rates below 300 g's/microsecond, seven of these occurred in the first twenty firings. At this point it was decided that extreme care must be taken to control the orientation of the detonator to the face of the fixture. The tests continued with the detonators held to a position of  $90^\circ \pm 5^\circ$  to the face of the fixture and only three of the following 182 shots yielded less than 300 g's/microsecond. Typical traces are shown in Illustration 3. The oscilloscope traces also showed that the shock lasted for an average duration of 20 microseconds.

## CONCLUSIONS

The early tasks involving detonator shock loading showed that high accelerations and rate of application of these accelerations were obtainable from standard explosive detonators. This allowed inertial impact switches to be tested to the high acceleration and  $dg/dt$  levels associated with high velocity impacts. The following series of tests demonstrated that the shock pulse could be varied to give shock inputs from 150 to over 2900 g's/microsecond depending on the detonator used. The pulse undoubtedly could also be varied to obtain particular pulse shapes by modifying the fixture to be used. The final series showed that use of a particular detonator-fixture combination yielded shock rates consistently over 300 g's/microsecond. The shock pulses usually were of 20 microseconds. The results of the explosive detonator shock tests have shown that high velocity impact shocks can be simulated inexpensively and quickly in contrast with the previous methods of projectile and rocket sled tests. It is quite probable that with further testing, the scope of these tests could be extended from the component level to the system level and quite possible to complete vehicle level. The detonator shock and fast shock loadings are encountered, such as simulation of shock waves. For these reasons, the explosive detonator test methods hold high promise as future test procedures that could increase the designers ability to simulate any shock pulses he may encounter in his product's usage.

## ACKNOWLEDGEMENT

The work described in this paper was performed at General Electric, Re-entry and Environmental Systems Division and The Franklin Institute Research Laboratories for United States Air Force Space and Missile Systems Organization.

Table I dg/dt Valves vs. Type of Detonator

Detonator	E94	E77	E1B(8)	E3B
Trial	dg/dt Valves - g's/microsecond			
1	400	450	1100	480
2	370	250	220	1350
3	320	180	1000	320
4	480	220	850	1000
5	350	530	1000	600
6	280	220	720	710
7	350	90	770	410
8	415	780	220	590
9	550	85	970	960
10	390	330	650	940
11	360	630	690	540
12	255	550	540	880
13	175	73	450	1100
14	390	480	650	1100
15	190	630	200	1100
Average	345	367	669	805

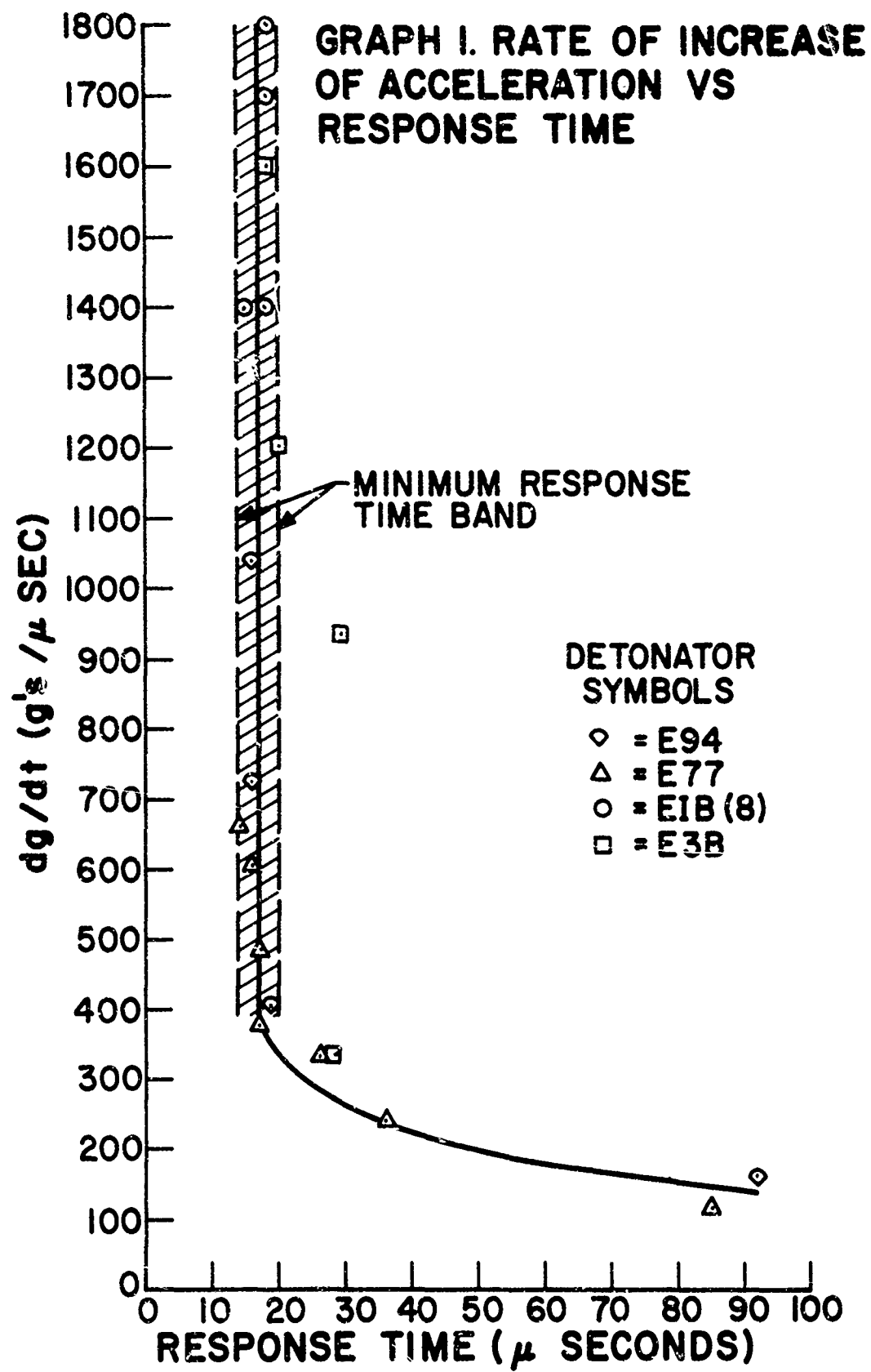




ILLUSTRATION 1. EXPLOSIVE SHOCK TEST SETUP

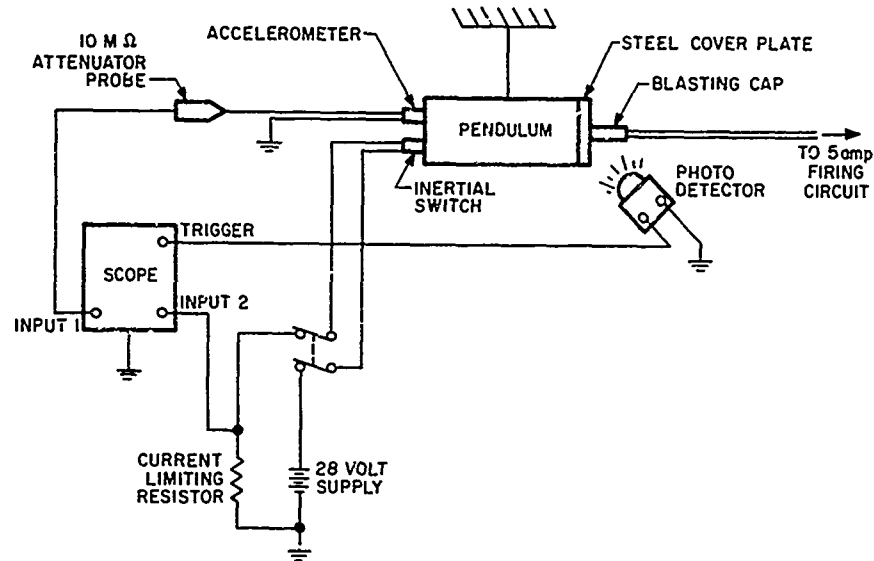
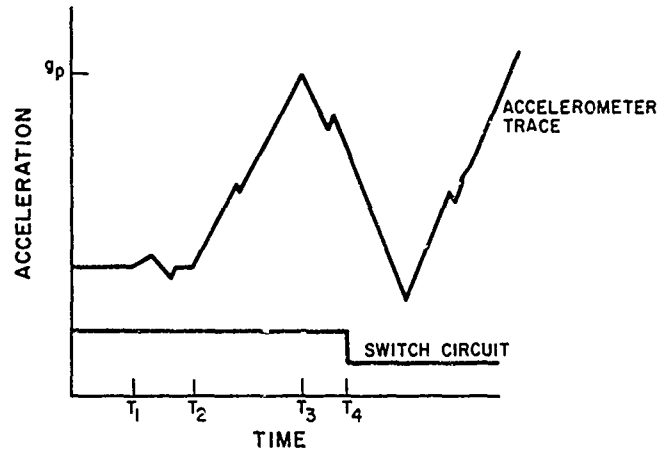


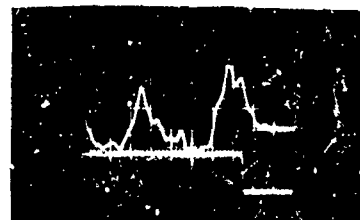
ILLUSTRATION 2. TYPICAL ACCELERATION TRACE



- $dg/dt = g_p / T_3 - T_2$   
RESPONSE TIME =  $T_4 - T_2$
- $T_1$  = INITIAL ACCELERATION
  - $T_2$  = START OF PEAK ACCELERATION CURVE BEFORE SWITCH OPENING
  - $T_3$  = PEAK ACCELERATION BEFORE SWITCH OPENING
  - $T_4$  = OPENING OF SWITCH
  - $g_p$  = MAXIMUM G LEVEL OF PEAK ACCELERATION CURVE



Vertical Deflection = 3625g/division  
Horizontal Deflection = 10 microseconds/  
division



Vertical Deflection = 7250g/division  
Horizontal Deflection = 10 microseconds/  
division

Illustration 3 Typical Acceleration and Switch Traces

### ABSTRACTS - SESSION THREE

3-1 Safety of EED's in the Naval Electromagnetic Environment

*F.J. Chesterman*

The paper describes the current practice in the Royal Navy of ensuring that EEDs are safe when being embarked and in operational use. The special problems arising when new weapons and new high power transmitters are introduced are outlined, and the methods of monitoring and passing the information to the Navy are discussed.

3-2 A Broadband RF Filter/Attenuator Plug for Wire Bridge Electroexplosive Devices

*Theodore Marshall,  
Paul F. Mohrbach*

A broadband rf filter/attenuator plug which replaces plastic type plugs in EED's has been developed. The filter/attenuator incorporates a novel approach to shield the materials within the plug which provides broadband rf protection. Typical dimensions are shown for one type EED. Worst case attenuation data indicate, this type approach can provide adequate rf protection for wire bridge or coaxial type EED's. Some specific aspects of design are discussed. Curves and data are shown for two designs utilizing different attenuating materials from various manufacturers, and some design considerations are discussed.

3-3 Sterilization-Environmental Testing of Initiators

*Laurence J. Ement*

Three types of initiators, developed for space applications, were subjected to six dry heat sterilization cycles (135°C - 36 hrs each), mechanical, and electrical environments. The as-received performance of the initiators was compared to the performance of units subjected to sterilization and mechanical environments. Results of various non-destructive, electrical and functional tests of these units indicate that two of the three units tested are promising candidates for use in interplanetary missions.

3-4 The E.M.I. Hazard Measurement System

*W.L. Watton and W.B. Scamaton  
Presented by W.S. Hall*

The system described was developed for the British Ministry of Technology, for use in EMC trials of complete guided weapons. An instrumented inert EED replaces each of the live ones for which information is required. A signal voltage derived directly from the inert device is converted into modulation of an audio frequency carrier. This low frequency signal is coupled electro-magnetically through the skin of the weapon under test. Once outside it is converted into an audio signal which is piped to a remote decoder/indicator unit where the audio signal and its modulation are further processed resulting in a meter reading calibrated in terms of equivalent dc signal at the detecting EED.

3-5 Discharge of an Electrostatically Charged Human

*John T. Petrick*

The common mechanisms for charging of the human and the duration and magnitude of that charge are discussed. The exact nature of the discharge produced when a charged human is grounded and methods of simulating that discharge to determine the electrostatic sensitivity of electroexplosive devices are explained.

3-6 Experiments in the Protection of EED's from Electrostatic Discharge

*E.G. Pierson*

Safety in the handling and application of EED's now specifies that such devices successfully withstand a 25 KV potential from a 500 picofarad capacitor applied between bridge-wire and case. What do we do with the many qualified EED's that would fail to withstand this test? Redesign and requalification might well be prohibitively costly. We have developed an inexpensive electronic component that can be relied upon to form an alternate preferential path for high voltage discharge that will safeguard handling and application of these devices. While conducting high voltage static discharge testing, we have observed an interesting phenomenon that changes the bridgewire resistance.

3-7 Plain Talk About Electrostatics

*L.D. Pitts*

Electrostatic discharges may have many significant effects on the safety and functioning of EED's in production, handling and applications. In this paper a number of aspects of electrostatics are pointed out and discussed briefly. These include the significance of electrostatic sensitivity tests of explosives and pyrotechnics, electrostatics in EBW design, application to RF sensitivity, protective devices, evaluation of different cases of series breakdown and production facility hazards.

3-8 Initiation of Electroexplosive Devices by Lightning

*Harvey S. North*

Experiments were fielded to study the effects of lightning-induced electricity on electro-explosive devices, when exposed in typical field setups. The data from these studies shows that most electroexplosive devices can be initiated by the electric fields associated with lightning and give some indication as to distances at which these fields were hazardous.

3-10 Liquid Desensitized Initiators

*Robert W. Heinemann*

This paper presents a novel approach to initiator safety. It is well known that explosives are desensitized by liquids. Could wetting the initiator make it safe to handle? To evaluate this idea, test detonators having porous caps were immersed in inert, volatile liquids. After a few minutes, they could not be initiated.

3-11 Instrumentation for Making Broadband Measurements on Electroexplosive Devices

*Jack G. Hewitt, Jr.*

Measurements are necessary to determine whether ordnance subsystems can be certified to conform to range safety specifications for accidental initiations. These measurements require special wideband instrumentation and sensors which (1) can be used to establish electroexplosive device sensitivities for all modes with a minimum of statistical firing tests and (2) can detect stray energy in an ordnance subsystem with a minimum of perturbation. Various instrumentation techniques including thermal energy sensors, microwave diodes, wideband microcircuit amplifiers and microstrip transmission lines are evaluated.

### 3-1 THE SAFETY OF EEDs IN THE NAVAL ELECTROMAGNETIC ENVIRONMENT

#### UNCLASSIFIED

by

F.J. CHESTERMAN, C.ENG., M.I.E.E.  
RADIATION SAFETY OFFICER  
ADMIRALTY SURFACE WEAPONS ESTABLISHMENT  
(PORTSDOWN, COSHAM, HANTS., ENGLAND)

**ABSTRACT:** The current practice of ensuring that EEDs are safe when being embarked on board ship, and in operational use is described. The methods of monitoring, measuring and passing the information to the Navy, when new weapons and new high power radars are introduced are discussed.

#### A. INTRODUCTION

1. A modern warship has special problems in this field. Many high power radiators and many electro-explosive devices (EEDs) are assembled on a metal superstructure in a comparatively small volume.
2. Weapons and radars can also be airborne in fixed wing aircraft and helicopters; both operating from the ship and flying in the vicinity of the ship. Therefore a warship represents possibly the biggest concentration of explosives and electromagnetic sources that is assembled in one volume. As an example the possible transmitters and EEDs for a warship are shown in Table 1.

#### B. GENERAL

1. The safety aspects of EEDs are considered separately as follows:-
  - (a) Transit, embarkation.
  - (b) Mounted on own ship for operational use.
  - (c) Ships alongside or ships in company.

2. Other aspects of safety which have a bearing on the policy of dealing with (a), (b) and (c) and are normally considered with them are:-

- (i) Safety of personnel.
- (ii) Reliability of weapons.
- (iii) Electrical shocks and r.f. burns.
- (iv) Electrical transients (switching transients in firing circuits).

In this paper (i), (ii), (iii) and (iv) will not be discussed in detail, and the emphasis will be primarily on EEDs in electromagnetic fields.

#### C. INTRODUCTION OF A NEW WEAPON AND NEW RADAR IN THE FLEET

1. Up to the present time the record of safety in the Royal Navy has been very good, and this has meant a slow evolution of measurement techniques and a small expenditure of resources.
2. The best way to study the machinery of safety is to consider a new missile and a new radar, which are on the drawing board.  
This missile and radar will eventually come together and be fitted in a new class of ship.
3. In figure 1 is shown the sequence of events. A most important stage is the scrutiny of the ship layout or antenna rig. This is the drawing board stage and the positions of antennae and explosive devices can be easily varied. Safety for personnel can also be injected at this stage, and a good layout pays handsome dividends when the ship or ships are built.
4. There are three stages of measurement:-
  - (a) Bare Missile (Handling, Transit and Embarkation).
  - (b) Own Ship Environment (Operational Use).
  - (c) Ship Alongside (Ships in Company).

##### Stage (a)

The bare missile is subjected to the strongest possible field in every band that is available or in use in the Services. These fields or power densities have been specified, and it is part of the contract with the makers, that the missile will be safe with a safety factor of 20 dB in these fields.

The missile is hoisted in front of a radar in the field maxima; it is rotated in the horizontal plane, and suspended nose down or up, to test for polarisation sensitivity whenever possible.

The 20 dB safety factor is specified to take account of:-

- (i) Variation in the firing level of the fuse.
- (ii) Deterioration of the missile in Service life.
- (iii) Errors introduced by the method of measurement and the site of measurement (site effect).

If a missile is already in Service and a new radar is introduced then the missile will be measured either by the makers or by the Navy Department, depending on the state of the contract.

#### Stage (b)

Own Ship Environment. A Ship Trial is done for the first of class or first fitting. The missile is mounted on its launcher and switching sequences and the orientation of the launcher are varied. All radars are beamed on to the missile if possible, and all communication transmitters are on. Several frequencies are radiated on each communication antenna, the frequencies being chosen and spaced so that any possible resonances in the missile are excited, e.g. 1 to 20 MHz seven spot frequencies.

The aim of this trial is to ensure that the missile is safe in its own ship environment with a safety factor of 20 dB.

#### Stage (c)

Ship Alongside. This trial is carried out in a similar manner to the Own Ship Trial. The radiation is from a ship alongside. In general antennae are mounted high and tend to "look over" or not illuminate a missile launcher in their own ship. Also some high power radars are fitted with cut outs to prevent superstructures and working spaces from being illuminated on own ship. Therefore a missile on its launcher can be subjected to a higher power density by a ship passing alongside or in company.

#### D. METHODS OF MEASUREMENT (WIRE FUZES)

##### 1. Heat Sensitive Paint

The paint is applied to the actual fuze wire, and the fuze assembled into the EED. The device is then subjected to the electromagnetic field.

The fuze is then removed and inspected under a microscope, if the paint has melted the weapon is unsafe, if the paint has not melted a direct current is passed through the fuze and increased in value until the paint melts. Depending on the paint used and the ambient temperature, the melt power is calculated, and safety factors of 14 to 20 dB are usually obtained.

##### 2. Vacuo Junction

The Vacuo Junction replaces the fuze, it has a bridge wire with a thermocouple in thermal contact, but not electrical contact with the wire. The temperature rise is measured by the change in thermal e.m.f. generated by the thermocouple.

##### 3. Acoustic Link/Thermistor

A Thermistor is attached to the actual fuze and is connected in one arm of an audio frequency bridge. The change in resistance of the Thermistor causes an out of balance current to flow through the primary of a split transformer, the primary half of which is attached to the inside skin of the missile. The secondary half is located on the outside of the missile skin and is connected to an acoustic transducer.

The acoustic tone is taken away from the missile by a plastic tube, to another transducer which converts the tone back to an electrical signal.

The reason for changing to an acoustic signal is to minimise the r.f. perturbation of the external r.f. field, i.e. there are no wires connected to the missile.

##### 4. These methods of measurement are summarised in Table 2.

5. Methods of Measurement General

Conducting carbon composition type igniters are measured with diode rectifying/d.c. amplifier circuits. The measuring circuits have been built into actual primers and the detected voltage level is related to the firing threshold level.

6. When the measuring devices so far described are being used, the electromagnetic field environment is measured in terms of  $\text{mW}/\text{cm}^2$  or  $\text{V}/\text{M}$ . Thus data is acquired about the relationship between the field external to the missile and the energy reaching the fuze. This data enables assessment of hazards to be made for subsequent fittings by analogy.

7. Standard laboratory and analytical techniques are also used in the assessment of hazard stages. Measurements are made of the physical constants of the electrical circuits of electro-explosives:- V.S.W.R., Transmission Loss, Impedance, Inductance, Capacity and Resistance. Data acquired in this manner is used in classical or numerical calculations. Analysis is normally carried out from the radiator to the fuze, and involves calculating the electromagnetic field at the EED, and the response of the EED to that field. In general calculations are always checked by trial and measurement, so that experience and confidence are gained in the methods used.

8. A photograph of a typical fuze is shown in figure 2. It can be seen that the two brass conductors which support the actual bridge wire, effectively form a parallel plate transmission line. Resonances can be measured in the actual fuze at microwaves, and the reflection coefficient varies by as much as 20 dB. Figure 3 is a comparison of an actual fuze with a Vacuo Junction, measured on the same bench under identical conditions. This figure (3) shows that at one frequency (4.5 GHz) the fuze accepts 25 dB more power than the Vacuo Junction.



#### E. INFORMATION PROMULGATED TO THE FLEET

1. The general aim is that there are no hazards or restrictions for EEDs when being embarked or used operationally on board ship. In the past if a device was Radhaz unsafe the frequency or band and the safe distance to the radiator was specified. The ship would thus make local rules for safety.
2. The present practice which is not complete will be as follows:-
  - (a) The specification of safe (20 dB) power densities or field strengths in all bands for bare missiles.
  - (b) The specification of safe (20 dB) power densities or field strengths for missiles on launchers.
  - (c) The specification of all radars in use in the Navy, plots of power density against distance, and specification of safe distances from communication transmitters.
3. Figure 4 shows a typical radar power density plot and Table A figure 4 shows some figures of power density safe level that could be measured for a missile. By projecting these power densities on the curve the safe distance can be obtained. Plots have been published in the Fleet of all radars in use. Curves for new radars and new EEDs will be published as new devices are introduced.
4. The curves and power densities should cover all situations i.e. a helicopter carrying an anti-submarine weapon landing on a frigate or a ship with a new radar fitted coming alongside.
5. The future trend in radar and communication design appears to be towards higher power. Since World War II powers have increased by ten times, and although there have been improvements in ordnance design, the problems will undoubtedly become more severe. This is particularly true from the hazards to personnel point of view.

6. Figure 5 is a plot of various bands and "dish" sizes for a mean power radiated of 5 kW. This was plotted for personnel hazards and safe distances of 1000 ft. are not unlikely. The efforts of the power valve designers in designing coherent sources, mean that power sources can be engineered into matrix arrays. It should also be remembered that the radar designer who wishes to increase the power transmitted, to double the detection range, must increase the transmitted power by sixteen times.
7. Communication transmitters, at present, are specified with a safe distance for EEDs. In general the problems are not serious as the radiation tends to be omni-directional, and not a pencil beam as in radar. However the fields around shipboard radiators of this kind are complex, so that clear cut curves of field strength cannot be issued as in the case of radars.

#### F. WIDER ASPECTS OF SAFETY

1. The following aspects of safety have been discussed:-
  - (a) EEDs in transit and embarkation.
  - (b) EEDs in use.
  - (c) EEDs illuminated by some radiation external to the ship.
2. The question then arises whether there is any situation where hazards could occur. Unfortunately there are, and they are in situations which require international co-operation as follows:-
  - (i) EEDs in transit by air or ship around the world. The carrier does not know what environment he is passing through. The UK has started to produce a specification for the transit of EEDs in a world-wide environment as a first step in this problem.
  - (ii) A warship passing a land based transmitter - exercising with ships of another Navy - or two warships of any nationality passing close to each other. It is in the mutual interests of all countries that there is no danger to personnel or EEDs.

### G. CONCLUSIONS

1. The practice of safety and methods used to ensure safety have been described and discussed. The methods have proven satisfactory and have reduced the risks to an acceptable safe level under conditions of operational activity.
2. Although the safety record is good it does not appear that restrictions can be relaxed, as the continuing trends in electromagnetic engineering are towards higher powers, and the problems will tend to become more acute.

TABLE 1

#### TYPICAL WARSHIP

Electromagnetic Sources	Electro-explosive Devices
Long Range Surveillance Radar	GW Long Range
Medium Range Acquisition Radar	GW Short Range
2 of Tracking Guidance GW Radar	Gun
Short Range Navigational Radar	Anti-submarine Mortars
Airborne Radar	Flares
Satellite Communications	Airborne Weapons
MF } HF } Communication UHF }	Airborne EEDs Army Weapons
Navigational Aids	

TABLE 2

SUMMARY OF METHODS OF MEASUREMENT (WIRE FUZES)

Advantages

Disadvantages

HEAT SENSITIVE PAINT

- |  |   |
|--|---|
| <ol style="list-style-type: none"> <li>1. No perturbation of r.f. characteristic of fuze.</li> <li>2. No wires added to fuze or missile.</li> <li>3. No modification of missile.</li> <li>4. Convenient to use on a launcher.</li> <li>5. Safety factor 14-20 dB.</li> </ol> | <ol style="list-style-type: none"> <li>1. Go-No Go test.</li> <li>2. No continuous indication of actual level of pick-up.</li> <li>3. Requires repetition of trial with paints of varying melting points to bracket the pick-up level.</li> </ol> |
|--|---|

VACUO JUNCTION

- |  |  |
|--|--|
| <ol style="list-style-type: none"> <li>1. Safety factors 20-30 dB.</li> <li>2. Measurement of level of pick-up.</li> </ol> | <ol style="list-style-type: none"> <li>1. Wires added to fuze and missile.</li> <li>2. Necessary to mount recorder or indicator inside or outside missile.</li> <li>3. Perturbation of electromagnetic field.</li> <li>4. Wires inconvenient when training launcher.</li> <li>5. Necessary to modify missile internally.</li> <li>6. Does not simulate fully the r.f. characteristic of fuze.</li> </ol> |
|--|--|

ACOUSTIC LINK/THERMISTOR

- |  |   |
|--|---|
| <ol style="list-style-type: none"> <li>1. Effectively no perturbation of r.f. characteristic of fuze.</li> <li>2. Safety factor 20-30 dB.</li> <li>3. Measurement of pick-up level.</li> </ol> | <ol style="list-style-type: none"> <li>1. Plastic tubes inconvenient when training launcher.</li> <li>2. Acoustic pick-up on tubes.</li> <li>3. Some internal modification of missile necessary.</li> </ol> |
|--|---|

**FIG.1.**  
**SAFETY OF EEDs. RADHAZ SEQUENCE.**

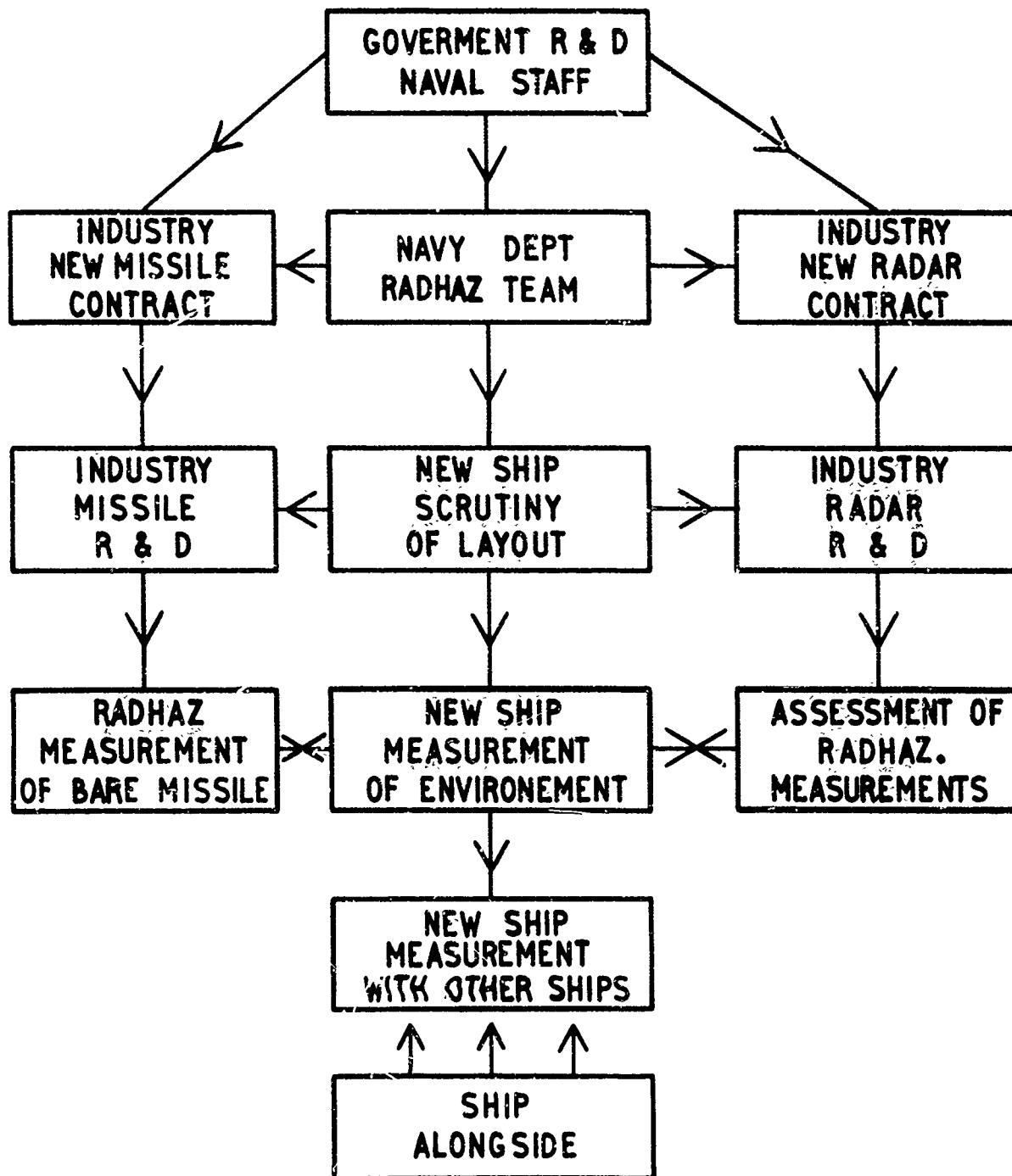


FIG. 2  
TYPICAL FUZE

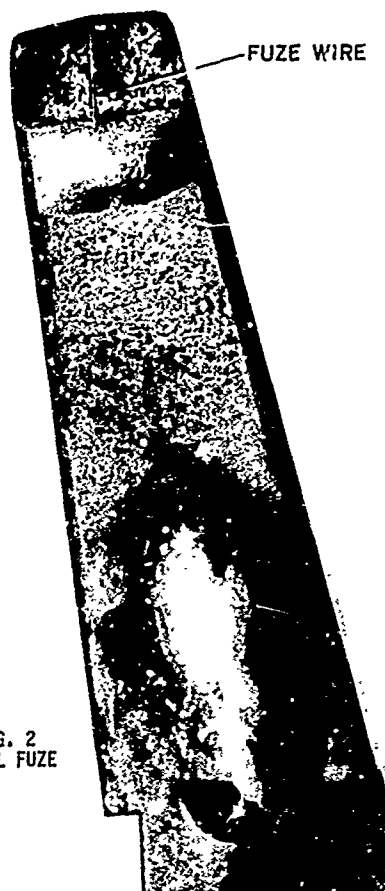


FIG. 3  
REFLECTIVITY OF FUZE

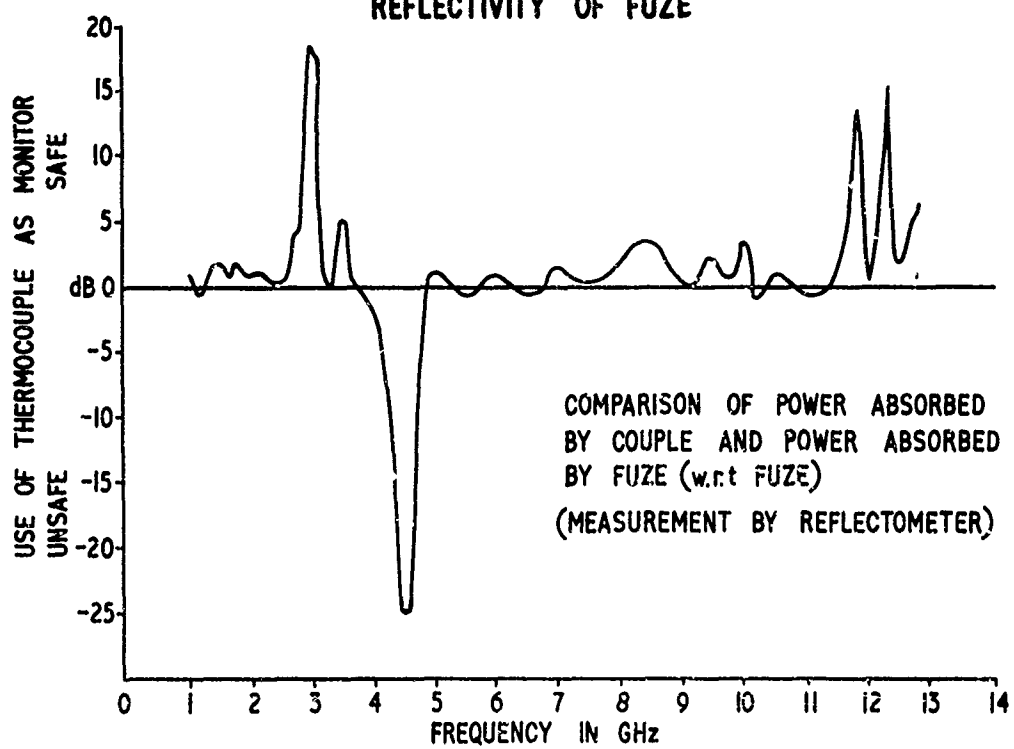
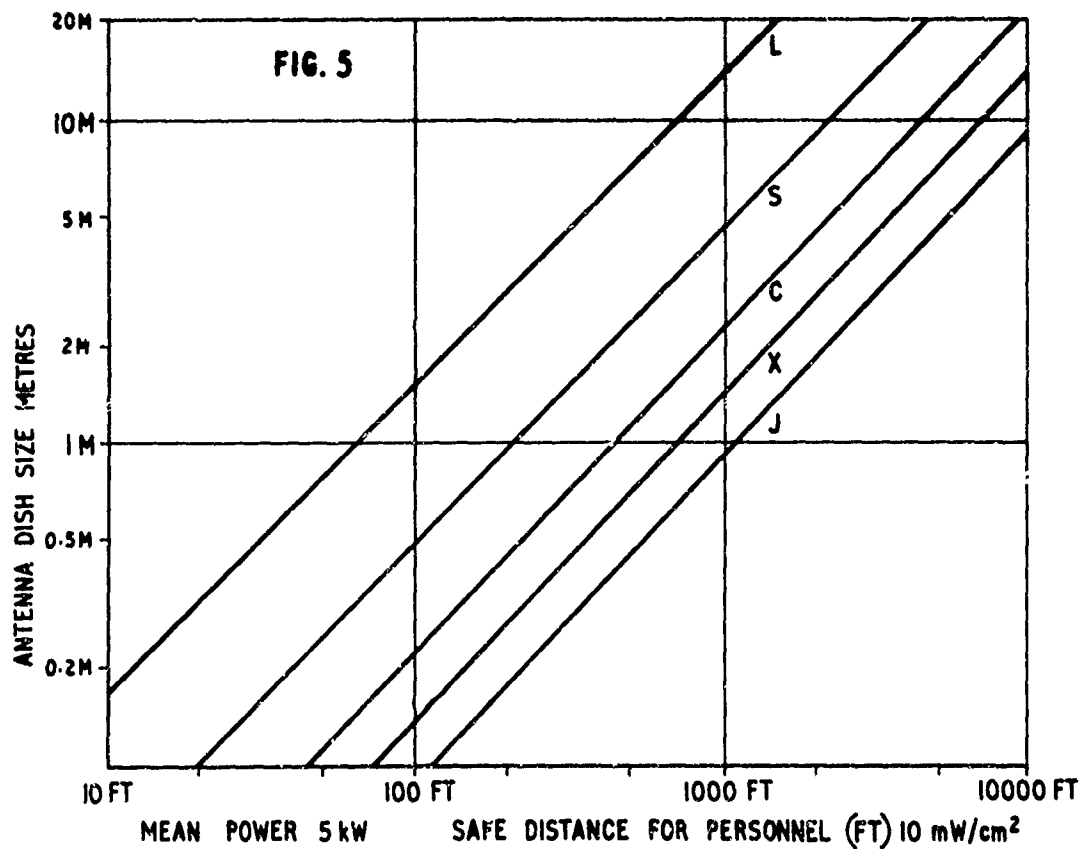
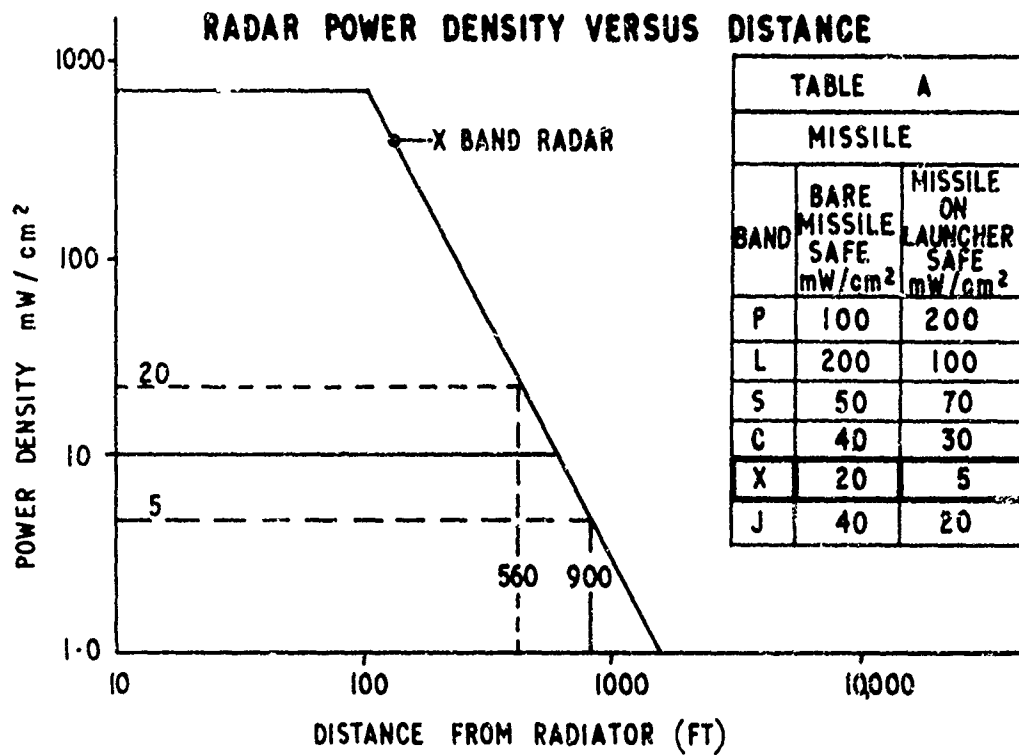


FIG. 4



3-2 A BROADBAND RF FILTER/ATTENUATOR PLUG FOR  
WIRE BRIDGE ELECTROEXPLOSIVE DEVICES (EED's)

*Theodore Marshall, Artillery Ammunition Lab, Picatinny Arsenal  
Paul F. Mohrbach, Franklin Institute Research Labs*

Introduction:

As a method to protect electroexplosive devices (EED's) against radio frequency (RF) energy, a broadband rf filter/attenuator plug which replaces plastic type plugs has been developed.

The T24E1 Electric Detonator is an example of an EED on which this approach has been attempted. Using samples from different manufacturing production lots, a comparison is made between the Picatinny Arsenal (PA) design and a black-box design.

Background:

Four groups of filter/attenuator plugs from one manufacturer were measured over the frequency range of 0.1 MHz to 10 GHz. Due to production delays, a minimum number of the PA design, was not available for comparison purposes. So that a valid comparison to the four groups evaluated could be made, a sample number of the PA design filter/attenuator plugs were constructed by the Franklin Institute Research Laboratories (FIRL). Using a special test fixture the evaluation for Worst Case Attenuation and Insertion Loss was made.

This was done to demonstrate (until additional production samples became available) that the specified attenuation level (Worst Case) could be obtained with this design. It was also thought this would serve as a standard against which filter/attenuator plugs of various construction and manufacture could be compared to.

Discussion and Test Results:

The plugs were placed in groups for identification purposes and marked as follows:

- |         |                            |
|---------|----------------------------|
| Group 1 | Initial Production         |
| 2       | Early Production           |
| 3       | Current Production (Mfr A) |
- 3-2.1



- 4 Latest Production
- 5 PA Design (FIRL) STANDARD
- 6 PA Design (Mfr B)

#### Group 1

The data on Group 1, Figure 1 was established by FIRL on contract DAAA21-68-C-0275. Although this is an insertion loss curve rather than worst case, it illustrates what effect plug variation can have on insertion loss. The top curve represents the maximum insertion loss obtained while the bottom curve is the minimum value. The wide variation in insertion loss at individual frequencies is an indication that the impedances of the plugs are not consistent. The construction of the plug was not uniform, and was confirmed later by X-ray photographs.

The circles containing an X are worst case values that were taken at 10, 20, 50 and 900 MHz. The spread in attenuation (Wc) values at 50 MHz and 900 MHz is 10 dB and these values are below the worst case specification level which is shown as a dashed line.

#### Group 2

The data obtained on Group 2 is shown in Figure 2. The two graphs represent the samples exhibiting the maximum and minimum worst case attenuation. Note, the sample with the greatest attenuation does not meet the specified level over much of the spectrum.

To illustrate how the attenuation varied from item to item at a given frequency, we have plotted all of the readings taken at 500 MHz. A rather uniform distribution from 10 dB to 20 dB occurs, indicating poor control over plug parameters.

### Group 3

A plot of Group 3's data is given in Figure 3. Once again we find that the spread in data is quite large; however, there is a definite improvement noted when compared to Group 2. One sample did exceed the specified attenuation at several frequencies, and the distribution is Gaussian rather than uniform.

### Group 4

To determine if crimping could damage the filter/attenuator plug when it is inserted into the detonator housing, we first measured the worst case attenuation of plugs at 100 MHz and 2 GHz. The plugs were then inserted into a detonator housing and crimped. They were later remeasured at the same frequency points of 100 MHz and 2 GHz.

The plug data before and after crimping is recorded in Table 1. The crimping procedure did not produce any change in attenuation at 100 MHz; however, at 2 GHz all of the plugs exhibited at least double the attenuation. (As can be seen by noting the data from Group 3 at 100 MHz and 2 GHz) the attenuation values for Group 4 is the same as those of Group 3 at the two frequencies tested, which substantiates the fact that proper contact within the case ID is paramount, if proper values of attenuation is to be achieved.

It is our thought that the pressure applied during the crimping operation has produced a better contact between the "S" spring and the ID of the case. Since Group 4 plugs are from the same lot as Group 3 plugs, it was not expected the attenuation would be larger for Group 4 samples than samples evaluated from Group 3 at the same frequency of 100 MHz and 2 GHz (see Figure 3).

The major problem with the group of plugs evaluated was that the "S" shaped spring inside the attenuator case was not soldered or welded. This can be seen illustrated in Figure 4. Note the potting compound has pushed the "S" spring away from the outer case. The results of the loose spring are shown by the decrease in the attenuation data at 2 GHz (Table 1).

### Statistical Analyses:

The data from Group 1, 2 and 3 were analyzed by statisticians at Picatinny Arsenal to determine if some correlation between worst case attenuation and insertion loss could be shown. Attenuation (Wc) and Insertion Loss (IL) data on the filter/attenuator plugs were plotted as a function of frequency to determine two frequencies at which the plug could be tested and still show an empirical relationship between the two types of measurements, Wc and IL.

No statistically valid relationship could be established due to lack of significance of the correlation coefficients at the 5% and 1% probability levels; however, an attempt was made to select two frequencies on the basis of (a) tight distribution for both Wc and IL, (b) the Wc data being well below the 25 db lower specification requirement, and (c) being from two different critical regions of the curves.

On this basis, Group 2 indicated 100 MHz and 2 GHz, while Group 3 was tighter at 3 GHz than at 2 GHz. Thus, the critical frequencies by the above are 100 MHz and either 2 or 3 GHz. The plotted points reflected the averages of 50 measurements from Group 1 and 3 and 25 measurements from Group 2.

### General Conclusions:

The goal was to measure a number of production filter/attenuator plugs and attempt to establish a correlation between Insertion Loss and Worst Case attenuation of a black-box design from manufacturer "A" and establish the possibility that MIL-Std 220A could be used in production testing of filter/attenuators. As indicated, the large variation in Worst Case Attenuation made it impractical to establish a comparison level when Insertion Loss measurements were attempted. In fact, the insertion loss spread was so great (Figure 3) that correlation was impossible.

#### Construction and Testing of Filter/Attenuators (PA Design):

Due to production delays, only a few of the PA design filter/attenuator plugs were available. It was therefore decided to construct an additional number of these plugs at The Franklin Institute Research Laboratories, evaluate their performance and compare them for worst case attenuation to the *four* groups evaluated. This would not only demonstrate that the specified attenuation could be obtained with this design, but would also provide a standard against which plugs of various construction could be compared.

##### Group 5

The PA plug design is intended to be a mass produced item. Since we were building laboratory quantities, it was found expeditious to build and test only the attenuator assemblies rather than the entire plug. The plug differs from the attenuator assembly only in the positioning of the wires and in the addition of a silicone sealant. It is not felt that these small differences will significantly affect the results of our evaluation.

The PA plug design incorporates two novel features: (1) the arrangement of the wires and solid state materials upon the ground-shield (2) the manner in which the ground-shield is constructed from two specially formed pieces of sheet stock. As neither feature had previously been studied, it was decided to proceed in two phases. First, the attenuator configuration was evaluated and its ability to attenuate established. This was accomplished by assembling the components on a one piece ground-shield which was milled from solid materials. Second, a group was constructed using the two piece ground-shield. Assembly of either *attenuator* is the same except for the ground-shields. Results were the same for both types of ground-shields.

Ordinarily, grounding and shielding are completed by the detonator case which is crimped into contact with the ground-shield. However, it is not possible to measure attenuation with the plug inside the detonator case since the lead wires are not accessible at the output. This difficulty is overcome by providing a brass sleeve into which the attenuator assembly is electrically connected. The outer diameter of the sleeve, is selected to fit the measuring fixture. Assemblies using the one-piece ground-shield are carefully cemented all around their circumference.

The assemblies are cemented only where the tabs make contact. This is done to simulate a worst case production condition and allow comparison between this and an optimized sample.

#### Measurements of PA Design (FIRL Constructed) Filter/Attenuator Plugs

##### Worst Case Attenuation:

Worst Case Attenuation was measured for the PA Design filter/attenuator plugs and the results are shown in Table 2 and Figure 5. It can be observed that the attenuator assemblies with one or two piece ground-shields are practically indistinguishable at all frequencies except 9000 MHz. The fall-off in attenuation at the high frequency is usually attributed to leakage of the RF energy through the device as a result of incomplete or inadequate shielding; however, in this situation we feel that the problem is in the attenuation measuring system. Specifically, the inability of the matching units to transfer the energy at this frequency due to multimode propagation. The coaxial line that is used during the measurements is assumed to support only TEM propagation. We suspect, however, that other modes do exist at 9 GHz which results in incorrect attenuation values. Because of this uncertainty, the 9 GHz values should not be considered as valid data

It should also be noted that the particular size, configuration and highly reactive electrical properties of this design and similar ones for this plug put very heavy demands on the matching systems and while the best general type systems are being used there may be excessive losses in the measuring system which would make the worst case attenuation measurements appear high. The problem is being investigated at this time.

Two samples are cemented to their outer sleeves only at the tabs, and might, therefore expect to be especially prone to leakage. They are, however, no different from the other specimens in this respect. This would seem to indicate that attachment to the outer sleeve is not so critical as was first supposed.

#### Insertion Loss:

Insertion Loss was measured and the results are shown in Table 3 and Figure 5. Very little, if significant difference, is noted between the one-piece and two-piece ground-shield assemblies. Since these assemblies require a different mount than the plugs evaluated in Group 1, a direct comparison of the insertion loss data for Group 5 (the PA Design) and (Group 1) is not made.

However, as is evident, the Insertion Loss data for Group 5 (Fig. 5) compared to Group 1 (Fig 1) shows no large variation and is uniform over most of the frequency band. At no point do the Group 5 values fall below the minimum level for either  $W_c$  or IL.

#### Group 6

The samples evaluated as made by manufacturer "B" showed they met the specification level ( $W_c$ ) requirements. Figure 6 data is for a filter/attenuator plug manufactured in accordance with Picatinny Arsenal detailed drawings.

The basic approach to attenuator construction encompassed by the PA designed filter/attenuator plug, and demonstrated by either one-piece ground-shield or two piece ground-shield samples, and by Figure 6 appears to be entirely satisfactory.

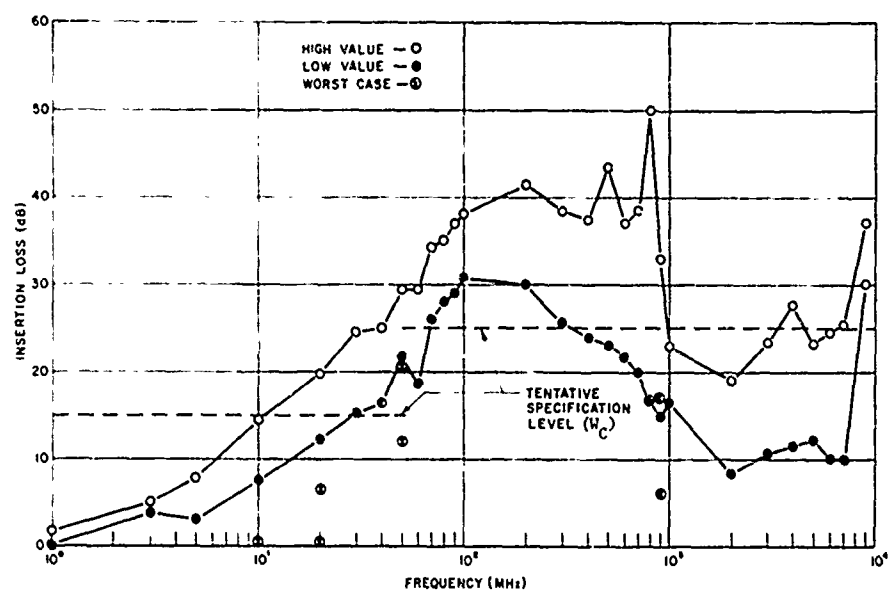


Fig. 1 Graph of Insertion Loss of the M78E1 Plugs (MIL-STD-220A) (Group No. 1)

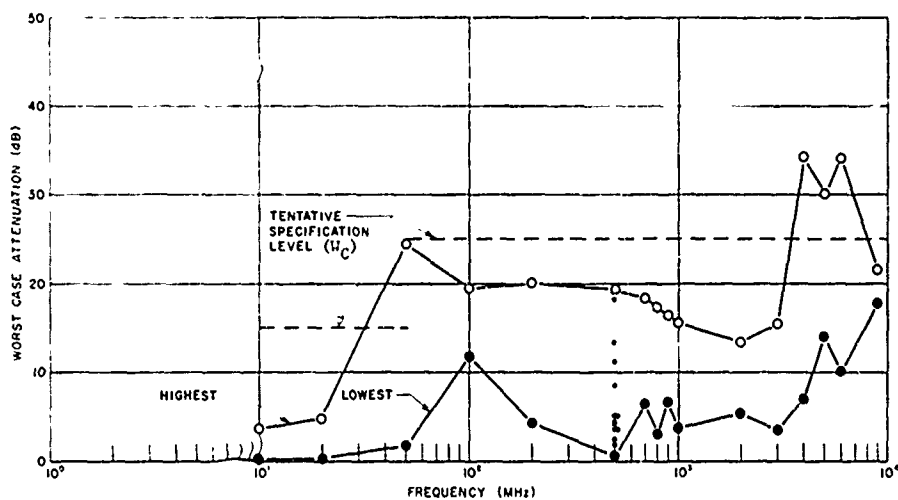


Fig. 2 Early Production, Group No. 2

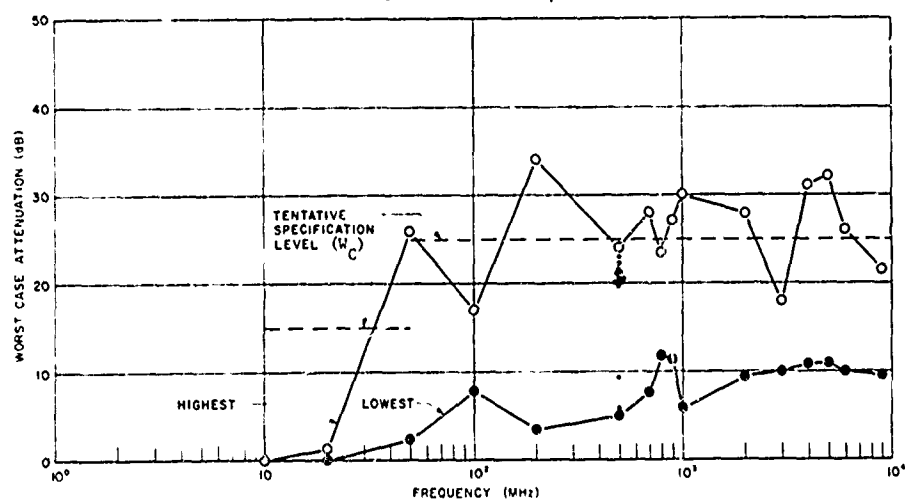


Fig. 3 Current Production, Group No. 3



Fig. 4 S Spring Pushed Away From Outer Case (Manufacturer A)



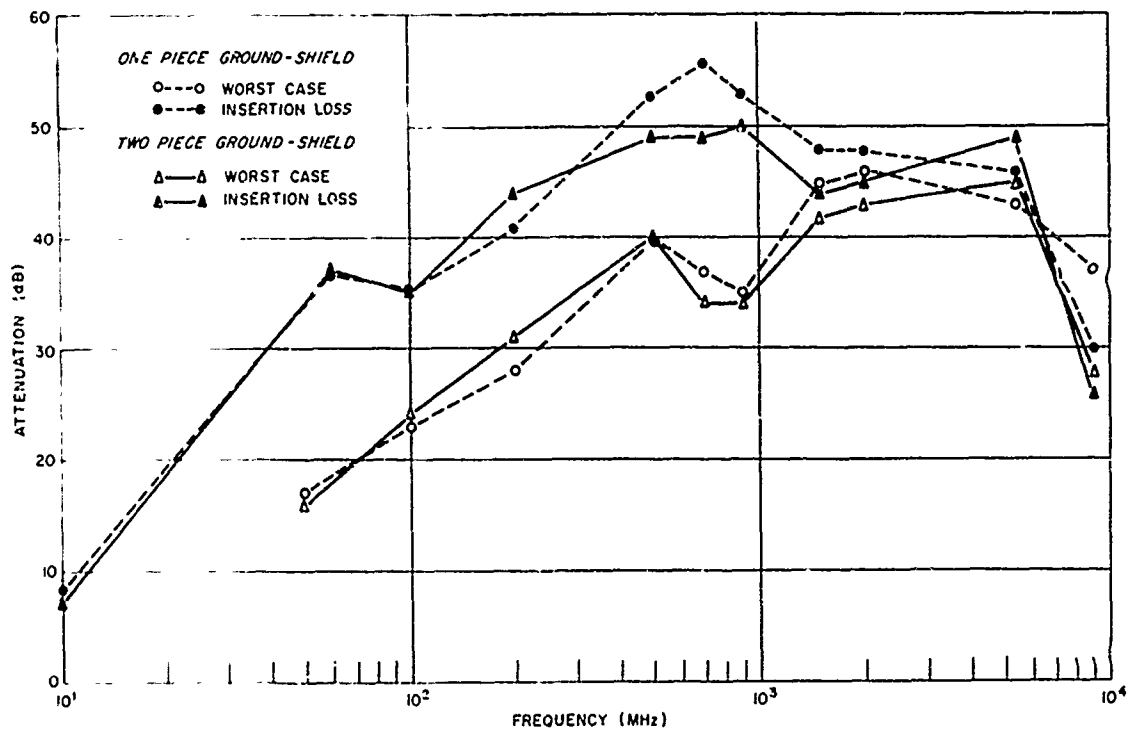


Fig. 5 Worst Case Attenuation and Insertion Loss

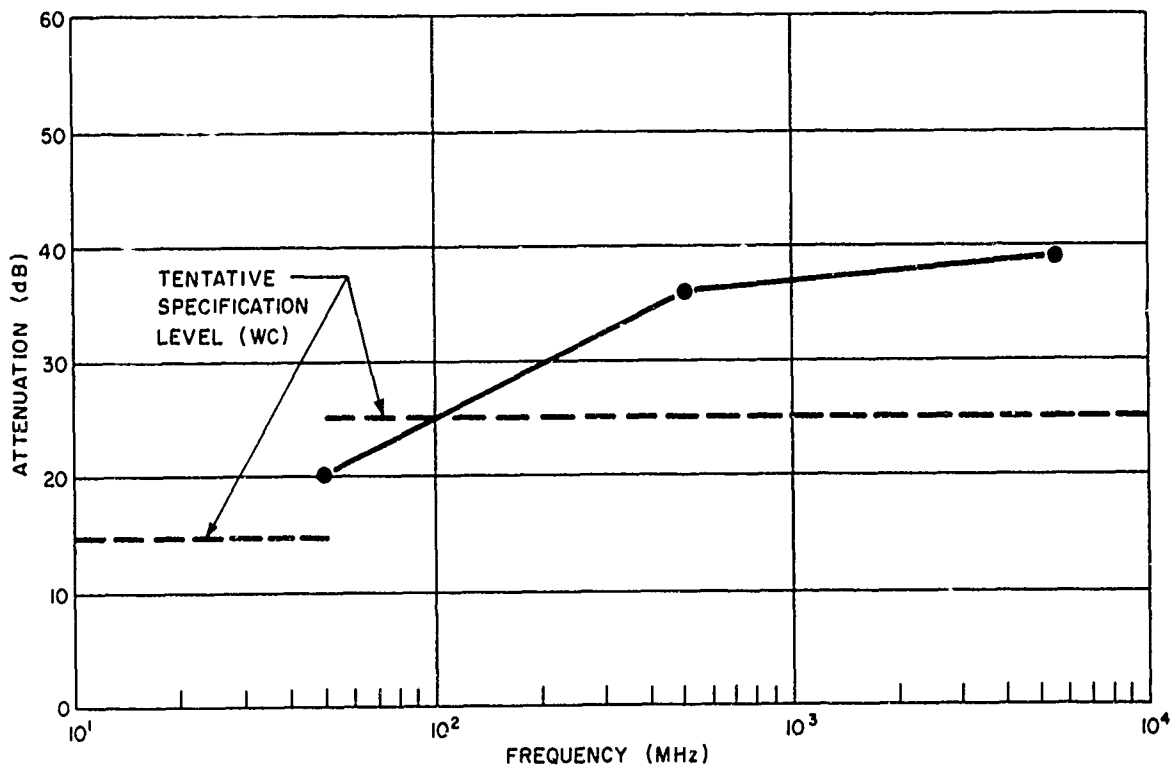


Fig. 6. Worst Case Attenuation

Table 1  
EFFECT OF CRIMPING

<u>Sample No.</u>	A	B	A	B
	<u>100 MHz</u>	<u>100 MHz</u>	<u>2 GHz</u>	<u>2 GHz</u>
102	23	22	9	27
103	26	24	11	27
104	18	19	4	29
105	22	22	12	28
106	21	17	9	27
107	21	21	12	27
108	22	22	9	26
109	21	21	9	27
110	23	22	9	27
111	22	22	9	26
112	23	23	9	26
113	22	22	12	25
114	22	21	12	28
115	21	21	6	26
116	20	21	20	27
117	22	20	11	28
118	22	22	5	28
119	23	21	11	27
120	23	21	9	27
121	23	22	12	27
122	14	22	6	28
123	20	18	11	27
124	18	20	9	28
125	22	23	8	26
126	20	20	11	27
127	21	20	9	27
128	22	22	9	27
129	22	23	9	26
130	21	22	12	27
131	21	21	12	29
132	22	22	9	27
133	21	20	14	28
134	22	21	10	26
135	20	21	6	27
136	21	20	9	28
137	21	20	9	28
138	21	18	10	25
139	20	19	12	27
140	19	20	4	27

Table 2  
WORST CASE ATTENUATION PA DESIGN ATTENUATOR ASSEMBLIES

Power Loss in dB

Frequency MHz	Sample No.	20	21	22	23	24	25	26	27	28	29
50		16	16	18	17	18	15	14	17	17	15
100		24	24	22	22	24	22	23	25	25	23
200		28	29	28	27	30	29	31	32	32	30
500		41	41	40	38	40	41	38	42	37	39
700		34	34	37	39	39	36	33	37	33	34
900		33	33	36	37	37	35	36	35	32	32
1200		31	35	45	45	45	36	35	40	35	37
1500		43	43	46	46	46	43	40	44	40	42
2000		48	48	44	45	45	44	41	45	42	44
5400		41	42	44	44	44	45	44	45	44	45
9000		36	37	37	38	37	31	26	26	28	28

Table 3  
INSERTION LOSS, PA DESIGN ATTENUATOR ASSEMBLIES

Power Loss in dB

Frequency MHz	One Piece Ground-Shield					Two Piece Ground Shield					
	Sample No.	20	21	22	23	24	25	26	27	28	29
10		8.5	9.2	8.0	7.7	8.2	7.5	8.5	8.9	9.2	8.0
50		37	36	36	37	38	37	37	37	39	36
100		36	36	34	33	35	33	35	36	37	35
200		43	43	40	40	41	41	45	44	46	43
500		52	53	52	52	54	49	48	52	47	50
700		55	54	57	59	57	49	47	52	48	50
900		51	51	54	54	54	50	49	53	48	52
1500		47	47	49	48	49	44	43	47	42	45
2000		47	48	49	49	48	45	44	47	44	47
5400		42	47	45	47	47	47	47	50	50	49
9000		30	30	30	30	30	27	27	27	24	25

### 3-3 STERILIZATION-ENVIRONMENTAL TESTING OF INITIATORS

Laurence J. Bement  
NASA-Langley Research Center

#### ABSTRACT

Three types of electro-pyrotechnic initiators, developed for space applications, were subjected to six dry heat sterilization cycles (135°C - 36 hrs. each), and to post-sterilization mechanical and electrical environments. The performance of units subjected to sterilization and the other environments was compared to the as-received performance of the initiators. Results of various non-destructive, electrical and functional tests conducted to compare performance of these units indicate that two of the three units tested are promising candidates for use in interplanetary missions.

#### INTRODUCTION

The international body, Committee for Space Research, (COSPAR), has issued a guideline that all spacecraft entering another planet's atmosphere, or contacting its surface must be biologically sterile; that is, probability of the spacecraft carrying a viable organism shall be less than one in a thousand. The most generally accepted technique of achieving sterility is to subject the spacecraft to dry heat cycles, the terminal cycle being 24.5 hours in duration at a temperature of 125°C, for the most thermally remote point within the spacecraft. All spacecraft components must demonstrate an ability to function following this heat cycle, as well as to resist the environments the spacecraft experiences in accomplishing its mission. The purpose of this paper is to describe the effects of sterilization heat cycles and post-sterilization environments on three types of electrical pyrotechnic

initiators, developed for space applications.

## PROCEDURE

Selection of Initiators - The factors upon which selection of initiators for this study was based are as follows:

- (1) High temperature resistant materials
- (2) Threaded cartridge body
- (3) Hotwire
- (4) One amp-one watt power dissipation
- (5) Electrostatically insensitive
- (6) Resistant to environments, (shock, vibration, vacuum, thermal cycling)

The temperature envelope of the heat cycle used in this study, which includes an overtest factor (greater than 24.5 hours at 125°C), is shown in Figure 1, and the environmental test levels are listed in Table 1.

The three initiators selected for testing, each having a different primary charge, were Hi Shear Corporation's dual-bridgewire PC 39-003, Space Ordnance Systems' dual-bridgewire Non-Conductive Apollo Standard Initiator, (NCASI, model No. S01-266-21) and the Single Bridge Apollo Standard Initiator, (SBASI, model No. S01-10197-11). The manufacturers of these initiators consider the chemical composition and internal design to be company proprietary; therefore, that information will not be included in this paper.

Performance Comparisons - The performance tests conducted in determining the effect of sterilization and environments can be divided into three areas; (1) non-degrading, such as X-rays, bridgewire resistance and ten-volt insulation resistance checks, (2) electrostatic tests, the energy stored

in a 500-picofarad capacitor with no series resistance, and (3) closed bomb constant current test firings. The block diagram of the closed bomb firing and monitoring system is shown in Figure 2.

Since the functioning time of these initiators is short, as low as 0.1 millisecond, a monitoring system with an overall frequency response of 20 kilocycles was employed, providing an accuracy of 0.05 milliseconds. Figure 3 shows a typical firing record which has an equivalent paper speed of 1100 inches per second, displaying a millisecond in 0.9 inches. The preset current causes the bridgewire to heat, changing its electrical resistance, which produces an increase in the voltage drop across the device. The ratio of the final resistance at bridgewire break to the original provides one basis of comparison,  $R_2/R_1$ . The times from application of current to bridgewire break,  $T_{BW}$ , and to first indicated pressure,  $T_p$ , are also displayed. The peak pressure and the time to peak pressure,  $T_{pp}$ , reveal the combustion performance of the propellant within the closed bomb. Compiling the times to bridgewire break,  $T_{BW}$ , and to first indicated pressure,  $T_p$ , over the range of expected current inputs, produces the function time plot shown in Figure 4. This plot represents the function times of nine different units of the same type, each fired at a preset constant current. For the ten amperes example shown, the bridgewire broke at 0.4 milliseconds and the pressure rose at 4.4 milliseconds, a 4-millisecond delay.

The performance comparisons made in this study are summarized in Table 2.

## RESULTS

Since a detailed report and analysis of the three hundred units tested in this study would be lengthy, only the major changes or accomplishments will be noted.

PC 39-003 - The test procedure for this initiator is shown in Table 3. The 80-unit lot was divided into eight groups of ten each. The groups were test-fired after being exposed to the environments indicated by an "X". Group 1 established the as-received performance, Group 2 the effect of mechanical environments, (vibration, shock and acceleration), and Group 3, the electrostatic sensitivity. Groups 4 through 7 were subjected to six heat cycles, and post heat-cycle environments. The units in Group 8 were preconditioned and fired at  $-195^{\circ}\text{C}$  ( $-320^{\circ}\text{F}$ ) and  $+250^{\circ}\text{C}$  ( $400^{\circ}\text{F}$ ).

The units subjected to six heat cycles experienced a change in bridge-to-bridge resistance, increasing incrementally after each heat cycle from 40 megohms to greater than 1000 megohms. This increase forewarned a change in electrostatic sensitivity which increased from bridge-to-case no-fires at 27 kilovolts and bridge-to-bridge firings at 23 kilovolts down to 3 kilovolts in both modes. It is believed that this is due to the binder utilized and could be corrected.

The effect of six heat cycles on firing performance is shown in the PC 39-003 function time plots (Figure 5), where a shift is noted in time to pressure rise. The minimum firing current decreased from 2.0 amperes to 1.6 amperes. The post-sterilization mechanical environment and thermal vacuum tests produced slightly more scattered data, but no misfires.

The peak pressure performance plot (Figure 6) shows a good consistency throughout the lot. The units test-fired at  $+205^{\circ}\text{C}$  ( $400^{\circ}\text{F}$ ) produced an expected high pressure, but the units test-fired at  $-195^{\circ}\text{C}$  ( $-320^{\circ}\text{F}$ ) produced abnormally high pressures which will be discussed later.

The resistance changes and times to peak pressure are shown in Table 4. The times to peak pressure nearly doubled after six heat cycles, and were

over four times longer after environmental tests, which indicated a change in propellant combustion. The time to peak pressure of the  $-195^{\circ}\text{C}$  ( $-320^{\circ}\text{F}$ ) firings is less than one-third of that of the reference group. It is believed that at  $-195^{\circ}\text{C}$  the propellant becomes brittle and is shattering on ignition, generating a large surface area which produces a more rapid combustion with higher pressures and shorter function times.

NCASI - The test procedure for this initiator is shown in Table 5. Twenty units were utilized in establishing the as-received performance in Group 1, and ten were used in each of the remaining groups. Extra groups were added to determine the effects of: electrostatic pulses on conventional ignition (Group 3), three heat cycles (Group 5), and six, 53-hour cycles (Group 7).

In the electrostatic tests, conducted in Groups 3 and 4, large changes in bridge-to-case resistance were observed, no matter what mode (bridge-to-bridge or bridge-to-case) was tested. The resistances decreased incrementally from greater than 1000 megohms to 30 megohms, leading to the conclusion that the breakdown path was from bridge-to-case. No ignitions were achieved up to 25 kilovolts in the bridge-to-bridge and bridge-to-case modes. The minimum voltage to achieve ignition through the bridgewire was 20 kilovolts. During the testing of this mode, several bridgewires broke and no ignitions were achieved. To determine the effect on function time and pressure performance of the electrostatic-induced change in bridge-to-case resistance, the units in Group 3 were pulsed repeatedly from bridge-to-bridge and bridge-to-case and test-fired with constant current in the closed bomb. No appreciable change was observed.

Figure 7 shows the NCASI function time plots for the reference group,



at currents of 15 amperes, or greater, there is a relatively large delay in time to pressure rise. Tests at the higher currents produced by the electrostatic tests evidently caused a complete decoupling of the ignition process, producing the misfires.

Subjecting the units to six heat cycles produced a shift in function times and an increase in minimum current firing from 2.0 to 2.25 amperes. (See Figure 7.) The electrostatic sensitivity remained unchanged. The bridge-to-bridge resistance dropped sharply in all units during the first heat cycles; in the worst case from 250 to 0.18 megohms. The extended heat cycles (53 hours) caused the minimum firing to increase to 2.5 amperes.

The group that had been aged six months after sterilization showed more data scatter than those fired immediately.

The peak pressure performance of the NCASI tests in Figure 8 shows some amount of data scatter which cannot be fully attributed to the effect of the environments, but more probably to manufacturing quality control. Again, high pressures were observed in the cold firings. The resistance change and time to peak pressure shows a measurable effect of the environments (Table 6).

SBASI - The test procedure for this 110-unit group is shown in Table 7. Twenty units established the as-received performance in Group 1. The electrostatic tests revealed no sensitivity to 25 kilovolts bridge-to-case, and the minimum voltage to achieve ignition through the bridge was 20 kilovolts.

The effect of six heat cycles on the function time was very minimal, as shown in Figure 9 which contains data from both the reference and the heat-cycled group. The same situation prevailed in the six 53-hour cycles, the post-sterilization environments and the units aged for six months.

The peak pressure performance in Figure 10 shows some data scatter which cannot be attributed entirely to the effect of environments. For

example the units in Group 6, (six 53-hour cycles), exhibited more consistent performance than those in Group 5, (six 36-hour cycles), a less severe test. Again, high pressures were observed in the  $-195^{\circ}\text{C}$  ( $-320^{\circ}\text{F}$ ) firings.

The resistance changes and times to peak pressure, (see Table 8), show a good degree of uniformity.

#### SUMMARY OF RESULTS

The three initiators selected for this study all met the initial requirements, that of one amp-one watt dissipation and low sensitivity to electrostatics and mechanical environments (shock, vibration and acceleration). Abnormally high pressures were observed at  $-195^{\circ}\text{C}$  ( $-320^{\circ}\text{F}$ ). All units functioned after being subjected to six 36-hour heat cycles, but some changes in performance were experienced.

The Hi Shear PC 39-003 initiator experienced a delay in function time, and decrease in minimum firing current of 0.4 amperes due to heat cycling which would not disqualify its use. However, the electrostatic sensitivity of this unit increased nearly ten-fold from ignitions at 23 kilovolts (as-received) to 3 kilovolts (sterilized). This lack of resistance to electrostatic voltages could result in inadvertent ignition.

The Space Ordnance Systems Non-Conductive Apollo Standard Initiator, (NCASI model No. S01-266-21), exhibited ignition failures at high current application, (greater than 20 amperes). Also, relatively low bridge-to-bridge resistance was caused by the sterilization cycling, (0.18 megohms). Heat cycling also produced an increase in minimum firing current of 0.5 amperes. Consideration should be given to these sterilization-induced changes in the application of these devices.

The Space Ordnance Systems Single Bridge Apollo Standard Initiator, (SBASI, model No. S01-10197-11), resisted all environments very well, the only possible problem being a scatter in peak pressure performance.

TABLE I  
ENVIRONMENTAL TESTS  
VIBRATION - ALL AXES

SINUSOIDAL	0.5" DA	5 - 52.5 cps	2 oct/min
	70 g $z$	52.5 - 2000 cps	2 oct/min
RANDOM	0.1 g $z$ /cps	5 - 50 cps	
	1 g $z$ /cps	50 - 2000 cps	5 min
SHOCK - $\pm$ ALL AXES			
TRAILING EDGE SAWTOOTH	80 g	7 ms	3 TESTS EACH DIRECTION
HALF sine	6000 g	0.2 ms	3 TESTS EACH DIRECTION
CONSTANT ACCELERATION - $\pm$ ALL AXES			
	300 g	5 min	
THERMAL - VACUUM			
$\leq 1 \times 10^{-6}$ torr	THREE THERMAL	- 60 <sup>0</sup> C	2 HOURS
72 HOURS TOTAL	CYCLES IN EIGHT	TO	
	HOUR WORKING DAY	120 <sup>0</sup> C	2 HOURS
		TO	
		22 <sup>0</sup> C	

TABLE 2  
INITIATOR PERFORMANCE COMPARISON TESTS

- |  |  |
|--|--|
| <p>1. NON DEGRADING</p> <p>A. BRIDGEWIRE RESISTANCES</p> <p>B. INSULATION RESISTANCE</p> <p style="padding-left: 20px;">a. BRIDGE TO CASE</p> <p style="padding-left: 20px;">b. BRIDGE TO BRIDGE</p> <p>C. X-RAY</p> | <p>2. ELECTROSTATIC SENSITIVITY</p> <p>A. BRIDGE TO CASE</p> <p>B. BRIDGE TO BRIDGE</p> <p>C. THROUGH THE BRIDGE</p> |
|--|--|
3. TEST FIRINGS - CLOSED BOMB
- A. VARIABLE CONSTANT CURRENT INPUT
- B.  $R_2/R_1$  - CHANGE IN RESISTANCE
- C.  $T_{BW}$  - TIME TO BRIDGEWIRE BREAK
- D.  $T_p$  - TIME TO FIRST PRESSURE INDICATION
- E. PEAK PRESSURE
- F.  $T_{pp}$  - TIME TO PEAK PRESSURE
- G. FUNCTION TIME PLOT
- H. PEAK PRESSURE PLOT

TABLE 3  
PC 39-003 TEST PROCEDURE

GROUP	REFERENCE			SIX STERIL. CYCLES	POST STERILIZATION TESTS				
	UNTESTED	MECH. ENVIRON.	ELECTRO- STATIC		MECH. ENVIRON.	THERMAL VACUUM	ELECTRO- STATIC	SIX MONTH AGING	COLD HOT FIRING
1	X								
2		X							
3			X						
4				X					
5				X	X	X			
6				X			X		
7				X				X	
8									X

TABLE 4  
PC 39-003 RESISTANCE CHANGE AND TIME TO PEAK PRESSURE

PC39-003 - GROUP	$R_2/R_1$ - RES. CHANGE AVERAGE	$T_{pp}$ - TIME TO PEAK PRESSURE - MS AVERAGE
1. REFERENCE	1.370	0.689
2. ENVIRONMENTAL REF.	1.136	0.613
3. SIX HEAT CYCLES	1.148	1.259
5. SIX HEAT CYCLES + ENVIRONMENTAL	1.181	3.2
8. -195° C, (-320° F)	1.148	0.160
+205° C, (+400° F)	1.192	0.363

TABLE 5  
NCASI TEST PROCEDURE

	REFERENCE					POST STERILIZATION TESTS				
GROUP	UNTESTED	MECH. ENVIRON.	ELECTRO- STATIC	STERIL. CYCLES		MECH. ENVIRON.	THERMAL VACUUM	ELECTRO- STATIC	SIX MONTH AGING	COLD HOT FIRING
				3	6					
1	X	X	X X	X	X X X X X	X	X	X	X	X
2										
3										
4										
5										
6										
7										
8										
9										
10										
11										

TABLE 6  
NCASI RESISTANCE CHANGE AND TIME TO PEAK PRESSURE

NCASI - GROUP	$R_2/R_1$ - RES. CHANGE AVERAGE	$T_{pp}$ - TIME TO PEAK PRESSURE-MS AVERAGE
1. REFERENCE	1.173	0.197
2. ENVIRONMENTAL REF.	1.560	0.194
3. ELECTROSTATIC PREPULSE	1.463	0.340
5. THREE HEAT CYCLES	1.506	0.218
6. SIX HEAT CYCLES	1.560	0.473
7. SIX 53 HOUR CYCLES	1.685	0.205
8. SIX HEAT CYCLES + ENVIRONMENTAL	1.652	0.188
10. SIX HEAT CYCLES + SIX MONTHS	1.532	0.174
11. -195°C, (-320°F)	1.851	0.316
+205°C, (400°F)	1.27	0.0668

TABLE 7  
SBASI TEST PROCEDURE

	REFERENCE					POST STERILIZATION TESTS				
GROUP	UNTESTED	MECH. ENVIRON.	ELECTRO- STATIC	STERIL. CYCLES		MECH. ENVIRON.	THERMAL VACUUM	ELECTRO- STATIC	SIX MONTH AGING	COLD HOT FIRING
				3	6					
1	X	X	X	X	X	X	X	X	X	X
2										
3										
4										
5										
6										
7										
8										
9										
10										

TABLE 8  
SBASI RESISTANCE CHANGE AND TIME TO PEAK PRESSURE

SBASI - GROUP	$R_2/R_1$ - RES. CHANGE AVERAGE	$T_{pp}$ - TIME TO PEAK PRESSURE-MS AVERAGE
1. REFERENCE	1.252	0.189
2. ENVIRONMENTAL REF.	1.422	0.228
4. THREE HEAT CYCLES	1.288	0.205
5. SIX HEAT CYCLES	1.095	0.518
6. SIX 53 HOUR CYCLES	1.328	0.244
7. SIX HEAT CYCLES + ENVIRONMENTAL	1.436	0.251
9. SIX HEAT CYCLES + SIX MONTHS	1.415	0.205
10. -195°C, (-320°F)	1.382	0.150
+205°C, (400°F)	1.25	0.117

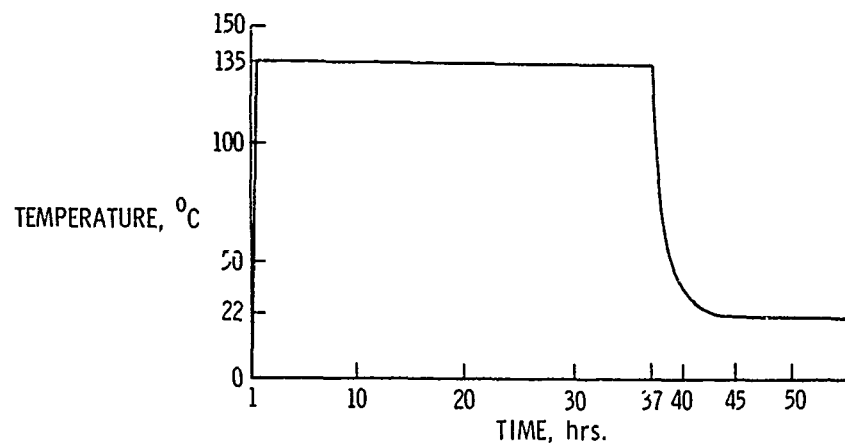


Figure 1.- Typical sterilization heat cycle.

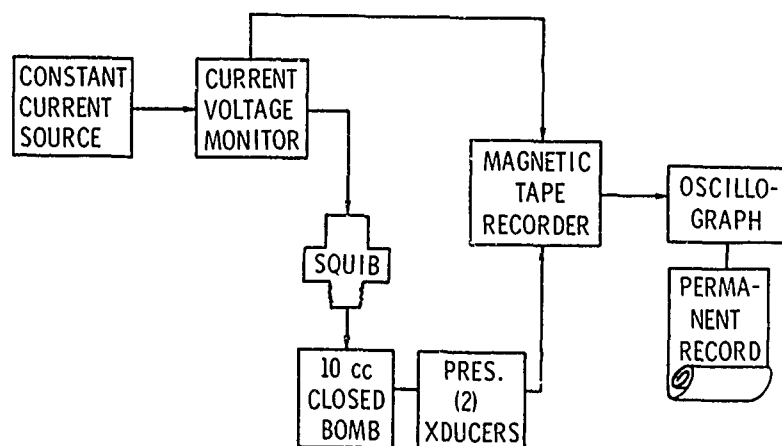


Figure 2.- Closed port firing and monitoring system.

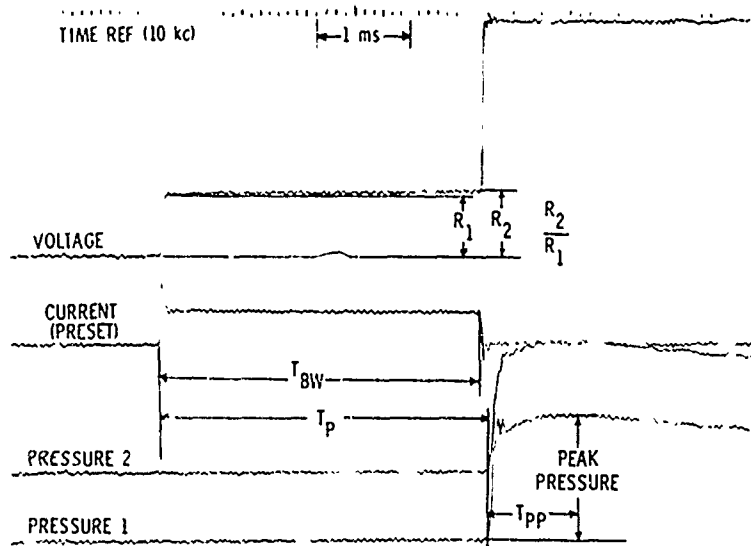


Figure 4 - Typical firing record for one initiator.

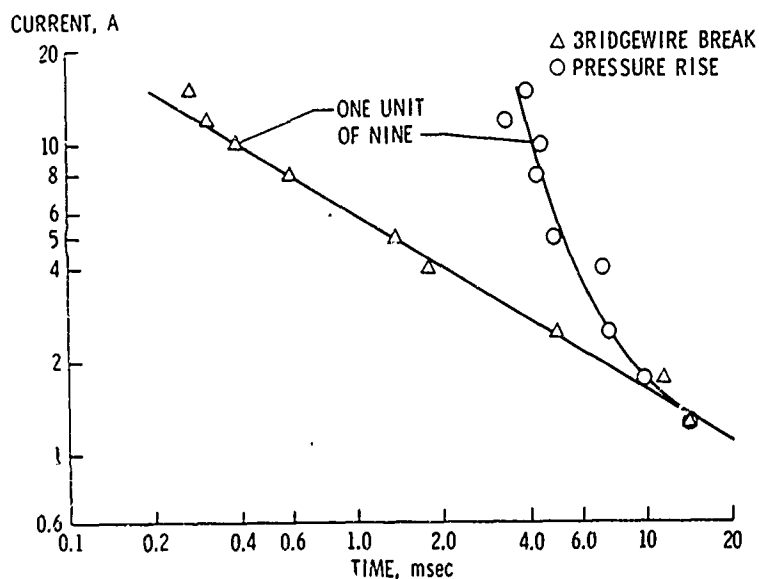


Figure 4a - Typical function time plot.

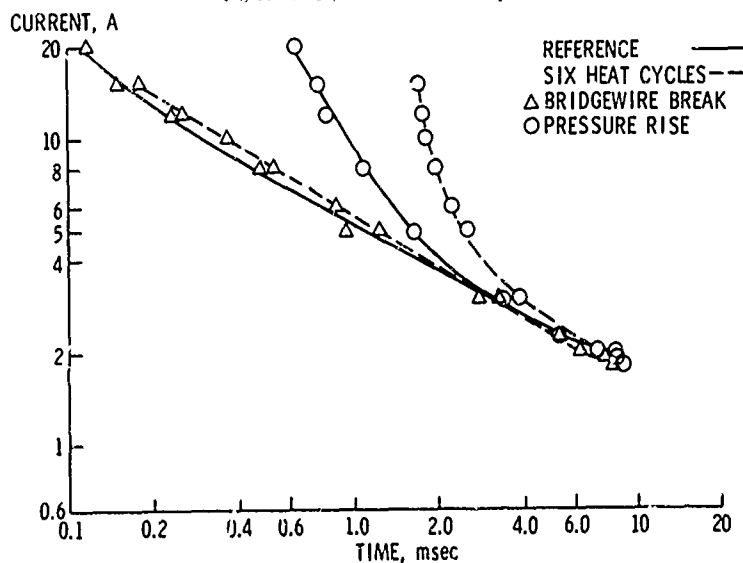


Figure 5 - FC59-003 function time plots

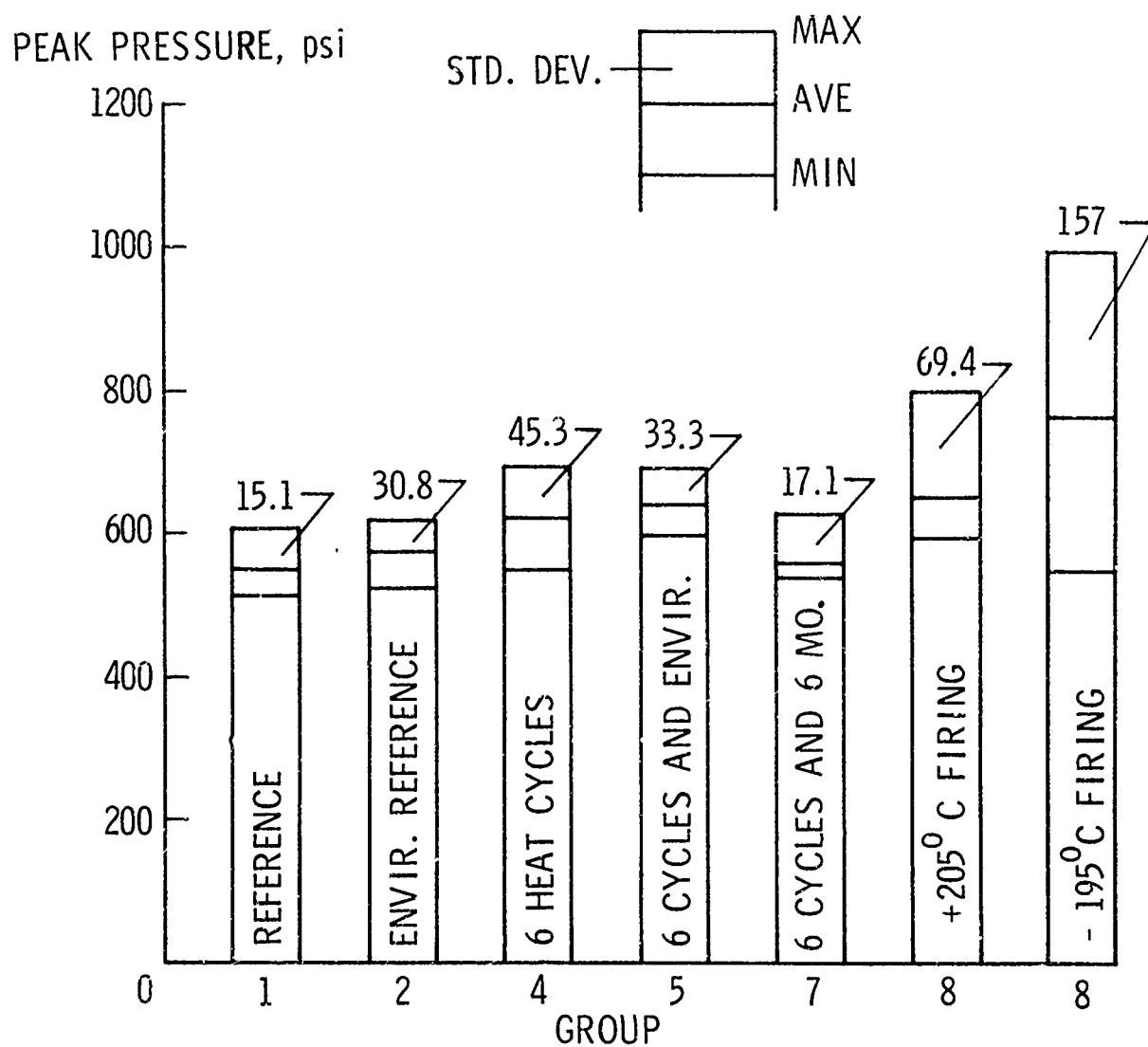


Figure 6.- PC59-003 peak pressure performance.



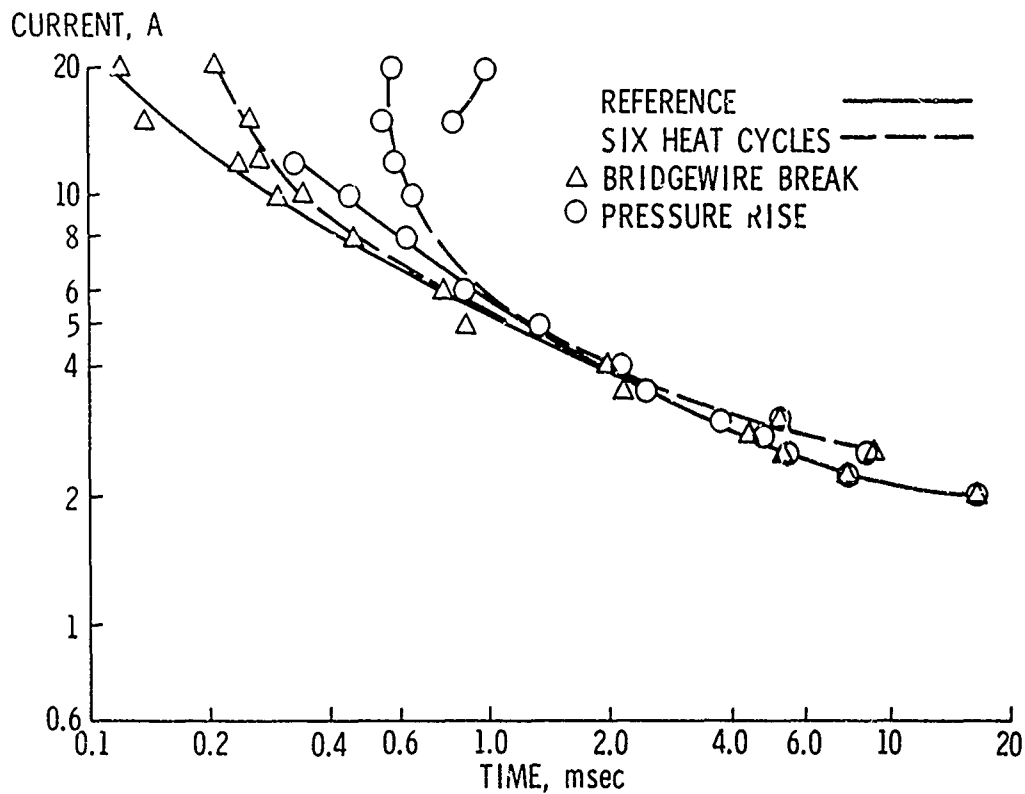


Figure 7.- NCASI function time plots.

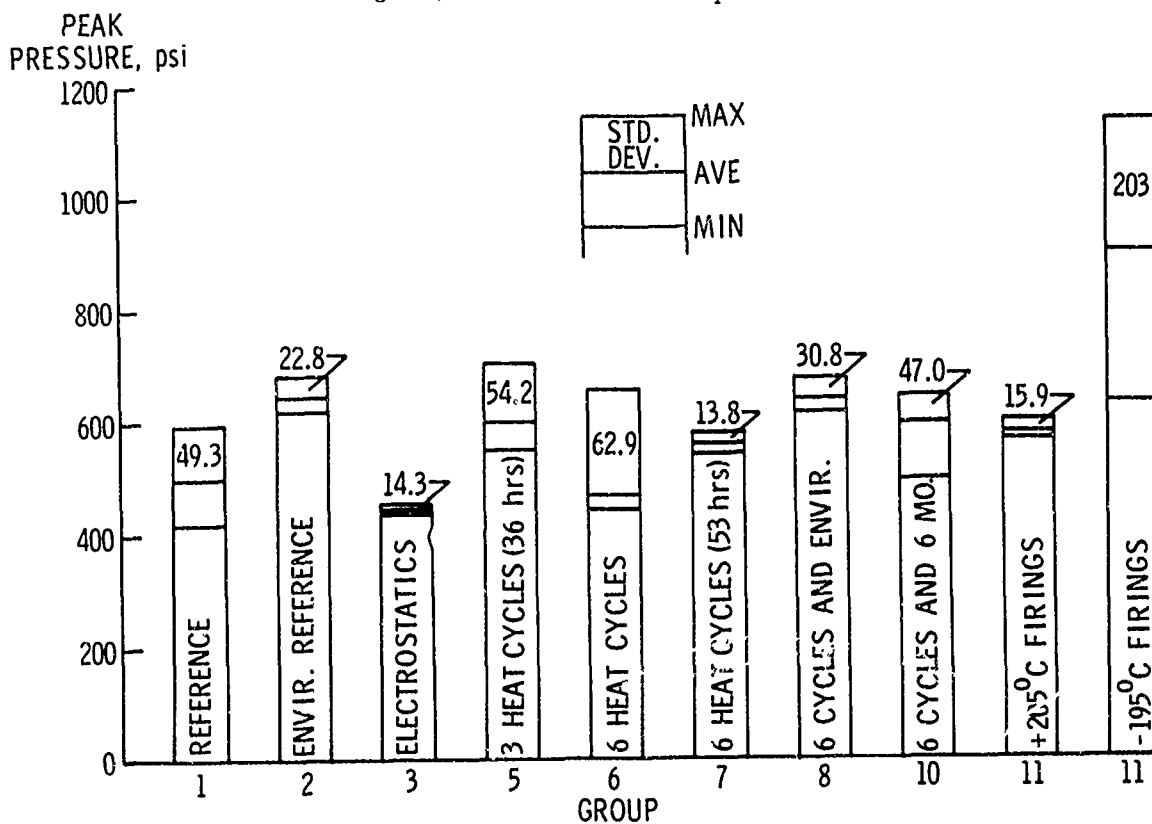


Figure 8.- NCASI peak pressure performance.

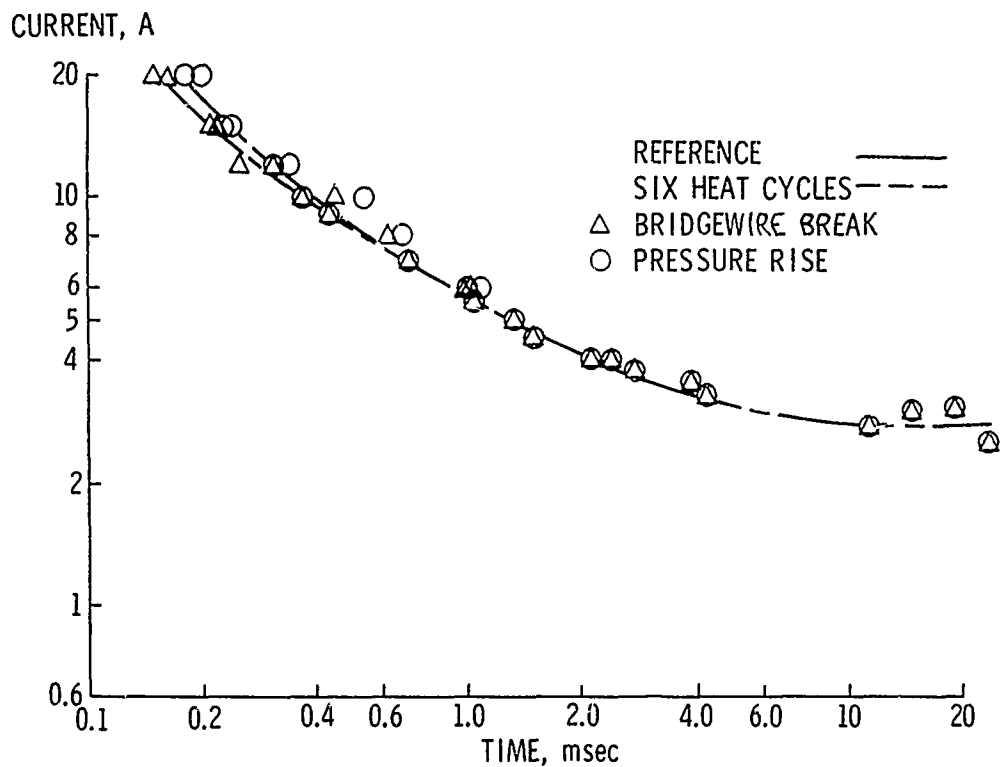


Figure 9.- SBASI function time plots.

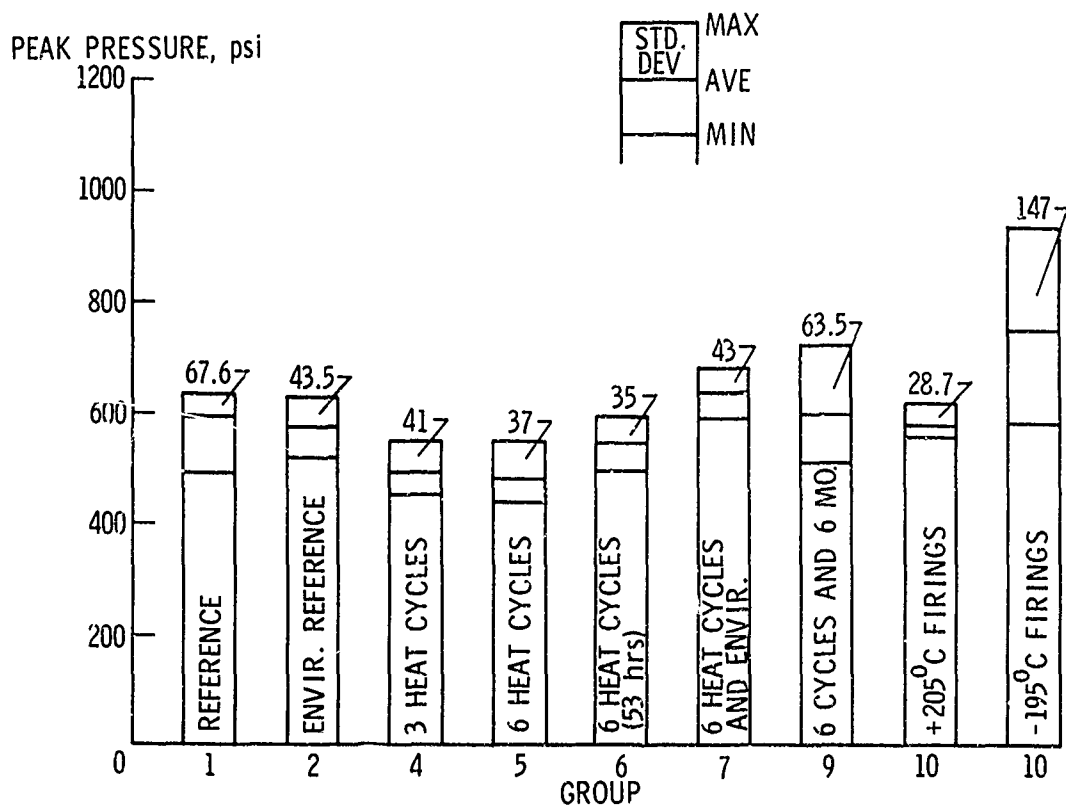


Figure 10.- SBASI peak pressure performance.

### 3-4 THE EMI HAZARD MEASURING SYSTEM

William L. Watton, Electric and Musical Industries (Electronic) Ltd, England, and  
Malcolm G. Brown and William B. Scamaton,  
Royal Armament Research and Development Establishment, Fort Halstead, England.

#### ABSTRACT

This paper describes an r.f. hazard measuring system developed under a contract funded by the British Ministry of Technology for use in electro-magnetic compatibility trials of complete guided weapons. An instrumented inert device replaces the actual E.I.E.D. for which information is required. A signal voltage derived directly from the inert device is converted into an audio frequency signal which is coupled electromagnetically through the skin of the weapon under test. It is then converted into an acoustic signal which is piped to a remote decoder indicator where it is displayed on a meter calibrated in terms of equivalent d.c. input to the instrumented inert device. Measurements can be made both on bridge wire and conductive mix E.I.E.Ds.

#### 1. INTRODUCTION

The radio hazard measuring equipment was designed as a field instrument for measuring r.f. pick-up in igniter firing circuits when these circuits are placed in intense e.m. fields, of the kind found in the vicinity of radio and radar aerials which are radiating a large amount of power. Ideally the equipment should neither interfere with the screening of the firing circuits nor modify the r.f. field distribution. To ensure this the system employs a specially developed telemetry link. Features of this link are:-

- a. The pick up information is transmitted through the skin of any screening enclosure, which may exist, without modification of this skin.

- b. From the outside of this skin the information is conveyed by non-electrically conducting means to a remote point. The observer is thus located outside the intense e.m. field. The equipment consists basically of two parts: one being the instrumentation of a dummy igniter, which replaces the live igniter in the weapon, the other being the telemetry link which conveys the output from this instrumentation to a remote observer.

Two systems have in fact been developed which, whilst operating on the same basic principle, differ somewhat in the method of processing the information for transmission; the Mk II version by improved instrumentation giving increased sensitivity, greater ease of use and longer battery life. Both systems have been used for assessing the r.f. hazard in bridge wire devices, both of the unsupported wire, (fusehead series F.) and the supported wire (Igniter series 200) types, which are shown schematically in figs. 1 and 2 respectively. Experimental work on hazard measurement in conducting-composition devices has also been carried out using both the Mk I and Mk II versions. Fig. 3 is a schematic diagram of the c.c. igniter.

## 2. IGNITER INSTRUMENTATION

### 2.1 Bridge Wire Igniters

The instrumentation, on both the supported and unsupported wire types, consists of a small thermistor cemented to the igniter bridge wire with a second thermistor located nearby; this latter giving ambient temperature compensation. An r.f. filter is also incorporated into this assembly and the whole is located within the normal dimensions of the igniter.

The two thermistors are connected as two arms of a bridge, thus any change in resistance of the sensing thermistor results in an unbalance of the bridge.

Fig. 4 is a schematic drawing of the series 200 igniter bridge wire instrumentation. A printed circuit board (0.45-0.5cm) is fitted to the end of the igniter and the components are attached. The circuit diagram of the instrumentation is shown in fig. 5. The compensating thermistor and the two filtering capacitors are embedded in Araldite and the three instrumentation leads emerge at the end opposite to the firing leads.

The instrumentation of wire bridge igniters is carried out by EMI(E) Ltd. to individual requirements and fig. 6 shows two types (supported and unsupported) of assembled, instrumented igniters.

## 2.2 Conducting-Composition (c.c.) Igniters

c.c. igniters are voltage sensitive devices and hence the parameter measured is the r.f. voltage appearing across the igniter electrodes. To this end a crystal diode voltmeter is used.

Since any device used to measure the r.f. voltage appearing across the igniter should disturb the circuit as little as possible, in particular the impedance characteristics should not be modified, an inert filled ignitor was used in order to simulate, as nearly as possible, the impedance/frequency characteristics of the live devices. Furthermore the d.c. resistance of this inert filled igniter was made similar to the maximum d.c. resistance likely to be found in the corresponding live igniter; it having been shown that the replacement of an igniter by one of lower resistance cannot lead to an increase in the r.f. voltage developed across the igniter. Since the normal junction diode becomes inefficient at frequencies above the VHF region, it was necessary, in the diode voltmeter, to use a point contact type diode. The point contact diode, because of its large physical size, cannot be mounted either inside or on the c.c. igniter and must be connected

across the igniter holder terminals. At high frequencies ( $>1\text{GHz}$ ), since the igniter impedance is low and reactive, standing waves exist in the firing circuit which feeds the igniter and large voltage differences exist between the point at which the diode is connected and the firing in the igniter. This fact has led to difficulties in calibration as will be seen in Section 4.2.

Figs 7(a) and (b) show the two possible circuit configurations which can be used for the diode voltmeter. The following points arise:-

- a. The series diode configuration relies, for its operation, on the existence of a d.c. path through the igniter and/or firing circuit. Provided that the d.c. resistance of this path is low, compared with the load for the diode, the two circuits will give identical d.c. outputs for identical r.f. voltages across the igniter.
  - b. The series diode will operate, albeit with reduced efficiency, down to very low frequencies whereas the shunt diode configuration has a definite low frequency cut off.
  - c. Any d.c. voltage existing across the igniter will have no effect when the shunt diode configuration is used.
- On balance it was considered that the shunt diode circuit was the better one for hazard measurement and the series diode circuit for diode calibration.

### 3. THE TELEMETRY LINK

As the telemetry link is almost identical for the bridge wire and c.c. systems it will be described with particular reference to the bridge wire system and any modifications required for use with c.c. igniters will be brought out in the text.

### 3.1 Hazard Measuring Equipment Mk I (HMEI)

A system block diagram of the HMEI is given in fig. 8. The thermistor bridge is fed by a 3.000 KHz oscillator. The out of balance signal from the bridge is amplified and then added to the output of a reference oscillator whose frequency differs from the first by 63Hz. The tracking components in the adjustment box provide a means of achieving an accurate balance over a wide range of ambient temperature.

The two oscillators and the amplifier are contained within the oscillator module and the output signal from this module, consisting of the combined reference and out-of-balance signals, is fed to the winding of a split core transformer. This half core is placed against the inner surface of the weapon skin whilst a second half core, which also carries a winding, is aligned with the first but on the outside of the skin. Sufficient magnetic field penetrates the skin to induce a workable current in the outside windings. The induced signal is then amplified by a tuned amplifier which incorporates an automatic gain control loop, operating on the reference signal. This provides a reasonably constant output and compensates for variations in the spacing of the split cores. This output provides the drive for the accoustic link transducer.

The sound produced passes down a plastic tube to a second transducer which, acting as a microphone, produces an electrical signal. The output from the link is fed via a screened input selector to the indicator unit.

The indicator unit has a 3KHz broad band tuned amplifier having an a.g.c. loop which maintains the level of the reference signal constant at the detector. The out-of-balance signal, and the reference signal are added in a mixer and the 63Hz beat signal selected and amplified in a tuned

amplifier and the output displayed on a meter. By maintaining the reference signal level constant, at the indicator unit detector, all gain variations throughout the system can be ignored.

For use with the c.c. igniter a chopper module is added and this, together with the crystal diode instrumentation replaces the thermistor bridge. The 3KHz bridge supply from the oscillator module drives a chopper circuit which alternately shorts and open circuits the d.c. output from the diode voltmeter at the igniter terminals. The resulting chopped d.c. is in a form which can be passed through the split-core transformer and is amplified and fed to the oscillator module as was the out-of-balance signal from the thermistor bridge. The complete modified data link system is shown in fig. 9.

### 3.2 Hazard Measuring Equipment Mk II (HME2)

A system block diagram of the HME2 is given in fig. 10. In this version the thermistor bridge operates at d.c. and the output is amplified and used to control the frequency of a pulse generator contained within the data coding module. When the bridge output changes, due to a temperature rise of the sensing thermistor, the pulse frequency also changes. The pulses are fed on to the primary winding of the split core transformer and from the external secondary winding to the indicator; the method of transmission is identical to that described in the HME1 system. However, at the indicator unit the incoming pulses are amplified and integrated giving a d.c. output, proportional to the unbalance of the bridge, which is displayed on a meter.

That part of the resultant d.c. from the integrator network, due to the slightly different resistances of the thermistors at ambient temperature, is backed off. These differences will vary with ambient temperature and



thus the backing-off facility is used to set the system zero and to correct for ambient temperature drift. Once the system has been 'zeroed,' heating of the igniter bridge wire, by flow of current in it, causes further unbalance of the d.c. bridge. This further unbalance gives an increase in the output voltage of the integrator network and this increase is displayed on the output meter.

The only modification to this system, required for use with the c.c. igniter, is the addition of a passive resistance network between the diode voltmeter output and the data coding module.

In cases where the weapon screening is not continuous the magnetic link may, if desired, be omitted from the system, in which case the amplifier module is not required. Fig. 11. shows the general arrangement of the HME2 for the bridge wire measuring system.

#### 4. CALIBRATION

##### 4.1 Bridge Wire Devices

On the bridge wire igniters calibration is a relatively simple task. It is achieved by injecting known d.c. current into the firing leads and observing the output meter reading. In this way a direct calibration of output meter reading against equivalent d.c. current is obtained. Fig. 12 shows a typical calibration curve.

##### 4.2 Conducting Composition Devices

The diodes used for the instrumentation are calibrated separately in a coaxial measuring jig. The r.f. voltage across the diode to produce fixed levels of d.c. at the output is determined for several frequencies.

Calibration of the c.c. system is complicated by the fact that the

diode instrumentation monitors the voltage, not at the igniter itself, but at its holder terminals for the reasons given in sect. 2.2. At higher frequencies voltage standing waves, between the igniter and its holder terminals, give rise to large differences between the measured voltage and the actual voltage appearing across the igniter. This phenomenon imposes a frequency limit of 500 MHz above which small changes in igniter-diode separation, which are inevitable with the different holders in use, leads to pronounced differences between the measured voltage and that appearing across the igniter. Also as there is a wide variety of igniter holders it is not possible to calibrate each type, as this would involve measurement of impedance at the point of voltage measurement and injecting a known power into this impedance. Hence calibration of individual combinations is extremely difficult and for this reason only one calibration is produced with the proviso that it is not accurate at frequencies in excess of 500 MHz.

Fig. 13 shows the voltage pattern at various frequencies on a 100 ohm line terminated with an impedance representing a typical c.c. igniter. The curves of this figure are calculated for a completely artificial case and are primarily intended to show the magnitude of the problem.

Work at EMI(E) is at present aimed to reduce the size of the instrumentation so that it can be contained within the body of the igniter. In this way lead lengths are very short and the instrumented igniter can be calibrated as a unit. Progress has been made possible by the recent introduction of very small diodes. Partly because of the resulting compactness, and partly because the diode can be connected much closer to the effective part of the igniter, it is hoped to extend the useful calibration to frequencies

in the region of 2GHz. Considerable extension of frequency has already been obtained, but techniques are not yet finalised.

## 5. CONCLUDING REMARKS

### 5.1 Comparison of the Performance of HME2 with HME1

A comparison of the performances of HME2 with that of HME1 is given in Table 1. Improvements not noted in the Table are:

- a. the use of 3000 Hz for driving the thermistor bridge in HME1 made it necessary to balance resistance and reactance. This was avoided in HME2 by using a d.c. bridge.
- b. HME1 required the use of thermistors selected for equality of resistance and temperature coefficient. The limits were tight and selection was tedious and costly. HME2 could work with wider tolerances, and commercially selected pairs were adequate and less costly.
- c. the accuracy of indication of current in the bridge wire is increased if calibration is carried out at an ambient temperature within  $5^{\circ}\text{C}$  of the working temperature. Provided this is done the accuracy of HME2 is within the stated limits for an ambient temperature range of  $-5^{\circ}\text{C}$  to  $+40^{\circ}\text{C}$ .

### 5.2 Use in the field

Both equipments have been used in the field to measure pick-up in production-type missiles when placed near high power transmitters. The extra sensitivity of HME2 has proved very useful, since an indication of pick-up can be obtained under unfavourable conditions, and orientation or other adjustment can then be made to maximize the reading. The equipments have been approved by the British Ordnance Board who accept the readings

obtained as valuable evidence in considering their recommendations of safety. Two of the larger British aircraft companies have sets of HME2, which are used in development of prototypes and another set, enabling six igniters to be monitored simultaneously, is held by a Government R & D establishment for testing overall systems.

British Crown copyright is reserved for the figures which are published with the permission of The Controller of Her Britannic Majesty's Stationery Office.

#### DISCUSSION

When using thermistors in detection circuitry coupled to EED's which are in an RF environment, the possibility of RF pickup by the detection circuit leads should be recognized. Shunt capacity of such magnitude that will provide a low impedance to the irradiation frequencies may help the situation.

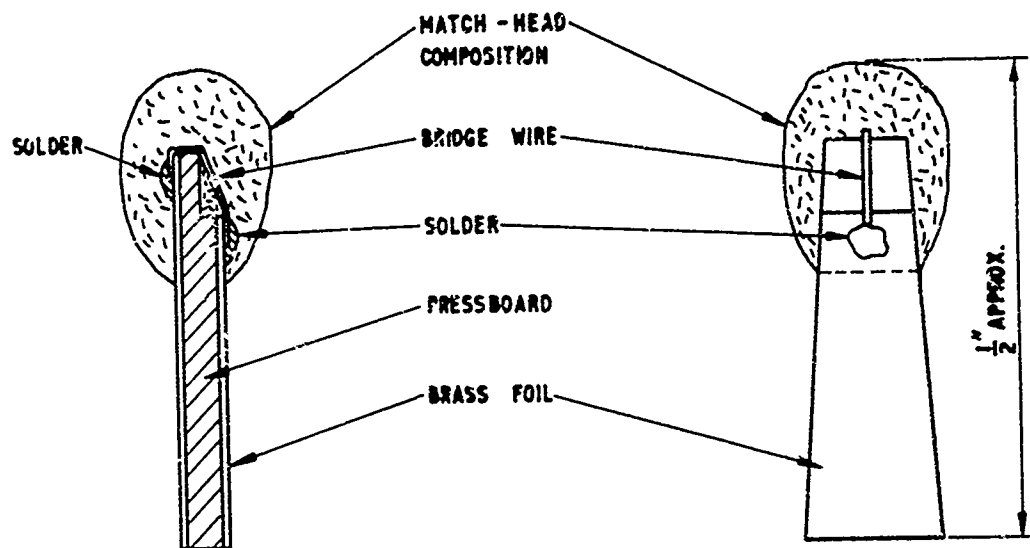
TABLE I. COMPARISON OF HAZARD MEASURING EQUIPMENTS MK I AND MK II BRIDGEWIRE DEVICES

	HME 1	HME 2
Basic Sensitivity	-26 dB	-40 dB
Dynamic Range	15 dB	26 dB
Accuracy of Current Indication	$\pm 1.5\text{dB}^*$	$\pm 2\text{ dB}^*$
Ambient Temperature Range	0-30° C	0-30° C
Continuous operating time of units mounted inside missile	80 hrs.	3 weeks

\*When calibrated at any temperature in Ambient Range.

#### c.c. Devices

The calibration and frequency range depends upon the instrumentation used, and this is still being developed.



ACTUAL SIZE

FIG. 1 LOW TENSION ELECTRIC FUSEHEAD

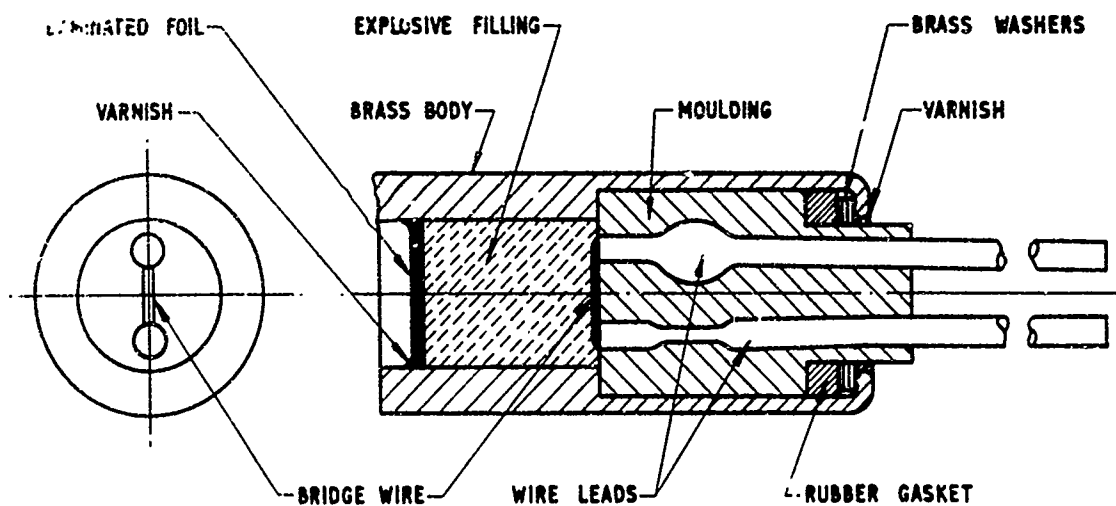


FIG. 2 X2/H ENCLOSED BRIDGE WIRE IGNITER

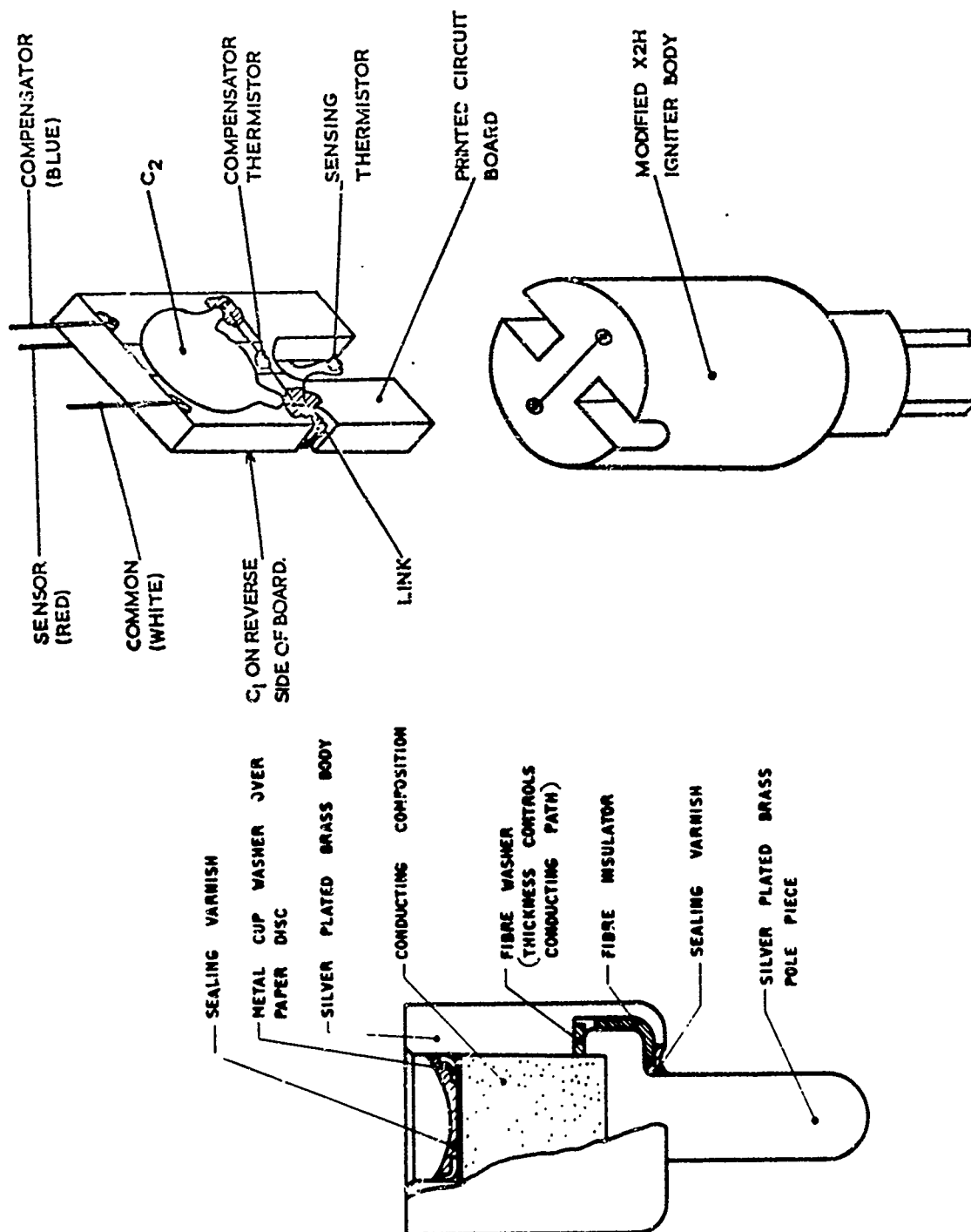


FIG. 3 MAIN FEATURES OF THE C.C. IGNITER

FIG. 4 INSTRUMENTED IGNITER ASSEMBLY

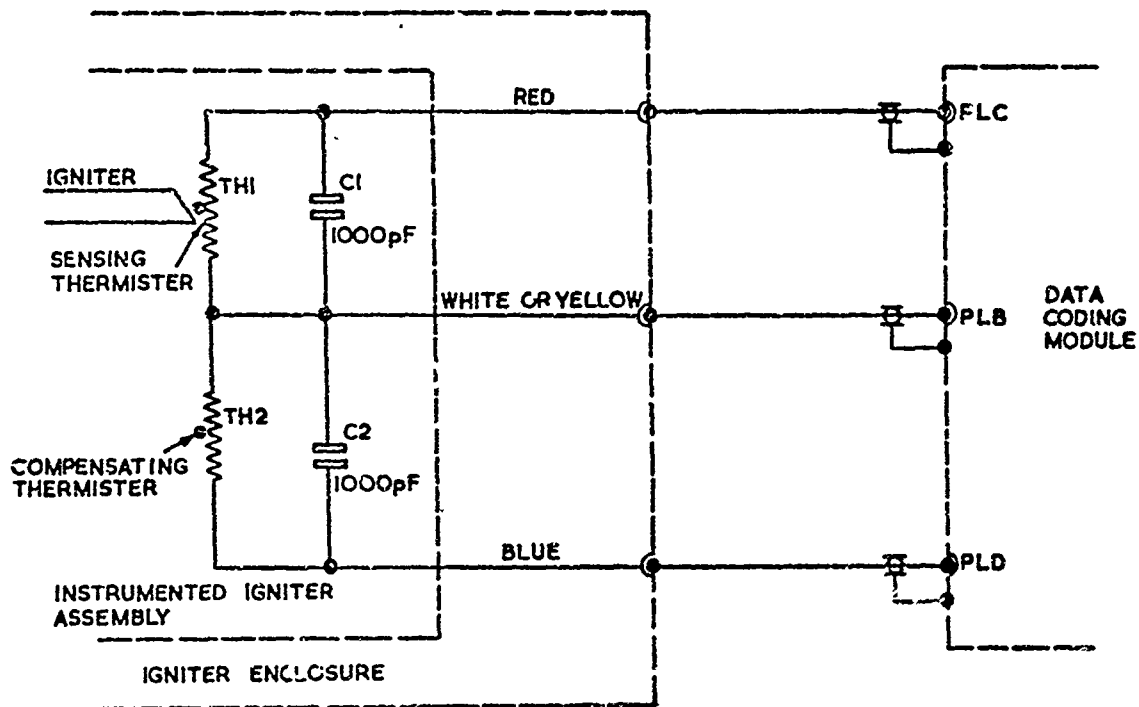


FIG.5 INSTRUMENTED IGNITER CIRCUIT.

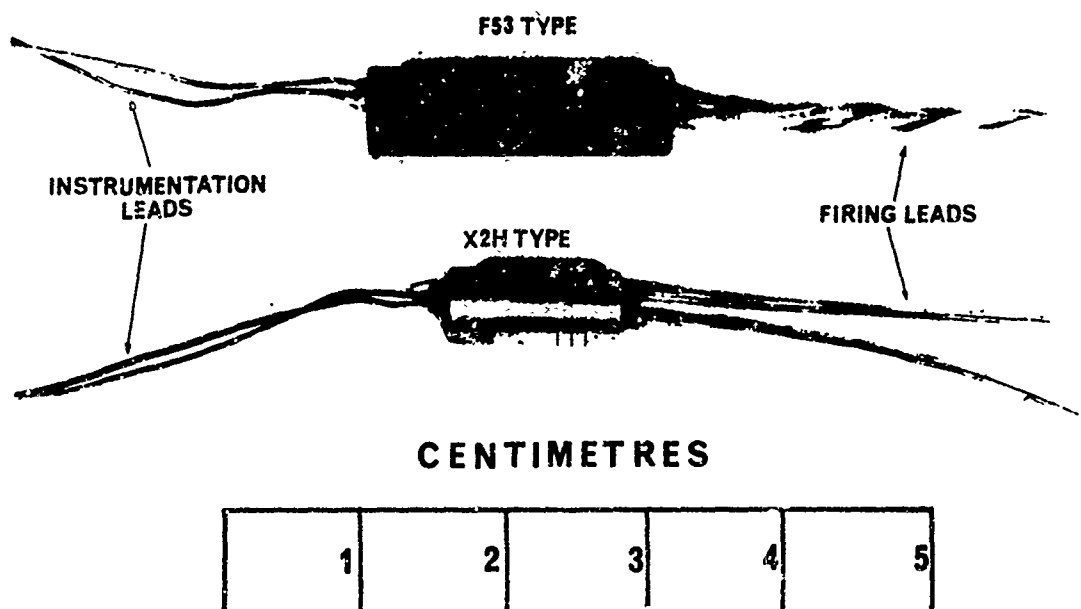


FIG.6  
INSTRUMENTED IGNITERS

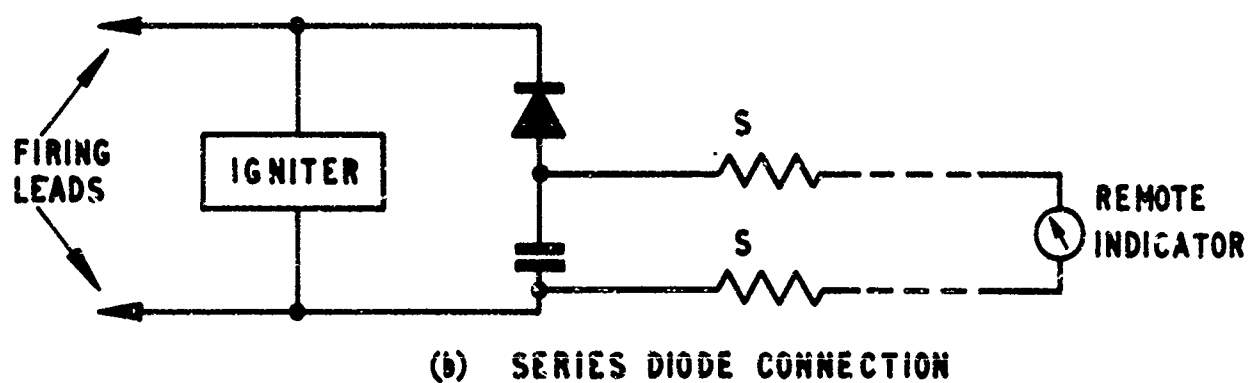
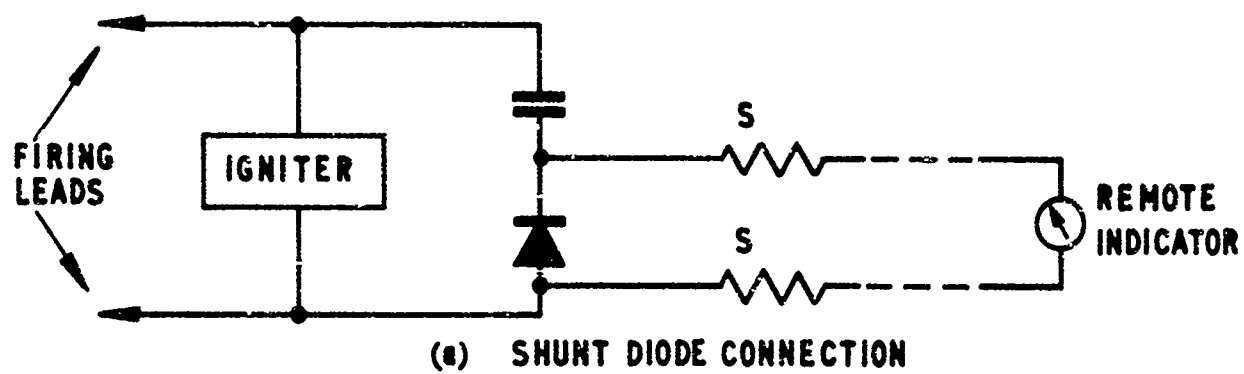


FIG. 7 BASIC VOLTMETER CIRCUITS



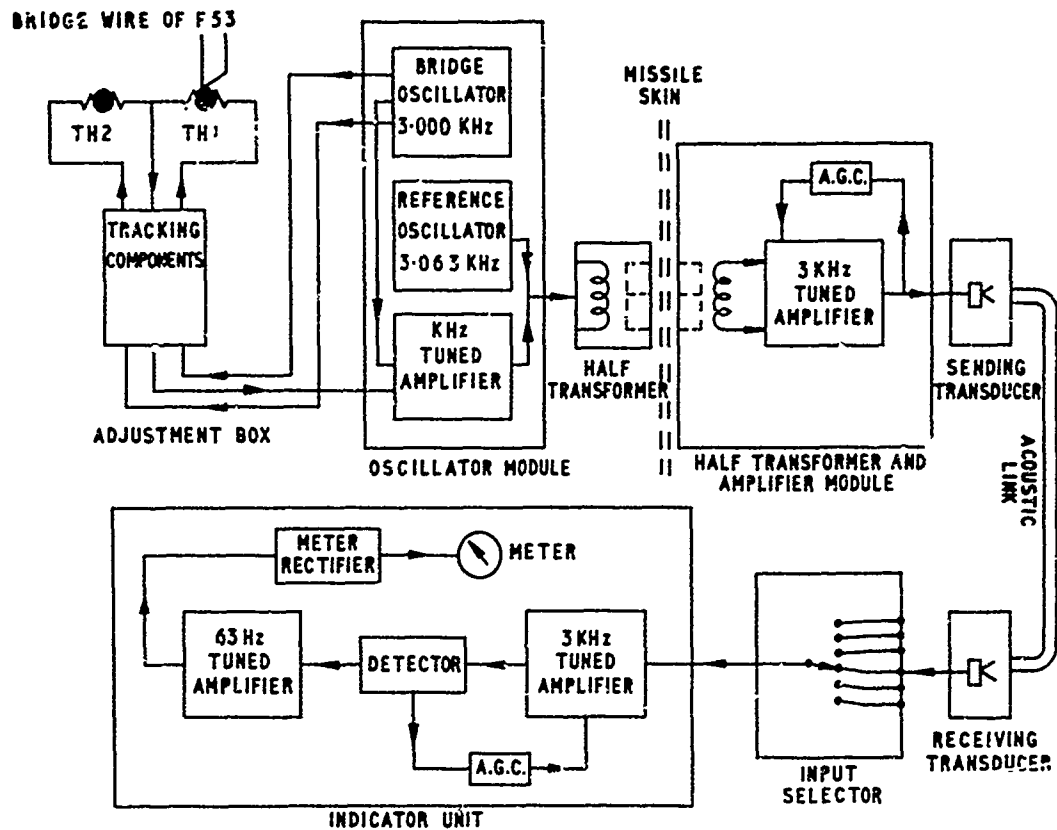


FIG. 8 SYSTEM BLOCK DIAGRAM

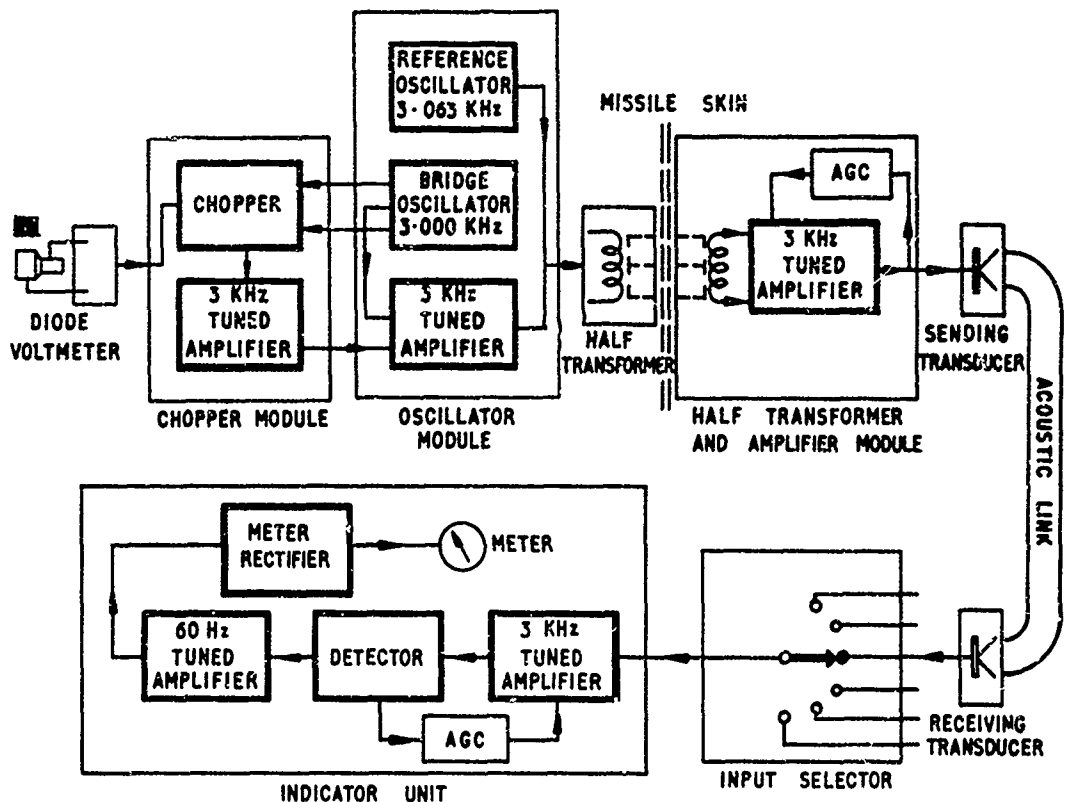


FIG. 9 MODIFIED HAZARD MEASUREMENT SYSTEM BLOCK DIAGRAM (CONDUCTING COMPOSITION DEVICES)

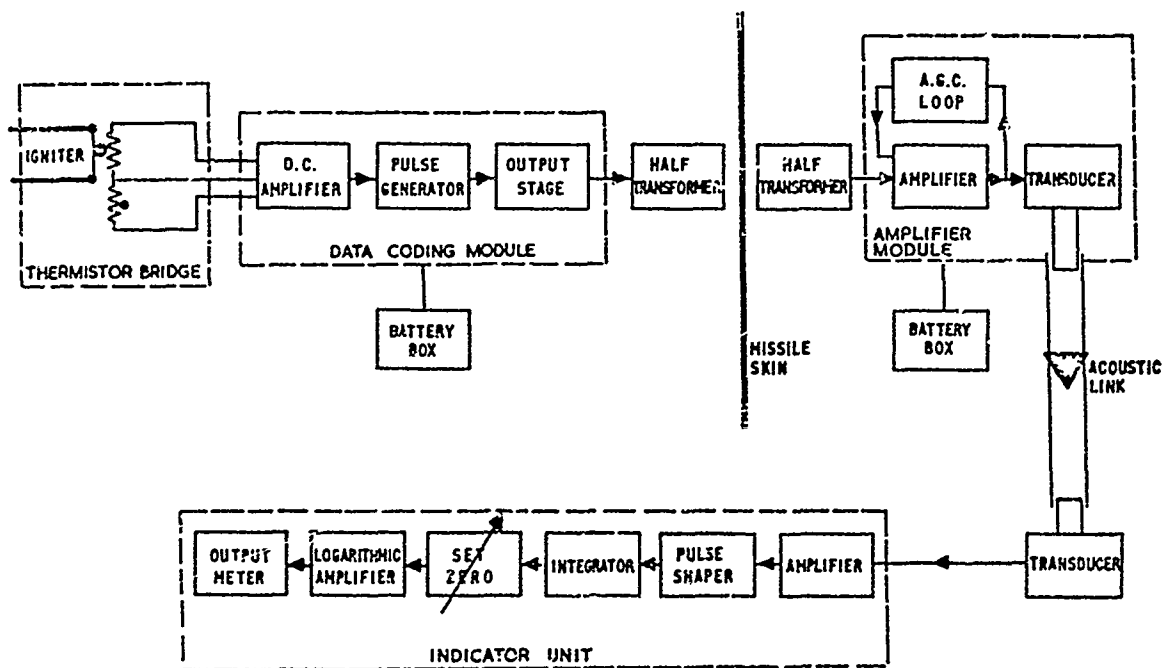


FIG.10  
BLOCK DIAGRAM OF HAZARD MEASURING EQUIPMENT MK II

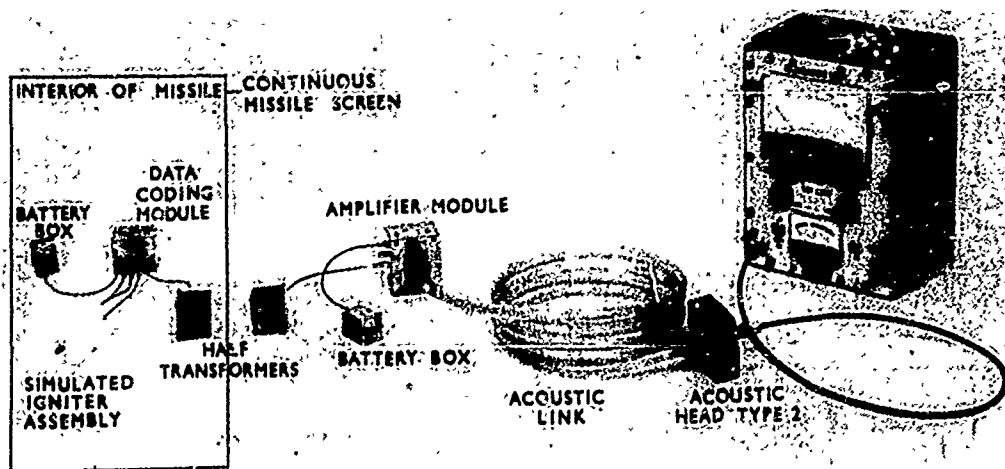


FIG.II HAZARD MEASURING EQUIPMENT MkII GENERAL ARRANGEMENT

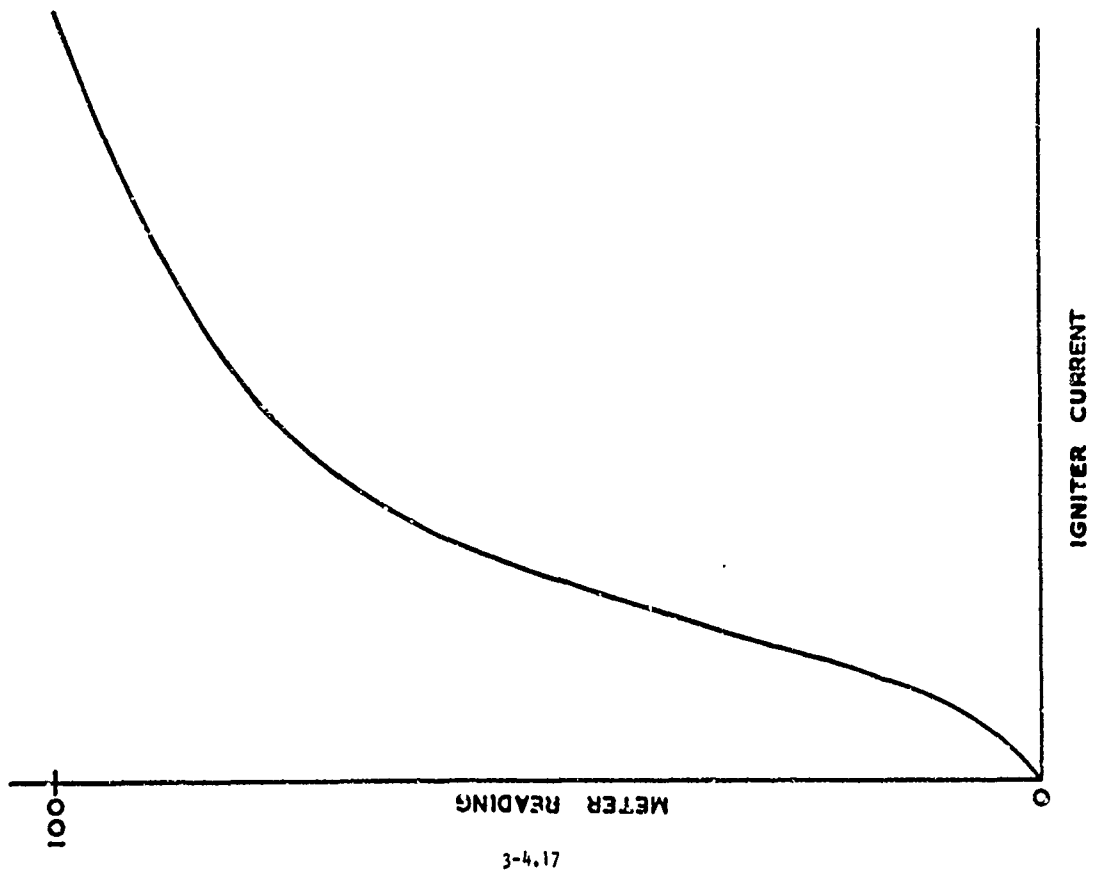


FIG. 12  
CHARACTERISTIC FORM OF CALIBRATION CURVE.

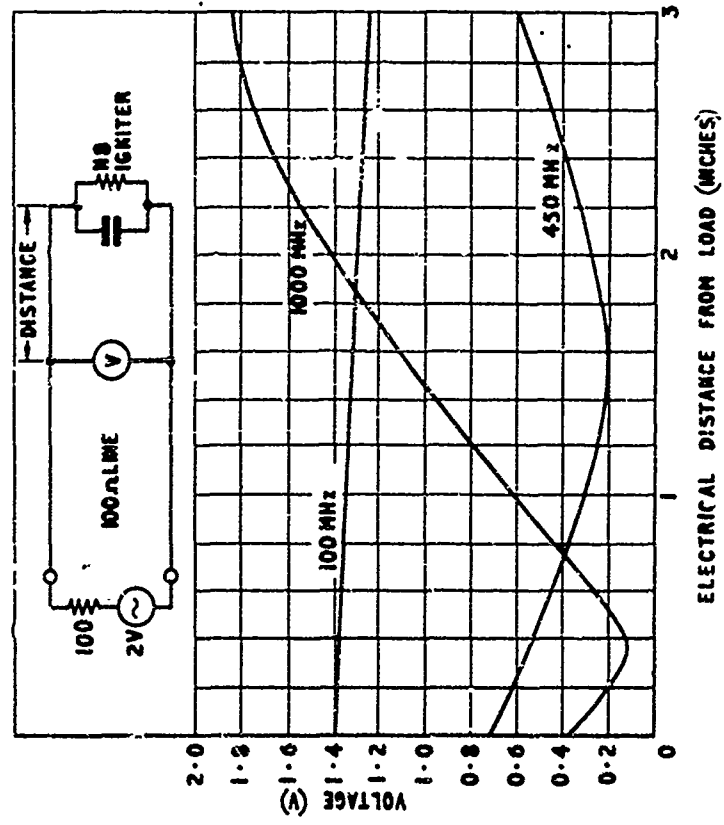


FIG. 13 VARIATION OF VOLTAGE WITH DISTANCE FROM IGNITER

### 3-5 DISCHARGE OF AN ELECTROSTATICALLY CHARGED HUMAN

John T. Petrick  
of  
The Naval Weapons Laboratory  
Dahlgren, Virginia

#### Charge Generation by Clothing:

Contact of various layers of clothing is the most common cause of personnel charging. This type of charging occurs whenever two dissimilar layers of clothing touch. The clothed human can be imagined as the spherical body shown in figure 1. The body is shown covered by four layers of fabric; the innermost being cotton undergarments, the next layer a wool jersey and the following two layers the inner and outer layers of a nylon jacket. The resistance, (R) is the total resistance to current flowing from the person to ground. In cases where the floor is quite conductive and the person's shoes are insulators this resistance will be the resistance of the shoes as measured by the Navy method outlined in OP5. In this case the capacitance is that measured with respect to the conductive floor. For example, consider a person with a capacitance of 200 pf and wearing rubber soled shoes. Now assume that the shoe resistance is such that if we charge the body to a particular level and then terminate the charging, the net charge will be reduced to almost nothing in a total time of about 200 seconds. This fixes the shoe resistance at about  $2 \times 10^{11}$  Ohms.

If the outer jacket is removed from our subject the charge generated at the interface of the wool jersey and the nylon inner lining of the jacket will be freed. The jacket will have charge of one polarity on its inner lining and the jersey will have an equal amount of charge of the opposite polarity on its outer surface. Since the body was not initially charged, the charge on the jersey will migrate, at a rate determined by the inner fabric layers' resistivity, through the inner fabric layer and be distributed over the body and the remaining fabric. Thus a potential difference is produced on the human capacitor (C) and the body will remain charged for about 200 seconds, provided that this potential is not excessive.

To determine the body potential which may be expected after removing this jacket, the charging characteristics of the jacket-jersey combination and the resistivity of each fabric layer must be known. The charging characteristics of any fabric combination may be measured by either of two methods currently used at the Naval Weapons Laboratory.

The first method for fabric evaluation is to place belt type test samples of all the fabrics involved on the device sketched in Figure 2. This device measures the charge generated when the sample belts contact and separate as they pass over rotating rollers. The charge produced is directly proportional to the total area of contact between the belts as they move. Measurement of this charge is used to predict the voltage expected during removal of various types and layers of clothing by using only fabric samples, not complete clothing articles or clothed personnel.

The other test method involves fabric covering of two metal drums, one with a sample of the jacket inner lining and the other with a sample of the jersey. The drums are then brought together and one is driven at a constant rate and grounded as shown in Figure 3. A Faraday cage placed around the ungrounded drum will provide a means for measuring any charge on the fabric cover of this drum and any charge which may have already been transferred to the drum. By connecting a capacitor to the Faraday cage the charge generating characteristics of the fabrics may be determined by measuring the capacitor voltage as the drums rotate. The rate at which the voltage rises ( $\Delta V / \Delta t$ ) is used in the following relations to determine the current flowing onto a person when he removes his jacket.

- (1)  $\alpha \equiv C' (\Delta V / \Delta T)$
- (2)  $A = 2\pi ab + l(w+c)/2$
- (3)  $V = 0.2A \alpha / C$

Where:  $C'$  = capacitance of Faraday cage and additional capacitor,

$\Delta V / \Delta T$  = measured rate of voltage rise

$a$  = sleeve length

$b$  = average sleeve diameter

$\alpha$  = charge/time/area

c = chest size

l = jacket length

w = waist size

C = human capacitance

A = calculated total contact area of jacket-jersey

At approximately 50% relative humidity the rate of voltage rise was found to be 0.12 volts per second for a NOMEX@nylon sample and a wool sample. For a size 36 jacket a total contact area was calculated to be 1,558 square inches. The expected voltage when removing a NOMEX jacket worn over a wool jersey is 2,057 volts for a person of 200pf body capacitance. This value is in good agreement with voltage measurements made on an individual in a similar environment when a nylon jacket worn over a woolen jersey is subsequently removed.

#### The Maximum Charge Level:

In our spherical model we assumed that essentially all the charge generated from removing a jacket or similar procedure will be drained from the individual in about 200 seconds. There is, however, another mechanism by which charge is drained from the body and it is this mechanism which limits the potential found on an individual after charging. This discharge phenomenon occurs when the electric field strength near the body becomes sufficiently high to ionize the surrounding air thereby causing a net efflux of charge from the body. Since objects having sharp points on their surfaces also have very strong fields in the vicinity of these points one expects these objects to begin losing charge by air ionization at far lower charge levels than smooth objects. A person's hair and even the individual fibers in his clothing will provide the high field site for this type of discharge to occur. Thus a voltage of about 30,000 volts is all that can be sustained by an individual for periods longer than a few seconds.

OUCH!

Consider the circuit shown in figure 4. Again the spheroid is the body and the resistance (R) and capacitance (C) have not changed. In this case the person has removed his jacket and is about to touch the grounded object labelled A which may be an ordnance @ Trade Mark

item. As he approaches his capacitance (C) increases; however, this increase is usually insignificant when compared to C, hence let his capacitance remain constant at 200pf.

At some body-objective separation the potential difference in the gap between body and object will cause the air in the gap region to ionize. The ionization will connect the individual to ground within a few nanoseconds; complete body discharge and, probably, exclamation of assorted profanities will ensue. The resistance of the ionized air is negligible; hence if bare skin contact is made the resistance of the body, skin, and the ground loop will be the only resistive components limiting the current flow. There is, however, sufficient evidence available to believe that the discharge circuit has a significant amount of inductance, a portion of which may rightly be called human inductance. This inductance limits the peak discharge current and may cause circuit ringing. The current flow in a pure R-C circuit is compared to that of a circuit with added inductance in figure 5.

The importance of the values of body capacitance, resistance, and inductance lies in providing a suitable test to evaluate ordnance and fuels for electrostatic safety. Since it is somewhat unsafe to charge a typical person to thirty thousand volts and see if he can ignite these materials the obvious recourse is to build a simple circuit which reproduces the discharge. By applying this reproduction to the ordnance or fuel we may determine whether ordnance or fuel is safe for handling.

Almost a year ago we began charging everyone within reach to voltages of about 5,000 volts. The person's capacitance was measured with an impedance bridge and the resistance and inductance were measured using the circuit shown in figure 6. The human capacitance was found to average about 200pf with a range of 100pf to 4,000pf for various shoes and personnel. The first discharge curves looked like the one shown in figure 7. From these curves the human resistance was found to decrease with increasing voltage and have a range of 25 to 60 Ohms for voltages from 2,000 to 8,000 volts. The inductance of the entire discharge circuit was found to be about 4 microhenrys.

A nitrogen filled pressurized spark gap, triggered by pressure release, several feet of RG 19 cable, some carbon resistors and a small coil were used with a 120,000 volt power supply to reproduce this discharge. The circuitry used is shown in figure 8 along with a typical

discharge current oscillogram of a 30,000 volt discharge. This circuitry, called the electrostatic discharge simulator, is currently used to evaluate electroexplosive devices and weapon systems for electrostatic safety

#### Measuring the Human Inductance and Resistance:

Recently, higher speed oscilloscopes have been used to record the discharge current of charged individuals. From these curves the fact became clearly evident that the measuring circuitry influences the shape of the recorded pulse

At first a 1 Ohm low inductance resistor was mounted in a General Radio insertion unit and connected directly to a Tektronix type 519 oscilloscope as shown in figure 9. Hopefully the skin resistance of the human would always be sufficiently large so that most of the voltage drop is across the skin and not the 1 Ohm sensing resistor. This was the case hence the oscilloscope did record the current flow occurring when a charged person was grounded through a low resistance path. The traces shown in figure 10 (a) were recorded from a person charged to 3,000 volts. The extremely short duration of this pulse and the values of resistance and inductance, (6ns, 10 Ohms, and 5nh respectively) indicated that the pulse was considerably different than the earlier ones and an explanation was sought.

The response of the earlier circuit was studied and apparently the inductance added by the measuring circuit was so high that the total discharge time ( $10L/R$ ) was extended far beyond its actual value. The response of the present circuit was also studied and it was found to have a natural resonance at almost the ringing frequency observed in figure 10. By increasing the 1 Ohm resistor to 10 Ohms the ringing appeared on the beginning of the pulse and was damped out before the discharge was complete. See Figure 10(b). This result confirmed the opinion that the response of the measuring circuit masked the actual discharge. A 10 Ohm resistor is too high to permit measurement of the human grounded through a low resistance ground, hence it cannot be used.

At this time a careful analysis of the measuring circuitry is being made and other methods are being considered. One of the alternate current measuring methods uses a Rogowski coil which produces a representation of the current flow during discharge without being directly connected to the discharge circuit. This circuitry is sketched in figure 11. Using



the Rogowski coil method the external circuit inductance and resistance can be minimized and the values of resistance and inductance for the human may be measured quite accurately. Design information for the Rogowski coil can be obtained from Huddleston and Leonard's text Plasma Diagnostic Techniques

#### Conclusion:

In conclusion it might be said that in the near future the results of those tests outlined herein will provide valuable information which will not only allow valid electrostatic sensitivity tests for explosives but will additionally aid in explaining the variation of human skin resistance with applied voltage, and determining the depth beneath the skin at which the charge most effective during human discharge resides. The results will also enable analysis of the possible bodily dangers involved in discharges of this nature, and give considerable insight into the radio frequency response of the human body.

#### DISCUSSION

The upper limit of the capacitance of the human body to ground is open to question. It has been noted that a person wearing conductive sole shoes (similar to being barefooted) standing on a mylar sheet approximately 2 mils thick, may show a capacitance ranging from 100 to 4000 picofarads, according to Mr. J.T. Petrick of the U.S. Naval Weapons Lab. The study was made to determine if it would be profitable to wear conductive shoes on naval vessels. The mylar sheet simulated the non-conductive paint common on decks of naval vessels.

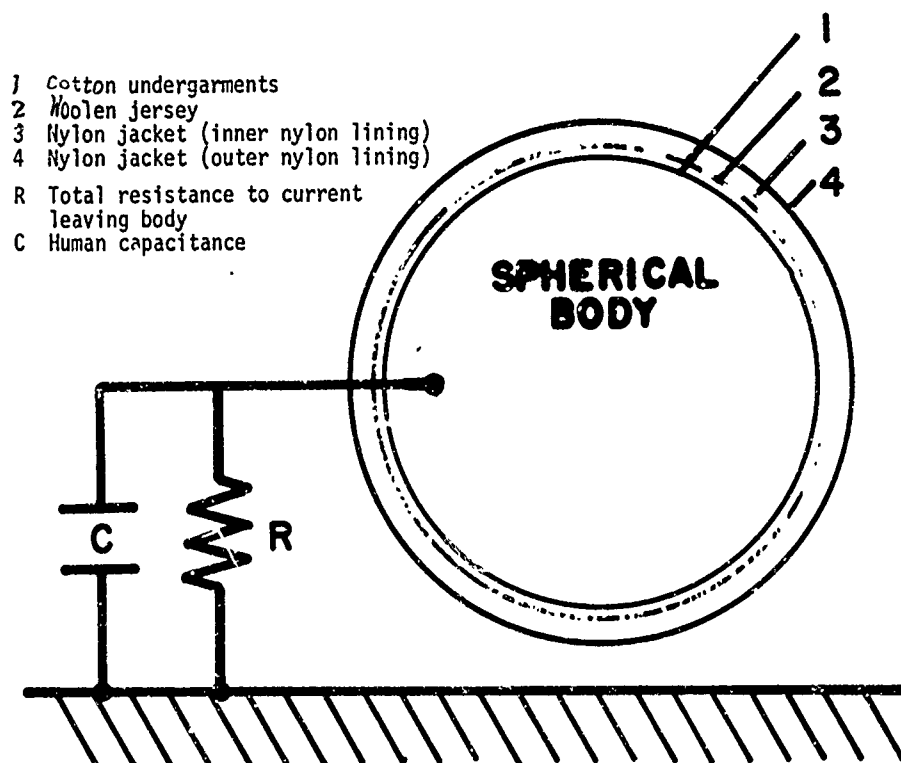
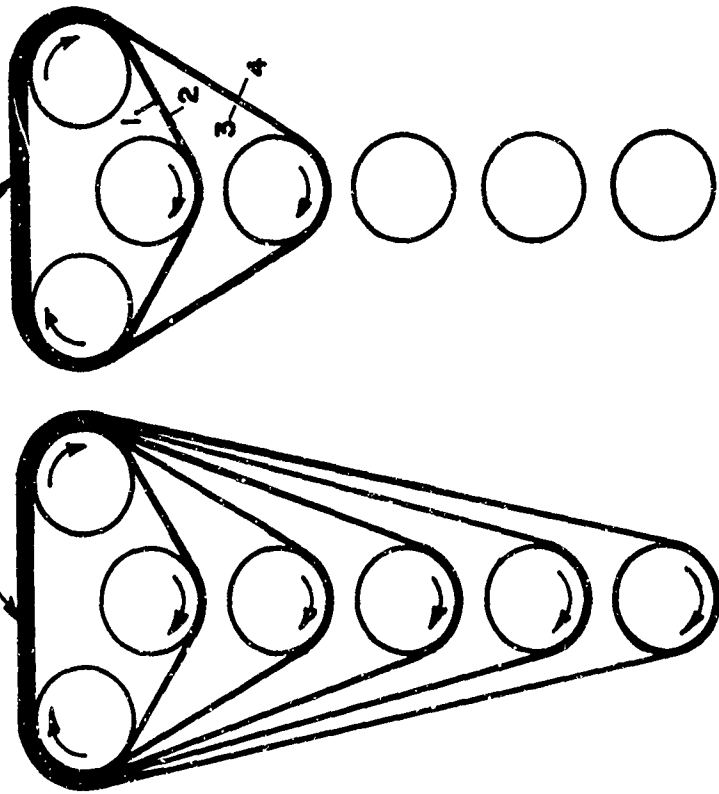


Figure 1. Spherical Body Model for Clothed Human

# FABRIC TEST DEVICE

CONTACT CHARGING OCCURS



- 1 - UNDERGARMENT SAMPLE
- 2 - SHIRT SAMPLE
- 3 - JACKET LINER SAMPLE
- 4 - JACKET EXTERIOR SAMPLE

3-5.7

# DEVICE FOR DETERMINING THE ELECTROSTATIC CHARGE AVAILABLE FROM FABRICS

BOTH DRUMS HAVE  
PROVISIONS FOR  
ATTACHING FABRIC  
SAMPLES

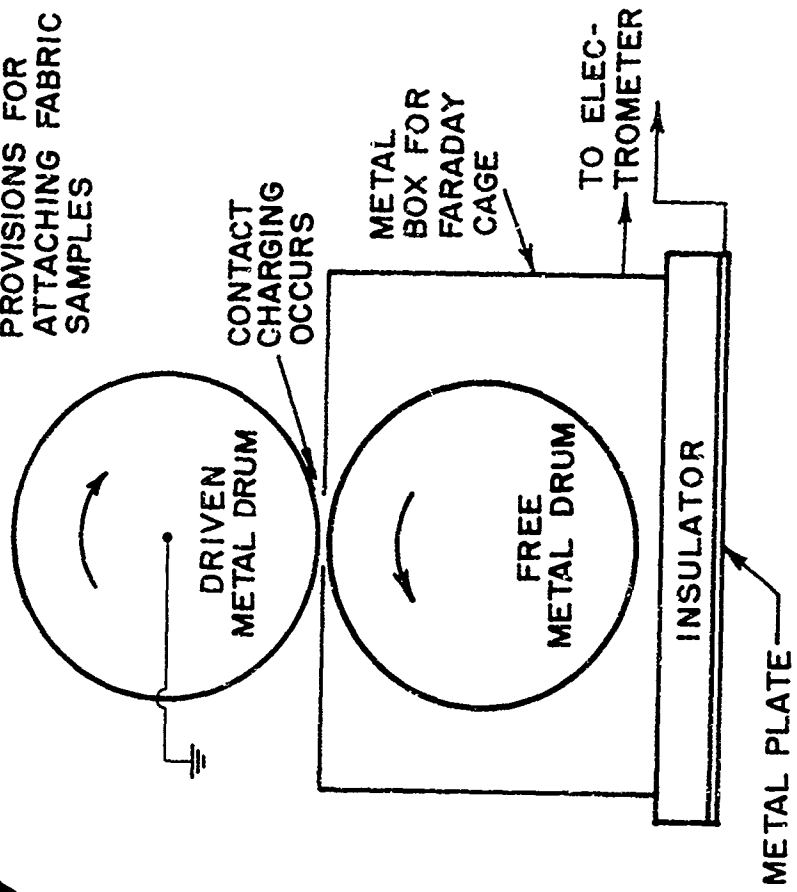
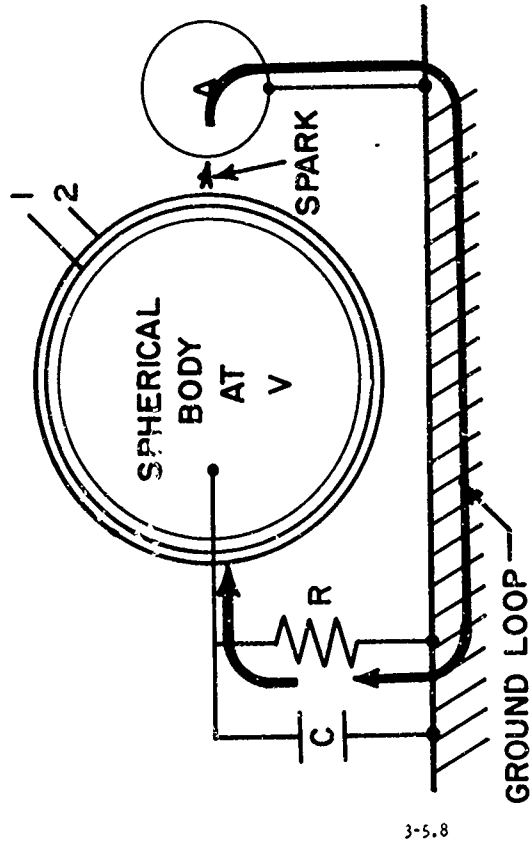


FIGURE 3

FIGURE 2

# HUMAN DISCHARGE CIRCUIT



- 1 COTTON UNDERGARMENTS
- 2 WOOLEN JERSEY
- A GROUNDING ORDNANCE
- V HUMAN VOLTAGE

FIGURE 4

# A COMPARISON OF RC and RLC DISCHARGE CIRCUITS

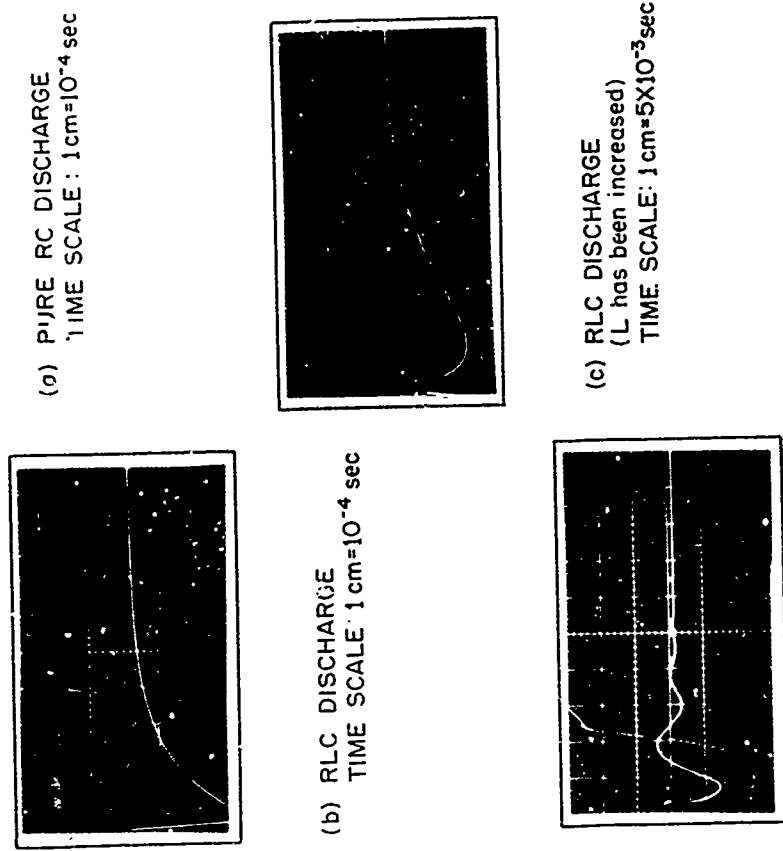
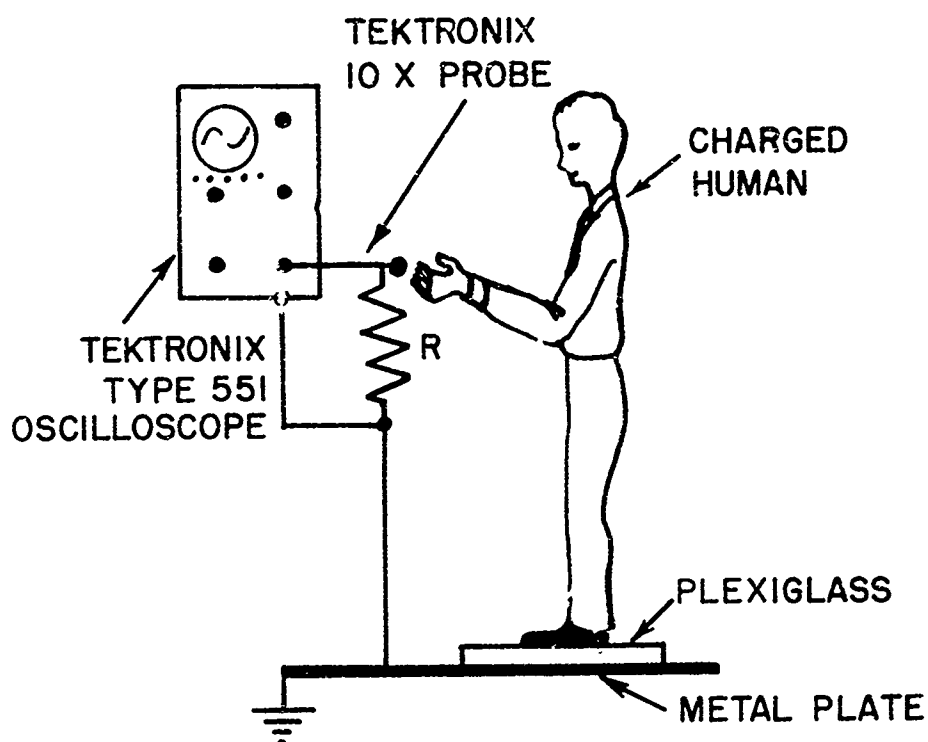


FIGURE 5

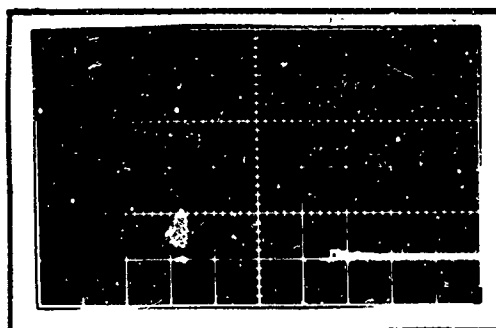
## THE FIRST CIRCUIT FOR MEASURING R AND L



$R = 1 \text{ Ohm}$

FIGURE 6

## AN EARLY HUMAN DISCHARGE CURVE



TIME SCALE:  $1 \text{ cm} = 0.5 \mu\text{s}$

FIGURE 7

# THE ELECTROSTATIC DISCHARGE SIMULATOR



30,000 Volt SIMULATED  
DISCHARGE  
TIME SCALE - 1 cm = 0.5  $\mu$ s

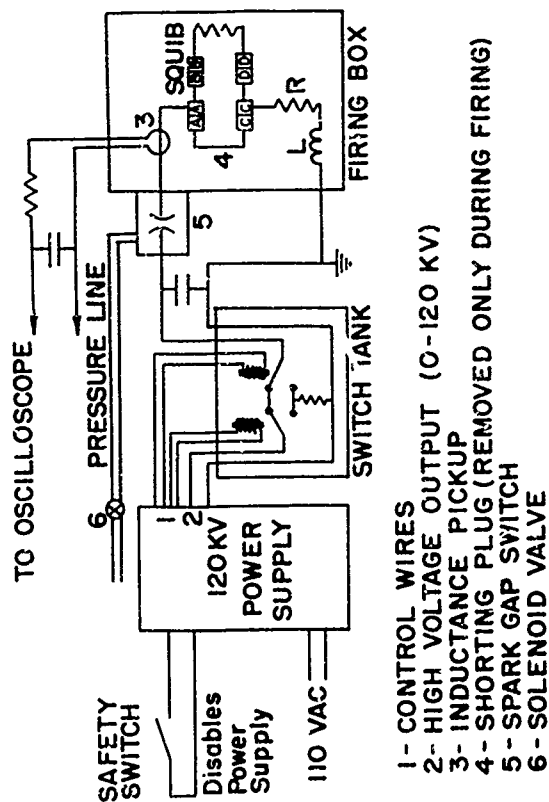


FIGURE 8

# CIRCUIT USED TO OBTAIN DISCHARGE CURVES FOR HUMAN EED DISCHARGE

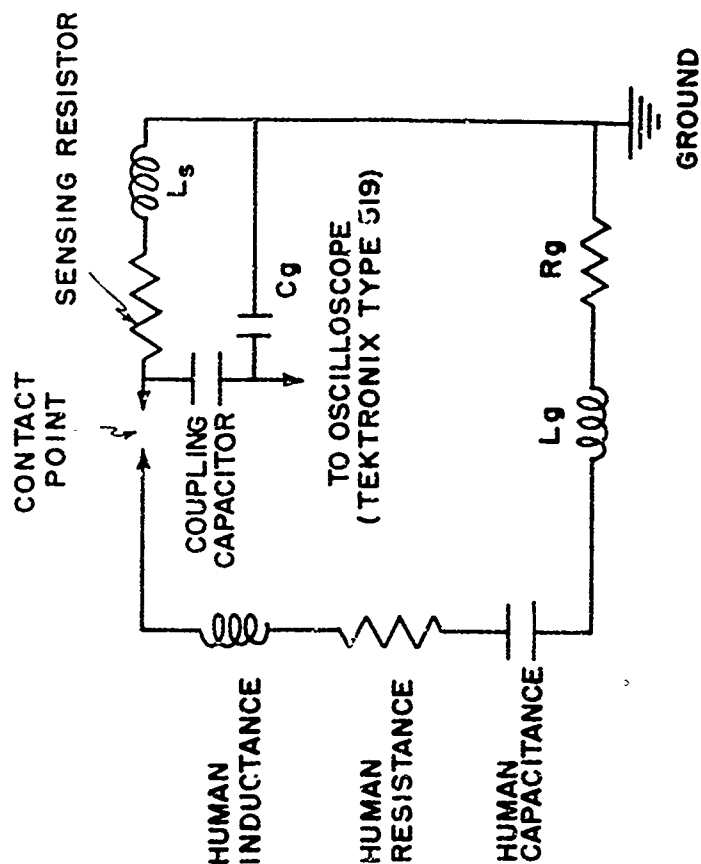
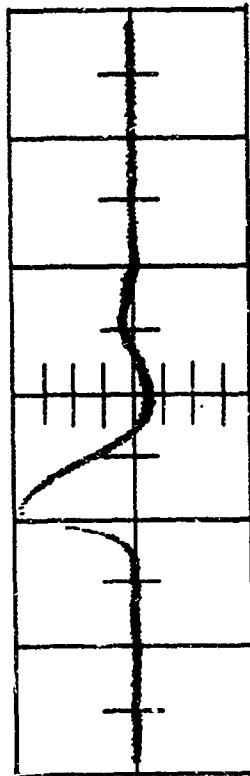
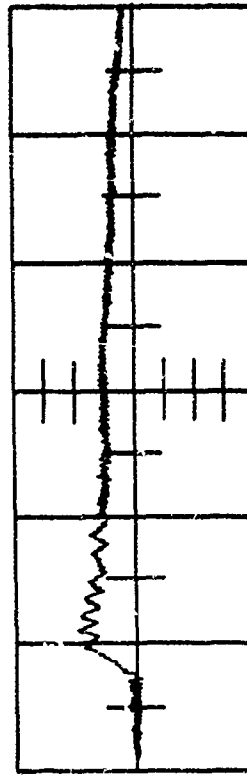


FIGURE 9

# HIGH SPEED OSCILLOGRAMS OF THE HUMAN DISCHARGE



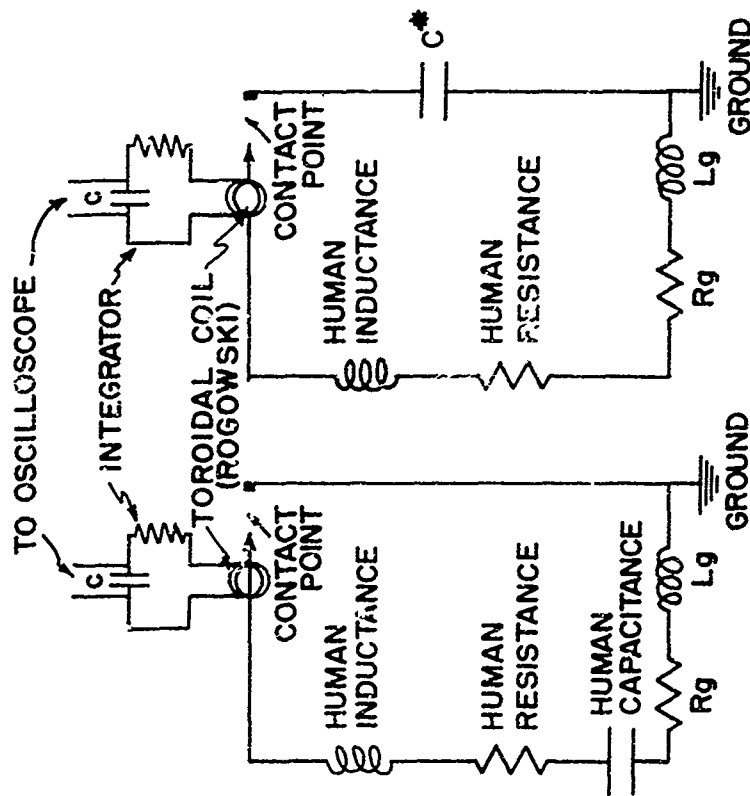
(a) HIGH SPEED TRACE USING 1 Ohm RESISTOR  
TIME SCALE: 1 cm = 5 ns  
(FIVE TRACES FROM HUMAN CHARGED TO  
3,000 Volts ARE SHOWN SUPERIMPOSED)



(b) HIGH SPEED TRACE USING 10 Ohm RESISTOR  
TIME SCALE: 1 cm = 5 ns

3-5.11

# TWO CIRCUITS USED TO MEASURE THE HUMAN DISCHARGE PARAMETERS



\* A COMMERCIAL CAPACITOR APPROXIMATELY EQUAL  
TO THE HUMAN'S

FIGURE 10

FIGURE 11

3-6 EXPERIMENTS IN THE PROTECTION OF EED'S  
FROM ELECTROSTATIC DISCHARGE  
EDWARD G. PIERSON  
CONAX CORPORATION  
BUFFALO, NEW YORK

INTRODUCTION

Specifications for safety in the handling and application of electro-explosive devices (EED's) now require that such devices successfully withstand a 25 KV potential from a 500 picofarad capacitor applied between bridgewire and case. Many disastrous accidents could have been avoided if the EED's involved had this capability. The build-up of a static charge capable of producing ignition has, for example, resulted from such simple operations as spraying insulated metallic surfaces with a cleaning solvent dispensed from a high velocity air gun. Inadvertent ignition occurs when the static discharge takes a path from bridgewire to case leading through the ignition mix.

The insertion of a barrier of high dielectric strength between the bridge-wire and the case that would withstand high static potentials is a common approach to solving the problem. An alternate approach would be the creation of a positive preferential discharge path free of ignitable material.

Dielectric barrier protection is complicated by the fact that many of the ignition mixes involved promote electrical conduction. Additionally, barrier protection may involve either excessive space or excessive inspection for dielectric faults.

In considering a preferential discharge path, the desired breakdown voltage should reliably occur somewhat above the system operating voltage. The preferential path should be self-healing to return to its initial breakdown level upon voltage drop. The current rise time should approximate one microsecond or less. While having infinite resistance below breakdown voltage, it must not be damaged by microsecond pulse discharges reaching hundreds of amperes.

At Conax Corporation, our chosen approach to safety from static discharge was the creation of the preferential discharge path. Consideration was given to the fact that there are many formerly qualified EED's which, except for their inability to meet the static discharge requirement, have demonstrated outstanding reliability. It was considered practical to add static protective circuitry to these devices while still retaining all of their know attributes.

#### PRELIMINARY TESTING OF COMPONENT

The major component required for a preferential discharge path was an automatic, voltage sensitive, avalanche switch that would function without regard to the polarity of the charge. Such a device might be (1) spark gap, (2) gaseous discharge lamp or (3) back-to-back solid state diodes. Cold cathode gaseous discharge lamps with two or three electrodes are readily available for test. Because small size and a non-conductive envelope were desirable, we chose to first evaluate the tiny AC1 high intensity neon lamp with two electrodes. This lamp is rated for only a few milliamperes continuous operation and requires a 47,000 ohm current limiting resistor for operation with 110 volts. Without the resistor, the lamp could fail at less than 110 VAC when the current and time effect of overheating resulted in electrode erosion or glass envelope rupture. The first question that needed an answer was: "Would this tiny lamp without benefit of a current limiting resistor withstand the 0.156 joules of energy to be dissipated from the 500 picofarad capacitor charged to 25 KV?"

Our electrostatic discharge equipment included an NJE Corp. Model HP-5 power supply of 0-30 KV with two 1,000 picofarad 20 KV capacitors. Series operation of the capacitors supplied a 500 picofarad capacitance chargeable to 30 KV. Parallel operation provided 2,000 picofarads at 20 KV. Low loss switching from charge to discharge was provided by Jennings Model 4401 actuator



with two Type RIG vacuum switches in SPDT arrangement.

To evaluate any instability of the breakdown voltage that might result from the high amperage discharge in the lamp, we conducted breakdown voltage evaluation tests before and after the high current pulses. For this we used the Microdot voltage breakdown tester Model 1901-A. This equipment provided a meter display of slow rising voltage until a selected breakdown current flow of 10, 100 or 1,000 microampere value stopped the meter movement at the indicated voltage level of conduction. Both one and four KV full scale deflections of the meter were available.

Evaluation of the peak discharge currents at a time constant of approximately ten nanoseconds was accomplished by using the single sweep trigger voltage adjustment in an oscilloscope. A fractional ohm non-inductive resistor was inserted with one terminal to ground in series with the AC1 lamp and the capacitor discharge equipment. The oscilloscope sweep trigger level connection was made across this resistor. As the capacitor discharges took place, the triggering level was lowered until sweep of the oscilloscope was accomplished. The value of the oscilloscope trigger setting was determined with a variable DC voltage supply and voltmeter. The peak current flow through the AC1 lamp was calculated by dividing the trigger sweep voltage setting by the value of the fractional ohm resistor.

From these preliminary tests it was observed that the AC1 lamps withstood repeated discharges from the 500 picofarad capacitor charge to 25 KV without benefit of any current limiting resistor. The same results were obtained with 2,000 picofarads charged to 20 KV. Microdot tests before and after the 25 KV discharges showed that the breakdown value of the lamps had not been greatly altered. The maximum deviation did not exceed a 6% rise and all readings were well under the 130 volt maximum rated breakdown value. The peak currents were

in hundreds of amperes.

#### FINALIZED DESIGN WITH EXPLOSIVE TESTING

Our next step involved the incorporation of the AC1 lamp into protective circuitry and testing with live EED's. It has been shown that the lamp alone can dissipate in excess of 0.156 joules per firing with intermittent duty. By adding resistance in the preferential discharge circuit, a greater energy dissipation can be handled without increasing the arc temperature in the lamp.

Figures 1 and 2 are schematic diagrams of our neon-resistor circuitry. One lead of a 10 ohm 1/4 watt carbon resistor is soldered to join with two AC1 lamps. The other lead from the resistor is grounded to the case of the EED. For a single bridgewire device, as shown in Figure 1, each terminal of the EED is connected to a free lamp lead. For a dual bridgewire device, as shown in Figure 2, the free lamp leads are connected to only one terminal of each bridgewire.

The carbon resistor performs a dual function. It limits the percentage of the total discharge energy that either the lamp or the bridgewire will be called upon to absorb. Again if for any reason a lamp should become shorted, the bridgewire would still receive better than 89% of the intended firing current.

Static discharge testing was performed on various EED types with and without the preferential discharge path circuitry. Voltages ranged from five to thirty KV. Capacitance was either 500 or 2,000 picofarads. (Figure 3 shows a test primer with protective circuitry). A small sampling of sequential tests, first with and then without protective lamp circuitry is given in Table I. The EED's in this sampling were single bridgewire, diazodinitrophenol base primers with lead styphanate spot and diazo-chlorate mix. The pulse discharges started at a 5 KV level and increased in 2 KV incremental steps. The

effectiveness of the system is clearly demonstrated.

#### OBSERVATIONS

During tests conducted At Conax, two phenomena worthy of mention were observed.

The first observation is in reference to the 1/4 watt, 10 ohm current limiting resistor. These resistors repeatedly decreased in resistance by as much as 20% with no visible outward signs of overheating. It is believed that this occurred because the high current density pulses have changed the carbonaceous composition to a graphitic state. This change in resistance agrees with a figure of 19-1/2% differential resistance given by National Carbon Co. for lampblack base carbon before and after graphitizing. In this application, the resistance change to a lower value is of no operational concern.

The second observation is of great concern. It relates to the possible effects of static discharge pulsing on bridgewire resistance stability. A group of fifteen EED's having Karma alloy bridgewires coated with an ignition mix of potassium perchlorate, powdered titanium metal and a silicone varnish binder were subjected to random static discharge pulses. The devices had received a previous two-hour thermal soak at 212°F with no indicated changes in resistance. Marked changes in bridgewire resistance for this device due to static pulsing were observed and are summarized in Table II. For example, one EED received thirteen pulses to reduce its resistance from 1.07 ohm to 0.82 ohm, a drop of 23-1/2%. Frequent reversal of the pulse polarity was employed. We explain this phenomena as follows: - - - The Karma alloy has a resistivity of 134 microhm per cm<sup>3</sup>, a coefficient of thermal expansion of  $14 \times 10^{-6}$  in/C° and is non-magnetic. Titanium has a resistivity of 55 microhm, a coefficient of thermal expansion of  $8.5 \times 10^{-6}$  in/C° and is also non-magnetic.

It is also assumed that the metal particles in the mix are charged both positive and negative. We believe that the mechanical bond on some of these particles is relatively weak. With proper stimulating force such as a high voltage positive charge applied to the bridgewire, any loose negatively charged particles in close proximity would be attracted to the bridgewire with sufficient force to make intimate contact and give up the excess electrons. Having done this, the metal particle would no longer be subject to repulsion if and when a reverse polarity pulse was applied to the bridgewire. With a change in polarity further migration of loose particles having a positive charge would take place. Titanium so deposited by electro-static precipitation has a unit conductivity nearly 2-1/2 times that of the Karma wire.

To partially restore the resistance of the bridgewire, it was found that a one ampere no-fire current applied to the bridgewire for five minutes increased the resistance by 17% when the previous decrease due to static pulsing had been 24%. Recovery to better than 89% of the original resistance was not accomplished.

Partial release of the titanium from intimate contact with the Karma wire is attributed to the 60% thermal expansion mismatch. Without resorting to a Bruceton statistical analysis, it can only be surmised that the reduced resistance of the bridgewire would not impair the operation of the device. However, devices which must contractually hold a fixed bridgewire resistance would be in serious difficulty if the required static discharge testing produced migration of metal particles in the ignition mix.

#### CONCLUSIONS

The tiny neon lamp AC1, chosen for ready availability, small size and low cost has met all of our special service requirements. While rated for only a

few milliamperes continuous operation, it has handled our high amperage pulsing without a single failure. The breakdown level is lower than the best of the crude spark gaps many devices are now depending on.

Previously qualified EED's known to be incapable of meeting the present static discharge requirements can now do so with the help of this preferential path circuitry. The neon/resistor combination can be incorporated in the EED proper or inserted as a plug-in unit between mating connectors. Figure 4 is a photograph of plug-in units for two and four pin connectors. Figure 5 is a photograph of a cutaway section of an explosive actuated gas energy release (EAGER-PAK) incorporating a pressure regulator and EED protected by our preferential discharge circuitry.

One word of caution should be given. With the preferential path of neon lamp and resistor circuitry installed, a few minor changes in check-out testing might be required. No changes would be required in methods of bridgewire resistance or in no-fire current testing. There would be no change in the 500 VAC dielectric testing if available lamps with 800 volt D.C. breakdown were used. With the AC1 lamp, however, dielectric testing with over 50 volt A.C. and a suitable current limiting resistor would only show the breakdown level of the lamp. Lamps can fail under sustained conduction when overheating results. To this we can only ask the question: - - - "Why should a 500 VAC dielectric test be required when the device performs its safety function at the 25 KV pulse level?"

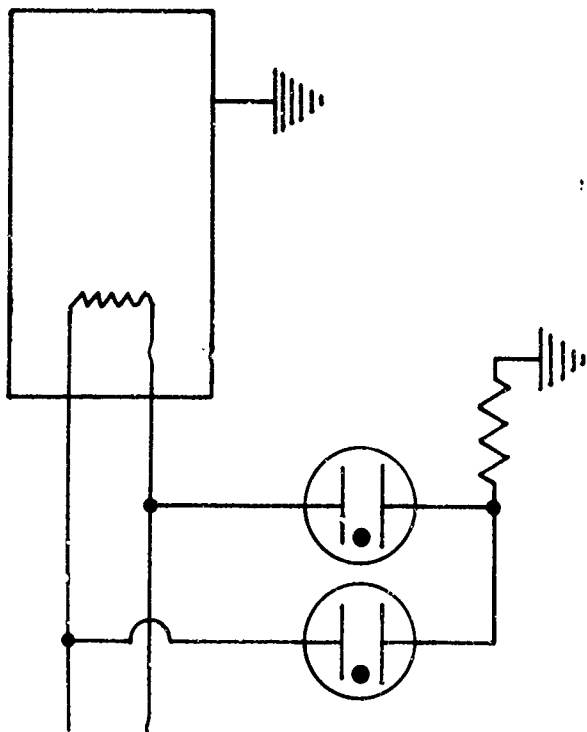


Fig. 1 Single Bridgewire EED with Static By-Pass

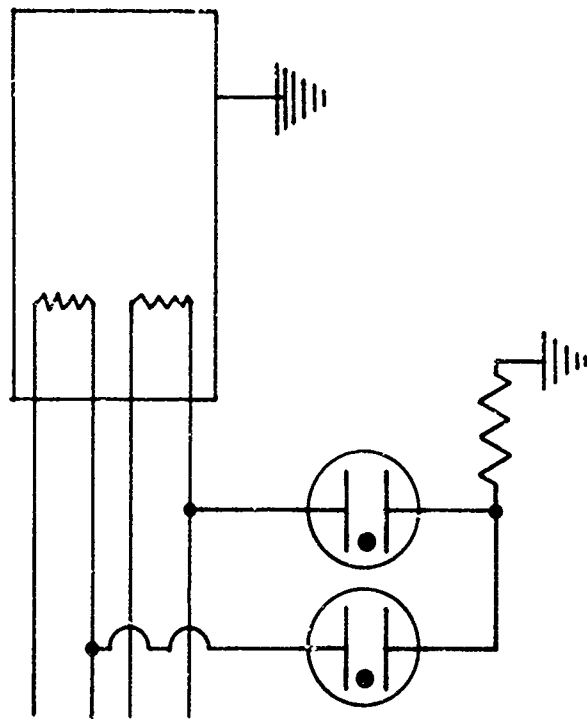
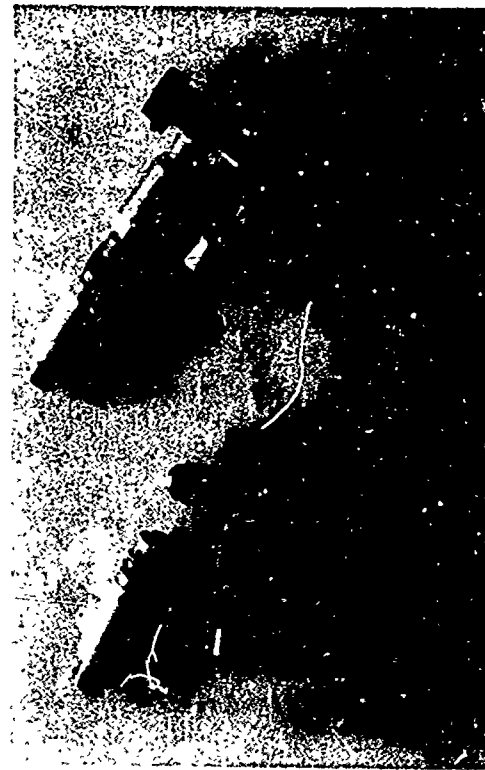
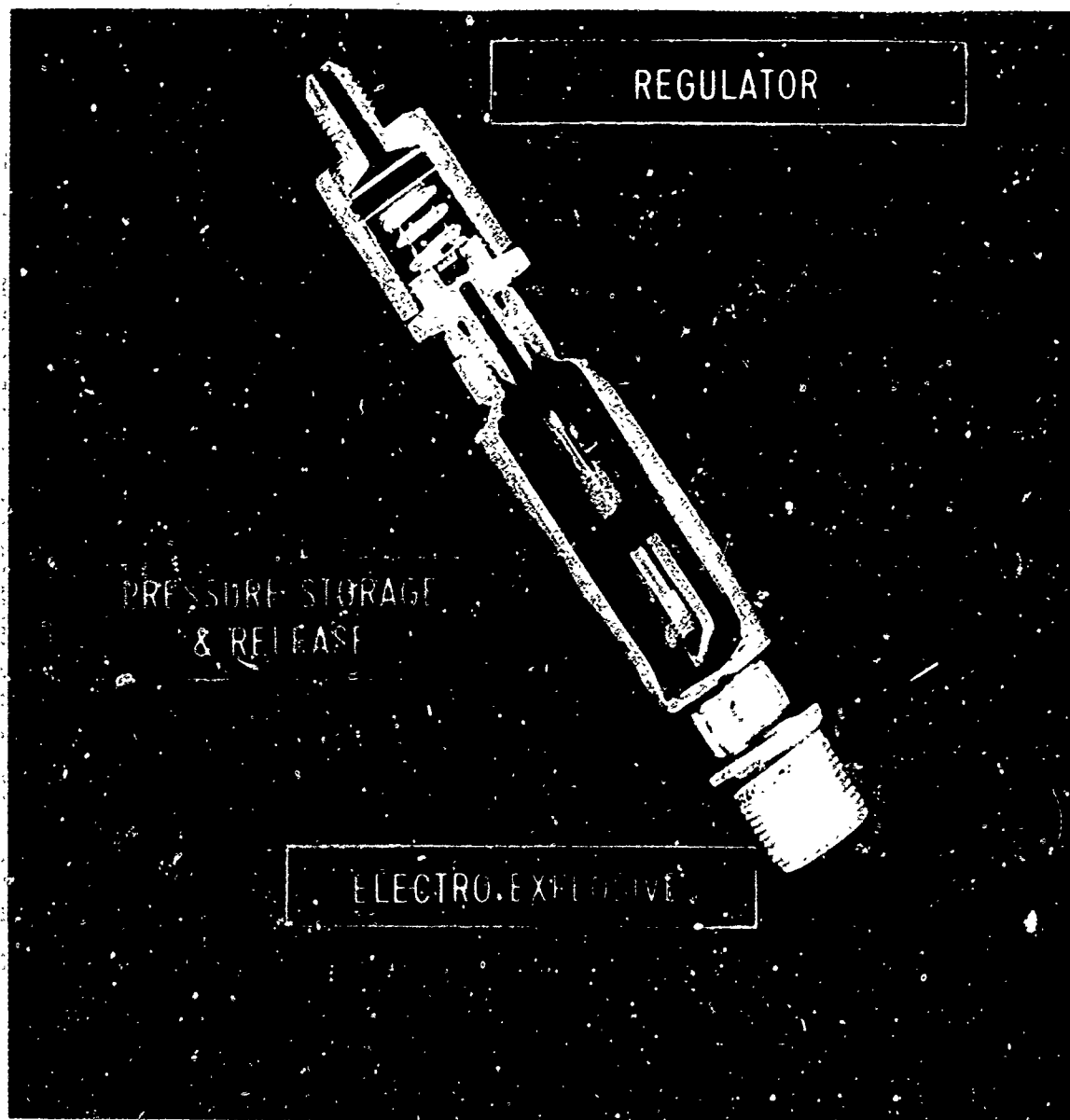


Fig. 2 Dual Bridgewire EED with Static By-Pass





**FIG.5 EAGER-PAK WITH BUILT IN  
STATIC PROTECTOR**

TABLE 1

STATIC DISCHARGE TEST SAMPLING OF LIVE PRIMERS

EED NO.	CAPACITANCE PICOFARADS	(A) WITH PROTECTIVE ACI NEON CIRCUIT		(B) WITHOUT PROTECTIVE CIRCUIT	
		KV*	- JOULES	KV*	- JOULES
1	500	25	0.156	5	0.00625
2	500	25	0.156	7	0.01225
3	500	25	0.156	5	0.00625
4	2000	15	0.225	7	0.049

"A" TESTS WITH PROTECTIVE PREFERENTIAL PATH CIRCUITRY IN PLACE  
PROCEEDED THE "B" TESTS WHERE PROTECTIVE CIRCUIT HAD BEEN REMOVED.

\* VOLTAGE PULSING STARTED AT 5KV LEVEL INCREASED IN 2KV STEPS.

"A" NO FIRINGS OCCURED WITH ACI NEONS.  
"B" ALL DEVICES FIRED AT 7KV OR BELOW.

TABLE 2

PERCENTAGE DECREASE IN BRIDGEWIRE RESISTANCE RESULTING  
FROM RANDOM STATIC DISCHARGE PULSING.

GROUP	PERCENTAGE DROP		UNITS	% OF TOTAL
	< 1			
A	1 TO 5	6 TO 10	1	7
B	11 TO 15	16 TO 20	3	20
C	21 TO 25	27	5	33
D			3	20
E			0	
F			2	13
G			1	7



## DISCUSSION

The problem of providing protection to EED's from electrostatic discharge is being approached by use of shunt elements that become conductive when a certain voltage is exceeded. Two ideas discussed were the use of a silicone carbide powder and small neon lights, in conjunction with carbon resistors. It is felt that the former type would, at present, occupy less volume, but specially made neon elements could conceivably be made more compact. Silicone carbide shunts can be tailor made to have breakdown voltages anywhere between about 200 and 1200 volts. The voltage breakdown of the neon lamps can also be varied. The overall idea of the shunts is to provide a conductive path to ground for high electrostatic voltages, but do not interfere with the normal signal used to initiate the EED.

### 3-7 DEMYTHOLOGIZING ELECTROSTATICS

By

L. D. Pitts

SINGER

Ordnance Products

#### INTRODUCTION

The lovely city of San Francisco was once popularly called "Baghdad-By-The-Bay". In those days, not so long ago, the citizens believed comfortably in many myths about their city's virtues and perfections. In the past decade, San Franciscans have had to shed their myths, often painfully, in order to face the very real problems of intolerance, water and air pollution, drug addiction, alcoholism, rising crime rate, traffic jams, and high taxes.

The ordnance industry, including manufacturers and users, is the victim of many myths about electrostatic discharges. These myths, ranging from the tragic to the ludicrous, are especially important today. EED's are much more commonly used than formerly; they are used in many potent weapons systems, including the most potent, and even astronauts' lives depend on them. In fact, aerospace specifications have been helpful in bringing many electrostatic myths to light.

My purpose in this paper is to attack the myths specifically and one at a time. I hope your favorite myth is included.

My comments are based on several years of experience in testing and designing EED's and on the analysis of data and comments in the references. In two previous papers (References 1 and 2) I have explored electrostatic design in a more orderly and generalized fashion than in this present paper. (4

I will discuss philosophical, design, hardware, and static sensitivity myths.

#### PHILOSOPHICAL MYTHS

Electrostatic design is so troublesome and confusing to many engineers that they surround themselves with vague dreams of perfect systems so that they can comfortably ignore electrostatics -- until reality confronts them with a failed acceptance test or a serious accident.

Myth 1 - Electrostatic design is unimportant because of new "safe" initiation systems.

Anti-myth - Laser, fluoric and other exotic initiation modes are under study and may be widely applied in specialized applications 10 years from now. But the EBW experience has shown the difficulty of competing with the hot wire EED, which has the virtues of low cost, light devices and power sources, easily available power supplies, proven reliability, rapid actuation, ease of installation, and immense application flexibility. There is considerable knowledge and experience in its design and production. As long as hot wire EED's are used, electrostatic design will be important, for many present designs are hazardous and electrostatic discharge has caused many unnecessary tragedies.

Myth 2 - Electrostatically insensitive primary materials make electrostatic design unnecessary.

Anti-myth - There is no way to prove that any material is absolutely insensitive in all possible discharge modes. The highly regarded secondaries, like PETN and RDX, have proved very sensitive in certain conditions. Some pyrotechnics are insensitive to contact discharges but fairly sensitive to discharges across an air gap.

Even if you have a primary material which is perfectly safe to discharges (also stable and fast acting, and with proper output), ignoring electrostatic discharges can permit bridge resistance changes, mix degradation, insulation resistance failure, or even EED firing if electrostatically sensitive materials are used as intermediate or output charges.

Myth 3 - Electrostatic discharge may be ignored for EBW's.

Anti-myth - Ignore electrostatic design and your EBW will fire from electrostatic discharge or lightning perhaps (Reference 3) or at least suffer bridgewire degradation or serious sensitivity variations.

A curious phenomenon we have observed on welded EBW bridges on unloaded headers when tested with EBW pulses is an energy robbing arc, visible from pin-to-pin, triggered (as in a triggered spark gap) by small arcs between the bridgewire and the inside edges of the pins.

Myth 4 - Electrostatic design is not pertinent to RF sensitivity.

Anti-myth - It is the most important factor after bridge system design. Mohrback and Wood of Franklin Institute (Reference 4), site of much RF sensitivity testing, have stated that there is often correlation between high discharge sensitivity and high RF sensitivity.

This sensitivity is most pronounced at the highest test frequencies, 1 to 10 GHz, where the breakdown voltage of air is very low, making arcing possible for a few hundred volts applied.

EED's, which should be less sensitive to RF than DC, can be designed for RF insensitivity by providing a protective path for as low a breakdown voltage as specifications allow, at least a 4:1 ratio of primer path to protective path (Figure 1) breakdown voltage, and as electrostatically insensitive a primer as other constraints permit. The 4:1 ratio usually implies a primary material with good insulation properties, particularly high dielectric strength. Production techniques should be employed which eliminate sharp points such as loose wire ends in the bridge system and remove metal particles from the cup surface (particles present after pin grinding).

Myth 5 - EED's cannot stand repeated discharges.

Anti-myth - If it is changed in any way by repeated discharges, it is an inferior EED. If the customer can guarantee a device will not see repeated discharges in its handling and application, he can guarantee it will not see even one. A person who swallows this myth would buy a car whose brakes were guaranteed to work well just once.

Myth 6 - A device safe to a 25 KV discharge from 500 pf (the standard discharge) is perfectly safe.

Anti-myth - These values are supposedly the human body maxima (Reference 5), though Tucker (Reference 6) suggests the voltage may be as high as 40 KV. However, other electrostatic sources such as plastic bags, missiles, large equipment, and lightning induction may store higher voltages or represent larger capacitances. Burger and Rost (Reference 3) have detailed the firing by lightning induction of an EED (containing  $\text{Al-KClO}_4$ , which is supposedly an insensitive mix, and pistol powder) which was specified as being safe when tested with a 25KV discharge from 600 pf.

For the pin-to-pin mode a broken bridgewire can compromise an otherwise adequate design.

Myth 7 - No one has ever proposed a standard electrostatic discharge development program.

Anti-myth - I have. Reference 2 also includes a more detailed electrostatic discharge specification than any I have seen.

Myth 8 - The electrostatic test circuit should have 5,000 ohms in series with the EED.

Anti-myth - If the test is intended to simulate non-human sources such as plastic bags and missiles, no resistance should be employed since such sources may have essentially zero resistance.

Even for simulation of human sources the 5,000 ohms determined by Franklin Institute (Reference 5) may be quite high since Tucker's data for humans (Reference 6) yields equivalent series resistances as low as 600 ohms.

Myth 9 - Lead styphnate EED's are inherently unsafe.

Anti-myth - Many are quite safe. A 25¢ lead styphnate-primed electric blasting cap is considerably less sensitive to electrostatic discharge than a \$10 power transistor, such as might be employed in a missile guidance system.

Of course, there are poorly designed \$10 EED's (using lead styphnate or a pyrotechnic) which are inferior to 25¢ transistors in discharge performance.

Generally what should be regarded as unsafe is any design which does not have insulation in series with the sensitive primary material or whose protective device has a breakdown voltage greater than 3KV.

## DESIGN MYTHS

Engineers I have known, including some very bright ones, calmly accept a variety of myths about electrostatic design, some sophisticated and some simply ridiculous.

EED users with no experience in EED design and manufacture are particularly liable to accept any plausible rumor about electrostatic design.

Myth 10 - Dielectric strength, expressed in volts/mil, is independent of dielectric thickness.

Anti-myth - Dielectric strength is the measure of critical electric field for breakdown at some particular distance. For distances typical of EED's the best simple approximation for breakdown voltage is:

$$V_B = N \sqrt{d}$$

where

$$V_B = \text{Breakdown voltage}$$

$$N = \text{Constant for material}$$

$$d = \text{Material thickness}$$

Thus the breakdown voltage is only three times as great at 9 mils as at 1 mil. Breakdown voltage increases but dielectric strength decreases with increasing distance.

CAUTION: Be very careful using single value dielectric strengths from vendor data sheets. Dielectric strength may have been tested for a thickness anywhere from 1 mil to 1 inch.

Myth 11 - Dielectric constant is related to dielectric strength.

Anti-myth - Dielectric constant enables calculation of the capacitance of a material in a particular geometry and has

no particular relationship to dielectric strength, the highest electric field intensity a material can withstand without arcing over.

Myth 12 - Breakdown voltage of two series dielectrics is always the sum of their separate breakdown voltages.

Anti-myth - If a gaseous dielectric develops corona (partial discharge), almost the entire source voltage will appear across a solid dielectric in series. Figure 2 illustrates this behavior in the Corona Region, where the breakdown voltage of air is a small fraction of that for mylar. Here system breakdown voltage is just the breakdown voltage of the mylar.

Beyond this region is the Partial Corona Region where corona also occurs, but not until the applied voltage significantly exceeds the breakdown voltage of air.

The divergence of the data from the curve predicted by summing the breakdown voltages of air and mylar is plainly evident in Figure 2.

Incidentally, our tests show that in common configurations electrostatic discharge corona will not initiate normal lead styphnate and other primaries. Corona energy is quite small and distributed throughout the primer volume.

Myth 13 - Electrical breakdown instantaneously follows application of overvoltage.

Anti-myth - If it did, protective gaps might not require a 4:1 breakdown voltage ratio.

Data for an air gap (Reference 7) show time to breakdown decreasing from 100 nanoseconds near the threshold electric field to .5 nanoseconds at four times the threshold field. Presumably, solid insulation has a different response time.



Myth 14 - Voltage division on series insulation paths inside an EED is determined by material resistances during discharge testing.

Anti-myth - All EED's break down someplace. Thus, the explosives and insulating materials are exposed to discharges for only a few microseconds, a period when the EED capacitances determine the voltage division.

Myth 15 - A protective gap (sometimes called "spark ring") is a dramatic new concept.

Anti-myth - Remember Ben Franklin's lightning rod.

Almost all EED's have such a mechanism, though it may not have been intentionally designed and may not work well.

There are many ingenious schemes for providing a protective breakdown path such as use of variable pin spacing, metal powders with low breakdown voltage and plated plastic films. A convenient protection device is a zener diode. Certain common zeners, when built into firing cables, can protect detonators which are very sensitive to discharges. Yet the zeners will not affect the normal firing pulse.

Myth 16 - A protective gap will work reliably if the breakdown voltage of the protective gap is less than that of the protected gap (primary explosive path, for instance.)

Anti-myth - Figure 3 refutes this for ratios (breakdown voltage of protected gap to protective gap) less than 3:1. A safe ratio should be 4:1 for air. It might differ somewhat for solid insulation.

For lesser ratios at slight overvoltages statistical considerations will permit some breakdowns of the protected gap prior to breakdown of the protective gap. At large overvoltages breakdown times are so short that the protective gap cannot serve its intended function and both gaps break down.

Significantly, Figure 3 predicts that a device with a 2.2:1 ratio would be safer for a 15 KV discharge than for a 9 KV discharge.

Inadequate protection ratios are the principal cause of erratic response (some fire, some don't) of certain EED designs to electrostatic discharge.

Myth 17 - Adequate protection ratio is obtained by protective path design only.

Anti-myth - The protected path is equally important in obtaining a 4:1 breakdown ratio. Concentrate on designing thick insulation of high dielectric strength (polyester films and ceramics, for instance) in series with the primer mix. For primary explosives, use of fine particles pressed at high pressures may be helpful in obtaining higher dielectric strength.

Myth 18 - Electrostatic discharge energy for ignition of a given EED type (pin-to-case) is about the same as its hot wire ignition energy.

Anti-myth - While the absolute minimum energy required to initiate the primary material in laboratory conditions might be of the same order of magnitude for hot wire and discharge stimuli, both initiation systems are extremely inefficient for EED's.

The hot wire system losses are primarily thermal conduction losses to the header or pins. Discharge losses are usually a function of the voltage required to overcome the dielectric strength of the primary material and other series insulation. A protective path can absorb most of the discharge energy.

Since the energy losses are independent, hot wire and electrostatic discharge initiation energies for a given EED type can easily differ by several orders of magnitude.

Myth 19 - A poor design will survive discharge tests if 5000 ohms is in series with the EED.

Anti-myth - Though the 5000 ohms may absorb most of the discharge energy, it does not prevent the full test voltage from appearing across the primer for some brief period before the system breaks down. If the primer should break down, due to poor design, there may still be enough energy available to ignite the primary material.

Our experiments show that both normal lead styphnate and  $Zr/MoO_3$  (both 3 mils thick) can be initiated from a 500 pf capacitor charged to 4 KV with 5000 ohms in series. Since specified test voltages for EED's are commonly 9 or 25 KV, these materials could be initiated in certain device configurations.

The 5000 ohms could be helpful with somewhat insensitive primers or in the pin-to-pin mode, though there is still the possibility of trouble due to pin-to-case-to-pin arcs.

#### HARDWARE MYTHS

There is a category of myths which are not evident until one gets to the test or hardware stage. These myths, often unstated assumptions, can be quite costly.

There is no substitute for intelligent experience.  
Aristotle would never have conceived the myth that men have more teeth than women if he had but looked in Mrs. Aristotle's mouth.

Myth 20 - If some EED's pass discharge testing and some fail, production personnel are to blame.

Anti-myth - Erratic response is usually caused by inadequate breakdown ratio (less than 4:1) provided by the design engineer. Prove it yourself by taking the units which survived and retesting them several times. Some will fire in the subsequent tests.

Production problems generally cause 100% failures, due for instance to use of cleaning solvents which leave conductive residues.

Myth 21 - It is sufficient to test a few prototypes at the specified voltage.

Anti-myth - The designer (or second-source engineer) should know from actual test data the failure voltage of an unprotected device, the protection breakdown voltage ratio, and assembly precautions. (See development program in Reference 2). Tests at the specification voltage are uninformative and often misleading.

Myth 22 - Nothing can happen to the bridgewire in discharge testing.

Anti-myth - Discharge testing (without series resistance) often causes bridgewire resistance change, particularly a decrease due to pseudo-welding near the inside edge of a pin. Resistance changes can also occur at the welds due to rewelding and electromechanical stress (which can actually make an unconfined bridgewire jump several mils). In certain cases at high voltages the resistance may increase due to spark erosion of the bridgewire.

Myth 23 - A needle electrode always has a lower breakdown voltage than a ball electrode for a constant gap distance.

Anti-myth - Most common metals develop thin oxides of relatively high dielectric strength on their surfaces in the presence of air. These oxides on a needle can triple the breakdown voltage required for a particular air gap. Round and flat electrodes have enough surface area that the oxide film has little effect. Thus, a ball electrode, which has a higher breakdown voltage than an unoxidized needle, may break down at half the voltage required for an oxidized needle.

Needles can be used reliably if cleaned with an abrasive before each test or if made of non-oxidizing materials such as platinum. Considerable static sensitivity testing is invalid due to the use of oxidized needles.

Myth 24 - Cleaning with a mild chemical reagent is sufficient for a ground header.

Anti-myth - Grinding imbeds small metal particles in the header surface, shortening the insulation path (particularly for RF) and lowering the breakdown voltage across the header.

We raised the breakdown voltage (for both 500 pf discharge and 60 Hz sources) for 10 "clean" ceramic headers more than 50% in each case by spraying them briefly with abrasive powder from an S. S. White Airbrasive tool.

Myth 25 - Insulation resistance is always a non-destructive test.

Anti-myth - I have seen quite a few poorly built *and* poorly designed EED's blow up in this test.

Myth 26 - Plastic bags are ideal packaging for EED's.

Anti-myth - Plastic bags can be killers. They easily build up and maintain sufficient electrostatic charge to be hazardous to completed or in-process EED's. Plastic safety shields and face masks can also be dangerous unless sprayed with an anti-static coating or plated with a thin metal film.

Myth 27 - Resistivities of lead styphnate and lead azide are unimportant to their handling qualities.

Anti-myth - The high resistivity ( $10^{13}$  ohm-cm) of lead styphnate can permit it to build up large charges on itself and cause autoinitiation. In some plants small quantities of graphite are added to lower resistance and minimize the self-charging, though the additional graphite significantly increases the lead styphnate sensitivity.

Lead azide has a much lower resistivity ( $10^{10}$  ohm-cm) which may in extreme cases cause autoinitiation by simple ohmic heating (no arcing). This condition is indicated in the interesting but alarmist work of Hanna and Polson (Reference 8). Calculations indicate it would be difficult to raise an entire .003 mm azide particle to ignition temperature with  $4 \times 10^{-3}$  ergs, but the energy may have been localized near the probes used to provide electrical contact.

#### ELECTROSTATIC SENSITIVITY MYTHS

Sad to say, present electrostatic sensitivity testing itself has the quality of myth. It does not measure what it is supposed to measure and it offers very little practical insight into explosive behavior.

Show me an engineer who really believes in electrostatic sensitivity testing and I will show you a man who believes in fairies and trolls - and who is rather weak in chemistry, physics, and electricity.

Myth 28 - Electrostatic sensitivity testing produces consistent data.

Anti-myth - Observe the "random numbers" for sensitivity compiled from various sources in Table I.

Myth 29 - Electrostatic sensitivity test parameters can be chosen arbitrarily.

Anti-myth - The wide range of data in Table I is due to this misconception.

Of the many parameters which can be significant in sensitivity testing capacitance, voltage, sample thickness, and consolidation pressure, can be singled out as especially important.

In many tests the voltage is held constant and the capacitance varied or vice versa. It is necessary to vary both, as in Figures 4 and 5 to obtain a practical insight into the material's behavior and to find a true minimum for the particular test configuration.

Sample thickness determines the voltage required to break down the explosive in a given test configuration, and thus has a strong effect on the minimum capacitor energy.

If the powder is not compressed it will be blown around in a dust by an arc. The result is an erratic test of a dust.

A partial list of the parameters which should be carefully examined and reported in a thorough electrostatic sensitivity test is presented below:

- |                                     |                             |
|-------------------------------------|-----------------------------|
| 1. capacitance                      | 12. contact or air gap      |
| 2. test voltage                     | 13. electrode configuration |
| 3. humidity                         | 14. consolidation pressure  |
| 4. sample thickness                 | 15. quality of contact      |
| 5. particle size                    | 16. spark location          |
| 6. oxidized needle electrode        | 17. temperature             |
| 7. confinement                      | 18. sample area             |
| 8. statistical effects              | 19. impurities              |
| 9. data presentation                | 20. stray capacitance       |
| 10. manufacturing process of powder | 21. circuit impedance       |
| 11. pulse rise time                 |                             |

Myth 30 - Primary explosives and pyrotechnics respond to electrostatic sensitivity testing in much the same way, even though minimum energies may be quite different.

Anti-myth - One would be surprised if the response were similar since primary explosives commonly have much smaller critical volumes than pyrotechnics and the initiation process very probably consists of the heating of the critical volume by the hot air in the discharge arc.

We performed a test to verify the different responses of lead styphnate and a  $\text{Zr/MoO}_3$  mix, a typical primary and a metal-metal oxide pyrotechnic.

In these tests the powders were compressed to 16,000 psi to prevent electrostatic repulsion effects. Steel phono needles (cleaned after each test) were used as top electrodes. The bottom electrode was flat except for a step to hold the plastic charge cup. Material breakdown was monitored with



an oscilloscope. The needle was moved to a different point on the  $\text{Zr/MoO}_3$  after each voltage application which produced breakdown. The top electrode was in contact with the explosive for these tests.

From the voltage vs capacitance graph of Figure 4 and the energy vs capacitance graph of Figure 5, a convenient method of presenting sensitivity data, two differences are clear.

First, the lead styphnate never breaks down without firing while the  $\text{Zr/MoO}_3$  breaks down at voltages far below the firing voltage for small capacitances.

Second, firing energy is a strong function of capacitance for lead styphnate but the  $\text{Zr/MoO}_3$  firing energy is independent of capacitance in this capacity range. Thus we cannot indicate which material is "more sensitive" unless the capacitance is specified.

One can conclude from this data that  $\text{Zr/MoO}_3$  (and probably many other pyrotechnics) can break down without the critical volume reaching initiation temperature and that many electrostatic sensitivity data for lead styphnate (and probably other primaries) are confused by the relatively large amount of energy the test capacitor must store in order to achieve the voltage necessary to break down the lead styphnate and release the small amount of energy (likely a few ergs) necessary for initiation.

Myth 31 - Electrostatic sensitivity testing yields reliable data pertinent to the handling and processing of explosives.

Anti-myth - How can even detailed sensitivity testing cover all the different handling situations an explosive

may be exposed to so that one can say what the likelihood of ignition is in any situation?

Below is a partial list of the different handling conditions an explosive may be exposed to:

- |  |                        |
|--|------------------------|
| 1. different shape implements (electrodes) | 8. density             |
| 2. moving air (air conditioning)           | 9. motion              |
| 3. light                                   | 10. pressure           |
| 4. fixed and moving "electrodes"           | 11. source resistance  |
| 5. stray electric fields                   | 12. source inductance  |
| 6. humidity                                | 13. source capacitance |
| 7. temperature                             | 14. source voltage     |

If you want to know how sensitive an explosive is in a given situation you just have to simulate that situation and vary the important parameters during your tests. Hanna and Polson did this somewhat with the Jones loader (Reference 8). Otherwise you are just making a guess and you might as well admit it. In one case explosive A may be 10 times as sensitive as explosive B. In another case the opposite may be true.

Myth 32 - Pyrotechnics are less sensitive than primary explosives.

Anti-myth - Some are; some are not. Pyrotechnics with fine zirconium and magnesium powders are particularly sensitive. For a 500 pf source  $\text{Zr/MoO}_3$  is appreciably more sensitive than normal lead styphnate (Figure 5).

Unfortunately the factors which make a pyrotechnic sufficiently heat sensitive for use on the bridgewire and the factors producing electrostatic sensitivity are not usually independent of each other.

## CONCLUSION

In light of the refutation of electrostatic myths, there are a few positive ideas to keep in mind.

- 1) Electrostatic design is very important to the ordnance industry and always will be.
- 2) An electrostatically safe EED can be designed using practically any primary material if adequate internal insulation and protection breakdown voltage ratio are provided.
- 3) EED hardware should be thoroughly and intelligently tested so that all anomalies present are observed and understood.
- 4) Electrostatic sensitivity testing is very interesting but not to be trusted.

If the winds of reason and experience will blow and dispell the mythy smog surrounding electrostatics, more EED's will be manufactured which reflect the increasing maturity of our industry.

TABLE I

### COMPARISON OF ELECTROSTATIC SENSITIVITY DATA

Initiation Energy (ergs)	<u>Lead Styphnate</u>	Information Source
1,100 - 9,000		Bureau of Mines (1944)
9,000		Bureau of Mines (1953)
4,000		Reynolds Lab, Atlas Chemical
20		ACD Lab, Atlas Chemical
3.8 - 112		Franklin Institute
	<u>Lead Azide</u>	
56,000 - 70,000		Bureau of Mines (1944)
70,000 (dextrinated)		Bureau of Mines (1953)
62,000 (dextrinated)		Reynolds Lab, Atlas Chemical
62,000 (PVA)		Reynolds Lab, Atlas Chemical
100 (dextrinated)		ACD Lab, Atlas Chemical
2 (PVA)		ACD Lab, Atlas Chemical
2 (RD 1333)		ACD Lab, Atlas Chemical
400 - 18,000		Franklin Institute
70,000 - 180,000 (dextrinated)		Franklin Institute
.004		Mason and Hanger

# BIBLIOGRAPHY

- Pitts, L. D., "Designing Electro-Explosive Devices for Electro-static Insensitivity," Franklin Institute, Proceedings of the Fifth Symposium on Electro-Explosive Devices, (June 13-14, 1967).
- Pitts, L. D., D. E. Davenport, and H. D. Peckham, "Designing Electro-Explosive Devices for Space," International Symposium on the Use of Pyrotechnic and Explosive Elements in Space Systems, Tarbes, France, (July 9-12, 1968).
- Burger, Joseph P., and D. L. Rost, "Preliminary Report of the Initiation of Various Types of Electro-Explosive Devices by Induced Lightning," Ninth Explosives Safety Seminar, Minutes, (August 15, 1967).
- Mohrback, P. F. and R. F. Wood, "Effects of Radio Frequency Stimuli on Electro-Explosive Devices," Franklin Institute, Proceedings of the Fifth Symposium on Electro-Explosive Devices, (June 13-14, 1967).
- Amicone, R. G., C. T. Davey, and J. B. Campbell, "Electrostatic Hazard to Electro-Explosive Devices from Personnel-Borne Charges," Franklin Institute, Monograph 65-1, (February 1965).
- Tucker, T. J., "Spark Initiation Requirements of a Secondary Explosive," New York Academy of Sciences, Prevention of and Protection Against Accidental Explosion of Munitions, Fuels, and Other Hazardous Mixtures, (1968).
- Molnar, J. P., "Conduction Phenomena in Gases", Electrical Engineering, (December 1950).
- Hanna, H. A., and J. R. Polson, "Investigation of Static Electrical Phenomena in Lead Azide Handling," Mason and Hanger-Silas Mason Co., Inc., Burlington, Iowa, Technical Report 98-A, (1967)

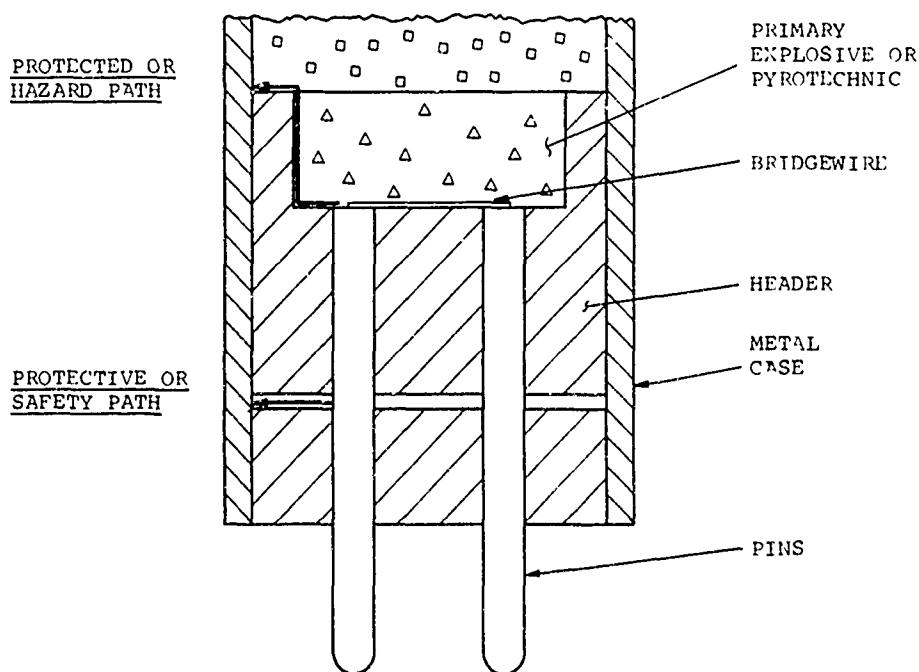


FIGURE 1 - TYPICAL EED HAZARD AND SAFETY PATHS

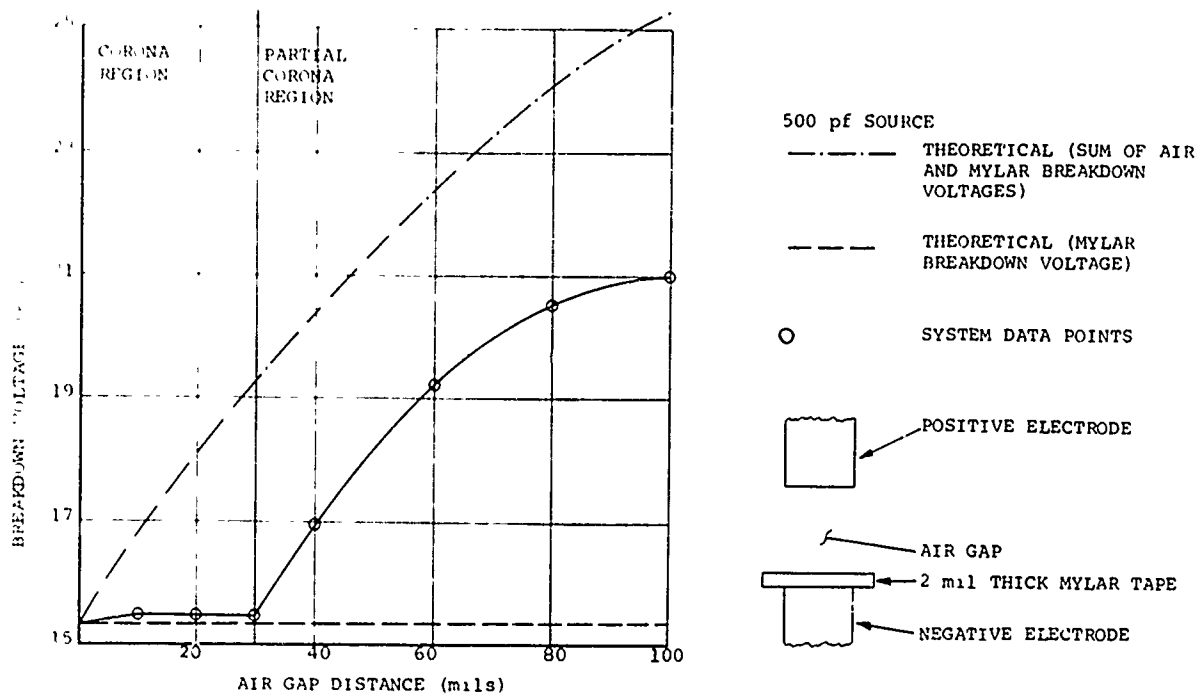


FIGURE 2 - BREAKDOWN CHARACTERISTICS OF AIR AND MYLAR IN SERIES

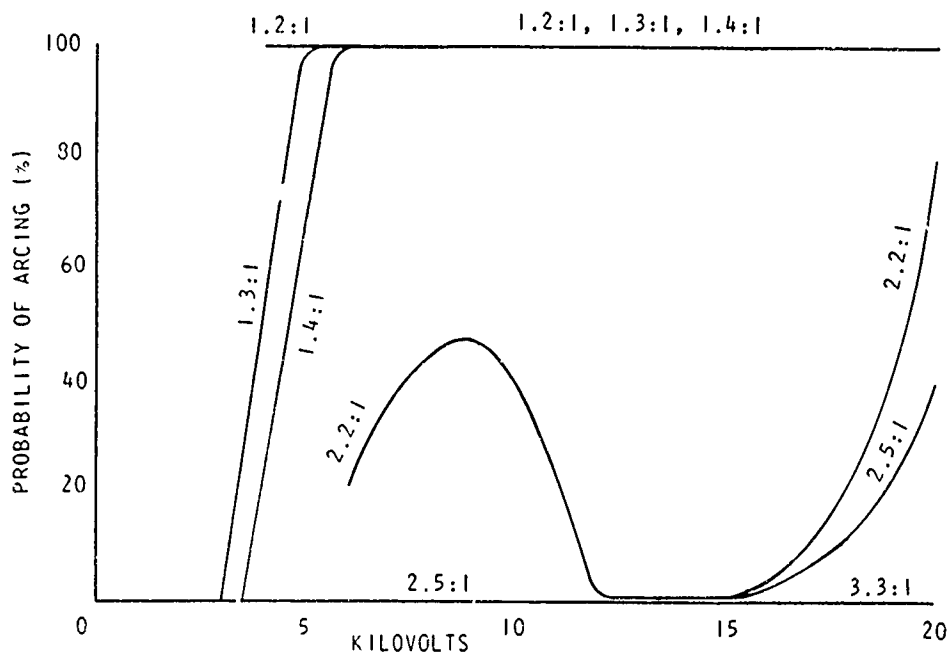


FIG. 3

PROBABILITY OF ARCING IN PROTECTED AIR GAP  
VS. TEST VOLTAGE FOR RATIOS OF  $\frac{V_B \text{ (AIR GAP)}}{V_B \text{ (SPARK GAP)}}$   
(FLAT ELECTRODE AIR GAP)  
(BENDIX SPARK GAP PROTECTION)

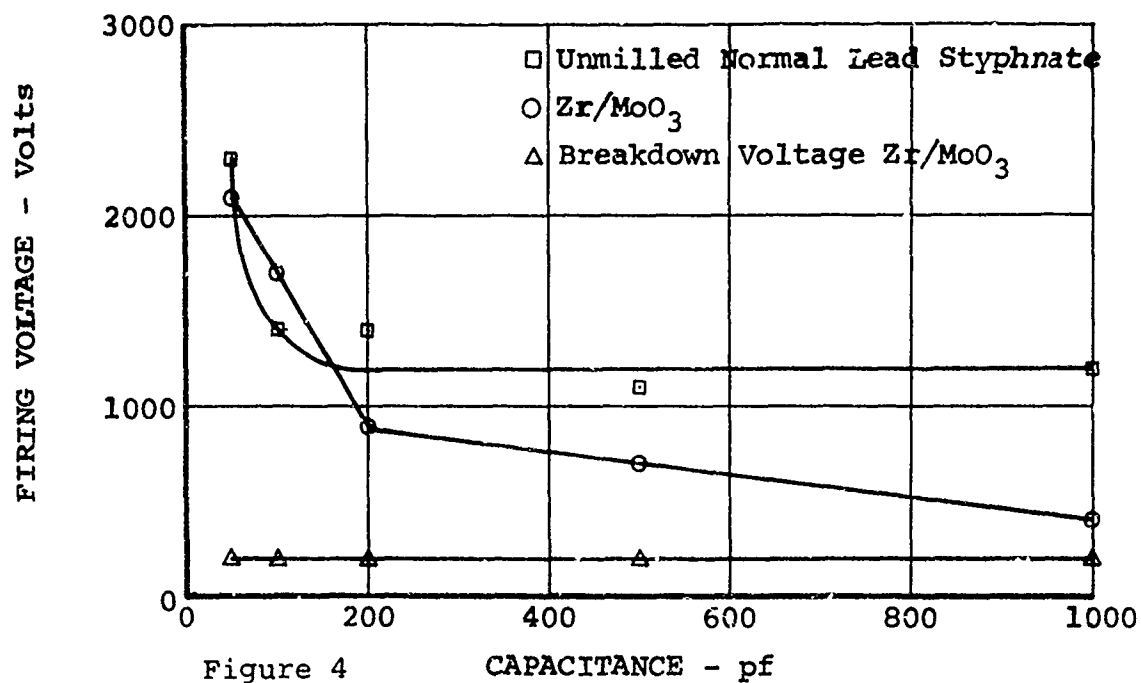


Figure 4

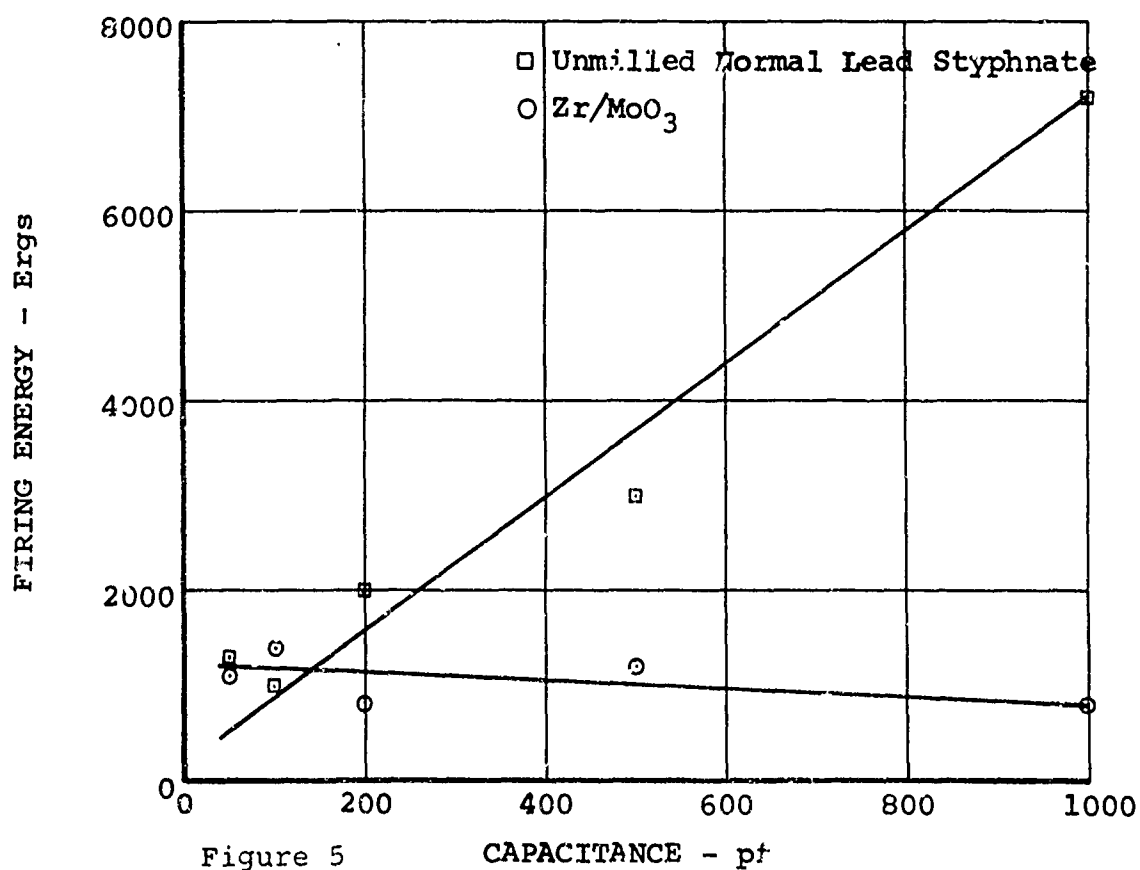


Figure 5

### ELECTROSTATIC SENSITIVITY TEST

### 3-8 INITIATION OF ELECTROEXPLOSIVE DEVICES BY LIGHTNING\*

By H. S. North, Safety Engineering  
Sandia Corporation, Albuquerque, N. M.

#### Introduction

The users of electroexplosive devices have been concerned about the effects of atmospheric potential gradient for many years, but the use of EED's was limited, and most facilities had lightning protection on buildings for assembly and testing. As the use of EED's has increased in numbers and applications, much of the assembly and testing is done in field locations where work is stopped when hazardous potential gradients exist. The approach of storm clouds with lightning is definitely a good time to shut down, but how about wind and dust-generated potential gradients? Most of our work is in the deserts of New Mexico and Nevada, where it is very dry and a moderate wind can generate 5000 v/m; if we do get any rain, it comes with much thunder and lightning. In fact, the mountains west of Socorro, New Mexico, are considered by atmospheric physicists as an excellent location to study lightning and, for this reason, is the site of the Langmuir Laboratory Atmospheric Research Facilities operated by the New Mexico Institute of Mining Technology (NMIMT).

Sandia Laboratories, operated for the Atomic Energy Commission by Sandia Corporation, is involved in extensive field testing of both conventional and nuclear explosives. This requires installation and handling of EED's under field conditions where the potential gradient is a major consideration. We use grounding straps and antistatic clothing to minimize the hazards, and have continuous recording potential gradient meters to warn of high potentials. This equipment is set to sound an

---

\*This work was done under the auspices of the U. S. Atomic Energy Commission.

alarm when a preselected potential is reached. We now use 2000 v/m as the value for stopping work in open areas, and the approach of electrical storms stops work in all areas, including lightning-protected facilities.

The 2000 v/m is for our test sites and may or may not be applicable at other locations. We used data from six to seven years of experience of recording potential gradients to arrive at this value. This data indicated that a value of 2000 v/m may be approached many times and then fall off; but if this value is exceeded, it will generally then go to much higher readings in a short time (15 to 30 minutes). The meter we use covers the range of -10,000 to +10,000 v/m, and these values are exceeded during storm conditions.

Other approaches to reducing the hazards of atmospheric electricity have been to make the EED less sensitive and to design firing circuits to shield against static electricity. There is no problem determining the firing energies required for the EED's; the problem is what energy can be expected from atmospheric potentials in the form of static charges and induced currents. The NMIMT had studies underway to measure the fine structure of lightning, and we discussed the problem with Dr. Marx Brook who was directing these studies at Langmuir Laboratories. He was interested in the problem and agreed to our fielding an experiment in conjunction with his study if Sandia Laboratory provided funds and instrumentation for the additional work.

#### Test Setup

We decided to use the go, no-go method of instrumentation. This consisted of placing fourteen different EED's, with lead wires 50 to 200 feet long, in an open meadow near the measuring instruments used for Dr. Brook's study. The devices and the lead wires were typical of field-test setups. The EED's ranged from sensitive lead azide and lead styphnate detonators through explosive bolts, blasting caps, squibs, pressure cartridges, and rocket initiators to exploding bridgewire detonators. Each EED was attached to a film switch to indicate firing



time, then placed in a box with a 1/2-inch plywood separator to prevent one device from initiating the next. The leads were placed on the ground radiating from the box. These leads or antennae, as you choose to look at them, were attached to one side of the EED bridgewire and the other side was attached to a common ground rod. As the EED's were fired by the lightning, they were replaced by a like device. All the types of EED's were fired during the 1-month exposure, and some types were fired several times.

#### Instrumentation

The instrumentation used to measure the lightning parameters consisted of:

1. Field measurement: NMIMT field mill
2. Field change:
  - a. Slow Antenna -- This is a high-input impedance instrument with a time constant of approximately 10 seconds. The long-time constant allows one to follow the field variations faithfully over the period of a flash, but the output returns to zero level between flashes. The output of this antenna system was recorded on an Ampex FR-1300 tape machine, along with thunder records from a capacitor microphone and the IRIG-B time code.
  - b. Fast Antenna -- This instrument has a very short-time constant and emphasizes the most rapidly changing events in the flash. The output of this antenna was recorded on an FR-1400 with a direct record response of 1.5 megahertz (MHz).

The film switch activation and the IRIG-B time code were recorded on a CEC recorder, and in this way the lightning stroke causing the EED's to fire could be identified.

The data from the field measurements was read from the records and reported by Dr. Brook (Ref 2). The type of device and time of firing was reported by Mr. Burger (Ref 1). The data is not complete for all

the strokes that caused EED's to initiate because of power loss or other damage from direct strikes on transmission lines and allied equipment. However, the results of these tests do give some indication of electrical fields that will initiate EED's.

### Conclusions

The electrical fields associated with firing EED's and some fields where no devices were fired are shown in the table. The electrical field was measured by the slow antenna to provide readings of the maximum potential. The distance to the stroke was determined by measuring the time from flash to thunder; also Dr. Brook (Ref 2) calculated the distance from electrical field changes. The data shown represents our initial attempt to find some correlation between potential gradients and hazards to field operations involving explosives; it is very meager and for only one location but does indicate orders of magnitude. Strokes of 17, 30, or even 56 kv per meter did not fire EED's, while 100 kv and up did fire them; and distances less than 3 kilometers provide such values.

Our objective was to determine safe limits of potential gradients for use during field operations. I believe our limit of 2000 v/m gives us an adequate factor of safety for this test setup. I want to point out here that this data did cover the full range of sensitivities of explosives, but only one type of antenna system was tested. There are many more systems as well as locations that could affect the limiting values. As an example, recently we had a case where a firing circuit was activated when static electricity provided the firing signal for a silicon-controlled rectifier used as a switch, thus detonating the explosive charge.

### Future

There is much work left to be done. In fact, we have created more questions than answers. I believe for future studies we would want to measure currents and potentials at the bridgewire, study potential gradient prior to the stroke as a possible means of forecasting high gradients, and to set limits for our warning systems. We would also

like to field-test design features of new firing systems and EED's. To do these things, it would be desirable to know in advance where the stroke will occur; and at Langmuir Laboratories they are installing a cable across a canyon that is expected to attract lightning strokes. They are also constructing a large lightning antenna on a mountain with a lead into instrumentation for measuring currents. Both of these facilities should provide strokes at a known location and measure their structure.

#### REFERENCES

1. Burger, J. P. and Rost, D. L., "Preliminary Report of the Initiation of Various Types of Electroexplosive Devices by Induced Lightning," Minutes of the Ninth Explosive Safety Seminar, Naval Training Center, San Diego, California, August 1967.
2. Brook, Marx, "Lightning Parameters Related to the Initiation of Electroexplosive Devices," Minutes of the Ninth Explosive Safety Seminar, Naval Training Center, San Diego, California, August 1967.

#### DISCUSSION

The manner in which an EED with attached antenna initiates in a lightning field may be difficult to detect and may depend on antenna configuration. Initiation may occur from current flow through the bridgewire, or from a static spark from bridgewire to case. Tests in a given field with EED's that had loop antennas with the case isolated from ground and loop antennas feeding through the bridgewire to ground initiated, while those with loop antennas with the case grounded did not. From these tests it was assumed that initiation was caused by current flow and not static spark.

<u>Date</u>	<u>Electrical Field (v/m)</u>	<u>No. of Devices Fired</u>	<u>Distance (km)</u>	
			<u>Calc.</u>	<u>Meas.</u>
8/4/66	242,000*	8	1.8	1.0
	30,400*			
	33,400*			
	26,600*			
	205,000*	2	1.9	2.2
8/7/66	9,000			
	11,000			
	9,500			
8/8/66	97,000	8	2.4	2.0
	16,000			
	15,000			
	56,000			
8/9/66	No record	1	NR	NR
	17,000			
	13,000			
	14,000			
8/17/66	4,200			
	3,500			
	9,000			
8/26/66	Recorder off scale	1	NR	NR
	38,000			
	35,000			
	38,000			

\*All five readings recorded in 10-minute period. EED's expended in first stroke could not be replaced prior to other strokes.

### 3-10 LIQUID DESENSITIZED INITIATORS

by  
Robert W. Heinemann

#### Background

The safety of initiators of hazardous reactions has always provided major technical problems. Thus, initiators should be safe to manufacture, assemble, store and transport, yet must function with a high degree of reliability in many military and commercial applications. Strong desire for maximum safety has led to the development of some highly insensitive electrical initiators, which require a vast amount of electrical energy for initiation. Exploding bridgewire (EBW) detonators, originally developed for the Atomic Energy Commission, are examples of such devices. These are relatively expensive and require special accessories for proper use. Consequently, they have found only limited acceptance to date. Most commercial and military initiators are capable of being functioned at relatively low energy levels and therefore present a degree of hazard when handled manually. Because of this hazard, most military initiator and fuze assembly operations are conducted remotely and under carefully controlled processes. The result has been a high safety record in United States munition plants.

Unfortunately, there are many operations in existence which do not lend themselves to such remote operations. These operations involve instances where initiators are manually placed in direct contact with relatively large quantities of hazardous materials. While numerous precautions are taken to provide "maximum protection" for the person performing this operation, there is a small, but finite probability, that the initiator may accidentally be functioned during the operation. While much progress has been made in providing safety equipment and procedures to reduce the

probability of an accident to a minute quantity, it has not altogether been eliminated. Reasons for accidental initiations include static electricity, electromagnetic radiation, induced voltages, accidental impact, equipment failure and human error.

#### Design Objective

The basic reason for the initiation is the fact that when an initiator sees the proper stimulus, irrespective of whether applied purposely or accidentally, it will function. While this is desired when the stimulus is purposely applied, it is extremely undesirable during the handling operations. It occurred to me that a process could be devised which would permit the initiator to be temporarily desensitized for a sufficient time frame to permit increased safety during the assembly operations. In my literature search for a process which would lend itself to implementation, I came across two pertinent facts. The first of these involves the desensitization of explosives by liquids. Numerous hazardous explosives are shipped under water, water/alcohol or other fluids in order to minimize or to eliminate the possibility of a premature explosion. The second fact was obtained through a study of initiator design requirements. The designer has been continuously plagued by a poor functioning reliability when the active materials contain trace quantities of moisture. It appeared to me that a liquid could be permitted to enter the initiator through a porous opening and fill the spaces between particles. In many initiators there is appreciable space for the entry of liquid between particles. Thus, lead azide, compressed into a detonator at 15,000 pounds per square inch, has only a density of 3.1 grams per cubic centimeter. Lead azide has a

crystal density of 4.6 grams per cubic centimeter. This leaves more than 30% space between the lead azide particles at the 15,000 psi loading pressure. This holds promise of meeting the objectives of permitting incorporation of a sufficient quantity of desensitizer to yield the desired quenching action. If the liquid were volatile, it could vaporize at a later time and permit the initiator to perform its normal function.

### Design

To evaluate this approach, two flash and one electric detonators were fabricated in such a way that at least one opening was closed off with a porous material, such as filter paper. The detonators were immersed in a volatile fluid and weighings conducted on some to determine the rate of fluid entering the detonators. It was found that most of the fluid capable of being held entered these initiators within a few minutes. Initiation attempts were completely futile on these wet initiators even when energies several times their functioning requirements were applied. The output of such detonators is normally measured by their ability to blow holes through or to dent metal discs. Exposure Time tests showed that such initiators became slowly armed and after some delay time began to exhibit signs of "output" in terms of dents. For the specific test conditions it was possible to obtain no "output" in less than 5 minutes of exposure, while obtaining proper output in 15 minutes. This data was obtained with several hundred test units, indicating that the original premise of temporary desensitization was valid. An extremely significant aspect was arrived at during weighing at various exposure times. It was found that only a few milligram quantities of desensitizer are required to produce the desired desensitization. This indicates that surface phenomena may control the

initiation process to a very high degree.

#### Alternate Designs

There are cases, especially in the testing phase, where considerable manual handling is involved, yet rapid arming is desired after the handling phase in order to maintain maximum safety during the assembly operation. The rapid arming can be obtained by providing the initiator with a means of heating in order to obtain the subsequent rapid arming. A small heating unit integral to or surrounding the initiator would meet the objective.

Some initiators, especially those containing pyrotechnic mixtures, are somewhat unstable, and some are deteriorated by exposure to air. Two approaches can be utilized to increase safety in their utilization. One approach is to seal off the open end with a cap, tape or the like to permit storage without deterioration. The seal is removed just before use. Another approach is to construct the initiator as a multi-component unit, with the units separated from each other by a porous tube containing a low density absorbent material. This material would absorb the desensitizer and prevent the propagation of the initiation between the components by stifling any flame. When dry, on the other hand, it would propagate through the material. Probably the best way to construct the components would be to separate the same into a primer and flash initiated acceptor unit containing the output material.

#### Desensitizers

In general, any inert liquid can act as the desensitizer for initiator constituent. The desensitizer must be so chosen as to meet the requirements of the conditions under which it is used. Thus, a desensitizer



with a relatively high volatility at the ambient temperature condition would not be practical for a test area where there is a long waiting time to arming. On the other hand, items which require extensive handling for assembly purposes and which will not be used for months or years subsequently would use desensitizers with a much lower volatility. Since the ambient temperature would range from Arctic to Tropics, a wide range of desensitizers may be desired. The inclosed table shows a chart of proposed desensitizers with their range of usable temperatures. It should be cautioned that any desensitizer selected would have to be checked for compatibility (non-reactivity) with all materials composing the initiator (although for short time exposure there will be little reaction in most cases.) From a theoretical viewpoint, the liquids with a higher specific heat will tend to be better desensitizers and are preferred.

#### Ramification

The ramification of this investigation is that it may open a new approach toward obtaining a considerable increase in safety in operations which require manual handling of initiators. This appears to be possible through a relatively minor modification of initiators. While it cannot be categorically stated that it can be applied to all initiators, it does appear to warrant serious consideration, based on the apparent considerable increase in safety which it could provide. It appears especially applicable to operations which require the manual insertion of initiators into high energy materials, such as explosives, propellants or pyrotechnics. The most likely areas to benefit involve the following:

- |   |                                 |
|---|---------------------------------|
| a. Blasting                             | c. Mining Operations            |
| b. Manual Fuze Assembly and Disassembly | d. Aerospace Device Connections |
| c. Testing                              |                                 |

# LIQUIDS FOR USABLE TEMPERATURE RANGE

°F		
<u>Max</u>	<u>Min</u>	<u>Chemical Compound</u>
190	160	n-propanol
170	140	sym. quatro-chloro difluoroethane
140	100	ethanol
130	90	methanol
100	70	1, 1, 2 trichloro; 1, 2, 2 trifluoroethane
100	60	sym-quatrofluoro dibromoethane
60	30	isopentane
55	20	trichloro fluoroethane
30	-10	dichloro fluoroethane
20	-20	sym. quatrofluoro dichloroethane
-20	-60	methyl chloride
-60	-90	dichloro fluoroethane

## DISCUSSION

Some liquids that can be utilized to desensitize high explosives used in initiators and primers are water, methyl chloroform, methanol, and ethanol. Desensitization is required during the handling and loading of explosives for initiators. Other compounds such as the Fluronote series sold by the 3M Company have been noted to break up under certain conditions and caused explosions. This has been noted particularly with the use of metallic powders in rather large quantities.

The incorporation of a small amount of bulking agent can also cause desensitization.

### 3-11 INSTRUMENTATION FOR MAKING BROADBAND MEASUREMENTS ON ELECTROEXPLOSIVE DEVICES

Jack G. Hewitt, Jr.  
Denver Research Institute  
University of Denver  
Denver, Colorado 80210

#### INTRODUCTION

Ordnance systems must be certified to compatibility with range safety requirements so that accidental initiations are prevented. Usually a worst-case mathematical analysis of a system in a specified environment is made to determine whether it meets range safety specifications. However, it is sensible to require that certain measurements be made to verify the applicability of the models used in the analysis. In particular, electroexplosive device sensitivities for all modes of initiation for all frequencies must be determined by measurement, and stray energy coming into the electroexplosive devices from ordnance subsystems in various environments should be measured.

Electromagnetic compatibility measurements on ordnance systems present some unique problems. Measurements must be made from DC to 10 GHz although ordnance subsystems are designed to operate only at DC and low frequencies. High frequency characteristics of these subsystems are difficult to predict due to uncontrollable variations of lead dress, parasitic impedances, connector contacts, shielding etc. In addition, broadband measurements are made with equipment usually having a characteristic impedance of 50 ohms so that some type of probe-coupler is required to connect to the ordnance circuit. Ideally the probe-coupler should not perturb the electrical characteristics of the ordnance circuit and its effect on the electrical measurements should be negligible or nulled by compensation.

Since the purpose of electromagnetic compatibility measurements is to search for stray energy which is supposed to be below a specified level, it is necessary to have equipment that can respond over an extremely wide frequency range without continuous adjustment or substitutions of components. The best available instrumentation for ordnance circuitry uses thermal sensors which detect stray energy dissipated as heat in the component measured or electrical detectors which respond to the peak voltage between the points of contact. The best method of measuring the broadband electrical characteristics of small ordnance components and circuits uses microstrip transmission line and microwave integrated circuit techniques as probe-couplers to assure accurate and meaningful data.

#### THERMAL SENSORS

Thermistors and thermocouples are commonly used for broadband power measurements. Thermistors are operated in pairs so that one senses ambient temperature while the other senses the heated element temperature. They are connected in a bridge circuit so that output is proportional to temperature difference. Sensitivity is limited by the slight but unavoidable difference in thermistor characteristics, which cause bridge unbalance as ambient temperature changes. Time response of thermistors depends on size and geometry. Thermocouples sense temperature difference between the hot and reference junctions and require no bridge circuit or balancing. They are self contained, low impedance power sources which can drive galvanometers, voltage controlled oscillators and level detecting circuits directly. Ambient temperature changes have no effect on a thermocouple and there is no intrinsic limit to thermocouple sensitivity. Sensitivity

is limited by the characteristics of the galvanometer or input amplifier. Time response depends on size and geometry.

Broadband electrical power measurements are made with a power head consisting of a heating element which is electrically isolated from a thermal sensor. The heating element is designed to have a constant specified impedance over an extremely wide frequency range and to provide maximum heating of the thermal sensor. VSWR and sensitivity are measures of how well the power heads are designed to meet these conditions. Commercial power meters designed with a 50 ohm coaxial input typically operate from a 10 MHz to 18 GHz with a maximum VSWR of 1.75. The useful range of power measurement for a thermistor type meter is 1 microwatt to 10 milliwatts and for a thermocouple type meter 0.03 microwatt to 1 milliwatt.

Broadband electrical power measurements on ordnance systems can be made in a similar manner by using inert electroexplosive devices instrumented with heat sensors. The instrumented electroexplosive device is the power head of a power meter. See Figures 1 and 2. The header and bridgewire assembly presents the same impedance characteristic as a real electroexplosive device. Sensitivity is maximized by selecting the best heat sensor and designing it to receive the maximum amount of heat without making electrical connection to the bridgewire circuit. Experience has shown that thin film thermocouples are the most sensitive heat sensors for this application and that the pattern of the films can be optimized to accommodate various types of electroexplosive devices. (See Figure 3). The minimum detectible power from DC to 10 GHz is 1 to 10 microwatts depending on the geometry of the electroexplosive device, and the upper limit of power is 10 to 100 milliwatts. This sensitivity is less than the commer-

cial thermocouple power head because the bridgewire-header configuration is small and has not been optimized as a heating element whereas the heating element in a commercial power head is larger and especially designed to transfer maximum heat to a larger sensor. Typical DC calibrations are shown in Table 1.

The response of thermocouple instrumented electroexplosive devices as a function of frequency can be determined by using the bridgewire as a bolometer for a reference measurement. Then the bridgewire of an instrumented electroexplosive device can be heated to the same temperature for all frequencies and thermocouple outputs recorded<sup>1,2</sup>. Tables 2 and 3 show the data referenced to thermocouple output at DC. Thermocouple instrumentation always becomes slightly more sensitive at microwave frequencies due to self heating of the hot junction by induced currents. These come primarily from the coupling of the bridgewire loop and the thermocouple loop as shown in Figure 2. Although these loops are supposed to be perpendicular, some coupling inevitably occurs. Data of Table 2 show less than a 3 db rise at microwave frequencies while the data of Table 3 show less than a 6 db rise except for 2 items which probably have misaligned or non-perpendicular loops. The difference between the geometries of the bridgewires and headers is why the frequency calibrations differ.

Time response is important for electroexplosive device instrumentation because actual devices are sensitive to heat resulting from single impulses of electrical energy and pulse trains. The thin film thermocouple is formed on a Formvar substrate which is thinner than the metallic films, thereby minimizing heat capacity. Time constants range from 5 to 20 milliseconds depending on size and geometry. Since inert

bridgewires have comparable time responses, the instrumented electroexplosive device can measure the effect of transients<sup>3</sup>. Transient response sensitivity is determined by measuring the peak thermocouple output voltage which is proportional to an impulse of input energy. See Figure 4. The constant of proportionality depends on bridgewire time constant, thermocouple time constant and DC sensitivity; it ranges from 100 to 500 microvolts per millijoule. This range of sensitivities is adequate to drive electronic compensating networks which can provide automatic readout that compares the effect of measured steady or pulsed stray energy with a predetermined electroexplosive device sensitivity level to various types of pulses and DC<sup>4</sup>.

Thermal detectors are particularly suited to ordnance measurements in the pin-to-pin mode because they respond to heat which is ultimately responsible for initiation. Also they sum the effects of heating over the entire frequency range.

Another mode of possible electroexplosive device initiation is pin-to-case or bridge-to-bridge. This mode is characterized by high impedance and requires high voltages to initiate breakdown and heat or to cause dielectric heating. Although thermal detectors for this mode have not yet been developed, it would be possible to simulate the effective resistance of the powder with a high resistance sheet heating element and use a thermal detector to make a power head for pin-to-case power measurements.

#### ELECTRICAL DETECTORS

Electrical detectors use miniature diodes to probe the voltage difference between two circuit points. See Figure 5. Diode detectors have

a high impedance input and sensitivity is limited by diode rectification efficiency, noise and output impedance, and by the noise, bandwidth and input impedance of the low frequency or DC amplifier. Small signal diodes are operated in the square-law region so that diode output current is proportional to the square of the input voltage. Intrinsic diode sensitivities are about 10 microamps per microwatt for silicon point contact types and 18 microamps per microwatt for hot carrier or Schottky types. Practical sensitivities are reduced by lead parasitics, etc. The dynamic diode resistance or video resistance is about 1000 ohms. Therefore, if the threshold sensitivity is limited by the amplifier at 1 microvolt with an input resistance of 100,000 ohms, the minimum detectible diode power is  $10^{-6}$  microwatts corresponding to a diode voltage of about 31 microvolts. Thirty one microvolts across a 1 ohm bridgewire is  $10^{-3}$  microwatts of power dissipated in the bridgewire. This sensitivity is about three orders of magnitude better than the thin film thermocouple.

Since the diode detector has a dynamic impedance around 1000 ohms it has negligible effect on electroexplosive device measurements in the pin-to-pin mode. However, in the pin-to-case mode the diode's loading is not negligible and measured data can be in error. It is possible to add a series resistance to the diode either externally or by obtaining a diode with a larger dynamic resistance, but then sensitivity is reduced. Note also that the addition of a resistor would increase diode noise eventually causing an even greater decrease of sensitivity.

The major disadvantage of electrical detectors is the frequency response calibration. Since the quantity measured is voltage, the impedance between the points of measurement must be known before power dissipation



can be determined. Also the parasitic impedances of the detector package and leads resonate to cause peaks and valleys in the calibration curve above 1 GHz.

A wideband microcircuit amplifier was developed to determine if the diode detector sensitivity could be increased and the input impedance changed for use in the pin-to-case mode<sup>5</sup>. The microcircuit amplifier is small enough to be inserted in an inert electroexplosive device as a pre-amplifier for the detector. The amplifier is shown in Figure 6. It is usable over a frequency range of 1 to 500 MHz and input and output impedances vary around 100 ohms. Table 4 shows a comparison of sensitivities of electroexplosive devices instrumented with diode detectors with and without the microcircuit preamplifiers in the pin-to-pin mode. No attempts were made to optimize impedances for the pin-to-case mode or to increase signal to noise ratio.

#### MICROSTRIP TRANSMISSION LINE ADAPTORS

Standard equipment for electromagnetic measurements from DC to 10 GHz usually has a characteristic impedance of 50 ohms and uses coaxial transmission line connections. It is best suited for measuring components which can be made an integral part of a coaxial geometry and which produce a low VSWR on the transmission line. Frequently broadband compatibility measurements must be made on miniature components not readily adaptable to a coaxial geometry or on low impedance components such as electroexplosive devices. Attempts to connect these devices to a 50 ohm coaxial system for broadband measurements are unsatisfactory for the following reasons: (1) the low impedance devices typically produce VSWR's in the range of 25 to 200 reducing accuracy to an impractical level, and

(2) the coaxial adaptor adds considerable impedance often masking the component under test, and although it is possible in principle to measure the adaptor impedance by itself so as to subtract its effect from the total, the degree of uncertainty of the resulting impedance is often greater than its value. It is possible to improve these measurements by using a transmission line geometry which allows for component insertion or connection with a minimum addition of spurious impedance. It should have the following characteristics: (1) transmission should be low loss TEM mode; (2) the structure should be open, exposing both the grounded and ungrounded conductors, and (3) the geometry should concentrate electromagnetic field energy in a small cross-section. The transmission line geometry best fitting these characteristics is microstrip.

Figure 7 shows a picture of the basic microstrip configuration. The transmission line is formed by a strip conductor of width  $w$  and thickness  $t$  on a dielectric slab of thickness  $h$ . The bottom side of the dielectric slab is covered with an extensive ground plane. Electromagnetic waves propagate in a quasi TEM mode as long as the half wavelength in the dielectric is less than  $w$  and/or  $h$ . If the dielectric is alumina ceramic with a relative dielectric constant of 9.6, the characteristic impedance is 50 ohms when  $w = h$ . Typically  $w=h=0.025$  inches and  $t=0.0004$  inches. It has been determined that 94% of the electromagnetic field energy is contained in the dielectric immediately under and within about 0.025 inches of the strip conductor<sup>6</sup>.

Microstrip transmission line adaptors have been used to connect electroexplosive devices to 50 ohm coaxial systems for high frequency pin-to-pin and pin-to-case electroexplosive device sensitivity

measurements. See Figure 8. This allows the system's 50 ohm characteristic impedance to be brought directly to the header of the electroexplosive device as shown in Figure 9 with negligible addition of parasitic impedance to obtain more meaningful and accurate firing sensitivity data. The receptacle on top of the microstrip transmission line as shown in Figure 8 adds less than 2 picofarads capacitance. Figure 10 shows a microstrip transmission line adaptor designed to make accurate impedance versus frequency measurements on a deposited film bridge for an electroexplosive device. These measurements which are necessary for obtaining power dissipation from diode detector measurements could not be made with practical accuracy using coaxial type adaptors.

#### CONCLUSION

Three most useful concepts of instrumentation for making electromagnetic compatibility measurements on ordnance components and systems have been discussed. These are: (1) the thin film thermocouple which measures heat generated by stray electromagnetic energy and is easily used from DC to over 10 GHz, (2) the electrical diode detector which measures stray voltages and is easily used from 0.1 MHz to 1 GHz and (3) the application of microstrip transmission line techniques to make connections to miniature components under test without adding parasitic impedances which destroy the accuracy and usability of the measured data. In general, instrumentation for the pin-to-pin mode is adequate while instrumentation for the pin-to-case mode is inadequate. Since pin-to-case problems such as dielectric heating are more likely to occur at higher frequencies it is reasonable to consider developing thermal detectors which simulate the pin-to-case impedance and heating characteristics.

Also use of microstrip transmission line techniques and miniature diodes in compatible beam lead packages should be investigated with the aim of improving impedance simulation.

TABLE 1

Typical Calibrations of Thermocouple  
Instrumented Electroexplosive Devices

100 ma no-fire			4.5 ohm cold bridgewire resistance
Bridgewire Current	Bridgewire Power	Average Bridgewire Temperature Rise	Thermocouple Output
(ma)	(Microwatts)	(°C)	(microvolts)
0.5	1.1	0.008	0.5
1	4.5	0.032	2
5	11	0.8	52
10	45	3.2	210
20	180	13	830
60	1,700	120	7700

1 amp no-fire		0.19 ohm cold bridgewire resistance
Bridgewire Current	Bridgewire Power	Thermocouple Output
(ma)	(Microwatts)	(microvolts)
5	5	0.5
10	19	2
25	120	12
50	480	48
100	1,800	180
250	12,000	1200
500	54,000	5400

TABLE 2

Frequency Response of Sandia Corp.  
Instrumented Electroexplosive Devices

Values are ratio of thermocouple output at frequency listed to DC output in db

Frequency (MHz)	Serial 3063	Serial 3106	Serial 3107	Serial 3109
500	0	0.3	0	0
1000	0.3	0.3	0	0.1
2000	0.7	0.8	0	0.1
3000	0.9	1.2	0.5	0.4
5000	1.1	---	0.5	0.6
7000	1.4	1.3	0.5	0.6
9000	1.9	2.2	0.7	1.2

TABLE 3

Frequency Response of Apollo  
Standard Instrumented Initiators

Values are ratio of thermocouple output at frequency listed to DC output in db

Frequency MHz	Serial 4289	Serial 4290	Serial 4292	Serial 4293	Serial 4491	Serial 4494	Serial 4503
100	0	0	0	0	0	0.1	0
200	0.5	0.2	0.9	0.5	0.3	0.3	0.4
450	0.7	0.5	1.2	0.8	0.6	0.4	0.8
960	1.4	1.4	2.7	1.4	1.5	1.0	2.3
2100	2.7	2.4	4.7	2.6	3.0	2.4	4.8
5000	4.1	3.7	6.7	3.9	4.4	3.7	6.7
9100	4.7	4.6	7.1	4.8	5.2	4.2	8.1

TABLE 4

Calibration of Sandia Corp. Electroexplosive Device  
With and Without Microcircuit Preamplifier

Values are voltages in millivolts across the 4.5 ohm bridgewire necessary to produce a 10 microvolt detector output

Frequency (MHz)	Bridgewire Voltage (Millivolts)	
	With Preamplifier	Without Preamplifier
10	0.16	1.3
20	0.15	1.3
60	0.18	1.3
100	0.22	1.5
140	0.31	1.5
180	0.33	1.2
220	0.35	1.1
260	0.36	1.2
300	0.40	0.91
340	0.40	0.73
380	0.40	0.82
420	0.36	0.64
460	0.35	0.58

## LIST OF REFERENCES

1. "Improvement of Instrumentation Used in RF Hazard Testing" Final Report, Sandia Corp., P.O. 73-5753, 30 September 1965.
2. "Electromagnetic Field Strength Measurement by Electroexplosive Devices", Final Report NAS10-5972, 31 October 1968.
3. "Transient Responses of Thermocouple Instrumented FED's," Task 1, Report of Sandia Corp., P.O. 73-2582, 15 September 1962.
4. "An EMC Measurement Technique for Ordnance Firing Circuits," C.D. Gronlund, Seventh Symposium on Electromagnetic Compatibility, IEEE New York, June 1965.
5. "Radio Frequency Instrumentation Amplifier," Final Report, Sandia Corp., P.O. 73-2948, 15 September 1967.
6. "Use of Microstrip Transmission Line to Improve Broadband Electromagnetic Measurements", Jack G. Hewitt, Jr., and Frank M. Roddy, International Symposium on EMC, Asbury Park, N.J., June 1969.

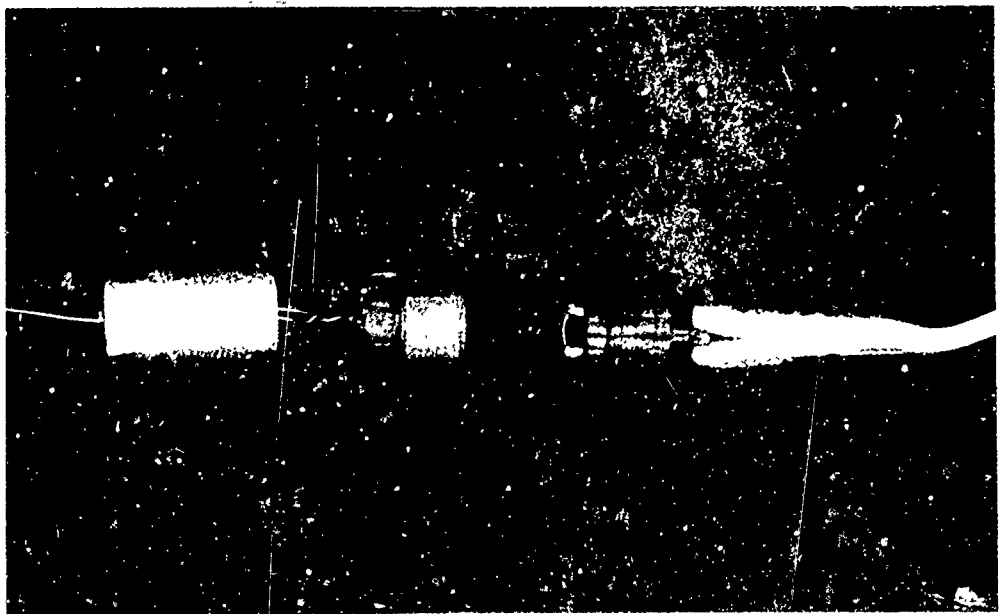


Fig. 1 Thermocouple, Instrumented  
Explosive Device Disassembled

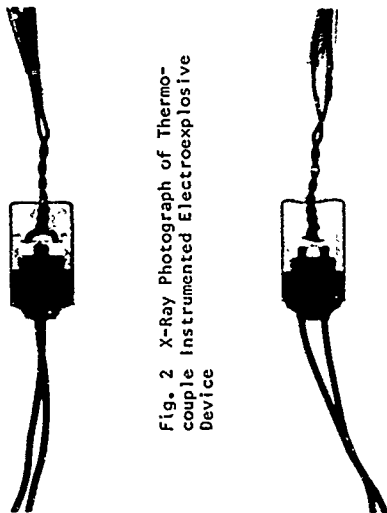


Fig. 2 X-Ray Photograph of Thermo-  
couple Instrumented Explosive  
Device

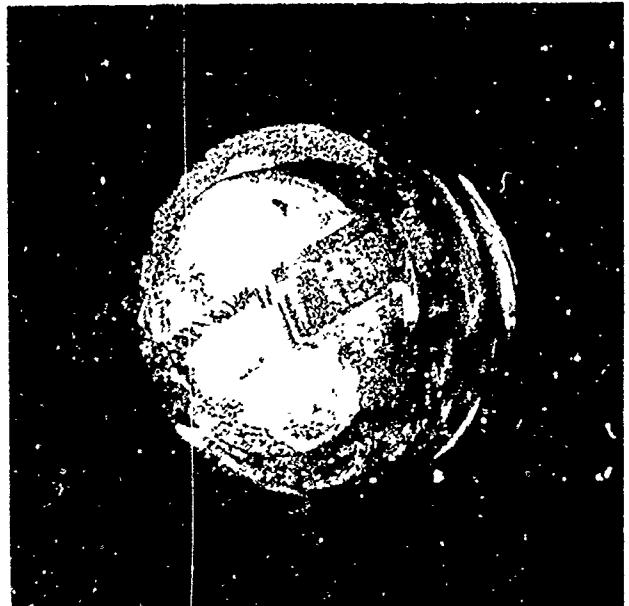
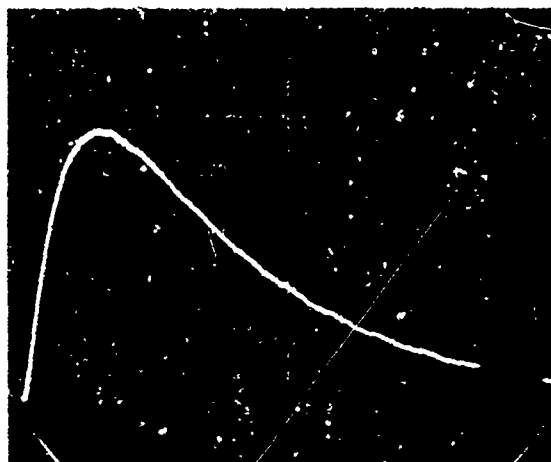


Fig. 3 Thin Film Thermocouple



Sweep Speed,  
20 mx/cm  
Vertical Sensitivi-  
ty, 200  $\mu$ v/cm  
Bridgewire Resis-  
tance, 1.14 ohms  
Impulse, 3 ampere -  
200  $\mu$ sec  
Impulse Sensitivi-  
ty, 440  $\mu$ volts/  
millijoule

Fig. 4 Impulse Response of Thermocouple Instrumented  
Apollo Standard Initiator

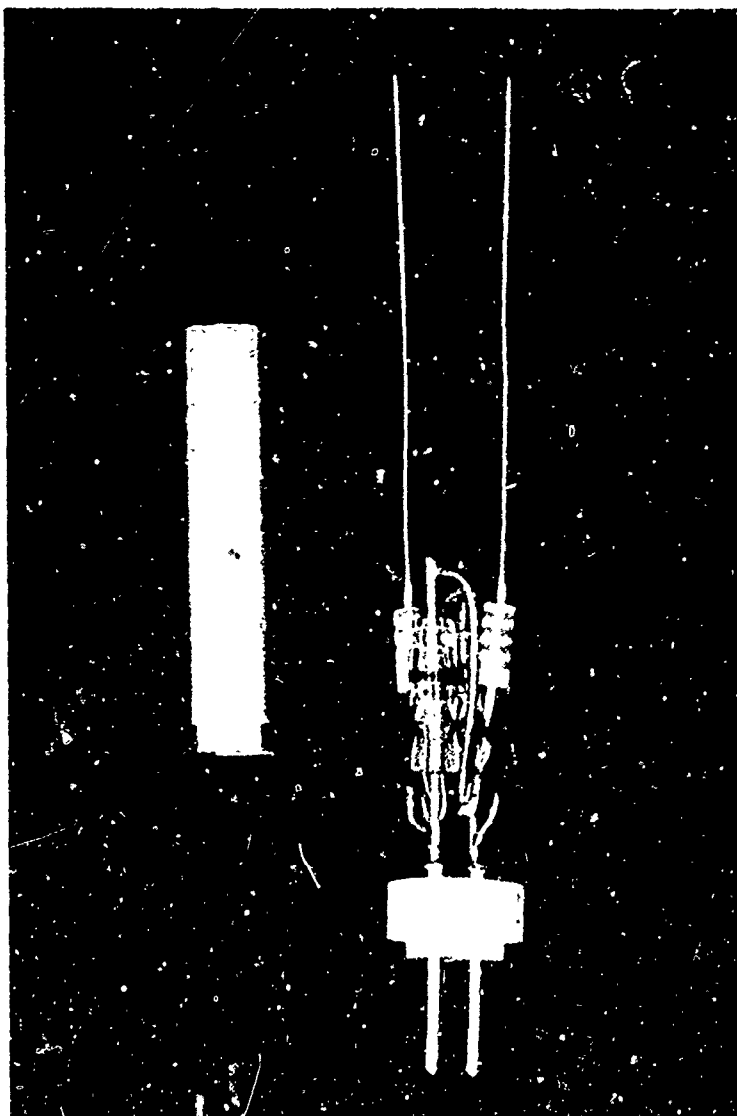


Fig. 5 Diode Detector  
3-11.14



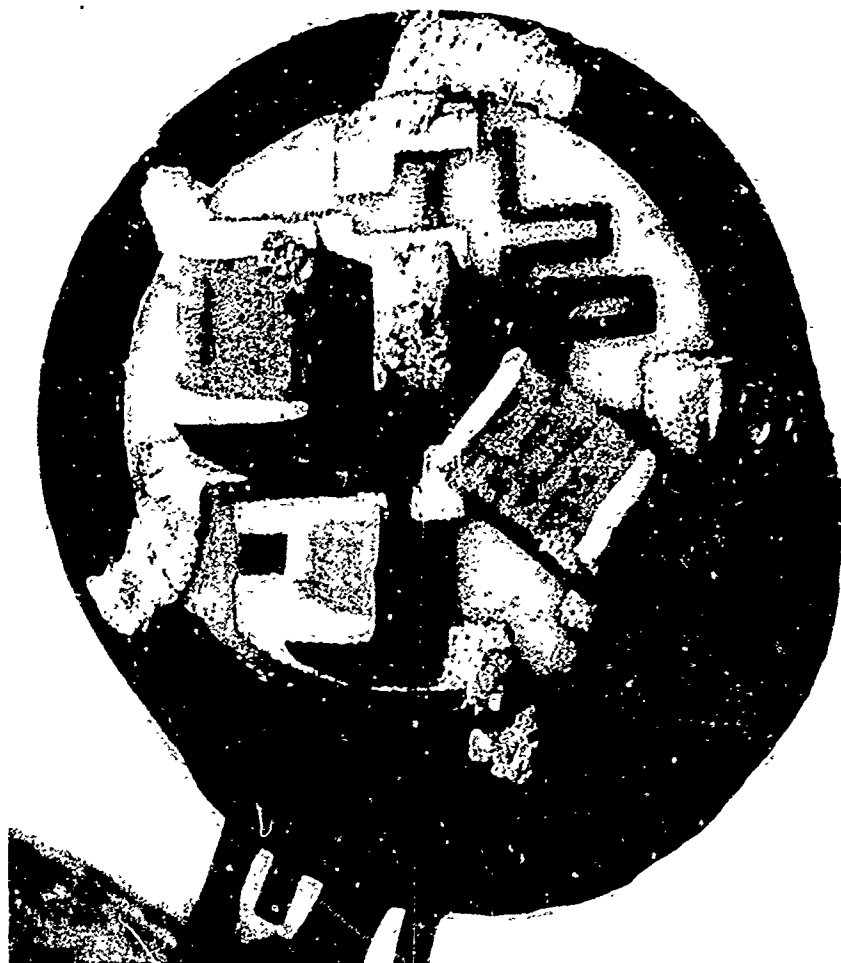


Fig. 6 Microcircuit Instrumentation Amplifier

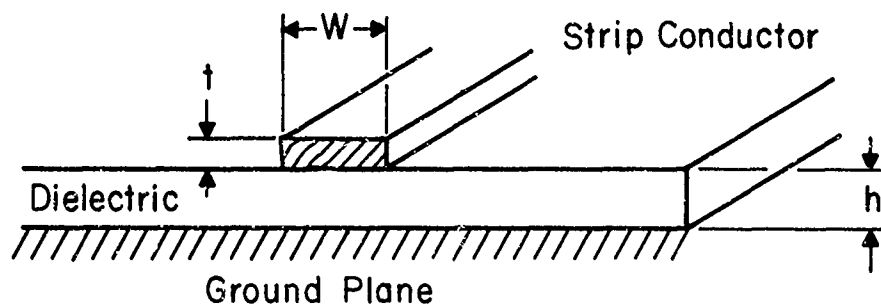


Fig. 7 Microstrip Transmission Line Cross Section

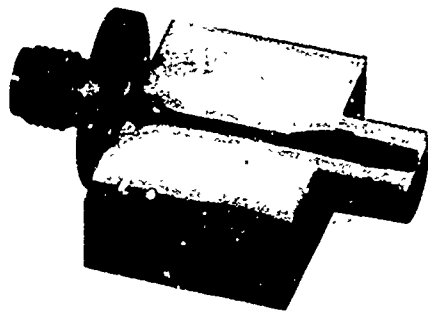


Fig. 8 Microstrip Transmission Line Adaptor

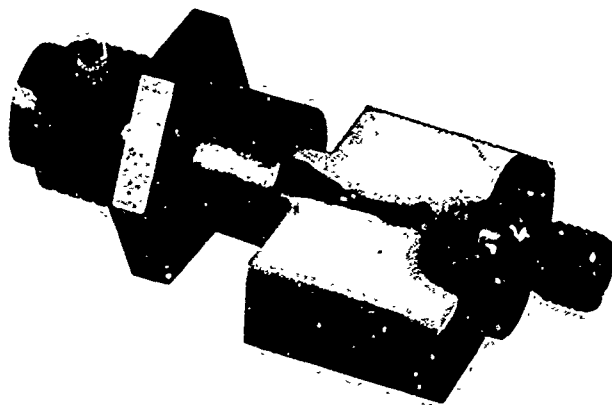


Fig. 9 Microstrip Transmission Line Adaptor with Electroexplosive Device Connected

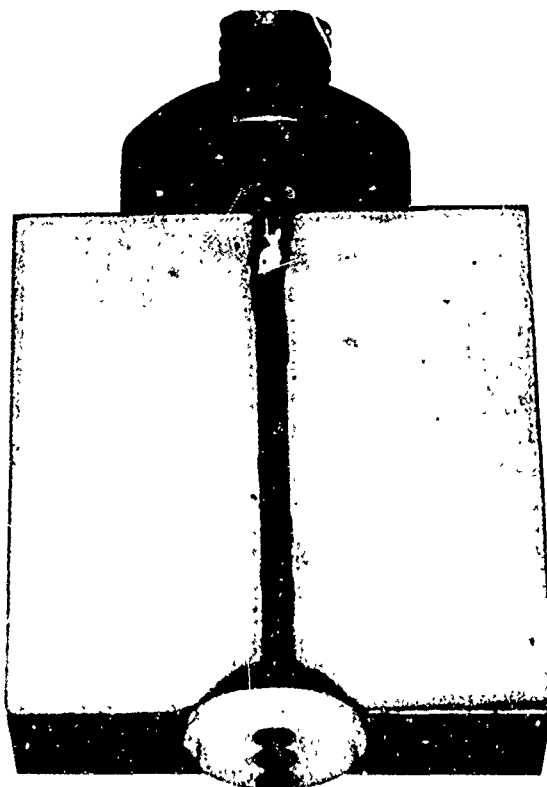


Fig. 10 Microstrip Transmission Line Adaptor for Measuring Deposited Film Bridge Characteristics

## DISCUSSION

A thermocouple placed near, but not touching, an exposed bridgewire can measure heating caused by electrical energy delivered to the EED. The response of the thermocouple must be faster than the bridgewire response, so it can be used as a valid detector. Measurements of this type to determine the response of exposed bridgewires to various stimuli can be correlated to actual firings of live EED's to help in defining what is actually setting the device off.

# ABSTRACTS - SESSION FOUR

## 4-1 Some Initial Investigations of the Laser Initiation of Explosives

*Modesto J. Barbarisi,  
Edward G. Kessler*

An experimental investigation was carried out to examine the feasibility of directly detonating secondary explosives using radiation from a ruby laser (6943A). Secondary explosives included PETN, HMX, RDX, and tetryl. Most of the effort was devoted to a statistical evaluation for the initiation energy of PETN. Findings show that, although a more sensitive mixture can be detonated through a light guide, attenuation of the radiation is too great to make this method practical for secondary explosives.

## 4-2 The Development of a Solid-State Explosive Initiator

*R.F. Flagg, E.J. Stecker and  
L.E. Hollander*

Detailed results are presented of the R&D of a new generation EED derived from solid state technology. The work includes a study of the basic resistance-temperature properties of a number of solid state materials, a theoretical and experimental investigation of both the steady state and the dynamic properties of the device. A mathematical model of the electro-thermodynamic system is constructed and various effects calculated and compared with measured values. Non destructive testing of key parameters has been demonstrated.

## 4-3 Effect of Reduced Ambient Pressure on the Hot-Wire Sensitivity of Primary Explosives, Metal-Oxidant Mixtures, and Black Powder

*H.S. Leopold*

The hot wire sensitivity of initiating materials can change under vacuum conditions. Lead azide, silver azide, black powder, and mixtures of  $Zr/KClO_4$  require slightly more energy for initiation under vacuum conditions. Basic lead styphnate and normal lead styphnate require slightly less energy for initiation under vacuum conditions. The loading density affects the energy differential. Hypotheses are proposed for the observed energy changes.

## 4-4 Functioning Time of a 1-Amp/1-Watt Detonator

*Soranton Nesbitt*

The insensitive electric initiator used in this study is a 1-ampere/1-watt no fire, 5-ampere/5-watt all fire detonator developed by the Navy and currently in use in several Naval and non-Naval applications. Functioning time characteristics are given for constant current inputs of 1 to 5 amperes and for various capacitance-charging potential combinations. Results of pulsed constant current and capacitor discharge Bruceton studies are also included.

## 4-5 The Propagation of Reaction Across a Lead Azide-PETN Interface

*Calvin L. Soott*

Lead azide was investigated for its ability to initiate PETN in the approximate dimensions and confinement commonly used for electro-explosive devices. Fixtures containing the explosives were viewed by a high speed smear camera. It was found in separate experiments that for the given conditions PETN was initiated high order at the lead-azide-PETN interface when: (1) the lead azide density was between 2.61 and 3.54 gm/cc (loading pressure of 5K to 30K psi), (2) the adsorbed moisture content was less than 0.8 percent for the lead azide pressed at 10K to 20K psi, and (3) the 0.150-inch diameter column contained 100 mg or more of the lead azide pressed at 10K psi.

## 4-6 On the Combustion Propagation of Tungsten Delay Powders

*Roswitha Zimmer-Galler,  
Martin Zimmer*

The combustion of tungsten delay powders containing bariumchromite and potassium perchlorate as oxidizing agent has been investigated under various environmental conditions. The results are interpreted to develop a semiqualitative combustion model and to provide a basis for predictably controlling the burning rate.

4-8 Development of RF Attenuators Utilizing Ferrite-Ceramic Component and the Effect of Nuclear Radiation of These Components *Nancy B. Killoughby and Stanley M. Adelman*

In the past 15 years, a multiplicity of hardware has been developed for protecting EED's and initiation circuits from the effects of RF radiation induced energy. Army programs have indicated the dissipative type attenuator utilizing ferrite components to be most desirable and have resulted in the operational use of such devices. It has been reported that ferrites can generate significant currents under nuclear radiation. Consequently, a program was initiated to determine the effects of nuclear radiation on various ferrites and on attenuators. Intrinsic electrical properties and attenuation were measured before and after exposure.

4-9 Response of SCOUT Destruct Charges to High Heat Fluxes *A.E. Pierard*

An experimental program was conducted to determine the sensitivity of the SCOUT missile destruct system to an abnormally high temperature environment such as might be caused by a combustion gas leak into the destruct system tunnels. Direct impingement failed to initiate the charge; however, detonation did occur when the gases engulfed the charges under the environment enclosure. This paper presents a description of the test apparatus, a discussion of the test procedures used, and an analysis of results of the tests.

4-10  $dx/dt$  vs. Time Detonation Monitoring *Donald Baker Moore*

Work was performed in continuous detonation velocity measurements. Using electronic differentiation,  $v/t$  plots (rather than the more usual  $x/t$  plots) produced interesting results. The technique is believed to be suitable to studying fundamental detonation propagation mechanism as well as being of immediate importance in quality control.

4-11 Evaluation of Detonating Cord by Framing Camera Technique *J.W. Blain, B.V. Carlson and A.H. Smith*

An experimental technique for evaluating detonating cord was developed using high speed motion picture photography. Explosive performance of 2.5 grain per foot to 13 grain per foot RDX - aluminum or lead jacket - detonating cords were photographed by the Cordin Camera technique at frame speeds of two microseconds and one microsecond per frame. Performance characteristics of each cord type were established and evaluated for missile design applications.

4-12P Comparative Effects of CW and Radar Signals on EED Bridgewire Temperature *O.W. Mayes and Charles Carlson*

The RF no-fire sensitivity of EED's in the bridgewire mode is often measured in terms of continuous wave (CW) power input. The no-fire power level thus determined is sometimes considered applicable to pulsed (radar type) RF signals, on an average power basis. This practice does not allow for bridgewire temperature fluctuation. An equation has been developed to account for bridgewire temperature fluctuation and implement the use of CW power sensitivity data under pulsed power conditions. The equation gives the effective relationship of CW and pulsed signals, based on the peak temperature of the bridgewire for the steady state pulse cycle.

4-13P EBW Firing Unit-Detonator Compatibility Tests *R.G. Amicone and M.G. Kelly*

Tests with a variable waveform EBW firing unit and an EBW spark gap detonator determined that the current parameters  $I_p$  (peak current) and  $t_p$  (time-to-first peak) of the damped sinusoidal output could not be used alone to define the compatibility between detonator and firing unit. Sensitivity tests at -65°F indicated that secondary current peaks may play a part in the initiation of the detonator.

4-14P Determining Ratings of RF Suppression Devices *P.F. Mohrhaach, R.F. Wood, and R.H. Thompson*

Surveying present methods of characterizing RF suppression devices indicated that there is no accepted standard of rating. Attention was focused on methods of determining minimum loss of a two port network. It was decided that, in general, there are two methods: (1) Measure the ratio of load power to input power for all possible terminations of the two port network and then select the maximum ratio; (2) Measure a transmission or transformation parameter of the network for a number of terminations and compute the minimum loss from the results. Various approaches to measuring the minimum loss of an RF suppression device are discussed.

#### 4-1 SOME INITIAL INVESTIGATIONS OF THE LASER INITIATION OF EXPLOSIVES

Modesto J. Barbarisi  
Edward G. Kessler

Feltman Research Laboratories  
Picatinny Arsenal, Dover, New Jersey

#### INTRODUCTION

Modern technology, especially in the military, would welcome the ability to safely detonate secondary explosives directly, without need for a sensitive primer. Ideally, the stimulus must not only be reliable but also offer increased safety over some of the other stimuli presently used. Primers, for example, are very sensitive to heat and friction, making them extremely dangerous to work with. EBW as well as hot bridgewire systems are in many applications sensitive to RF radiation, thereby presenting the danger of premature firings.

With the development of efficient lasers, a new stimulus has been made available. This form of coherent radiation seems to lend itself well to such an application. Focusing properties of coherent radiation are capable of producing high temperatures, while intense shocks might be produced with the higher power Q-switched lasers. The concept proposed is to use laser radiation as a stimulus for detonating secondary explosives directly. Such a system in cases where applicable, would greatly decrease the dangers involved in the employment of secondary explosives. This would be accomplished by eliminating the need for a sensitive primary to induce high order detonation. Simultaneity of explosions as well as immunity to RF radiation and electrostatic hazards are other advantages of laser initiation. Direct ignition by intense

electromagnetic radiation would be safer as well as more reliable than systems using primers since no arming devices which might result in mechanical or electrical failure would be necessary.

The ability to reliably detonate a secondary explosive with laser radiation would also be extremely useful in explosive sensitivity tests. Presently in the production of secondary leads, boosters, and chargers, reliability tests are usually performed in conjunction with detonators involving a primary explosive. These detonators exhibit considerable energy variation and therefore good sensitivity tests are difficult. Sensitivity tests employing EBW devices are limited, since although one might have an accurate knowledge of the energy input to the wire, the amount of energy imparted to the explosive is not accurately known especially in cases where exothermic materials are used. With the use of a laser system precise energy and power measurements would be possible with the desired result of extremely accurate sensitivity measurements.

The approach used is an experimental one for the chief purpose of establishing feasibility and justification for continuing programs of this nature. Experimental possibilities involve enough work to keep investigators busy for years. All of the theories and information applicable to conventional stimuli might be investigated for laser initiation. Such things as initiation by the adiabatic compression of trapped gas,<sup>1</sup> hot spot theory, addition of a suitable grit to induce hot spots are just some of the many avenues open to investigators. Since nearly all secondary explosives do not begin to absorb appreciably until below 3500Å, and available laser radiation does not approach the ultra violet, investigations involving second harmonic generation might be particularly interesting.

Dielectric breakdown of explosive materials due to the extremely intense electric fields present in laser radiation offers other interesting possibilities.

A complete research program to investigate the laser initiation of explosives would include a large effort to understand and describe the mechanism by which the light energy is transported into the initiation of the explosive and the following growth into an explosion. Such a description has yet to be fully defined for stimuli presently used.<sup>2</sup> It should be understood therefore that the chief aim of this program was not to investigate the coupling mechanism, but rather to first establish feasibility and secondly to set some limits on the conditions necessary for reliable detonations.

This present investigation was limited to the radiation of a ruby laser. Free running as well as Q-switched techniques were used. The selection of secondary explosives was influenced only by their relative use in the military today. PETN, Tetryl, HMX, and RDX are some of the widely used explosives in military items.

In such an investigation there were many variables to consider. Such things as explosive grain size, density, confinement pressure, and relative humidity are just some of those associated with the explosive. Other variables characteristic to the laser are power, energy, frequency, etc. We considered the variation only of those parameters which would seem to have the greatest effect on our results. Energy and pressure for example were considered variables while such things as temperature and grain size were assumed constant.



## EXPERIMENTAL PROCEDURE

The laser used in these experiments was a pulsed ruby rod ( $6943\overset{\text{O}}{\text{\AA}}$ ), with a plano total internal reflectance configuration. The ruby rod had a diameter of  $5/32$  inch and a length of 6 inches. A 50% reflecting mirror at the front end was found to give excellent lasing action. Pumping action was provided by two FX47 Xenon flash lamps manufactured by EG&G. With the configuration described above, Q-switching was only possible from the front end of the rod. In cases where Q-switching was desired, a cell filled with a passive liquid Q-switch solution (Maser Optics, Inc.) was placed in the beam path between the front end of the rod and the external 50% mirror.

Although a passive liquid gives excellent switching, it is, in certain respects, less reliable than other means of Q-switching such as Pockel cells, rotating mirrors, etc. First, the liquid is a self activating device and cannot be controlled as easily as some of the other devices. Secondly, the switching characteristics of the liquid depend on both the concentration of the liquid and the energy output of the laser. This makes it more difficult to obtain a good single pulse using a liquid switch. However, with proper monitoring, the liquid solution can give good results.

The laser head was aimed to fire through a hole into an explosive barricade. A front surface mirror was placed in the barricade to reflect the beam down onto the explosive sample (See Figure 1). The mirror was used to displace the laser head from a direct line of sight of the explosive and thus protect the laser from flying fragments.

A hydraulic ram was placed under the test sample. Its purpose was to compress the explosive when necessary, inside a die against a glass block. The glass block allows the laser light a path to the sample while keeping the sample under pressure.

To monitor energy, we had placed a glass beam splitter outside the barricade in the laser path at an angle, to reflect 5% of the incoming beam into a thermopile. This external thermopile was calibrated as to include losses introduced by lenses, mirrors and other sources of light attenuation which might be present in the beam path. Thus the thermopile was calibrated as to give the amount of energy hitting the explosives.

For initiation time measurements, we had run a DuPont "Corfon" light guide into the barricade. The interior end was pressed against the glass block. There it conducted both the light of the laser striking the test sample indicating relative power, and the light of the detonation, to an EG&G "Lite Mike". The resultant output was displayed on a Tektronix 585 oscilloscope. We define the term 'initiation time' to be the time between the arrival of the first laser spike at the target and the onset of the detonation. When necessary, a lens was inserted in the path of the laser beam so as to focus it onto the top surface of the test sample.

Energy measurements were taken by sampling a portion of the beam with a high speed light detector operated in an integration mode (not shown in figure). This integrated picture of the laser output, combined with both the thermopile reading of total energy and the initiation time measurement, allows one to calculate the amount of energy imparted before initiation. Energy could be varied by using filters, or a variable aperture in the beam path.

## EXPERIMENTATION

### Preliminary Trials

Our first attempts were designed to determine feasibility of laser initiation of explosives. These first experiments were not detailed considerations, but rather a gross effort to determine whether or not explosives could be detonated using a laser. We fired at a pyrotechnic mixture (consisting of 50%  $\text{KNO}_3$ , 25% nickel powder and 25% aluminum powder) lead styphnate, lead azide, HMX, PETN, and tetryl.

The laser power supply has a capacity of 1600 mfd. giving energy input to the laser cavity of 7200 Joules when fired at 3000 volts. These first experiments were conducted with the laser fired at 3000 volts since this was well above the lasing threshold of our cavity assuring us of lasing on each shot. The laser output [0.1 - 20 Joules depending on both the mode of operation and the temperature of the rod] was focused onto the sample surface using a 9 cm focal length lens. These first attempts gave the following results:

The pyrotechnic mixture responded readily to the laser radiation. With the laser operating in the free running mode, it was found that this mixture had an average initiation threshold of approximately .0053 Joules per square millimeter exposed (Table I). When the laser mode was changed to Q-switch, it was found that the initiation threshold of this same mixture was lowered below the measuring limits of our instruments. The pyrotechnic mixture was also initiated by focusing the laser beam into a plastic light guide and placing the other end of the light guide into the mixture. It can be mentioned here that none of the secondary

explosives could be detonated using this light guide method. If, however, the secondary powder was mixed with the pyrotechnic mixture, then the light guide proved successful in achieving detonation. These few initial attempts at using light guide as a means of transporting energy seem to indicate simply that the light guide attenuates the radiation to the point where it is no longer effective as a stimulus for the explosive. Consider however, the possibility that with second harmonic generation of the beam, the absorption coefficient of the explosive might be high enough to permit reliable laser initiation of secondary explosives through a light guide.

Attempts at initiating lead styphnate and lead azide resulted in information similar to that for the pyrotechnic mixture. With a free running laser lead styphnate required about  $.0007 \text{ J/mm}^2$  for initiation, and lead azide about  $.007 \text{ J/mm}^2$ . Initiation times for both were  $7 \mu\text{sec}$ . However, when these same explosives were radiated with a Q-switched laser, the energy sensitivity of both was increased beyond the measuring limits of our equipment. The initiation times decreased to below  $0.5 \mu\text{sec}$ .

For the secondary explosives, no detonation could be excited in the loose powder, using either the free running or the Q-switched laser. By adding a black coloring agent to the powder we achieved partial consumption. This coloring agent probably had the effect of inducing hot spots (because of its greater absorption coefficient) which in turn increases the probability of initiation. Consumption by using a coloring agent was only completed when the sample was compressed to 7500 psi.

This confinement pressure proved to increase the sensitivity of the secondary powders enough so as to cause detonation even without the aid of a coloring agent. This might be explained by the fact that initiation by adiabatic compression of trapped gas is more probable at higher confinement pressures. PETN confined at 7500 psi would detonate with reliability. At this same pressure, Teteryl would partially detonate, however if the pressure is increased to 13,500 psi, reliable detonation is achieved. HMX was unaffected at 7500 psi but at 13,500 it showed reliable sensitivity. Again, in all cases, the probability of response was much increased when radiated by a Q-switched rather than a free running laser. This, combined with the fact that the Q-switched laser has considerably less total energy than a free running laser (See Figure 2) gives strong indication that a functional relationship between threshold of detonation and applied stimulus would not be simply energy dependent, but depend also on power. It is recalled that the pyrotechnic mixture mentioned earlier as well as lead azide and lead styphnate also followed this behavior.

#### Initiation Threshold for PETN

From initial experimental work we learned that the control of all parameters is of extreme importance. Such things as grain size, temperature, pressure, energy all influence experimental results. Thus it soon became apparent that in order to get meaningful and reproducible results it would be necessary to monitor all experimental parameters. In certain cases this presented no real problem. For instance, temperature

and pressure could be kept reasonably constant. In the case of grain size an attempt was made to acquire a relatively pure and uniform explosive powder. Properties of the radiating source such as power, energy and frequency are particularly important since it is the functional dependence of detonation on these parameters which is under investigation.

Our initial work was to define the energy sensitivity of the explosive assuming power to be relatively constant. As there is no exact go-no-go point, a statistical evaluation of the results had to be undertaken. The energy threshold should be of the form shown in Figure 3.

In order to adequately define the cumulative distribution function from the data, it is important that energy be varied enough to assure energy levels in the data that provide 100% detonations and energy levels that provide no detonations. If these limits were not reached, the threshold curve could not be adequately defined. In attempting to define the energy threshold, we often exceeded the limits of sensitivity of our measuring equipment without covering the lower bounds of the threshold curve.

The following sets of experiments were carried out in an attempt to completely cover the energy threshold curve. If the energies were varied over an order of magnitude, yet still failed to cover the threshold curve, the deviation was considered too great to provide useful information. Then some parameter was varied for the next series in an attempt to reduce the deviation.

The first set of experiments were run at 7,500 psi with the PETN placed inside the focus of a 9 cm focal length lens. The beam covered an area of 2 cm<sup>2</sup>. We thought that although there might be local dissimilarities in sensitivities due to any variations in grain size, by covering a large number of grains with the beam, the differences should average out, and we should get better consistency. The incident energy was varied from .09 to 1.95 Joules without covering the threshold.

We then switched to focusing the beam on the surface, using the 9 cm focal length lens. The area of illumination at the target was 2 mm<sup>2</sup>. We covered an energy range from .013 to .055 Joules with erratic results.

Recalling that Tetryl failed to detonate at 7500 psi, and initiated at 13,000 psi, we decided to increase the confinement pressure on our PETN samples to 13,000 psi. Our hope was to reduce the spread of initiation energies previously encountered. With this increase in pressure, reliable detonations were achieved at a somewhat lower input.

When the data provided reasonable coverage of the curve, we used a maximum likelihood method to estimate the mean ( $\mu$ ) and standard deviation ( $\sigma$ ) of the curve.

The equation of the probability curve is

$$1) \quad P(E) = \frac{1}{\sqrt{2\pi}\sigma} \int_{-\infty}^E \exp\left[-\frac{(t-\mu)^2}{2\sigma^2}\right] dt$$

The best estimates of  $\mu$  and  $\sigma$  are chosen according to the maximum likelihood method. In this procedure the best estimates of  $\mu$  and  $\sigma$  are taken to be those which maximize the quantity  $L = \prod_{i=1}^5 P_i(E) \prod_{j=1}^{m-5} (1 - P_j(E))$

where  $P_i$  is the probability of success in the  $i$ th trial and  $s$  is the number of successes, and  $(1-P_j)$  is the probability of failure in the  $j$ th trial and  $n-s$  is the number of failures. A full analysis of this method has been given by Golub and Grubbs<sup>3</sup> and Kessler<sup>4</sup> has adapted it in a manner suitable for use on a high speed computer.

The data, while more consistent than our previous results, indicate a spread of more than an order of magnitude was necessary to completely define the threshold curve.

$$\begin{aligned}\mu &= .1486 \text{ J/mm}^2 \\ \mu + 2\sigma^* &= .5035 \text{ J/mm}^2 \\ \mu - 2\sigma &= .0439 \text{ J/mm}^2\end{aligned}$$

Initiation time = 50  $\mu$ s

With the accumulation of data and its statistical evaluation, the reasons for our large deviations of threshold energy were becoming apparent. First, our assumption that power was relatively constant during these experiments was incorrect. Statistical results became more consistent if approximate values of power levels were injected as a variable along with energy.

The free running laser was giving us unequally spaced spikes of more or less randomly distributed power levels. Also, as the initiation time varied, we could not accurately estimate which portion of the laser train was responsible for the actual detonation. Our new need to know the exact power output of our laser caused us to switch from a free running to Q-switched mode. An exact measurement of power would require knowledge of the time duration of each energy pulse. With our

\*When normalizing the stimulus-response curves for explosives, it is necessary to transpose the stimulus input to a log base.



present equipment exact measurement of such ultra fast pulses ( $< 15$  ns) was impossible. Approximations were used one of which assumed that our newly installed liquid Q-switch was giving a clean single pulse.

The deviation was reduced by use of the Q-switched laser, however we have no accurate estimation of the power. It was discovered during the tests that the Q-switching solution would deteriorate with time and produce several giant spikes. This could introduce considerable error in the data.

$$\begin{aligned}\mu &= .025 \text{ J/mm}^2 \\ \mu + 2\sigma &= .080 \text{ J/mm}^2 \\ \mu - 2\sigma &= .008 \text{ J/mm}^2\end{aligned}$$

$$\text{Initiation time} = < 20 \mu\text{s}$$

It is apparent that the energy threshold is reduced by the increased power of the Q-switched spikes, thus it appears that our thresholds are a function of power as well as energy. Our experiments could not accurately take into account the power relationship.

A good evaluation of the power threshold will require an ultra fast detector as well as a scope of similar rise time. Such equipment is now on order. We also hope to be able to resolve any fine structure associated with the Q-switched pulses, which is beyond the capabilities of our present detection system. If such fine structure exists, a knowledge of its form would improve power estimates.

#### DISCUSSION

It is our contention that the laser detonation of explosives is a function of both power and energy. At this time we cannot fully resolve the power as the rise times are beyond the capabilities of our present

equipment. In the analysis of present data, we get a variation of apparent threshold energies greater than an order of magnitude. We believe that if we were to hold power at a constant value, the energy threshold deviation would be reduced to a reasonable value.

We suspect that if we were to monitor both power and energy in our coverage of the threshold, we would find a normal bivariate distribution of the form.

$$2) \hat{P}(E, P) = \frac{1}{2\pi\sigma_E\sigma_P\sqrt{1-\rho^2}} \iint_{-\infty}^{\infty} \exp\left[-\frac{1}{2(1-\rho^2)}\left(\frac{(E'-\mu_E)^2}{\sigma_E^2} - 2\rho\frac{(E'-\mu_E)(P'-\mu_P)}{\sigma_E\sigma_P} + \frac{(P'-\mu_P)^2}{\sigma_P^2}\right)\right] dP'dE'$$

where  $\sigma_E^2$  is the variance of E,  $\sigma_P^2$  is the variance of P and  $\rho$  is the correlation coefficient between P and E.

The cumulative distribution function of  $\hat{P}$  is of the form of Figure 4. There is a minimum rate of application of energy below which detonation will not take place. Above the threshold, the amount of energy necessary for initiation decreases as power increases. Finally there should be a point where further increase in the rate will not reduce the energy requirement.

We feel we can adapt an analysis similar to the monovariant case to the bivariate distribution to find best estimates of the five parameters involved when power is accurately measured.

An energy-power relationship of this form has been obtained using various sources of power and energy<sup>5</sup> such as stab initiators, hot bridge-wire electric initiators and conductive mix electric initiators.

McGirr<sup>6</sup> made mention of the fact that superfine RDX required about 500,000 ergs to detonate in a capacitor discharge spark sensitivity test, with a capacitor voltage of 100 volts. However, this same explosive required only 22,500 ergs to detonate when the discharge voltage was increased to 300 volts. This seems to be a clear indication that considerably less energy is needed for detonation if the rate of application (power) is increased.

#### CONCLUSIONS

With the experimental work thus far completed, we feel very strongly that the direct initiation of secondary explosives is not only possible, but also very practical. Such a system has potential not only in devices but also in explosive sensitivity analysis as well as experimentation. At this point we do not draw any conclusions concerning the type of initiation mechanism except to note that most of the results in this report would fit into a thermal initiation theory.

Without having gone into any investigations concerning variation of the radiating source such as second harmonic generation, to effect absorption, or any variation of the explosive itself, such as grain size, ambient temperature, or introduction of foreign material, we feel that the initiation of secondary explosives is dependent on both power and energy of the radiating source.

Reliable detonations have been achieved with energy inputs as low as  $.025 \text{ J}/(\text{mm})^2$ . There is no reason to doubt that this value can be reduced since the bivariate distribution predicts lower energy requirements for higher power inputs.

With the ultra fast rise time equipment which we expect to have shortly, we will attempt to define the exact form of this bivariate distribution. The natural course to follow after that would be to investigate some of the many variables mentioned earlier and to see how they effect this distribution.

#### REFERENCES

1. F. P. Bowden and A. D. Yoffe, Initiation and Growth of Explosion in Liquids and Solids, (Cambridge at the University Press, London, 1952).
2. A. D. Yoffe, Proc. Roy. Soc. (London) A 246, 254 (1958).
3. A. Golub and F. E. Grubbs, American Statistical Association Journal, 51, 257 (1956).
4. E. G. Kessler, "Estimation of Bivariate Distribution Parameters from Go, No-Go Data" ESL-IR 427 (to be published March 1969). Picatinny Arsenal.
5. "Explosive Trains", U. S. Army Materiel Command Pamphlet 706-174, March 1965.
6. R. McGirr, "Sensitivity of Explosive to Sparks" Proceedings 5th Symposium on Electroexplosive Devices. (Philadelphia) (1967).

Table I

#### INITIATION ENERGY OF PYROTECHNIC MIXTURE

ENERGY/AREA	DETONATION*
0 - .0037 J/mm <sup>2</sup>	0 0 0 0
.0037 - .0042	0 0 0 0 0 0 0 X
.0042 - .0047	0 0 0 0
.0047 - .0052	0 0 X X X X X X
.0052 - .0057	0 X X
.0057 - .0062	X X
.0062 +	X X X X

$$\mu = \text{mean} = .0053 \text{ J/mm}^2**$$

$$\sigma = \text{standard deviation} = .0015 \text{ J/mm}^2$$

$$\mu + 2\sigma = .0083 \text{ J/mm}^2$$

$$\mu - 2\sigma = .0022 \text{ J/mm}^2$$

\*Each experiment is characterized in the following manner:

X = ignition

0 = no ignition

\*\*For an explanation of the method of calculation see Page 4-1.10

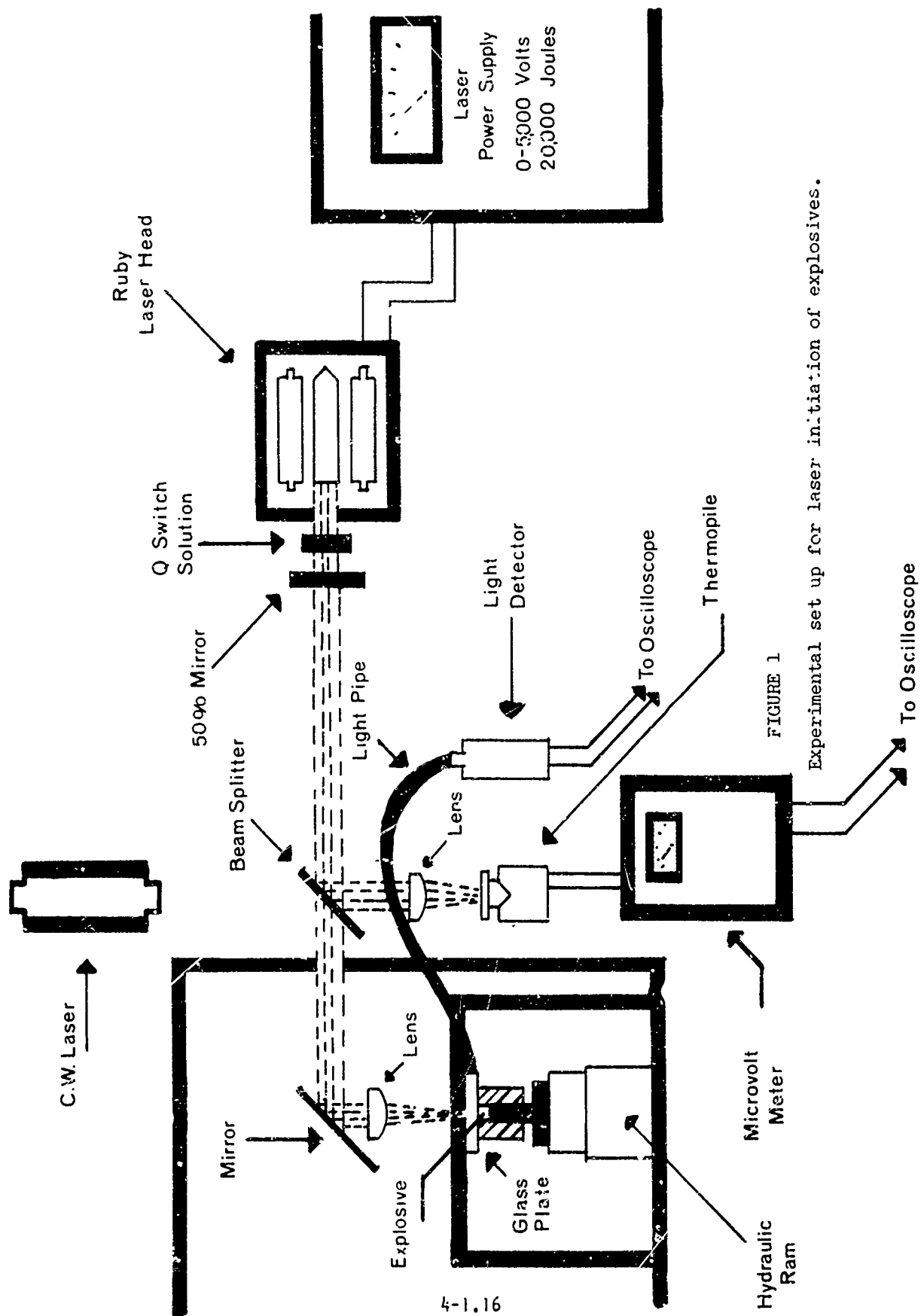


FIGURE 1

Experimental set up for laser initiation of explosives.

FIGURE 2  
LASER OUTPUT

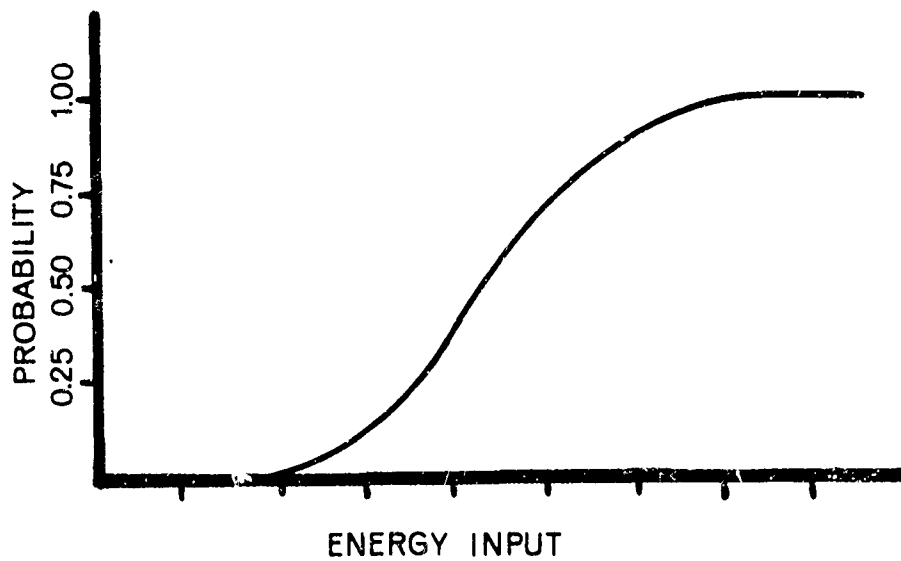
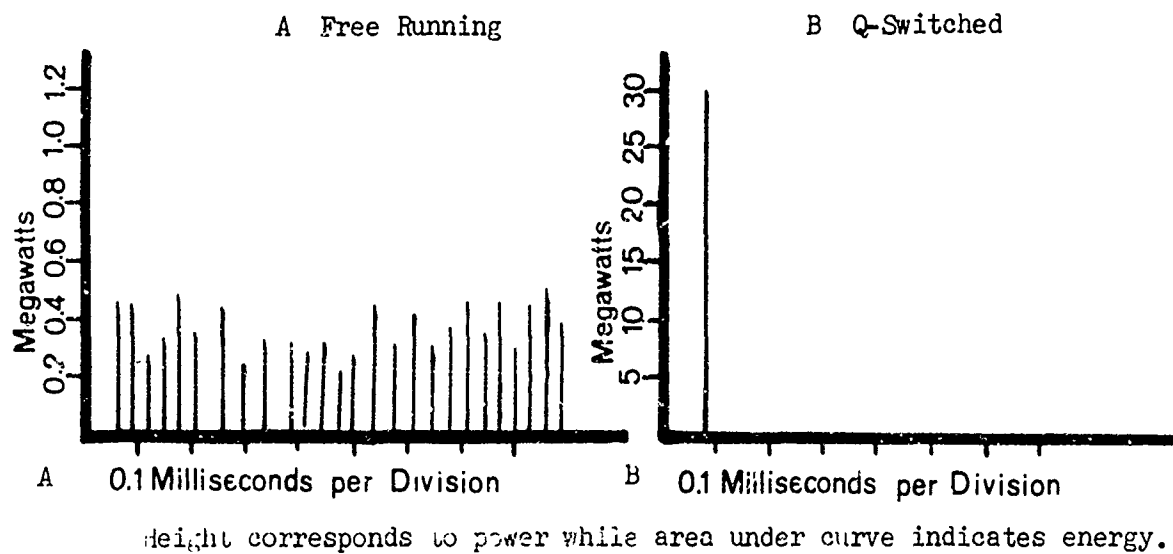


FIGURE 3  
Energy threshold of detonation

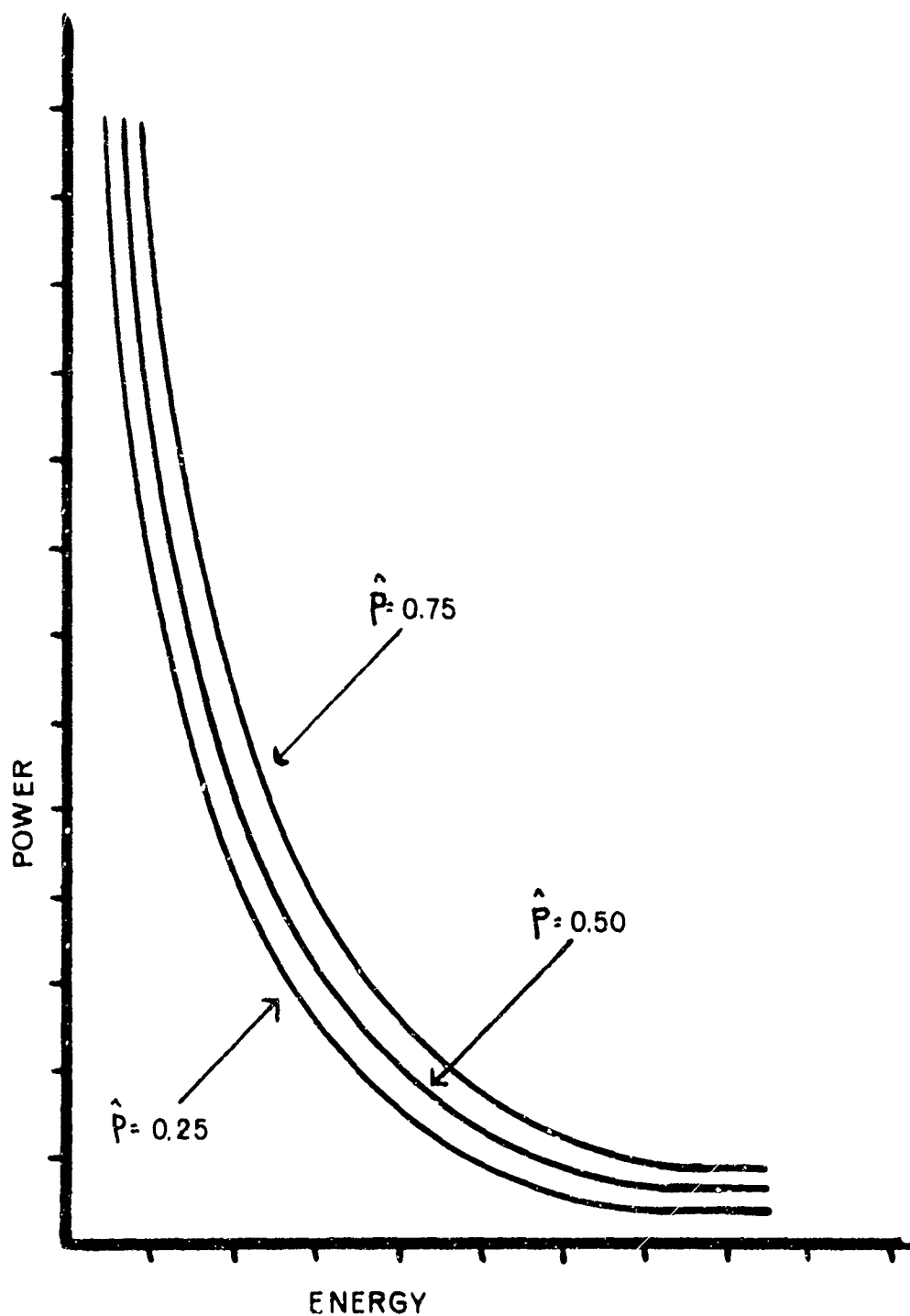


FIGURE 4  
Bivariate probability of initiation

4-1.18

## DISCUSSION

A luminescent plume emanates from a surface impacted with a laser beam. A questioner asked for ways of determining if the observed light output was the result of detonation or this plume and whether the explosive was detonating or deflagrating.

Results of back-up plate examination indicated that the explosive had detonated (this results in a definite indentation with characteristic markings). Without a detonation one sees the laser spike itself on the photocell trace. When detonation occurs, the laser spike is obscured. This indicates strongly that detonation is taking place.

In reply to a question concerning the photocell lens focal length, Mr. Barbarisi indicated that a lens with a 9-cm focal length was used.

With partial switching using a long Q switch, functioning time (delay from arrival of laser light to arrival of explosive light) was on the order of 20 microseconds. A single giant probe resulted in functioning times of less than one microsecond.

The energies per unit area applied to the PETN were on the order of  $10^{-5}$  joules/mm<sup>2</sup>. A good reliable detonation may require as much as 0.02 joules/mm<sup>2</sup>. The spot size used in these experiments was on the order of 0.5 mm<sup>2</sup> and only the center of the beam was used in order to obtain a uniform pattern.

Other agencies reported difficulty in obtaining uniformly intense laser spots. Alignment of the beam generally causes non uniform spots. A good alignment technique and good optical equipment help to eliminate this problem and simplify alignment.

Explosive geometry effects were asked for including sensitivity to initiation and time to detonation. It was stated that originally a weight of 1 gram of PETN was used. This was cut to about 1/4 gram because of damage to components. Other geometry effects have not been investigated.

A comment was made concerning the use of a glass bead at the light explosive interface. The bead acted as a lens, focusing the light on explosive. The direction of the incoming light was not critical. It worked very well.

It was suggested that the explosive materials be pressed into a column contained in a transparent material and that a smear camera be used to determine propagation velocity.



## 4-2 THE DEVELOPMENT OF A SOLID STATE EXPLOSIVE INITIATOR

Robert F. Flagg, Ernest J. Stecker  
and Lewis E. Hollander, Jr.\*

Holex Incorporated  
Hollister, California, 95023

### 1. INTRODUCTION

Since the advent of the first true electroexplosive devices several decades ago, a number of novel techniques for initiating explosives have been proposed. Some of these have had attendant physical limitations and shortcomings which prevented their wide acceptance, others have enjoyed only limited acceptance. A few have received widespread acceptance and make up the bulk of the explosive initiators installed in military, space and commercial explosive systems today.

Generally, up until the early 1960s, the bridgewire electroexplosive device initiated by from a few volts to tens of volts potential, made up the bulk of the electroexplosive devices in use. With the increasing power and number of RFI generating sources, the problem of premature initiation of these devices became acute<sup>1</sup> and alternative methods sought to perform the initiating function. The exploding bridgewire concept sought to avoid this failing, and has been generally successful, except that increased complexity and weight is necessary for most systems. To counter this problem and to recover the original simplicity of the bridgewire, the heat-sinked bridgewire capable of dissipating 1 watt continuously, i.e., the 1 amp, 1 watt cartridge, was developed.<sup>2</sup> We feel the trends presently favor this general approach. However, the exploding bridgewire devices have their supporters and even more complex systems such as the LEED<sup>3</sup> have recently been introduced. While these specialized systems have merit in unique situations and warrant our careful inspection, in our opinion there is, and will be for an indefinite time, a requirement for a simple, low cost, low weight, reliable initiator, capable of being nondestructively tested and operated from existing common power sources without complex interface equipment.

\* Consultant

The solid state (semiconductor) initiator, SSI\*, has these properties. It is basically a standard bridgewire initiator that has had its bridgewire replaced by a small piece of a semiconducting material. The exterior of the SSI appears identical to the standard bridgewired part; however, its electrical and functioning characteristics are markedly different and much improved over the original characteristics.

For example, most conventional bridgewires have a resistance which generally increases with temperature, although some designs use alloys which attempt to maintain an approximately constant resistance. The resistance of the semiconductor element of the SSI has both large positive and negative temperature coefficients, being positive in regions where positive coefficients are advantageous and negative in regions where negative resistance coefficients can be put to advantage. This nonlinear behavior of the resistance is the crux of the SSI.

There are two key parameters of interest to the user of electroexplosive devices. These are the firing threshold condition and the firing time at a given firing signal. For conventional devices a "no-fire" current and an all-fire current are generally specified. These describe the boundary and account for the fact that for the conventional bridgewire part, it is a broad diffuse boundary, rather than a sharply defined one. In contrast, a single value characterizes the fire-no fire boundary of the SSI. The firing time description for both kinds of electroexplosive devices is generally very similar.

## 2. THEORETICAL CONSIDERATIONS

### 2.1 Resistance-Temperature Properties of Semiconductors

The ideal material for the initiating element of an electroexplosive device would have three properties 1, an initial increase in resistance with increasing input power 2, a sharp well-defined maximum and 3, a rapidly decreasing resistance with further increase in power. This immediately suggests a material having two types of conduction, selected by the level of input power. Precisely, this effect can be found in doped semiconductors.

There are two basic types of conduction in semiconductors, intrinsic and extrinsic. Intrinsic conduction

\* U.S. Patent 3,392,576, L. Hollander, July, 1968.

is the thermal activation of carriers from the valence band into the conduction band. This occurs only in very pure specimens of semiconductors where there are no interlying impurity atoms which are activated at temperatures lower than the basic intrinsic band gap of the semiconductor material. Thus the higher the temperature the larger number of carriers that are activated from the valence band to the conduction band, the lower the resistance for the material. The resistivity ( $\rho$ ) of a semiconductor material is given by

$$\rho = (n_e e \mu_e + n_h e \mu_h)^{-1} \quad (1)$$

where  $n_e$  is the number of electrons,  $n_h$  is the number of holes in the valence band,  $e$  is electronic charge, and  $\mu_e$  is the mobility of the electrons, and  $\mu_h$  is the mobility, or drift velocity per unit electric field for the holes. This resistivity has a nearly  $1/T$ , (where  $T$  is the absolute temperature) temperature dependency. The temperature dependence of  $\rho$  will vary as

$$\rho = A \exp (E_g/2KT) \quad (2)$$

where  $E_g$  is band gap of the semiconductor,  $K$  is Boltzman's constant,  $T$  is in absolute temperature. Thus, the larger the band gap, the steeper the temperature dependence of the intrinsic conductivity, which as noted is desirable for the devices discussed here.

The second type of conduction of importance is impurity conduction (extrinsic) where into the basic host lattice are introduced impurity atoms which are either donors (for n-type) which supply excess electrons, or acceptors which supply excess holes (for p-type). Since these acceptor and donor sites are activated by energies far smaller than the basic band gap, they are activated at much lower temperatures by virtue of the fact that the activation energy required is smaller.

It is now apparent that we have two sources of carriers activated at different temperatures. At low temperatures the impurity sites contribute the majority of the carriers and are responsible for the conductivity of the material. As the temperature is raised, all the impurities of the impurity band are used up, and as the temperature is increased further, the carriers from the valence band begin to contribute to conduction. In the region where the carriers from the impurity band are already ionized and in the conduction band but no significant contribution from the valence band has yet been achieved, the mobility,  $\mu$ , plays a major role. This is the region in which we are interested. The mobility has

a temperature dependence in the reverse direction; i.e., the higher the temperature, the greater the lattice vibrations resulting in lower carrier mobility and higher resistance. For example, boron in the silicon lattice has an activation energy of the order of .045 e.v. (electron volts), as shown in Fig. 1, and is almost completely ionized at room temperature. The intrinsic band gap for silicon is 1.106 e.v. Therefore, as the temperature is raised above room temperature, the resistance of silicon, boron doped, will in general rise, as shown in Fig. 2. However, at some point, depending on the density of the boron doping, the intrinsic carriers from the valence band become predominant. Beyond this point, the resistivity drops rapidly with a  $1/T$  temperature dependence. The temperature at which this occurs is precisely fixed by the relationship of the boron doping density and the energy band gap of the silicon lattice. The higher the doping level the higher the temperature at which this inflection takes place. For a practical design, one need only to match the inflection point of the semiconductor material with the ignition temperature of the primer that one wishes to initiate.

It should be noted silicon was selected in the present work primarily because it is readily available, very strong and the processing techniques for it are well developed. In principle, other semiconductors also have promise, but to date none have demonstrated superior all-around performance.

## 2.2 Mathematical Model of the SSI

It is very desirable in any investigation of a new concept to construct a mathematical model of the physical system under study. The complexity of the model need not be great, only of sufficient detail to accurately describe the effects of interest. The model serves three purposes. It provides a focus for understanding the device, it aids in directing the experimental efforts which would otherwise have to rely on intuition, or "cut and try" methods, and most importantly, it provides a tool for design.

Consider the thermodynamic system shown schematically in Fig. 3 consisting of a semiconductor element of length, width and thickness;  $l$ ,  $w$ ,  $d$  respectively, having a volume  $V$  and a mass  $m$ . Electrodes are attached to either end over the entire cross section  $A$  and assumed to have a negligible resistance compared to the resistance  $R$  of the semiconductor element. The junction between the electrode and the semiconductor is assumed ohmic. The resistance of the element

is given from first principles by

$$R = \rho l/wd \quad (3)$$

where  $\rho$  is the resistivity of the material.

The First Law of Thermodynamics requires that the rate of change of the internal energy of the element,  $E_{int}$  be equal to the power input minus the loss power, or

$$m C_p \frac{dT}{dt} = \frac{E^2}{R} - h(T-T_o) \quad (4)$$

The heat transfer coefficient,  $h$ , and the specific heat,  $C_p$ , are assumed constant.

No general solution to Eqn (4) is possible in the present case because of the behavior of  $R(T)$  which can only be represented in a tabular fashion or at best, as an exponential over only a very limited range of temperature. However, special cases are possible and warrant inspection for the insight they allow into the behavior of the SSI.

### 2.3 Steady State Behavior

Under "no-fire" steady conditions, when the temperature,  $T$ , of the semiconductor mass is in a state of equilibrium, the electrical power to the element is just balanced by the power lost through heat conduction. Since time variant terms are absent, the equation describing the system reduces to

$$\frac{E^2}{R(T)} = h(T-T_o) \quad (5)$$

It is important to note that for the SSI, equilibrium at any arbitrary temperature is not possible. For  $h$  constant, and noting that  $T$  has no physical limitations on its maximum, but that  $R(T)$  does have a maximum, it is clear that there is a maximum potential that is permitted under equilibrium conditions, which is given by:

$$E_{to} = \left[ R_o \cdot \frac{R_{to}}{R_o} \cdot h(T_{to} - T_o) \right]^{1/2} \quad (6)$$

This voltage, the maximum voltage that may be applied to the device and steady state conditions obtained, is given the name "turnover voltage." The temperature and resistance ratio corresponding to the turnover condition can be obtained from a knowledge of  $R(T-T_o)$  versus  $T$ . Steady

voltages beyond this value are not possible.

In practice one can expect that at any voltage less than the turnover voltage, the temperature will approach a steady temperature asymptotically and then remain at this temperature indefinitely. If the ignition temperature of the explosive is greater than this value, the part will experience "no-fire."

## 2.4 Dynamic Behavior

The dynamic case is of interest since it enables one to predict the electrical functioning time of the device. Eqn (4) can be nondimensionalized to yield

$$dT/d\bar{t} = Z/(R/R_0) - (T-1) \quad (7)$$

where

$$T = T/T_0$$

$$\bar{t} = t/\tau$$

$$\tau = m C_p / \bar{I}$$

$$Z = E^2 / R_0 T_0$$

Z is effectively a "driving potential function" and is a constant for any given problem. Z<sub>to</sub> is defined as that value of the driving potential which will just cause firing at  $t = \infty$ , i.e., Z evaluated at the turnover voltage.

Z<sub>to</sub> may be evaluated independently of the actual turnover voltage since from Eqn (6) it can be written in terms of  $R_{to}/R_0$  and  $T_{to}/T_0$  directly.

Generally, numerical solutions of Eqn (4) are required since  $R(T)$  data exists only in tabular form. However, closed form solutions are possible for special descriptions of  $R(T)$ , and while they will not give accurate answers that can be used directly in design calculations, they provide insight into the dynamic response, hence are of interest.

For example, consider an ideal case where the resistance temperature characteristics are given by

$$\frac{R}{R_0} = 1 \quad T \leq T_{t0} \quad (8)$$

$$\frac{R}{R_0} = 0 \quad T > T_{t0}$$

The nondimensional dynamic equation reduces to

$$\frac{dT}{dT_{t0}} = 1 + Z - T \quad (9)$$

which may be integrated directly to yield:

$$\bar{T} = \text{Ln} \left[ \frac{Z/Z_{t0}}{Z/Z_{t0} - 1} \right] \quad (10)$$

If losses were negligible, then the terms  $1 - T$  would not appear in Eqn (4) and the equation for the response becomes

$$\bar{T} = \frac{1}{Z/Z_{t0}} \quad (11)$$

Eqn (7) and its corresponding lossless relation were programmed for solution on an IBM 360 computer, using an interpolation scheme for  $R(T)$  based on an exponential fairing of two adjacent points. No particular programming problems occur. Values were obtained for a range of driving functions from  $1.25 Z_{t0}$  to  $6 Z_{t0}$ . The results are shown in Fig. 4.

It can be seen that the nondimensionalized temperature time curves have a negative curvature as a result of the resistance increasing with temperature, up to the turnover temperature. Beyond the turnover temperature the curvature is positive and increasing with temperature and time. At the later stages the curves are nearly vertical, indicating a very rapid deposition of energy into the semiconductor mass as the resistance of the device goes to zero. The curve corresponding to  $Z_{t0}$  is asymptotic to the turnover temperature at  $\bar{T} = \infty$ .

This behavior is to be contrasted to a constant resistance wire which gives a straight line in  $T - \bar{T}$

space or a  $1 + \alpha T$  type resistance wire which gives an negative curvature parabola in this space.

The functioning time versus driving potential curves are shown in Fig. 5.

It can be seen that in the idealized lossless case that  $Z_{t0}$  corresponds to that driving potential which causes turnover at  $t = T$ . Increasing the driving function decreases the amount of time required to function. Since  $Z \propto E^2$ , it can be seen that the functioning time decreases as  $1/E^2$ .

For the idealized lossy cases, the firing time approaches  $\infty$  as  $Z \rightarrow Z_{t0}$ , i.e., as  $E \rightarrow E_{t0}$ . Increasing the driving function results in a marked reduction in firing time and for  $Z \gg Z_{t0}$  the firing time approaches the lossless case as the shorter firing times do not permit losses to be significant.

It can also be seen that the data for real materials, in this case, 0.2ohm-cm silicon, follows generally these two ideal curves.

### 3. COMPARISON WITH EXPERIMENT

#### 3.1 Steady State Experiments

Knowing the resistance-temperature characteristics of the semiconductor material and using the steady state equation, (5), enables one to calculate the voltage-resistance or the voltage-current characteristics of an actual device. This has been done for a typical device and the results appear in Fig. 6. The voltage has been nondimensionalized by the turnover voltage and the resistance by the maximum resistance. Included on the figure is V-R data obtained for several SSI devices.

The data corresponding to the upper part of the curve is obtained by using an adjustable potential power supply. The lower part of the curve can be obtained using an adjustable current supply to limit the current. It can be seen from the figure that the agreement between the predicted and measured voltage-resistance values is good, indicating that the  $R(T)$  values measured for the initial calibration and the  $R(T)$  of the actual device are similar, and that the heat transfer coefficient is indeed nearly constant. As the semiconductor material that was used in these tests was "off the shelf" grade with a very wide tolerance in resistivity  $\pm 25\%$ , this variation is understandable. For production, resistivity



tolerance can be narrowed significantly with only minor increase in cost.

This particular property, the predictability of the V-R curve, provides a nondestructive means of determining the turnover voltage from a simple single point test, by measuring the voltage and resistance ratio at one point and knowing the shape of the curve.

For example, consider Eqn. (5) evaluated at the turnover point and at some test potential less than the turnover voltage. Taking the ratio of these two values yields

$$\frac{E_{to}}{E_{test}} = \left[ K \cdot F \left( \frac{R}{R_0} \right) \right]^{1/2} \quad (12)$$

where

$$K = \frac{R_{to}}{R_0} \cdot (T_{to} - T_0)$$

and

$$F \left( \frac{R}{R_0} \right) = \frac{R_0}{R} \cdot (T - T_0)^{-1}$$

K is a constant and is known from a "calibration" of the semiconductor material. F can be evaluated from a knowledge of R(T).

Some typical predicted and measured values are given in Table 1 from which it can be seen that the turnover voltage can be predicted within a few percent.

An instrument\* that determines the turnover voltage automatically, which has been developed at HOLEX for field and laboratory use, is the subject of a separate report. This instrument operates on a somewhat different principle than given here, but produces the same result.

### 3.2 Dynamic Measurements

The parameters which control the firing time are the heat transfer coefficient, the mass of the element, and the driving potential. Decreasing the mass of the element reduces the time, since there is less material to

---

\* Pat. Pending

be raised to the turnover temperature. The firing time decreases approximately as  $(E/E_{t0})^2$ , except near the turnover voltage, where the time approaches infinity as the firing voltage approaches the turnover voltage from above.

In principle, firing time can be predicted from a knowledge of  $E/E_{t0}$ ,  $\Phi$  and  $m$ . The turnover voltage and heat transfer coefficient can be determined, using the steady state procedures previously noted. The mass of the chip can be accurately determined by direct measurement.

Measured and predicted firing times for typical devices are included in Fig. 5. It is seen that the measured electrical functioning times are generally longer than the predicted values, but having the same general behavior and trends as the predicted values. The discrepancy is that the present heat transfer representation does not account for transient effects. Recall that in the model,  $\Phi$  is assumed constant. In reality there are two components to the heat transfer, a transient component and a steady component. Since the "transient heat transfer coefficient" is initially added to steady state coefficient, losses are greater and the time to reach the turnover temperature will be proportionately longer. However, in the present simplified analysis, the trends are properly represented, only the absolute values are in error.

This same general type of transient behavior is observed in transistors,<sup>7</sup> a near-neighbor of the present device, and for them allows a higher power rating for pulse duty than for steady state duty. It should also be appreciated that for the SSI, the total firing time is made up of the electrical functioning time, plus a chemical time which accounts for the finite length of time it takes for the chemistry to progress. Detailed measurements indicate that of the total function time, approximately 30% is due to the chemistry.

#### 4. QUALIFICATION TESTS

Detonators embodying the principles set forth in the previous sections have been designed and manufactured. The detonators, shown in Fig. 7, are presently being tested according to MIL-23659, and to date have passed with no problems. It would be appreciated that this particular specification was written for the standard 1 watt-1 ohm bridge and EBW devices, hence some

of the specifications had to be modified to accommodate the SSI. However, the spirit of the specification is being religiously respected.

The initiators have been "no-fire" tested by applying 0.8 of the turnover voltage for a period of one hour. The measured resistance change was 1.5%, which is approximately the noise level of the instrumentation used. Other units were given 2000 cycles of 0.8  $E_t$  15 seconds on--15 seconds off, with the same result. The chip temperature of this condition was approximately 300°C. The units functioned normally when fired at 2  $E_t$ .

## 5. CONCLUSIONS

The above theoretical and experimental study has given the physical basis of the solid state initiator, SSI, and demonstrated that practical devices can be made which embody these physical principles.

It has been shown that the use of semiconductor material permits a great latitude in bridgewire resistance and in locating the fire-no fire boundary, as well as a high degree of accuracy in defining that boundary.

This will permit devices whose electrical characteristics are optimized to minimize EMI and/or to allow optimum matching to existing power supplies, be they 1 volt or 100's of volts.

Further, it has been demonstrated that the turnover voltage, i.e., the "fire-no fire" boundary, can be accurately predicted using nondestructive techniques. Presently firing times can be predicted up to an empirical constant, which reflects our present ignorance of the transient heat transfer coefficient. However, a more accurate determination of the transient heat transfer should permit much better accuracy. Present efforts at HOLEX are directed to this end.

# REFERENCES

1. Proceedings of the HERO Congress, Franklin Institute, May, 1961.
2. Stecker, E. J. Susceptibility of Electrically Fired Parts, Proceedings of the HERO Congress, Franklin Institute, May, 1961.
3. Lewis, D. Laser Energized Explosive Device System, Proceedings of the Fifth Symposium Electroexplosive Devices, Franklin Institute, June, 1967.
4. Pearson, G. K. Bardeen, J. Electrical Properties of Pure Silicon Alloys Containing Boron and Phosphorus, Phy. Rev., Vol. 75, pp. 865-883, 1949.
5. Chapman, P. W. Tufte, O. N. Zook, J. D. Long, D. Electrical Properties of Heavily Doped Silicon, J. Appl. Phys., Vol. 34, pp. 3291-3295, 1963.
6. Runyan, W. R. Silicon Semiconductor Technology, McGraw-Hill, 1965.
7. Gutzwiller, F. W. Sylvan, T. D. Power Semiconductor Ratings Under Transient and Intermittent Loads, Communication & Electronics Journal, AIEE, Jan. 1961.

TABLE 1 Comparison of Measured and Calculated Turnover Voltages

R <sub>0</sub> (ohms)	E <sub>to calc</sub> (volts)	E <sub>to meas</sub> (volts)
92	23.2	23 ± 0.5
45	17.6	18 ± 0.5
49	18.0	18 ± 0.5
49	20.9	21 ± 0.5
49	21.5	20.5 ± 0.5
47	22.2	21.5 ± 0.5
29	13.6	14.2 ± 0.5

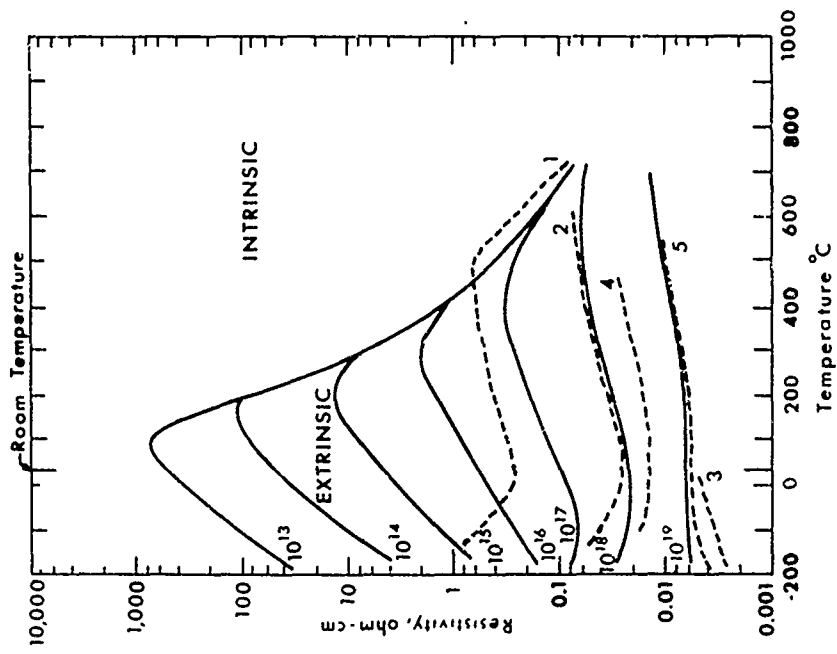


Figure 2. Resistivity versus Temperature for n-type Silicon. Solid lines are calculated values for Sb-doped silicon. Dashed lines are experimental: (1)  $1 \times 10^{17}$  phosphorus; (2)  $1.3 \times 10^{18}$  phosphorus; (3)  $1.7 \times 10^{19}$  phosphorus; (4)  $1.7 \times 10^{18}$  arsenic; (5)  $1.1 \times 10^{19}$  arsenic. (from Ref 6)

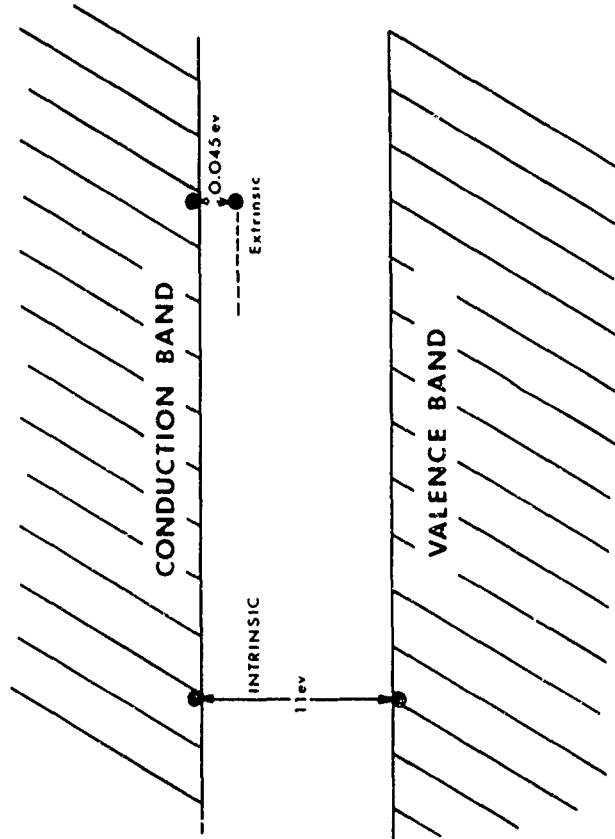


Figure 1. Energy band diagram for P-type Silicon doped with Boron.

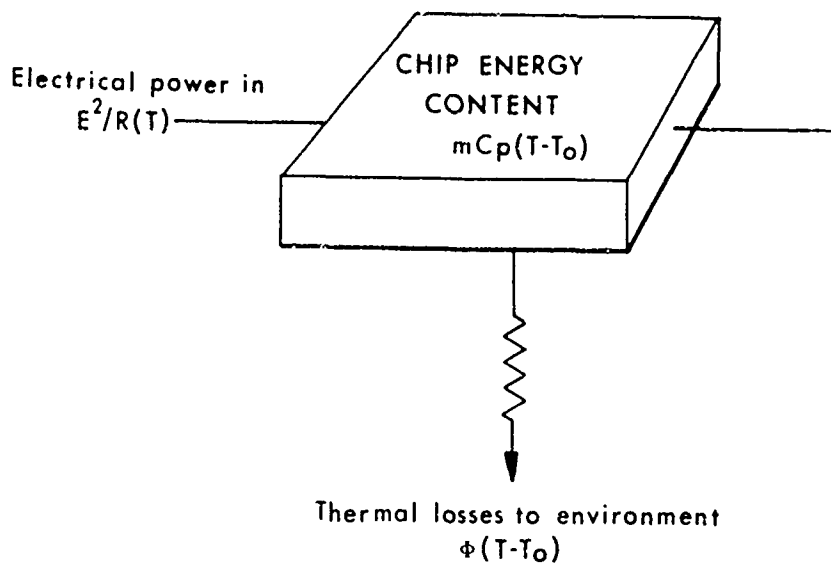


Figure 3. Schematic of the Thermodynamic System.

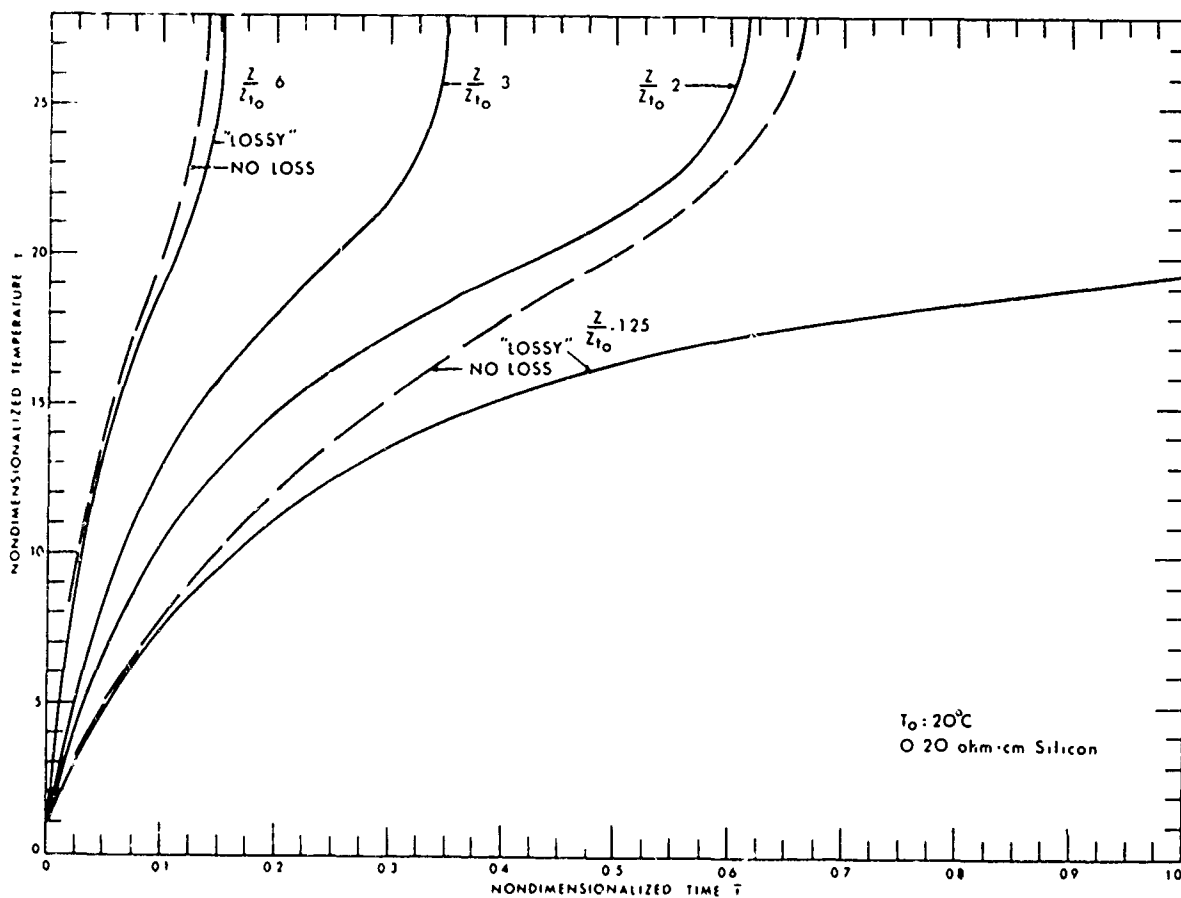


Figure 4. Nondimensionalized Temperature versus Nondimensionalized Time.

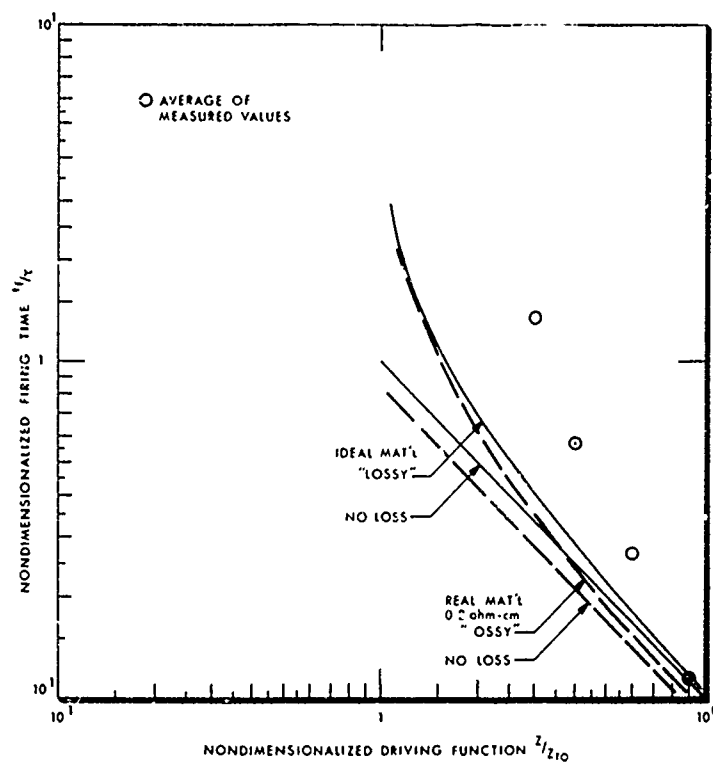


Figure 5. Nondimensionalized Firing Time versus Nondimensionalized Driving Function.

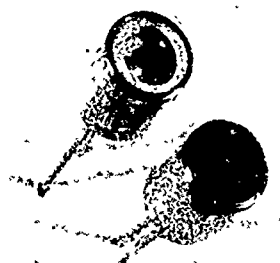


Figure 7. Views of the Halex Solid State Initiator (SSI).

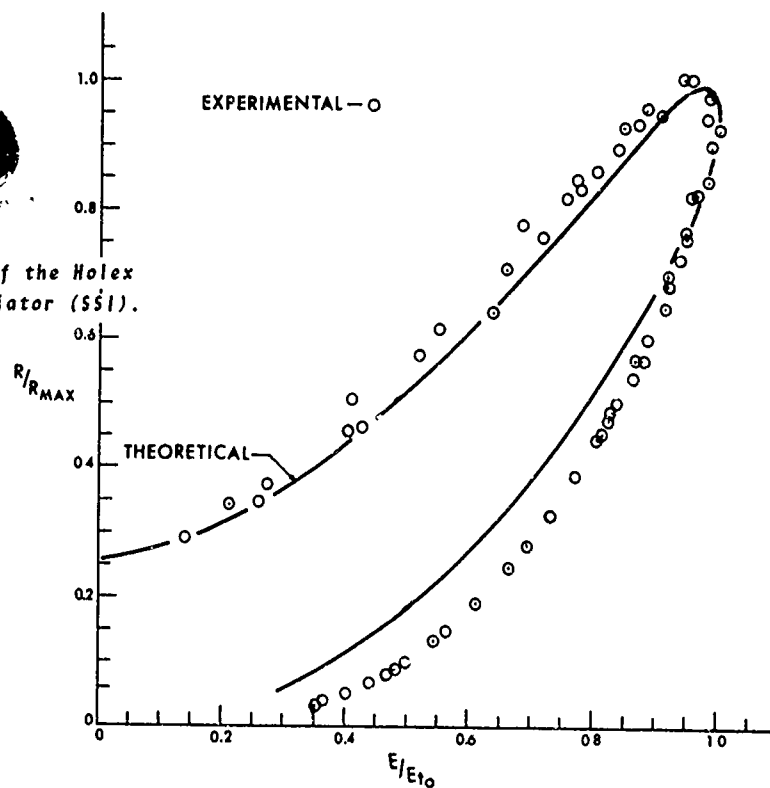


Figure 6. Resistance versus Voltage Steady State.

## DISCUSSION

The firing of the solid state initiators (SSI) which have a negative resistance characteristic in parallel may cause one squib to take more than its share of power. A circuit composed of a couple of capacitors, perhaps separated by diodes, which prevent one from feeding back to the other after the fashion of an ionization probe which is used for measuring detonation velocity, may be the answer according to Mr. Flagg of Holec Corp.

The SSI's are very temperature dependent and the turnover voltage will change with temperature, also the fire-no-fire boundary will shift with temperature, as is true with conventional EED's. The turnover voltage at a particular temperature can be determined by actual measurement at the temperature in question.

The resistance-voltage characteristics of the SSI can also be presented as resistance-current. The SSI appears to act as a current limiter.

The SSI can be designed for use with almost any chosen power supply, but at the moment are made compatible with a 28-volt source. If the supply is overpowered (100 volts) the functioning time would decrease.

The nondestructive tests will not detect whether the primary explosive is in contact with the semiconductor element. The bulk of the heat transfer is through the leads, so any change in heat transfer due to the explosive mix in contact with the semiconductor material cannot be seen.

The turnover voltage is independent of the functioning time. The units discussed in this paper have the following characteristics:

1. designed for 28-volt power supplies;
2. cold resistance of 50 ohms;
3. 0.2 ohm-cm material; and
4. functioning time less than 20 millisecond at 28 volts.



4-3 EFFECT OF REDUCED AMBIENT PRESSURE ON THE  
HOT WIRE SENSITIVITY OF PRIMARY EXPLOSIVES,  
METAL-OXIDANT MIXTURES, AND BLACK POWDER

Howard S. Leopold

U. S. Naval Ordnance Laboratory  
White Oak, Silver Spring, Maryland

INTRODUCTION

The high altitude use of electroexplosive devices (EED's) in the Polaris and other missiles and the increasing amount of vacuum chamber experiments have created another pressure environment for Navy EED's. Previously, EED's were designed to function at tropospheric pressures\* or the higher pressures of various ocean depths. To overcome any possible low pressure effects, hermetically sealed EED's are usually employed so that the hot wire/explosive interface is not exposed to the reduced pressure. The possibility of air leakage out of defective hermetically sealed devices and reports of both decreased and increased EED sensitivity under vacuum conditions made it advisable to examine in greater detail the effect of reduced pressure on the hot wire sensitivity of initiating materials.

EXPERIMENTAL METHOD

The explosive material under test was loaded into an aluminum charge holder force-fitted onto a standard two-pin

\*Sea level up to 7-10 miles from earth's surface.

phenolic initiator plug, as shown in figure 1. The initiator plug had been previously bridged with a 1-mil diameter nichrome wire.

The loaded initiator plug was mounted in a test chamber as shown in figure 2. The test chamber was fitted with a transparent plastic window so that the intensity of the explosive flash could be observed. The test chamber was pumped down by a two-stage vacuum pump to the desired vacuum test range of 5-15 microns and a McLeod gauge was used to measure the pressure. The vacuum test range used corresponds to an altitude of 80 kilometers or 260,000 ft. as shown in figure 3. The pump down of the test chamber and measurement of the vacuum usually required 3 to 5 minutes, which is the duration of the explosive or pyrotechnic exposure to the chamber conditions.

Bruceton tests were used to determine the mean firing energy.<sup>1</sup> When paired Bruceton tests were run, such as a comparison of the explosive hot wire sensitivity under ambient and vacuum conditions at the same loading pressure, the tests were made by first firing 10 shots under vacuum conditions and then 10 shots under ambient conditions with the procedure repeated until the two Bruceton tests were completed.

## EXPERIMENTAL RESULTS

### Zirconium/Potassium Perchlorate Mixtures

To test the effect of vacuum on the hot wire sensitivity of fuel/oxidizer mixtures,  $\text{Zr/KClO}_4$  was used. This mixture is typical of mixtures being used by commercial producers to obtain 1-amp/1-watt no fire electroexplosive devices.

Zirconium in the subsieve size state is an easily ignited fuel. In this fine size it will ignite at a temperature of 180-200°C in air.<sup>2</sup> Larger size zirconium particles will generally require higher temperatures. Potassium perchlorate shows incipient decomposition at 400°C, melts at 588°C, and decomposes rapidly above 600°C.<sup>2</sup> Ellern has reported that in pairing an active fuel with an inactive oxidizer, the fuel determines essentially the ignition point.<sup>2</sup> The energy required for hot wire ignition of  $\text{Zr/oxidizer}$  mixtures has been found to be relatively independent of the type of oxidizer, agreeing with Ellern's statement.<sup>3</sup>

Five  $\text{Zr/KClO}_4$  compositions ranging from fuel poor ( $\frac{1}{3}$  and  $\frac{2}{3}$  amount of stoichiometric fuel) to stoichiometric (chemically balanced) to fuel rich ( $1\frac{1}{3}$  and  $1\frac{2}{3}$  amount of stoichiometric fuel) were prepared by dry tumbling  $\text{Zr(JAN-Z-399A, } 3\pm 1 \text{ micron average diameter)}$  and  $\text{KClO}_4 (< 44 \text{ microns})$ . These mixes were pressed into the charge holders at 10,000 psi, a commonly used loading pressure.

Figure 4 shows the results of fifty shot Bruceton tests run to determine the mean firing energy and dispersion under both ambient and vacuum conditions. In general, more energy is required for ignition under vacuum than under atmospheric conditions, with the least amount of additional energy required with the stoichiometric composition. Mixtures differing the most from stoichiometric require more energy for ignition under both vacuum and ambient conditions. It is believed that the higher energy needed for the ignition of the  $1\frac{2}{3}$  fuel rich mixture is due to the higher concentration of zirconium which rapidly conducts heat away from the wire/mixture interface. The heat is dissipated throughout a larger mass of the mixture, thereby requiring greater energy input to reach the ignition temperature. On the extreme fuel poor side, the volume of fuel (zirconium) in the mixture is now fairly low (~ 15%) and more difficult to ignite. The dispersion of the energy required for igniting the mixtures is much higher than the dispersion for single primary explosives. The  $\frac{1}{3}$  fuel poor mixture had very poor pressing properties and an extremely large energy dispersion probably due to movement of the mixture when exposed to vacuum. The other mixtures had good pressing properties and stayed intact under the test conditions.

It is believed that when  $\text{Zr/KClO}_4$  mixtures are fired under ambient conditions, the Zr can initially react with

the interstitial air in the voids of the mix. A possible explanation for the greater energy requirement under vacuum conditions where interstitial air is not present is that additional energy is required to decompose the  $\text{KClO}_4$  so that it can furnish the necessary oxygen for ignition. The results are indicative only of the energy required for ignition and not indicative of the strength of the ensuing propagation which appears to be much weaker under vacuum conditions. Russian investigators have found the ignition of stoichiometric  $\text{Zr/KClO}_4$  pellets under vacuum conditions results in the reaction of only 10% of the  $\text{Zr}$ .<sup>4</sup>

Extreme care should be taken if extrapolations are made from the test results to other fuel/oxidizer combinations. The reported results are for short term exposure to vacuum. If the vapor pressures of the mixture constituents differ widely, long term exposure could result in drastic changes in composition. The results reported should be typical of an active metal fuel paired with a fairly inactive oxidizer. If the fuel is a poor conductor instead of a metal, an energy increase under vacuum conditions may not be observed.\* If there is specific interest in the use of an active metal/oxidizer composition under vacuum conditions, various loading pressures should be investigated to determine if a loading pressure effect also exists.

---

\*See Basic Lead Styphnate results.

### Primary Explosives

Figure 5 shows the results of fifty shot Bruceton tests with four different primary explosives under both atmospheric and vacuum conditions. The explosives were loaded at 10,000 psi. Both styphnate explosives appear to require less energy under vacuum conditions, while both azides appear to require more energy under vacuum conditions.

Additional Bruceton tests were run at different loading pressures to further examine the sensitivity changes. Dextrinated lead azide and basic lead styphnate (BLS) were used for the additional tests since these two explosives exhibited the largest sensitivity change of each type of explosive.

### Basic Lead Styphnate

Figure 6 shows the Bruceton test results with BLS. The sensitivity of the BLS remains fairly constant under atmospheric conditions as the loading pressure is varied.\* Under vacuum conditions, the decrease in initiation energy is greatest at the lower loading pressures where the most voids are present. The sensitization effect disappears at the high loading pressure with approximately the same amount of energy required as under atmospheric conditions.

The following hypothesis is offered as an explanation for the decreased ignition energy of BLS under vacuum conditions when abundant voids are present. The bridgewire when heated by the electrical discharge under ambient

---

\*Previous unpublished experiments with normal lead styphnate (NLS) have shown the same effect.

conditions can transfer heat to the initiator plug, explosive particles, and interstitial air as shown in figure 7. Under vacuum conditions, heat can only be transferred to the initiator plug and explosive, since a vacuum cannot conduct heat. This results in a greater heat transfer efficiency to the explosive. Since the difference between ambient and vacuum can be readily observed with Bruceton testing, it appears that air can remove a portion of the heat from the bridgewire which is not utilized in the explosive ignition.

To partially confirm the hypothesis offered, further Bruceton tests were run with BLS in an atmosphere of helium which has a lower heat capacity than does air and in an atmosphere of sulfur hexafluoride which has a higher heat capacity than does air. The BLS was loaded in the initiator plug at 10,000 psi. The test results are shown in Table 1. The 50% firing energy appears to vary with the heat capacity of the gas. E. Jones has shown that as the excitation time approaches zero, (such as we might observe with a capacitor discharge) the quantity of heat absorbed presumably varies with the thermal capacity of the gas (if the gas is thermally stable).<sup>5</sup> With longer excitation times, the diffusibility of the gas becomes more important and the heat loss should vary with the thermal conductivity of the gas. The results support the original hypothesis. It is believed that this

effect was not observed with the  $\text{Zr/KClO}_4$  mixtures because the thermal conductivity of Zr is approximately 1000 times greater than that of air, making any heat transfer through air negligible in comparison.

#### Lead Azide

Bruceton tests were conducted with milled dextrinated lead azide over the same loading range used for the BLS. As shown in figure 8, less initiation energy is required as the loading pressure is increased. Stregau and Rowe<sup>6</sup> have reported this effect for PVA, Service, and dextrinated lead azide and also for silver azide. Under vacuum conditions, the same decrease in initiation energy is observed as the loading pressure is increased. The extra initiation energy required under vacuum conditions diminishes as the loading pressure is increased.

Lead azide, though also a fairly poor conductor like the styphnates, exhibits an opposite effect from the styphnates in that it requires more energy under vacuum than under ambient conditions. It appears that whatever the operative mechanism, it is strong enough to outweigh the air heat loss factor. Investigative tests eliminated the possibilities of a catalytic effect of oxygen or air upon the decomposition of lead azide, loss of a sensitizing volatile component under vacuum conditions, and azide crystal strains as possible causes of the observed phenomenon. This led to the following



hypothesis as a common explanation to account for the dual phenomena of both increased hot wire sensitivity at higher densities and the decreased hot wire sensitivity under vacuum conditions. It is an extension of Yoffee's explanation for the decomposition of liquid azides under vacuum conditions.<sup>7</sup> In lead azide the burning stage is absent with detonation commencing almost immediately. If the decomposition of lead azide is examined on an expanded time scale before detonation commences, the following phenomena occur:

- 1) Heat from the hot wire raises azide electrons to a conduction band  $N_3^- \rightleftharpoons N_3 + e$
- 2) These electrons combine with lead ions to form lead nuclei  $Pb^{++} + 2e \rightarrow Pb$
- 3) The azide radicals form nitrogen molecules in an exothermic reaction  $2N_3 \rightarrow 3N_2 + 232 \text{ K cal}^{(8)}$

The nitrogen molecules formed are quite hot and energetic. It is believed at the lower loading densities where the interstitial spaces are quite numerous, these hot molecules can rapidly move away from their origin at the wire/lead azide interface. See figure 9. As the density of the lead azide is increased and the interstitial spaces and paths become less numerous, the diffusion of the hot molecules is hindered. The extreme case might be a small closed air pocket, where the hot wire in addition to heating adjoining lead azide crystals, also heats the air, creating a slight

pressure rise which tends to momentarily restrain the nitrogen molecules keeping them close to the crystal surface. Some restraint of the hot nitrogen molecules assists in the transfer of part of their energy to the decomposing crystals, accelerating the decomposition. Though this might first appear to be in contradiction to LeChatelier's Principle, experiments on ignition temperatures and thermal decomposition have shown there is only a small pressure coefficient for pressures as high as 25,000 atmospheres.<sup>8</sup>

It is believed that the reason more energy is required for initiation under vacuum conditions is that there are no gaseous molecules to restrict the movement of newly formed nitrogen molecules away from their formation sites. Hence more energy is required to produce a faster initial decomposition so that sufficient hot nitrogen molecules will remain in situ to accelerate the decomposition. It appears that though the primary mechanism for initiation of the azides is thermal, there is a very definite secondary gaseous effect. This effect manifests itself in the increased sensitivity at higher loading pressures and in the decreased sensitivity under vacuum conditions.

#### Black Powder

Black powder is occasionally used as an initiating agent. It requires much higher initiation energies than needed for

the commonly used primary explosives. Bruceton type and Probit type tests were run under vacuum and ambient conditions with black powder meal (finest granulation available) loaded directly on the bridgewire as shown in figure 10. Note that less initiation energy is required for black powder, a material whose burning rate is pressure dependent, as the loading pressure is increased. Under ambient conditions, the energy dispersion is quite high and a forceful ejection of red sparks is observed when firings occur. When fired under vacuum conditions more energy is required for initiation, the energy dispersion decreases considerably, and the combustion is weaker appearing as a blue flash. A blue flash was considered the criterion for a fire under vacuum conditions.

The initiation of a 3 component mixture such as black powder ( $\text{KNO}_3/\text{C}/\text{S}$ ) is considerably more complicated than a single explosive. Though the actual mechanism of initiation and burning is still obscure, the main functions of each mix ingredient are known. The  $\text{KNO}_3$  is the oxygen producer and the C is the main combustible material. The S makes the powder more readily inflammable and forms K-S complexes, preventing part of the  $\text{CO}_2$  evolved from forming potassium carbonate and reducing the amount of gas evolved.

It is well known that the burning rate of black powder is pressure dependent and the performance below one atmosphere

pressure is poor - decreased light output and considerable unburnt residue are observed.<sup>9</sup> It has also been observed that increasing pressure lowers the delay to ignition by a hot wire.<sup>9</sup> It is interesting to compare the increased sensitivity of black powder as the loading pressure is increased to that of the azides for which a pressure dependent initiation has also been postulated.

More energy is required under vacuum conditions for black powder and lead azide as would be expected for a pressure dependent initiation. However, there is a difference between the black powder and lead azide in that the vacuum and ambient initiation energy of lead azide tend to converge as would be expected with higher loading pressures while those of black powder tend to diverge. It appears that the initiation energy curves obtained for black powder under ambient and vacuum conditions should not be compared too closely since different reactions occur under each condition. The red sparks observed under ambient conditions are typical of a carbon combustion with all 3 components reacting, while the blue flash observed under vacuum conditions is probably indicative of a reaction dominated by  $\text{KNO}_3$  combining with the more inflammable S.

#### SUMMARY

In summary, the most important practical implication is that there is no drastic change in the 50% firing energy

for styphnates and azides between atmospheric conditions and vacuum at practical loading pressures. Trouble would only be expected when marginal firing units are used with azides. Firing reliability using marginal firing units would actually be increased with styphnates under vacuum conditions. Multi-ingredient initiating materials such as fuel/oxidant mixtures or black powder, which require an oxygen transport mechanism for functioning, are poor materials for use under vacuum conditions.

This work was supported by the Naval Ordnance Systems Command.

#### REFERENCES

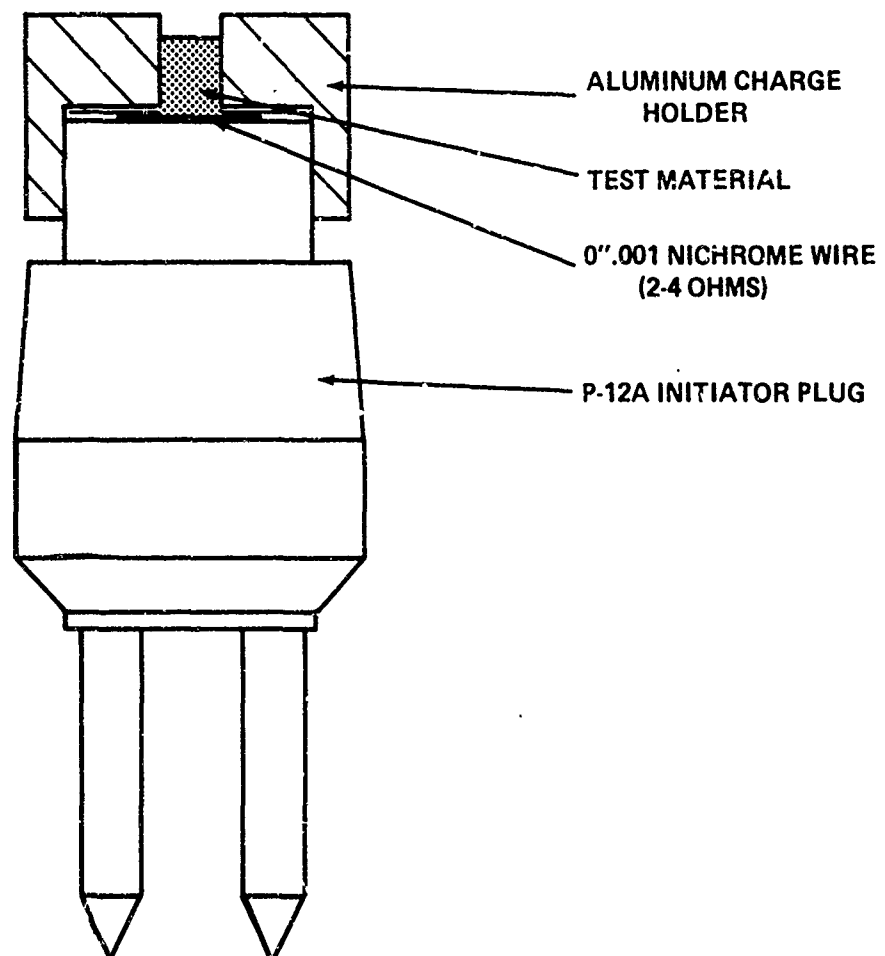
1. "Statistical Analysis for a New Procedure in Sensitivity Experiments", AMP Report No. 101.1R SRG-P, No. 40, 1944; a report submitted by the Statistical Research Group, Princeton University
2. Ellern, H. "Modern Pyrotechnics" Chemical Publishing Co., Inc., New York 1961
3. Summary Report No. 3 Contract NORD 13466 Task 2, 1 Jan 1958 to 30 April 1961, Universal Match Corp., St. Louis, Mo. (Confidential)
4. Pokhil, P. F. and Romodanova. L. D., "Zhurnal Fizicheskay Khimni", V39, no. 11, 1965, 2757-2759
5. Jones, E., "Heat Transfer in Hot Wire Ignition" Fourth Symposium on Combustion, p. 151, Williams and Wilkins Co. Baltimore, 1953
6. Stresau, R. and Rowe, M. H., "Observations of the Effects of Loading Density on the Initiation and Growth of Detonation in Azides", Proceedings of Electric Initiator Symposium 1960 (Confidential)
7. Yoffee, A. D., "Thermal Decomposition and Explosion of Azides", Proc. Royal Soc. A208 (1951) 188
8. Bowden, F. P., and Yoffee, A. D., "Fast Reactions in Solids", Butterworths Scientific Publications, London 1958
9. Blackwood, J. D. and Bowden, F. P., "The Initiation, Burning, and Thermal Decomposition of Gunpowder", Proc. Roy. Soc. A213 (1952) 285

Table 1

Effect of Atmosphere on 50% Firing Energy of BLS

Atmosphere	Heat Capacity (STP)	50% Firing Energy (ergs)	Sigma (log units)
Vacuum	---	13,310	0.019
Helium	$0.21 \times 10^{-3} \text{ cal/cm}^3/^{\circ}\text{C}$	14,370	0.035
Air	$0.35 \times 10^{-3} \text{ cal/cm}^3/^{\circ}\text{C}$	14,590	0.013
Sulfur hexafluoride	$1.03 \times 10^{-3} \text{ cal/cm}^3/^{\circ}\text{C}$	14,910	0.016

**FIGURE 1**  
**INITIATOR PLUG ARRANGEMENT**



**FIGURE 2  
TEST CHAMBER**

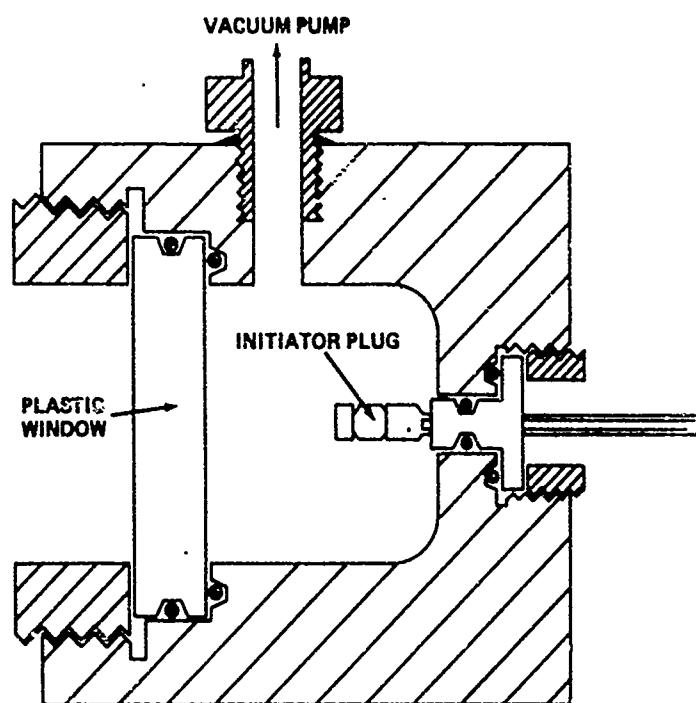


**FIGURE 3  
PRESSURE VS. ALTITUDE**

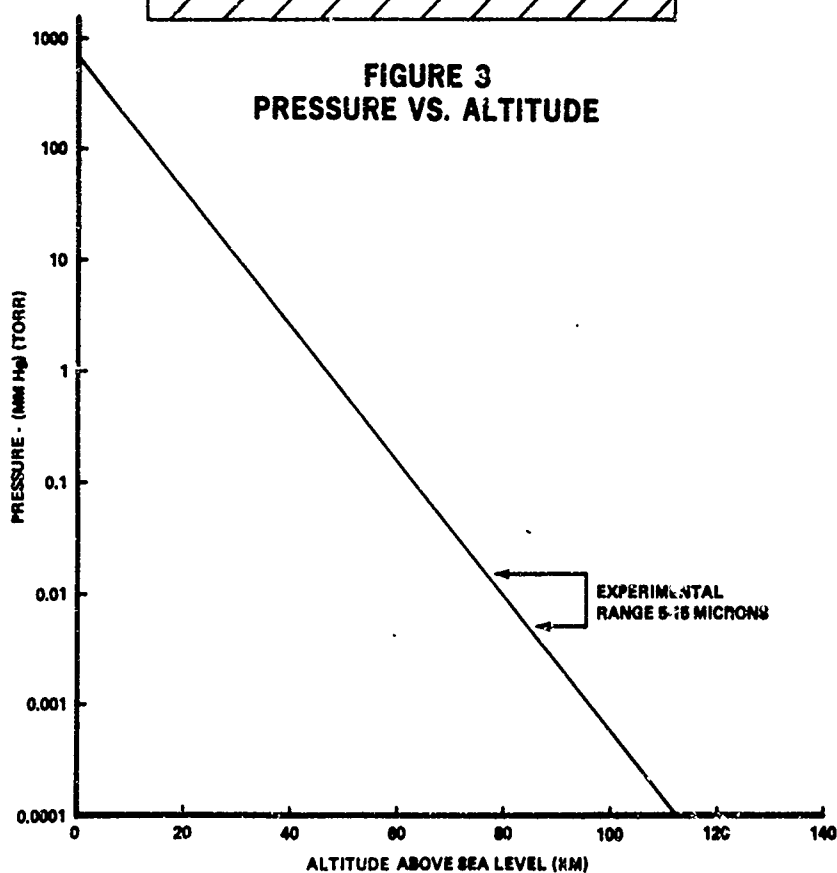
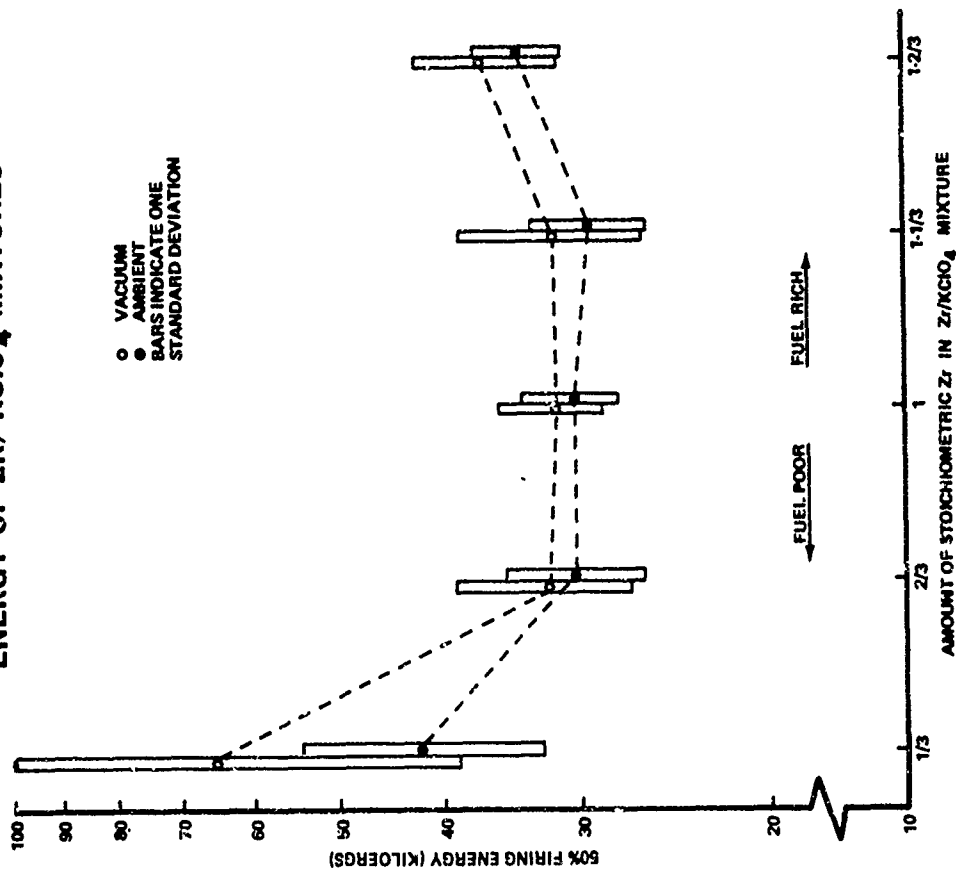




**FIGURE 4**  
EFFECT OF VACUUM ON 50% FIRING  
ENERGY OF ZR/KCIO<sub>4</sub> MIXTURES



4-3.17

**FIGURE 5**  
EFFECT OF VACUUM ON 50% FIRING  
ENERGY OF SEVERAL PRIMARY EXPLOSIVES

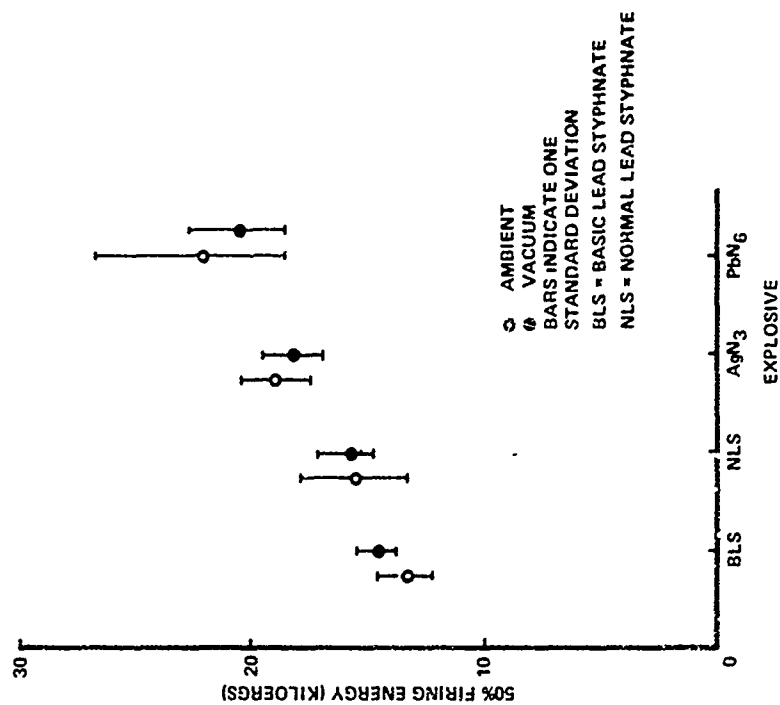


**FIGURE 7**  
**HEAT LOSS FROM BRIDGEWIRE**

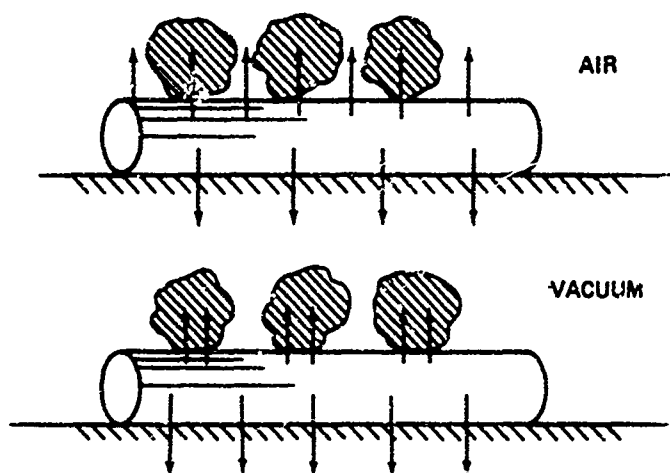


**FIGURE 6**  
**EFFECT OF LOADING PRESSURE ON**  
**50% FIRING ENERGY OF BASIC LEAD**  
**STYPHNATE IN AIR AND VACUUM**

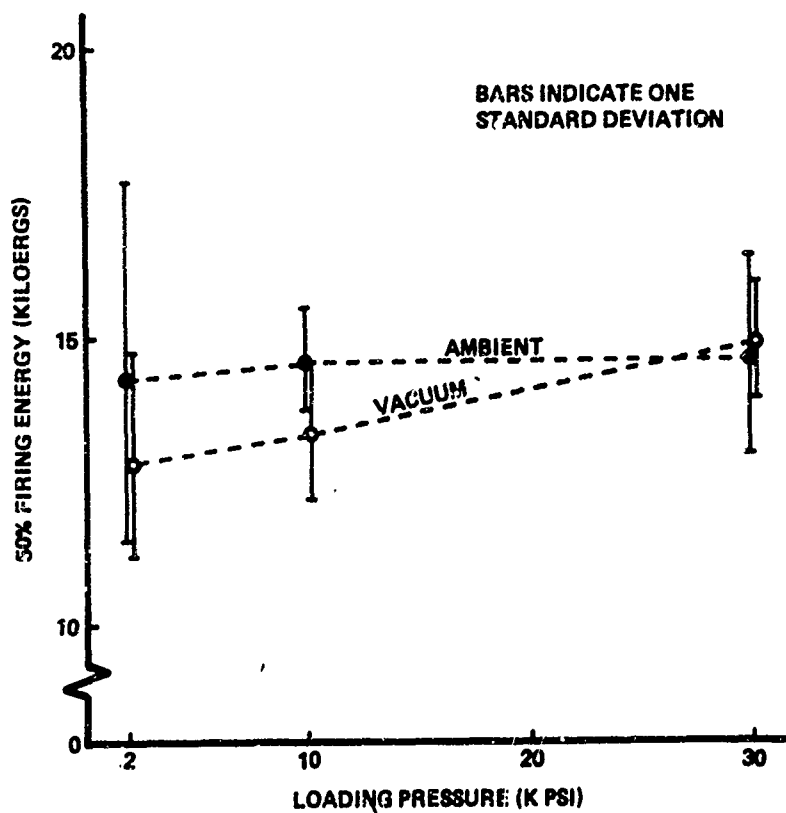


**FIGURE 8**  
**EFFECT OF LOADING PRESSURE ON**  
**50% FIRING ENERGY OF MILLED DEXTRINATED**  
**LEAD AZIDE IN AIR AND VACUUM**

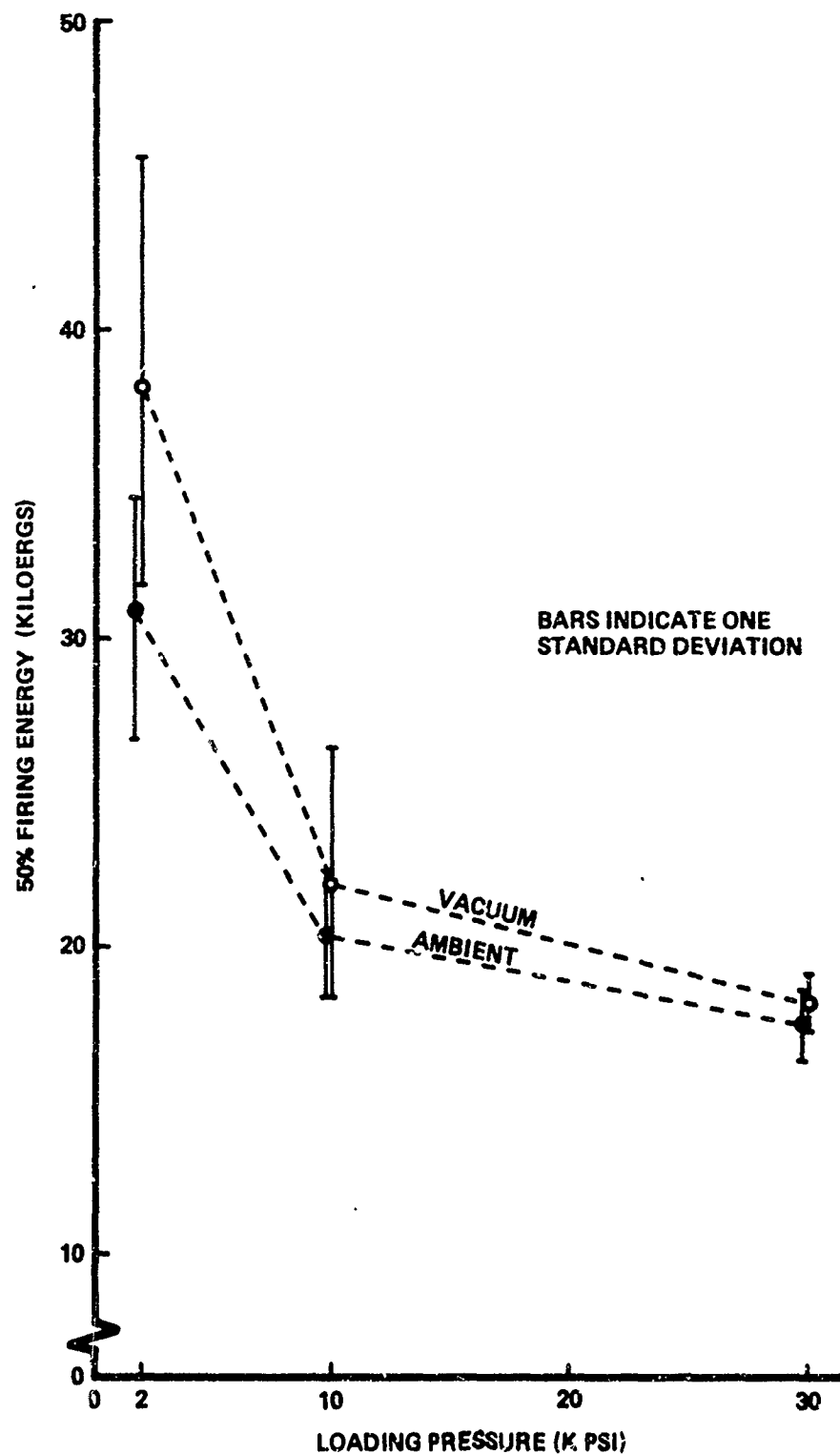


# **FIGURE 9** **DECOMPOSITION OF LEAD AZIDE**

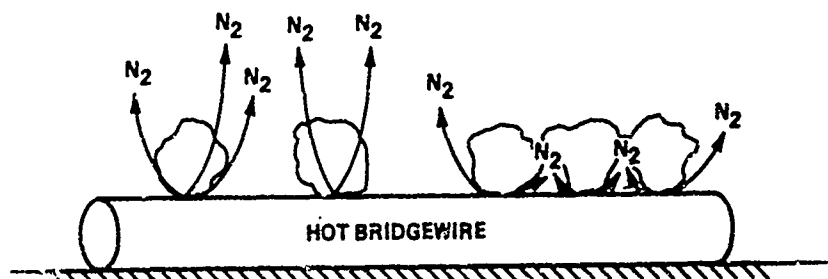
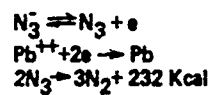
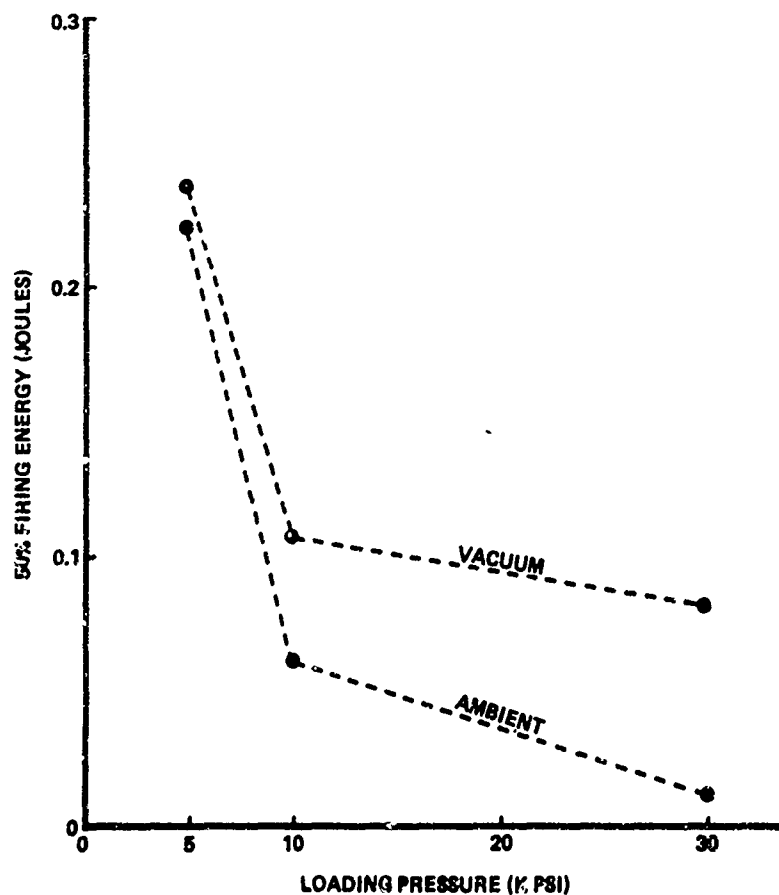


# **FIGURE 10** **EFFECT OF LOADING PRESSURE ON** **50% FIRING ENERGY OF BLACK** **POWDER MEAL IN AIR AND VACUUM**



#### 4-4 Functioning Time of 1-Amp/1-Watt Detonator

Scranton G. Nesbitt II

U. S. Naval Ordnance Laboratory  
White Oak, Silver Spring, Maryland

#### INTRODUCTION

Recently there has been a great deal of interest shown in the functioning characteristics of the Mk 101 type 1-amp/1-watt insensitive electric detonator. The characteristics of greatest interest are the required firing energy for various types of electrical inputs and the functioning times of the detonator for these inputs.

A ribbon type bridge element is used to obtain the desired electrical characteristics. Figure 1 shows the bridge element on a glass/kovar plug as it is used in the detonator. The bridge element is photoetched from 1 mil thick evanohm material. The ribbon part of the element, on which the lead azide ignition charge is loaded, is 10 mils wide. The "sawtooth" pattern around the perimeter of the element provides a relatively safe electrostatic discharge path from the bridge element to the charge holder. The resistance of the bridged plug is between 1.0 and 1.5 ohms.

The Mk 101 type detonator assembly is shown in Figure 2. The ignition assembly of this detonator consists of the

conventional glass/kovar plug, the evanohm bridge element, a plastic insulator, and an aluminum charge holder. Dextrinated lead azide is pressed at 10K psi into the charge holder cavity and onto the bridge element. It is primarily this ignition assembly that determines the functioning characteristics of the detonator.

This detonator is a revised version of the WOX-69A detonator that was developed by the Navy about four years ago<sup>1</sup>. This detonator meets the recommended no-fire requirements of Specification MIL-I-23659<sup>2</sup>. That is, it will pass 1-ampere of current or dissipate 1-watt of power, whichever is greater, for five minutes without initiating. This requirement is designed to help reduce the hazard of initiation from electromagnetic radiation or other spurious electrical sources.

#### EXPERIMENTAL ARRANGEMENT

Experimental apparatus was built to study the functioning time for constant current and capacitor discharge inputs to the detonator. The constant current input was accomplished with wet cell storage batteries and a solid state constant current regulator<sup>3</sup>. A mercury switch provided a relatively sharp current step to the detonator. A Millisecond (pulse)

Switch\* was used for pulsed constant current Bruceton tests. This device provides a sharp square wave current pulse which can be set to any duration from 10 to 250 millisec. At a given setting the pulse duration is reproducible within 1 millisecond<sup>3</sup>.

The firing circuit for the capacitor discharge tests consisted of a variable potential power supply which charged the capacitors through a 10K ohm resistor. This firing circuit also employed a mercury switch which allowed the capacitors to discharge directly through the detonator<sup>4</sup>.

A Tektronix 551 Dual Beam Oscilloscope and a Polaroid camera were used to record the functioning times. The potential drop across the detonator, when the mercury switch closed, provided the triggering signal for the oscilloscope.

Several methods are available for determining the time of detonator output. Sensitive mechanical switches, ionization gauges, and optical schemes have been used for this measurement in the past. In the tests reported here an optical method which has proven to be reliable and convenient was used. In this method the light emitted from the detonator when it ruptures was transmitted by a Crofon Light Guide (light pipe) to a silicon photo-diode. The electrical signal from the photo-diode was amplified and transmitted

\*Developed by Professor L. A. Rosenthal of Rutgers University and consultant to the Naval Ordnance Laboratory, White Oak.

to the input of one channel of the oscilloscope. The functioning time was measured as the time from the beginning of the oscilloscope sweep to the beginning of the light signal. The light pipe transmits radiation of wavelengths from 3,100 to 13,300 angstroms, while the photo-diode responds to radiation of wavelengths from 4,000 to 11,000 angstroms. The "light pipe amplifier"\*, which contained the photo-diode has an overall rise time of 4 microseconds<sup>5</sup>.

It was found that if the light pipe was pointed directly at the end of the detonator, it would pick up enough light to give a sharp output signal on the oscilloscope even if the light pipe were 10 or 15 cm from the detonator. When used at this distance a sharp signal was obtained with a minimum of damage to the detection equipment; on the average, less than 1/4 inch of light pipe was destroyed in each shot.

#### FUNCTIONING TIMES

##### Continuous Constant Current Results

Even though there are probably not too many actual applications where a true constant current power supply is used to fire an electro-explosive device, constant current functioning data are useful in characterizing such items. The data provide a functioning characteristic by which different devices can be compared. Using an evanohm bridge element, an Ohm's law conversion of the constant current data

---

\*Developed by Professor L. A. Rosenthal



should give reasonably good information for constant potential firing sources, because the resistance of the bridge element changes very little as its temperature increases.

Constant current functioning times were studied at five current levels ranging from 2.0 to 5.0 amperes. The term "functioning time" refers to the time between the beginning of the electrical input and the rupturing of the detonator cup. The results of these five tests are shown in Table 1. Twenty-five detonators were fired at each of the five current levels.

Since the bridge resistance of this detonator is held within the limits of 1.0 to 1.5 ohms, the input power ( $P = I^2R$ ) will be within the limits given.

In Military Specification MIL-I-23659<sup>2</sup>, previously mentioned in connection with the 1-amp/1-watt no-fire stimulus, there is also an all-fire stimulus given. It states that an electro-explosive device of this general group should function within 50 milliseconds from a 5.0-ampere input. From Table 1 it is apparent that the 5.0 ampere stimulus is easily met. Inspection of Table 1 shows in addition that at a 2.0 ampere input the functioning time at the 5-watt level could be greater than 50 milliseconds. At 2.0 amperes besides having a rather long average functioning time, 81.7 milliseconds, the spread of the observed functioning times for the detonator

is very wide - 32 to 164 milliseconds. From the data it appears that if it were desirable to have relatively accurate control of detonator functioning time, 3.0 amperes would be about the minimum constant current which should be considered.

From these constant current tests it was also possible to get an idea of how the differences in bridge resistance affect the functioning times. Table 2, which is divided into five sub-tables, one for each current level, shows the relationship between the bridge resistance and the average of the functioning times for the detonator at each resistance level. The detonators for these tests were picked at random, and thus without consideration to bridge resistances. Even though the number of detonators in each resistance level varies widely, there is a definite trend established. As expected, the average functioning time decreases as the bridge resistance increases.

A curve of firing current versus average functioning time is shown in Figure 3. From this it is evident that the functioning times for currents below 2.0 amperes would become very long. However, this type of detonator can function at a current input of 1.5 amperes. When prolonged currents between 1.1 and 1.5 amperes were used there were cases in which the detonators become hot enough to melt the solder seal between the cup and the plug before the detonator fired.

In these cases the cup with the PETN base charge was blown off the ignition assembly by the internal pressure that built up during heating. If the current was continued the lead azide in the charge holder fired several seconds later. Thus it is recommended that currents less than 1.5 amperes not be used to initiate this type detonator.

#### Pulsed Constant Current Results

Pulsed constant current Bruceton tests were conducted at 2.5 and 3.0 amperes. Tests were not conducted at currents above 3.0 amperes because the appropriate Bruceton step sizes were of the same order of magnitude as the inaccuracy of the pulse length settings. The results of these two tests are given below.

Current (amps)	Sample Size	Pulse Length for 50% Firing (millisec)	$\sigma$ (milli-sec)	Observed Functioning Times of Fires (millisec)		
				Average	Minimum	Maximum
2.5	50	26.4*	8.03*	20.6	7.0	30.0
3.0	48	18.1	1.97	16.4	12.1	19.5

\*(These values should be considered as approximate values, since the ratio of  $\sigma$  to the Bruceton step size was  $\sim 4$  and the recommended limit is about  $2.5^6$ .)

The information in the last three columns of this table was collected by observing the light output from the detonators that fired in the Bruceton test. In the 2.5 amperes test there were 27 fires out of 50 samples and in the 3.0 amperes test there were 24 fires out of 48 samples.

### Capacitor Discharge Results

Capacitor discharge firing circuits are used in many applications, and there have been many inquiries concerning capacitance-charging potential combinations and the energy needed to initiate this type of detonator. Similarly, interest has been expressed concerning the functioning times associated with capacitor discharge initiation.

Capacitors ranging from 50 $\mu$ f to 3000 $\mu$ f were used both in Bruceton tests to find the 50% firing potentials and in tests to find the functioning times at each capacitance for various charging potentials.

Table 3 gives the results of the capacitor discharge Bruceton Tests. Logarithmic Bruceton steps were used for the variable charging potentials. Thus the standard deviation is expressed in log units.

The Bruceton 50% Firing Potential is the charging potential at which half of the items tested should initiate. The 50% Firing Energy is the energy stored in the capacitor as calculated from the 50% firing potential and the capacitance of the capacitor.

Because of the wide range of capacitances needed for these tests and in consideration of what capacitors were immediately available, more than one type of capacitor had to be used. The two smallest capacitors, 50 $\mu$ f and 100 $\mu$ f were high quality oil-paper capacitors (meeting MIL-C-25); the 350 $\mu$ f, 700 $\mu$ f,

and 3000 $\mu$ f capacitors were high quality Compulytic<sup>®</sup> aluminum electrolytic capacitors (meeting MIL-C-62); and the 1000 $\mu$ f capacitor was a Tantalum electrolytic (non-solid electrolyte) capacitor (meeting MIL-C-3965). The 1000 $\mu$ f capacitor is under consideration for use in a Navy Fuze to fire the 1-amp/1-watt detonator. Since inquiries have been received about using electrolytic capacitors in actual applications, they were used in these tests. However, it should be noted that electrolytic capacitors are not normally considered accurate enough for characterizing electro-explosive devices. Thus, the part of these data generated from this type capacitor should be considered accordingly. When measured at 120 cps the electrolytic capacitors used were found to be within approximately 10% of their stated values.

In the actual Bruceton test approximately half of the detonators will fire; however, the charging potential at which they fire will range from one or two Bruceton steps below the 50% Firing Potential to a couple of steps above. The data in the last three columns of Table 3 was obtained by recording the functioning time of those detonators which fired. It should be noted that each number in the "Average Observed Functioning Time" column is not the average functioning time at the 50% potential, but is the average time associated with all the fires. The average of the charging potentials for the fires ranged from about 0.3 to 1.6 Bruceton steps above the 50% potential.

As expected the 50% firing energy increases as the capacitance increases. Since the RC discharge time constant becomes larger as C increases, there is an increasing thermal loss from the bridge element to the surrounding material, particularly to the glass/kovar plug. This leads to the increase in the Average Observed Functioning Times shown in Table 3. The data also show the detonator to act rather adiabatically as far as firing energy is concerned for RC input times of less than ~1.0 millisecond. However, firing time continues to decrease as the firing potential is raised. Besides the value of the capacitance, there are other characteristics of the capacitors which affect the energy required for initiation as well as the functioning time. However, no attempt was made to measure or account for such characteristics as impedance, equivalent series resistance, power factor, and leakage which are considered to be secondary factors. The solid line of Figure 4 is a plot of the 50% firing potential versus capacitance. The broken line is an iso energy line of  $1 \times 10^6$  ergs. Generally, the 50% firing energy increases as the capacitance increases.

The results of fixed potential capacitor discharge functioning time tests are given in Table 4. The same capacitors were used in these tests as were used in the Bruceton tests. Except for the 50uf capacitor, tests were made with each capacitor charged to each of these charging potentials. Because of power supply limitations the 50uf capacitor was only tested at two potentials. Fifteen detonators

were tested at each charging potential; their functioning times were recorded photographically from an oscilloscope as previously described.

There are two numbers given in each space in the charging potential columns. The first number is the charging potential; while the second number, in parenthesis, is the calculated energy stored in the given capacitor at the given potential.

The average functioning times in column  $T_1$  are associated with capacitors charged to energies of from  $2 \times 10^5$  to  $7 \times 10^5$  ergs above their 50% firing energy. At these energies, which were the lowest studied, the observed functioning times had quite a large spread. However, all the charging potentials listed in column  $V_1$ , except the one for the 100uf capacitor, are considered adequate for the reliable initiation of Mk 101 type detonators for the capacitors used in this study. Of course, at higher potentials the functioning time spreads become smaller and the average functioning time becomes shorter.

#### CONCLUSION

The Mk 101 type detonators used in this study meet the 1-amp/1-watt no-fire requirement. Functioning times for two types of electrical inputs, constant current and capacitor discharge, have been studied. This type detonator can be reliably initiated by a constant current of 2.0 amperes or greater and by capacitor discharges of  $15 \times 10^5$  ergs from a

50uf capacitor or  $20 \times 10^5$  ergs from a 3000uf capacitor. Average functioning times as low as 3.38 milliseconds for a 5.0 ampere constant current input and .023 milliseconds for a capacitor discharge input from a 50uf capacitor at a potential of 100 volts were observed. Tables 1 and 3 give complete functioning time results.

These studies were supported by the Naval Ordnance Systems Command.

#### REFERENCES

1. NOLTR 66-186, "Development of WOX-69A Detonator," V. J. Menichelli, 23 Jan 1967.
2. Military Specification, "Initiators, Electric, Design, and Evaluation of," MIL-I-23659, revision of 17 Aug 1965.
3. NOLTR 65-103, "An Investigation of Insensitive Initiators I, 1-amp/1-watt No-Fire Initiator", V. J. Menichelli, 6 Jul 1965.
4. NOLTR 65-115, "An Investigation of Insensitive Initiators II, Development of the WOX-63A Detonator", V. J. Menichelli, 20 Jul 1965.
5. Personal communication between L. A. Rosenthal and S. G. Nesbitt.
6. Statistical Analysis for a New Procedure in Sensitivity Experiments, AMP Report No. 101.1R, SRG-P No. 40, Jul 1944.



**TABLE 1**  
**CONSTANT CURRENT FUNCTIONING TIMES**

CURRENT (AMPS)	FUNCTIONING TIMES (MILLISEC)			POWER LIMITS (WATTS)	
	AVERAGE	MINIMUM	MAXIMUM	1 OHM	1.5 OHMS
2.0	81.7	32	164	4.0	6.0
3.0	12.9	7.5	22	9.0	13.5
3.5	7.84	3.0	10	12.3	18.4
4.0	5.24	.1*	7.2	16.0	20.0
5.0	3.38	2.6	5.0	25.0	37.5

\* (THIS TIME IS NOT CONSISTENT WITH OTHER TEST DATA AND COULD HAVE RESULTED FROM FAULTY SCOPE TRIGGERING; NEXT MINIMUM-3.8 MILLISECONDS)

**TABLE 2**

**FUNCTIONING TIMES AS A FUNCTION OF BRIDGE RESISTANCE**

R- RESISTANCE IN OHMS	AVERAGE FUNCTIONING TIME-MILLISEC	NUMBER OF DETONATORS AT R	R- RESISTANCE IN OHMS	AVERAGE FUNCTIONING TIME-MILLISEC	NUMBER OF DETONATORS AT R
<b>A - 2.0 AMPERES</b>			<b>C - 3.5 AMPERES</b>		
1.0	164	1	1.2	8.9	13
1.1	111	2	1.3	7.5	6
1.2	81.4	15	1.4	5.8	6
1.3	69.0	5			
1.4	45.0	2			
<b>B - 3.0 AMPERES</b>			<b>D - 4.0 AMPERES</b>		
1.1	20	2	1.1	6.8	1
1.2	14.6	5	1.2	5.4*	10
1.3	12.9	10	1.3	5.4	9
1.4	10.4	7	1.4	4.4	5
1.5	7.5	1			
<b>E - 5.0 AMPERES</b>			1.2	5.0	1
			1.3	3.7	10
			1.4	3.2	9
			1.5	2.9	5

\* (IF THE QUESTIONABLE TIME OF 0.1 MILLISECONDS IS DROPPED, THIS AVERAGE FUNCTIONING TIME BECOMES 6.0 MILLISEC.)

TABLE 3  
CAPACITOR DISCHARGE BRUCETON RESULTS

CAPACITANCE (f)	50% FIRING		$\sigma$ (LOG UNIT)	SAMPLE SIZE	OBSERVED FUNCTIONING TIME OF FIRES (MILLISECONDS)		
	POTENTIAL (VOLTS)	ENERGY (ERGS)			AVERAGE	MINIMUM	MAXIMUM
50	61.7*	$9.5 \times 10^5$ *	.0096*	25	.129	.07	.32
100	45.3	$10.3 \times 10^5$	.0212	27	.247	.09	.83
350	24.3	$10.3 \times 10^5$	.0205	25	.691	.47	> .95
700	17.5	$10.7 \times 10^5$	.011	25	1.00	.70	1.6
1000	16.7	$13.9 \times 10^5$	.0125	50	1.15	.70	1.8
3000	10.1	$15.3 \times 10^5$	.0147	25	3.24	1.8	4.7

\*(THESE VALUES SHOULD BE CONSIDERED AS APPROXIMATE VALUES, SINCE THE RATIO OF  $\sigma$  TO THE BRUCETON STEP SIZE DID NOT FALL WITHIN THE RECOMMENDED LIMITS.<sup>6</sup>)

TABLE 4 CAPACITOR DISCHARGE FUNCTIONING TIME

CAPACITANCE ( $\mu$ f)	V <sub>1</sub> (VOLTS) (E-ergs)	T <sub>1</sub> * (MILLISEC)	V <sub>2</sub> (VOLTS) (E-ergs)	T <sub>2</sub> (MILLISEC)	V <sub>3</sub> (E-ergs)	T <sub>3</sub> (MILLISEC)
50	77.5 ( $15 \times 10^5$ )	.045	100.0 ( $25 \times 10^5$ )	.023		
100	50.0 ( $12.5 \times 10^5$ )	.1227	65.0 ( $21.2 \times 10^5$ )	.0513	100.0 ( $50.0 \times 10^5$ )	.0238
350	30.0 ( $15.75 \times 10^5$ )	.2943	41.4 ( $50.0 \times 10^5$ )	.1137	53.5 ( $50.0 \times 10^5$ )	.070
700	20.7 ( $15.0 \times 10^5$ )	.543	25.4 ( $22.5 \times 10^5$ )	.341	29.3 ( $30.0 \times 10^5$ )	.211
1000	20.0 ( $20.0 \times 10^5$ )	.627	24.5 ( $30.0 \times 10^5$ )	.313	30.0 ( $45.0 \times 10^5$ )	.214
3000	11.5 ( $20.0 \times 10^5$ )	2.21	14.1 ( $30.0 \times 10^5$ )	1.05	18.3 ( $50.0 \times 10^5$ )	.52

V (E) - CHARGING POTENTIAL (ASSOCIATED ENERGY)

\* T<sub>1</sub> - AVERAGE FUNCTIONING TIME ASSOCIATED WITH POTENTIAL V<sub>1</sub>, ETC.

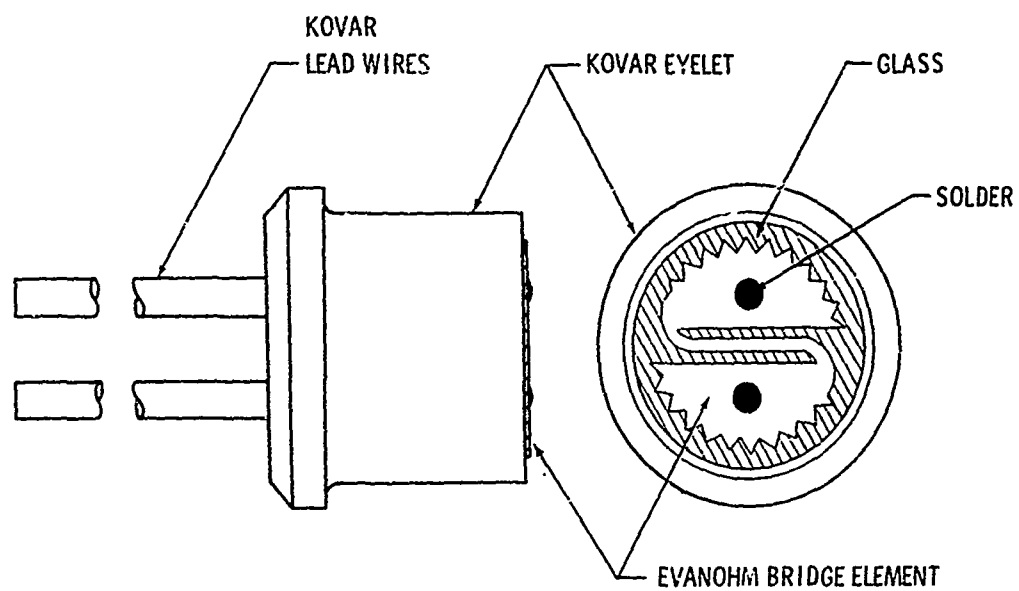


FIG. 1 EVANOHM BRIDGE ELEMENT ON GLASS/KOVAR PLUG

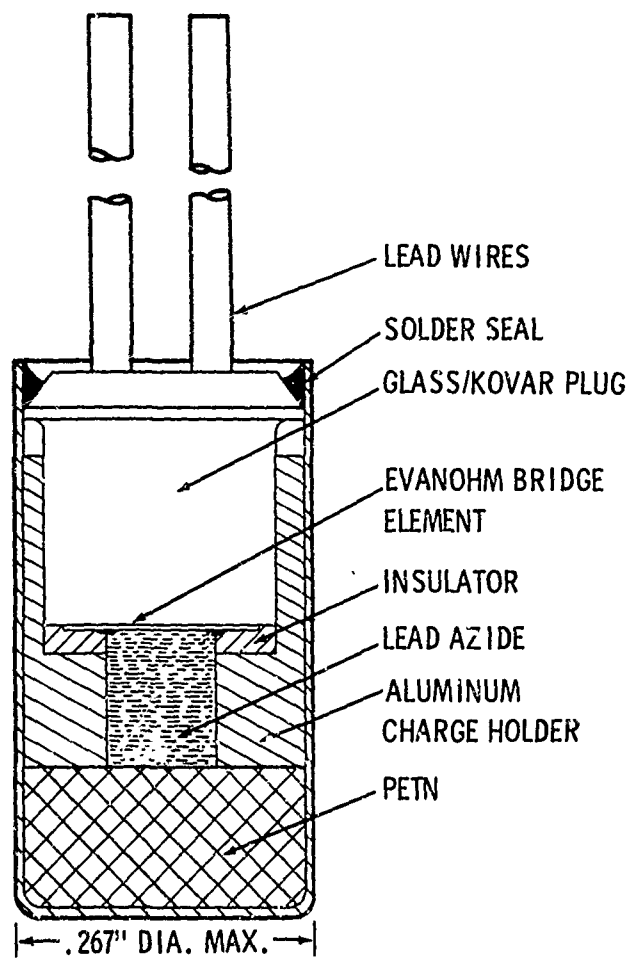


FIG. 2 MK 101 TYPE DETONATOR ASSEMBLY

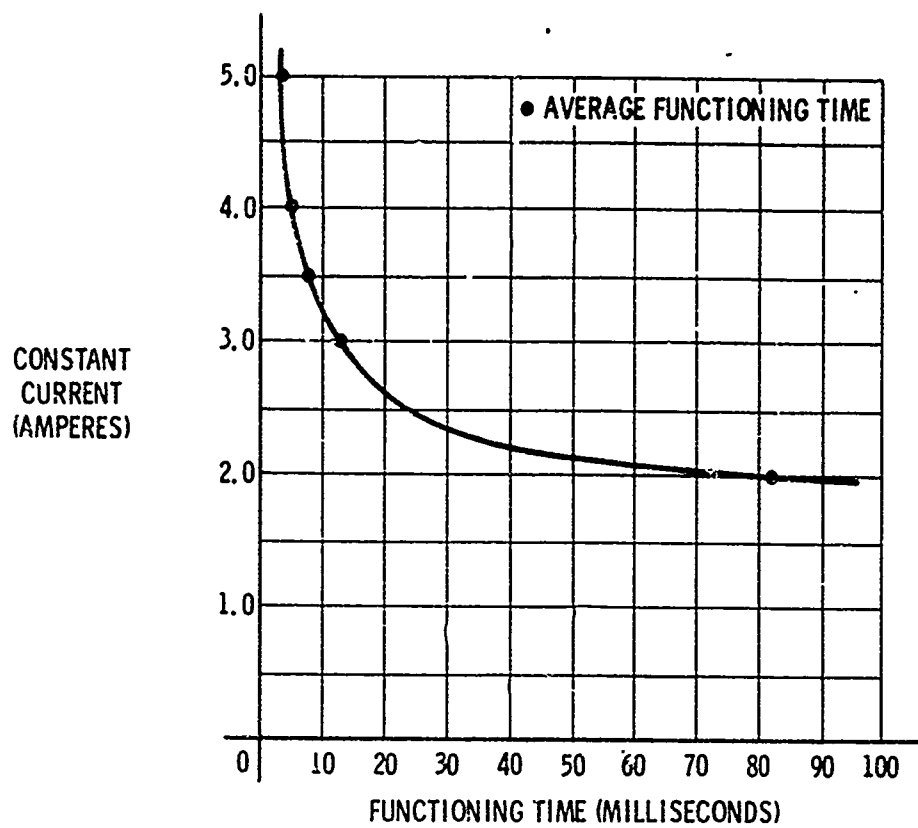


FIG. 3 CONSTANT CURRENT FUNCTIONING TIMES

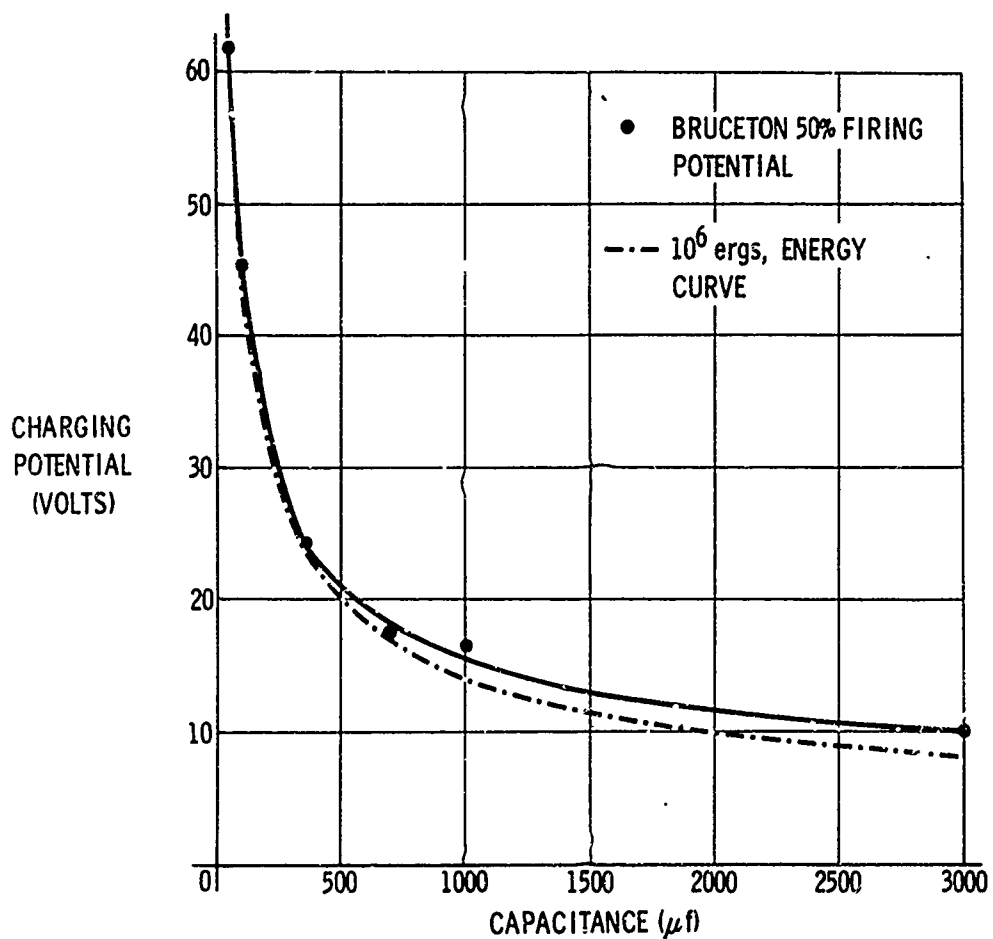


FIG. 4 CAPACITOR DISCHARGE BRUCETON RESULTS

#### 4-5 THE PROPAGATION OF REACTION ACROSS A LEAD AZIDE-PETN INTERFACE

Calvin B. Scott

U. S. NAVAL ORDNANCE LABORATORY  
White Oak, Silver Spring, Maryland

#### INTRODUCTION

In a fuze train, the transition from deflagration to detonation normally occurs in the detonator.<sup>1</sup> Detonators, generally, have been designed empirically. The main consideration being whether or not the detonator could reliably initiate the succeeding train element. Little was known about what happened within the explosive column of the detonator.

Many electric detonators, such as the one shown in Figure 1, contain lead azide ( $\text{PbN}_6$ ) as the intermediate charge and pentaerythritol tetranitrate (PETN) as the base charge. The build-up from deflagration to detonation of these explosives in typical detonator dimensions was the subject of this study.

Some of the parameters which affect the build-up to detonation of  $\text{PbN}_6$  and PETN are loading density, particle size, column length, column diameter, confinement, and moisture content. The parameters which were varied in this study were:

- (a) Density (loading pressure)
- (b) Moisture content
- (c) Column length of  $\text{PbN}_6$

## EXPERIMENTAL TECHNIQUES

A high speed smear camera was used to photograph the explosive events occurring in an arrangement of normal lead styphnate (NLS),  $\text{PbN}_6$  and PETN. From the photographs, measurements were made of the velocity of burning and/or detonation in each explosive column. The photographic observations could be followed to the end of the PETN column.\*

The camera record was obtained by observation of the explosive system in an aluminum-PMMA\*\* cylinder shown in Figures 2a and 2b (type A fixture). A PMMA rod pressed into and parallel with the side of an aluminum cylinder formed a window which served as a section of both the outside and the inside surfaces of the cylinder. Preliminary experiments showed this fixture to be adequate for use with explosives pressed to 45 K psi.

Another type of fixture, shown in Figure 3 (type B fixture) was also used in this work. A PMMA block on the front of the fixture forms the window for viewing the loaded explosive. This fixture was used for explosives pressed from 5 to 50 K psi.

\*A thin layer of an inert mixture of graphite and plaster of Paris separated the explosive column from the air. This thin layer isolated the end point of the PETN explosion from the subsequent reaction of the shocked air.

\*\*Polymethyl methacrylate (a transparent plastic)

Figure 4 is an actual photographic record. An accelerating detonation wave in the  $\text{PbN}_6$  can be seen. This detonation wave propagates to the  $\text{PbN}_6$ -PETN interface where the PETN is initiated. Almost immediately, a stable detonation wave propagates through the PETN column.

A detailed analysis of the preceding photographic record is shown on Figure 5. At a distance 0.25 mm into the  $\text{PbN}_6$  the propagation velocity is 1350 meters per second. Approximately one microsecond later - 3.25 mm into the  $\text{PbN}_6$  - the detonation velocity has reached 4300 meters per second. Less than one-half microsecond later the PETN is initiated. The PETN detonates stably at 7900 meters per second.

#### DENSITY STUDY

This study was done to find the effect of the  $\text{PbN}_6$  density on the initiation and growth to detonation of the PETN.

Both types of fixtures were used. In one part of the study the  $\text{PbN}_6$  and PETN were both loaded at the same pressure and the resulting densities were measured. Loading pressures of 5 to 50 K psi were used.

In a second part of this study, the  $\text{PbN}_6$  and the PETN were loaded at different pressures in the type B fixtures as follows:

(a)  $\text{PbN}_6$  at 30 K psi and PETN at 10 K psi

(b)  $\text{PbN}_6$  at 50 K psi and PETN at 10 K psi

These two systems permitted a study of the effect of the  $\text{PbN}_6$  detonation velocity on the initiation of PETN of constant density.

#### RESULTS AND DISCUSSION OF THE DENSITY STUDY

The results for the  $\text{PbN}_6$  and PETN loaded at 5 K psi and 10 K psi, respectively, were similar. A photographic record (Figure 6) representing the 10 K psi loading condition shows that after the NLS is initiated, an accelerating detonation wave proceeds from the  $\text{PbN}_6$  to the PETN. The PETN appears to detonate immediately.

For loading pressures between 15 K and 30 K psi, immediate detonation of the  $\text{PbN}_6$  no longer occurs. Figure 7 is typical of the group. It can now be observed that the  $\text{PbN}_6$  begins low order then makes the transition to high order detonation. When the transition occurs, the  $\text{PbN}_6$  detonates both forward toward the PETN and rearward toward the NLS. The PETN initiation at the interface seems unaffected by the density variation and the change in the  $\text{PbN}_6$  detonation. In other words, the transition to high order detonation takes place in the  $\text{PbN}_6$  at a sufficient distance from the PETN interface to create a pressure pulse sufficient to detonate the PETN upon its arrival.



As the  $\text{PbN}_6$  loading pressure was increased from 30 to 40 K psi, the transition to detonation did not occur in the  $\text{PbN}_6$ . The low order firing of the  $\text{PbN}_6$ , however, was sufficient to initiate the PETN, which then grew to high order detonation. See Figure 8.

For  $\text{PbN}_6$  loading pressures of approximately 45 and 50 K psi, the photographs showed no detonation waves. These photographs show only burning throughout the  $\text{PbN}_6$  column across the  $\text{PbN}_6$ -PETN interface and through the PETN column. This phenomenon is indicated by the luminous trace in the photograph, see for example Figure 9, for 50 K psi loading conditions.

In the preceding experiments, the  $\text{PbN}_6$  and the PETN columns were loaded at the same pressure. The next two photographs (Figure 10 and Figure 11) show characteristics for the  $\text{PbN}_6$  pressed to 30 K psi and 50 K psi, respectively, and the PETN loaded at only 10 K psi.  $\text{PbN}_6$  at 30 K psi initiated PETN to a high order detonation; at 50 K psi, it only caused the PETN to deflagrate.

#### MOISTURE STUDY

The objective of this phase of the work was to determine the effects of moisture on the initiation and growth to detonation of the  $\text{PbN}_6$  and PETN.

Dextrinated  $\text{PbN}_6$  and PETN were exposed to an atmosphere of 90% relative humidity at 30°C. The  $\text{PbN}_6$  equilibrates

at 0.8% water by weight and the PETN is nonhygroscopic.<sup>2</sup> One percent and higher moisture contents in  $\text{PbN}_6$  or PETN were obtained by the mechanical addition of water.

Aluminum-PMMA cylinders (Type A, Figure 2a) were loaded with NLS (60 mg),  $\text{PbN}_6$  (4 increments of 30 mg each) and PETN (6 increments of 25 mg each) as shown in Table 1. When water was added mechanically, it was introduced from a micrometer syringe into an explosive increment by putting the desired amount on the surface of the previously pressed increment, then pouring and pressing the explosive on top of it. Pressure was applied slowly until the water was taken up into the explosive. Then the final required loading pressure was applied.

The average densities, where determined, are given in Table 1. Included also in Table 1 are density values of the dry explosives which were used as standards. Density values for explosives with moisture contents of 5, 10, and 20% were not recorded. The densities of the wet explosives are in good agreement with the standards except that of  $\text{PbN}_6$  loaded at 10 K psi. Here, the density values are significantly higher than those of the standards. No attempt was made to explain this condition.

#### RESULTS AND DISCUSSION OF THE MOISTURE STUDY

The results of this phase of the investigation can be divided into the following groups:

(a) Explosives having moisture content less than 2%.

(b) Explosives having moisture content of 2% or greater.

For the 10, 20 and 30 K psi loading pressures (both  $\text{PbN}_6$  and PETN) the test shots containing less than 2% moisture achieved high order detonation. Test shots numbered 47A, 52A and 72A, show detonation velocities for PETN of the same order as those of the standard 36A--7900 m/sec. Even the time interval of about 11 microseconds for the initiation of the PETN, after the NLS initiation, is approximately the same.

In the case of the photograph obtained for Fixture No. 77A which had the  $\text{PbN}_6$  and the PETN with a very small amount of water added mechanically to each increment, the final PETN detonation velocity was also about the same as those of the dry explosive--7900 m/sec. However, unlike the others, stable detonation did not occur until the end of the third PETN increment. Also, the initiation of the PETN occurred some 6 microseconds later than the 11 microseconds cited for test shots 36A and 72A.

The mechanically added water decreases the detonation velocity of the  $\text{PbN}_6$ . For 10 K psi loading conditions, Figure 12 shows the comparison of reactions of dry explosives, explosives with adsorbed moisture, and explosives with mechanically added water. Figure 12 was composed from the analysis of some of the photographs where the  $\text{PbN}_6$  contained <0.8% adsorbed moisture and was pressed at 10 K psi. It shows that the reaction time of  $\text{PbN}_6$  has been significantly slowed due to the mechanically added water.

Also, tests were run with  $\text{PbN}_6$  and PETN exposed to 94% relative humidity and then loaded at 20 K psi. The  $\text{PbN}_6$  and the PETN detonation velocity curves are shown in Figure 13. The  $\text{PbN}_6$  curve has two regimes with the second regime representing the transition to high order detonation, sufficient to cause the PETN to detonate at the  $\text{PbN}_6$ -PETN interface. At a loading pressure of 20 K psi, the absorbed moisture in the  $\text{PbN}_6$  has no appreciable effect on the normal reaction as compared with dry  $\text{PbN}_6$ .

The effect of adsorbed moisture is evident at the 30 K psi loading pressure. The  $\text{PbN}_6$  did not make the transition to high order detonation within the  $\text{PbN}_6$  column. Even so, the PETN did attain stable detonation in the fourth PETN increment. Figure 14 shows the comparison of the velocity curves of the  $\text{PbN}_6$  and of the PETN of 59A with the standard 44A. Note, also, that the moisture laden explosive system took more time to propagate to the end of the column.

In the tests of the systems containing 2% or more moisture no photographs were obtained that showed either  $\text{PbN}_6$  or PETN burning or detonating. Upon examination of the damaged fixtures, it appeared that the PETN did not detonate or burn, but was blown away by a low order reaction of the  $\text{PbN}_6$ . Figure 15 shows a comparison of the damage of the fixtures (c to g) as the amount of moisture was decreased

in the  $\text{PbN}_6$  and the PETN. Note that the damage to the fixtures increased as the amount of moisture decreased.

#### COLUMN LENGTH STUDY

In the test shots 36A and 37A (Table 1) which were prepared as standards, 120 mg of  $\text{PbN}_6$  loaded in 30 mg increments was sufficient to initiate PETN. Discrete reaction velocity curves of the  $\text{PbN}_6$  and the PETN were observed on the photographs. Since the quantity of  $\text{PbN}_6$  was more than sufficient to initiate the PETN, a determination was made of the amount necessary to initiate PETN to immediate high order detonation.

The aluminum-PMMA fixtures were loaded with NLS,  $\text{PbN}_6$ , and PETN. Loading of the  $\text{PbN}_6$  and the PETN was at 10 K psi. The test plan called for varying the amounts of  $\text{PbN}_6$  downward from the 120 mg. All the fixtures were tested in the usual manner using smear camera photography.

#### RESULTS AND DISCUSSION OF THE COLUMN LENGTH STUDY

When the  $\text{PbN}_6$  weight was about 5 mg, high order detonation of the PETN occurred only in one of six tests. Burning of the PETN occurred in the others. The burning velocity near the end of the PETN column was about 900 meters per second and is apparently on the increase. This would suggest that a longer column of PETN may attain high order detonation. These tests show that when about 5 mg of  $\text{PbN}_6$  is used, initiation of PETN to high order detonation is marginal.

When more than 10 mg of  $\text{PbN}_6$  was used, detonation occurred in the PETN in every case; but where it occurred varied from shot to shot. As the amount of  $\text{PbN}_6$  was increased, stable detonation of PETN occurred closer and closer to the  $\text{PbN}_6$ -PETN interface. Only when the  $\text{PbN}_6$  weight was 100 mg or more did the detonation of PETN start high order at the  $\text{PbN}_6$ -PETN interface.

#### CONCLUSIONS

The results of this investigation show that due consideration must be given to all parameters affecting the operation of a typical electric detonator to obtain maximum efficiency. Loading pressures, explosive materials, column diameters, and column lengths used in this investigation were typical of production detonators that perform satisfactorily.

In the typical detonator configurations, burning dextrinated  $\text{PbN}_6$  such as that encountered at loading densities of 45 K and 50 K psi has insufficient power to initiate PETN high order. To initiate the PETN immediately to high order detonation, the density of the  $\text{PbN}_6$  should correspond to loading pressures of 5 K to 30 K psi in a column of  $\text{PbN}_6$  long enough to allow the  $\text{PbN}_6$  to attain stable detonation. For  $\text{PbN}_6$  loading pressures between 35 K and 40 K psi, PETN will be initiated but must build-up to stable detonation.

47  
18

Small amounts of moisture in  $\text{PbN}_6$  have an adverse effect. Moisture can cause a low velocity detonating regime for the  $\text{PbN}_6$  before it makes the transition to high order detonation. If most of the  $\text{PbN}_6$  column undergoes low velocity propagation before the transition to high order detonation, PETN will be initiated but not high order. The attainment of stable detonation will be, then, dependent upon a long enough column of PETN. If more than 2% moisture is present in the  $\text{PbN}_6$ , it will not make the transition to detonation and the PETN will not be initiated. Secondly, even with the small amount of moisture that  $\text{PbN}_6$  adsorbs at 90% RH, the loading pressure must be reduced if the normal explosive reaction of the  $\text{PbN}_6$  is to be obtained. For ideal functioning, the  $\text{PbN}_6$  moisture content should be less than 0.8% at loading pressures from 5 to 30 K psi.

For a column diameter of 0.150 inch with heavy confinement, at least 10 mg of  $\text{PbN}_6$  is required to reliably initiate 120 mg of PETN when both are pressed at 10 K psi. However, the PETN does not detonate immediately. It burns first and finally makes a transition to detonation. Only when the  $\text{PbN}_6$  weight is about 100 mg or greater does the PETN detonate at the  $\text{PbN}_6$ -PETN interface.

The data obtained from this study and, in part, the conclusions drawn are highly dependent on the geometry, confinement, and explosives used in the experiments. Nonetheless, the general trends of what can be expected in a

detonator are believed to be valid. Absolute values, however, can be expected to change as the parameters are altered.

This work was supported by the Naval Ordnance Systems Command.

#### ACKNOWLEDGEMENT

The author acknowledges with pleasure the helpful suggestions of Mr. Vicent J. Menichelli, Mr. Howard Leopold, and Mr. Irving Kabik in the preparation of this manuscript. Thanks are also due to Mr. Horace C. Dowdy for his careful and patient work in preparing the fixtures used in this investigation.

#### REFERENCES

- (1) NOLR 1111, Ordnance Explosive Train Designer's Handbook, 1952.
- (2) TM 9-1910, Military Explosives, April 1955.
- (3) Leopold, H. and McVaney, D., "High Speed Photography Applicable to the Development of Electroexplosive Devices", Proceedings of Electric Initiator Symposium, 1963.

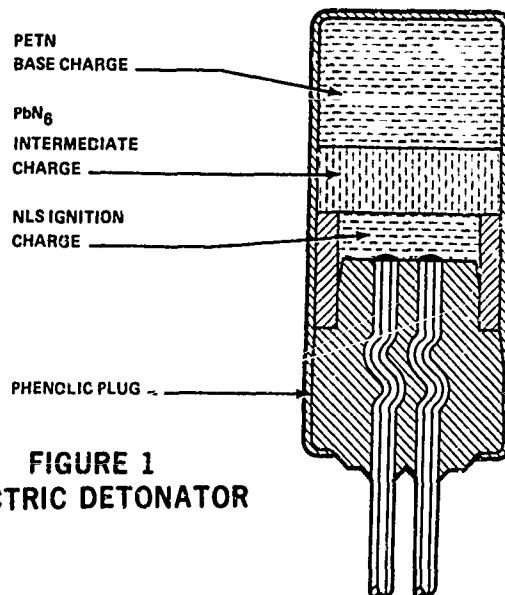
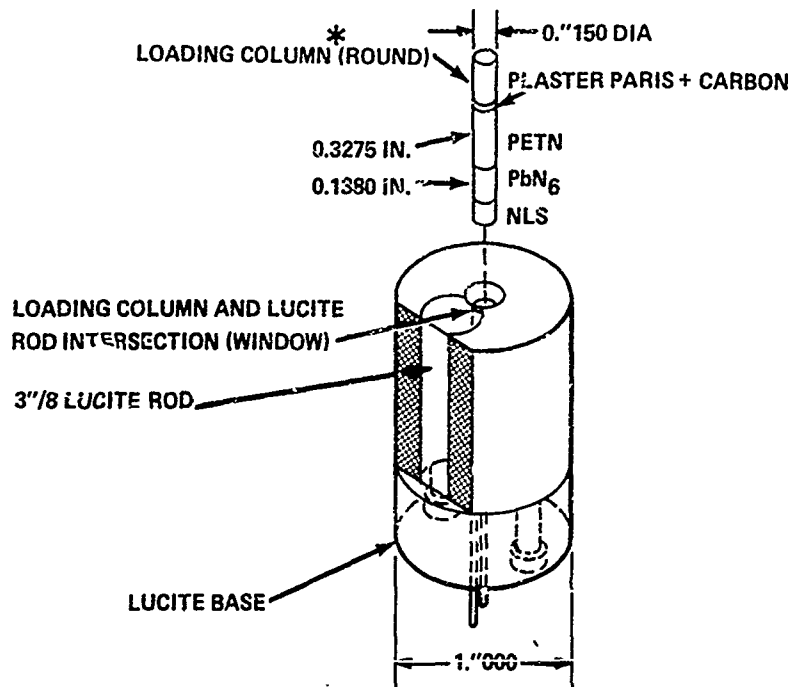


FIGURE 1  
ELECTRIC DETONATOR



**FIGURE 2A**  
**ALUMINUM-LUCITE FIXTURE WITH A CIRCULAR LOADING**  
**COLUMN ( FIXTURE, TYPE A)**



\*EXPLOSIVES LOADED DIRECTLY IN FIXTURE. DETAILS SHOWN OUT OF FIXTURE FOR CLARITY OF DRAWING.

**FIGURE 2B**  
**CROSS-SECTIONAL VIEW OF FIXTURE,**  
**TYPE A, AT THE BASE**  
**OF THE LOADING COLUMN**

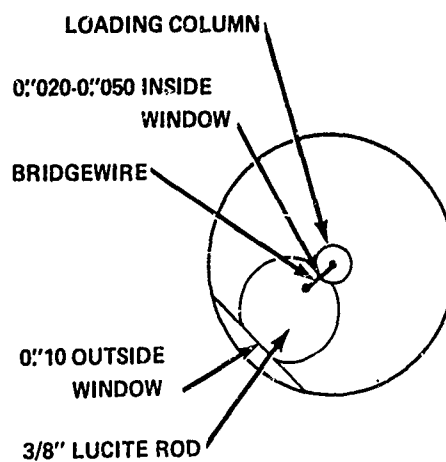
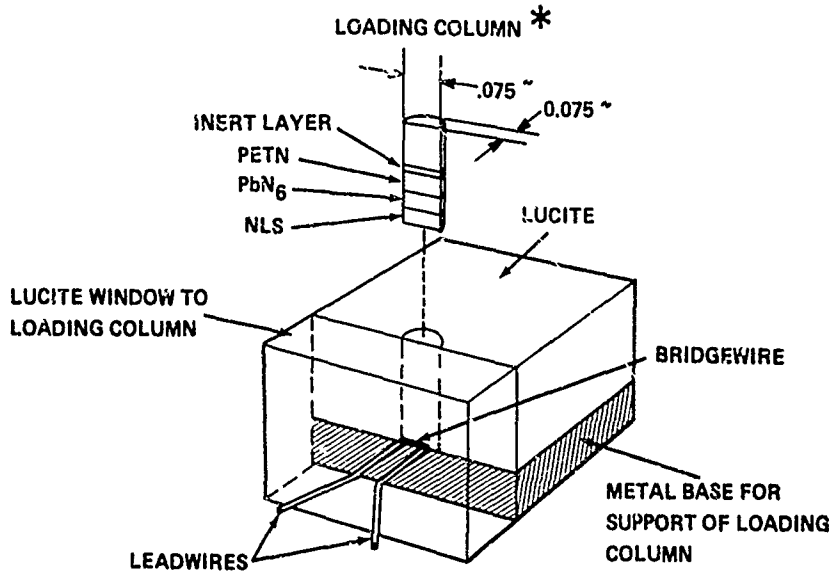


**FIGURE 3**  
**LUCITE BLOCK TYPE FIXTURE WITH A**  
**HEMICYLINDRICAL LOADING COLUMN (FIXTURE TYPE B). ③**



\*EXPLOSIVES LOADED DIRECTLY IN FIXTURE. DETAILS SHOWN OUT OF FIXTURE FOR CLARITY OF DRAWING.

**FIGURE 4**  
**TYPICAL HIGH-SPEED CAMERA PHOTOGRAPH**

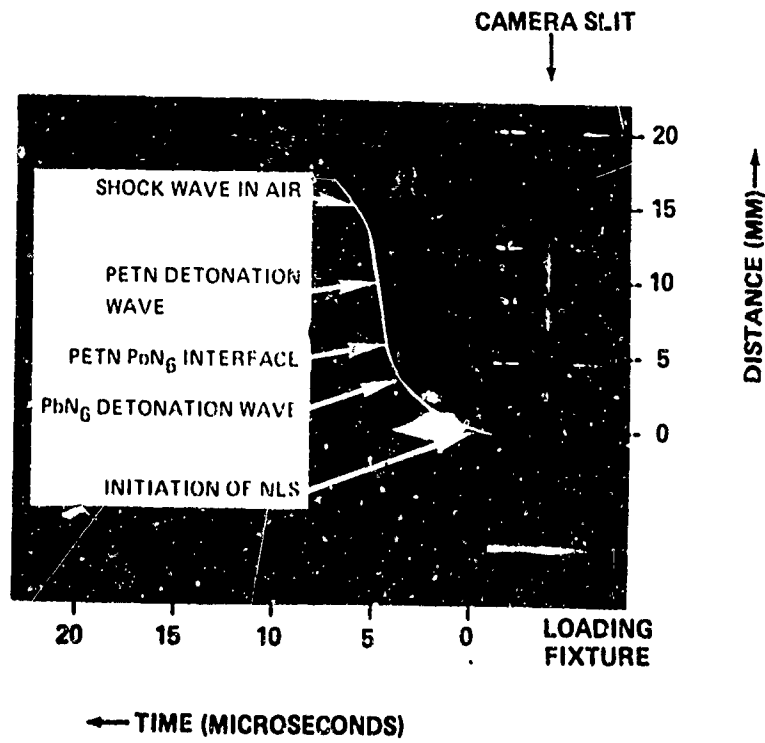


FIGURE 5  
 DETONATION VELOCITY CURVES OF  $\text{PbN}_6$  AND PETN WITH SOME  
 ACTUAL VELOCITIES INDICATED AT POINTS A, B AND ALONG CC'

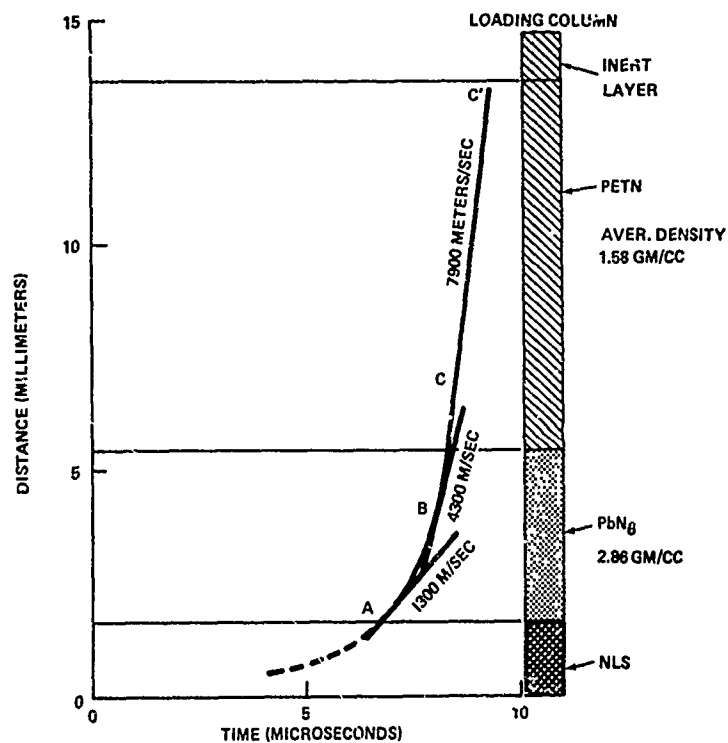
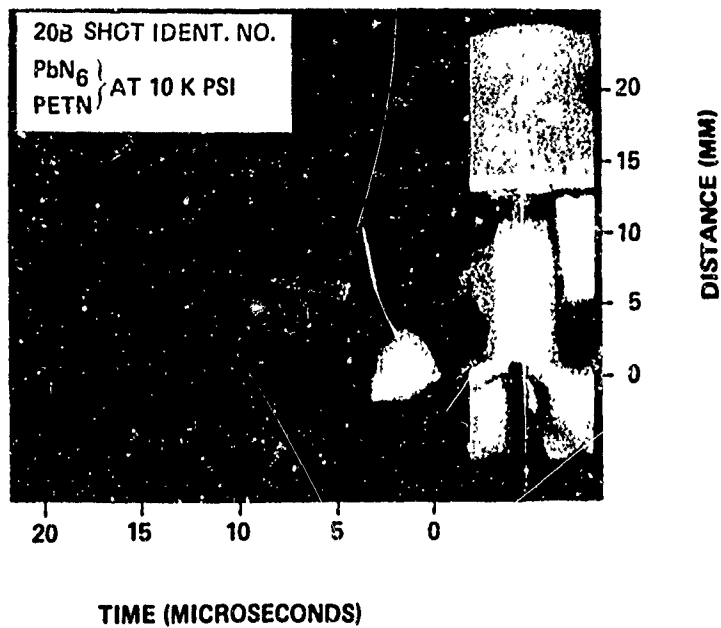
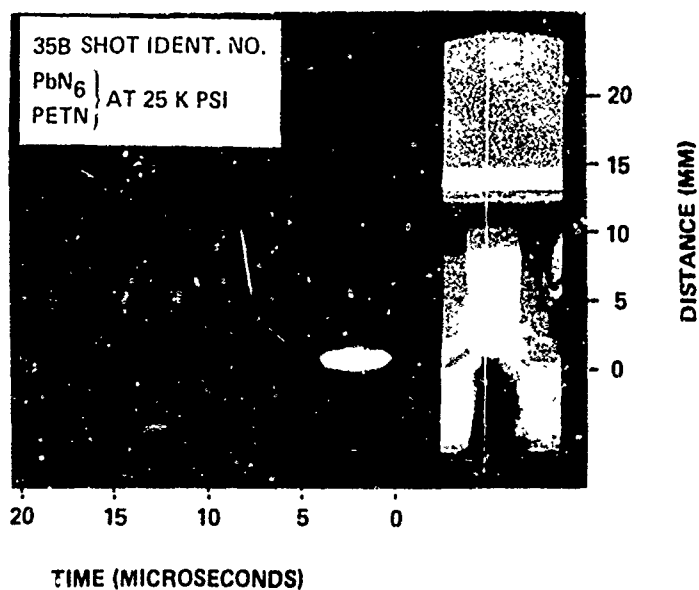


FIGURE 6  
 HIGH VELOCITY DETONATION  
 IN  $\text{PbN}_6$  AND PETN



**FIGURE 7**  
**LOW VELOCITY DETONATION IN  $\text{PbN}_6$ , FOLLOWED BY**  
**HIGH VELOCITY DETONATION IN  $\text{PbN}_6$  AND PETN**



**FIGURE 8**  
**LOW VELOCITY DETONATION IN  $\text{PbN}_6$**   
**AND HIGH VELOCITY DETONATION IN PETN**

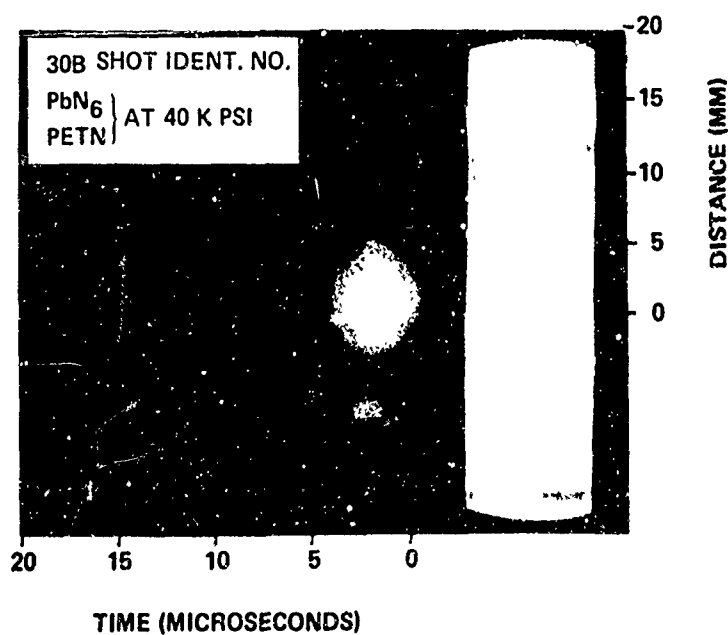


FIGURE 9  
LOW VELOCITY DETONATION IN  $\text{PbN}_6$  AND  
DEFLAGRATING PETN

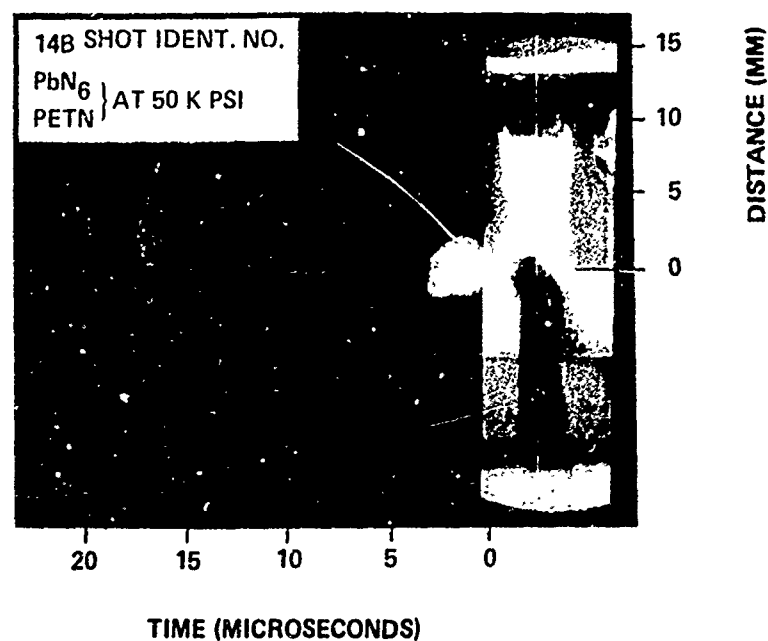
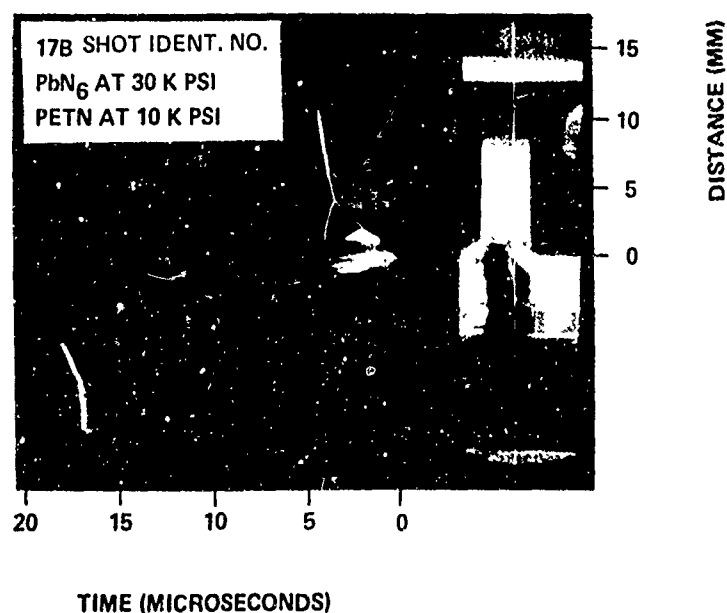
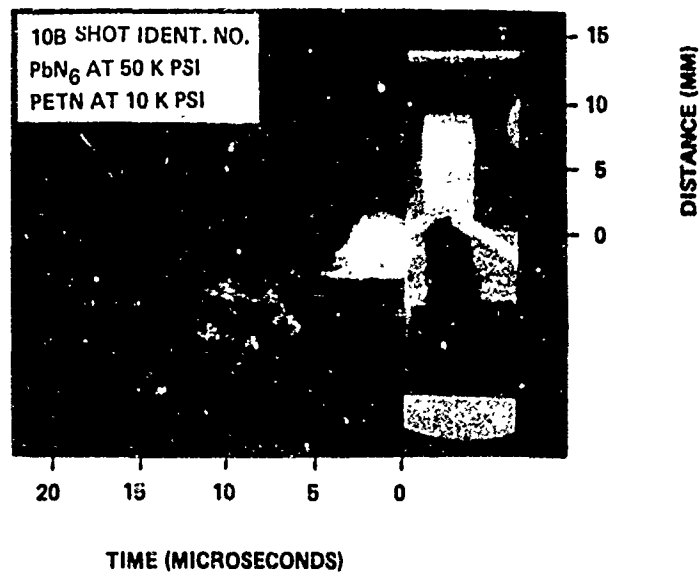


FIGURE 10  
LOW VELOCITY DETONATION IN  $\text{PbN}_6$  FOLLOWED  
BY HIGH VELOCITY DETONATION IN  $\text{PbN}_6$  AND PETN



**FIGURE 11**  
**LOW VELOCITY DETONATION OF  $PbN_6$  AND**  
**DEFLAGRATING OF PETN**



**FIGURE 12**  
**REACTION OF EXPLOSIVES LOADED AT 10 K PSI**

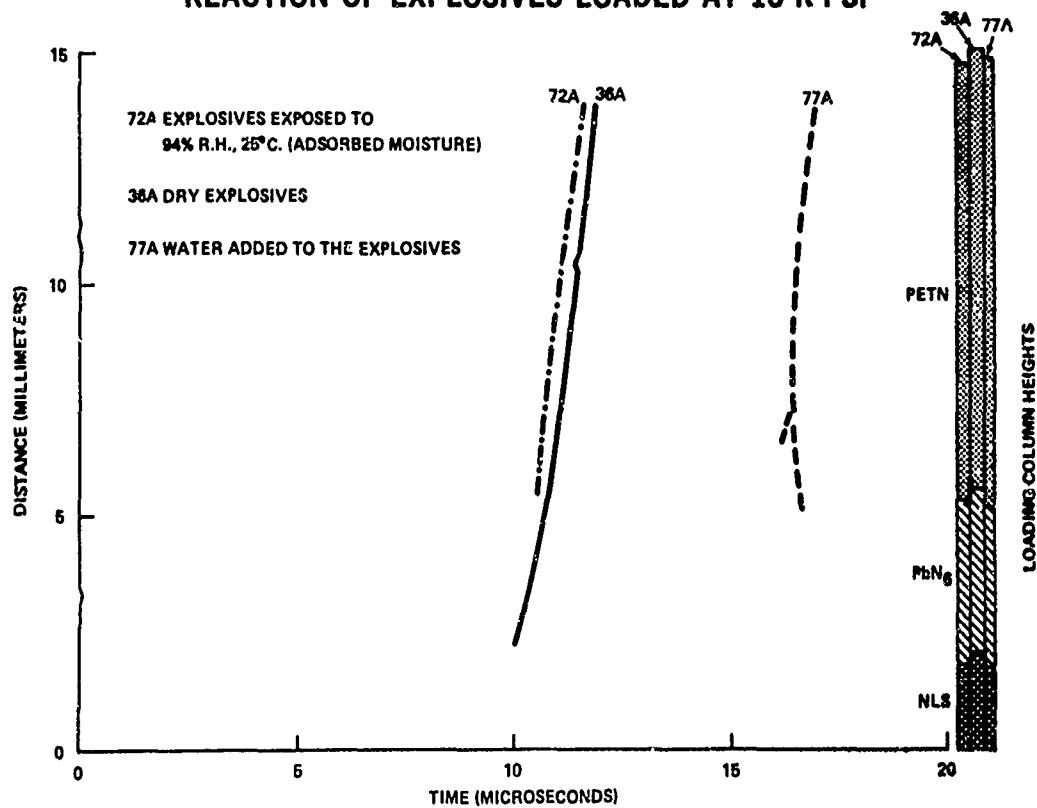


FIGURE 13  
REACTION OF EXPLOSIVES LOADED AT 20 K PSI

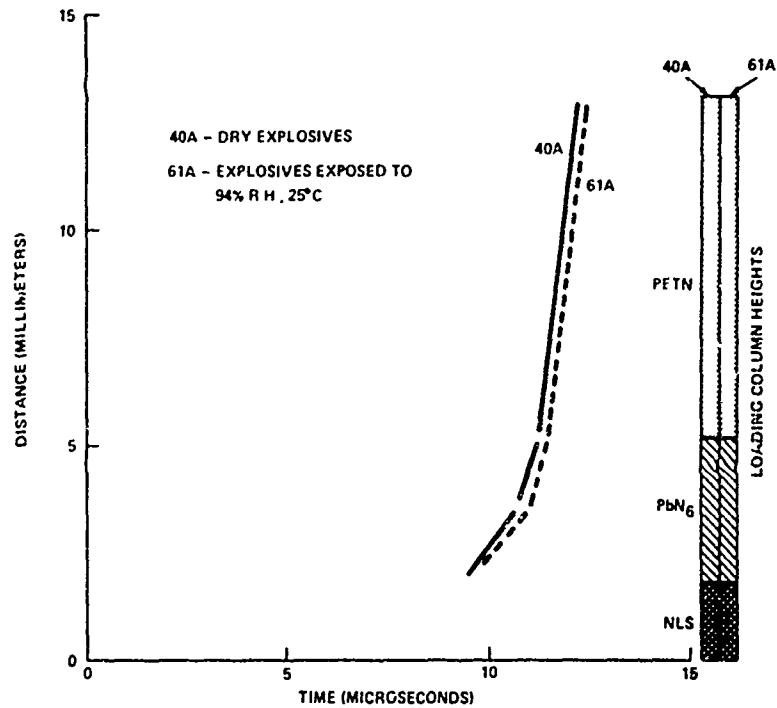
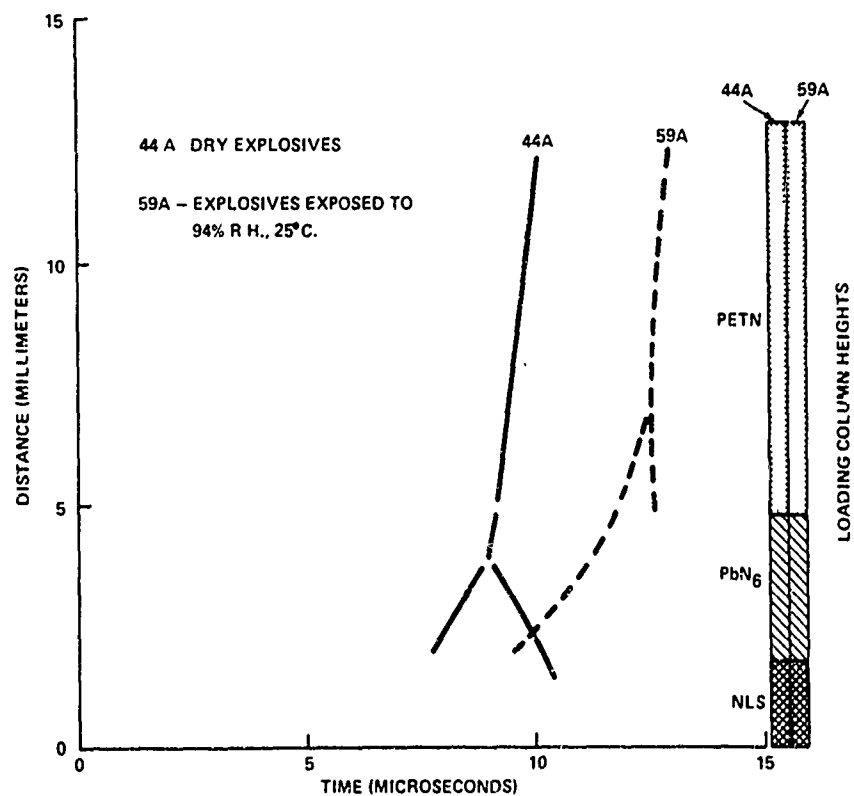
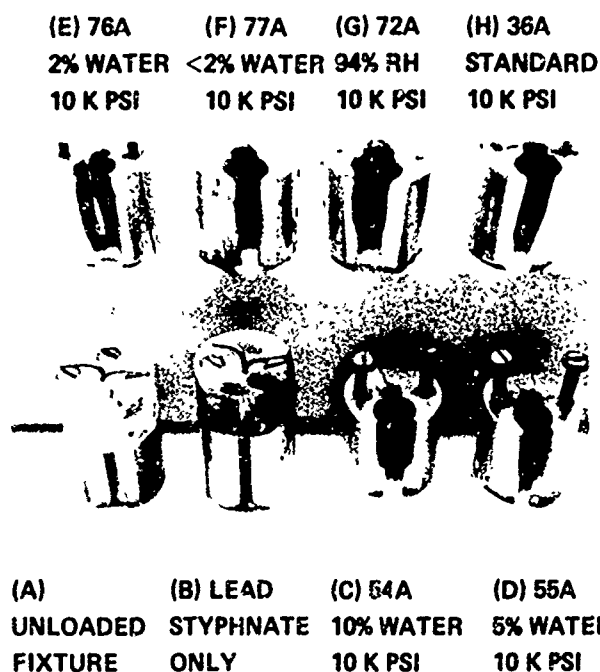


FIGURE 14  
REACTION OF EXPLOSIVES LOAD AT 30K PSI



# **FIGURE 15** **DAMAGE TO FIXTURES AS THE AMOUNT OF** **WATER IN THE EXPLOSIVES VARIED**



**TABLE 1**  
**AVERAGE DENSITY OF  $PbN_6$  AND PETN INCLUDING MOISTURE CONTENT**

FIXTURE NO.	MOISTURE CONTENT (%)	DENSITY OF $PbN_6$ (G/CC)	DENSITY OF PETN (G/CC)
<b>EXPLOSIVES AT 10K PSI.</b>			
47A	0.8 <sup>+</sup>	3.08	1.59
52A	0.8 <sup>+</sup>	3.03	1.56
72A	0.8 <sup>+</sup>	3.02	1.55
77A	<2.0 <sup>#</sup>	3.30	1.58
76A	2.0 <sup>#</sup>	3.43	1.62
36A	•	2.99	1.57
37A	•	2.97	1.57
<b>EXPLOSIVES AT 20K PSI.</b>			
61A	0.8 <sup>+</sup>	3.29	1.69
40A	•	3.29	1.69
41A	•	3.30	1.69
<b>EXPLOSIVES AT 30K PSI.</b>			
59A	0.8 <sup>+</sup>	3.52	1.74
60A	0.8 <sup>+</sup>	3.55	1.75
44A	•	3.54	1.75
45A	•	3.54	1.74

<sup>+</sup> ADSORBED MOISTURE

<sup>#</sup> WATER ADDED FROM MICROMETER SYRINGE

<sup>\*</sup> DRIED EXPLOSIVES FOR USE AS STANDARDS

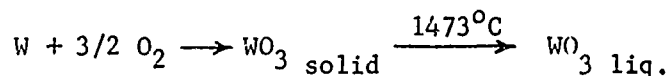
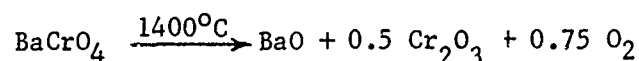
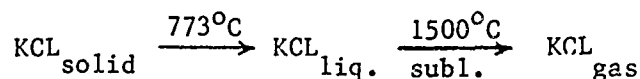
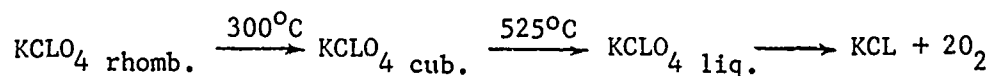


#### 4-6 THE COMBUSTION PROPAGATION OF TUNGSTEN DELAY POWDERS

by  
R. Zimmer-Galler  
Naval Ordnance Station  
Indian Head, Md.

##### INTRODUCTION

A predictably controllable and consistent burning rate is a primary requirement for delay compositions used in cartridge-actuated devices. To find proper ways in which the reaction rate may be influenced, it is necessary to gain some understanding of the physical and chemical reactions involved in the burning process. Investigations are carried out on the combustion of delay compositions with varying proportions of tungsten, barium chromate, potassium perchlorate, and diatomaceous earth. The different components are characterized as individual compounds by the following elementary physical and chemical reactions:



The oxidation of tungsten by gaseous oxygen is known to start under formation of oxide particles on the surface of the metal<sup>(1,2)</sup>. Therefore, diffusion of oxygen through the oxide layer is to be considered as a possible rate-determining step.

In this report, the physical states are determined at which the main reactions take place. There is a discussion of how the different components are involved in the burning process, how they interact with each other, and how changes in composition affect the burning.

## DISCUSSION

### HETEROGENEOUS REACTIONS

Although tungsten delay powders often are called "gasless compositions", it is quite obvious that gaseous reactions are involved in the burning process. Potassium chloride, as a product of potassium perchlorate, is subliming. The formation of smoke and a pressure-buildup in the delay composition, which results in an increase in volume and large cracks in the composition after cooling, is observed in high-speed motion pictures (Figure 1). The extent of solid phase/gas phase reactions in the overall chemical process has been determined by gas-volumetric measurements. Reactions with the outside atmosphere depend on the oxygen balance of the system. Whereas in an overoxidized system, oxygen is released, in an underoxidized system, atmospheric oxygen is consumed. The formation of subliming potassium chloride depends on the burning temperature and on the pressure of the system.

The following methods have been applied to search for a possible liquid phase:

#### High-Speed Motion Photography with Magnification

No melting is observed when a sample of tungsten delay powder containing diatomaceous earth is burned (Figure 2). Partial fusion of the reacted product is seen in a burning sample of tungsten delay powder without diatomaceous earth (Figure 3).

## Microscopic Investigation of the Structure of the Cooled Slag

The sample with diatomaceous earth shows little indication that partial melting had taken place during burning, while the sample without diatomaceous earth shows evidence of melting (Figure 4).

## Differential Thermal Analysis

No melting endotherm had been detected before the exothermic reaction occurred nor thereafter at the investigated temperature up to 1000°C.

From these results, it is concluded that there is no homogeneous liquid-induction zone. Only partial melting is observed in the reacted zone.

## DECOMPOSITION OF THE OXIDIZER

Since the burning of tungsten compositions is affected by environmental conditions, a solid/solid phase reaction between tungsten and potassium perchlorate or barium chromate appears unlikely. It is assumed that the first step in the burning process of tungsten delay compositions is the decomposition of the oxidizing agent under formation of gaseous oxygen.

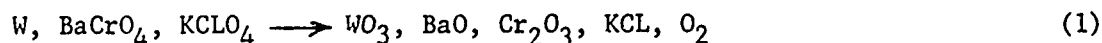
Differential thermal analyses (DTA), of tungsten -  $\text{BaCrO}_4$  mixtures in inert atmosphere do not show any thermal reaction in the investigated temperature range up to 1200°C. Attempts to burn tungsten delay powder without potassium perchlorate failed. This indicates that  $\text{KClO}_4$  is important to initiate the burning process. Differential thermal analysis of tungsten- $\text{KClO}_4$  mixtures, as well as the regular delay compositions (Figure 5), show an endotherm at about 300°C, characteristic for the crystalline transition of  $\text{KClO}_4$  from the rhombic to the cubic lattice. The decomposition temperature is re-

duced in presence of tungsten below the melting temperature ( $570^{\circ}\text{C}$ ) of  $\text{KClO}_4$ . No melting endotherm is detected for any of the mixtures. The main exothermic reactions occur at approximately the same temperature ( $503\text{-}509^{\circ}\text{C}$ ) for tungsten -  $\text{KClO}_4$  and tungsten -  $\text{KClO}_4\text{-BaCrO}_4$  compositions with tungsten concentrations from 30 to 75% covering a large burning rate range (approximately 0.1 to 3 cm/sec). Therefore, thermal decomposition of the oxidizer does not seem to be rate-determining.

#### THE REACTIONS OF TUNGSTEN

##### Heats of Reaction

The heat of reaction ( $\Delta H_r$ ) is used as a design criteria for the overall chemical reaction of burning tungsten delay powder. As shown in Table 1, the heats of reaction measured in a Parr bomb calorimeter  $\Delta H_{r\text{Parr}}$ , are higher than the heats of reaction  $\Delta H_{f(1)}$ , calculated from heats of formation for the following chemical reaction:



This leads to the assumption that other reactions are involved in the combustion process. The formation of barium tungstate (3) is considered as a reaction which accounts for additional heat release:

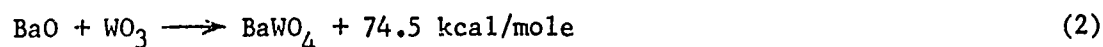


TABLE 1: CALCULATED AND MEASURED HEATS OF REACTION OF TUNGSTEN DELAY  
POWDERS IN CAL/G.

W(%)	BaCrO <sub>4</sub> (%)	KClO <sub>4</sub> (%)	SiO <sub>2</sub> (%)	$\Delta H_f(1)$	$\Delta H_f(2)$	$\Delta H_{rParr}$
30.5	59.5	10	-	177.3	300.9	285
30.5	54.5	10	5	190.6	314.2	317
75.0	15.0	5	5	117.25	161.35	181

The values  $\Delta H_{f(2)}$  calculated for the total heat released in reactions (1) and (2) are comparable with the measured heats of reaction  $\Delta H_{rParr}$ .

The following correlation is used for an estimation of the temperature  $T_r$  at which the reaction takes place:

$$\Delta H_r = \sum_i \int_{T_a}^{T_r} X_i C_i dT + \sum_i L_i + \sum_j \int_{T_r}^{T_f} X_j C_j dT + \sum_j L_j \quad (3)$$

where

- $X_i$  = weight fraction of the i-th component of unreacted product
- $Q_i$  = heat capacity in (cal/g degree) component of unreacted product
- $L_i$  = latent heat of each phase change i of unreacted product in (cal/g)
- $X_j$  = weight fraction of the j-th component of reaction product
- $Q_j$  = heat capacity of the j-th component of reaction product in (cal/g degree)
- $L_j$  = latent heat of each phase change j of reaction product in (cal/g)
- $T_a$  = ambient temperature, 25°C
- $T_f$  = final temperature

Since the thermal properties of tungsten are rather well defined, the calculations have been carried out for the 75% - tungsten composition. For  $\text{BaCrO}_4$  a specific heat of  $0.108 \text{ cal/g } ^\circ\text{C}$  and for diatomaceous earth a value of  $0.183 \text{ cal/g } ^\circ\text{C}$  at room temperature have been experimentally determined. The specific heat of tungsten is described over a temperature range between  $100^\circ\text{C}$  and  $900^\circ\text{C}$  by the following expression<sup>(4)</sup>:  $C_p = 0.032036 + 0.045292 \times 10^{-4}t$ . The specific heats of the other components are also taken from the literature<sup>(5)</sup>:

For the crystal - phase change of potassium perchlorate, a value of  $L = 27 \text{ cal/g}$  has been derived from the endotherm in a thermogram measured with a differential scanning calorimeter. The heat of transition for tungsten trioxide is reported to be  $1.77 \text{ cal/g}$ <sup>(5)</sup>. The final temperature  $T_f = 1192^\circ\text{C}$  has been experimentally determined. Heat losses to the surroundings have been neglected. According to the calculated value  $T_r$ , reaction takes place at a temperature higher than that measured by differential thermal analysis ( $507^\circ\text{C}$ ), at a heating rate of  $20^\circ\text{C/min}$ , however, before the final burning temperature  $T_f$  is reached.

In contrast to most other compositions, tungsten delay powders do not reach a maximum burning rate for a stoichiometric composition with maximum heat of reaction and maximum reaction temperature. The burning rate increases with tungsten concentration, independent of the oxygen balance of the system.

#### Particle Size Effects

The effect of particle size on the oxidation reaction of tungsten in oxygen atmosphere has been investigated by differential thermal analysis. As illustrated in the thermograms (Figure 6), the temperature at which tungsten reacts with oxygen is a direct function of the metal-particle

size. As the metal surface becomes smaller by increasing the particle size of tungsten or by decreasing the tungsten concentration in the delay powder, diffusion of oxygen through a metal-oxide layer on the surface of tungsten particles is considered as a rate-controlling reaction. The effect of tungsten-particle size on the burning rate becomes more pronounced the smaller the tungsten content of a delay composition.

#### Temperature Profiles

Temperature profiles along the lateral surface of cylindrical samples of burning delay powder, pressed at 30,000 psi, have been measured with a two-color pyrometer operating at 0.56 and 0.65  $\mu$ . As the reaction front passes a 1-mm slit arrangement, the recorded temperature changes exhibit three (3) regions: induction zone, main reaction zone, and cooling zone.

From the temperature-time and temperature-distance profiles (Figure 7), the thermal diffusivities  $\alpha = \frac{\lambda}{\rho c}$  have been derived. Neglecting heat losses to the surroundings and assuming that heat is transferred by conduction only, the general heat transfer equation has been used:

$$\frac{\partial T}{\partial t} = \frac{\lambda}{\rho c} \frac{\partial^2 T}{\partial x^2}$$

The burning rate is directly proportional to the thermal diffusivity, but inversely proportional to the temperature-distance gradient of the system.

An increase in potassium perchlorate concentration from 5 to 10% increases the burning rate and raises the burning temperature of the under-oxidized 75% tungsten composition. It does not have a measurable effect

on the burning rate or the temperature of the 30.5% tungsten composition in which enough oxygen for complete combustion of tungsten is furnished.

#### The Effect of Diatomaceous Earth on the Burning

Diatomaceous earth is used in delay powders to improve the loading characteristics. It does not undergo or catalyze any chemical reaction during the combustion process, as shown by differential thermal analysis or microscopic investigation of the slag. The differential thermogram of tungsten delay powder without diatomaceous earth shows the same exothermic peak temperature as samples containing 5, 10 or 15% of diatomaceous earth. Under the microscope, silica particles could not be mechanically isolated from the bulk of the burned material. However, by repeated fuming with hydrochloric acid, adding water, and filtering off water-soluble chlorides, and by separating the silica from undissolved tungsten with a density column, diatoms were found.

The effect of diatomaceous earth on the burning temperature of delay compositions is shown in Table 2 and Figure 8. The burning temperature is reduced, and the linear-burning rate  $r$  is raised with increasing amount of diatomaceous earth. The drastic difference in the mass-burning rate  $\dot{m}$  between the composition without diatomaceous earth and the compositions with diatomaceous earth is related to different physical states. The burning temperature of the sample without diatomaceous earth is high enough as to cause liquefaction of tungsten trioxide (m. p.  $1473^{\circ}\text{C}$ ), which possibly forms a molten layer on the surface of tungsten.



TABLE 2: THE EFFECT OF DIATOMACEOUS EARTH ON THE COMBUSTION OF 30.5%  
TUNGSTEN DELAY POWDER<sup>\*)</sup>

SiO <sub>2</sub> (%)	Density(g/cm <sup>3</sup> )	r(cm/sec)	$\dot{m}$ (g/cm <sup>2</sup> sec)	Temp(°C)
0	5.218	0.0905	0.472	1512, 1512
5	4.878	0.1365	0.666	1437, 1427
10	4.908	0.1367	0.670	1285, 1328
15	4.472	0.1428	0.639	1140, 1134

<sup>\*)</sup> 10% KClO<sub>4</sub>, rest BaCrO<sub>4</sub>

#### CONCLUSIONS

1. Solid phase/gas phase reactions are involved in the burning of tungsten delay powder. There is no evidence of a liquid-induction zone.  
Partial melting of the reaction products, which depends on the temperature of the system, has been observed.
2. Tungsten trioxide, as a primary reaction product, undergoes secondary reactions with decomposition products of barium chromate.
3. There is no correlation between the burning rate and heat-of-reaction or the reaction temperature.
4. Diatomaceous earth, which acts as a heat sink, increases the burning rate. The inverse correlation between burning temperature and mass-burning rate is related to changes in the physical state.
5. The specific surface area of tungsten is considered as the main burning-rate-controlling factor.

## REFERENCES

- (1) Louis-Claude Dufour & Ph. Dufour, Bulletin de la Société de France, 8, 3161, (1968).
- (2) S. S. Brenner & W. J. McVeagh, J. Electrochem. Society, 115, No. 12, 1247, (1968).
- (3) Gmelins Handbuch der Anorganischen Chemie, 54, 146
- (4) A. Magnus, H. Holzmänn, Ann. Phys., (5), 3, 598, (1929)  
(Gmelin 54, 56)
- (5) JANAF Thermochemical Data, Dow Chemical Company, Thermal Lab.,  
Midland, Michigan (1966)

## ACKNOWLEDGEMENT

The author thanks T. D. Austin, W. C. Eller, R. H. Spatz and F. Valenta for their support during this investigation.

The work was supported by the Naval Air Systems Command, AIR-53222A, (AIRTASK No. A-35-532-068/286-1/F008-17-01).

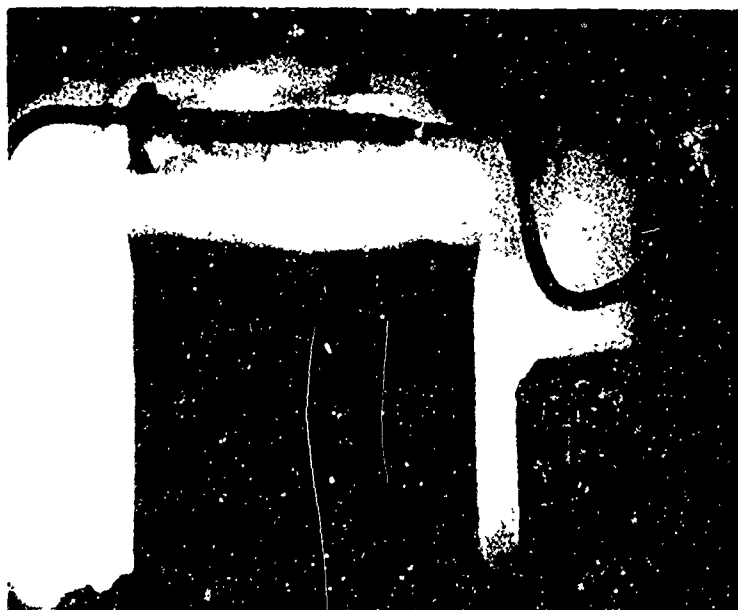


FIGURE 1: BURNING TUNGSTEN DELAY POWDER



FIGURE 2: BURNING TUNGSTEN DELAY POWDER CONTAINING DIATOMACEOUS EARTH



FIGURE 3: BURNING TUNGSTEN DELAY POWDER CONTAINING NO DIATOMACEOUS EARTH

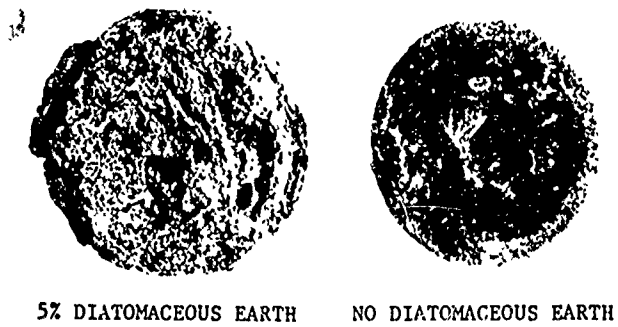


FIGURE 4: BURNED TUNGSTEN DELAY POWDER

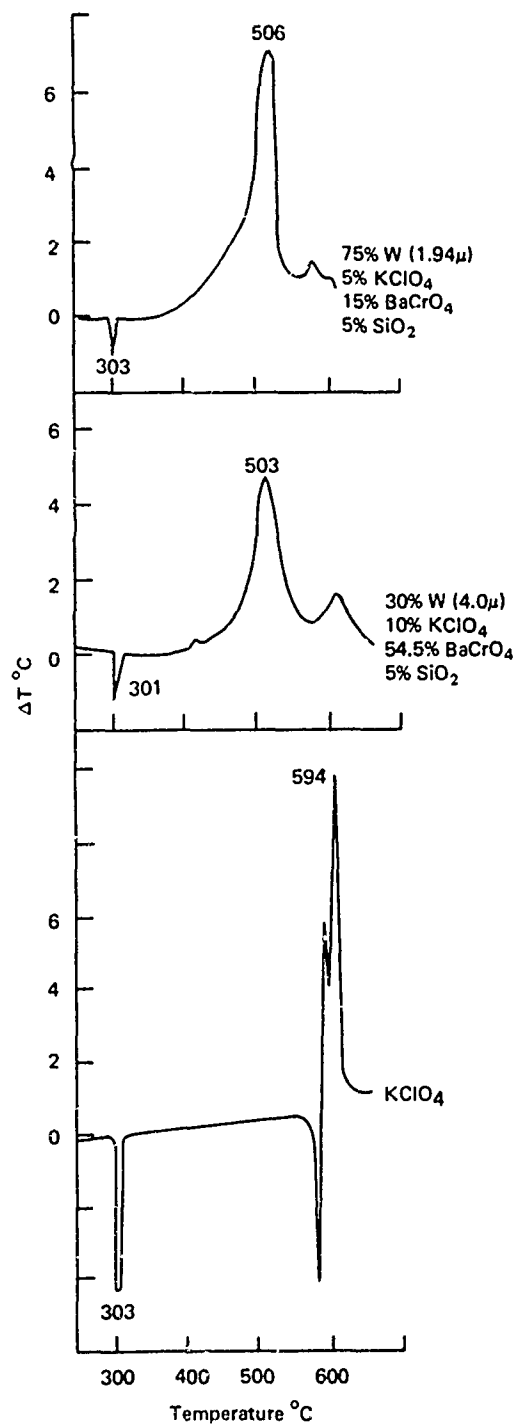


Figure 5 Differential Thermal Analysis of Potassium Perchlorate and Tungsten Delay Powders

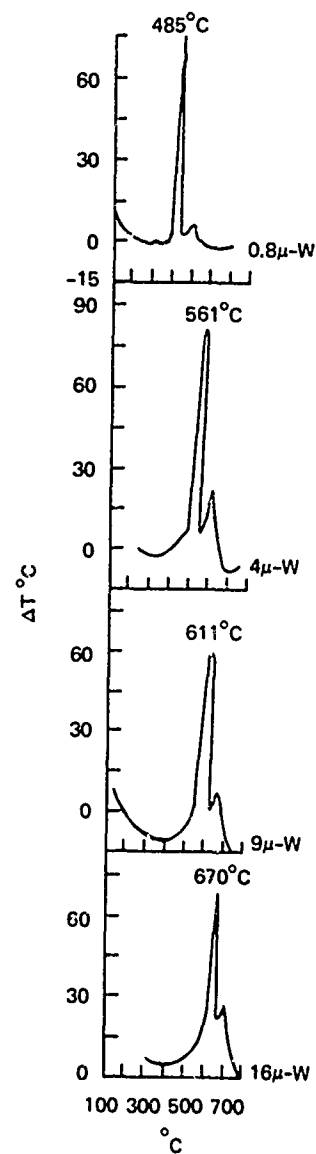


Figure 6 Differential Thermal Analysis of Tungsten Powder with Varying Particle Size in Air.

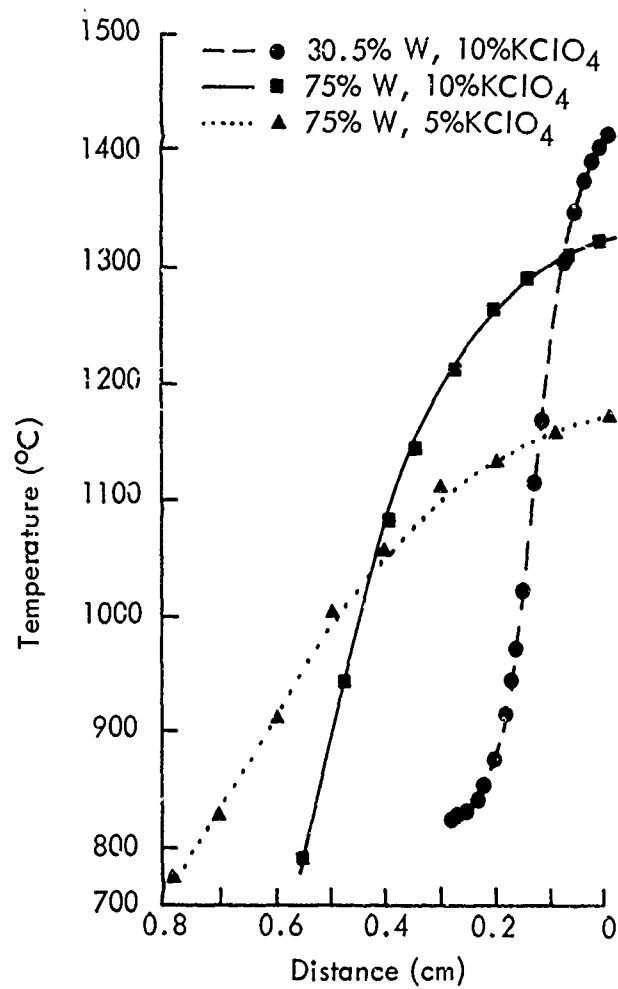


Figure 7 Temperature vs. Distance from the Reaction Zone of Burning W-Delay Powder

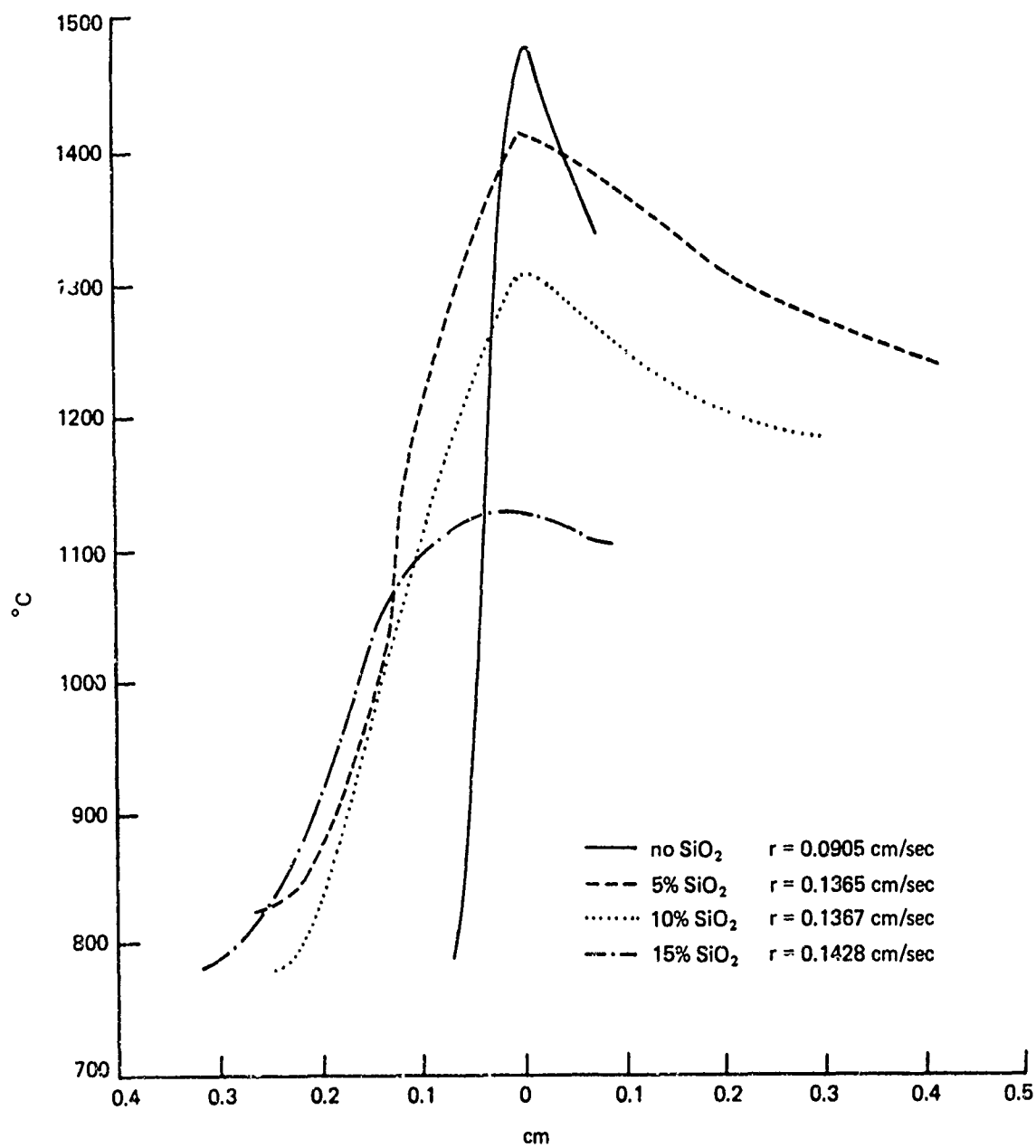


Figure 8 Temperature vs. Distance from the Reaction Zone of Burning 30%-Tungsten Delay Compositions with Varying Amount of Diatomaceous Earth

Stanley M. Adelman  
Nancy B. Willoughby  
Artillery Ammunition Laboratory  
Picatinny Arsenal

#### 4-8 DEVELOPMENT OF RF ATTENUATOR UTILIZING FERRITE - CERAMIC COMPONENTS AND THE EFFECT OF NUCLEAR RADIATION ON THESE COMPONENTS

In the past fifteen years, a multiplicity of devices have been developed for protecting electric initiators and initiation circuits from the effects of energy induced by RF radiation. Most of these have been reflective type filters, some have been of the dissipative variety; others have combined both features. I am all in favor of dissipation but I must admit there is a place for reflection also. So let us now reflect.

The dissipative type attenuator is basically an energy converter. RF energy is converted into heat. Therefore, one need not be concerned with the possibility of reflected RF energy introducing problems elsewhere in the system. Moreover the dissipative attenuator can be designed so that it has practically no effect on a normal firing pulse. This is of great importance in most systems where space and weight limitations are rigorous and power supplies are not much better than marginal as a consequence. The energy differential between 90% reliability and 50% reliability is not very great for many initiators and degradation of the firing pulse cannot be tolerated no matter how efficient the RF suppressor utilized. Additionally, the dissipative filter has no resonant points.

On the debit side it is theoretically possible for the heat generated by the dissipative attenuator to cook off the explosive charge in the initiator if the design does not provide a suitable heat sink. However, it is extremely unlikely that such a situation would be encountered because prolonged exposure at very high levels would be required to obtain an

initiation in this fashion. Of more import is the difficulty frequently involved in obtaining ferrites with the desired characteristics. Here our requirements run counter to those usually specified for the manufacture of ferrites. We seek lossy material while the manufacture strives to produce non-lossy material. One man's gold is another man's garbage.

Reflective filters are more readily available than are dissipative attenuators, do not present even a theoretical cook-off problem and do not require hard-to-obtain ferrites. However, they integrate the normal firing pulse so that system reliability may be degraded; or, if the power supply in the system is marginal, may even prevent firing the initiator at all. The RF energy reflected may introduce problems elsewhere in the initiation system, telemetry, or other electronic and electrical components. Resonant points which are open windows for the admittance of RF energy may exist at certain frequencies.

Some devices are hybrids which combine both dissipative and reflective elements. In effect they make use of the capabilities peculiar to both approaches. Unfortunately, they also preserve some of the disadvantages of both. For particular applications where the advantages outweigh the drawbacks or where they are not significant, hybrid filters may provide an excellent solution of RF problems.

In point of fact, one of the two general types or the hybrid type may be suitable for a specific application; unsuitable for others. A knowledge of the merits and demerits of each particular device and a thorough understanding of the system to which it is to be applied is necessary for a judicious selection to be made. My personal opinion is that dissipative type attenuators should be used in all cases because they are relatively



foolproof, have no resonant points, and do not affect firing current.

As I remarked before, I am in favor of all types of dissipation.

A major objective in all our RF suppressor development programs has been good attenuation (20 db or better) at frequencies as low as 100 KHz. It has been difficult to get appreciable attenuation below 1MHz while still maintaining good attenuation across the rest of the frequency range of interest, i.e. 100 KHz to 20GHz. We have conducted programs to develop improved ferrites and ferro-ceramic components to give us better low frequency attenuation. This has met with some success but we are not yet at the point where we can unequivocally recommend the incorporation of a particular material into electric initiators on a production basis. One of the problems has been that improvement in one characteristic essential to good attenuation usually results in degrading another important characteristic. We must seek some combination of generally improved parameters rather than fruitlessly attempt to optimize individual factors.

We know that RF attenuation of ferrites is increased by high initial permeability and high loss tangents. These are the important properties which are the key to successful ferrite attenuators. Of equal import is the ability of the attenuator to withstand the "thousand natural shocks to which electroexplosive devices are heir" to paraphrase Shakespeare slightly. A "natural shock" which we must consider is the effect of nuclear radiation on these components.

Investigations of surface space-charge layers on barium titanate have indicated this material to be sensitive to radiation in that significant voltages may be generated under certain conditions. Similar effects have been observed in other ferroelectrics. The use of such materials in electronic circuits and as initiation system components which might be

exposed to a nuclear radiation environment compelled us to determine the effect of such exposure on these components. The effects of immediate interest were magnitude of voltage generated and energy transferred under different levels of radiation, effect on attenuator capability and the possibility of physical breakdown. We embarked upon a preliminary investigation to gain insight into the problem before conducting any large-scale program.

One inch diameter, silvered, unpoled, flat barium titanate discs were exposed to flash electron radiation and monitored for voltage generation. (Fig. 1) Secondary effects and extraneous noise had to be eliminated or at least suppressed in order to obtain meaningful information. The samples were placed in the direct central beam of the electrons using appropriate sample holders. (Figs. 2, 3) Cables, electrodes, etc were well shielded to reduce noise levels. Oscillographs were taken without a sample to obtain the imprimatur of the triggering signal so as to differentiate it from signals generated by the sample. Readings taken with the samples indicated voltage generation, the amount being dependent on the dose. The character of the pulse generated varied with the side of the sample facing the beam. About 1.7 to 1.9 volts maximum initial pulse was generated in four microseconds at 0.7 to 3.5 Megarads. This was followed by a damped oscillation starting with an amplitude of  $\pm 0.4$  volts which was damped out in 130 microseconds. At 7 to 10 Megarads, the maximum initial pulse was two volts and at about 12 Megarads it was 2.4 volts. Similar damped oscillations followed. Reversing the sample; a maximum voltage of 1.5 volts was generated in two microseconds at 12 Megarads. Characteristic oscillation started with an amplitude of  $\pm 1$  volt and damped out after 140 microseconds. The highest voltage pulse obtained with any sample was 3.5 volts after 0.7 Megarads.

Lead zirconium titanate in the form of circular discs of various sizes was irradiated by flash electrons to doses from 1.1 to 14 Megarads. Capacitance and dissipation factor measurements were made before irradiation, (Fig. 4) and two days and ten days after irradiation. In some cases these values changed with time. No definable trend could be discerned because different mixes of the same material and supposedly identical materials from different manufacturers exhibited wide differences in behavior.

Insertion loss measurements on actual attenuators before and after irradiation indicated improved attenuation below 150 MHz and slightly decreased attenuation at the higher frequencies. The true significance of this data is questionable because the devices tested had low attenuation in the low frequency range to begin with so that an increase of 2 db looms very large on a percentage basis. However, a definite pattern of improved low frequency performance did emerge and the possibility of improving low frequency capability of attenuators by irradiating them or their ferro-electric components merits further exploration.

Again using flash electron techniques, the change in magnetic properties of different groups of ferrites was investigated. In general, the attenuating properties of a ferrite are governed by complex permeability, complex permittivity and magnetic and electrical loss tangents. Absorption is increased by high initial permeability and high loss tangents. These requirements are directly opposite to those called for in commercial use.

Four samples of five different groups of manganese-zinc-iron ferrite systems were studied. Permeability and Q as a function of frequency were plotted for each sample before and after irradiation. (Figs. 5, 6) Three groups (T-1, 9170 - D/10 and O-7) exhibited an increase in permeability (up to 1 MHz) which decreased after two weeks but remained higher than that before irradiation.

There was a minor increase in permeability from 1-4 MHz and a decrease in permeability above 4 MHz. In general Q increased at lower frequencies up to 5 MHz.

One ferrite (9170-AE) exhibited an increase in permeability around 1 MHz which became greater after two weeks. At higher frequencies this trend was reversed. Q followed the same pattern except for a significant decrease at higher frequencies.

Ferrite H showed decreased permeability at low frequency. Part of the decrease was eliminated after two weeks. At 5 MHz there was no significant change. Q increased over the range 0.5-5 MHz.

These tests indicated the possibility of increasing low frequency permeability of the Manganese-Zinc ferrites by irradiation. More intensive investigation at higher dose levels is in order. However, the increase in Q noted in some cases is undesirable.

#### DOSE MEASUREMENTS

The dose from the flash electron tube was measured at different distances from the window by cellophane dosimetry. Blue cellophane paper (commercially available) was used as the dosimeter. Radiation bleaches the dye in the cellophane resulting in a change in transmittance which is approximately linear with dose at 6,550 Angstroms. Small pieces of cellophane were cut off from different sections of a sheet and were sandwiched between rigid cardboard shaped to fit the sample holder of the Beckman Spectrophotometer. The percentage transmittance of seven samples was measured at 6,500 Angstroms before and after irradiation. Since the dose per pulse

was not high enough, each cellophane piece was radiated for more than three pulses. Cellophane samples were located at different distances and were radiated at different times through the duration of the experiment. This was to monitor the repeatability of the electron dose from the tube as it was used. The percent transmittances of the samples were taken at different times before irradiation to check any changes due to time duration.

Spectrophotometer settings:	Scanning Time	2
	Scale Expansion	2X
	Time Constant	0.2
	Range	0-10
	Sensitivity	20

It was more convenient to get a trace of percentage transmittance vs. wavelength in a convenient range and then read the value of percentage transmittance at 6,550 Angstroms. (Fig. 7)

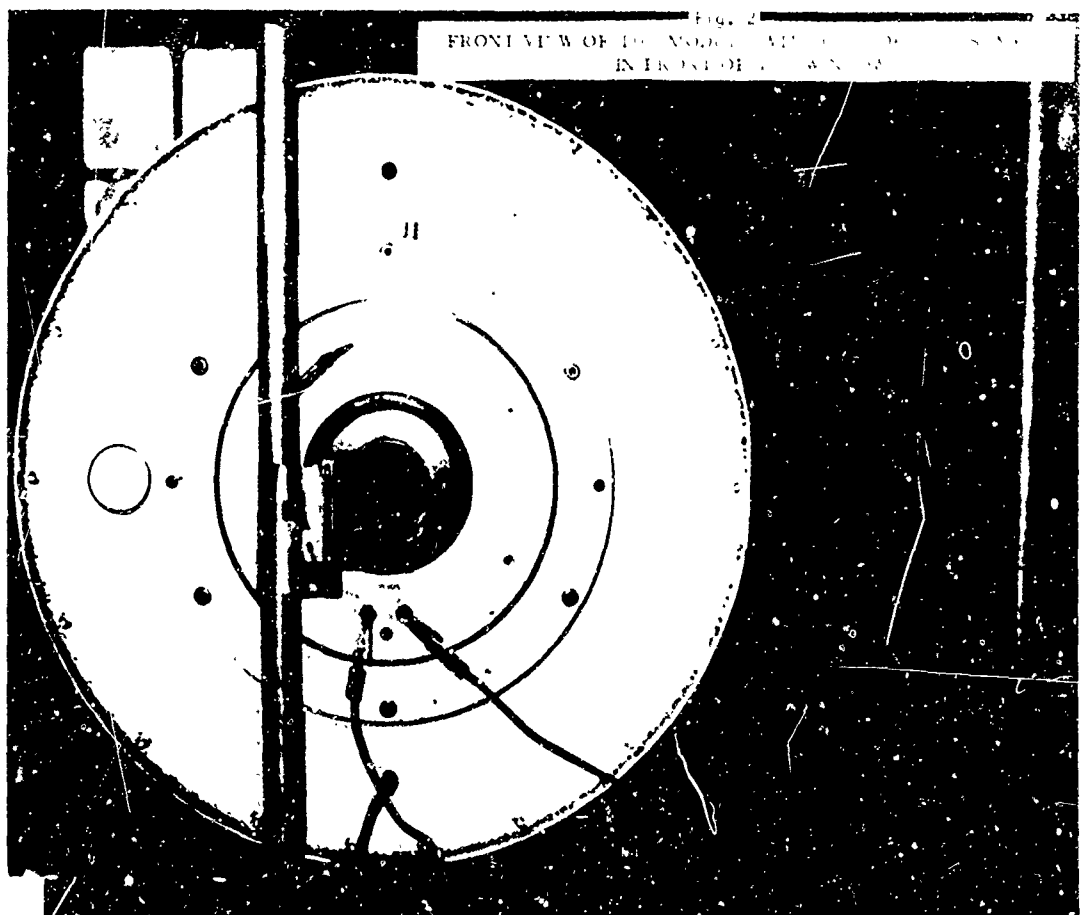
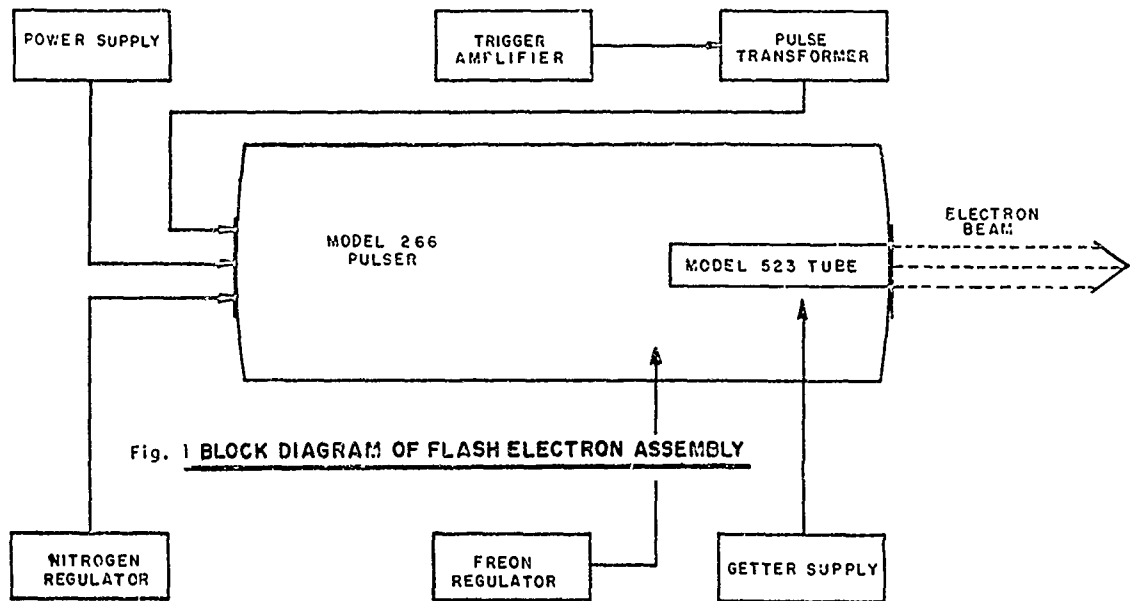
Distance from Source (inches)	Average Dose/Pulse (megarads)
5/16	1.4
7/16	1.33
1/2	1.07
9/16	0.89
5/8	0.67
1-7/16	0.22
1-5/8/3	0.08
1-3/4	0.075
42 @ 85°	Negligible

The flash electron tube was operated by the trigger system at 24KV instead of the maximum 30K in order to conserve tube life. The dose was monitored at different time intervals. Maximum energy was 540Kev. According to specification the dose was one Megarad pulse at  $\frac{1}{2}$  inch from the face of the tube.

The work reported on nuclear radiation effects indicates the need for developing a program to determine not only the nature and magnitude of these effects but the mechanism by which they occur. This brings us into the somewhat esoteric realm of crystal mechanics, surface space charge layer, and charge release mechanisms. Perhaps we shall be in a position to report from that rarefied atmosphere at the Seventh EED Symposium.

#### DISCUSSION

It appears that no work has been done with ferrites in the area of ferrite phase shift and disparity effect in respect to RF attenuators for EED's.



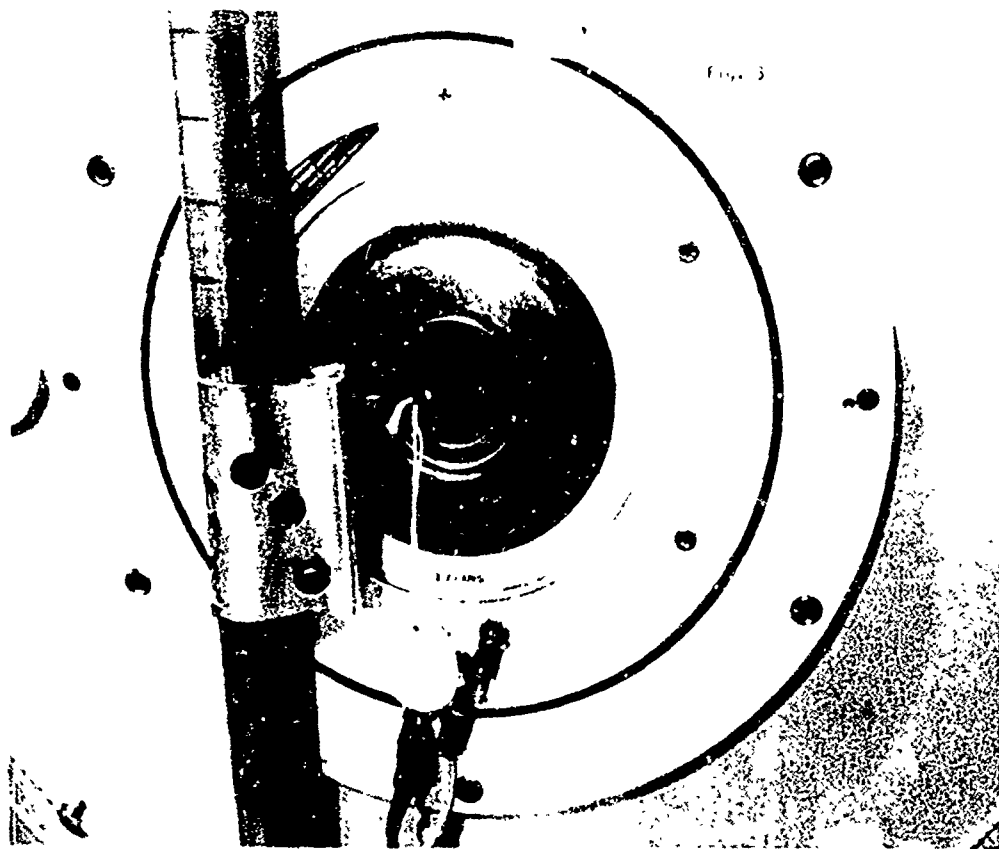


Figure 3

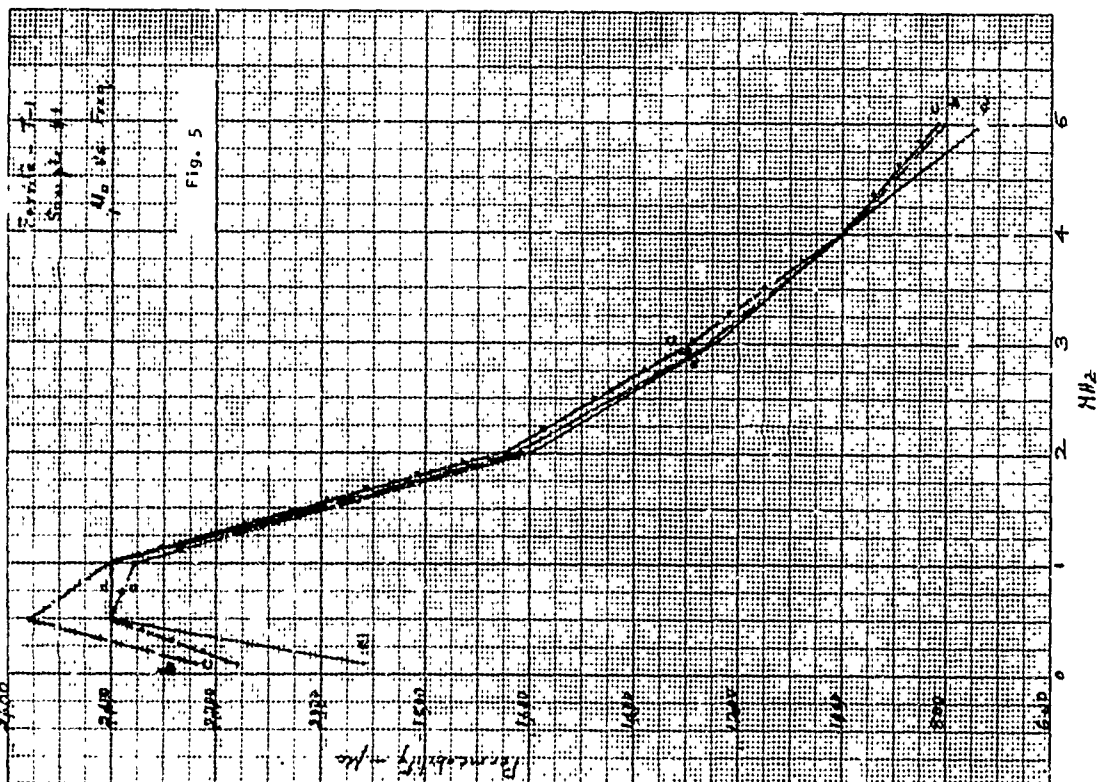


Fig. 5



Fig. 4

Frequency	Prior Irradiation	After Irradiation		Prior Irradiation	After Irradiation		
	8/16/68 $M_o(1)$	8/23/68 $M_o(2)$	9/6/68 $M_o(3)$	Q (1)	Q (2)	Q (3)	
<u>SAMPLE #1 -- 20 pulses</u>							
.1	5497	4718	5392	24	28	28	cm. OD= .575 ID= .305 H= .150
.5	4196	3707	4179	2	1	1.80	
1.0	2623	2528	2443	1	1	1.07	
2.0	1452	1685	1495	0.9	0.9	0.85	
3.0	1301	1357	1222	0.8	0.9	0.78	
4.0	995	982	868	0.8	0.7	0.60	
5.0	806	725	650	0.6	0.6	0.48	
<u>SAMPLE #2 -- 20 pulses</u>							
.1	4390	4064	4810	28	31	31	cm. OD= .580 ID= .305 H= .150
.5	3474	3649	3815	2	1	2.0	
1.0	2716	2322	2405	1	1	1.14	
2.0	1639	1555	1410	1	0.96	0.88	
3.0	1343	1271	1137	1	0.96	0.77	
4.0	1013	937	856	0.8	0.71	0.63	
5.0	768	697	631	0.6	0.57	0.50	
<u>SAMPLE #3 -- 10 pulses</u>							
.1	4266	3941	4414	22	28	25	cm. OD= .570 ID= .305 H= .150
.5	3460	3153	3405	2	1.9	1.98	
1.0	2654	2365	2365	1	1.36	1.30	
2.0	1482	1754	1577	1	1.1	1.01	
3.0	1278	1372	1216	0.8	0.92	0.77	
4.0	1006	945	840	0.8	0.66	0.57	
5.0	637	652	557	0.5	0.49	0.41	
<u>SAMPLE #4 -- 85 pulses</u>							
.1	4736	4976	5474	19	21	23	cm. OD= .580 ID= .305 H= .150
.5	3805	3981	3981	2	1	1.62	
1.0	2623	2488	2364	1	1	1.02	
2.0	1639	1576	1451	0.9	0.84	0.81	
3.0	1197	1218	1063	0.7	0.79	0.66	
4.0	866	818	743	0.6	0.56	0.51	
5.0	599	579	517	0.4	0.45	0.39	

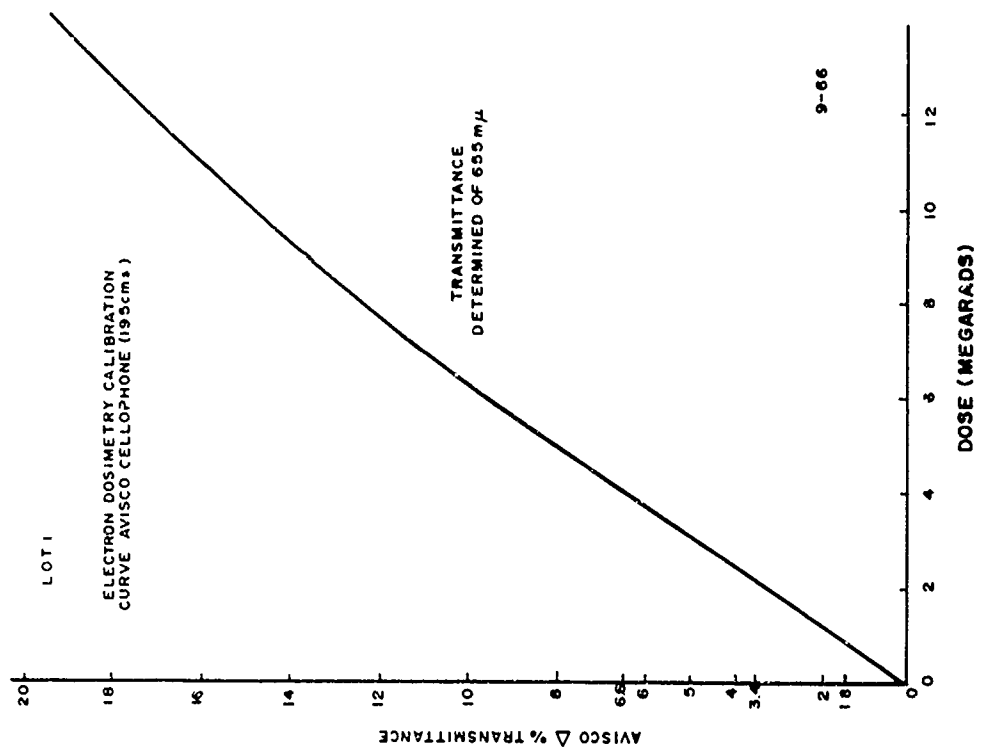
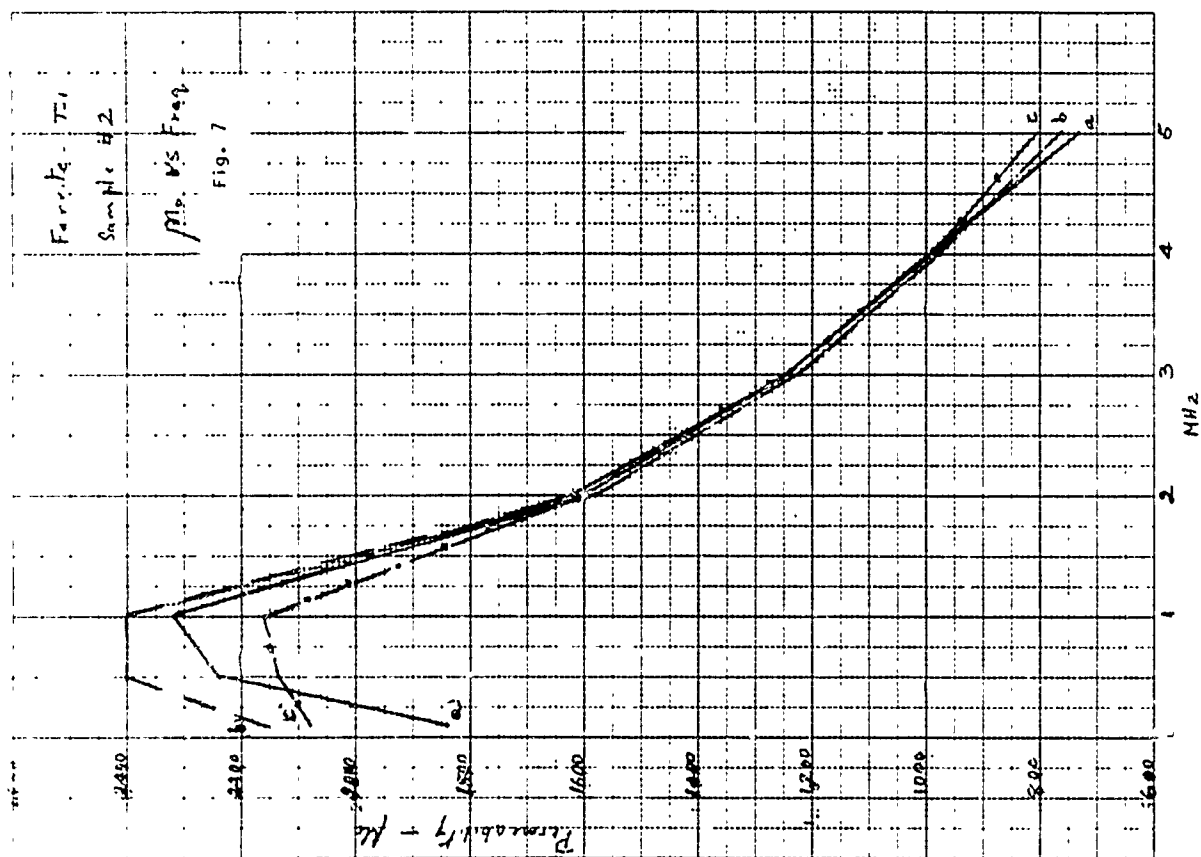


Fig. 6



4-9 RESPONSE OF SCOUT DESTRUCT  
CHARGES TO HIGH HEAT FLUXES

A. E. Pierard  
J. A. Bottorff

MISSILES AND SPACE DIVISION  
LTV AEROSPACE CORPORATION

A B S T R A C T

An experimental program was conducted to determine the sensitivity and possible premature operation of the Scout missile destruct system when subjected to an abnormally high temperature environment such as might be caused by a combustion gas leak into the vehicle Destruct Environmental Enclosure. Linear shaped charges, loaded with 180 grain/foot waxed RDX, were tested by subjecting them to radiant heat fluxes from 20 to 420 BTU/ft<sup>2</sup>-sec and measuring ignition time versus heat flux. Ignition times ranged from 37 milliseconds at 420 BTU/ft<sup>2</sup>-sec to 26 minutes at 20 BTU/ft<sup>2</sup>-sec. Test specimens were also subjected to heat by solid rocket motor exhaust gases. The latter experiments provided for direct impingement of the high velocity rocket exhaust gases on the test specimen and also for the hot gases to fill the volume under an environment cover normally employed around the charges. Direct impingement failed to initiate the charge; however, detonation did occur when the gases engulfed the charges under the environment enclosure. Witness plates in the latter tests indicated that part of the charge merely burned whereas part of the charge underwent a high order detonation.

INTRODUCTION

The investigation discussed in this paper was conducted by the Missiles and Space Division (MSD) of LTV Aerospace Corporation under NASA Langley

Contract NAS 1-6020 to study the effect of a high heat flux on the Scout Vehicle destruct charges.

The ASD-NASA Scout is a four stage vehicle, each stage being powered by a solid rocket motor. Linear shaped charges are located on the first three stages to provide the capability for flight termination. The linear shaped charges are located under an environmental cover along the entire length of each motor.

The explosive charges are fabricated by loading 2% waxed RDX into 3/8 inch O.D. aluminum tubing and pressing into a chevron shape. The charge loading is approximately 180 grains/foot. The 0.028 inch thick aluminum walls are primed with zinc chromate and painted with Enamel Gloss.

Stage separation on the Scout Vehicle is accomplished by gas pressure developed on ignition of the next motor. The build up in pressure from the exhaust gases causes release of the burned-out motor from the vehicle. Although the vehicle has been designed to prevent exposure of the destruct system of the spent stage from the hot exhaust gases of the thrusting stage at separation, the possibility of an accidental initiation of the destruct system does exist. Such an occurrence could cause damage from flying debris to the thrusting stage.

Another possible mode of failure is the accidental initiation of the destruct system by the impingement of hot gases from a leak in a solid rocket motor, although again, the system is designed to avoid such an occurrence.

Both of these possible modes of failure involve rapid exposure of the destruct system charges to a hot gas environment. Such a situation is not amenable to theoretical analysis because of the unknowns such as convective heat transfer coefficients to the specimens, the radiative and conductive heat transfer properties of the painted surfaces and structural weakening of the aluminum sheath during heating which can reduce confinement of the

explosive. Therefore, it was decided to conduct experimental tests in which test specimen destruct charges were subjected to rapid heating to determine the autoignition time and characteristic of the ignition.

The tests described in this paper consisted of two different types. In the first type of test, the specimens were subjected to static radiant heating. Radiant heat tests were conducted because of the relative ease in providing a range of heat flux conditions and the predictability of the environments. In the second type of test destruct charges were exposed to flow of hot gases from a small solid rocket motor. These latter tests more closely duplicated the conditions of a potential failure mode. The non-alumized propellant of the small rocket motors had a lower combustion temperature and different gas composition than the alumized propellant used in the Scout rocket motors. However, by correlating the test data with the results of the radiant heat tests, the specimen ignition time that would be obtained with the Scout motor propellant could be predicted.

#### RADIANT HEAT TESTS

The objective of this series of tests was to evaluate the sensitivity of the destruct charges to high heat fluxes by exposing samples to known radiant heat fluxes ranging from 20 to 420 BTU/ft<sup>2</sup>-sec and to measure the time required for the sample to autoignite.

Two different series of radiant heat tests were conducted; one series of three tests was conducted at low heat flux and the other series of three tests was conducted at high heat flux. The high heat flux tests, 160 to 420 BTU/ft<sup>2</sup>-sec, were conducted after experimental results revealed that testing at lower flux levels produced ignition times longer than three seconds. These long delays are not considered significant because a motor leak of this duration would in itself cause catastrophic destruction of the stage. On the other hand, a delay of this magnitude, at stage separation, would

provide time for the spent stage to move a safe distance from the thrusting stage before charge initiation.

#### Low Heat Flux Tests

The three specimen used for this series of tests were identical and consisted of sections of production destruct charges similar to those used on Scout Vehicle.

The test apparatus consisted of a low temperature furnace in which radiant heat was applied by pyrometric reflectors No. PM 99685-B. Each reflector was fitted with five 10 inch - 2000 watt G.E. tublar lamps No. 2MP-3. The reflectors were air cooled. The reflectors were adjusted so that the distance from the nearest lamp to the specimen was one inch.

The radiant heat was manually controlled by means of a 200KW Research Incorporated "Thermac". This controller is essentially an ignitron tube type pulser using single phase 60 cycle current.

Following the design and fabrication of the test equipment, operational checks and calibration runs were performed to assure that the test requirements could be met. The system was calibrated using a copper slug type calorimeter, Alabama Automation Model C-7. This calorimeter measures heat by the rate of temperature rise in a thin plate. A continuous writing, single channel, Minneapolis - Honeywell, Brown Recorder was used to record the temperatures. The heat flux measured by the calorimeter was correlated with its distance from the lamps and the voltage drop across the lamps. This calibration data was used to determine the heat flux to a test specimen knowing the specimen distance from the lamps and the voltage drop across the lamp.

To conduct a test, a specimen was placed in position, the voltage drop was adjusted to the proper value and the lamps were turned on and were allowed to remain on until the charge initiated. The time to initiation was determined

by monitoring a thermocouple mounted on the specimen. The thermocouple, facing toward the lamps, provided a first indication of heat to the specimen and indicated when initiation occurred by a termination in the signal. Temperatures as measured by the thermocouple were not considered valid because of direct exposure to the incident radiation.

Tests were conducted at flux levels of 20, 50 and 75 BTU/ft<sup>2</sup>-sec. The results are shown below in Table I and graphically in Figure 1.

TABLE I  
RESULTS OF LOW HEAT FLUX TESTS

<u>FLUX LEVEL (BTU/ft<sup>2</sup>/sec)</u>	<u>TIME TO IGNITE (sec)</u>
20	26
50	8
75	3.5

#### High Heat Flux Tests

The test specimens for this series of tests were specially prepared by loading a 13 inch length of 3/8 inch O.D. aluminum tubing with eight inches of waxed RDX to a loading of 180 grains/ft and the remaining 5 inches with Boraxo soap as an inert filler. The inert filler was used in the low temperature tests in order to reduce the total quantity of explosive, and hence, the amount of required shielding. The tube was crimped to the configuration of the Scout shaped charge and end caps were installed. Figure 2 shows a typical specimen. All samples were painted similar to the production hardware except for some stripes on the inert section which aided in reducing the data which was recorded by a high speed movie camera.

A special high temperature resistance furnace shown in Figure 3 was used to provide the required heat fluxes. The furnace consisted of a 12-inch long, 2-inch I.D., by 3/8-inch thick wall graphite tube oriented vertically and clamped at both ends with copper electrodes. The electrodes were supported on a one-inch thick, 12-inch wide by 18-inch long Supramica high temperature board. Power cables connected the furnace electrodes to the power supply. The furnace tube was plugged at the bottom with a graphite block and was thermally insulated circumferentially to a thickness of two inches with layers of 1/4 inch carbon felt. Two layers of fiberglass cloth were wrapped around the outside of the carbon felt to inhibit burning of the felt. A 1/2-inch diameter hole cut through the thermal insulation in line with a 1/4-inch diameter hole drilled through the wall of the graphite tube provided a line of sight into the furnace for the optical pyrometer temperature measurements. The furnace was observed to heat uniformly over a 6 to 8 inch long section at the furnace center.

The power supply for the furnace consisted of a 150 kw, ignitron tube controlled, power circuit with a multi-tapped, impedance matching, output transformer. The resistance of the graphite tube was approximately  $10^{-2}$  ohms and the 10 volt, 15,000 amp, secondary tap was used for these tests. A special power supply remote control potentiometer was installed to allow the operator to be stationed behind a blast shield.

A guided free fall drop tower, shown in Figure 4, was used as a means of inserting the test article into the furnace. This system allowed positioning of the specimen in the furnace with an elapsed time from initial entry in the furnace to final positioning of only 40 milliseconds. The drop tower consisted of a vertical pole 20 feet long, anchored at the base to the furnace structure and supported by four guy wires at the top. A carriage was made



to slide on two taut cable guides attached to the vertical pole. A 3/8 inch I.D. coupling was used to attach the specimen to the carriage. Set screws held the specimen in the coupling. The carriage with a dummy specimen installed can be seen in Figure 3. A quick release latch was installed at the top of the drop tower and the latch was actuated by means of a string extending to the operator's station behind the blast shield shown in Figure 4. The drop tower was adjusted such that the lower nine inches of the specimen would extend into the furnace along the furnace's vertical centerline. Movies of the tests indicated that the specimens did not touch the furnace wall. The free fall travel of the carriage was 16 feet.

Instrumentation was provided to measure furnace temperature, timing of events, and power supply voltage and current. The furnace temperature was measured with a Pyrometer Instrument Co. Micro Optical Pyrometer, Serial No. M-4936 with a 1300 to 5800°F range. Timing of events was recorded by a Fairchild Model HS 100, 16 mm high speed camera at a film speed of 1000 frames per second. The accuracy of the timing of events was  $\pm 5$  ms.

Checkout of the apparatus consisted of approximately two dozen drops made with a dummy specimen installed on the drop tower. High speed movies were taken of four drops. Prior to conducting the series of tests, the furnace was heated to approximately 4500°F to demonstrate its design adequacy.

A test specimen was prepared prior to each test and loaded on the drop tower. The furnace was heated to the required temperature and monitored with the optical pyrometer located approximately five feet from the furnace behind the blast shield. After recording temperature and power supply readings, a ten second countdown was initiated. At 0 minus one second the camera was turned on at 0 seconds the latch mechanism was released allowing the specimen to enter the furnace at approximately 0 plus 1 second.

The heat flux for these tests ranged from 160 to 420 BTU/ft<sup>2</sup>-sec. The high speed film revealed that the paint burned off prior to ignition. The furnace temperature and event timing data are presented below. A plot of ignition time versus heat flux for these tests conducted at low heat flux is shown in Figure 1.

TABLE II

RESULTS OF HIGH HEAT FLUX TESTS

<u>Furnace Temp (°F)</u>	<u>Heat Flux (BTU/ft<sup>2</sup>-sec)</u>	<u>Time of Insertion (Milliseconds)</u>	<u>Time to Ignite After Insertion (Milliseconds)</u>
3850	160	43	547
4500	289	33	625
5000	420	37	375

The resulting shock after initiation of the charge caused the graphite furnace tube and its thermal insulation to disintegrate, requiring replacement of these components after each test. Figure 5 shows the furnace after one of the tests. The timing data was obtained from the high speed movies. The explosive yield (noise) of the 4500°F test seemed to be lower than the other two tests, although there is no plausible explanation for this. Figure 2 shows the 4500°F specimen after the test. The aluminum appeared to have been near its melting point at the bottom end, and all paint had been burned off on the lower 6 inches. The specimens painted with the yellow paint appeared dull, rusty colored near the top. Not enough of the lower 8 inches of the specimens were recovered to make an observation of their appearance.

HOT GAS IMPINGEMENT TESTS

The objective of these tests was to evaluate the vulnerability of the Scout destruct charges to hot propellant gases which might be vented under

the tunnel and impinge directly upon the destruct charges. The test specimens were section of actual Scout production charges consisting of standard aluminum tubing of 3/8" O.D. loaded with 180 grains per foot of waxed RDX explosive and pressed to a chevron configuration. The charges were cut to provide a length slightly longer than the third stage X-259 motor case. Two charges were then assembled over a previously fired X-259 motor case, and covered with a fiberglass tunnel cover to simulate actual Scout installation. The assembly just prior to testing is shown in Figure 6.

The hot gas for impingement on the specimens was provided by .6KS 40 or 1KS40 solid rocket motors used as spin motors on the Scout Vehicle. The propellant in these motors is Atlantic Research Corporation Arcite 362 M which is a nonaluminized composite propellant having a flame temperature of 2284°K. The .6KS40 motor has a nominal burn time of 0.642 seconds and a mass flow of 0.192 pounds/second. The nominal burn time of the 1KS40 motor is 1.07 seconds and the mass flow is 0.199 pounds/second. Variation of mass flows and exposure times could be achieved by employing combinations of motors.

Instrumentation was provided to measure the outside surface temperature of the destruct charge tubes as a function of time. Temperatures were measured at six different locations with iron-constantan thermocouples and were recorded on a visicorder. Timing events were obtained with a high speed movie camera operating at 1000 frames/second. Witness plates were placed under each charge at each end of the motor case. These witness plates were identical to those used for acceptance testing of destruct charges for the Scout Vehicle. High order detonation of the RDX is necessary to cause the destruct charges to cut the witness plates.

The motors were positioned internal to the X-259 chamber and located with the nozzle pointing toward the case as shown in Figure 7. A hole drilled through the X-259 motor case allowed gas to vent into the destruct tunnel. High speed motion picture cameras were turned one second before current was applied to the gas generator squibs.

The first test firing utilized a .6KS40 motor exhausting through a 1/4 inch diameter hole in the motor case. The hole in the case was located between the two destruct charges. The hot exhaust gases eroded the underside of the fiberglass case but did not enlarge the drill hole. The only effect inside the tunnel was smoke deposits.

The conditions of the second test were similar to those of the first except that the motor exhausted through a 3/4" diameter hole in the motor case. After this test, it was found that the wiring insulation had started to melt and a heavy smoke deposit was produced. Slight erosion of the fiberglass at the top of the tunnel was noted.

The third test consisted of firing three (3) 0.6KS40 motors through a 1" x 4" rectangular hole in the fiberglass motor case. The results of this test are shown in Figure 8. All materials in the vicinity of the rocket exhaust suffered severe damage, but no detonation occurred. Three or four inches of each charge were melted away and the explosive was missing from another 5 to 7 inches on both sides of the burned out section, leaving the hollow aluminum tube. All of the insulation was burned away from the exposed section of the wire bundles and some of the wires were burned through. The wire at the left side of the photograph was used to support the destruct tube and wire bundle for the purpose of indicating their location in the photograph. The mounting bracket had broken loose from the case.

The fourth test utilized a 1KS40 rocket motor for the gas generator and the gases were directed through a 1/2" hole into the tunnel region. The damage was more extensive than for firing of the 0.6KS40 motor but less severe than for firing of three 0.6KS40 motors. Ignition of the destruct charges still did not occur even though the thermocouples recorded 800 to 900°F on the surface of the destruct tubes.

Test Number five employed two 1KS40 spin motors placed side by side and each fired through a separate 1/2 inch hole drilled in the case. The motors were programmed to fire sequentially with an approximate overlap in burning of 20 milliseconds. After 1.268 seconds of burn time the destruct tube initiated and failed the motor case the entire length of its cylindrical section. Figure 9 is a view of the motor case (a section of case between the two charges was wired into its original position for the photograph). Fraying of the fiberglass is also obvious at the top of this picture. Figure 10 is a photograph of the retrieved witness plates. The two plates joined by tape were originally located at the aft end of the motor case. The other two plates, shown as 3 pieces, were located at the forward end of the motor case. These witness plates indicate that the two charges did not undergo a high order detonation aft of the gas vent hole but forward of the vent one charge underwent high order and the other was in a transition from low order to high order detonation over the witness plate. The relationship of the radiant heat flux from the gas to time of ignition produced by these two motors is shown by a point on Figure 1.

A review of the high speed film indicated a very bright puff of smoke 1.034 seconds after ignition of the spin motors and detonation 0.230 seconds later. This indicates that the charges may have ignited and separated into two pieces without undergoing high order detonation at the time of the first bright puff of light. This action could explain one half of the charge going low

order and the other half going high order. The results of five tests are summarized in Table III.

TABLE III  
SUMMARY OF HOT GAS IMPINGEMENT TESTS

<u>GAS SOURCE</u>	<u>NUMBER OF GAS GENERATORS</u>	<u>VENT HOLE (in)</u>	<u>APPROX. GAS FLOW TIME (sec.)</u>	<u>RESULTS</u>
.6KS40	1	0.25 dia	0.64	Smoke Damage Only
.6KS40	1	0.75 dia	0.64	Slight Erosion of Fiberglass
.6KS40	3	1 x 4	0.64	Melted Charge-No Detonation
1KS40	1	0.5 dia	1.0	Damage more Severe than one .6KS40 But no Ignition
1KS40	2	0.5 dia each	1.264	Detonation of Charge

#### CONCLUSIONS

1. High heat fluxes, as may be experienced by engulfing the destruct charges in rocket motor exhaust gases, can cause ignition in less than 1 second.
2. Initiation does not appear likely with direct impingement of the high velocity exhaust gases. These tests results concur with previous testing conducted on the destruct system.
3. Engulfment of the charges in the hot exhaust gases will cause initiation. This action may be high or low order detonation. A more extensive test effort is required to resolve the mechanism for initiation to high or low order.
4. Prediction of function time appears feasible based only on radiation from the gas.

#### DISCUSSION

At Lockheed, RDX in lead sheaths that were subjected to gas flames of about 4500°F at velocities of 2000 fps did not detonate the RDX. All that occurred was burning of the RDX that was in direct contact with the hot gases. The gases melted and eroded the lead and left the RDX core mostly unburned. The compression pressures used in forming shaped charges (FLSC) composed of RDX and 2 percent wax in a 3/8 in. O.D. aluminum tubing was estimated to be between 20,000 and 25,000 psi.

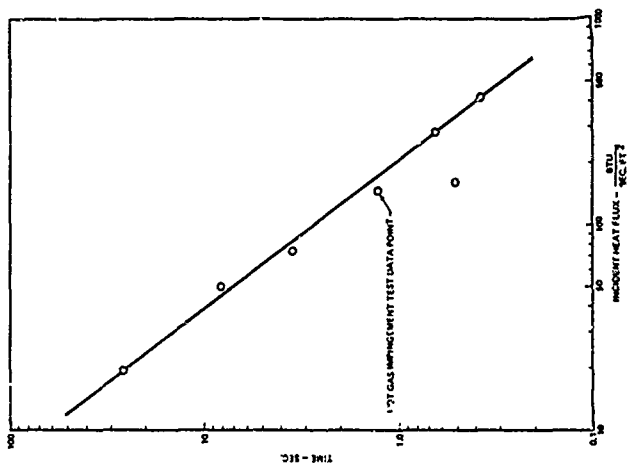


**FIGURE 1 IGNITION TIMES FOR RADIANT HEAT TESTS**



**FIGURE 2 HIGH HEAT FLUX TESTS SPECIMEN - BEFORE & AFTER TEST**



### FIGURE 3 HIGH TEMPERATURE FURNACE



**FIGURE 4 DROP TOWER**

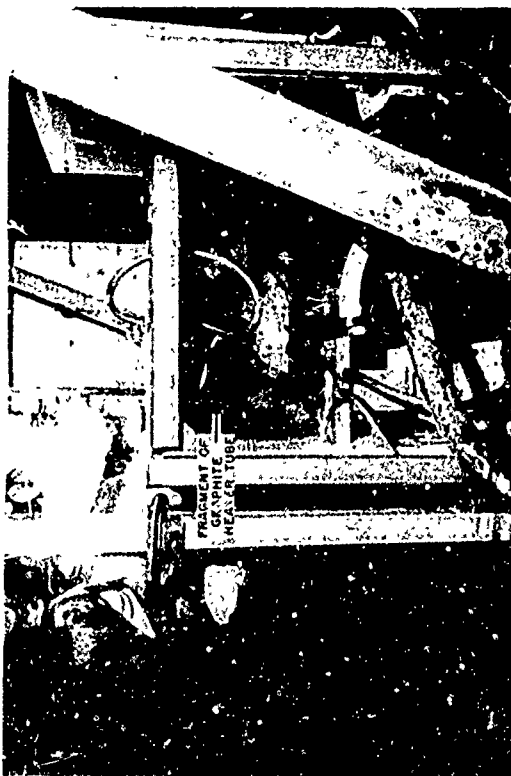


FIGURE 5 HIGH TEMPERATURE FURNACE AFTER TEST

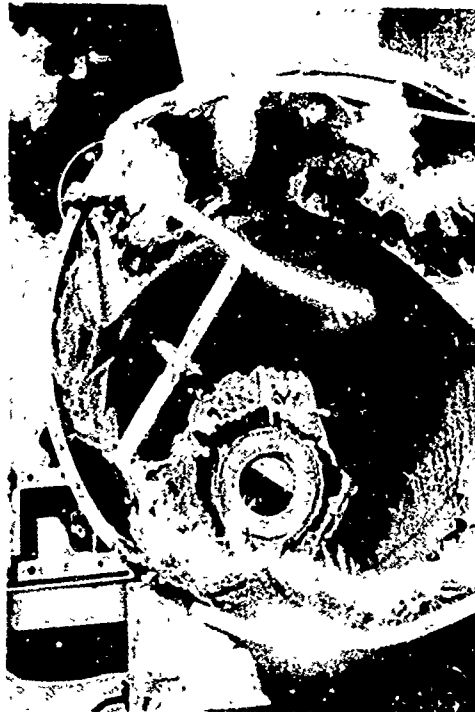


FIGURE 7 .6KS40 ROCKET IN POSITION FOR TEST

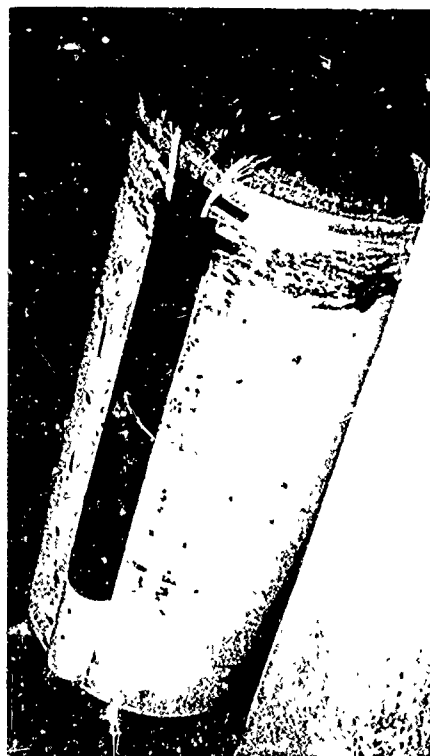


FIGURE 6 DESTRUCT SYSTEM ASSEMBLY PRIOR TO TEST



FIGURE 8 POST FIRE VIEW -- THREE .6KS40 MOTORS FIRED SIMULTANEOUSLY





FIGURE 9 MOTOR CASE AFTER TEST OF TWO 1KS40 MOTORS FIRED SEQUENTIALLY

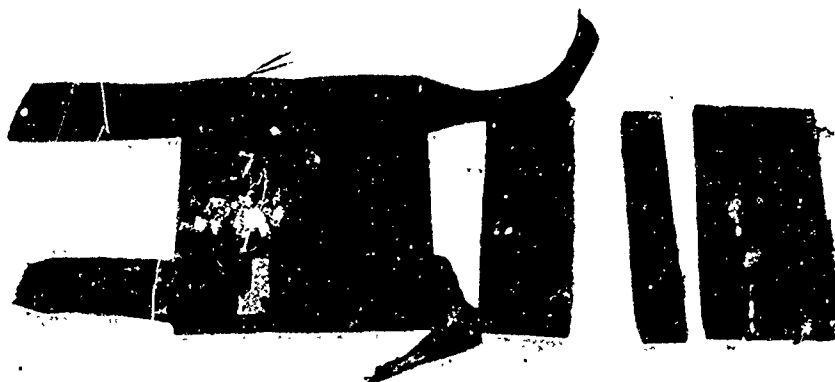


FIGURE 10 WITNESS PLATES AFTER TEST WITH TWO 1KS40  
MOTORS FIRED SEQUENTIALLY

## 4-10 dx/dt vs TIME DETONATION MONITORING

Donald Baker Moore and Roy McLeod

### Explosive Technology

#### INTRODUCTION

Detonation Velocity measurement in explosives and explosive products is of considerable interest as a means to understanding basic phenomena as well as being a practical measure of performance and quality. Most commonly detonation velocity is estimated by monitoring the elapsed time between arrival of some manifestation of detonation progress between two or more known positions. In the ideal case this manifestation may be the ionization zone within the detonation front short circuiting switches or ionization probes. More commonly the observable will be the motion of a surface, or the result of motion of a surface of some material in contact with the explosive, if not the explosive surface itself. This paper presents results obtained from metal sheathed explosive cord, but the technique is applicable to and has been used with bare cast and extruded explosives.

Frequently it is desired to measure the reproducibility of detonation velocity in explosive cord, or other items. It is immediately apparent that when elapsed time measurements are made over fixed distances the standard deviation of the velocities calculated should be proportional to the square root of the distance measured, but the relative standard deviation, or coefficient of variation, which is a more common measure of precision, should be inversely proportional to the square root of the distance measured. From this it follows that, unless care is used in stating exact experimental conditions, an explosive cord with velocities estimated over two inch distances might show a coefficient of variation of two percent, where if the same product were measured over one meter

distances it could be expected to appear to be better than one-half percent.

Considerations of this nature, in addition to questions of fundamental detonation mechanics, indicate the desirability of point estimates of detonation velocity, or continuous detonation monitoring as a function of distance.

#### TECHNIQUE

The "continuous wire" method has been in use for some years as a means of measuring detonation front displacement as a function of time. This technique consists of installing a resistance wire or wires either in the explosive, or immediately adjacent to a metal sheath about the explosive in such a manner that either the ionization front in the explosive, or the motion of the metal sheath will progressively short the resistance wire. This short will proceed along the resistance wire with a displacement more or less directly relatable to the displacement of the detonation front. If either a constant voltage or constant current source is connected in series with the resistance wire, a change in current or voltage across the wire will be observed whose magnitude can readily be determined and which can be then directly related to the location and motion of the progressive short.

Early measurements by the authors and others using constant voltage sources were inconvenient to interpret, however, later measurements by Amster (Ref. 1), and others using constant current sources yielded output voltages directly proportional to displacement and were directly readable. The exact details of the circuitry and connections are not given here but are fully documented by others such as Price, et al. (Ref. 2) and Pirts (Ref. 3).

The results of the continuous wire method yield displacement vs time data which can then be graphically differentiated to get estimates of velocity vs distance or time. Although other means have been used in special circumstances for measuring displacement or velocity directly, particularly those using microwaves (Refs. 4 and 5), the continuous wire method remains the simplest and for most purposes the most useful. Considering the limitations of precision in using an oscilloscope, and that this technique is most useful for observing relative velocity variations than for absolute measurement, elaborate constant current power supplies and temperature compensation have proven unnecessary. In fact we have had considerable success with a single transistor biased so that its current output is only a negligible function of load variation within the limits used.

It was remarked above that what is frequently desired is not simply an average detonation velocity, but point estimates or, preferably, a continuous record of detonation velocity as a function of displacement. This has usually been obtained from the continuous wire technique output by graphical differentiation of the resultant oscilloscope trace. The authors have for some time eliminated this step by the comparatively simple means of electronically differentiating the displacement-time data as it is generated by the progressive shorting of the continuous resistance wire.

This is accomplished readily by inserting the normal displacement-time, or  $x-t$ , data into an operational amplifier set up for differentiation, and displaying the output  $dx/dt$  vs  $t$ , on a dual beam oscilloscope on one channel, using the second channel for displaying the usual  $x$  vs  $t$  information. The results shown in the figures were obtained using a Tektronix Type O preamplifier in a Type 555 oscilloscope. Input and Feedback impedance were adjusted to obtain satisfactory gain and frequency response. ( $Z_1 \approx 0.0001$

microfarad,  $Z_f = 0.01$  megohm). With these settings and using 15.2 milliamperes through 199.1 ohm/foot single silk insulated Karma wire, output voltage changes of 10 millivolts per centimeter change in resistance wire length were obtained. This gives for the x-t trace at a vertical scope sensitivity = 0.5 volt/centimeter a scale of 50mm (displacement)/scope vertical centimeter and two microseconds/horizontal centimeter. For the dx/dt trace with a vertical scope sensitivity = 0.05 volt/centimeter, a scale of dx/dt = 5mm/microsecond corresponds to one centimeter vertical deflection. These scales are indicated in the figures.

### RESULTS

Figure 1 is a record using the above parameters to monitor the detonation of five grain per foot, lead sheathed, RDX filled explosive cord. The bottom trace is the usual x-t record, the top trace is the electronically differentiated dx/dt record. It will be observed that the record shows an instrumented cord length of 100mm and that the dx/dt record shows a varying "velocity" ranging from about six to eight millimeters/microsecond.

As mentioned in the beginning the word velocity must be used carefully, particularly in this measurement, since what we actually observe is a closure, or rate of closure, produced by the motion of the lead jacket expanding and shorting the resistance wire. Variations in rate will be due to both real variations in explosive detonation velocity, and variations in jacket thickness from point to point along the explosive column length.

Figures 2 and 4 show similar observations on the same lot of cord except that in both cases the cord had been carefully bent in two places ninety degrees about a one-quarter inch radius and then straightened. Effort was taken to prevent perturbing the cord between the bends. The results clearly show disturbances in both the x-t and dx/dt traces and indicate that in spite of precautions, the cord performance has been altered along its entire length, in addition to the two anticipated major effects.

Figure 3 is another example of the same cord which was handled carefully; with every attempt being made to preserve its integrity before firing and is representative of observed velocity variations in good cord.

Figure 5 is a reference shot showing the electrical noise in the circuit when steady state current existed in the resistance wire and the cord was not detonated, but an electrical detonator was fired near the cord. This figure is included to demonstrate that while the electronic differentiation technique can be notably noisy, in this case the major variations observed are appreciably in excess of the electrical noise level.

#### CONCLUSIONS

We have used a modification of the continuous wire technique for monitoring the detonation velocity in explosives, and the velocity of propagation of metal sheath disturbance in metal clad explosive cords. The device of electronically differentiating the normal  $x$  vs time curve to obtain a  $dx/dt$  vs time plot has proven useful, and challenging. While it has lent itself well to examination of the performance of products, it has simultaneously given us a means of detailed examination of that performance such as we have not previously known. Further work will be required to enable us to differentiate between that portion of the observed effects which is due to real variation in explosive detonation velocity, and that which is contributed by variations in the sheath thickness or hardness. In the meantime, while this technique does not yield numbers of the apparent precision and accuracy obtainable by simple elapsed time measurement, neither does it conceal what may be real and significant variables in explosive performance.

#### REFERENCES

1. Amster, A. B., Kendall, P. A., Veillette, L. J., and Harrell, E., "Continuous Oscillographic Method for Measuring the Velocity and Conductivity of Stable and Transient Shocks in Solid Cast Explosives," Review of Scientific Instruments, 31, pp 188-192, 1960
2. Price, D., Toscano, J. P., and Jaffe, I., "Development of the Continuous Wire Method Progress Report III. Measurement in Cast DINA," NOLTR 67-10, United States Naval Ordnance Laboratory, White Oak, Silver Spring, Maryland 1967
3. Pitts, Locha D., "Electrical Probe Technique for Measurement of Detonation and Deflagration Velocities," Proceedings of the Fourth Symposium on Detonation, ACR-126, Office of Naval Research, Washington, D.C., 1965
4. Cook, M. A., Doran, R. L., and Morris, G. J., "Measurement of Detonation Velocity by Doppler Effects at Three-Centimeter Wavelength," Journal of Applied Physics, 26, pp 426-428, 1955
5. Johnson, Edgar G., "A Microwave Technique for Studying Detonation Phenomena," Proceedings of the Fourth Symposium on Detonation, ACR-126, Office of Naval Research, Washington, D.C., 1965

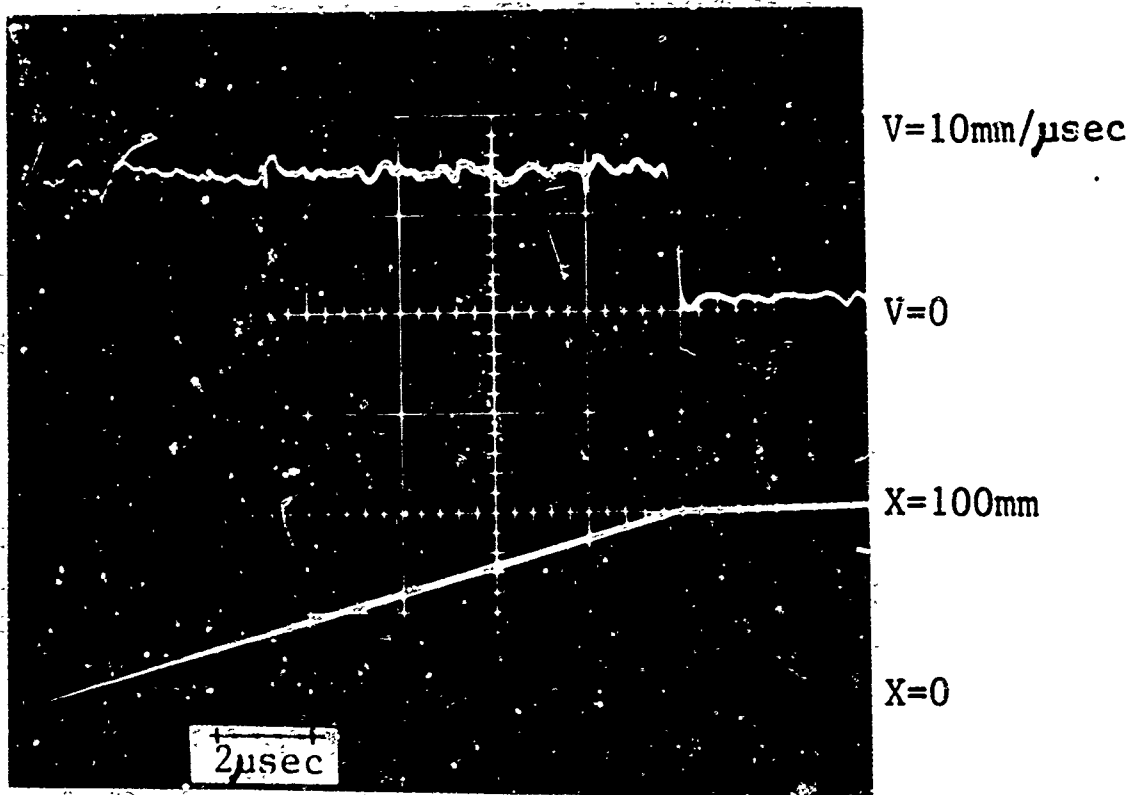


Fig. 1  $dx/dt$  vs  $t$ , and  $x$  vs  $t$  record of detonation in five grain per linear foot, lead sheathed, RDX filled explosive cord, undamaged.

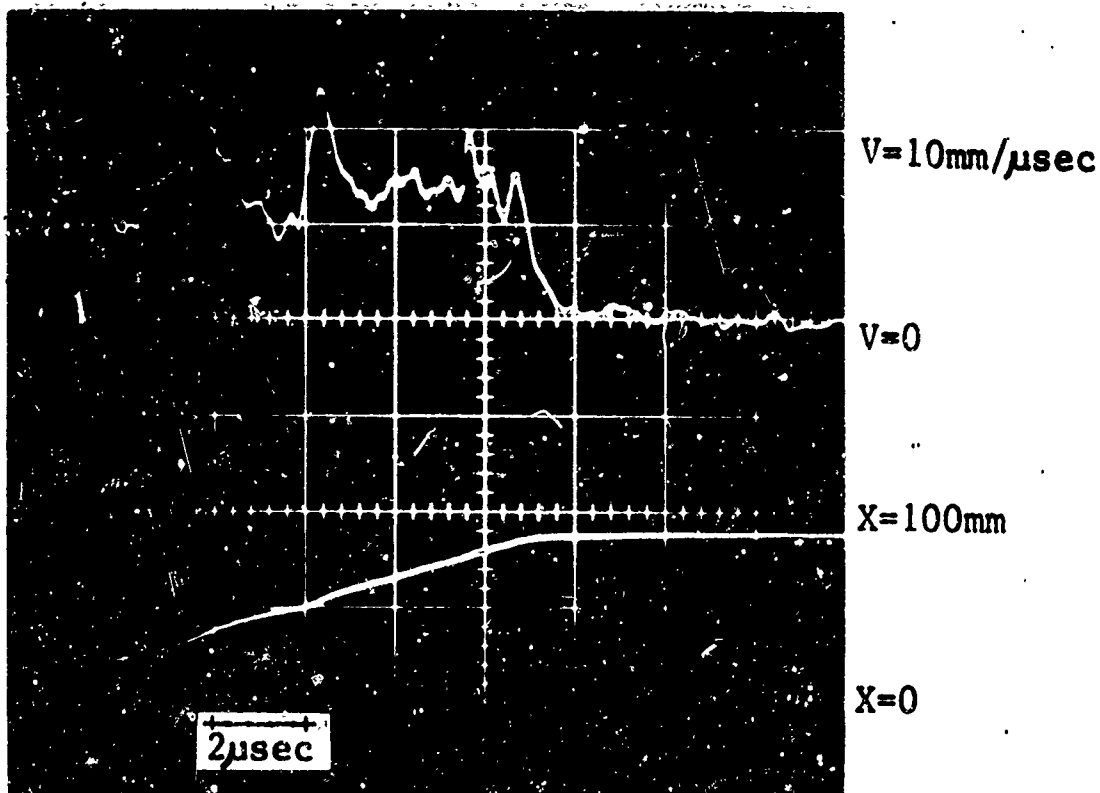


Fig. 2 Record obtained from similar cord bent and restraightened.

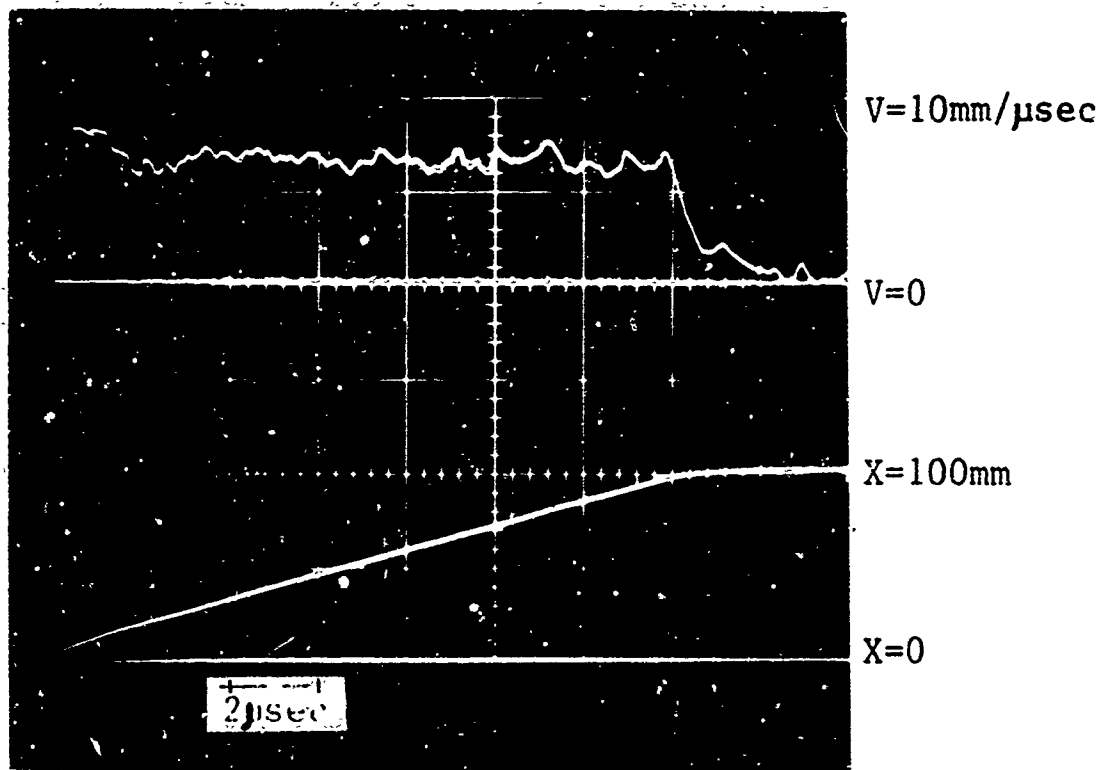


Fig. 3 Record from undamaged cord, similar to Fig. 1.

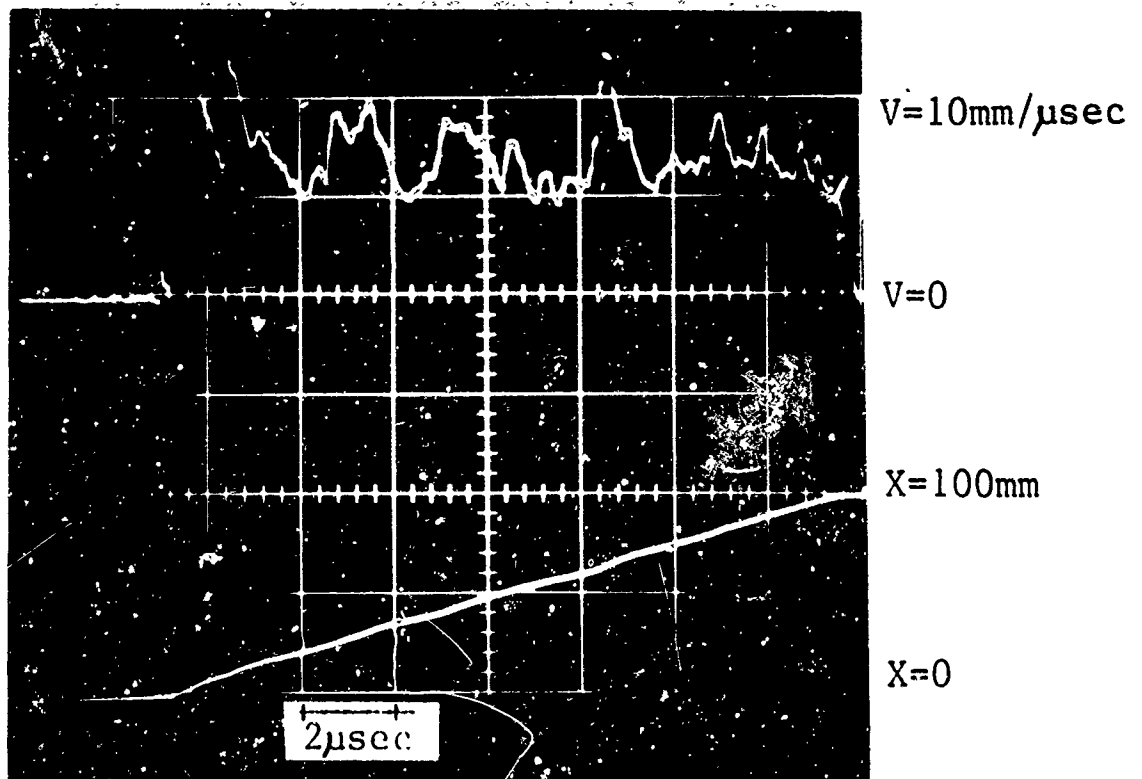
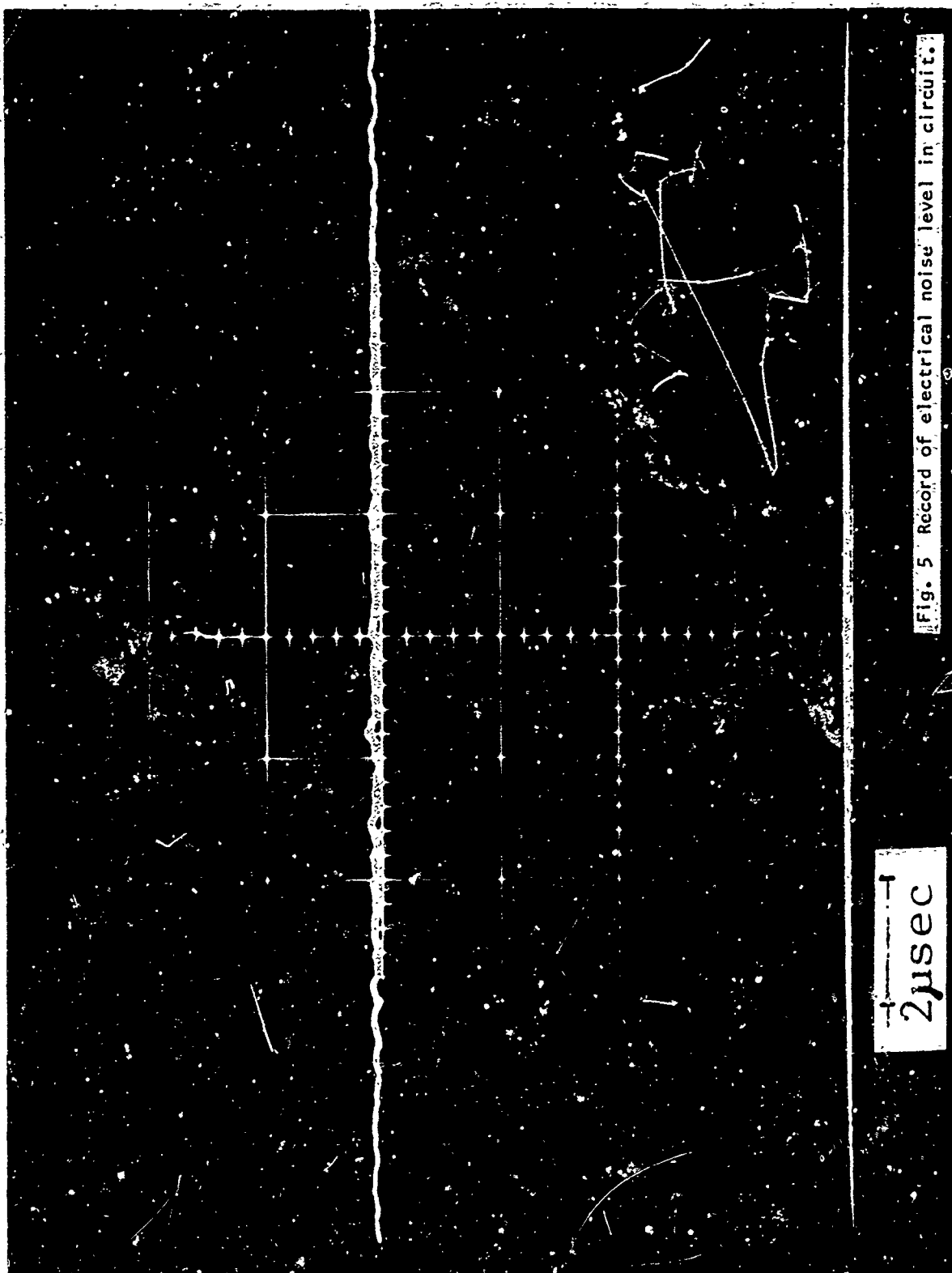


Fig. 4 Record from cord bent and restrengthened as in Fig. 2.





#### 4-11 EVALUATION OF DETONATING CORD BY FRAMING CAMERA TECHNIQUE\*

JIM W. BLAIN, BERTIL V. CARLSON, ALLAN H. SMITH

LOCKHEED MISSILES & SPACE COMPANY

##### ABSTRACT

An experimental technique for the evaluation of detonating cords was developed based on high speed motion picture photography. Explosive performance of several RDX-metal sheath systems were photographed using the framing camera technique at frame rates of  $5 \times 10^5$  and  $1 \times 10^6$  frames/second (2 microseconds and 1 microsecond per frame). Performance characteristics of each system were established and evaluated for missile design applications.

##### INTRODUCTION

One of the most important uses of detonating cord in the design of a missile is to separate structural members (i.e., separate two sections of the missile body). There is a scarcity of published information on the fundamental behavior of the detonating cord relating the detonation products of the explosive to the behavior of the metal sheath and further, to the ability of the metal sheath to perform useful work such as breaking a metal joint or separating a metal skin. The designer now has to rely on his past experience with similar applications of detonating cord and on destructive tests which empirically relate basic design parameters of the detonating cord to the final destructive action of breaking the metal. Unfortunately, these tests do not always predict the ability of the detonating cord to break the metal joint.

\* The work reported in this paper was performed at Lockheed Missiles & Space Company under U.S.N. Contract N0003066C0186

Recently we experienced this non-predictability when attempting to correlate the joint separating capability of detonating cords which were manufactured by different vendors who used dissimilar manufacturing processes and which were tested at different time phases in a long range program. In addition, variations in explosive behavior were observed between lead sheathed detonating cord and aluminum sheathed detonating cord when it was confined inside either IMSC Zipcord, polyurethane plastic tubing or fiberglass sheathing.

In order to better understand the performance of the detonating cord, its ability to break a metal joint and its ability to expand a polyurethane tubing, a special high speed photographic technique was developed to observe the detonation process and subsequent fragmentation of the metal sheath. In this technique, a sample of detonating cord was detonated and the detonation process was recorded by a framing camera at frame rates of one microsecond per frame. The details of this technique, the analysis of the detonation process and the detonating cord characteristics that are pertinent to the application of breaking a metal joint are discussed in this paper. Experimental correlation of the performance of the detonating cord to actual separation joint design or to confinement in plastic tubing was not completed in time for presentation in this paper.

#### EXPERIMENTAL PROCEDURE

Since the purpose of the study was to investigate the dynamic behavior in the micro-second time region of small size detonating cords, a technique was developed using the Cordin 1.2-million frames/second framing camera. Figure 1 depicts the overall test setup, comprising of a camera, strobe lamp and sample test fixture.

The procedure for accomplishing the test program was as follows:

An 8-inch (20 cm) long sample of detonating cord was secured in the test fixture exposing an approximate 6-inch (15 cm) length to the camera field. Replaceable adapter collets were made to fit the various sample diameters. Immediately behind the sample was placed a 1 mm x 1 mm paper grid. This grid was used as a reference scale in data reduction. The test fixture also accommodated a 1/4-inch thick plexi-glass window (placed approximately 1.5 inch in front of the sample) which protected the camera lens from the blast and fragments.

In order to obtain the high speed initiation event necessary for camera timing, the samples were initiated with an EBW detonator. For this particular test series, a Reynolds Industry's P/N 167-4314 EBW Detonator was employed (Reference 1). The detonator was attached to the end of the cord and placed in a protective tubular member which indexed the initiation point approximately 1 inch (2.5 cm) away from the start of the length passing through the camera field.

Initial calibration tests indicated that the sample was not sufficiently self-illuminating for proper definition of the metal jacket. Consequently, a high intensity xenon strobe lamp in the front lighting mode was found necessary to provide maximum jacket fragment resolution.

The Cordin camera was positioned on center with the sample at a distance giving a field-of-view of 6 x 6 inches (15 x 15 cm) - appropriate connections were made with the strobe lamp, high pressure nitrogen supply (camera mirror drive) and EBW firing circuit. Sequencing of the camera, detonator and strobe was accomplished automatically through the Cordin Instrumentation Console. Vendor data (Reference 2) claims a total system accuracy (jitter) of  $\pm 0.016$  microsecond.

The end product of the test was a length of 35 mm film (black and white or color) which usually contained 21 - 25 frames of information. As noted, the majority of the tests were made at a frame rate of one million frames/second. Data acquisition was accomplished by analysis of enlarged 8 1/2" x 11" still photographs and tabulation was made of the desired measurements, time increment, etc., necessary for parametric computation. To illustrate the behavior of lead and aluminum sheath detonating cords, a short, animated-type film has been prepared for presentation at this symposium. Beginning with 2.5 grain and progressing through 13.0 grain detonating cord sizes, each detonation process event is displayed on the screen several times.

#### EXPERIMENTAL RESULTS

This particular test series was comprised of approximately 30 tests involving 2.5, 3.5, 4.0, 7.0, 11.0 and 13.0 grain per foot detonating cord which contained either RDX or HMX explosives in either lead or aluminum sheaths. Each test sample was detonated in the test fixture (Figure 1) and the resultant detonation process was recorded by the framing camera (Figure 1). As dramatically illustrated in Figures 2 and 3, selected frames taken at a rate of  $5 \times 10^5$  or  $1 \times 10^6$  frames per second clearly show different detonation processes and fragmentation patterns between lead and aluminum sheaths. Several frames from each film strip were enlarged to 8 1/2" x 11" prints for analysis of the detonation process and fragmentation patterns.

All of the tested detonating cords exhibited the same destructive patterns: A nonreactive zone, an expansion zone and a metal fragmentation zone. These zones are illustrated in Figure 4 along with the various measurements that were used in

the data reduction process. The nonreactive zone was the undetonated detonating cord ahead of the detonation front. The expansion zone was selected to start at the detonation front and to cover the expansion of the detonation products and the metallic sheath until the sheath started to rupture and fragment. A slight error was introduced into the calculation of the specific volume of the detonation products by this selection since the expansion front was assumed to be at a fixed angle with the centerline of the detonating cord. Analysis of the radial expansion of a Comp B/Copper cylinder system (References 3 and 4) with respect to time indicated the radial expansion to be linear except for the first 15% of the total expansion. The fragmentation zone was selected to start to the beginning of the sheath fragmentation and extend over the sheath fragmentation and expended detonation products.

A representative print was measured for the detonation parameters: Expansion of the metal sheath (both linear and angular radial expansion) length of expansion zone, linear and angular displacement of the metal fragmentation pattern. These parameters were then combined with other detonating cord parameters such as core weight, explosive detonating velocity, and physical dimensions to calculate several detonation characteristics: Metal fragmentation velocity, expansion time, expansion wall velocity, volume of detonation products when metal sheath starts to fragment, and mass ratio of explosive to metal and/or plastic materials. Tables 1 and 2 present a summary of the measurements and calculated detonation characteristics for the test detonating cords.

COMPARISON OF EQUATION OF STATE  
FOR DETONATION PRODUCTS WITH EXPERIMENT

The behavior of the detonation products in the expansion section of the detonating cord can be analyzed by a simplified method and then compared to the theoretical equation of state for detonation products from a RDX system and from a metal-explosive system. This comparison allows a relative assessment of the capability of the explosive to expand, accelerate, and fragment the metal sheath for several mass ratios (mass of explosive to metal or to metal and plastic). In addition, it can be used to determine the relative pressure of the detonation products at the end of the expansion zone.

The pressure-volume-energy behavior (P-V-E) of the detonation products for a metal-explosive system was most thoroughly described by J. W. Kury, et al., (Reference 3) at the Fourth Symposium (International) on Detonation. This metal-explosive system was selected for comparison of the detonation process because of its similarity to the detonating cord in explosive to metal mass ratio and in the explosive and metal materials and on the availability of experimental data on the detonation behavior.

The experimental system used by Kury was a 1.0 inch diameter cylinder of Comp B confined in a copper tube with a 0.102-inch thick wall. Results from the expansion of the copper wall indicated the detonation products expanded essentially along the Chapman-Jouquet (C-J) isentrope and that this expansion relationship was not sensitive to the explosive used. Another fundamental relationship of interest to the expansion of the copper tube was the pressure-volume region. The relative volume expansion relationship is presented in Figure 5 and the pressure-volume relationship

in Figure 6. Also presented is the theoretical relationships for the detonation products of RDX and Comp B (Reference 3 and 5).

A comparison (Figure 5) of sheath expansion and the related detonation products volume for the various detonating cord configurations is made with the theoretical curve for RDX and the curve for the experimental Comp B/Copper system.

For a lateral detonation system, Kury (Reference 3) predicted the detonation products would effectively transfer energy to the metal wall until the specific volume ( $V$ ) reached an approximate value of 7 at an expansion ratio ( $R/R_0$ ) of approximately 2. The experimental data for the detonating cords indicate the detonation products volume ( $V$ ) is between values of 5 to 7.5 for expansion ratios of 4.5 to 5. This is good experimental agreement for the effectivity of energy transfer since the detonating cords are starting to rupture and fragment at this state. The higher expansion ratio is attributed to the lower mass ratio ( $M_e/M_s = 0.01$  to  $0.23$ ) of the detonating cords. It is readily apparent the detonating cord system does not approach the theoretical relationship for RDX nor for the Comp B/Copper cylinder system with a mass ratio of 0.43.

Based on the expansion of the detonation products in the copper cylinder and on the experimental results (Reference 3) which indicated the expansion relationship is not sensitive to the explosive used, one can use the pressure-volume relationship (Figure 6) to estimate the pressure of the detonation products when the metal sheath ruptures and fragments. To further support the applicability of the P-V relationship for the Comp B/Copper cylinder system to the detonating cord systems, the data for both RDX and Comp B fall on the theoretical curve of Figure 6 within experimental error. The experimental detonation products specific volume ( $V$ )



range of 5 to 7.5 cc/gm would relatively correspond to a detonation pressure range from 2.1 to 3.9 K bars (30,870 to 57,330 psi) at the time of metal sheath rupture.

#### MATERIAL EFFECTS

Major physical parameters of the detonating cords evaluated for their effects on performance are:

1. Explosive
  - a. RDX, HMX
  - b. Core Weights 2.5, 3.5, 7.0, 11.0 and 13.0 grain/foot
2. Sheath
  - a. Type - Lead (Pb), Aluminum (Al), Nylon
  - b. Combination - Metal, Metal and Plastic

Detonation characteristics of the detonating cords experimentally determined are:

1. Expansion zone time, expansion angle, ratio ( $R/R_0$ ), specific volume ( $V$ ) of detonation products, mass ratio ( $M_e/M_g$ ) and sheath wall velocity.
2. Fragmentation zone-fragmentation angle, pattern and size of fragments, and fragment velocity.

Experimental values for the detonation characteristics are presented in Table 1 for the expansion zone and in Table 2 for the fragmentation zone.

A review of the expansion zone characteristics presented in Table 1 shows the lead sheathing either with or without a plastic covering gave the smaller angle of expansion ( $2.8^\circ$  to  $4.8^\circ$ ) when compared with aluminum ( $3.9^\circ$  to  $10.6^\circ$ ). An increase in the explosive weight (grain/foot) gave a similar increase in expansion angle. Also, the wall velocity of the expansion zone is slower (0.33 to 0.65 mm/ $\mu$ second)

for lead sheaths than for aluminum sheaths (0.49 to 1.30 mm/ $\mu$ second). HMX explosive detonating cords were not studied in sufficient detail to draw any firm comparisons as only one HMX detonating cord was studied. Another significant fact is the apparent insensitivity of the experimental mass ratio (0.013 to 0.23) on the specific volume and on the expansion ratio ( $R/R_0$ ).

Kury (Reference 3) showed the Comp B/Copper cylinder system had a maximum metal wall velocity of 1.63 mm/ $\mu$ second before the wall ruptured. For comparison, he presented a maximum velocity of 1.71 mm/ $\mu$ second for a 90% RDX-10% Kel F explosive and 1.86 mm/ $\mu$ second for HMX explosive for similar explosive - copper cylinder systems. Hoskins (Reference 5) gives an experimental value of 1.64 versus a calculated (Gurney theory) value of 1.70 mm/ $\mu$ second for the metal wall velocity just before rupturing of the same Comp B/Copper cylinder system. Hoskins also showed the plate velocity relationship for metal plates at mass ratios in the detonating cord range to be insensitive to the type of metal tested: i.e., mild steel, aluminum, copper and brass.

The results for the fragmentation section (Table 2) showed several important factors. One, in particular, is the different fragmentation pattern and particle sizes for the metal sheaths. Another interesting comparison between lead and aluminum sheaths showed the expansion angle and the fragmentation angle were the same for lead while the fragmentation angle was greater than the expansion angle for aluminum. Fragmentation pattern are shown in Figures 7, 8 and 9. These represent the fragmentation size and pattern for lead and aluminum metal sheaths. Of note, is the very small fragment sizes for lead as compared to the long, sliver fragment sizes for aluminum. The more ductile lead sheath exhibited a more uniform fragmentation pattern.

An interesting explosive detonation pattern and resultant fragmentation pattern was observed with the 3.5 grain/foot aluminum sheath (Figure 9). The long slivers appeared to be generated in a spiral motion by a detonation front that was rotating. This rotation caused the slivers to be formed at an angle of approximately  $30^\circ$  to the normal direction of detonation. The spinning detonation wave front (Reference 6) has been recognized as a marginal propagating detonation condition in gaseous detonation systems over long runs. It may represent the same condition in condensed explosive systems. Also the spiral pattern may be the result of the manufacturing process which induced a spiral stress pattern in the aluminum sheath. The 4.0 grain RDX pictures in Figure 2 also show the spiral fragmentation pattern.

Fragment velocities which were measured at the beginning of the fragmentation zone are presented in Table 2 for the experimental detonating cords. Also presented for comparison is a calculated fragment velocity for each experimental detonating cord. The calculated fragment velocities were based on the simplified Gurney equation (Reference 7) for cylinders which related mass ratio ( $M_e/M_s$ ) to the fragment velocity. Both the experimental and calculated fragment velocities are rearranged as a ratio with the maximum achievable velocity for RDX and are presented in graphical form in Figure 10 as a function of the mass ratio. It was assumed for the Gurney equation that the maximum velocity for the Comp B systems could be used for the RDX systems within experimental error. Hoskins (Reference 5) indicates a value of 2.91 mm/ $\mu$ seconds for the preferred Comp B/Copper cylinder system. His experimental value for the fragment velocity ratio is presented in Figure 10 for reference purposes. The experimental fragment velocities show fairly good agreement with the calculated Gurney fragment velocities for the experimental mass ratio range of 0.01 to 0.4.

Several generalities for the experimental fragment velocities are observed in the comparison with the Gurney equation values. The lead sheath detonating cords show

excellent agreement while the aluminum detonating cords exhibit more variability. This relationship has been observed in applications where both metal sheathed 2.5 grain/foot detonating cords have been encased in polyurethane plastic tubing. A lot-to-lot variability of approximately 14% is observed between the two samples of 7.0 grain/foot aluminum and nylon sheath detonating cords. No significant effect can be attributed to the plastic sheathing. The overall variability indicated in Figure 10 suggests a more rigorous or a refinement of the analytic method for data reduction and should be made to reduce experimental error and to obtain a more precise detonating cord evaluation.

#### SUMMARY

The framing camera technique does provide a method for obtaining data useful in characterizing detonating cords. Expansion parameters of the detonation cords can be used to predict gaseous pressure levels of the detonation products at the time of sheath rupture. Fragment patterns, sizes and velocities can be predicted for various sizes and types of detonating cord. Fragment velocities agree fairly well with those predicted by the Gurney equation for cylinders in the mass ratio level below 0.5.

Information resulting from the detonation cord study is presently being utilized in development of missile separation systems. It is also planned to use the same information in establishing improved manufacturing processes for the aluminum detonating cord in the 2.5 and 11.0 grain/foot RDX sizes. It is also evident that analysis of basic detonation phenomena and related physical parameters for detonating cords and probably including flexible linear shaped charge cord, can be applied and translated into design criteria in aerospace ordnance applications.

Examples where this type of information is needed and useful are -

- evaluating detonating cord for use in separation joints and other energy and shock loading designs.
- evaluating destructive forces, overpressures and fragmentation damage to surrounding structures and equipment.
- evaluating detonating cord for use inside plastic and/or metal tubing.
- completely characterizing detonating cord.
- determining performance and quality of detonating cord.
- for research and development of new detonating cords and for improvement of present detonating cords.
- failure mode analysis of detonating cord (i.e., initiation and propagation anomalies).

#### REFERENCES

1. "EBW Detonator", Reynolds Industries Catalog #28, Explosive Components Section, 28 July 1967, page 2.
2. Cordin Camera, Model 114, Operational Instruction Sheet
3. J. W. Kury, H. C. Hornig, E. L. Lee, J. L. McDonnell, D. L. Ornellas, M. Finger, F. M. Strange, M. L. Wilkins, Fourth Symposium on Detonation, "ONR Symposium Report ACR-126", (1965), pp 3-13.
4. N. E. Hoskins, J. W. S. Allan, W. A. Bailey, J. W. Lethaby, I. C. Skidmore, Fourth Symposium on Detonation, "ONR Symposium Report ACR-126", (1965), pp 14-26.
5. M. J. Kamlet and H. Hurwitz, "The Chemistry of Detonations. V. Pressures of C-H-N-O Explosives at Various Stages of the Isentropic Expansion", Report NOLTR 68-44, United States Naval Ordnance Laboratory, White Oaks, Maryland, 6 May 1968.
6. G. L. Schott, Fourth Symposium on Detonation, "ONR Symposium Report ACR-126", (1965), pp 67-77.
7. R. W. Gurney, "The Initial Velocities of Fragments From Bombs, Shells and Grenades", BEL Report No. 405, 14 September 1943.

TABLE I COMPARISON OF EXPANSION ZONE CHARACTERISTICS

CORD SIZE & EXPLOSIVE (gr/ft)	SHEATH MATERIAL	MASS RATIO $M_e/M_s$ (5)	TIME $\mu$ sec	ANGLE $\alpha^\circ$	EXPANSION RATIO R/Ro	DETONATION PRODUCTS VOLUME (cc/gm)	DETONATION VELOCITY mm/usec.	WALL VELOCITY ( $V_w$ ) mm/usec.
2.5 - RDX	Pb + Nylon	0.013	7.72	2.8	8.6	19.4	6.65	0.33
2.5 - RDX	Pb	0.020	2.72	3.5	3.5	4.3	6.65	0.41
2.5 - RDX	Al	0.095	2.75	3.9	4.3	5.5	7.18	0.49
3.5 - RDX (1)	Al	0.131	3.19	4.0	4.9	6.9	7.49	0.53
3.5 - RDX (2)	Al	0.223	4.24	3.3	5.0	7.6	7.59	0.43
4.0 - RDX	Al	0.383	N.D.	7.8	N.D.	N.D.	8.10	1.10
7.0 - RDX (3)	Al + Nylon	0.103	2.44	6.8	4.5	5.4	7.37	0.94
7.0 - RDX (4)	Al + Nylon	0.103	1.9	5.6	4.1	5.0	7.90	0.77
11.0 - RDX	Al + Nylon	0.21	2.35	8.1	4.4	5.1	7.66	1.09
13.0 - RDX	Al + Nylon	0.23	2.70	10.6	5.0	5.2	7.09	1.30
11.0 - RMX	Pb + Polyethylene	N.D.	5.40	4.8	N.D.	N.D.	7.85	0.65

NOTES: (1) Lot 1712-1  
 (2) Lot 1711-1  
 (3) Lot 1713-4  
 (4) Lot 1715-1  
 (5)  $M_s$  - mass of sheath includes plastic where indicated.  
 N.D. = Not Determined

TABLE 2 COMPARISON OF FRAGMENTATION ZONE CHARACTERISTICS

CORD SIZE EXPLOSIVE (gr/ft)	SHEATH MATERIAL	MASS RATIO $M_e/M_s$	PATTERN (5)	PARTICLE SIZE (approx. -inch)	ANGLE $\beta^\circ$	FRAGMENT VELOCITY ( $V_f$ ) mm/usec.	GURNEY FRAGMENTATION VELOCITY ( $V_o$ ) mm/usec.
2.5 - RDX	Pb + Nylon	0.013	pellets	0.2 x 0.05	2.8	0.33	0.33
2.5 - RDX	Pb	0.020	rods	0.5 x 0.05	3.5	0.41	0.41
2.5 - RDX	Al	0.095	slivers	1 x 1/32	5.8	0.73	0.88
3.5 - RDX (1)	Al	0.131	slivers	3 x 1/32	9.3	1.23	1.02
3.5 - RDX (2)	Al	0.223	slivers	3 x 1/32	8.3	1.09	1.31
4.0 - RDX	Al	0.383	pellets	0.1 x 0.05	9.3	1.31	1.65
7.0 - RDX (3)	Al + Nylon	0.103	slivers	2 x 1/32	8.3	1.14	0.91
7.0 - RDX (4)	Al + Nylon	0.103	slivers	2 x 1/32	7.3	1.00	0.91
11.0 - RDX	Al + Nylon	0.21	rods	1/2 x 1/16	11.5	1.53	1.27
11.0 - RMX	Pb + Polyethylene	N.D.	rods	1/4 x 1/32	4.8	0.65	N.D.
13.0 - RDX	Al + Nylon	0.23	rods	1/2 x 1/32	11.7	1.42	1.32

NOTES: (5) slivers  
 pellets  
 rods  
 (1) Lot 1712-1  
 (2) Lot 1711-1  
 (3) Lot 1713-4  
 (4) Lot 1715-1  
 N.D. = Not Determined  
 (6) Fragmentation velocities calculated from Gurney Equation for Cylinders (Ref. 7).

$$\frac{V_o}{V_1} = \sqrt{\frac{M_e/M_s}{1 + 1/2(M_e/M_s)}} \quad \text{where } V_1 = 2.91 \text{ mm/usec. (Ref. 5)}$$

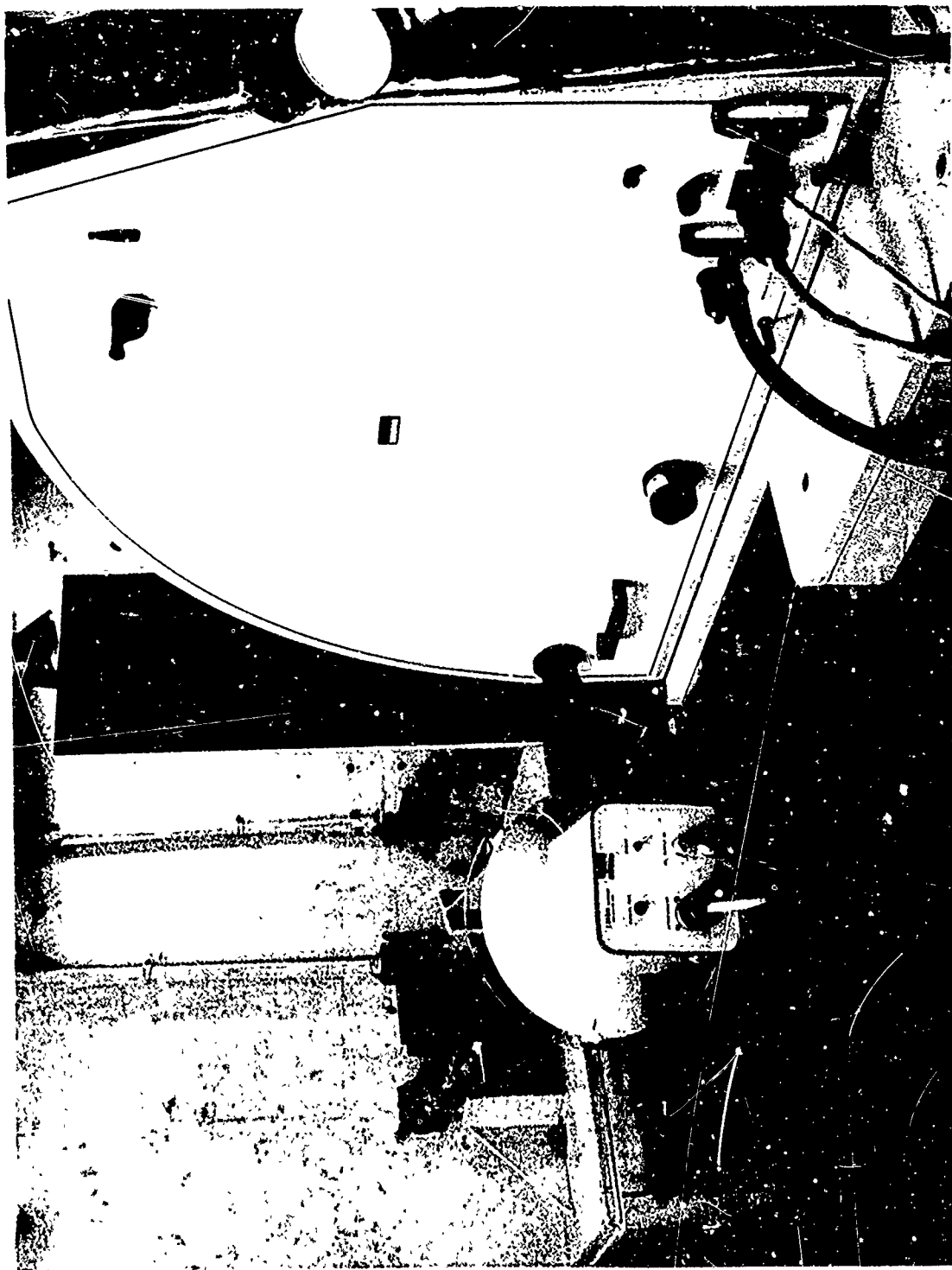
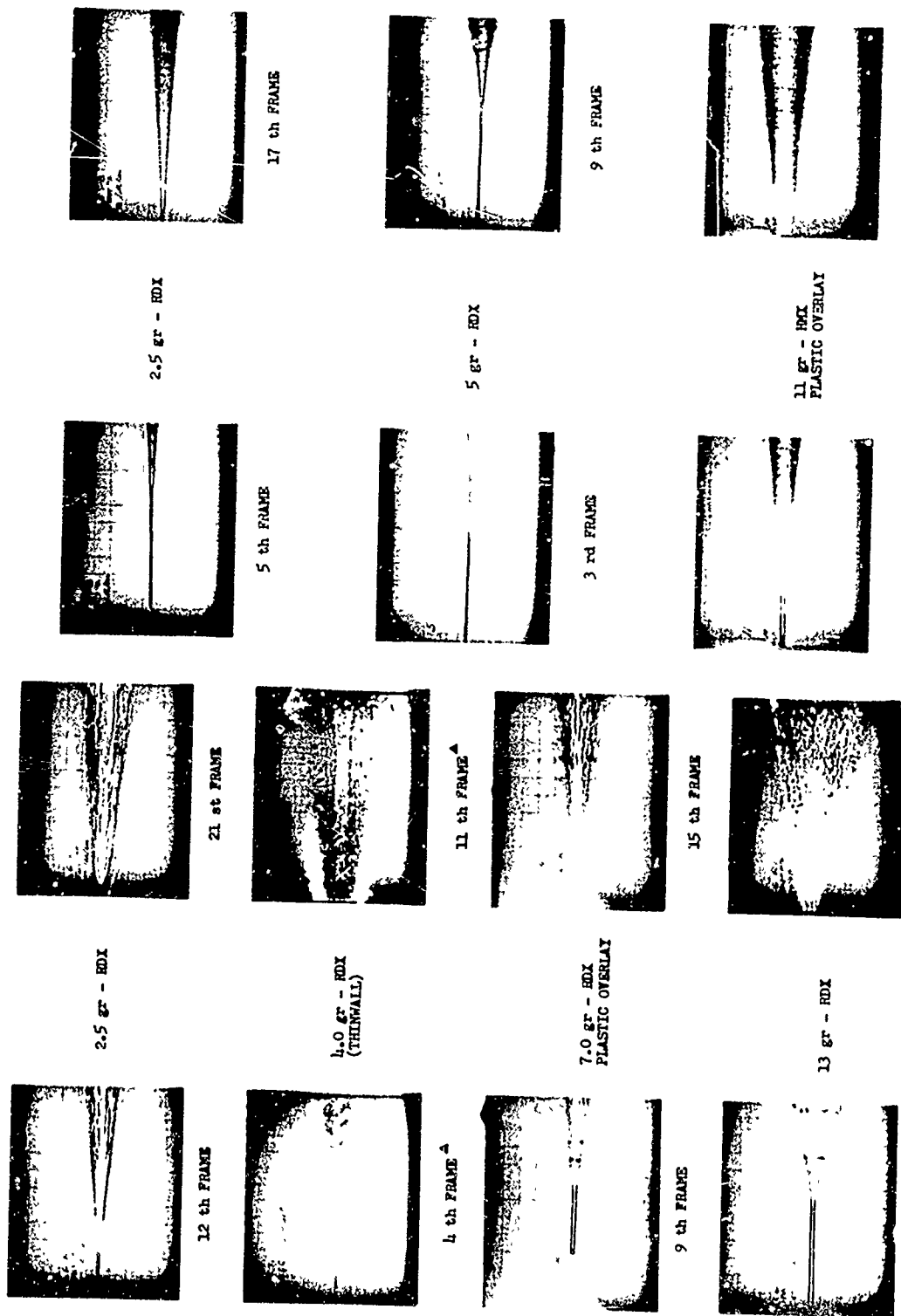


FIGURE 1  
TEST SETUP - COORDIN CAMERA



SELECTED FRAMES OF ALUMINUM JACKET MDP TAKEN  
AT  $5 \times 10^3$  AT  $1 \times 10^4$  f/SEC - CORDIN CAMERA  
FIGURE 2

SELECTED FRAMES OF LEAD JACKET MDP TAKEN  
AT  $1 \times 10^4$  f/SEC - CORDIN CAMERA  
FIGURE 3



NOTES:

1 - Wall Velocity -  $(V_w) = V_D \sin \frac{\alpha_1 + \alpha_2}{2}$

2 - Fragment Velocity -  $(V_f) = V_D \sin \frac{\beta_1 + \beta_2}{2}$

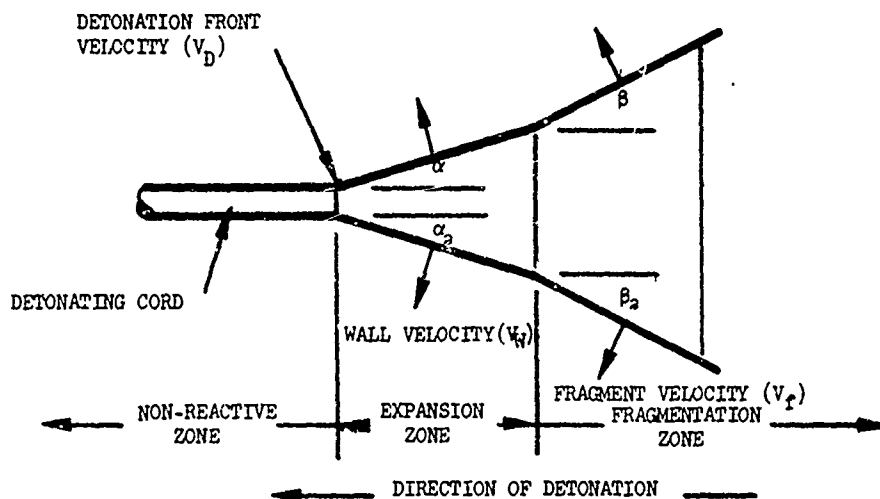


Figure 4  
DETONATION PROCESS DIAGRAM FOR DETONATING CORD

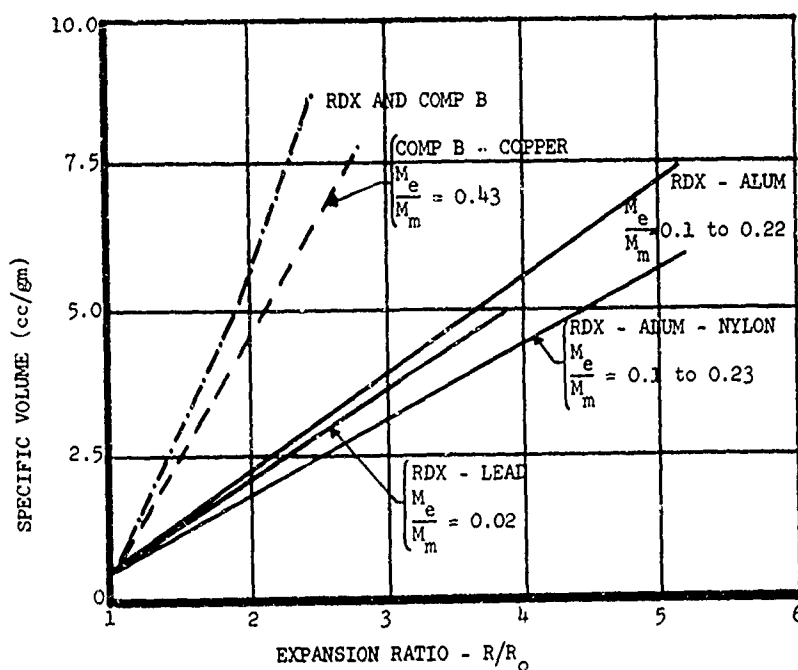


Figure 5  
COMPARISON OF DETONATION PRODUCTS - SPECIFIC VOLUME  
VERSUS EXPANSION RATIO FOR VARIOUS EXPLOSIVE SYSTEMS

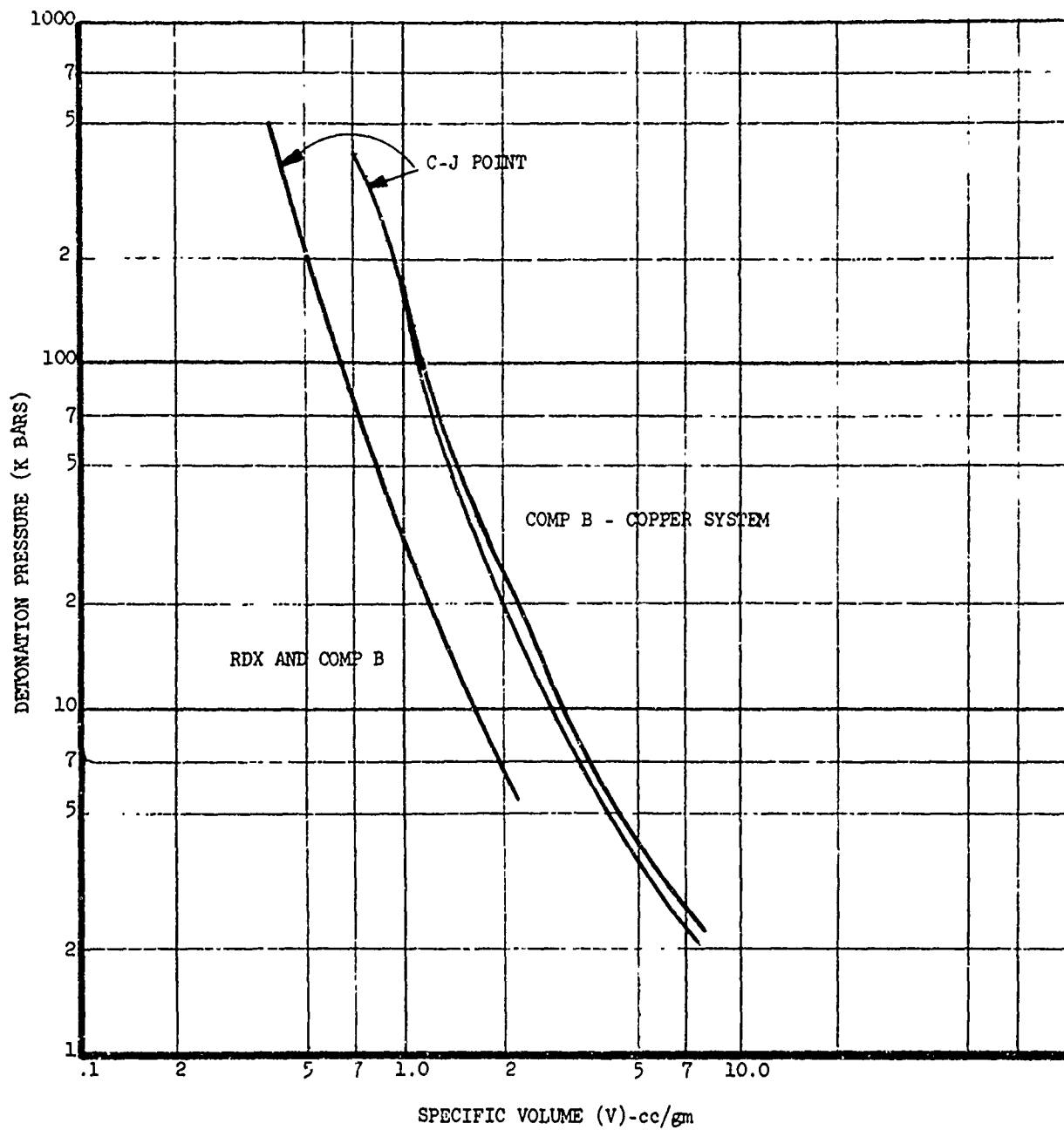
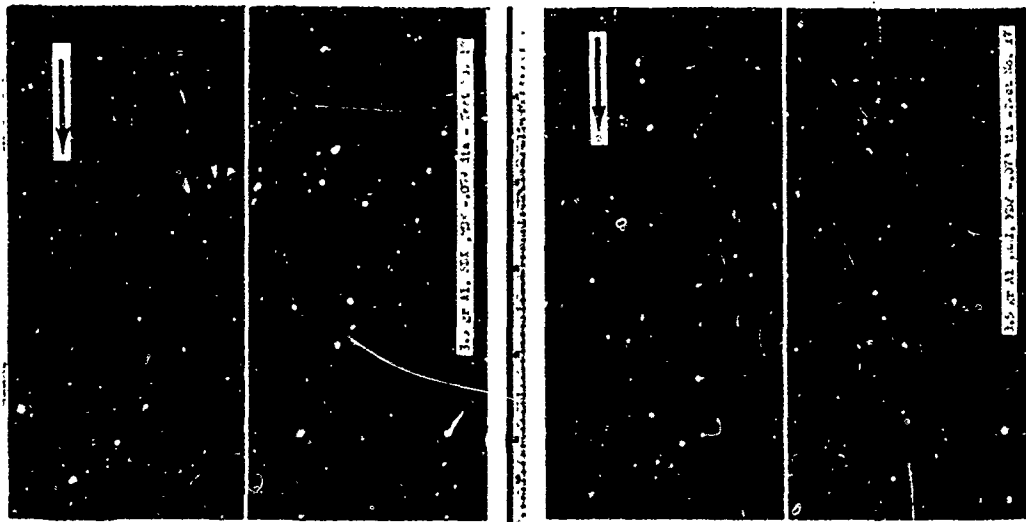


Figure 6  
EQUATION OF STATE RELATIONSHIP FOR DETONATION  
PRESSURE AND SPECIFIC VOLUME

**Fig. 9**



**Fig. 8**

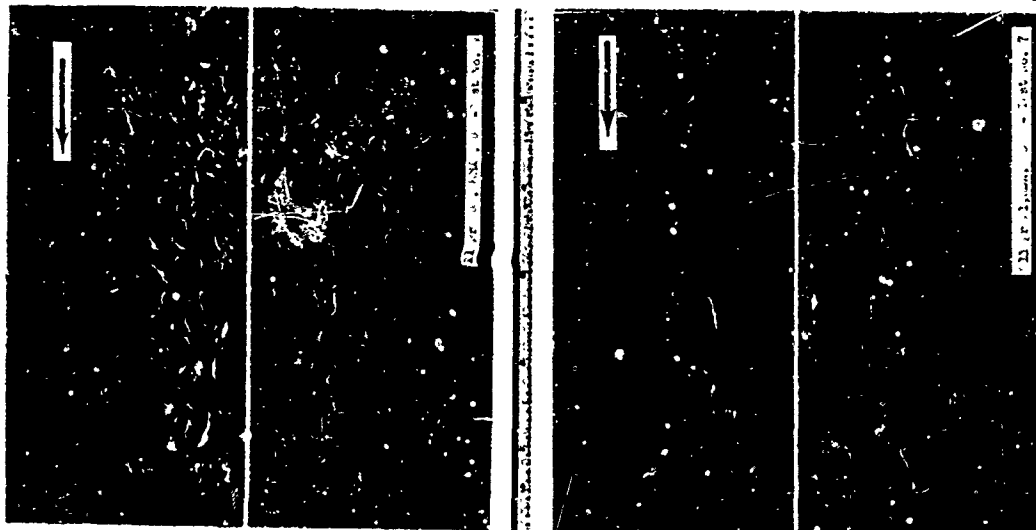
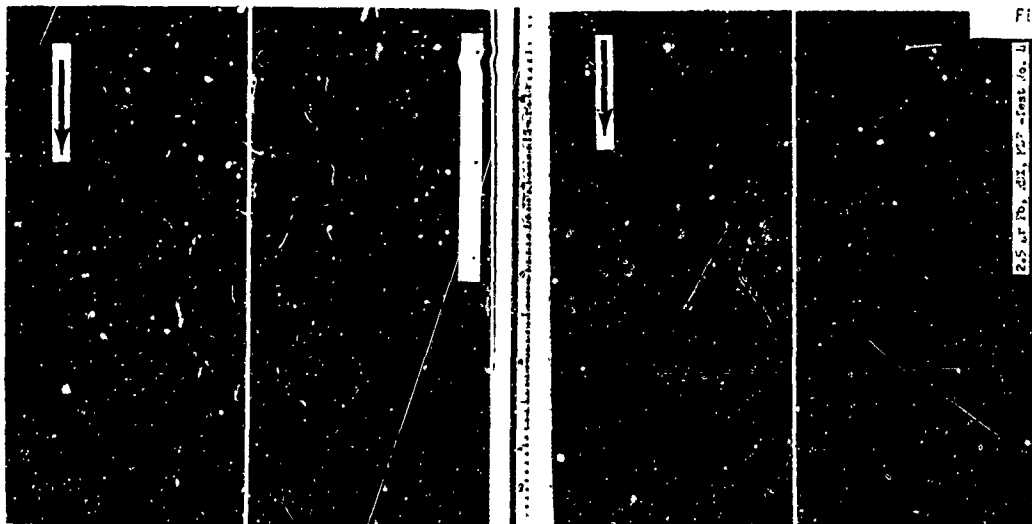


Fig. 7



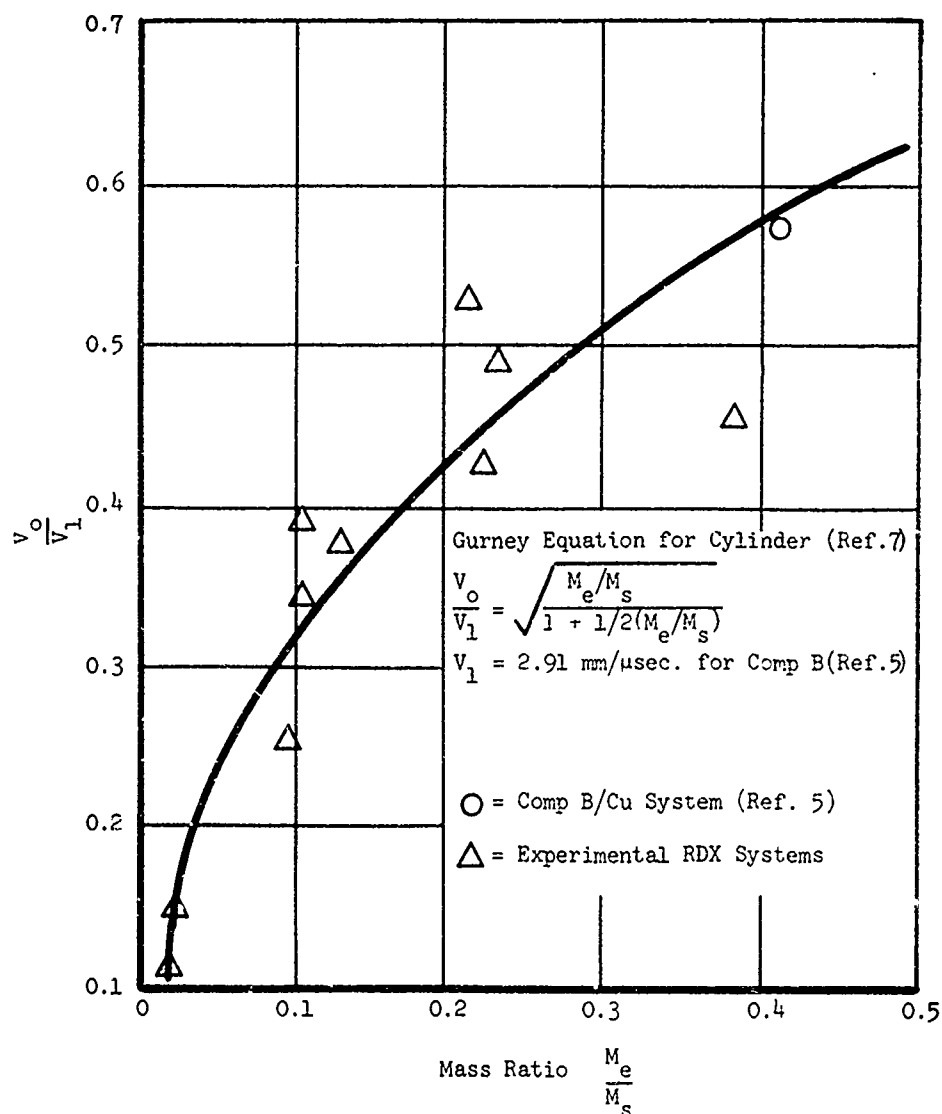


Figure 10. Comparison of Experimental Fragment Velocity Ratio with Gurney Equation for Cylinders

#### DISCUSSION

A question was aimed at determining how close to critical the explosive diameters were. The reason for the question was to attempt to explain differences in framing pictures between the work of Dr. Cook and the study reported here. The answer was that standard cord of from 2-1/2 to 13 grains per foot were used. If a half grain is not below critical diameter then the others were over it. There is no correlation to Dr. Cook's aquarium method. The environment for these studies was air. The cord was manufactured by Ensign Bickford by a swaging process that displayed the spiral fragment pattern. Some of the cord was supplied by another vendor.

## 4-12P COMPARATIVE EFFECTS OF CW AND RADAR

### SIGNALS ON EED BRIDGEWIRE TEMPERATURE \*

O. W. Mayes, McDonnell Douglas Astronautics Company, Western Division

and

Charles Carlson, formerly Douglas Aircraft Company, Inc.

### INTRODUCTION

The engineer who evaluates EED circuits for RF susceptibility faces many quandaries. One of these concerns the sensitivity of the EED itself. EED sensitivity is commonly expressed in terms of continuous wave (CW) power input. But the RF environments for susceptibility evaluations usually include radar signals. The question arises: how much error is introduced by assuming that EED sensitivity is identical for radar and CW signals? This paper provides an answer for one mode of EED sensitivity, namely, the normal (pin-to-pin) bridgewire heating mode.

While power input is used as a practical index of EED sensitivity, it is an indirect measure, at best. A more fundamental but intangible measure is temperature of the prime charge. A fairly direct measure, and one that lends itself to analysis, is temperature of the bridgewire. It is therefore convenient to use EED bridgewire temperature as a *common* reference in comparing the effectiveness of different types of power input signals.

Such a comparison between CW and radar type RF signals is made here, in two parts: a qualitative approach to the problem, followed by a parametric analysis to provide a working formula.

---

\* Based on work done for Bell Telephone Laboratories, Inc., under contract DA-30-069-AMC-333Y.

## QUALITATIVE APPROACH

The relationship between bridgewire power input and temperature is time variant because of thermal lag within the EED. Consequently, as shown in Figure 1, the temperature response trace does not resemble the power input trace.

Figure 1 also illustrates that the EED thermal lag damps out any significant temperature fluctuations at radio frequency. Thus, a DC pulse and an RF pulse of the same average power produce essentially identical temperature responses in the bridgewire. Therefore, it is conventional to refer to average power in describing a single RF pulse. Note, however, that it is the peak temperature of the bridgewire that provides a common reference for EED sensitivity levels.

Consider an RF power input pulse of relatively long duration, so the bridgewire temperature rises to a maximum value and stabilizes. As shown in Figure 2, this typifies the CW condition often used in measuring EED RF sensitivity levels.

Next, assume that the long pulse is broken up into a series of short pulses, maintaining the same average power per cycle. This requires that the average power per pulse (or simply pulse power) be increased in proportion to the power-off time between pulses, as shown in Figure 3. For actual radar signals, the ratio of pulse-on time to pulse-off time is much less than that shown in Figure 3; hence the ratio of pulse power to cycle average power is much greater, ranging in order from  $10^2:1$  to  $10^4:1$ .

It is seen from Figure 3 that the bridgewire temperature fluctuates about a value which would be produced by applying the cycle average power. Accordingly, an RF susceptibility evaluation based on EED CW sensitivity

levels and radar cycle average powers does not account for the peaks of temperature fluctuation. On the other hand, an evaluation assuming continuous application of the pulse power is unduly conservative.

However, as shown in Figure 4, there is some lesser value of cycle average power input which produces a steady state peak temperature rise equal to the stabilized temperature rise at the CW sensitivity power level. If that equivalent cycle average power value were known, it could be used in place of the CW sensitivity power level to provide a more accurate susceptibility evaluation. The objective of this paper is to provide a simple means of making such a conversion.

The problem may be viewed in terms of bridgewire temperature fluctuation. As seen from the previous illustrations, there are four factors which condition the fluctuation, namely:

1. Pulse duration )  
(Radar signal characteristics)
2. Time between pulses )
3. Bridgewire heating response )  
(EED thermal characteristics)
4. Bridgewire cooling tendency )

From the considerations thus far, it may be estimated that the pulse duration, being a very small part of the cycle period, is of secondary importance (assuming constant pulse energy). Further, it is apparent that an increase in any of the other three items tends to increase the fluctuation.

In 1961, a report entitled The Response of Electroexplosive Devices to Transient Electric Pulses, by Kabik, Rosenthal, and Solem,<sup>(1)</sup> described the thermal behavior of EED's in terms of the following properties:

- $C_p$  = Bridgewire effective heat capacity (energy/ $\Delta t$ )  
 $\gamma$  = Bridgewire effective heat loss coefficient (energy rate/ $\Delta t$ )

(1) U.S. Naval Ordnance Laboratory, White Oak, Maryland, Report NOLTR 61-20, June 1961.

The report used these parameters as the basis for a differential equation which related instantaneous bridgewire temperature to a time-variant power input. From this equation, the report derived: an expression for the bridgewire peak temperature rise produced by a radar signal; an expression for the bridgewire stabilized temperature rise produced by a CW signal.

The following analysis briefly reviews the equations of the referenced report and uses them to give the power relationship between radar and CW signals for equivalent bridgewire temperature rise. This provides a conversion factor for application to EED CW power sensitivity levels.

#### ANALYSIS

The differential equation giving the temperature-time relationship of the EED bridgewire is:

$$C_p \frac{d\theta}{dt} + \gamma\theta = P(t) \quad (1)$$

where

$C_p$  = heat capacity of device, watt sec/°C

$\gamma$  = heat loss coefficient, watts/°C

$\theta$  = temperature rise above ambient, °C

$P(t)$  = power input, watts

Under steady-state conditions, the temperature rise of the bridgewire during the time that a radar pulse is present is equal to the temperature



drop during the interval between pulses. The magnitude of the temperature fluctuation is given by

$$\theta_2 - \theta_1 = \frac{I_p^2 R_1}{\gamma - I_p^2 R_1 \alpha} \left[ 1 - \exp \left\{ \frac{-(\gamma - I_p^2 R_1 \alpha) t_r}{C_p} \right\} \right] \quad (2)$$

where

- $\theta_2$  = peak temperature rise, °C
- $\theta_1$  = minimum temperature rise, °C
- $I_p$  = pulse current caused by radar signal, amp
- $R_1$  = resistance of bridgewire at temperature rise  $\theta_1$ , ohms
- $\alpha$  = temperature coefficient of resistivity, ohms/°C
- $t_r$  = duration of radar pulse, sec

The peak temperature rise in the bridgewire is given by

$$\theta_2 = \frac{I_p^2 R_1}{\gamma - I_p^2 R_1 \alpha} \left[ 1 - \exp \left\{ \frac{-(\gamma - I_p^2 R_1 \alpha) t_r}{C_p} \right\} \right] \frac{1}{\left[ 1 - \exp \left( -\frac{\gamma}{C_p} t_d \right) \right]} \quad (3)$$

where

- $t_d$  = time between pulses, sec

The relationship between these temperatures and times is shown in Figure 4.

For a typical radar signal,  $t_r$  is in the order of microseconds. Also,  $I_p^2 R_1$  is normally less than 100 watts. For typical values of  $\gamma$ ,  $C_p$ , and  $\alpha$ , a good approximation to

$$\exp \left\{ \frac{-(\gamma - I_p^2 R_1 \alpha) t_r}{C_p} \right\}$$

is

$$1 - \frac{(\gamma - I_p^2 R_1 \alpha) t_r}{C_p}$$

Equations (2) and (3) can then be simplified to

$$\theta_2 - \theta_1 = \frac{I_p^2 R_1 t_r}{C_p} \quad (4)$$

and

$$\theta_2 = \frac{I_p^2 R_1 t_r}{C_p} \frac{1}{\left[ 1 - \exp \left( -\frac{\gamma}{C_p} t_d \right) \right]} \quad (5)$$

Equation (5) gives the steady-state peak temperature rise of the bridgewire for a radar signal.

The quantity  $I_p^2 R_1$  is the power dissipated in the bridgewire at the beginning of the radar pulse. If the bridgewire resistance increases with increasing temperature ( $\alpha > 0$ ), the power dissipated will decrease slightly

during the time of the pulse. For practical purposes, the power dissipation may be assumed constant, then

$$\theta_2 = \frac{P_p t_r}{C_p} \left[ \frac{1}{1 - \exp\left(-\frac{\gamma}{C_p} t_d\right)} \right] \quad (6)$$

where

$P_p$  = power dissipated in the bridgewire during the radar pulse, watts.

The time variant temperature rise of the bridgewire upon application of a constant RF current,  $I_{cw}$ , is

$$\theta'_{cw} = \frac{I_{cw}^2 R_a}{\gamma - I_{cw}^2 R_a \alpha} \left[ 1 - \exp\left\{ \frac{-(\gamma - I_{cw}^2 R_a \alpha) t}{C_p} \right\} \right] \quad (7)$$

where

$\gamma > I_{cw}^2 R_a \alpha$   
 $\theta'_{cw}$  = bridgewire temperature rise at time  $t$ , °C  
 $I_{cw}$  = constant amplitude RF current, amp  
 $R_a$  = Bridgewire resistance at  $\theta = 0$ , ohms  
 $t$  = elapsed time from application of signal, sec

Under steady-state conditions,  $t$  approaches infinity, and equation (7) reduces to

$$\theta_{cw} = \frac{I_{cw}^2 R_a}{\gamma - I_{cw}^2 R_a \alpha} \quad (8)$$

where

$\theta_{cw}$  = the steady state temperature rise of the bridgewire for  
a CW signal.

If the bridgewire resistance changes with temperature, the actual power  
dissipated in the bridgewire is

$$P_{cw} = I_{cw}^2 R_{cw} = I_{cw}^2 R_a (1 + \alpha \theta_{cw}) \quad (9)$$

where

$P_{cw}$  = steady state CW power dissipated in the bridgewire, watts

$R_{cw}$  = resistance of the bridgewire at temperature rise  $\theta_{cw}$

Rearranging equation (8) to

$$\gamma \theta_{cw} = I_{cw}^2 R_a (1 + \alpha \theta_{cw})$$

and substituting in equation (9),

$$P_{cw} = \gamma \theta_{cw} \quad (10)$$

Equation (10) gives the steady state CW power dissipated in the bridgewire  
and is seen to be a restatement of the basic differential equation (1) for  
conditions of constant power input. Equations (6) and (10) provide the

means for relating equivalent radar and CW power dissipation levels in terms of bridgewire maximum temperature rise, as follows:

For the condition  $\theta_{cw} = \theta_2$

$$P_{cw} = \gamma \theta_2 = \frac{\gamma P_p t_r}{C_p} \frac{1}{\left[ 1 - \exp \left( -\frac{\gamma}{C_p} t_d \right) \right]} \quad (11)$$

By definition  $\frac{C_p}{\gamma} = \tau$ , the EED thermal time constant, sec

Rewriting equation (11)

$$P_{cw} = \frac{P_p t_r}{\tau} \frac{1}{(1 - e^{-t_d/\tau})} \quad (12)$$

It is convenient, however, to work with the radar cycle average power,  $P_{ra}$ , instead of the pulse power,  $P_p$ .

Considering cycle energy

$$P_p = P_{ra} \frac{(t_r + t_d)}{t_r} \quad (13)$$

Substituting in equation (12)

$$P_{cw} = P_{ra} \frac{(t_r + t_d)}{\tau} \frac{1}{(1 - e^{-t_d/\tau})} \quad (14)$$

Since  $t_d$  is measured in milliseconds and  $t_r$  is at most a few microseconds,  $t_d$  may be approximated by  $(t_r + t_d)$ .

Also,

$$t_r + t_d = \frac{1}{F_{pr}}$$

where

$F_{pr}$  = radar pulse repetition frequency, cycles/sec

Rewriting equation (14)

$$\frac{P_{ra}}{P_{cw}} = \tau F_{pr} (1 - e^{-\frac{1}{\tau F_{pr}}}) = K \quad (15)$$

Where K is a multiplication factor to convert EED CW power sensitivity values to radar power sensitivity values.

## RESULTS AND DISCUSSION

Figure 5 is a plot of equation (15). If the thermal time constant ( $\tau$ ) and the pin-to-pin CW sensitivity are known for a particular EED, its sensitivity to radar signals of known pulse repetition frequencies ( $F_{pr}$ ) may be found from Figure 5. The largest sensitivity corrections result from the smallest  $\tau$ 's and  $F_{pr}$ 's.

Figure 6 is an inverse plot of equation (15). It is of interest mainly to show that for large values of  $[\tau F_{pr}]^{-1}$  the exponential function vanishes, and the power sensitivity ratio  $\left(\frac{P_{CW}}{P_{ra}}\right)$  is simply equal to  $[\tau F_{pr}]^{-1}$ .

Figure 7 plots bridgewire temperature fluctuation  $(\theta_2 - \theta_1)$  as a function of peak temperature  $(\theta_2)$ . For small fluctuations the increase is nearly linear with  $(\tau F_{pr})^{-1}$ . Beyond the knee of the curve, however, a condition of complete fluctuation is approached, where the temperature decays during each pulse cycle to essentially the ambient value. In this region, EED's may be treated as being "energy" sensitive rather than "power" sensitive, since "thermal stacking" is absent, and the peak temperature is derived from the energy of a single pulse.

As noted in the introduction, this paper deals with EED sensitivity in the normal, bridgewire heating mode. The results should be used with the knowledge that EED's have anomalous modes of RF sensitivity that may govern in a particular susceptibility evaluation. Where voltage sensitivity is a factor, radar signals may be an aggravation, since the ratio of radar pulse voltage to CW voltage (for a given power input) ranges, in order, from 10 to 100.

Consider, however, the fact that there is no basic requirement for an EED to be sensitive in modes other than its normal firing mode. The existence of anomalous sensitivity in modern EED designs has caused a defeatist attitude in some quarters. Spurious RF behavior of EED's is accepted as inevitable. It is submitted that a bonafide need exists for applied research effort to advance the state-of-the-art in this area.

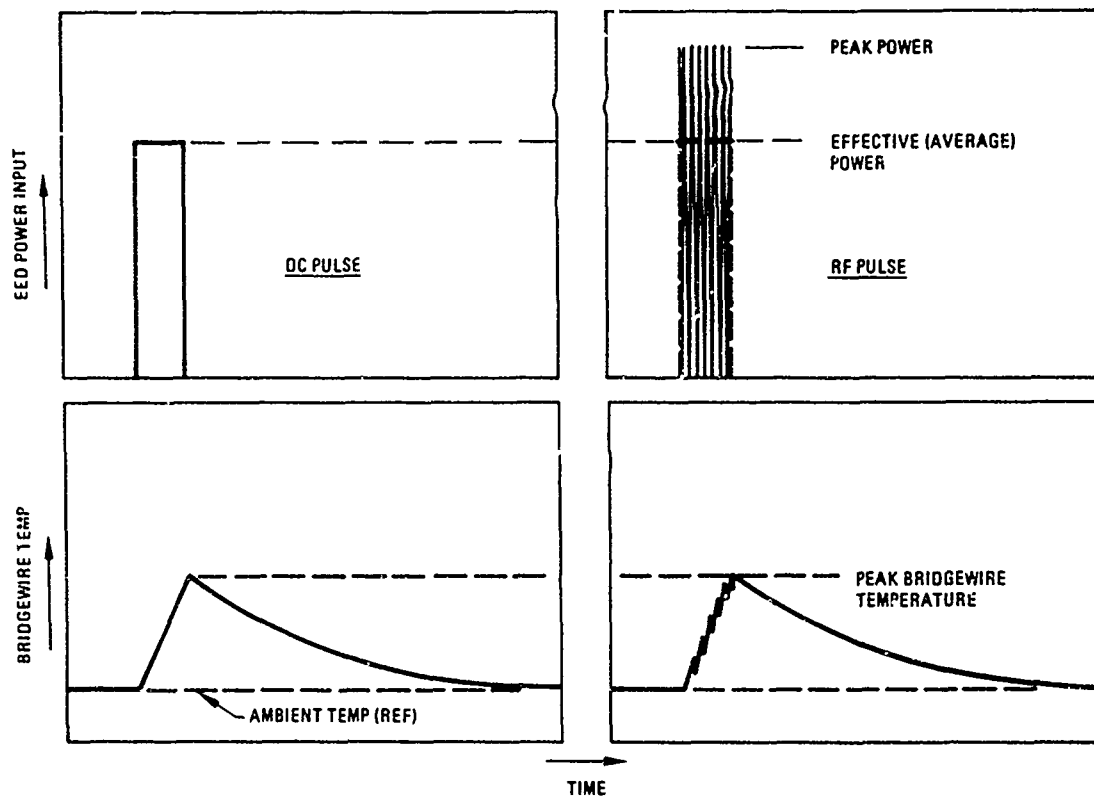


Figure 1. Bridgewire Temperature Response to Transient DC and RF Pulses

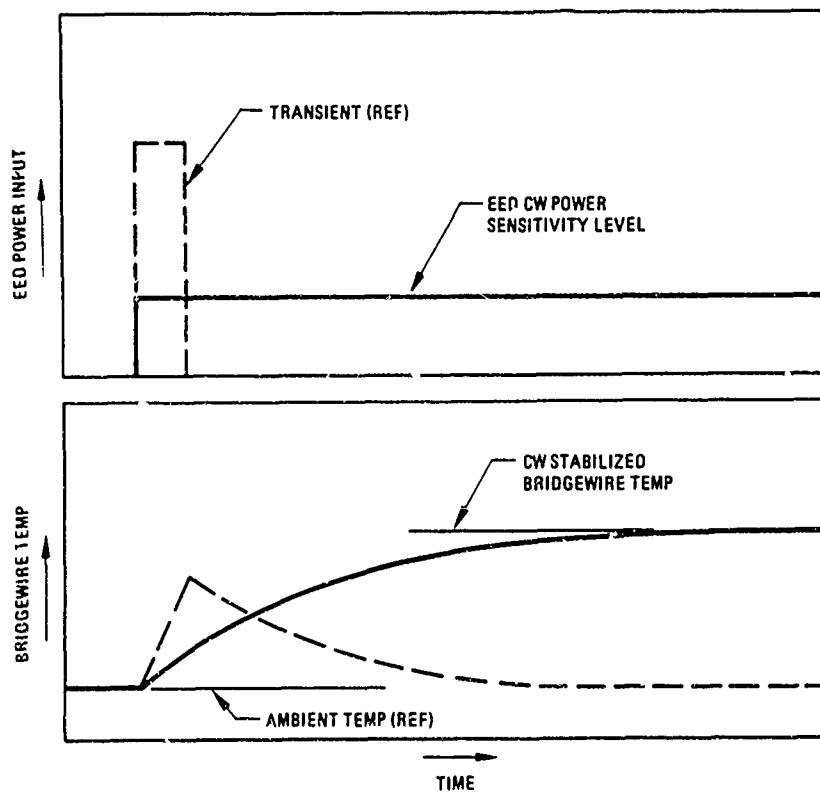


Figure 2. Bridgewire Temperature Response to a Very Long (CW) RF Pulse



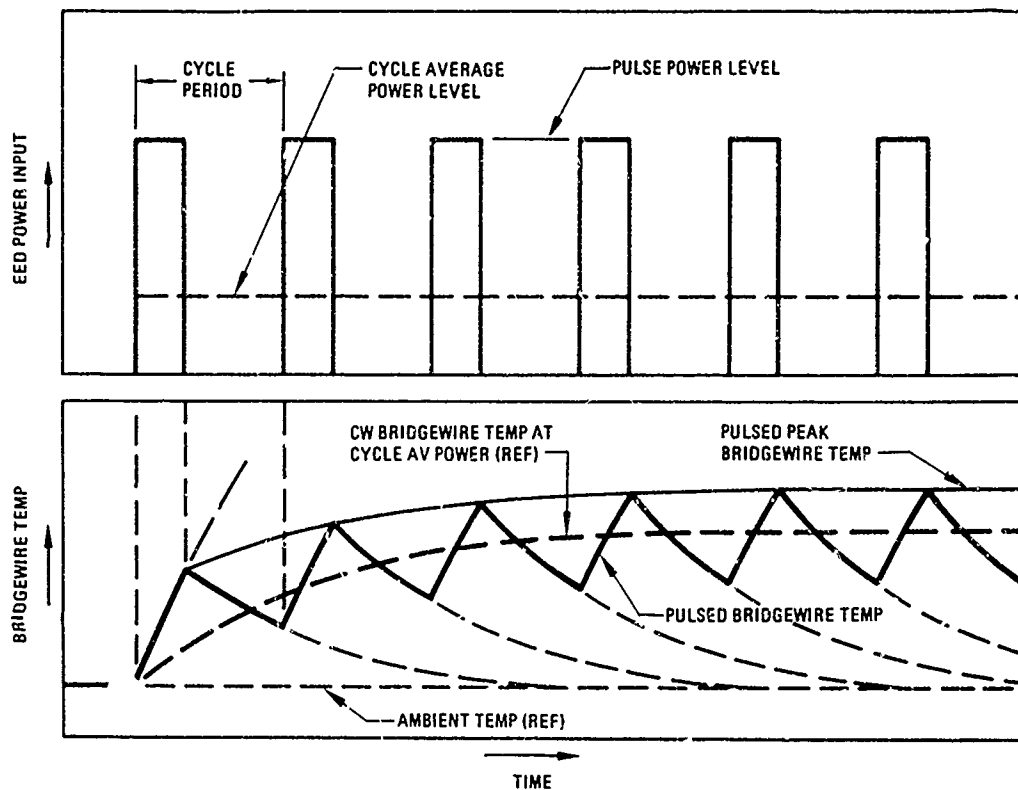


Figure 3 Bridgewire Temperature Response to a Series of Short RF Pulses

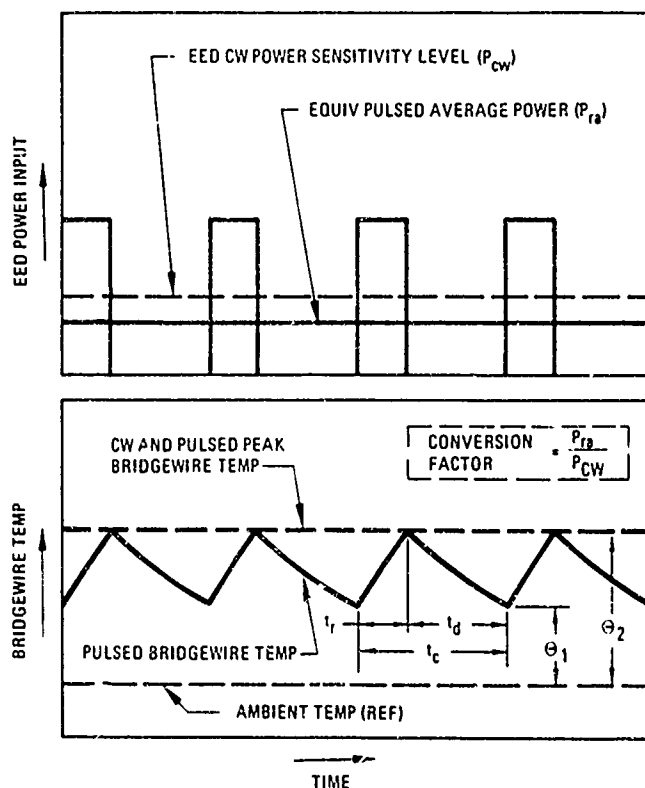


Figure 4 Effect of Bridgewire Temperature Fluctuation on EED Sensitivity

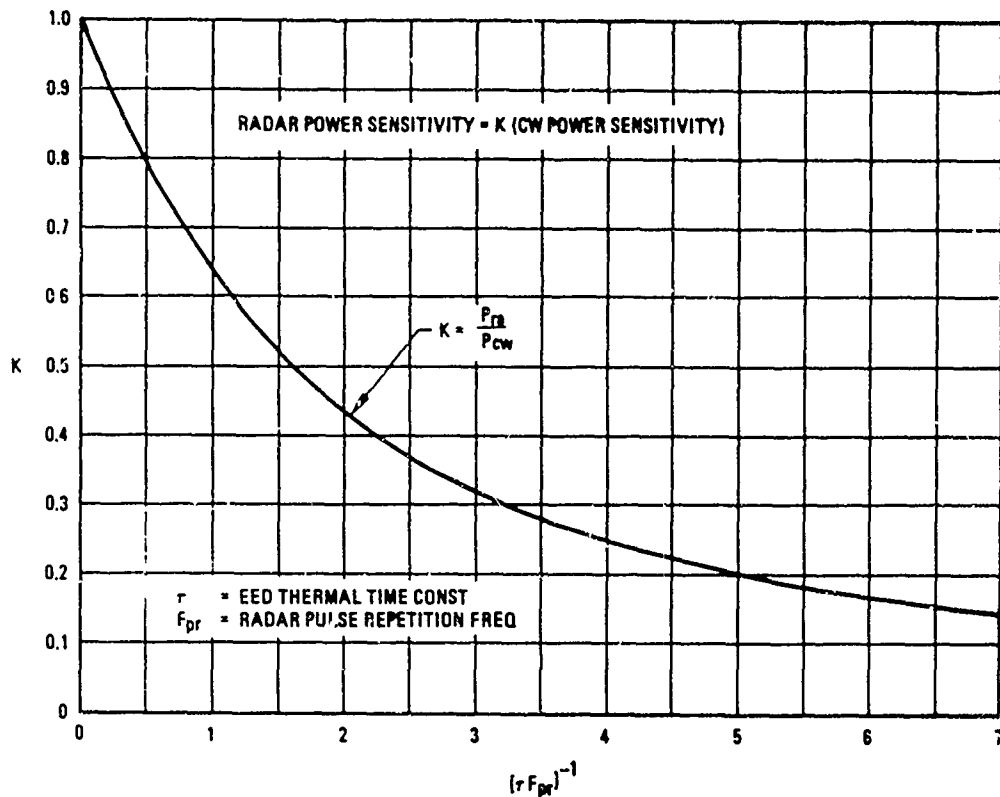


Figure 5. Conversion of EED CW Sensitivity to EED Radar Sensitivity

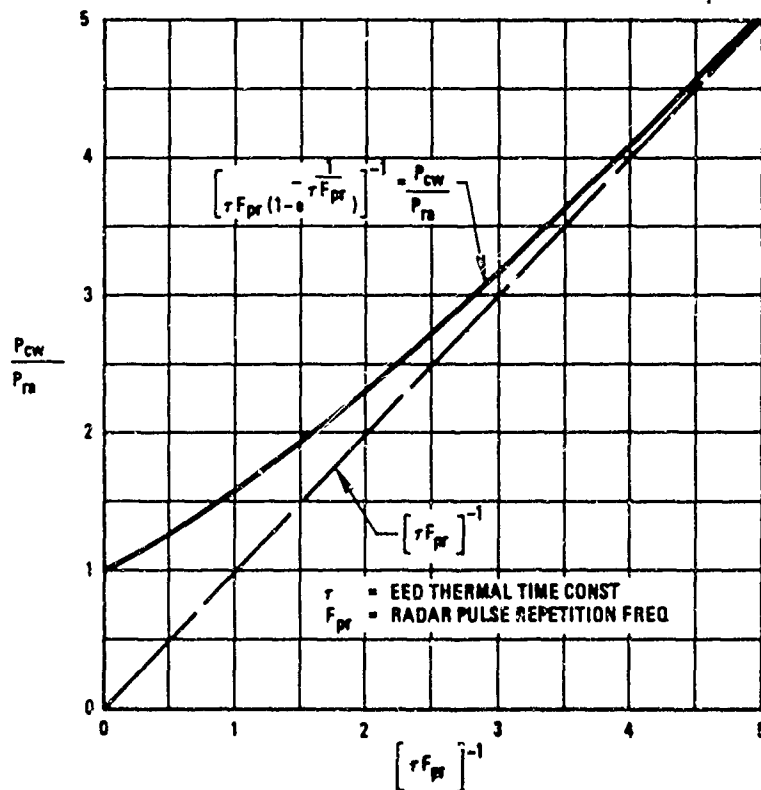


Figure 6. CW/Radar Power Ratio for Equivalent Bridgehead Temperature Rise

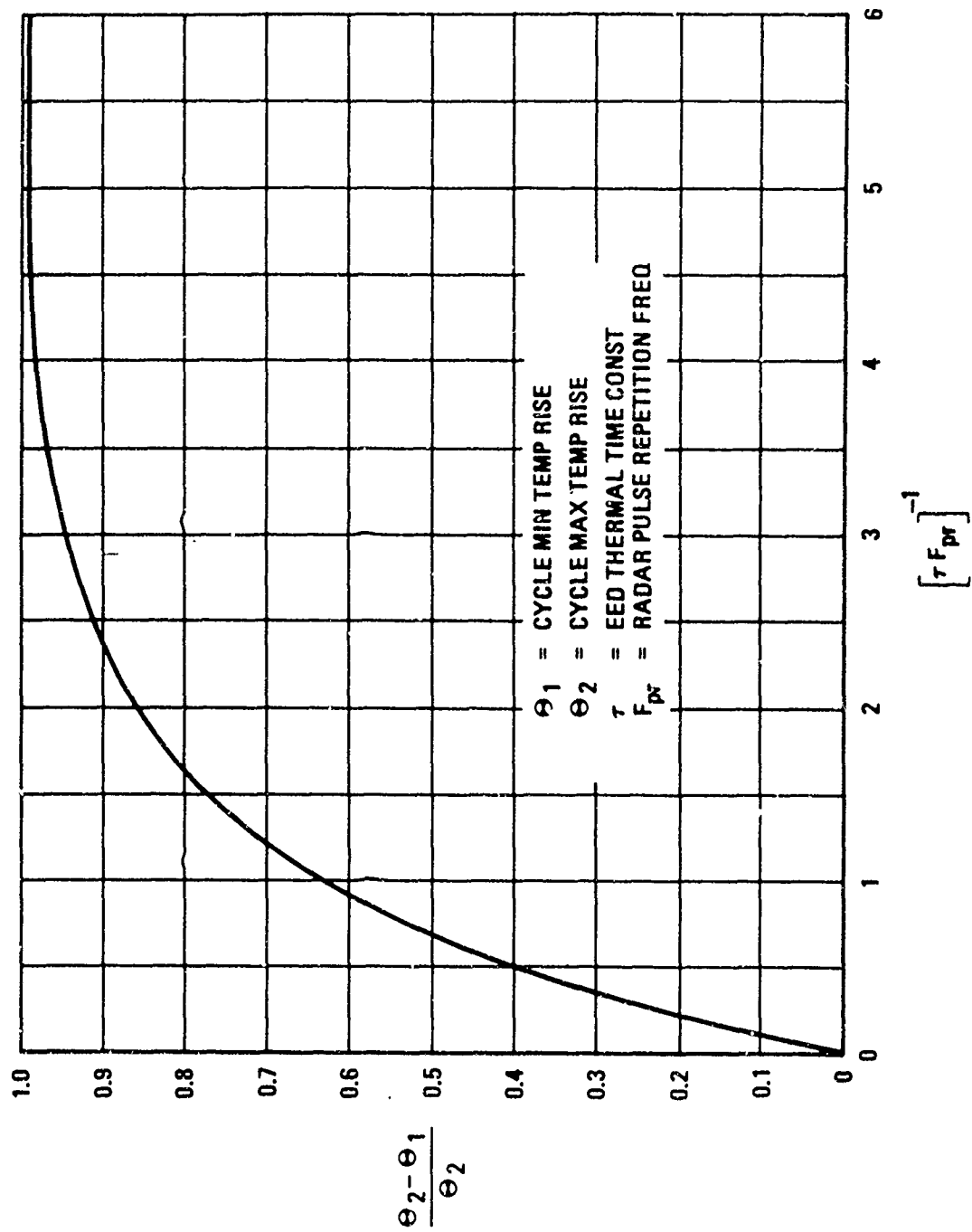


Figure 7. Bridgewire Temperature Fluctuation with Radar Signals

## 4-13P EBW FIRING UNIT-DETONATOR COMPATIBILITY TESTS

by Raymond G. Amicone, Michael G. Kelly

*The Franklin Institute Research Laboratories*

### INTRODUCTION

The prime objective of this program was to determine if the current waveform parameters, peak current ( $I_p$ ) and time-to-peak ( $t_p$ ) are adequate criteria to define the capability of a firing unit used to supply an EBW detonator with the proper electrical input. If these parameters can, indeed, define EBW detonator-firing unit compatibility then both detonator and firing unit designers will have a common basis for their designs.

The EBW detonator used in these studies<sup>1</sup> was the McCormick-Selph Part No. 805630K, Douglas Aircraft No. 7865742-1-005 "N" (Fig. 1). The firing unit that produced current waveforms of variable amplitude and duration was the General Laboratories Associates P/N 42439-B, Serial No. 001.

### INSTRUMENTATION

A General Laboratories Associates (GLA) Variable Waveform Firing Unit P/N 42439-B was used for the majority of the tests. It is designed to provide an exponentially damped sinusoidal waveform (within the limits of the minimum breakdown voltage of the internal spark gap tube) with an adjustable time to first peak ( $t_p$ ) of from 0.46 to 3.4  $\mu$ sec and a first peak amplitude ( $I_p$ ) between 340 and 9200 amperes. Variations in these parameters are obtained by changing cable length, capacitor size, and series inductance.

For calibration, the Shunt Isolator (GLA P/N 42063) is used in place of the EBW detonator. The isolator's input resistance is similar to that of the EBW and such that a 500 ampere current peak into the isolator will yield a 1 volt peak across the output. A Tektronix, Model 551 Dual Beam oscilloscope was used to observe the shunt isolator output and, thus, calibrate the firing unit. Oscillographs of firing unit waveforms (Fig. 2) were taken with the aid of the shunt isolator.

The GLA Variable Waveform Firing Unit contains storage capacitors which must be charged to voltage levels ranging from 700 to 3000 volts dc. A meter on the front panel of the firing unit monitors the voltage on the storage capacitor with an accuracy of 1%. External electrostatic voltmeters were used periodically to check the panel meter accuracy.

---

<sup>1</sup>Amicone, R.G. and Kelly, M.G., "EBW Firing Unit-Detonator Compatibility Tests", Franklin Institute Research Laboratories, Final Report F-C1968, November 1968. Contract NAS8-20404 NASA/Marshall Space Flight Center

## FIRING PROCEDURE

An EBW initiator checkout unit, Model 421A1, S/N 5 was supplied by NASA to check voltage breakdown between each of the two pins and case (resistance should exceed 100 megohms at 1200 volts) and the gap breakdown voltage (between 0.6 and 1.2 kilovolts). The McSA 805630K detonators (diagrammed in Figure 1) were mounted on steel plates  $\frac{1}{4}$  inch thick, 2- $\frac{1}{2}$  inches square and conditioned for a minimum of 2 hours before firing in the environmental test chamber at either  $+125^{\circ}\text{F}$  or  $-65^{\circ}\text{F}$  depending on the test run. The detonator to be tested was positioned in the protective firing fixture so that the steel witness block was sandwiched between the output end of the detonator and a backup positioning block. The connector end of the detonator extended through a hole in the firing fixture. The detonator shorting plug was removed and the detonator was mated with a keyed firing cable. A stream of dry nitrogen was continually directed at the connector to insure a moisture free fitting.

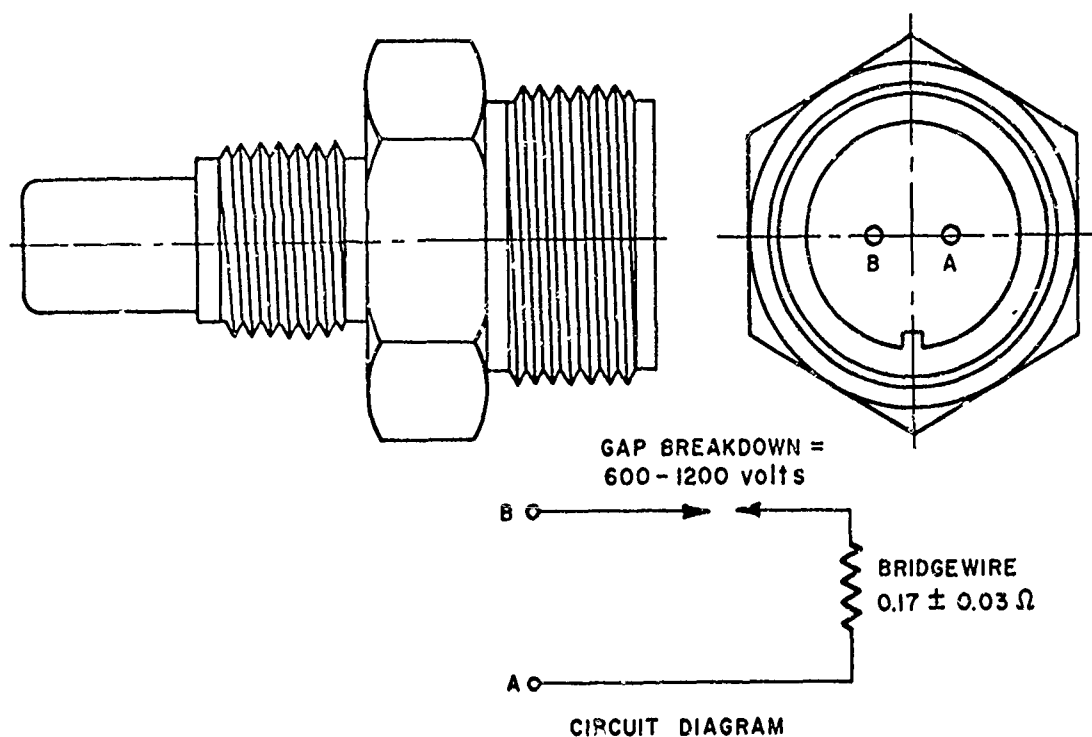


*Fig. 1 McSA 805630K EBW Detonator*

A set of curves giving the relationship between firing unit capacitor voltage and peak output current ( $I_p$ ) for each  $t_p$  value are shown in Figures 3A, B and C where Figure 3A, B and C represent each of the three possible capacitor values, 0.5, 1.0 and 2.0F, respectively. For any given capacitor value the values of  $t_p$  may not be exactly 0.57, 0.8 and 1.6  $\mu\text{sec}$  as

mentioned earlier, rather, they are as close as the variables of the firing unit would permit. In the case of the  $2\mu\text{F}$  capacitor (Figure 3C) only two pulse times were attainable. These curves, which were derived from numerous calibrations were used throughout this program to define the capacitor voltage-peak current relationship.

A go, no-go type of firing criteria had to be established for use in the staircase and probit type test procedures. In tests of the detonator alone, a burst, even a small one, in the output end of the detonator was considered evidence of a fired item. Anything less than this, such as a "pimple" on the end or a case sheared off near the base of the detonator were considered misfires. In the case of the detonator-MDF combinations the firing criteria was the complete consumption of the explosive core of the MDF test lead.

## TEST PLAN AND RESULTS

### Sensitivity of EBW-MDF Combination

Although not the prime objective, the first part of the test program called for a definition of the peak current ( $I_p$ ) sensitivity of the EBW detonator-MDF combination at an ambient temperature of  $-65^\circ\text{F}$  for pulse conditions of 0.57, 0.8,  $1.6\mu\text{sec.}$  to first peak ( $t_p$ ). These pulse widths were achieved with the GLA variable waveform firing unit using a  $1.0\mu\text{F}$  capacitor and variable cable length and inductance. Approximately 20 detonators and MDF assemblies were used at each pulse width and the firing plan was as specified by the Bruceton technique which follows the procedure outlined in the Bruceton report<sup>2</sup>. With this technique the pulse width is fixed and the stimulus (in this case the voltage on the firing unit capacitor) is either raised or lowered by a fixed logarithmic increment, depending upon whether the preceeding observation was a non-fire or a fire. When the data are properly analyzed an estimate of the mean and standard deviation may be made.

The criteria for a fired EBW-MDF combination is the complete consumption of the explosive core of the MDF test lead. Figure 6 shows expended test leads and detonators from one of the Bruceton tests. The MDF assembly is shown above the EBW assembly in each grouping. The small ring shown in some groupings is the main charge sleeve, a part of the EBW detonator which may be seen still partially intact on serial numbers 1380, 1110 and 1667. Fragments of the casing are also shown in some groupings. The lower right of Figure 4 shows the remains of the EBW detonators and dent blocks which were used to approximate the starting level for the above test.

---

<sup>2</sup>Statistical Analysis for a New Procedure in Sensitivity Experiments, July 1944, Prepared by Statistical Research Group, Princeton University (SRG Report No. 40) for the Applied Mathematics Panel NRDC and redesignated AMP Report 101.R.

Although the test plan called for three tests using nominal  $t_p$  values of 0.57, 0.8 and 1.6  $\mu$ s with a 1  $\mu$ F capacitor, two additional tests were run. The first was at a nominal  $t_p$  value of 0.57  $\mu$ s with a 0.5  $\mu$ F capacitor; the second at  $t_p = 0.8 \mu$ s with a 1  $\mu$ F capacitor but at +125°F. The results of the five sensitivity tests are summarized in Table 1. The actual pulse time-to-peak ( $t_p$ ) is given in this table as well as the mean value of peak current obtained when the capacitor is discharged into the shunt isolator.

It may be seen in Table 1 that there is a large increase in the peak current sensitivity of the EBW-MDF combination when the ambient temperature is raised from -65°F to +125°F, all other factors being held constant. The magnitude of the change is 5 amperes per °F or about 0.25% per °F. This temperature dependence seems normal for the gold alloy wire (Secon 443) used in the EBW detonator. A second point of much interest is the large difference in the peak current sensitivity when the time-to-peak is held nearly constant and only the size of the firing capacitor is changed. In particular, with a 1.0  $\mu$ F capacitor and  $t_p = 0.65 \mu$  sec. the mean  $I_p$  was 3300 amperes; with a 0.5  $\mu$ F capacitor and  $t_p = 0.57 \mu$  sec. the mean  $I_p$  was 1780 amperes. These results seemed to indicate that  $t_p$  and  $I_p$  would not completely define the compatibility between the detonator and firing unit; and subsequent tests were modified accordingly.

#### Sensitivity of EBW Detonator as a Function of Input Parameters $I_p$ and $t_p$

The second part of the test plan called for a definition of the "all-fire" probability level (99.9% with 95% confidence) of the EBW detonator as a function of time-to-first-peak ( $t_p$ ) and storage capacitor size (C). The mean or 50% peak current ( $I_p$ ) sensitivity was first to be established at nominal  $t_p$  values of 0.57, 0.80 and 1.60  $\mu$ s, with  $C = 1.0 \mu$ F. Fixed level testing was then continued at the projected 66% and 90% firing level for capacitor values of 0.5, 1.0 and 2.0  $\mu$ F and the three nominal  $t_p$  values. Steel dent blocks were to be used to measure relative output.

The test plan was modified to make preliminary test of approximately 15 EBW's at each capacitor value and pulse time. The results of these tests are summarized in Table 2. To conserve detonators the test at  $C = 0.5 \mu$ F,  $t = 0.57 \mu$ s was not fired; rather, the voltage and current sensitivities were extrapolated from the EBW-MDF combination test results listed in Table 1. This action was justified by a comparison of the 1.0  $\mu$ F, peak current sensitivities (at all  $t_p$  values) in Tables 1 and 2 that showed the mean peak current required to fire the EBW's alone is less than that required by the EBW-MDF combination by a constant logarithmic increment (this may be seen in Figure 5).

In Figure 5 all values of mean peak current sensitivity except the two high temperature tests from Tables 1 and 2 are plotted as a function of time-to-peak for each capacitance value. Figure 6 is a plot of the mean capacitor voltage sensitivity data of Table 2 (excepting

the high temperature test) as a function of time-to-peak. The data of Table 1 were not plotted in Figure 6 because the difference is relatively small.

The curves of Figure 5 convincingly illustrate that the parameters peak current and time-to-peak current cannot be used to define the compatibility between the EBW spark gap detonator and a firing unit used in these studies. As an example, if we selected a  $t_p$  value of  $1.0\mu s$  in Figure 5, the peak current value necessary to produce 50% firing of the EBW would be 930, 1860 or 2850 amperes depending on the firing capacitor used to achieve the desired  $t_p$ . Since the output waveform of the firing unit employed in these tests is a damped sinusoid we may conclude that the detonator used in these tests is being initiated, in part, by energy supplied after the first current peak.

Whereas Figure 2 showed oscillographs of only the first current peaks as recorded with the shunt isolator, Figure 7 shows a major portion of the entire current waveform for fixed values of  $t_p$  and  $I_p$  ( $1.5\mu s$  and 1300 amperes) but for three different capacitor values. It is apparent from this figure that when the capacitance,  $C$ , is increased from 0.5 to  $2.0\mu F$  the magnitude and the number of peaks after the first peak decreases. If we concede that current peaks in addition to the first peak contribute to initiation then the results shown in Figure 8 are not surprising.

It must be stressed that the above conclusions are specifically applicable to the detonator we tested and that we have no right to generalize since the input requirements with other EBW detonators may vary considerably depending on their construction. Leopold<sup>3</sup> discusses this in detail and suggests mechanisms whereby these differences may occur.

When we compare the peak currents for 50% fire at  $+125^{\circ}F$  with the corresponding test at  $-65^{\circ}F$  (Table 2), the difference is 490 amperes or about 2.5 amperes per  $^{\circ}F$ . This is about half the change discussed for the high temperature EBW-MDF combination. We may infer from this difference that the high temperature in the EBW-MDF test not only affects the EBW input sensitivity but also the relative output strength of the EBW.

#### Determination of "All-Fire" Levels for EBW Detonator

An additional objective of this test program was to establish the "all-fire" (99.9% firing probability with 95% confidence) level in terms of  $I_p$  and  $t_p$ . Originally, this objective applied to all three capacitance values and was later modified to include only the 0.5 and  $1.0\mu F$  values. The results of the Bruceton tests summarized in Tables 1 and 2 were used to estimate capacitor charging voltages required for 66% and 90% probability of fire for each  $C$  and  $t_p$  value. Approximately 17 detonators were tested at the 66% and 43 at the 90% level. Steel dent measurements were made on all firings and the ambient temperature was  $65^{\circ}F$  throughout testing. The data are summarized in Table 3.

<sup>3</sup>Leopold, H., "Initiation of Explosives by Exploding Wires: VII Effect of Energy Termination on the Initiation of PETN by Exploding Wires" NOLTR 65-56, June 1965 (AD618-675)



The data in Table 3 were combined with the Bruceton data and analyzed by the Probit<sup>4</sup> and Logit<sup>5</sup> techniques. The results of these analysis are listed in Table 4 and plotted in Figures 8 and 9. Although both the 99.9% and 0.01% firing probability points, with 95% confidence were computed in the Logit and Probit analyses, only the 99.9% with 95% confidence points are plotted in Figures 8 and 9. It should also be noted that in the Logit analyses in Appendix B the figures shown in parenthesis in the "Number Fired, %" and "1" columns are estimates based on an initial calculation. This technique is described in the cited reference on the Logit analysis and is useful for making more accurate  $\chi^2$  calculations.

Figures 8 and 9 represent the response of the 805630K EBW detonator to the first current peak of the GLA Variable Waveform Firing Unit output for various  $t_p$  values and storage capacitor sizes of  $0.5\mu\text{F}$  and  $1.0\mu\text{F}$ , respectively. The  $\chi^2$  analysis showed that there was no pronounced advantage in the fit obtained by either the Probit or the Logit method.

The Logit method does give wider limits to the predicted "all-fire" and "no-fire" (0.1% with 95% confidence) values. The overall results shown in Figure 9 for the  $1.0\mu\text{F}$  firings are in fairly close agreement with data derived previously<sup>6</sup> on the same detonator under similar firing conditions.

## CONCLUSIONS

The main objective of this program was to determine if the current waveform parameters  $I_p$  and  $t_p$  could adequately define the capability of a firing unit to supply an EBW detonator with the proper input requirements. If these criteria were proven adequate, then both EBW detonator designers and firing unit designers would have a common ground to assess compatibility. It seems clear from the results that parameters other than  $I_p$  and  $t_p$  will be required to define the sensitivity of the Mc/SA 805630K EBW spark gap detonator to the output of the GLA Variable Waveform Firing Unit. The probable reason is that the GLA firing unit, and the majority of other EBW firing units, produce a damped sinusoidal waveform which has secondary current peaks after the first peak ( $I_p$  and  $t_p$  pertain to the first peak) and the 805630K detonator is apparently sensitive to a combination of energy provided by the main peak and the secondary peaks. Another EBW detonator would not necessarily behave in this manner.

---

<sup>4</sup>Finney, D.J., Probit Analysis, A Statistical Treatment of the Sigmoid Response Curve, Cambridge Press, 1947

<sup>5</sup>Berkson, J., "A Statistically Precise and Relatively Simple Method of Estimating the Bio Assay with Quantal Response, Based on the Logistic Function", Journal of the American Statistical Association, Sept 1953

<sup>6</sup>Amicone, R.G., Goldie, V.G., "Compatibility Test of Firing Unit and EBW Detonator", prepared for General Laboratory Associates, Inc. under NASA Contract No. NAS8-14004.

The 805630K detonator contains a spark gap in one of the two input pins (in the header) which is set to break down at  $900 \pm 300$  volts. Thus, unless the potential supplied by the firing unit exceeds  $900 \pm 300$  volts no current is applied through the bridgewire. Since the voltage from the GLA firing unit is also a damped sinusoid, the spark gap itself may contribute to the secondary peak sensitivity of the 805630K detonators.

Figure 6 brings out an interesting and possibly useful fact. As the time to first peak is reduced, the firing voltage needed on the storage capacitor becomes relatively independent of the size of the capacitor. This fact might be useful for the design of a firing unit where restricted space is a consideration.

Since we have shown that  $I_p$  and  $t_p$  are inadequate for defining the compatibility between the GLA firing unit and McSA 805630K detonator the question as to the existence of a "compatibility" parameter or parameters arises. The recent literature<sup>7,8</sup> gives much evidence indicating that parameters such as the rate of energy input to the bridgewire, secondary energy input after initial current burst, and burst current may be significant in predicting the performance of EBW detonator-firing set systems. A means of monitoring the actual current while firing and a knowledge of the RLC parameters of the firing circuit are usually required for these parameter measurements.

No actual firing currents were observed during this test program since it was not within our province to tamper with the parameters of relatively fixed firing systems; however, if further investigation of compatibility parameters is to be pursued it is recommended that both current and voltage of the firing waveform into the EBW be observed. The presence of a spark gap within the 805630K detonator may make the dynamic firing voltage an important parameter.

#### ACKNOWLEDGEMENT

This work was carried out under Contract NAS8-20404 with NASA/Marshall Space Flight Center the authors wish to acknowledge the guidance, cooperation, interest and patience of Messrs. John Atkins and James Stulting of NASA/MSFC.

---

<sup>7</sup>Cnare, E.C., "Exploding Wire Detonator: An Approximate Method of Predicting Exploding Wire Detonator-Capacitor Discharge System Performance," from Exploding Wire, Vol. 3, W.G. Chace and H.K. Moore, 1964.

<sup>8</sup>Leopold, H.S., "Effect of Bridgewire Parameters on Explosive Initiation," from the same source.

**Table 1**  
**PRELIMINARY SENSITIVITY ESTIMATES**  
**OF EBW-MDF COMBINATION**  
**(Bruceton Tests)**

<u>Storage Capacitor (<math>\mu</math>F)</u>	<u>Actual Pulse Time (<math>\mu</math>s)</u>	<u>Ambient Temperature (<math>^{\circ}</math>F)</u>	<u>Sample Size</u>	<u>Mean Capacitor Voltage (volts)</u>	<u>Std. Dev. (log volts)</u>	<u>Mean Peak Current (amperes)</u>
1.0	0.65	-65	15	1681	.0060	3300
1.0	0.80	-65	15	1697	.0188	2600
1.0	0.80	+125	15	1108	.0141	1650
1.0	1.5	-65	15	1341	.0147	1130
0.5	0.57	-65	15	1800	.0076	1780

**Table 2**  
**PRELIMINARY SENSITIVITY ESTIMATES**  
**OF EBW DETONATORS**  
**(Bruceton Tests)**

<u>Storage Capacitor (<math>\mu</math>F)</u>	<u>Actual Pulse Time (<math>\mu</math>s)</u>	<u>Ambient Temperature (<math>^{\circ}</math>F)</u>	<u>Sample Size</u>	<u>Mean Capacitor Voltage (volts)</u>	<u>Std. Dev. (log units)</u>	<u>Mean Peak Current (amperes)</u>
0.5	0.57	-65	15	1730*	.0076	1640*
0.5	0.80	-65	15	1802	.0142	1090
0.5	1.40	-65	8	1540	.0148	670
1.0	0.65	-65	20	1639	.0107	3200
1.0	0.80	-65	20	1551	.0458	2350
1.0	0.80	+125	17	1243	.0316	1860
1.0	1.50	-65	17	1264	.0121	1065
2.0	0.80	-65	15	1485	.0186	3730
2.0	1.50	-65	14	1171	.0399	1580

\*Extrapolated from Table 1. See Text

Table 3

TESTS AT ESTIMATED 66% AND 90% LEVELS  
(EBW Alone)

Storage Capacitor ( $\mu F$ )	Actual Pulse Time ( $\mu s$ )	Applied Capacitor Voltage (volts)	Detonators		
			Number Tested	Number	Fired %
0.5	0.57	(mean from Bruceton data = 1730 volts)			
0.5	0.57	1734	17	13	76
0.5	0.57	1785	43	40	93
0.5	0.80	(mean from Bruceton data = 1602 volts)			
0.5	0.80	1634	17	15	88
0.5	0.80	1643	43	35	81
0.5	1.40	(mean from Bruceton data = 1540 volts)			
0.5	1.40	1568	17	8	47
0.5	1.40	1650	42	36	86
1.0	0.65	(mean from Bruceton data = 1639 volts)			
1.0	0.65	1672	17	12	71
1.0	0.65	1749	43	41	95
1.0	0.80	(mean from Bruceton data = 1551 volts)			
1.0	0.80	1582	17	14	82
1.0	0.80	1630	43	42	98
1.0	1.50	(mean from Bruceton data = 1264 volts)			
1.0	1.50	1289	17	8	47
1.0	1.50	1360	43	40	93

Table 4

FIRING PROBABILITY AS FUNCTION OF PEAK CURRENT  
(Analyzed by Probit and Logit Methods)

Storage Capacitor ( $\mu F$ )	Actual Pulse Time ( $\mu s$ )	Sample Size	Type of Analysis	Amperes for Indicated Firing Probability (*with 95% confidence)			Degrees of Freedom	$\chi^2$
				*99.9%	50%	*0.1%		
0.5	0.57	83	Probit	1970	1650	1395	8	8.21
0.5	0.57	82	Logit	2380	1590	1097	6	1.51
0.5	0.80	75	Probit	1250	1080	950	4	1.42
0.5	0.80	75	Logit	1325	1080	875	3	0.97
0.5	1.40	71	Probit	825	680	560	8	1.06
0.5	1.40	69	Logit	895	680	520	5	0.58
1.0	0.65	80	Probit	3730	3210	2790	4	1.07
1.0	0.65	80	Logit	3875	3210	2660	3	0.44
1.0	0.80	80	Probit	2810	2275	1860	6	12.10
1.0	0.80	80	Logit	3250	2270	1570	5	6.67
1.0	1.50	77	Probit	1260	1080	925	4	2.45
1.0	1.50	77	Logit	1325	1080	820	3	1.21

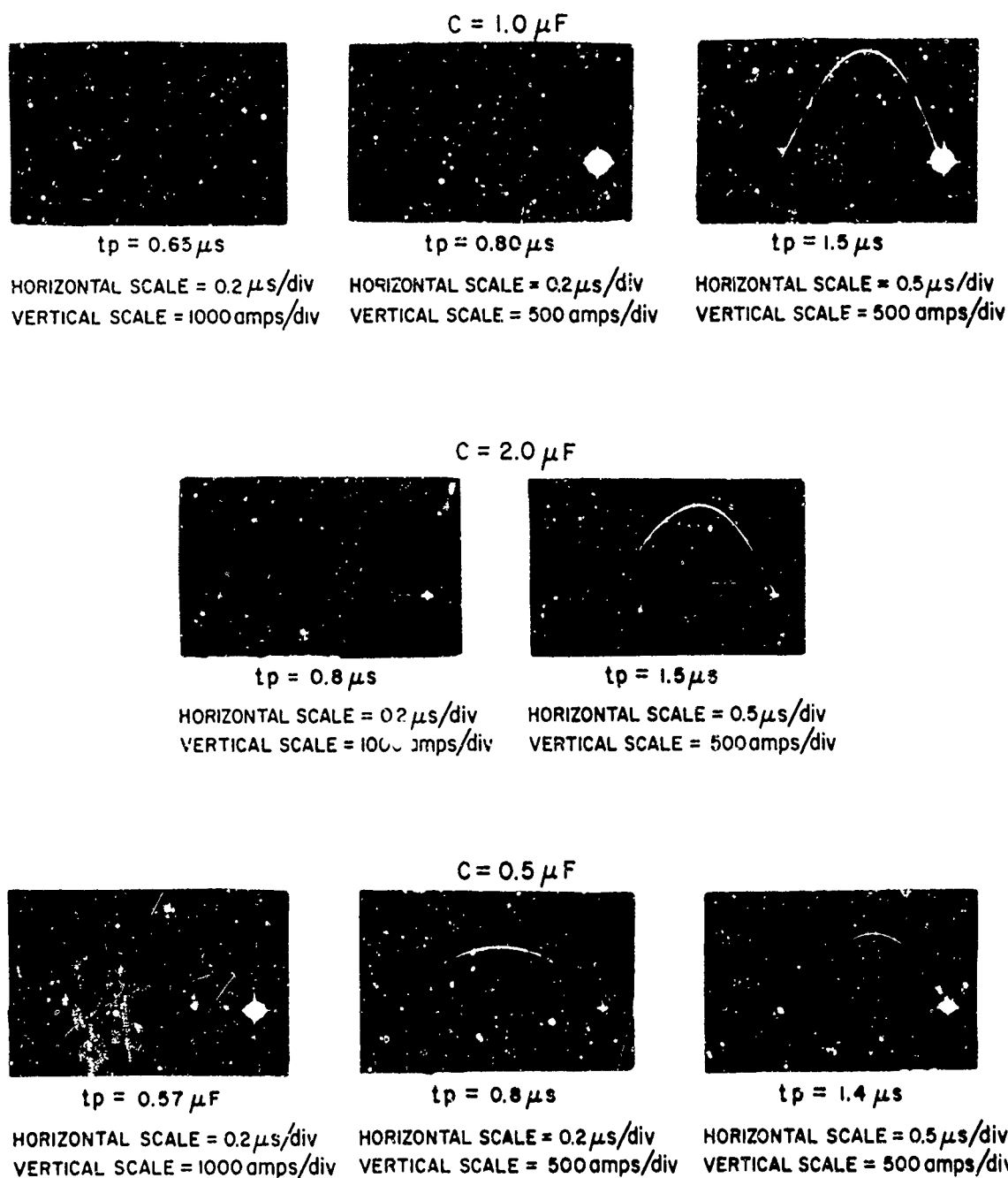
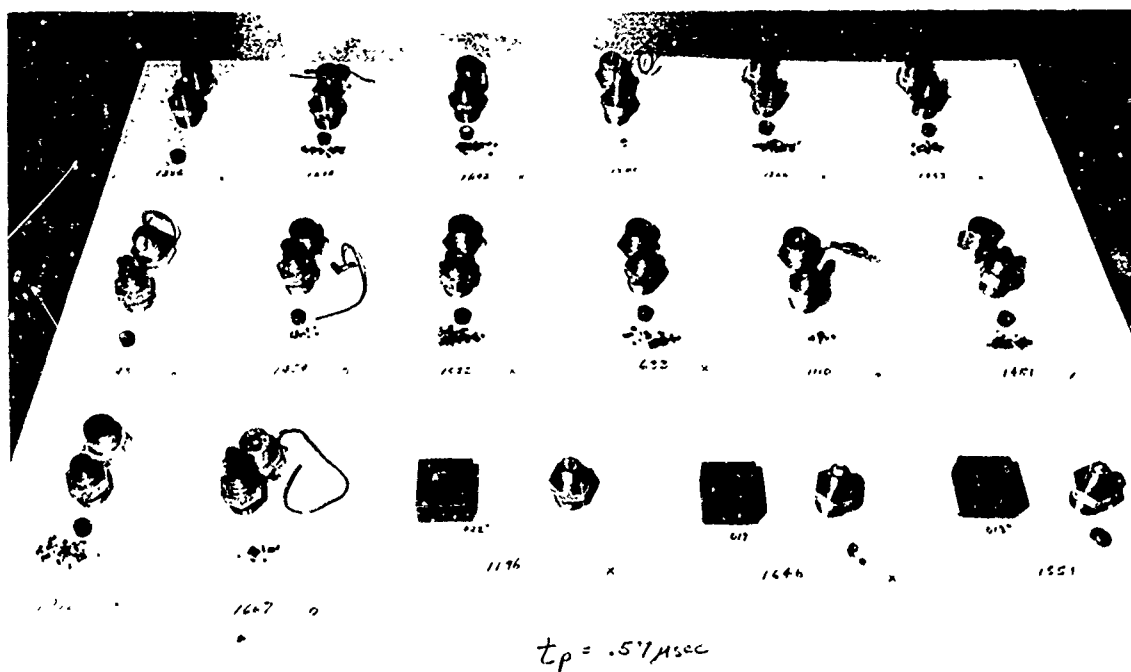
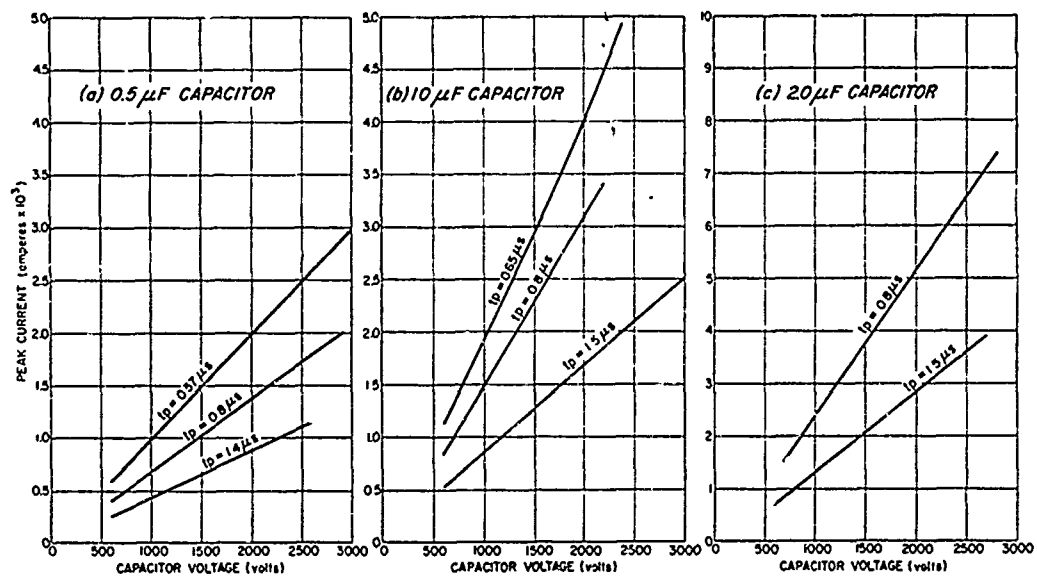


Fig. 2. Current Waveforms Into Shunt Isolator (GLA Firing Unit)



H 1007-1

Fig. 4. Expended MDF Test Leads and EBW Detonators (From 0.57  $\mu$ s Bruceton Test)  
4-13,11

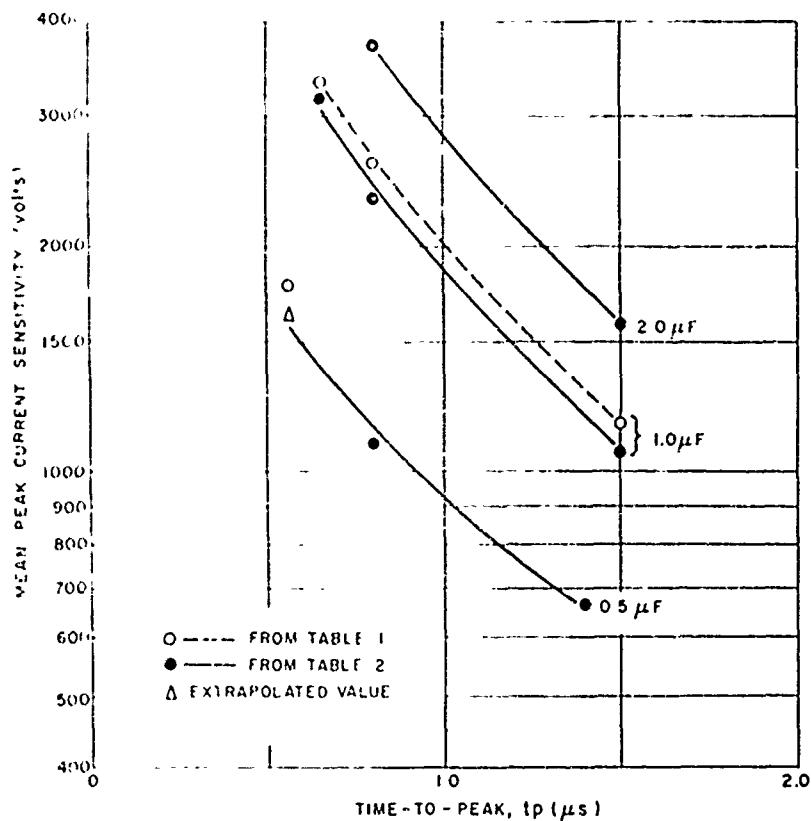


Fig 5 Mean Current Sensitivity As A Function of Time-to-First Peak

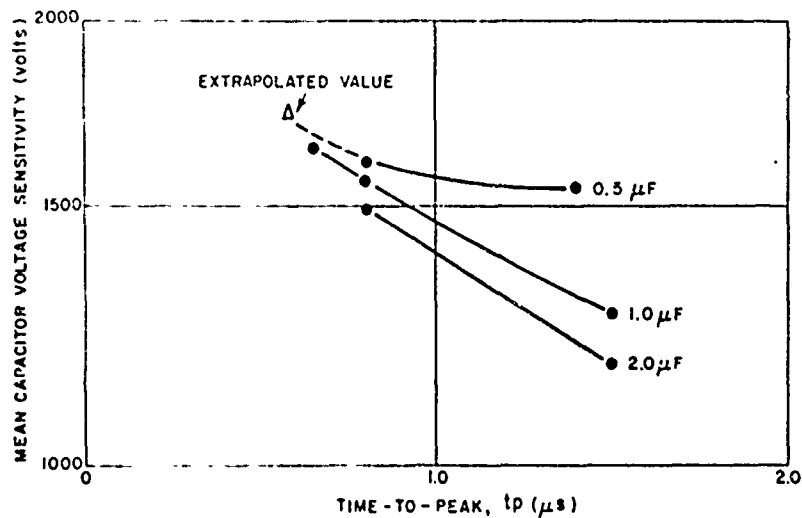


Fig 6 Mean Capacitor Voltage Sensitivity As A Function of Time-to-First Peak

VERTICAL SCALE = 1000 amps/div  
HORIZONTAL SCALE =  $2 \mu s$ /div



Fig 7 Current Waveforms From GLA Firing Unit  
( $I_p = 1.300$  amperes,  $t_p = 1.5 \mu s$ , Variable Capacitance)

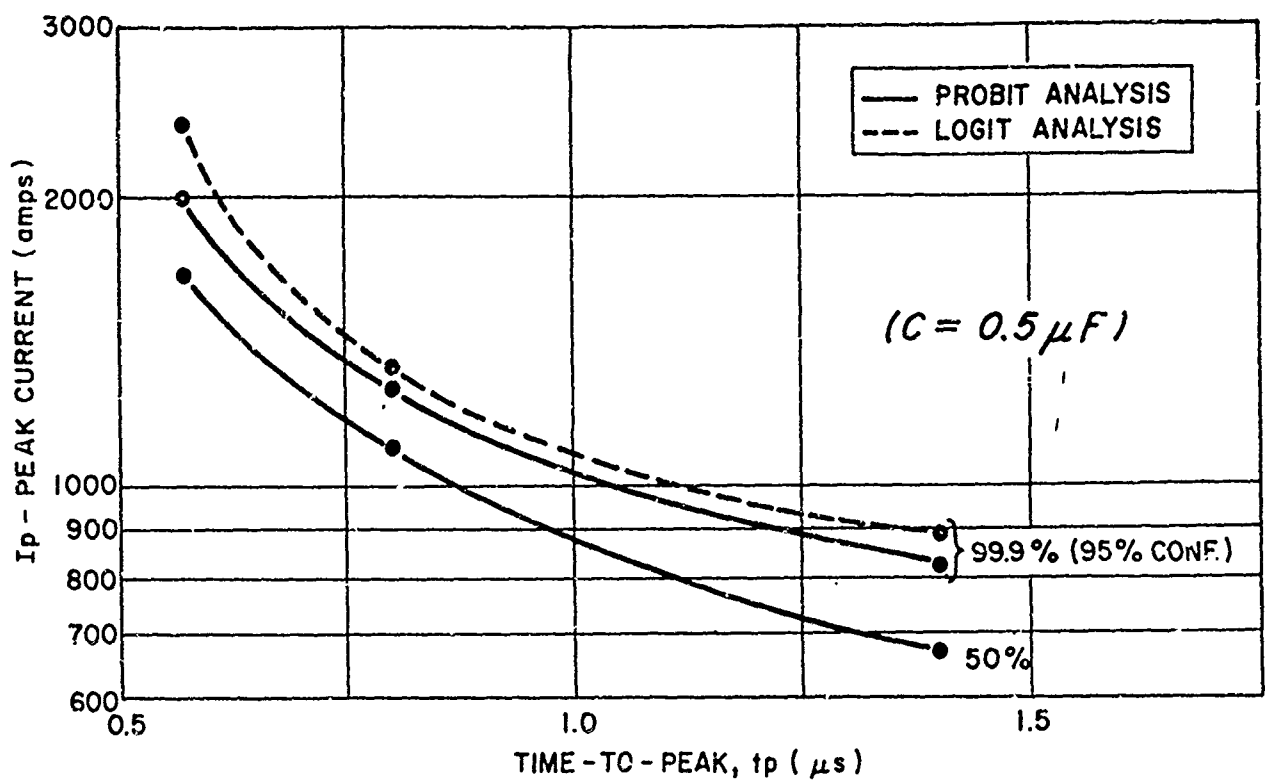


Fig. 8. Peak Current Sensitivity of EBW Detonator At Two Probability Levels

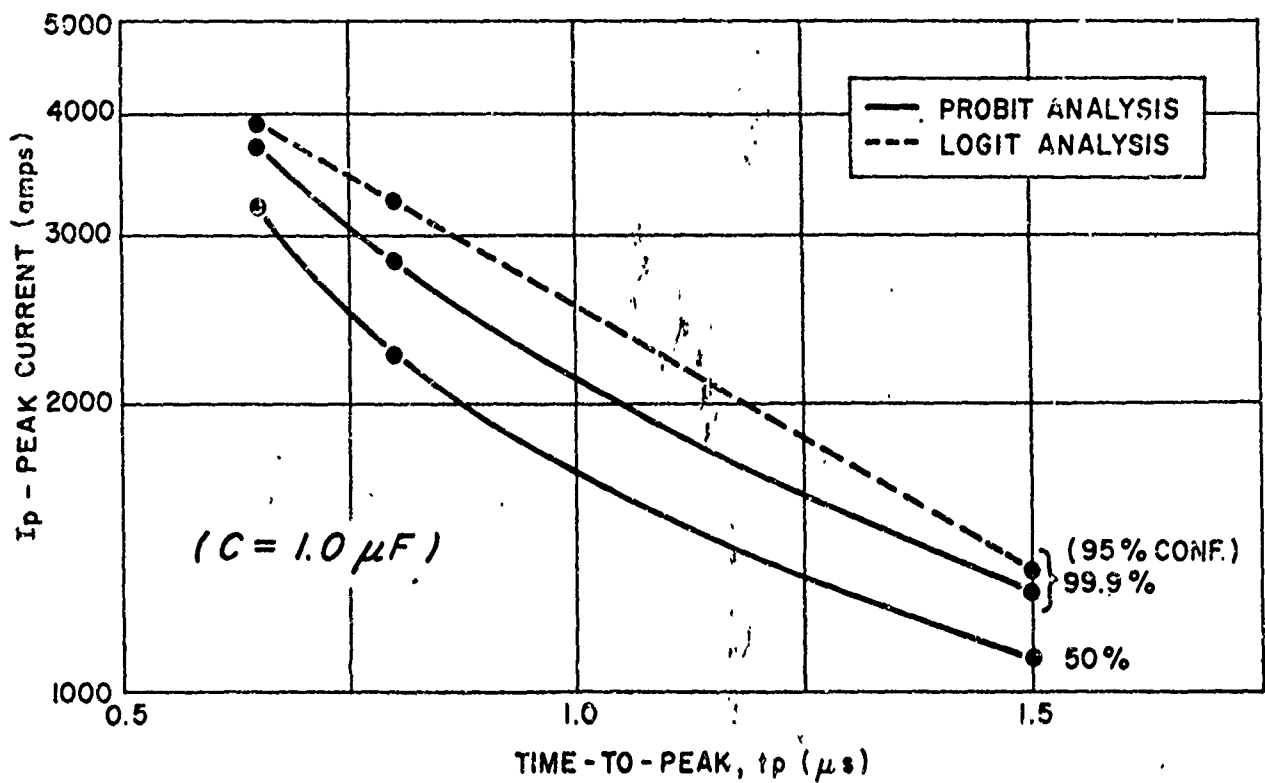


Fig. 9. Peak Current Sensitivity of EBW Detonator At Two Probability Levels



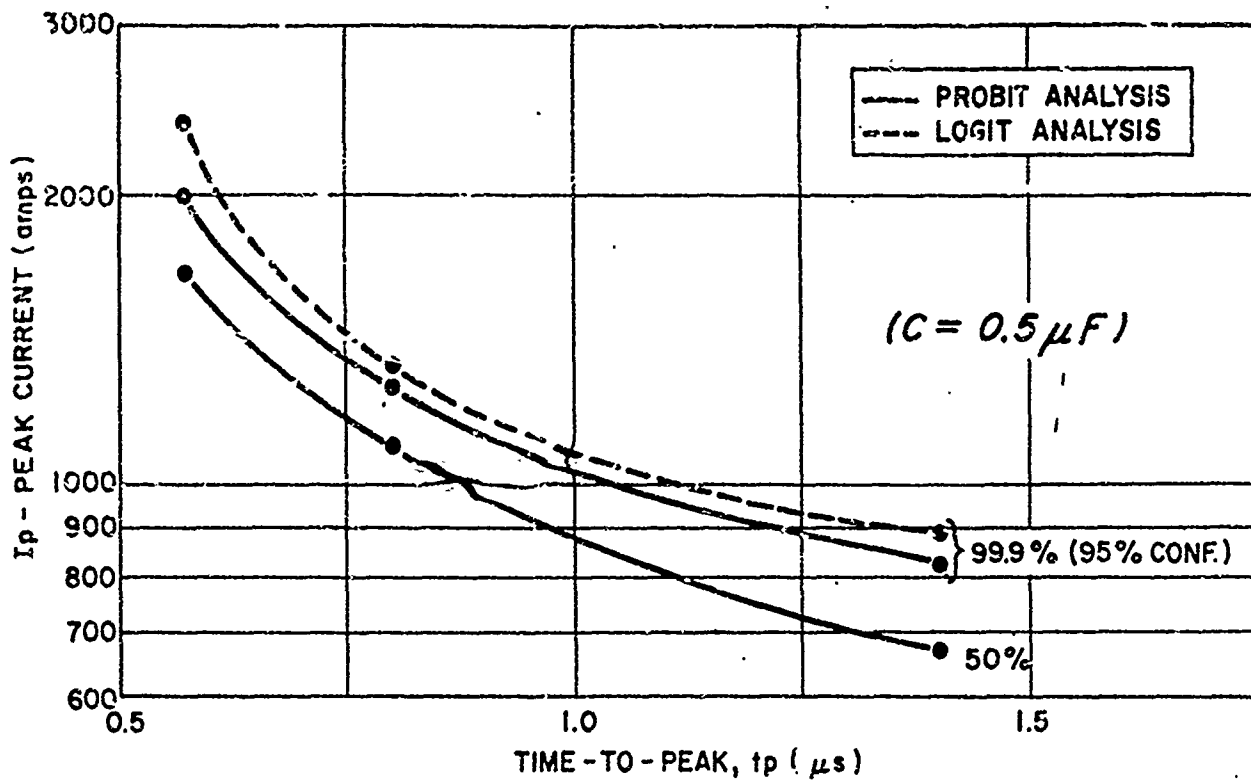


Fig. 8. Peak Current Sensitivity of EBW Detonator At Two Probability Levels

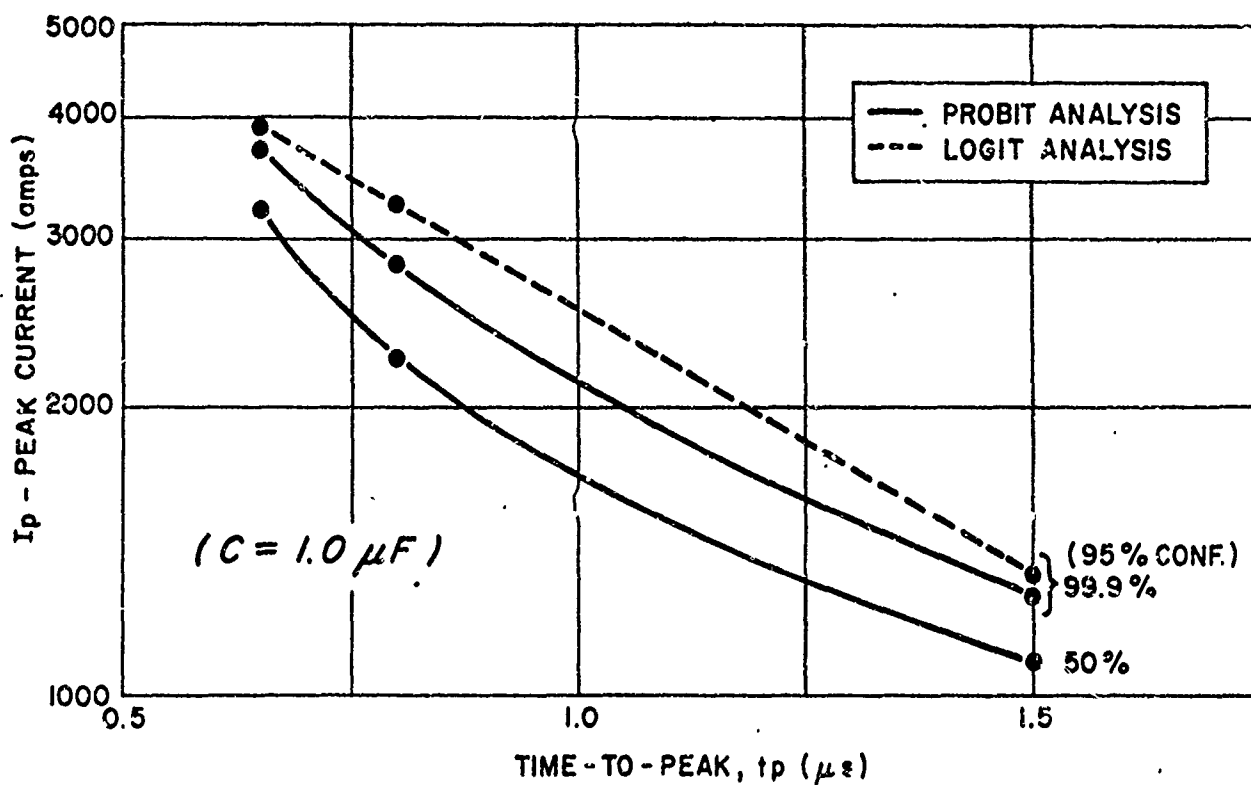


Fig. 9. Peak Current Sensitivity of EBW Detonator At Two Probability Levels

#### 4-14P DETERMINING RATINGS OF RF SUPPRESSION DEVICES

P. F. Mohrbach, R. F. Wood, R. H. Thompson

#### ABSTRACT

Surveying present methods of characterizing RF suppression devices indicated that there is no accepted standard of rating. Attention was focused on methods of determining minimum loss of a two port network. It was decided that, in general, there are two methods:

- (1) Measure the ratio of load power to input power for all possible terminations of the two port network and then select the maximum ratio;
- (2) Measure a transmission or transformation parameter of the network for a number of terminations and compute the minimum loss from the results.

Various approaches to measuring the minimum loss of an RF suppression device are discussed.

#### 1. INTRODUCTION

Present day weapon systems use numerous electrically initiated explosive devices to accomplish many functions. These devices are subject to inadvertent initiation or degradation by stray electromagnetic energy from communication and radar transmitters. Electroexplosive system designers must choose components and designs that will reliably fulfill their intended mission and yet be safe from electromagnetic energy. The designers' problems are particularly difficult in today's weapons because they seldom know the electromagnetic environments in which the system must operate.

One of the techniques employed to minimize the hazard to radio-frequency (RF) energy is to insert an RF suppression device between the EED and the circuit that picks up the energy. These suppression devices can protect the EED by causing a mismatch to occur between the EED and its circuit (reflecting the power); it can absorb the energy and dissipate it in the form of heat, or a combination of the two can be utilized. Obviously these devices must be able to handle the normal firing current, withstand the input voltage, and dissipate the power without failing.

This paper discusses some of the methods of testing such devices for these parameters.

The overall object of this project was to develop equipment capable of determining the overload ratings of RF suppression devices in the frequency range of 0.1 MHz to 10 GHz. Input powers as high as 100 watts were to be considered. The Naval Weapons Laboratory (NWL) and The Franklin Institute Research Laboratories (FIRL) agreed early in the project that the parameter of interest in evaluating RF suppression devices is the worst case attenuation. When the prospect of obtaining a single high power system over the entire frequency range of interest appeared bleak, it was then agreed that we would devote our effort to specification of  $\text{dB}_{\text{wc}}$  measurement systems that would function, each perhaps only in its own frequency band, over the entire frequency band of interest. In addition, these systems were to be capable of measuring any RF suppression device but could use low power techniques in contrast to the high input power requirement considered previously. Networks with worst case attenuation up to 50 dB were to be included. Measurement systems that were as simple as possible to operate, without sacrificing too much in accuracy, were to be specified wherever possible.

It should be noted in the ensuing discussion that only the high points of various measuring systems are touched upon due to time limitations. In most cases a considerable amount of mathematical development, specialized equipment development and proof tests support the findings. The bulk of this supporting material can be found in The Franklin Institute Research Laboratories Report F-C2050, "Determining the Maximum Continuous and Maximum Overload Ratings of Radio Frequency Suppression Devices", November, 1968. This report was prepared for the U. S. Naval Weapons Laboratory, Dahlgren, Virginia, on Contract No. N00178-67-C-0171.

## 2. $DB_{WC}$ MEASUREMENT SYSTEMS

### 2.1 Matched Input and Output System

One of the most direct methods of determining  $dB_{WC}$  is by means of a system such as shown in Figure 1. While such a system can be set up for any part of the RF frequency spectrum, it is most easily used where distributed component matching systems (double stub and line stretcher-shortened stub combinations) are available. This is normally in the range above 40 MHz. If in a system of this type, a matching system is lossless and capable of matching a device's impedance, all the recorded loss can be attributed to the device; however, if the matching system is lossy and/or cannot match a device's impedance, some of this recorded loss is not truly the device's worst case attenuation but is the combined loss of the device and the matching system.

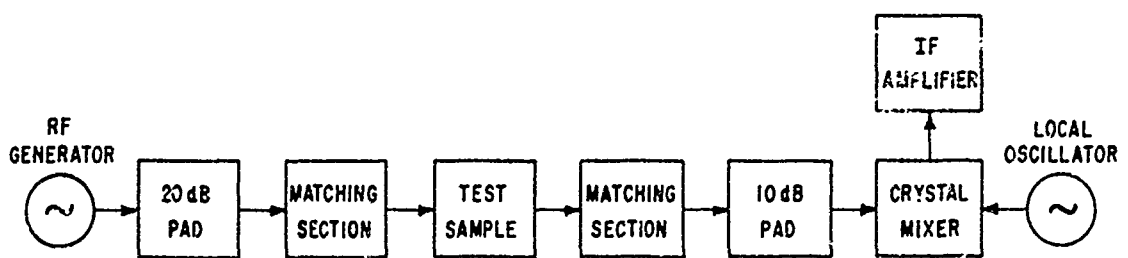


Figure 1. Worst Case Attenuation Measurement System

Some specification for matching system loss must be made if duplicate measurement systems are to be constructed and their results compared. Such a loss parameter could be developed if a specification of loss (in dB for instance) in terms of VSWR is acceptable. Obviously, VSWR is not a sufficient parameter to completely define loss since the same VSWR can be associated with an infinity of impedances to be matched; however, a specification of this type (VSWR) ignores losses due to line length variation which is always less than a half wavelength. Since most of the loss in a distributed matching system is associated with the variable line's contacts (finger stock) such a parameter specifying

loss might be an acceptable error parameter. We tried to evaluate the losses of our distributed matching systems in terms of VSWR in order to determine the ease of measurement of such a parameter as well as to get a general idea of our matching system losses.

To obtain a wide range of VSWR values, a series of test samples was constructed using disk resistors of 0.1, 0.5, 1.0, 5.0, 10 and 50 ohms which shunted the input of a 50 ohm attenuator pad. In addition, since all of the components in the measuring system had a 50 ohm characteristic impedance (except the disk resistor), it was possible to eliminate the second matching section so that the loss in one matching section at a time could be determined. The final results of this study are shown in Figure 2 where the VSWR values were computed from impedance measurements of the disk resistor networks, and the matching loss was obtained by subtracting the losses of the disk resistor and 10 dB pad (which were computed) from the actual dB readings made with the measuring system. It can be noted that the matching error increases both with VSWR and with frequency. Indications are that the bulk of the loss occurs at the sliding fingers in the tuning sections.

## 2.2 Attenuation as a Function of Input Impedance Loc

It can be shown that the worst case attenuation ( $\text{dB}_{wc}$ ), the minimum loss, of a passive linear two port network can be determined from a plot of the input impedance of the network when the network is terminated in all possible reactive loads. Specifically

$$\text{dB}_{wc} = +4.34\theta \quad (1)$$

where  $\theta = \cosh^{-1} (\tau/\rho)$  and  $\tau/\rho$  can be determined from the input impedance plot. In general, the input impedance ( $Z_{in}$ ) plot of the network for reactive termination of the network will be a circle as shown in Figure 3. It is assumed that all possible reactances have been used as terminations.

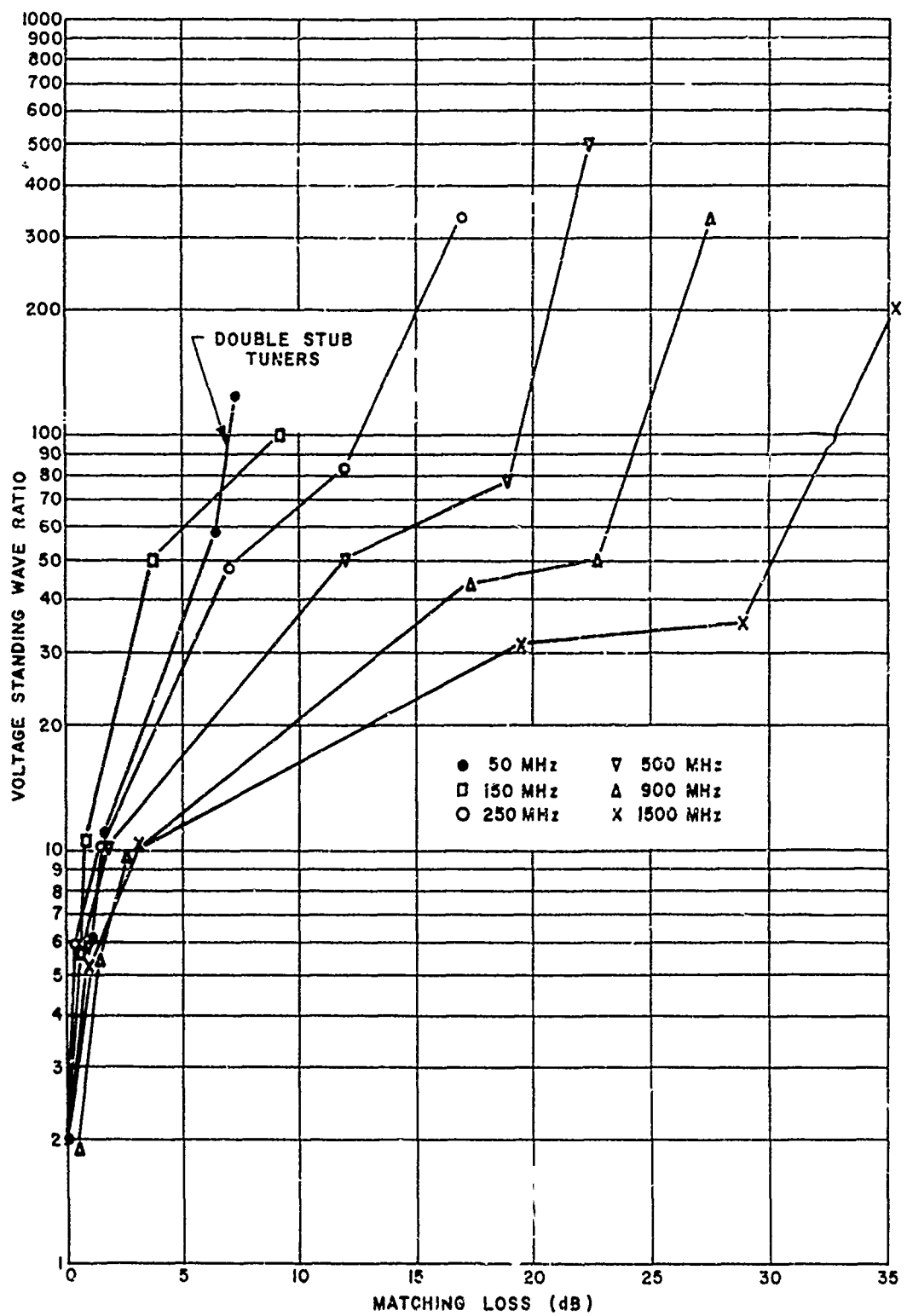


Figure 2. Matching Section Losses Versus Input VSWR

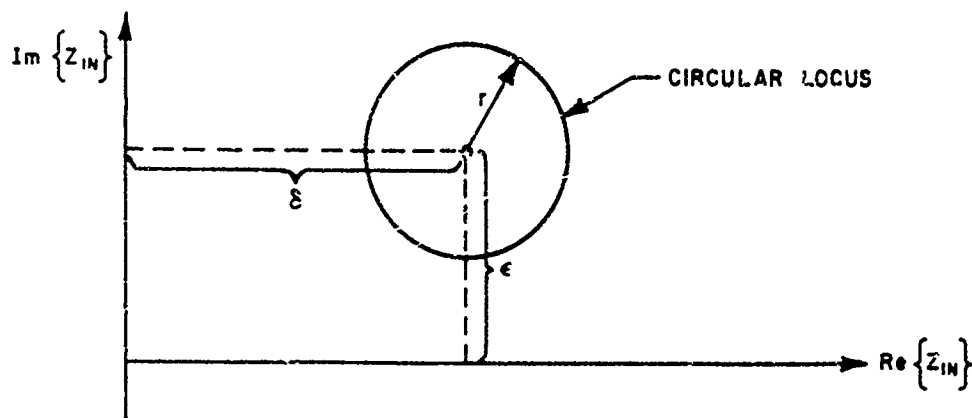


Figure 3. Input Impedance Locus for Reactive Termination of a Two Port Lossy Network

Assuming that the circle is centered at a real coordinate  $\delta$  and imaginary coordinate  $\epsilon$  and has a radius  $r$ , then  $\tau/\rho$  for the network can be shown to be

$$\tau/\rho = \frac{\delta}{r} \quad (2)$$

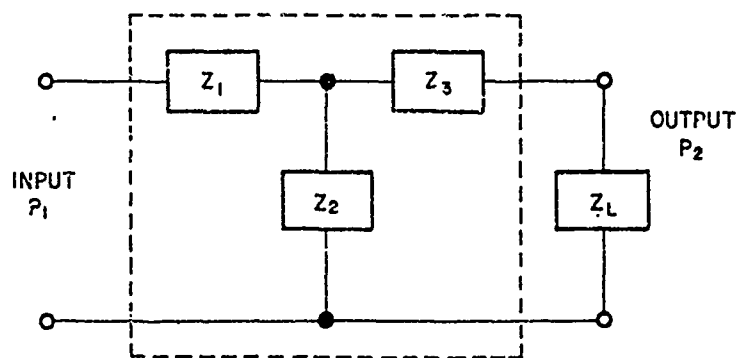
and  $\text{dB}_{wc}$  can be computed directly from Equation (1).

As an example, consider the ideal network in Figure 4a. We may calculate  $Z_{in}$  for three reactive loads and obtain

$Z_{Load}(\text{ohms})$	$Z_{in}(\text{ohms})$
+j0	4.40 +j5.92
-j10	6.10 +j3.98
+j10 <sup>8</sup>	6 +j8

If we plot these three points on linear paper with  $\text{Re}\{Z_{in}\}$  as the abscissa and  $\text{Im}\{Z_{in}\}$  as the ordinate, a circle can be constructed, and the center of the circle and radius can be determined. This is shown in Figure 4b.

From this figure  $\delta = 6.46$ ;  $\epsilon = 6.0$ ; and  $r = 2.06$  (all in ohms). The  $\tau/\rho$  ratio of this plot is 3.14 and the  $\text{dB}_{wc}$  from Equation (1) is 7.87 dB.



ASSUMED  
NETWORK VALUES

$$Z_1 = 2 + j3$$

$$Z_2 = 4 + j5$$

$$Z_3 = 6 + j7$$

Figure 4a. Ideal Network

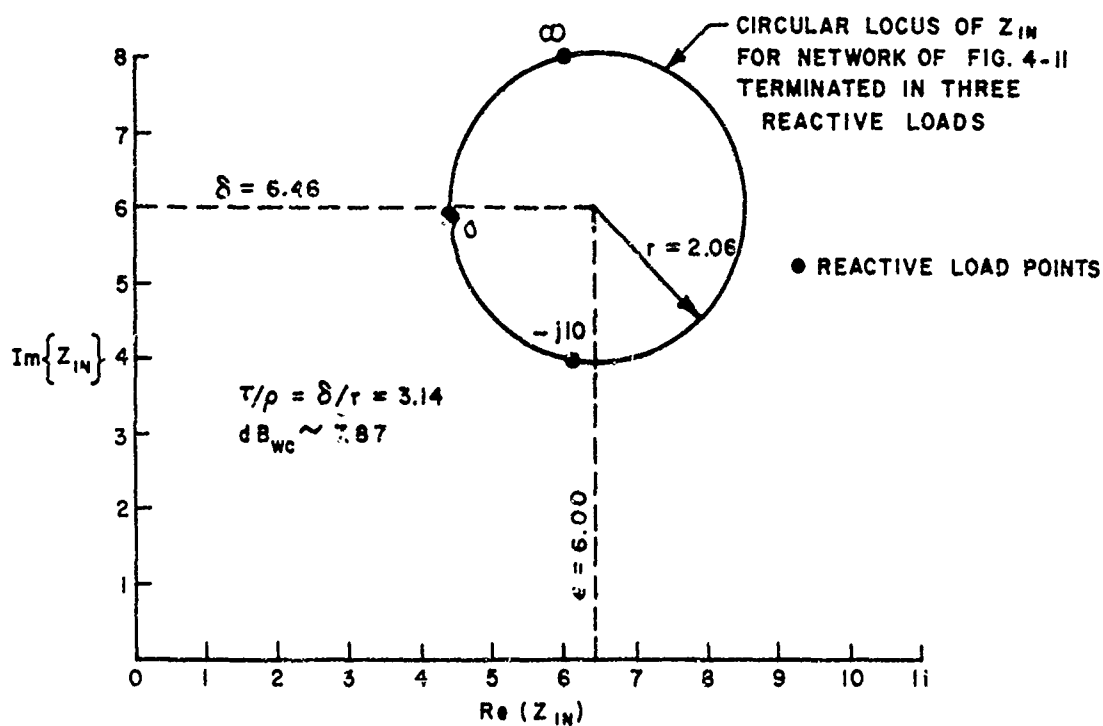


Figure 4b. Input Impedance Locus Method Applied to Network of Figure 4a.



For high attenuation filters, the  $\delta/r$  ratio becomes large and extreme accuracy in measuring  $Z_{in}$  becomes necessary. For example, for a 23 dB 50-ohm pad, at the same three load conditions, the input impedances are,

$Z_{Load}$ (ohms)	$Z_{in}$ (ohms)
+j0	49.50 +j0
-j10	49.54 -j0.190
+j10 <sup>8</sup>	50.50 +j10

The radius of this impedance circle is 0.50 ohms,  $\delta = 50$  ohms,  $\tau/\rho = 100$  and  $\epsilon = 0$ . For these loads the input impedance varies only about 2% and extreme measurement accuracy would be required.

### 2.3 Attenuation as a Function of Reflection Coefficient

A scheme similar to the above and which requires that the input impedances be known for various reactive loads deals with reflection coefficient locus in the following manner.

If the input reflection coefficient  $\gamma$  of the network is measured in relation to a real characteristic impedance  $Z_0$  then

$$\gamma = \frac{Z_{in} - R_0}{Z_{in} + R_0} \quad (3)$$

It can be shown by conformal mapping techniques that the reflection coefficient locus will also be circular for purely reactive terminations. This circle is defined by

$$\left. \begin{aligned} r_\gamma &= \frac{2r_R}{(\delta_R + 1)^2 - r_R^2 + \epsilon_R^2} \\ u_\gamma &= \frac{2(\delta_R + 1)}{(\delta_R + 1)^2 - r_R^2 + \epsilon_R^2} \\ v_\gamma &= \frac{2\epsilon_R}{(\delta_R + 1)^2 - r_R^2 + \epsilon_R^2} \end{aligned} \right\} \quad (4)$$

where  $Z_0 \delta_R = \delta$ ,  $Z_0 \epsilon_R = \epsilon$ ,  $Z_0 r_R = r$  and  $r_Y$ ,  $u_Y$  and  $v_Y$  are respectively the radius, real coordinate and imaginary coordinate of the center of the circle in the reflection coefficient plane.

Noting from Equation (2) that

$$\tau/\rho = \frac{\delta}{r} = \frac{\delta_R}{r_R}$$

and solving Equation (4) for the  $\frac{\delta_R}{r_R}$  ratio

$$\tau/\rho = \frac{\delta_R}{r_R} = \frac{r_Y}{2} + \frac{1-A^2}{2r_Y} \quad (5)$$

where  $A^2 = u_Y^2 + v_Y^2$ ; i.e.,  $A$  is the distance from the origin of the  $y$  plane to the center of the reflection coefficient circular locus.

A 23 dB<sub>WC</sub> attenuation is associated with a  $\tau/\rho$  value of 100. If we insert this value in Equation (5) and remember that both  $A$  and  $r_Y$  must be less than one, we can see that the  $r_Y/2$  term of Equation (5) must be of very small value; hence,

$$200 r_Y \approx 1 - A^2 \quad (6)$$

for dB<sub>WC</sub> equal to 23 dB. The most favorable measurement condition (that which gives the largest radius  $r_Y$ ) is that in which  $A = 0$ . Manipulation of Equation (5) shows that this condition can be obtained by selecting

$$Z_0 = \sqrt{\delta^2 - r^2} \quad (7)$$

Even under this special selection, however,

$$r_Y \approx \frac{1}{200} \quad (8)$$

and the diameter of the reflection coefficient circular locus is only 1% of the maximum reflection coefficient magnitude of one.

If the accuracy of the reflection coefficient measuring equipment was approximately  $\pm .02$  (on a reflection coefficient plot whose maximum magnitude must be one) then the determination of  $dB_{wc}$  with this equipment for a 23 dB network would be extremely difficult.

In summary, we find that the reflection coefficient method suffers from the same limitation as the input impedance method: very high accuracy equipment is necessary for the measurement of high values of worst case attenuation.

## 2.4 Multiple Impedance Measurements

With this method, we are dealing with a technique that has been used by FIRL for several years. We measure the input impedance of a network with a short circuit termination ( $Z_{sc}$ ) of the network and then with a 50-ohm termination ( $Z_{50}$ ). This is repeated with the network reversed. A computer program then calculates the  $dB_{wc}$  case and  $Z_{wc}$  from these measurements. An accurate impedance bridge is required to obtain meaningful answers. It was found with this technique that if devices with high attenuation are to be measured (above 25 dB) the input impedance is changed very little by output load terminations and accuracy is lost. This approach appears to be valid, however, for devices having attenuation values of 20 dB or less.

## 2.5 Attenuation From a Knowledge of the Network's TPL Surface

### 2.5.1 General Characteristics of the TPL Surface

It can be shown that a two port four terminal passive network can be completely defined by three real parameters,  $\rho$ ,  $\tau$ , and  $\sigma$ . The load/input power ratio then can be expressed in terms of real (x) and imaginary (y) parts of the load impedance and the three parameters as,

$$Z = P_{load}/P_{in} = \frac{2\rho x}{(x+\tau)^2 + (y+\sigma)^2 - \rho^2} \quad (9)$$

In using Equation (9) we are only interested in the surface in  $x, y, z$  space for which  $x \geq 0$ ,  $-\infty \leq y \leq +\infty$ , and  $z \geq 0$ . These restrictions dictate that  $\tau/\rho \geq 1$ ,  $\tau > 0$ ,  $\rho > 0$ ,  $-\infty \leq \sigma \leq +\infty$ . If we plot this function in the  $xy$  plane,  $xz$  plane and  $yz$  plane we obtain typical sections as shown in Figure 5 to 7 respectively.

The practical significance of Equation (9) is only appreciated if we attempt to determine accurately the three real parameters from measurements on an actual network.

### 2.5.2 Solutions by Assuming Measured Values to be Roots to a Real TPL Surface

The report referenced in the introduction presents the algebra which solves three equations of the form of Equation (9) simultaneously for  $\rho$ ,  $\tau$ , and  $\sigma$ . Three inputs are required and one load must be complex, otherwise the  $\sigma$  parameter will be undefined. A computer program was written in Fortran IV coding, and trials were made with ideal inputs from assumed paper networks as well as measured values on a ferrite filter at 0.1, 1 and 3 MHz. It was observed from this work that deviations as small as  $\pm 1\%$  from true inputs resulted in imaginary values for  $\rho$ ,  $\tau$ , and  $\sigma$ . It was reasoned that, every combination of  $\rho$ ,  $\tau$ , and  $\sigma$  has a TPL (terminated power loss) surface, but every TPL surface defined by arbitrary measured points is not associated with real values of the parameters. Since overall measurement errors could easily approach  $\pm 10\%$ , the above method will not serve our purpose too well. A little thought into the matter, however, indicated that if we were able to generate a real TPL surface that represented the best fit in a root mean square (rms) sense to the measured points we would have a fairly valid approach.

### 2.5.3 Solutions by RMS Fitting of Measured Values to a Real TPL Surface

A computer program is absolutely essential for this technique since it is based on an iterative process that is repeated thousands of times. In essence, the technique is based on the following steps:

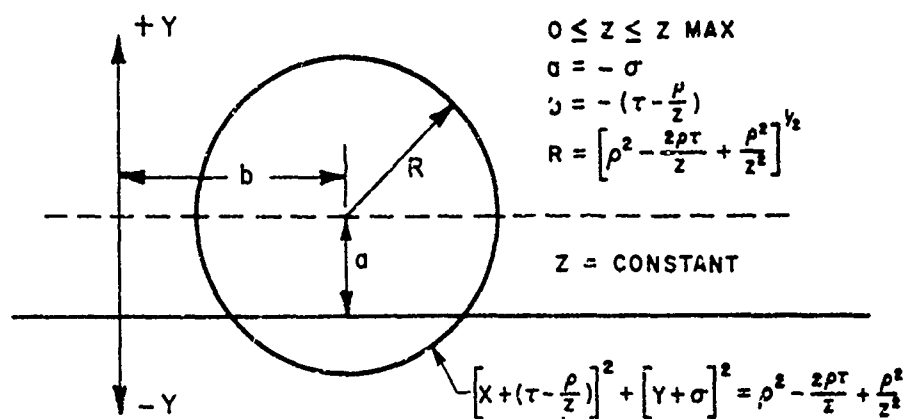


Fig. 5 XY Section of TPL Surface

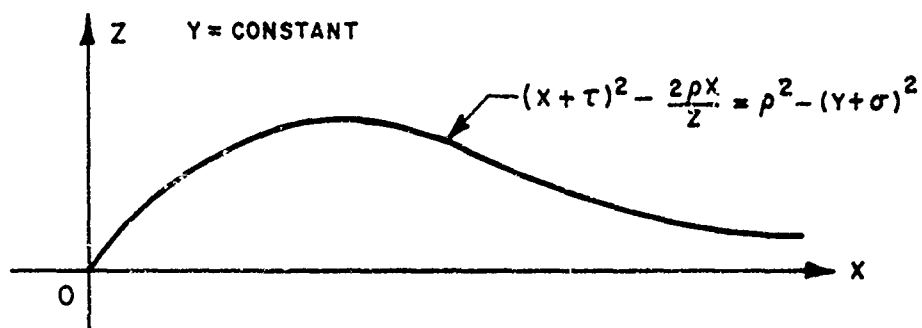


Fig. 6 XZ Section of TPL Surface

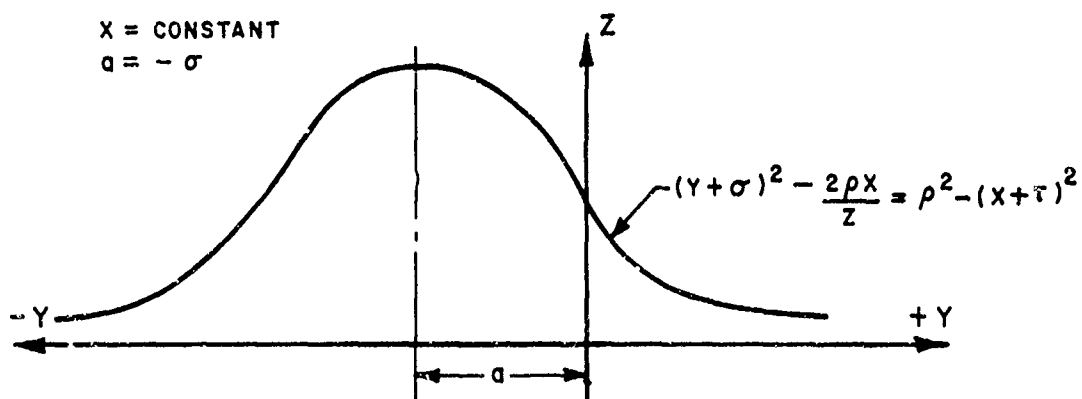


Fig. 7 YZ Section of TPL Surface

- (1) Measure various output/input power ratios at known load impedances for the given network.
- (2) Make an initial choice for a TPL surface by selecting real values for the  $\rho$ ,  $\tau$ , and  $\sigma$  parameters.
- (3) Using the loads from 1 and the parameters from 2 or 5, calculate a set of output/input power ratios from the general TPL Equation (9).
- (4) Compare these with the measured ratios in 1.
- (5) Increment  $\rho$ ,  $\tau$ , and  $\sigma$  in the direction of decreasing error and form a new TPL surface; repeat steps 3, 4, and 5.
- (6) Stop the process after a given fit has been obtained or after  $n$  iterations.

Based on present computer costs, a network can be analyzed for about \$6 or less. Redundant measurements can also be made and various combinations can be run and results averaged. The method is limited in frequency range to the extent that it is dependent on whether input power and load power can be determined with any degree of accuracy and if the true value of the load impedances are known. The system is also most effective for attenuations greater than 10 dB.

### 3. SUMMARY OF THE ADVANTAGES AND DISADVANTAGES OF THE VARIOUS MEASUREMENT SCHEMES

#### 3.1 Matching

The matching system method has several desirable features:

1. A relatively inexperienced person can make the measurements although maintenance of the system requires considerable skill.
2. Only one measurement need be made at each frequency.
3. The system can be made almost direct reading--often nothing more than a simple subtraction of two dB values is necessary for a final reading.
4. The theory is simple and readily comprehended.
5. The equipment, at least in the coaxial tuner frequency range, is available commercially.

6. The method allows measurement of the power transfer of the network directly and since the load power measuring equipment is voltage measuring equipment having very high gain, very high values of worst case attenuation can be measured. For present detector systems and available low power generators the upper limit on measurable attenuation is on the order of 80 dB.

The disadvantages of this system are all attributable to the matching sections. At the higher frequencies where coaxial line stretchers and shorting stubs can be used as matching sections, the loss in the matching components when the components are used under high VSWR conditions can cause fairly large errors in worst case attenuation readings. In its frequency range the matching components, if perfect, could match any impedance to any other; hence, the error in the measurement is due only to the loss. As mentioned earlier the loss in a matching section contributes to the error by two separate means, (1) it limits the impedance transferring qualities of the matching system so that a true match is not achieved and (2) it actually dissipates power. Both of these contributions tend to make any measurement of  $dB_{wc}$  appear higher than it actually is.

At the lower frequencies, where variable length coaxial components are still commonly used as matching sections, the variable length may not be sufficient to match any impedance to any other. Here the matching approach may indicate a value of  $dB_{wc}$  much higher than the actual value since the network being measured will not be correctly terminated or the input line to the network will not be flat, or both. The flatness of the input line can be checked with a directional coupler in most cases; however, the correct termination is not known, therefore, it can not be checked. Higher frequency systems that use double stub tuners are also susceptible to this source of error.

At the lower frequencies where distributed parameter components, such as coaxial line stretchers and shorting stubs can not be economically applied, variable lumped components are employed. In general, lumped variable components suffer from the same problems as their higher frequency counterparts. At frequencies between 1 and 10

MHz a lossless (or hi Q) variable inductance is extremely difficult to construct and is, in general, severely limited in its range of variable reactance.

In summary, the matching approach to measuring worst case attenuation has many desirable features but it has practical problems particularly at the lower frequencies where the systems must be hand tailored to the network to be measured. It has been our experience that any practical RF suppression device can be evaluated by this method but much engineering effort may be necessary.

### 3.2 Reflection Coefficient and Multiple Impedance Measurements

#### A. Reflection Coefficient

Determination of the input impedance or input reflection coefficient locus, has the following advantages:

1. Equipment is commercially available.
2. The concept is simple.
3. Relatively unskilled personnel may be employed.

The most important disadvantages are:

1. Even under the most favorable conditions, worst case attenuations of greater than 23 dB can not be determined with presently available equipment.
2. At the lower frequencies the purely reactive terminations necessary for the required measurements are difficult to obtain.

#### B. Multiple Impedance Measurements

The advantages are:

1. The equipment required is available commercially.
2. Results can be cross checked by further measurements.
3. A complete characterization of the network is obtained from the equivalent circuit.
4. The theory is straight-forward.



The disadvantages are:

1. Use of a computer is almost mandatory.
2. High values (23 dB or more) of worst attenuation can not be measured accurately with presently available equipment.
3. A large variety of equipment is necessary to cover the frequency band of interest.
4. A skilled technician is essential to make the measurements.

### 3.3 Relating to a Network's TPL Surface

#### A. Root Method

We have shown that power measurement errors as small as 1% can completely invalidate the approach. Since the power measurements across highly reactive impedances may well be 10% or more in error, we consider this approach untenable.

#### B. RMS Approach

The determination of three real power transmission constants by a "best fit" procedure, has not been thoroughly investigated but based on our present knowledge, the advantages appear to be as follows:

1. Results can be checked by further measurements.
2. Measurements of both very high and very low dB<sub>WC</sub> networks can be handled with available equipment.
3. The necessary computations give the three real power transmission constants as a by-product of the dB<sub>WC</sub> computations and hence TPL can be calculated for any known load.
4. The power measurements that make up the input data can sometimes be checked by other measurement methods.
5. The measured input data are essentially TPL ratios. These, in themselves, are useful for certain applications of many RF protective devices.

The disadvantages are:

1. A computer is absolutely necessary to evaluate the input data economically.
2. The power input data, especially that associated with highly reactive impedances, can be seriously in error with available measurement equipment.

3. The theory is relatively complicated.
4. A skilled measurement technician is necessary to obtain reliable data.
5. Several measurements are necessary to evaluate any one protection device.
6. Several different sets of measurement equipment would be necessary to use this approach over the entire frequency band of interest.

In conclusion, there appears to be no completely satisfactory universal system for determining the worst case attenuation of a device over the entire frequency range of interest and for all values of attenuation and input impedance. However, if one has some information on possible attenuation and input conditions, one can choose a system which, when properly applied, can be expected to give reliable results. All of the system suffer somewhat from present equipment limitations especially in terms of accuracy of equipment, possible losses in sliding contacts, components and frequency range of the equipment. Our technology is constantly improving the quality of instruments and such improvements should be constantly monitored and incorporated into the measuring systems whenever feasible.

## ABSTRACT - SESSION FIVE

### 5-1 Evaluation of the Susceptibility of SPRINT Ordnance to Electromagnetic Radiation (U)

*E.D. Kiehm and  
W.D. Raymond*

(U) During the transportation sequence of a missile system, such as SPRINT, between factory and launch site it is exposed to known and unknown RF fields. Rather than totally depend upon a "worst case analysis" alone, it was elected to empirically determine that SPRINT ordnance presented no hazard to life or property when immersed in the EMR environment in the so-called "transportation mode." This paper will present the preliminary tests, field test instrumentation design and calibration, and data analysis.

### 5-2 The Application of Heat-Resistant Explosives to Advanced Weapons and Space Systems (U)

*E.E. Kilmer*

(U) This paper concerns some of the properties and applications of several Naval Ordnance Laboratory developed heat resistant explosives. Applications of these materials, in new weapon systems and manned spacecraft systems such as APOLLO will be discussed. In addition, comparison of the performance of conventional RDX-MDF's and heat resistant MDF's after extended periods of heating will be presented.

### 5-3 A Simplified Approach to the Sensitivity of Conductive Mixes (U)

*W.S. Hall*

(U) In order to explain fully the behaviour of conductive mix EED's, it is necessary to admit at least three firing mechanisms. For each of these a separate and independent sensitivity threshold can be recognised. From measurements on devices based upon carbon as the conductor, values for each of the thresholds can be deduced. Predictions may be made concerning the future potential of conductive mixes particularly in relation to the low voltage system which would match some important future requirements.

### 5-4 Detonator Initiation by a Remotely Located Flash Charge (U)

*M.E. Anderson and  
James E. Means;  
Vincent J. Menichelli;  
Lien C. Yang*

(U) Analytical and experimental studies have been performed to establish the feasibility of remotely initiating a detonator with the radiant energy emitted from a small pyrotechnic or explosive flash charge. Two types of flash charges were used: (1) The M123 photo-flash cartridge, and (2) an explosively excited argon gas bomb. The primary requirements for the flash charge were that it be small, rugged, and emit radiation isotropically. Two techniques were examined for initiation of the detonator. The primary requirements for the detonator and sensor were that it be inexpensive, safe, and reasonably insensitive to critical alignment toward the flash charge. Several field tests were performed to establish at what distances from the flash charge each of the techniques could be expected to function.

### 5-5 An Experimental Investigation of a Fluoric Explosive Ignition Device (U)

*E.L. Rakowsky;  
A.P. Corrado*

(U) The objective of this study was to define the geometry and operating parameters affecting the performance of a resonance tube as a fluoric ignition device. Several models of varying geometric proportions were designed, fabricated and tested over a range of inlet pressures using both air and helium as the working fluids. The conclusion is postulated that the "Pneumatic Match" represents a quantum increase in safety, reliability, and simplicity of initiation devices.

5-6 Nuclear Hardened Explosive Devices (U)

*Stephen P.D. Smith  
Robert E. Betts, and J.E. Turrentine*

(U) This paper presents work done in an attempt to overcome the adverse effects of a nuclear environment on an electroexplosive device. One method being tried is the use of laser light for EED ignition. Both Neodymium and Ruby type lasers are being used in our exploratory program to determine the effects of frequency. Investigation is being carried out to determine various levels of laser light energy and how parameters affect the transmission of laser light to the EED fiber optics. Materials of construction of EED igniters are also being investigated.

5-7 A Percussion/Electric Primer for Machine Gun Ammunition (U)

*D.A. Schlachter and  
M.J. Puig*

(U) The design of a combination percussion/electric primer for 20mm gun systems is discussed. This primer will provide greater interchangeability of 20mm ammunition among various gun systems. One major design consideration has been to provide protection from inadvertent initiation by radio frequency energy. This has been accomplished by a capacitive voltage divider to decrease the induced rf voltage across the conductive mix. Both ceramics and plastic-clad metals have been studied for use as dielectrics in the capacitive network.

5-8 Remote Actuation of Line Controlled EED's by  
Electromagnetic Illumination (U)

*Jack O'Krepky;  
R.H. Thompson*

(U) This research program and paper presents an approach to clear enemy line controlled mines by induced heating of EED's using long waves. The presentation is expected to include Target Definition, Test Data, Analyses of Data and Proposed Hardware.

4-7 Pressure Thresholds for the Initiation of  
Composition B

*L.N. Cosner and R.G.S. Sewell,  
J.E. Sinclair*

Experiments were conducted in which the donor-receptor and related techniques were used to study the initiation of explosives by shock waves. The distance traversed by the accelerating wave and the time required to traverse that distance are shown to be directly related to the initial shock strength. An empirical equation of the exponential type is shown to fit the experimental observations. Analytical expressions to describe the general case are derived from the empirical equation.

# ATTENDANCE LIST 6EED

Adelman, Stanley	Picatinny	Burson, Joseph H.	NASA-Marshall
Agard, L.Cdr. C. C.	French Navy	Burwell, William R.	Naval Torpedo Station
Ainslie, Robert E.	Nav.Air Devel.Ctr.	Busby, Capt. Arthur	Norton AFB
Akst, I. B.	Mason & Hanger	Butterfield, Neil J.	Martin-Denver
Allen, Robert C.	McCormick Selph	Caldwell, Arnold	Franklin Inst.
Anderson, M.C.	Expl. Tech.	Campbell, LaVere A.	Thiokol-Brigham City
Anderson, Matthew E.	NWC-Corona	Cardie, William J.	Atlas Chem.Ind.
Andreasen, Wayne P.	North Amer.Rockwell	Carson, Robert M.	Harry Diamond Labs
Armstrong, H.T.	LTV Aerospace	Carter, Sam	Space Ord. Sys. Inc.
Austin, William	Bell Tele Labs	Chesterman, F. J.	Admiralty Surface Weapons
Austing, James	IIT Res.Inst.	Chisel, Dean M.	NASA-Ames
Ayres, James N.	NOL-White Oak	Cohn, Gunther	Franklin Inst.
Bach, L. B.	NWL-Dahlgren	Colburn, W. H. Jr.	Singer Gen.Prec. Sys.Inc.
Bacquet, Eugene A.	Bendix Msl.Sys.Div.	Cole, M. W. Jr.	Esso Prod. Res. Co.
Baihets, Roy	Singer Gen.Prec.Inc.	Colpitts, David A.	NWC-China Lake
Barbarisi, M.	Edwards AFB	Conner, Allan L.	Los Alamos Scientific Lab
Baron, Michael	Picatinny	Cornack, Charles M.	Naval Air Sys. Cmd
Barron, Dr. Saul	Dept.of Navy	Corrado, Anthony P.	Picatinny
Beard, Lawrence W.	Conax Corp.	Corsey, Roland	Naval Ord. Station
Becker, Gerald H.	Sprague Elec.Co.	Cosner, L. N.	NWC-China Lake
Bement, Laurence J.	Thiokol-Elkton	Cote, William I.	Hercules
Benedict, A. G.	NASA-Langley	Craig, James R.	Sandila Corp.
Bennett, David E.	ARC Assoc. Inc.	Craig, Ralph R.	Keynolds Ind.Inc.
Bicks, Lt. D. E.	Sandia Lab	Crain, E. L.	McCormick Ind. Inc.
Blackshire, Robert	Ministry of Def.(Navy)	Daly, J. L.	Lockheed-Naval Plt.Rep. Office
Blake, T. Gaynor	Unidynamics/Phoenix	Davenport, D.E.	Singer Gen.Prec.
Boggs, Brian F.	Hanley Ind. Inc.	Deleray, A. L.	MBAssociates
Boliveau, C. W.	Ensign Bickford	Delskey, S.	General Electric Co.Phila.
Bowers, Francis X.	Thiokol-Brigham City	DesRochers, L. Geo.	Canadian Ind. Ltd.
Bradley, Edward L.	Grumman Aircraft Engr.	Disher, E. Odell	Bell Telephone Labs
Bratton, Dr. F. H.	The Boeing Co.	Doellner, Leonard	The Boeing Co.
Breakey, William S.	Ensign Bickford	Dondero, Andrew	Fairfield Scientific Corp.
Brocce, L. R.	McCormick Selph	Drinkard, G.L.	Hughes Aircraft Co.
Broske, Wm.	Goodyear Aerospace	Dunphy, John B.	Sanders Assoc.
Brown, Paul A.	AMP Inc.	Durham, Dough	Lockheed M&S Co.
Brown, Richard	Naval Air Test Ctr.	Eckert, N.C.	Atlantic Res. Corp.
Bruscino, J.	Atlas Chem. Ind.Inc.	Eisenhart, Robert W.	Amron Corp.
Burkdoll, F. B.	Picatinny	Eliezer, Efrati	Gov't of Israel
Burnett, R. J.	Expl. Tech.	Ellena, James	Atlantic Res. Corp.
	Sandia Labs.	Fedowitz, Frank	TRW Systems Group

Ferguson, R. M.	Canadian Arsenal Ltd.	Harlan, Jere G.	Sandia Labs
Ferrell, Robert B.	Los Alamos Scientific Lab	Harrell, Fred	DCASR- San Francisco
Fillippi, Ernest A.	Special Devices Inc.	Hassler, John W.	Holox Inc.
Finochio, D.F.	Quantic Ind. Inc.	Hauser, Ralph I.	Westinghouse Elec.
Fitzgerald, W. J.	Aerospace	Hedden, S. E.	NWL-Dahlgren
Fitzgerald, William	Colt's Firearms Div.	Heidelbach, R. G.	Johns Hopkins Univ.
Fitzhugh, Robert S.	Los Alamos Scientific Lab	Heinenmann, Robert W.	Picatinny
Flagg, Dr. Robert F.	Holox Inc.	Heiney, Otto K.	Jet Propulsion Lab
Fleming, Bert	AVCO -Stratford, Conn.	Hepner, Richard R.	E.I. Dupont
Flowers, Bobby J.	NASA-Wallops	Hevesy, Louis W.	Aerojet
Folsom, Robert E.	Hercules Inc.	Hewitt, Jack G.	Denver Res. Inst.
Ford, James A.	Fairfield Scientific Corp.	Hickman J. D.	NWL-Dahlgren
Fox, Edward A. Jr.	Atlas Chem. Ind.	Hillman, J. T.	Sandia Lab
Freeman, William B.	Martin-Orlando	Holfard, John E.	Army Materiel Cmd
Fyfe, Donald	Unidynamics/Phoenix	Huber, John F.	Unidynamics-Phoenix
Gaither, Don	Naval Ammo Depot	Huntington, John	Physics Internat'l Co.
Gallant, W. Keith	Honeywell Inc.	Ingham, R. W.	McCormick Selph
Gartenberg, Allan	Aerospace	Inglis, R. T.	General Dynamics Pomona
Garvin, Lawrence	DCASR -San Francisco	Jablovskis, Janis	NWL-Dahlgren
Gay, Benjamin	Networks Elec. Corp.	Johnson, C. D.	Honeywell Inc.
Gerber, F.	Dayton T. Brown Co.	Johnson, Theodore	Remington Arms Co.
Gigas, G.	Atomics International	Jones, Jerry O.	NWC-Corona
Gluckman, I. B.	Lockheed MAS Co.	Kabik, I.	NOL-White Oak
Goldberg, Ernest	Raytheon	Kaeding, G. G.	TRW Systems
Goldfarb, George	Aerospace	Kahl, F. A.	Joslyn Elec. Systems
Goldie, Victor	G.E. Co.-Chestnut St.	Kaszupski, Stanley	Frankford Arsenal
Goodall, Roger A.	Singer Gen. Prec.	Kawka, John H.	Norton AFB
Goudy, Joseph R.	NASA-Langley	Kent, E. H.	Atlantic Res. Corp.
Gower, W. R.	E.I. DuPont Expl. Dept.	Kestler, George	Autonetics/Div. of N. Amer. Rockwell
Green, Arden	DCASR -San Francisco	Kiehm, Erdman D.	Martin-Orlando
Greenough, Clarence	North Amer. Rockwell	Kilmer, Eugene E.	NOL-White Oak
Griffin, D. N.	Quantic Ind. Inc.	Laughlin, R.C.	United Tech. Ctr.
Grimes, P. M.	Unidynamics-Phoenix	Lawhill, Ronald C.	Central Tech. Inc.
Guay, Roland	Naval Plt.-Rep. Office Lockheed	Laybourn, Lt. Col. Wm.	Defense Atomic Support Agency
Gunter, Wayne D.	NASA-Wallops	Leavitt, L. F.	Reynolds Ind. Inc.
Hall, Wilfred S.	British Embassy	Leeman, L. E.	Monterey Tech Inc.
Haluza, D. J.	United Tech. Ctr.	Leopold, Howard S.	NOL-White Oak
Hamilton, Ralph H.	G.E. Co. Phila.	Lewis, Don	Space Ord. Sys. Inc.
Hamister, Don B.	Joslyn Elec. Sys.	Lilly, James L.	G.E. Co. Phila.
Hannum, Edward E.	Franklin Inst.	Lockard, Charles W.	Naval Supply Ctr.

Locklin, H. W.	G.E.-Houston	Peckham, Herbert D.	Singer Gen.Prec.
LoFiego, Louis	Bermite	Petrack, John T.	Nav. Weapons Lab
Luth, Percy A.	HiShear	Piccoli, Syl C.	Singer Gen.Prec.
Lyn h, Robert W.	HiShear	Pierard, A.E.	LTV Aerospace
Lytic, Dell	Space Ord. Sys.	Pierce, David M.	Sandia Lab
MacDonald, Bert	Physics Internat'l	Pierson, Edward G.	Conax Corp.
Macdonald, W. G.	Canadian Forces Hdq	Pitts, Locha	Singer Gen.Prec.
MacFarlane, B. F.	Atlantic Res. Corp.	Plummer, W. A.	The Zippertubing Co.
Marshall, Tyler	McGraw-Hill	Pokraka, R. G.	McCormick Selph Assoc.
Maxwell, Billy Ray	Expl. Tech.	Pratt, Alexander	Sanders Assoc.
McLain, J. H.	Wash. College	Puech, Louis	D.C.A.N. France
McLellan, Quinton A.	Harry Diamond Labs	Puig, Michael J.	NWL-Dahlgren
Means, James E.	Naval Weapons Ctr.	Quinn, A. S.	SAFECOM-DER
Menichelli, Vincent J.	Jet Propulsion Lab	Radke, Harold H.	Aerospace
Miller, Paul H.	Atlas Chem. Ind.	Rakowsky, Edward L.	Singer Gen.Prec.Inc.
Mohrbach, Paul	Franklin Inst.	Randall, Howard J.	DCASR-San Francisco
Montesi, Louis J.	NOL-White Oak	Ray, E. R.	TRW Systems
Montgomery, Jeff	Varian Assoc.	Reed, Lt. Col. Leon	DCASR - San Francisco
Moore, Donald Baker	Expl. Tech.	Reinhardt, Jack R.	Atlantic Res. Corp.
Morris, Edmond J. Jr.	Nav. Underwater Weapons Stat	Rexon, C. J.	DCASR -Los Angeles
Motchok, Emil	Sylvania Elec. Sys.	Richardson, Neil	Tech. Ord. Inc.
Moyant, D. A.	Atlas Chem. Ind.	Riester, James J.	U.S. Nav.Amm. Depot
Mumma, Douglas	Physics Internat'l Co.	Rieter, Howard	Sanders Assoc.
Murphy, Arthur J.	Jet Propulsion Lab	Riley, B. J.	Allison Div. GMC
Myers, Robert C.	Lawrence Rad. Lab.	Ritchie, R.	Singer Gen.Prec.
Nagengast, Crosby	Pyronetics Inc.	Roberts, J. R.	Canadian Arsenal's Ltd.
Neff, William K.	Fairfield Scientific Corp.	Rojas, Octavio	Space Ord. Sys.
Nellis, Stewart	Tech. Wire Products Inc.	Romine, E. A.	Sandia Corp.
Nelson, Gary R.	Chamberlain Mfg. Corp.	Roper, R. L.	General Dynamics
Nesbitt, Scranton	NOL-White Oak	Rose, W. E.	Unidynamics-Phoenix
Norman, William D.	TRW Systems	Ryle, Bernard G.	AMP Inc.
North, H. S.	Sandia Corp.	Saldarini, Walter	EG&G
Numbers, Gary L.	Monsanto Res. Corp.	Salzman, Paul K.	General Dynamics Pomona
Nye, Charles D.	Pyronetics Inc.	Schellman, Armond	Fairfield Scientific Corp.
O'Krepky, Jack E.	Picatinny	Schimmel, M.L.	McDonnell Douglas
Ollikkala, W. A.	Twelfth Coast Guard Dist.	Schor, Ferdinand	Consultant
Ozenghar, Homer H.	DCASR--Anaheim	Scott, Calvin L.	NOL-White Oak
Parker, Robert	Lawrence Rad. Lab	Schroll, Oscar M.	Sandia Lab
Patrick, Wayne	Mason & Hanger	Schwarz, Alfred C.	Sandia Lab
Patton, James B.	Physics Internat'l Co.	Schwerdtfeger, Lee H.	Johns Hopkins Univ.

Sells, Rodney, R.	FMC Corp.	Warner, Clyde, W.	Harry Diamond Labs.
Shackelford, Walter E.	Maxson Elec.	Warner, Robert Keith	Harry Diamond Labs.
Shani, Bezadei	Gov't of Israel	Warren, C. E.	Lundy Tech. Ctr.
Sheppard, Donald C.	JFK Space Ctr.	Marshall, Theodore	Picatinny
Sheridan, George E.	Reynolds Ind. Inc.	Wattstreet, Irv. A.	Space Ord. Sys. Inc.
Shirley, Noel C.	G.E. Co.-Pleasanton	Watts, Harry	British Embassy
Silva, Joseph W.	Olin Math.Chem. Corp.	Maxler, Daniel	Picatinny
Simmons, W. H.	NASA-Houston	Weinman, Lawrence	Colt's Pyrodynamics Oper.
Sinclair, Prof. James	Nav.PostGraduate School	Weintraub, Herbert S.	MBAssociates
Sincock, Richard E.	Northrop Electro-Mech.Div.	Weisman, S. D.	Atlantic Res. Corp.
Small, B. B.	Singer Gen.Prec. Inc.	West, Troy L.	White Sands Msl.Range
Smith, Allan H.	Lockheed M&S Co.	Wiard, Thomas D.	Univ. of Calif.
Smith, Robert D.	Unidynamics-Phoenix	Williams, J.L.T.	McDonnell Douglas Corp.
Smith, Steven P.	U.S. Army Msl.Cmd.	Williams, V.D.	Quantic Ind. Inc.
Smith, William M.	Ensign Bickford Co.	Wilson, C. R.	G.E. Co.-Pleasanton
Stark, William E.	Colt's Firearms Div.	Witzerman, M. Allyn	Monsanto Res. Corp.
Stecker, Ernest J.	Holox Inc.	Wood, J. M.	Quantic Ind. Inc.
Steeves, Cameron W.	Fairfield Scientific Corp.	Wood, William A.	Aeronutronic Div.Of Philco Ford
Steinberg, E.	TRW Systems	Worden, Bruce	Sandia Corp.
Sterling, Walter	TRW Elec. Tech.	Worwag, W. R.	Martin-Denver
Stresau, R. H.	R. Stresau Lab	Young, Galen R.	Holox Inc.
Sullivan, R. R.	Douglas Aircraft Corp.	Zablocki, Henry S.	Markite Corp.
Syrop, Leroy J.	Del Mar Engr. Lab	Zacharin, Alexey	Picatinny
Taylor, Boyd	Ballistic Res. Lab	Zimmer-Galler, R.	Nav.Ordnance Station
Taylor, Philip R.	Brown Engr. Co.	Zimmerschied, Alan B.	The Boeing Co.
Tharp, Mitchell, D.	Central Tech. Inc.		
Thomas, W. R.	Hercules, Inc.		
Thompson, A. L.	Singer Gen. Prec.		
Thompson, Ramie H.	Franklin Inst.		
Tuchto, Jess	Amphenol Canada Ltd.		
Valenti, R. M.	Singer Gen.Prec.		
Van Landingham, Earl	NASA-Langley		
Varnado, G. Bruce	Sandia Lab		
Vlahos, Petro	Motion Picture Res. Ctr.		
Voreck, W. E.	Picatinny Arsenal		
Voznick, H. P.	William Wahl Corp.		
Wagner, Robert	Picatinny		
Walbancke, Cmdr. Fred W.	Ministry of Def.(Naval)		
Walker, N. N.	N. Amer. Rockwell		
Ward, John	Space Ord. Sys.		